TRACE ELEMENT DISTRIBUTIONS AND PARTITIONING TRENDS IN HYDROTHERMAL BASE METAL SULPHIDE ORES COMPRISING SPHALERITE, GALENA, CHALCOPYRITE AND TETRAHEDRITE-TENNANTITE

LUKE GEORGE

This thesis is submitted for the degree of Doctor of Philosophy

in the

School of Physical Sciences, Department of Earth Sciences,

at

The University of Adelaide

THE UNIVERSITY of ADELAIDE

March 2017

TABLE OF CONTENTS

ABSTRACT

This study addresses trace element concentrations and distributions in hydrothermal base metal sulphide (BMS) ores using samples from a wide variety of ore deposits and conditions of ore formation. The ranges of trace elements that can be incorporated into natural sphalerite, galena, chalcopyrite and tetrahedrite-tennantite are determined, as are the preferred equilibrium trace element partitioning trends among these sulphides.

The previously documented coupled substitution $Ag^{+}+(Bi, Sb)^{3+}\leftrightarrow 2Pb^{2+}$ in galena is confirmed, yet should also be modified to include Cu^{+} and Tl^{+}. However, when Bi and/or Sb are present at concentrations above ~2000 ppm, incorporation likely includes the creation of site vacancies. Thallium is always principally hosted in galena when BMS assemblages including sphalerite and chalcopyrite are mapped with LA-ICP-MS. Trace element mapping also reveals oscillatory and sector compositional zoning of various elements in galena for the first time. It is inferred that the partitioning of certain minerals between galena and sphalerite pairs is both predictable and systematic.

This systematic partitioning is explored and it is shown that the primary factors controlling the preferred BMS hosts of almost all trace elements in sphalerite-galena-chalcopyrite assemblages are element oxidation state, ionic radii of the substituting elements, element availability and the maximum trace element budget that a given sulphide structure can accommodate. In contrast, it is revealed that temperature, pressure, redox conditions at time of crystallization and metal source, do not significantly affect the preferred BMS host of almost all trace elements. The only exceptions to this recognized in the study are the critical metals Ga, In and Sn in assemblages recrystallized at high metamorphic grades. Observed partitioning patterns can be used to assess whether a particular BMS assemblage co-crystallized.

Compared to sphalerite and galena, trace element concentrations in chalcopyrite are typically quite low (tens to hundreds of ppm). Nevertheless, it is shown that chalcopyrite can host a wide range of trace elements, and the concentrations of such elements generally increase in chalcopyrite in the absence of other co-crystallizing sulphides. Importantly, chalcopyrite is generally a poor host for most elements considered harmful or unwanted in the smelting of Cu (except for Se and Hg on occasions), which suggests it is rarely a significant contributor to the presence of such elements in copper concentrates. The concentrations of Zn and Cd in chalcopyrite show systematic variation that depends, at least in part, on the temperature of BMS crystallization. The Cd:Zn ratios in coexisting chalcopyrite and sphalerite may be used to assess if the physiochemical conditions remained constant during BMS crystallization.

Since minerals of the tetrahedrite isotypic series are also common components in base metal ores, investigation into the trace element chemistry of tetrahedrite-tennantite is relevant to understanding the controls on trace element partitioning in such ores. It is shown that tetrahedrite-tennantite will always be the primary host of Ag, Fe, Cu, Zn, As and Sb, and will be the secondary host of Cd, Hg and Bi in co-crystallizing BMS assemblages. Conversely, tetrahedrite-tennantite is a poor host for the critical metals Ga, In and Sn, all of which will prefer to partition to co-crystallizing BMS.

DECLARATION

I certify that this work, to the best of my knowledge, contains no material previously published or written by another person, except where due reference has been made in the text, and that, unless otherwise indicated (see preface), no material has been accepted for the award of any other degree or diploma in my name, in any university or other tertiary institution. In addition, I certify that no part of this work will, in the future, be used in a submission in my name, for any other degree or diploma in any university or other tertiary institution without the prior approval of The University of Adelaide and, where applicable, any partner institution responsible for the joint-award of this degree.

I acknowledge the support I have received for my research through the provision of an Australian Government Research Training Program Scholarship.

I give consent to this copy of my thesis, when deposited in the University Library, being made available for loan and photocopying, subject to the provisions of the Copyright Act 1968. I also give permission for the digital version of my thesis to be made available on the web, via the University's digital research repository, the Library Search and also through web search engines, unless permission has been granted by the University to restrict access for a period of time.

I acknowledge that copyright of published works contained within this thesis resides with the copyright holder(s) of those works.

Signed _____ Date 26/05/17

ACKNOWLEDGEMENTS

The completion of this PhD would not have been possible without the support and encouragement from numerous people.

Firstly, I would like to recognise the staff at Adelaide Microscopy, in particular, Mr. Angus Netting, Dr. Animesh Basak, Mr. Ken Neubauer, Ms. Aoife McFadden, and especially Dr. Benjamin Wade. Thank you for training me in various analytical techniques, tirelessly providing assistance whenever needed and creating such a great place to work in.

I would like to acknowledge our research group led by Prof. Nigel Cook and Dr. Cristiana Ciobanu. This group has provided the ideal environment in which to learn and grow. It has been exciting working with such a diverse group that has achieved many significant scientific outcomes. I would particularly like to thank Alkis, Sasha and Matt, who began their projects at the same time as me. This journey would not have been anywhere near as enjoyable without you.

I would also specifically like to thank my two supervisors, Prof. Nigel Cook and Dr. Cristiana Ciobanu for always being available and ready to help in any way needed. Your unwavering support and encouragement have helped me develop in so many ways over the last 3 years. Cristi, I thank you for always being willing to push me to be better and not settle for 'good enough'. Your tireless pursuit of excellence is evident in your own work, and I hope it has rubbed off on me. Nigel, I could not have asked for a better primary supervisor. You have been so easy to get along with, both on professional and personal levels. Communicating with you has been effortless and I'm thankful that we have almost always seen eye to eye on things. Never have you sent me away when I needed assistance, no matter

how trivial the matter. Yet you have also given me much freedom to develop my project myself, try things, and make mistakes. I have come to deeply respect you, not just as a scientist, but also as a person.

I have been undeservedly blessed with the family and close friends that I have. They have been a constant source of support over the last 3 years and I hope that I have made them all proud. I specifically thank my Mum and Dad who have raised me selflessly, loved me unconditionally and have constantly encouraged me to pursue whatever I wanted. I hope I am becoming a person like you both. To my beautiful wife Steph, thank you for being by my side throughout this journey, putting up with many late nights in the lab and cheering me on. You have continually inspired me to push on and have always believed I had what it takes, even when the task seemed overwhelming. Thank you for providing a loving place of escape from the world of research when I've needed it. I love you!

Lastly, and most importantly, I give all glory and honour to my God and Saviour Jesus Christ, who loves me and gave his life for me, though I do not deserve it. You are the giver of intellect and logic, the one who created a rational and orderly world, and thus the one who makes science possible. In some small way, I hope, like many of the founding fathers of modern science, to have uncovered more of the beauty in your world.

"To know the mighty works of God, to comprehend His wisdom and majesty and power; to appreciate, in degree, the wonderful workings of His laws, surely all this must be a pleasing and acceptable mode of worship to the Most High, to whom ignorance cannot be more grateful than knowledge."

-Nicolaus Copernicus

PREFACE

This thesis comprises of a portfolio of manuscripts which have been published, or accepted for publication, in international peer-reviewed journals. The journals in which these papers have been published and/or accepted are *'American Mineralogist'* (Chapter 3), *'Ore Geology Reviews'* (Chapter 4), *'Mineralogical Magazine'* (Chapter 5) and *'Minerals'* (Chapter 6). All of the manuscripts are closely related, and summarise the sulphide trace element analytical data, observations and interpretations that were made as part of this project. Recommendations have been made at the end of this thesis as a direct result of the key findings of this research, and it is hoped that many of these are explored at a later date.

The four papers which form the basis of this thesis are:

1. George, L., Cook, N. J., Ciobanu, C. L., Wade, B. P., 2015. Trace and minor elements in galena: A reconnaissance LA-ICP-MS study. American Mineralogist 100, 548-569. (*This paper builds on research undertaken during the candidate's honours year.)*

2. George, L. L., Cook, N. J., Ciobanu, C. L., 2016. Partitioning of trace elements in co-crystallized sphalerite–galena–chalcopyrite hydrothermal ores. Ore Geology Reviews 77, 97-116.

3. George, L. L., Cook, N. J., Crowe, B. B. P., Ciobanu, C. L., 2017. Trace elements in hydrothermal chalcopyrite. Mineralogical Magazine (accepted for publication at time of thesis submission).

4. George, L. L., Cook, N. J., Ciobanu, C. L., 2017. Minor and trace elements in natural tetrahedrite-tennantite: effects on element partitioning among base metal sulphides. Minerals 7, 17. doi: 10.3390/min7020017.

Chapter 8 contains all additional material* for the main papers outlined above, as well as additional conference abstracts, and other co-authored publications that have been produced. The additional material is as follows:

A. Additional material for Chapter 3 (Paper 1).

B. Additional material for Chapter 5 (Paper 3).

C. Additional material for Chapter 6 (Paper 4).

D. Cook, N., Ciobanu, C. L., George L., Zhu Z. Y., Wade B., Ehrig K., 2016. Trace element analysis of minerals in magmatic-hydrothermal ores by laser ablation inductively-coupled plasma mass spectrometry: Approaches and opportunities. Minerals 6, 111. doi: 10.3390/min6040111.

E. George, L. L., Cook, N. J., Ciobanu, C. L., 2016. Trace element partitioning between sphalerite, galena and chalcopyrite (Abstract). 35th International Geological Congress, Cape Town, South Africa, August 27th – 4th September.

F. George, L., Cook, N., Ciobanu, C., 2015. Controls on trace element partitioning between sphalerite and galena (Abstract and Poster). Society of Economic Geologists Conference 2015, 'World-Class Ore Deposits: Discovery to Recovery', Hobart, TAS, Australia, September 27th – 30th.

* Appendix A for Chapter 4 (Paper 2) may be found in Chapter 4

G. George, L., Cook, N. J., Ciobanu, C. L., 2015. Trace element partitioning between co-existing sphalerite, galena and chalcopyrite (Extended abstract). In: André-Meyer, A. -S., et al., Eds., Mineral Resources in a Sustainable World. Proceedings of the 13th SGA Biennial Meeting, Nancy France, ISBN: 978-2-85555-065-7, 24-27.

H. Cook, N. J., Ciobanu, C. L., George, L. L., Crowe, B., Wade, B. P., 2014. Trace Element Distributions in Sulphides: Progress, Problems and Perspectives (Extended abstract), 14th Quadrennial Symposium of the International Association on the Genesis of Ore Deposits, 'Mineral Resources: Discovery and Utilization, "Let's brainstorm"', Kunming, China 19th – 22nd. August 2014, Acta Geologica Sinica (English Edition) 88, 1444-1446.

The final chapter of this thesis consists of a complete reference list of all publications cited within any of the manuscripts, chapters and additional material of this thesis.

CHAPTER 1

INTRODUCTION

CHAPTER 1: INTRODUCTION

This chapter provides an overview of the history of trace element analysis of sulphide minerals, details of the laser ablation inductively-coupled plasma mass spectrometry used extensively in this study, common applications of trace element data and the objectives and structure of this thesis.

1.1 A brief history of trace element data for common sulphides

Metal sulphides represent some of the most economically important minerals in the Earth's crust. They are the principal sources of base metals and are also abundant components of precious metal deposits. About a dozen of the 400 or so sulphide minerals are sufficiently common that their mineralogy, geochemistry and paragenesis have become of widespread interest to geologists concerned with understanding geological processes (Bowles et al., 2011).

Interest in sulphide-hosted trace elements began in the 1930s. Much of the research at that time was focused on understanding the hosts of economic elements in sulphide ores (e.g., Noddack and Noddack, 1931; Warren, 1932; Warren and Loofbourow, 1932; Lord, 1933; Oftedahl, 1940; Stoiber, 1940). At the same time, the treatment of such ores for optimum extraction of economic elements was also being pursued (e.g., Hoffman, 1934; Park, 1934; Sebba and Pugh, 1937). Element analysis during this period was generally conducted using wet chemistry techniques, and as such all analyses were made on bulk mineral separates. These bulk methods were greatly limited in their ability to recognize inhomogeneity in

minerals (e.g., inclusions, or compositional zoning). These studies were compiled into the authoritative paper published by Fleischer (1955).

From the late 1950s to 1960s, the development and commercialization of electron probe microanalysis (EPMA) initiated significant development in the quality of element analysis in all minerals, including sulphides. The technique provided microanalysts with the ability to truly measure elements *in-situ*. This permitted researchers to accurately determine concentrations of minor elements in sulphides as part of ore deposit studies (e.g., Fujiki, 1963; Urasima, 1968), contributed to an expansion of synthetic experiments (e.g., Kano and Nambu, 1967; Takenouchi and Fujiki, 1968), and led to the recognition of many solid solution series in nature (e.g., Nakamoto et al., 1969; Sugaki et al., 1970). In a similar way, the development and popularization of secondary ion mass spectrometry (SIMS) and particle-induced X-ray emission (PIXE) through the 1980s caused the next revolution in microanalysis (e.g., Duchesne et al., 1983; Harris et al., 1984; McIntyre et al., 1984; Cabri et al., 1984, 1985; Chryssoulis et al., 1986, 1987, 1989; Remond et al., 1987; Cathelineau et al., 1988; Chryssoulis 1989). Such techniques allowed the quantification of elements at much lower minimum detection limits than offered by EPMA.

Through each new development in microanalysis over the last six decades, numerous new opportunities have arisen for sulphide research. Yet despite the many changes to microanalytical techniques, the main drivers for such sulphide research has largely remained the same; notably, the desire to understand how elements of interest are hosted in ore bodies, what controls their distribution, and how they can best be exploited.

For example, research targeted at the characterization of trace element distributions in pyrite and arsenopyrite has been driven by the desire to understand how ‘invisible gold’ is hosted in the Fe-sulphides with the purpose of determining its role in refractory ores, in which recovery by conventional methods is unsatisfactory. It has long been recognized that

pyritic Au ores can contain Au that is neither visible under the microscope, nor recoverable using conventional processing techniques (e.g., Bürg, 1935), and that the proportion of this invisible gold can significantly influence the economic viability of some ores in a negative way (Henley, 1975; Gasparrini, 1983; Cabri, 1988; Harris, 1990).

In a series of papers in the late 1980's and early 1990's, Cabri, Chryssoulis and co-workers applied new microanalytical techniques (proton microprobe, SIMS) to the problem of invisible gold. These studies not only confirmed the presence of invisible gold as lattice-bound or nanoparticulate Au within the structures of common sulphides (pyrite and arsenopyrite; see below), but were able to generate accurate quantification of such Au at concentrations down to the ppb-level (Cabri, 1987, 1988, 1992; Chryssoulis et al., 1987, 1989; Cabri et al., 1989; Cook and Chryssoulis, 1990). These pioneering studies also demonstrated that chalcopyrite and other base metal sulphides were poor hosts for invisible gold. It was recognized that Au-rich pyrite is generally also enriched in As, and that pyrite is typically less efficient at hosting Au than coexisting arsenopyrite, often by concentrations of an order of magnitude or more. The role of pyrite as an economically significant Au carrier was, however, potentially high or dominant where arsenopyrite was rare or absent. The relationship between Au and As was also consistent with work on Au-rich arsenopyrite being undertaken at the same time (Cathelineau et al., 1988). Throughout the subsequent 20 years or so, many dozens of studies (e.g., Arehart et al., 1993; Huston et al., 1995; Large et al., 2009; 2014; Cook et al., 2013a) have contributed to a now sizeable dataset for Au and other trace elements in pyrite.

Most of these studies have largely confirmed the important role of As as a 'catalyst' for the incorporation of Au in pyrite. This relationship, and the occurrence of lattice-bound versus particulate Au, was quantified by Reich et al. (2005), who showed a wedge-shaped area on a Au vs. As plot, under which Au may be expected to occur in solid solution, and

above which it would form nanoparticles or larger inclusions of visible Au. This implies that nanoparticle nucleation is controlled by concentration of Au and As above the saturation limit in the crystal lattice, i.e., at Au/As > 0.02. Reich et al. (2006) were also able to show that the size of Au nanoparticles in As-bearing pyrite controls their thermal stability, and they observed size-dependent coarsening or dissolution of Au nanoparticles in arsenian pyrite under thermally-induced gradients at temperatures above 370 °C. The association between Au and As has also fueled effort to derive the chemical state of Au incorporated in pyrite and the substitution mechanism(s) by which this takes place (e.g., Cook and Chryssoulis, 1990; Friedl et al., 1995; Fleet and Mumin, 1997; Simon et al., 1999; Savage et al., 2000; Deditius et al., 2014).

The paradigm of arsenic-mediated incorporation of Au was also discussed by Cook et al. (2009a), who demonstrated enrichment of several hundreds of ppm Au in arsenic-free pyrite from the Dongping deposit, Hebei Province, China. It was suggested that other elements, such as Bi, Pb and Te, may also play a role as catalysts for Au incorporation in a similar way to As. Subsequent work on the same material (Ciobanu et al., 2012) revealed the presence of abundant nano and fine particles of Au-bearing phases, notably a range of Au-(Ag)-tellurides.

The abundance of literature addressing trace element incorporation in pyrite (and arsenopyrite) has emerged largely in the absence of similar studies on common base metal sulphides (BMS). This is despite the fact that many BMS are common in a range of different hydrothermal ore types and environments, and can be significant hosts of economically important elements. Of particular relevance here are sphalerite, galena and chalcopyrite, the three most common BMS and the principle ores of Zn, Pb and Cu, respectively. These BMS may host elements representing valuable by-products that can be extracted from an ore (e.g., Cd and In in sphalerite, Ag in galena), or impurities that may reduce the value of an ore or pose an environmental hazard should such an ore be treated incorrectly (e.g., Bi in galena;

Lane et al., 2016). In spite of the advances in microanalysis that have occurred over the previous 50 years, the distribution and partitioning of trace elements in base metal sulphide ores remains poorly understood.

In addition to the relative lack of literature on trace elements in BMS, the development and rapid expansion of high-resolution scanning electron microscopy and chemical mapping techniques has shown extraordinary inhomogeneity in many natural materials, inferring that much of the published minor and trace element data for sulphides may simply be an average of more than one compositionally-distinct zone. Many of the contemporary techniques that provide reliable, quantitative analytical data for sulphides (EPMA, SIMS, PIXE and laser ablation inductively-coupled plasma mass spectrometry; LA-ICP-MS) remain 'bulk' methods, inasmuch as the offered spatial resolution may be less than that of individual micro-inclusions or chemical-structural features in the analyzed grain (e.g., micron-scale lamellar banding). Nevertheless, if researchers are aware of the limitations of such techniques, and where applicable use processes that may indirectly indicate the presence of inhomogeneity, such microanalytical techniques can provide reliable data with direct application to geological problems.

1.2 The Laser Ablation Inductively-Coupled Plasma Mass Spectrometry technique

The continual growth in popularity of microanalytical techniques amongst researches in the geosciences has been largely due to the continual technological advancement of such techniques and the constantly expanding range of geological problems microanalytical data can be applied to. In regards to LA-ICP-MS, analytical resolution, sensitivity and speed have greatly improved over the last 20 to 30 years, coupled with increased access to a wide range

of homogeneous reference calibration standards and a reduction in instrument price. This has led to the technique being extensively used by researchers in laboratories all over the world to acquire trace element data for many different minerals. LA-ICP-MS boasts detection limits much less than 1 ppm for many heavy elements while still maintaining a relatively small spatial resolution (typically in the tens of μm range). Despite allowing hundreds of analyses within a day, and the simultaneous measurement of more than 25 elements per analysis, the technique remains relatively cheap to run. Details on the history of the LA-ICP-MS technique over the past 20-30 years are given in Fryer et al. (1995), Sylvester (2008a) and Sylvester and Jackson (2016). In addition, descriptions of LA-ICP-MS hardware, software, methods and routine applications are given in Sylvester (2001, 2008a), Vanhaecke and Degryse (2012), Thomas (2013) and Jenner and Arevalo (2016).

Significant advances to LA-ICP-MS systems have come through the development of multi-collector ICP-MS instruments, which allow greater trace element sensitivity than their quadrupole counterparts (e.g., Blichert-Toft and Albarede, 1997; Lee and Halliday, 1995; Marechal et al., 1999; White et al., 2000), and femtosecond laser ablation systems, as opposed to traditional nanosecond alternatives (Russo et al., 2002; Koch and Günther, 2007). Perhaps most notable, however, is the flexibility users now have in utilizing different laser functions to tackle geological problems; lasers ablation systems may be used to create ‘spots’ (deep craters at a single point), ‘trenches’ (shallower craters along a line) or ‘maps’ (many trenches adjacent and parallel). Spot analysis provides the best spatial resolution, and is the most widely used technique in determining trace element compositions. However, it is possible that compositional variation across a mineral or sample can be missed using spot analysis alone. Trenches and maps lower spatial resolution due to a greater analysed surface area, but compositional changes can usually be monitored and measured. LA-ICP-MS ‘maps’ are ideal for providing visualization of compositional variability (assuming such variability

does not occur below the spatial resolution provided by the laser), and have clearly revealed complex chemical zoning in a range of minerals (e.g., pyrite; Large et al., 2009, molybdenite; Ciobanu et al., 2013a). Maps can either be used to display qualitative information (expressed as counts-per-second) or quantitative compositions (typically ppm) based on an assigned internal standard.

Despite the widespread popularity of LA-ICP-MS amongst geological researchers, the method is not without its limitations. Compared to microanalytical techniques such as EPMA, sample volumes analysed by LA-ICP-MS are quite large. Thus, there is potential that LA-ICP-MS spots or trenches can unknowingly analyse fine-scale inclusions of distinct mineral phases beneath the sample surface. If such inclusions are large enough and are heterogeneously dispersed within a laser spot, then it is possible to recognise their presence on time-resolved down-hole ablation profiles (e.g., Cook et al., 2009b). However, if inclusions are small (e.g., nanoparticles) and homogeneously distributed, then they will be invisible on such profiles. Therefore, it is imperative that the locations of LA-ICP-MS spots be selected by other techniques (e.g., scanning electron microscopy [SEM]) before analysis to ensure the mineral surface is free of any noticeable inclusions. This, along with careful inspection of all time-resolved down-hole ablation profiles, generally provides reliable trace element data (Cook et al., 2016). Additionally, areas directly adjacent to laser craters can be extracted by focussed ion beam scanning electron microscopy (FIB-SEM) and examined using transmission electron microscopy (TEM; Ciobanu et al., 2011). This technique allows one to distinguish between trace elements hosted in solid solution as opposed to fine-scale inclusions, and also potentially allows for the identification of such inclusions (Ciobanu et al., 2012).

Problems may also be encountered by repeatedly analysing similar areas in different grains of the same mineral. Consistently placing LA-ICP-MS spots in the centres of mineral

grains that are oscillatory zoned from core to rim can result in a large systematic error in the data set. Similarly, issues are encountered if some trace elements are only present in mineral pores, fractures or cleavage plains. The presence of such trace element rich zones will likely be overlooked since such areas are typically not selected for spot analysis. For example, Au is concentrated in specific inclusion rich zones in pyrite from Dongping, China; areas that would generally be avoided by when placing laser spots (Cook et al., 2009a). This highlights the danger of relying on a single technique for providing trace element data. Ideally, spot analysis should be accompanied by compositional mapping, especially if the analysed mineral is suspected of heterogeneity.

Integral to applying LA-ICP-MS data to geological problems is the correct identification and interpretation of data trends, patterns and groups. However, the speed and ease of the LA-ICP-MS technique, and thus its ability to generate large amounts of data quickly, can mean that data is not properly processed or interpreted. Prior to LA-ICP-MS analysis, it is vital that thorough optical microscopy and SEM work be carried out on a wide range of representative sample material, focusing on the identification of mineral textures including different mineral generations, overgrowths, compositional zones and replacement reactions. This should provide insights for the separation of compositional data into groups that reflect actual temporal or textural phenomena, as well as allowing data trends to be placed in their proper geological contexts. For example, at the Chang'an gold deposit, Sanjiang region, China, diagenetic pyrite is preserved as cores within euhedral pyrite overgrowth rims formed during metamorphic recrystallization (Zhang et al., 2014). These two pyrite generations can be recognized from their textures, as well as from their vastly different trace element signatures.

In addition to recognizing mineral textures, sulphide mineral solutions, stability relationships and solid solution series are also of importance for understanding trace element

distributions. Key publications on sulphide thermochemistry and phase equilibria include Barton and Skinner (1967, 1979), Barton (1970), Craig and Scott (1976), Vaughan and Craig (1997), Fleet (2006) and Sack and Ebel (2006). These sources also contain compilations of published phase relation data for geologically important binary, ternary and higher-order sub-systems.

It is also important to determine the right statistical treatments for a particular dataset as these directly influence geological interpretations. Different treatments have been discussed by a range of authors (e.g., Winderbaum et al., 2012; Marques de Sá, 2014; Frenzel et al., 2016; Makvandi et al., 2016a; 2016b), and their application depends primarily on the purpose of a given study.

Although typically disregarded, factors related to the LA-ICP-MS hardware and function may also impact data quality and precision. Fractionation can occur due to different processes taking part during LA-ICP-MS analysis, e.g., if melting is induced at the sample during ablation. This problem seems to be reduced using femtosecond lasers (Wohlgemuth-Ueberwasser and Jochum, 2015). Recent research has also investigated fractionation of ablated material as it moves from the sample to the plasma and into the mass spectrometer (Gilbert et al., 2014). Particle size, selective ionization and various chemical reactions may cause different elements to be transported within the LA-ICP-MS system differently. For example, it has recently been shown that sulfur isotopes may fractionate up to 2 ‰ $\delta^{34}S$ during laser ablation of pyrite with a 193 nm ArF laser (Zhu et al., 2017). This is due to variable decomposition of pyrite under different laser conditions. Similarly, fractionation may also be caused during spot analysis as the laser ablates deeper into the sample with time. Most fractionation problems can be mitigated or eliminated using suitable matrix-matched standards and properly regulating operating parameters (e.g., Günther et al., 2001; Jackson

and Günther, 2003; Günther and Koch, 2008; Sylvester, 2008b; Norman et al., 1996; 2003; Wohlgemuth-Ueberwasser et al., 2007; Danyushevsky et al., 2011; Zhu et al., 2017).

1.3 Applications of trace element data

Although there are issues and limitations that need to be considered when using any microanalytical technique, including LA-ICP-MS, such techniques have proven powerful in their ability to collect reliable trace element data that can be applied to a wide range of geological problems and contexts. As such, trace element data has become crucial to studies in economic geology, as well as to the mining industry directly. Applications are wide, varying and contrasting and so only a few selected applications will be described here to illustrate this range. First and foremost, essentially all minerals that are mined contain trace elements, and sometimes such trace elements, if valuable and present at high enough concentrations, can be recovered and exploited as by-products of the primary ore. As discussed above, much of the now sizeable body of work relating to trace elements in pyrite and arsenopyrite was driven by the desire to understand how invisible Au is hosted in the Fe-sulphides with the purpose of determining its role in refractory ores. In a similar way, many critical metals (e.g., In, Ge, Ga, Sc, Re) that generally do not form discrete economically exploitable minerals must be extracted from ores primarily concentrating other metals. In contrast, trace elements can also become impurities in concentrates, usually because they reduce the overall grade of the concentrate, and sometimes because the element in question represents an environmental hazard (e.g., Lane et al., 2016). If a concentrate contains too much of an impurity element, then a significant financial penalty will be incurred from the smelter. Thus, in a given ore system it is often necessary to know which minerals host either

valuable by-product elements, or penalty elements, and at what concentrations, so that the ore can be processed accordingly.

Understanding the genesis of ore bodies is vitally important, particularly for those in the minerals industry who need conceptual models for exploration of new deposits. Trace element data can provide crucial information relating to the evolution of mineralizing fluids and the mineralizing system. Through analysis of minerals in host rock and ore, the sources of mineralizing fluids and stages of mineralization and overprinting can often be determined. For example, Large et al. (2013) use LA-ICP-MS trace element maps of pyrite from the Carbon Leader Reef in the Witwatersrand basin, South Africa, to argue that Au concentration at Witwatersrand initially resulted from a sedimentary accumulation of Au-rich detrital pyrite, followed by an addition of Au in hydrothermal pyrite overgrowths on detrital pyrite during peak metamorphism. This interpretation is supported by the fact that detrital pyrite has similar trace element composition to digenetic pyrites of the West Rand Group, and is intergrown with alumina silicates and organic matter, while later pyrite overgrowths are enriched in the same trace elements concentrated in altered brecciated pyrite associated with brittle fracture zones in the Carbon Leader Reef.

Smith et al. (2004) also investigate the origin and evolution of skarns in the Beinn an Dubhaich Aureole, Isle of Skye, Scotland, by measuring the trace element contents in garnets. Variations in the rare earth element (REE) and U compositions of garnets reflect crystallization under near equilibrium conditions to almost super-saturation, as well as from essentially small amounts of fluid in a closed system to a larger more open system. Most garnets are light REE (LREE) enriched with flat heavy REE (HREE) distributions. These trends are interpreted to result from essentially closed system fractional crystallization from a fluid at equilibrium with pre-existing minerals. Iron-rich garnet with positive Eu anomalies and increased LREE contents relative to HREEs represent crystallization following the

addition of new externally buffered fluid into the skarn system. In contrast, Fe-poor garnet with HREE enrichment and negative Eu anomalies are thought to be the result of REE surface sorption during disequilibrium growth from a super-saturated solution.

Reich et al. (2016) report pyrite geochemical data from the Los Colorados iron oxide-apatite (IOA) deposit, Chile. They show that the high Co/Ni ratios in pyrite are typical of a magmatic-hydrothermal origin related to more mafic magmatism than pyrite from porphyry Cu deposits. Compositionally and texturally, Los Colorados pyrite is also similar to pyrite from iron oxide copper gold (IOCG) deposits. They thus infer that metals hosted within pyrite (e.g., Cu, Au, Ag, As, Zn, Pb, Cd, Sb, Se and Te) are sourced from fluids related to mafic or intermediate magmas, and that Fe-Cu-Au-rich fluids that form IOA systems may continue to migrate up through the crust to form IOCG deposits.

Heidarian et al. (2016) show different magnetite generations in the Chadormalu magnetite-apatite deposit, Bafq district, Central Iran, can be differentiated based on their trace element signatures. Using FeO, SiO_2, Al_2O_3 and CaO concentrations, it is shown that primary magnetite is likely related to magmatic-hydrothermal fluid and that secondary magnetite that replaces primary magnetite is related to more of a meteoric brine-dominated fluid. These two magnetite generations also show evidence of fluid assisted recrystallization to form a third late stage magnetite. The authors suggest that Chadormalu is a Kiruna-type iron-oxide deposit formed through the evolution of an ore fluid from magmatic-hydrothermal to more brine dominant, and that Fe contents increase during fluid evolution.

The recent increased interest in vector approaches to mineral exploration is also an application of trace element data related to the search for new deposits. These approaches are based on there being systematic trace element variation in a specific mineral or mineral group in various rock types across an ore deposit and alteration envelope. Such variation is attributable to the fact that even subtle physiochemical changes in the ore environment as a

function of distance to mineralization are typically reflected in trace element incorporation into minerals. If predictable compositional trends relating to distance from mineralization can be identified for a given mineral in a specific terrane, then it may be possible to be directed towards potential mineralization in a similar terrane by measuring trace element abundances in the same mineral. A number of studies have investigated the viability of this method in specific terranes, using different minerals (see Cook et al., 2016, and references therein), though none have been applied generally outside their immediate contexts. For example, numerous studies (e.g., Nadoll et al., 2012; Boutroy et al., 2014; Acosta-Góngora et al., 2015; Canil et al., 2016; Makvandi et al., 2016a; 2016b) have shown the potential of magnetite as an indicator mineral in a range of different systems including Ni-Cu-PGE, IOCG, porphyry, skarn and VMS deposits. Gahnite has also been used as a pathfinder to mineralization in the Proterozoic Broken Hill terrane, and more recently, trace element analysis has defined certain gahnite compositional fields that allow the mineral to be used as an exploration guide to high-grade sulphide rich ore (O'Brien et al., 2015).

Also worth mentioning is the use of trace elements in geochronology, perhaps the most common application of trace element data (e.g., Cocherie and Robert, 2008). U-Pb zircon geochronology was first developed on mineral separates during the 1950s using thermal ionisation mass spectrometry (TIMS). Subsequently, *in-situ* geochronology analysis was allowed by SIMS, and later, specially designed sensitive high-resolution ion microprobe (SHRIMP). LA-ICP-MS U-Pb dating was then established in the early 1990s after considerable development of laser ablation systems, including the reduction of operating wavelengths and use of matrix matched reference standards (e.g., Fryer et al., 1993; Feng et al., 1993). Whereas original TIMS techniques could only analyse at the scale of whole zircon grains, *in-situ* methods generally allow zircons with complex internal structures and evolutionary histories to be dated through the analysis of individual growth zones related to

specific temporal events. Since the 1990s, *in-situ* geochronology by LA-ICP-MS has been applied to a wide range of additional minerals including allanite (Pal et al., 2011; Darling et al., 2012; Gregory et al., 2012), apatite (Chew et al., 2011; Thomson et al., 2016), xenotime (Liu et al., 2011), rutile (Zack et al., 2011), hematite (Ciobanu et al., 2013b, Courtney-Davies et al., 2016), cassiterite (Li et al., 2016) and epidote group minerals (Mcfarlane, 2016). The development of multi-collector ICP-MS has allowed for high-precision isotope ratio determination, greatly aiding the simplicity and ease of isotope systematics (Woodhead et al., 2016). Thus, although LA-ICP-MS geochronology techniques are less sensitive compared with SHRIMP or ID-TIMS, they can nevertheless provide rapid, cost-effective and sufficiently accurate data.

Various geothermobarometers have also been developed utilizing trace element data. For example, Watson and Harrison (2005) define a geothermometer based on Ti substitution into zircon. As Ti^{4+} substitutes directly for Si^{4+} in the zircon structure, the thermometer is based on the simple $TiO_{2(rutile)} = TiO_{2(zircon)}$ reaction in a TiO_2 saturated system. Measuring the Ti content in 54 Hadean zircons from Jack Hills, Western Australia, they infer that the zircons crystallized at ~700 ^{o}C, essentially identical to zircon crystallization temperatures in modern water saturated granitoids. They conclude that within ~100 million years of the earth's formation, granites were forming through crustal anatexis, and the processes of erosion and sediment recycling had begun. A similar geothermobarometer has been defined by Hayden et al. (2008) based on Zr replacing Ti in the crystal lattice of titanite. Analysis of Zr in titanate from seven rocks of well constrained crystallization conditions shows that the thermobarometer reliably estimates temperatures consistent with independent constraints to within 20 °C over the temperature range of 600 to 1000 $^{\circ}$C.

1.4 Research objectives and thesis structure

As applications for trace element data have expanded, this has naturally led to a substantial increase in the number of individual minerals in which trace elements have been measured. Similarly, research focussing on experimentally determining the maximum solubility limits of many trace elements in a variety of minerals has also grown (e.g., Kojima and Sugaki, 1985; Liu and Chang, 1994; Lepetit et al., 2003; Chutas et al., 2008). Emerging from this work is a broad understanding of the common trace elements expected to be hosted in different minerals, at what concentrations, and the underlying reasons for the observed trends (Table 1.1). This has further led to knowledge of the expected partitioning behaviours of key trace elements in different geological systems (e.g., the platinum group elements and gold, between pyrrhotite, pentlandite, pyrite and BMS in magmatic sulphide ore deposits; Holwell and McDonald, 2010; Dare et al., 2011, and references therein). Such an understanding is fundamental to the range of economic applications for trace element data since such data is directly related to the genesis of ore systems and their optimal processing. Nevertheless, some minerals and systems are far better understood than others (e.g., pyrite and arsenopyrite compared to the base metal sulphides), and therefore there is significant opportunity to expand our knowledge of trace element partitioning behaviours, and in particular, their incorporation into certain minerals in specific systems.

Table 1.1. Selected studies that address the trace element composition of common sulphides, iron-oxides, rock-forming silicates and accessory minerals. After Cook et al. (2016).

Minerals	**Reference(s)**
Sphalerite	Cook et al. (2009b); Ye et al. (2011); Cook et al. (2012); Murakami and Ishihara (2013); Lockington et al. (2014); Belissont et al. (2014); Cook et al. (2015)
Chalcopyrite	Butler and Nesbitt (1999); Wohlgemuth-Ueberwasser et al. (2015)
Bornite, chalcocite-group	Cook et al. (2011)
Pyrite	Large et al. (2007); Cook et al. (2009a); Large et al. (2009); Winderbaum et al. (2012); Ingham et al. (2014); Large et al. (2014)
Arsenopyrite	Morey et al. (2008); Sung et al. (2008); Cook et al. (2013a); Lawley et al. (2015)
Enargite	Deyell and Hedenquist (2011)
Molybdenite	Ciobanu et al. (2013a)
Pyrrhotite-pentlandite-(pyrite, Ni-arsenides) in magmatic ores, including PGE deposits	Barnes et al. (2008)
Bismuth chalcogenides and sulphosalts	Ciobanu et al. (2009)
Hematite	Ciobanu et al. (2013b)
Magnetite	Nadoll et al. (2014); Dare et al. (2014)
Chromite	Pagé and Barnes (2009)
Gahnite	O'Brien et al. (2015)
Scheelite, wolframite, ferberite	Goldmann et al. (2013); Song et al. (2014); Hazarika et al. (2016); Raju et al. (2016)
Xenotime, florencite	Cook et al. (2013b)
(Calcic, skarn) garnet and other skarn calc-silicates (pyroxenes, clinozoisite etc.)	Smith et al. (2004); Gaspar et al. (2008); Ismail et al. (2014); Xu et al. (2016)
Feldspars	Kontonikas-Charos et al. (2014)
Rutile and titanite	Smith et al. (2009); Ismail et al. (2014); Fu et al. (2016)
Apatite	Ismail et al. (2014); He et al. (2016); She et al. (2016)
Fluorite	Gagnon et al. (2003)

This project aims to better understand the trace element composition of minerals in the BMS group, and, in turn, trace element partitioning patterns between them. This work principally focuses on the BMS sphalerite, galena and chalcopyrite, three of the most common BMS, and the principle ores of Zn, Pb and Cu respectively. In addition, tetrahedrite-tennantite, a sulphosalt solid solution series that commonly co-crystallizes with BMS is also considered. This project was carried out using a variety of microanalytical techniques, most notably the LA-ICP-MS technique, and the methods employed are described in **Chapter 2**.

Of the three BMS focussed on here, sphalerite has been the object of the most thorough trace element studies (e.g., Bethke and Barton, 1971; Johan, 1988; Axelsson and Rodushkin, 2001; Cook et al., 2009b; Ye et al., 2011; Cook et al., 2012; Murakami and Ishihara, 2013; Lockington et al., 2014; Belissont et al., 2014; Cook et al., 2015), in large part to understand the distribution of critical elements (e.g., In, Ge, or Ga). Such elements generally do not form discrete minerals that are economically exploitable, rather are typically produced as by-products of Zn mining. In contrast to sphalerite, trace element studies of galena are relatively scarce and have mostly focused on the elements Ag, Bi and Sb (e.g., Van Hook, 1960; Foord et al., 1988; Foord and Shawe, 1989; Jeppsson, 1989; Lueth et al., 2000; Costagliola et al., 2003; Chutas et al., 2008; Renock and Becker, 2011), elements commonly hosted at relatively high concentrations in the Pb-sulphide. **Chapter 3** thus outlines a broad LA-ICP-MS study of galena specimens from a range of different galena-bearing ores. It is shown that galena can be a significant host of a number of important trace elements including Sn, Tl and Cu. Both Cu and Tl appear to partition into galena as part of the coupled substitution $(Ag, Cu, Tl)^{+} + (Bi, Sb)^{3+} = 2Pb^{2+}$. Bismuth is the most abundant trace element measured in galena with concentrations reaching over 36,000 ppm, however the incorporation of concentrations above ~2,000 ppm likely involves the creation of vacancies in the galena lattice. For the first

time, trace element oscillatory and sector compositional zoning is observed within epithermal galena.

For some trace elements, it is noted that partitioning patterns are generally predictable between galena and co-crystallizing sphalerite. However, the presence of other co-crystallizing minerals, especially chalcopyrite, affects the distributions of some elements. These findings are the basis for the subsequent study detailed in **Chapter 4**, which investigates the systematic partitioning of trace elements between co-crystallizing sphalerite, galena and chalcopyrite in hydrothermal ores. The aim is to identify the primary controls on trace element partitioning and determine the preferred BMS hosts of a suite of trace elements. It is shown that partitioning is governed principally by element oxidation state, ionic radius of the substituting element, element availability and the maximum trace element budget that a given sulphide mineral can accommodate. All trace elements have a single preferred BMS host under all investigated physiochemical conditions. The only exceptions are Sn, Ga and In where partitioning behaviours change at high metamorphic grades during BMS recrystallization.

One additional observation is that chalcopyrite trace element concentrations are typically quite low, especially when compared to sphalerite and galena. Furthermore, the majority of prior studies investigating the trace element composition of chalcopyrite have focused on a limited suite of elements and often the minimum detection limits of the microanalytical techniques used were too high to accurately determine trace element ranges and concentrations (e.g., Harris et al., 1984; Cabri et al., 1985; Kase, 1987; Brill, 1989; Huston et al., 1996; Scott et al., 2001; Moggi-Cecchi et al., 2002; Serranti et al., 2002; Shalaby et al., 2004; Demir et al., 2008; Layton-Matthews et al., 2008; Monteiro et al., 2008; Demir et al., 2013; Gena et al., 2013; Reich et al., 2013; Cioacă et al., 2014; Helmy et al., 2014; G. Wang et al., 2015; Wohlgemuth-Ueberwasser et al., 2015; Sadati et al., 2016). Therefore, **Chapter**

5 explores chalcopyrite trace element chemistry in detail, aiming to establish which trace elements may be hosted by chalcopyrite in a wide variety of settings. It is shown that chalcopyrite may host a wide range of elements, some of which are rarely if ever reported in previous studies. As chalcopyrite is often present in far greater abundance compared to other sulphides in many Cu-ores, it may be the main host of many trace elements in a given system. An important consideration is that chalcopyrite may even host enough Se and Hg to cause an associated Cu-concentrate to incur a monetary penalty from a smelter. The Zn:Cd ratio of chalcopyrite systematically varies depending in part on temperature of crystallization. If the Zn:Cd ratios of co-crystallizing chalcopyrite and sphalerite are approximately constant and equal, it implies the sulphides formed under constant physiochemical conditions.

In addition to sphalerite, galena and chalcopyrite, minerals of the tetrahedrite isotypic series are also widespread components of base metal ores, where they commonly co-crystallize with BMS. Thus **Chapter 6** considers the trace element chemistry of tetrahedrite-tennantite to determine which trace elements can be incorporated, at what levels of concentration, and how the presence of tetrahedrite-tennantite influences patterns of trace element partitioning in base metal ores. It is shown that tetrahedrite-tennantite is a significant carrier of a range of trace elements, which should be recognized when assessing the main hosts of trace elements in any given assemblage. The presence of tetrahedrite-tennantite in co-crystallizing BMS assemblages will influence the distribution patterns of Fe, Cu, Zn, As, Ag, Cd, Sb, Hg and Bi. Perhaps most noteworthy, tetrahedrite-tennantite will always be the primary host of Ag in a co-crystallized BMS ore. In contrast, tetrahedrite-tennantite is a poor host for the critical metals Ga, In and Sn, all of which prefer to partition to co-crystallizing BMS.

Chapter 7 summarises all the key findings of this project, outlines current research gaps as well as further opportunities for additional investigation. **Chapter 8** provides all additional material for this thesis, and finally, **Chapter 9** collates all references cited within the thesis.

Acosta-Góngora, P., Gleeson, S. A., Samson, I. M., Ootes, L., Corriveau, L., 2015. Trace Element Geochemistry of Magnetite and Its Relationship to Cu-Bi-Co-Au-Ag-U-W Mineralization in the Great Bear Magmatic Zone, NWT, Canada. Econ. Geol. 109, 1901-1928.

Arehart, G. B., Chryssoulis, S. L., Kesler, S. E., 1993. Gold and arsenic in iron sulfides from sediment-hosted disseminated gold deposits; implications for depositional processes. Econ. Geol. 88, 171-185.

Axelsson, M. D., Rodushkin, I., 2001. Determination of major and trace elements in sphalerite using laser ablation double focusing sector field ICP-MS. J. Geochem. Explor. 72, 81-89.

Barnes, S. J., Prichard, H. M., Cox, R. A., Fisher, P. C., Godel, B., 2008. The location of the chalcophile and siderophile elements in platinum-group element ore deposits (a textural, microbeam and whole rock geochemical study): Implications for the formation of the deposits. Chem. Geol. 248, 295-317.

Barton, P. B., 1970. Sulfide petrology. Mineralogical Society of America Special Paper 3, 187-198.

Barton, P. B., Skinner, B. J., 1967. Sulfide mineral stabilities. In Barnes, H. L., Ed., Geochemistry of Hydrothermal Ore Deposits, 236-333.

Barton, P. B., Skinner, B. J., 1979. Sulfide mineral stabilities. In Barnes, H. L., Ed., Geochemistry of Hydrothermal Ore Deposits 2, 278-403.

Belissont, R., Boiron, M. C., Luais, B., Cathelineau, M., 2014. LA-ICP-MS analyses of minor and trace elements and bulk Ge isotopes in zoned Ge-rich sphalerites from the Noailhac - Saint-Salvy deposit (France): Insights into incorporation mechanisms and ore deposition processes. Geochim. Cosmochim. Acta 126, 518-540.

Bethke, P. M., Barton, P. B., 1971. Distribution of some minor elements between coexisting sulfide minerals. Econ. Geol. 66, 140-163.

Blichert-Toft, J., Albarede, F., 1997. The Lu–Hf geochemistry of chondrites and the evolution of the mantle–crust system. Earth Plan. Sci. Lett. 148, 243–258.

Boutroy, E., Dare, S. A. S., Beaudoin, G., Barnes, S. J., Lightfoot, P. C., 2014. Magnetite composition in Ni-Cu-PGE deposits worldwide: application to mineral exploration. J. Geochem. Explor. 145, 64-81.

Bowles, J. F. W., Howie, R. A., Vaughan, D. J., Zussman, J., 2011. Rock-forming Minerals: nonsilicates: oxides, hydroxides and sulphides. Geol. Soc. Lond.

Brill B., 1989. Trace-element contents and partitioning of elements in ore minerals from the CSA Cu–Pb–Zn deposit, Australia. Can. Mineral. 27, 263-274.

Bürg, G., 1935. Natur des in den Pyriten nichtsichtbar enthaltenen Goldes. Zeits. prakt. Geol. 43, 17-32.

Butler, I. B., Nesbitt, R. W., 1999. Trace element distributions in the chalcopyrite wall of a black smoker chimney: insights from laser ablation inductively coupled plasma mass spectrometry (LA–ICP–MS). Earth Plan. Sci. Lett. 167, 335-345.

Cabri, L. J., 1987. The mineralogy of precious metals: new developments and metallurgical implications. Can. Mineral. 25, 1-7.

Cabri, L. J., 1988. The role of mineralogy in gold metallurgy. Proceedings of Symposium on Heap Leaching of Gold in a Canadian Environment Timmins, Ontario, Canada. Can. Mineral Processors, CIM, Paper No. 2, 11.

Cabri, L. J., 1988. The role of mineralogy in gold metallurgy. Proceedings of Symposium on Heap Leaching of Gold in a Canadian Environment Timmins, Ontario, Canada. Can. Mineral Processors, CIM, Paper No. 2, 11.

Cabri, L. J., 1992. The distribution of trace precious metals in minerals and mineral products. Mineral. Mag. 56, 289-308.

Cabri, L. J., Blank, H., El Goresy, A., Laflamme, J. G., Nobiling, R., Sizgoric, M. B., Traxel, K., 1984. Quantitative trace-element analyses of sulfides from Sudbury and Stillwater by proton microprobe. Can. Mineral. 22, 521-542.

Cabri L. J., Campbell J. L., Laflamme J. H. G., Leigh R. G., Maxwell J. A., Scott J. D., 1985. Proton-microprobe analysis of trace elements in sulfides from some massive-sulfide deposits. Can. Mineral. 23, 133-148.

Cabri, L. J., Chryssoulis, S. L., de Villiers, J. P. R., Laflamme, J. H. G., Buseck, P. R., 1989. The nature of "invisible" gold in arsenopyrite. Can. Mineral. 27, 353-362.

Canil, D., Grondahl, C., Lacourse, T., Pisiak, L. K., 2016. Trace elements in magnetite from porphyry Cu–Mo–Au deposits in British Columbia, Canada. Ore Geol. Rev. 72, 1116-1128.

Cathelineau, M., Boiron, M. C., Holliger, P., Marion, P., 1988. Gold-rich arsenopyrites: crystal chemistry, gold location and state, physical and chemical conditions of crystallization. In: Proc. Gold '88 (Melbourne), 235-244.

Chew, D. M., Sylvester, P. J., Tubrett, M. N., 2011. U-Pb and Th-Pb dating of apatite by LA-ICPMS. Chem. Geol. 280, 200-216.

Chutas, N. I., Kress, V. C., Ghiorso, M. S., Sack, R. O., 2008. A solution model for high-temperature PbS–$AgSbS_2$–$AgBiS_2$ galena. Amer. Mineral. 93, 1630–1640.

Chryssoulis, S. L., 1989. Ion probe microanalysis of gold in common sulphide minerals and implications for enhanced recovery from refractory gold ores. CANMET Contract Report # 79037-01-55.

Chryssoulis, S. L., Chauvin, W. J., Surges, L. J., 1986. Trace element analysis by secondary ion mass spectrometry with particular reference to silver in the Brunswick sphalerite. Canadian Metallurgical Quarterly 25, 233-239.

Chryssoulis, S. L., Cabri, L. J., Salter, R. S., 1987. Direct determination of invisible gold in refractory sulphide ores. In: Gold Metallurgy--Proceedings of the International Symposium, 235-244.

Chryssoulis, S. L., Cabri, L. J., Lennard, W., 1989. Calibration of the ion microprobe for quantitative trace precious metal analysis of ore minerals. Econ. Geol. 84, 1684-1689.

Cioacă M. E., Munteanu M., Qi L., Costin G., 2014. Trace element concentrations in porphyry copper deposits from Metaliferi Mountains, Romania: A reconnaissance study. Ore Geol. Rev. 63, 22-39.

Ciobanu, C. L., Cook, N. J., Pring, A., Brugger, J., Danushevsky, L., Shimizu, M., 2009. 'Invisible gold' in bismuth chalcogenides. Geochim. Cosmochim. Acta 73, 1970-1999.

Ciobanu, C. L., Cook, N. J., Utsunomiya, S., Pring, A., Green, L., 2011. Focussed ion beam - transmission electron microscopy applications in ore mineralogy: bridging micron- and nanoscale observations. Ore Geol. Rev. 42, 6-31.

Ciobanu, C. L., Cook, N. J., Utsunomiya, S., Kogagwa, M., Green, L., Gilbert, S., Wade, B., 2012. Gold-telluride nanoparticles revealed in arsenic-free pyrite. Amer. Mineral. 97, 1515-1518.

Ciobanu, C. L., Cook, N. J., Kelson, C. R., Guerin, R., Kalleske, N., Danyushevsky, L., 2013a. Trace element heterogeneity in molybdenite fingerprints stages of mineralization. Chem. Geol. 347, 175-189.

Ciobanu, C. L., Wade, B., Cook, N. J., Schmidt Mumm, A., Giles, D., 2013b. Uranium-bearing hematite from the Olympic Dam Cu-U-Au deposit, South Australia; a

geochemical tracer and reconnaissance Pb-Pb geochronometer. Precambr. Res. 238, 129-147.

Cocherie, A., Robert, M., 2008. Laser ablation coupled with ICP-MS applied to U–Pb zircon geochronology: a review of recent advances. Gondwana Res. 14, 597-608.

Cook, N. J., Chryssoulis, S. L., 1990. Concentrations of invisible gold in the common sulfides. Can. Mineral. 28, 1-16.

Cook, N. J., Ciobanu, C. L., Mao, J. W., 2009a. Textural control on gold distribution in As-free pyrite from the Dongping, Huangtuliang and Hougou gold deposits, North China Craton, (Hebei Province, China). Chem. Geol. 264, 101-121.

Cook, N. J., Ciobanu, C. L., Pring, A., Skinner, W., Shimizu, M., Danyushevsky, L., Saini-Eidukat, B., Melcher, F., 2009b. Trace and minor elements in sphalerite: A LA-ICPMS study. Geochim. Cosmochim. Acta 73, 4761–4791.

Cook, N. J., Ciobanu, C. L., Danyushevsky, L. V., Gilbert, S., 2011. Minor elements in bornite and associated Cu-(Fe)-sulfides: a LA-ICPMS study. Geochim. Cosmochim. Acta 73, 4761-4791.

Cook, N. J., Ciobanu, C. L., Brugger, J., Etschmann, B., Howard, D. J., de Jonge, M., Ryan, C. G., Paterson, D., 2012. Determination of the oxidation state of Cu in substituted Cu-In-Fe-bearing sphalerite via μ-XANES spectroscopy. Amer. Mineral. 97, 476–479.

Cook, N. J., Ciobanu, C. L., Meria, D., Silcock, D., Wade, B., 2013a. Arsenopyrite-pyrite association in an orogenic gold ore: tracing mineralization history from textures and trace elements. Econ. Geol. 108, 1273–1283.

Cook, N. J., Ciobanu, C. L., O'Rielly, D., Wilson, K., Das, K., Wade, B., 2013b. Mineral chemistry and element partitioning in hydrothermal Rare Earth Element (REE) mineralization, Browns Ranges, Western Australia. Lithos 172–173, 192–213.

Cook, N. J., Etschmann, B., Ciobanu, C. L., Geraki, K., Howard, D. L., Williams, T., Rae, N., Pring, A., Chen, G., Johannessen, B., Brugger, J., 2015. Distribution and substitution mechanism of Ge in a Ge-(Fe)-bearing sphalerite. Minerals 5, 117-132.

Cook, N. J., Ciobanu, C. L., George, L., Zhu, Z., Wade, B., Ehrig, K., 2016. Trace element analysis of minerals in magmatic-hydrothermal ores by laser ablation inductively-coupled plasma mass spectrometry: approaches and opportunities. Minerals 6, 111.

Costagliola, P., Di Benedetto, F., Benvenuti, M., Bernardini, G. P., Cipriani, C., Lattanzi, P. F., Romanelli, M., 2003. Chemical speciation of Ag in galena by EPR spectroscopy. Amer. Mineral. 88, 1345–1350.

Courtney-Davies, L., Zhu, Z. Y., Ciobanu, C. L., Wade, B. S., Cook, N. J., Ehrig, K., Cabral, A. R., Kennedy, A., 2016. Matrix-matched iron-oxide laser ablation ICP-MS U-Pb geochronology using mixed solution standards. Minerals 6, 85. DOI: 10.3390/min6030085.

Craig, J. R., Scott, S. D., 1976. Sulfide phase equilibria. In Ribbe, P. H., Ed., Sulfide mineralogy. Rev. Mineralogy vol. 1.

Danyushevsky, L., Robinson, P., Gilbert, S., Norman, M., Large, R., McGoldrick, P., Shelley, M., 2011. Routine quantitative multi-element analysis of sulphide minerals by laser ablation ICP-MS: Standard development and consideration of matrix effects. Geochem. Explor. Env. Anal. 11, 51-60.

Dare, S. A., Barnes, S. J., Prichard, H. M., Fisher, P. C., 2011. Chalcophile and platinum-group element (PGE) concentrations in the sulfide minerals from the McCreedy East deposit, Sudbury, Canada, and the origin of PGE in pyrite. Mineral. Deposita 46, 381–407.

Dare, S. A. S., Barnes, S. J., Beaudoin, G., Méric, J., Boutroy, E., Potvin-Doucet, C., 2014. Trace elements in magnetite as petrogenetic indicators. Mineral. Deposita 49, 785-796.

Darling, J. R., Storey, C. D., Engi, M., 2012. Allanite U-Th-Pb geochronology by laser ablation ICPMS. Chem. Geol. 292-293, 103-115.

Deditius, A. P., Reich, M., Kesler, S. E., Utsunomiya, S., Chryssoulis, S. L., Walshe, J., Ewing, R. C., 2014. The coupled geochemistry of Au and As in pyrite from hydrothermal ore deposits. Geochim. Cosmochim. Acta 140, 644-670.

Demir Y., Uysal I., Burhan Sadiklar M., Sipahi F., 2008. Mineralogy, mineral chemistry, and fluid inclusion investigation of Köstere hydrothermal vein-type deposit (Gümüşhane, NE Turkey). Neu. Jb. Mineral. Abh. 185, 215-232.

Demir Y., Uysal İ., Sadıklar M. B., 2013. Mineral chemical investigation on sulphide mineralization of the Istala deposit, Gümüşhane, NE-Turkey. Ore Geol. Rev. 53, 306-317.

Deyell, C. L., Hedenquist, J. W., 2011. Trace element geochemistry of enargite in the Mankayan District, Philippines. Econ. Geol. 106, 1465-1478.

Duchesne, J. C., Rouhart, A., Schoumacher, C., Dillen, H., 1983. Thallium, nickel, cobalt and other trace elements in iron sulfides from Belgian lead-zinc vein deposits. Mineral. Deposita 18, 303-313.

Feng, R., Machado, N., Ludden, J., 1993. Lead geochronology of zircon by laserprobe-inductively coupled plasma-mass spectrometry (LP-ICP-MS). Geochim. Cosmochim. Acta 57, 3479–3486.

Fleet, M. E., 2006. Phase equilibria at high temperatures. Rev. Mineral. Geochem. 61, 365-419.

Fleet M. E., Mumin A. H., 1997. Gold-bearing arsenian pyrite and marcasite and arsenopyrite from Carlin Trend gold deposits and laboratory synthesis. Amer. Mineral. 82, 182–193.

Fleischer, M., 1955. Minor elements in some sulphide minerals. Econ. Geol. Fiftieth Anniversary Volume: 1905-1955. 970-1024.

Foord, E. E., Shawe, D. R., 1989. The Pb-Bi-Ag-Cu-(Hg) chemistry of galena and some associated sulfosalts; a review and some new data from Colorado, California and Pennsylvania. Can. Mineral. 27, 363–382.

Foord, E. E., Shawe, D. R., Conklin, N. M., 1988. Coexisting galena, PbSss and sulfosalts: evidence for multiple episodes of mineralization in the Round Mountain and Manhattan gold districts, Nevada. Can. Mineral. 26, 355–376.

Frenzel, M., Hirsch, T., Gutzmer, J., 2016. Gallium, germanium, indium, and other trace and minor elements in sphalerite as a function of deposit type — A meta-analysis. Ore Geol. Rev. 76, 52-78.

Friedl J., Wagner F. E., Wang N., 1995. On the chemical state of combined gold in sulfidic ores: Conclusions from Mössbauer source experiments. Neues Jahrb. Miner. Abh. 169, 279–290.

Fryer, B. J., Jackson, S., Longerich, H., 1993. The application of laser ablation microprobe-inductively coupled plasma-mass spectrometry (LAM-ICP-MS) to in situ (U)–Pb geochronology. Chem. Geol. 109, 1–8.

Fryer, B. J., Jackson, S. E., Longerich, H. P., 1995. Design, operation and role of the Laser-Ablation Microprobe coupled with an Inductively-Coupled Plasma - Mass-Spectrometer (LAM-ICP-MS) in the earth-sciences. Can. Mineral. 33, 303-312.

Fu, Y., Sun, X. M., Zhou, H. Y., Lin, H., Yang, T. J., 2016. In-situ LA–ICP–MS U–Pb geochronology and trace elements analysis of polygenetic titanite from the giant Beiya gold–polymetallic deposit in Yunnan Province, Southwest China. Ore Geol. Rev. 77, 43-56.

Fujiki, Y., 1963. Study on the Nickel-and Cobalt-bearing Sulphide Minerals from the Komori Mine by Means of Electron Probe Microanalyzer. Min. Geol. 13, 333-338.

Gagnon, J. E., Samson, I. M., Fryer, B. J., Williams-Jones, A. E., 2003. Compositional heterogeneity in fluorite and the genesis of fluorite deposits: Insights from LA-ICP-MS analysis. Can. Mineral. 41, 365-382.

Gaspar, M., Knaack, C., Meinert, L. D., Moretti, R., 2008. REE in skarn systems: a LA-ICP-MS study of garnets from the Crown Jewel gold deposit. Geochim. Cosmochim. Acta 72, 185–205.

Gasparrini, C., 1983. The mineralogy of gold and its significance in metal extraction. Canad. Inst. Mining Metall. 76, 144-153.

Gena K., Chiba H., Kase K., Nakashima K., Ishiyama D., 2013. The Tiger Sulfide Chimney, Yonaguni Knoll IV Hydrothermal Field, Southern Okinawa Trough, Japan: The first reported occurrence of Pt–Cu–Fe-bearing bismuthinite and Sn-bearing chalcopyrite in an active seafloor hydrothermal system. Resour. Geol. 63, 360-370.

Gilbert, S. E., Danyushevsky, L. V., Goemann, K., Death, D., 2014. Fractionation of sulphur relative to iron during laser ablation-ICP-MS analyses of sulphide minerals: implications for quantification. J. Anal. Atom. Spectrom. 29, 1024-1033.

Goldmann, S., Melcher, F., Gäbler, H. E., Dewaele, S., De Clerq, F., Muchez, P., 2013. Mineralogy and Trace Element Chemistry of Ferberite/Reinite from Tungsten Deposits in Central Rwanda. Minerals 3, 121-144.

Gregory, C. J., Rubatto, D., Hermann, J., Berger, A., Engi, M., 2012. Allanite behaviour during incipient melting in the southern Central Alps. Geochim. Cosmochim. Acta 84, 433-458.

Günther, D., Koch, J., 2008. Formation of aerosols generated by laser ablation and their impact on elemental fractionation in LA–ICP–MS. In Sylvester, P., Ed., Laser Ablation ICP-MS in the Earth Sciences: Current Practices and Outstanding Issues. Mineralogical Association of Canada Short Course Volume 40, 19-34.

Günther, D., von Quadt, A., Wirz, A., Cousin, H., Dietrich, V. J., 2001. Elemental analyses using laser ablation-inductively coupled plasma-mass spectrometry (LA-ICP-MS) of geological samples fused with $Li_2B_4O_7$ and calibrated without matrix-matched standards. Mikrochim. Acta 136, 101–107.

Harris, D. C., 1990. The mineralogy of gold and its relevance to gold recoveries. Mineral. Deposita 25, S3-S7.

Harris D. C., Cabri L. J., Nobiling R., 1984. Silver bearing chalcopyrite, a principal source of silver in the Izok lake massive-sulfide deposit: confirmation by electron and proton-microprobe analyses. Can. Mineral. 22, 493-498.

Hayden, L. A., Watson, E. B., Wark, D. A., 2008. A thermobarometer for sphene (titanite). Contrib. Mineral. Petrol. 155, 529–540.

Hazarika, P., Mishra, B., Pruseth, K. L., 2016. Scheelite, apatite, calcite and tourmaline compositions from the late Archean Hutti orogenic gold deposit: Implications for analogous two stage ore fluids. Ore Geol. Rev. 72, 989-1003.

He, H. L., Yu, S. Y., Song, X. Y., Du, Z. S., Dai, Z. H., Zhou, T., Xie, W., 2016. Origin of nelsonite and Fe–Ti oxides ore of the Damiao anorthosite complex, NE China: Evidence from trace element geochemistry of apatite, plagioclase, magnetite and ilmenite. Ore Geol. Rev. 79, 367-381.

Heidarian, H., Lentz, D., Alirezaei, S., Peighambari, S., Hall, D., 2016. Using the chemical analysis of magnetite to constrain various stages in the formation and genesis of the Kiruna-type chadormalu magnetite-apatite deposit, Bafq district, Central Iran. Mineral. Petrol. 110, 927-942.

Helmy H. M., Shalaby I. M., Rahman H. A., 2014. Large-scale metal zoning in a late-Precambrian skarn-type mineralization, Wadi Kid, SE Sinai, Egypt. J. Afr. Earth Sci. 90, 77-86.

Henley, K. J., 1975. Gold-ore mineralogy and its relation to metallurgical treatment. Minerals Sci. Engng. 7, 289-312.

Hoffman, J. I., 1934. Preparation of pure gallium. Bur. Stand. J. Res. 13, 665.

Holwell, D., McDonald, I., 2010. A review of the behaviour of platinum group elements within natural magmatic sulphide ore systems. Platin. Met. Rev. 54, 26–36.

Huston, D. L., Sie, S. H., Suter, G. F., Cooke, D. R., Both, R. A., 1995. Trace elements in sulphide minerals from eastern Australian volcanic-hosted massive sulphide deposits; Part I, Proton microprobe analyses of pyrite, chalcopyrite, and sphalerite, and Part II, Selenium levels in pyrite; comparison with delta 34 S values and implications for the source of sulfur in volcanogenic hydrothermal systems. Econ. Geol. 90, 1167–1196.

Huston D. L., Jablonski W., Sie S. H., 1996. The distribution and mineral hosts of silver in eastern Australian volcanogenic massive sulfide deposits. Can. Mineral. 34, 529-546.

Ingham, E. S., Cook, N. J., Cliff, J., Ciobanu, C. L., Huddleston, A., 2014. A combined chemical, isotopic and microstructural study of pyrite from roll-front uranium deposits, Lake Eyre Basin, South Australia. Geochim. Cosmochim. Acta 125, 440-465.

Ismail, R., Ciobanu, C. L., Cook, N. J., Schmidt Mumm, A., Wade, B., Giles, D., Teale, G. S., 2014. Rare Earths and other trace elements in minerals from skarn assemblages, Hillside iron oxide-copper-gold deposit, Yorke Peninsula, South Australia. Lithos 184-187, 456-477.

Jackson, S. E., Günther, D., 2003. The nature and sources of laser induced isotopic fractionation in laser ablation-multicollector-inductively coupled plasma-mass spectrometry. J. Anal. Atom. Spectrom. 18, 205-212.

Jenner, F. E., Arevalo, R. D., 2016. Major and Trace Element Analysis of Natural and Experimental Igneous Systems using LA–ICP–MS. Elements 12, 311-316.

Jeppsson, M. L., 1989. Mineral chemistry of silver in antimony and bismuth rich sulphide ore in Bergslagen, central Sweden. Neu. Jb. Mineral. Mh. 5, 205–216.

Johan, Z., 1988. Indium and germanium in the structure of sphalerite: an example of coupled substitution with copper. Mineral. Petrol. 39, 211–229.

Kano, S., Nambu, M., 1967. The study of the equilibrium in the system FeS-S_2 (I) Dissociation equilibrium of pyrite at the low temperature. The Journal of the Japanese Association of Mineralogists, Petrologists and Economic Geologists 57, 81-97.

Kase K., 1987. Tin-bearing chalcopyrite from the Izumo vein, Toyoha Mine, Hokkaido, Japan. Can. Mineral. 25, 9-13.

Koch, J., Günther, D., 2007. Femtosecond laser ablation inductively coupled plasma mass spectrometry: achievements and remaining problems. Anal. Bioanal. Chem. 387, 149-153.

Kojima, S., Sugaki, A., 1985. Phase relations in the Cu–Fe–Zn–S system between 500 degrees and 300 degrees C under hydrothermal conditions. Econ. Geol. 80, 158–171.

Kontonikas-Charos, A., Ciobanu, C. L., Cook, N. J., 2014. Albitization and redistribution of REE and Y in IOCG systems: Insights from Moonta-Wallaroo, Yorke Peninsula, South Australia. Lithos 208-209, 178-201.

Lane, D. J., Cook, N. J., Grano, S. R., Ehrig, K., 2016. Selective leaching of penalty elements from copper concentrates: a review. Miner. Eng. 98, 110-121.

Large, R. R., Maslenikov, V. V., Robert, F., Danyushevsky, L. V., Chang, Z., 2007. Multistage Sedimentary and Metamorphic Origin of Pyrite and Gold in the Giant Sukhoi Log Deposit, Lena Gold Province, Russia. Econ. Geol. 102, 1233-1267.

Large, R. R., Danyushevsky, L., Hollit, C., Maslennikov, V., Meffre, S., Gilbert, S., Bull, S., Scott, R., Emsbo, P., Thomas, H., Singh, B., 2009. Gold and trace element zonation in pyrite using a laser imaging technique: implications for the timing of gold in orogenic and Carlin-style sediment-hosted deposits. Econ. Geol. 104, 635-668.

Large, R. R., Meffre, S., Burnett, R., Guy, B., Bull, S., Gilbert, S., Goemann, K., Danyushevsky, L., 2013. Evidence for an intrabasinal source and multiple concentration processes in the formation of the Carbon Leader Reef, Witwatersrand Supergroup, South Africa. Econ. Geol. 108, 1215-1241.

Large, R. R., Halpin, J. A., Danyushevsky, L. V., Maslennikov, V. V., Bull, S. W., Long, J. A., Gregory, D. D., Lounejeva, E., Lyons, T. W., Sack, P. J., McGoldrick, P. J., Calver, C. R., 2014. Trace element content of sedimentary pyrite as a new proxy for deep-time ocean-atmosphere evolution. Earth Plan. Sci. Lett. 389, 209-220.

Lawley, C. J. M., Creaser, R. A., Jackson, S. E., Yang, Z. P., Davis, B. J., Pehrsson, S. J., Dubé, B., Mercier-Langevin, P., Vaillancourt, D., 2015. Unraveling the Western Churchill Province Paleoproterozoic Gold Metallotect: Constraints from Re-Os Arsenopyrite and U-Pb Xenotime Geochronology and LA-ICP-MS Arsenopyrite Trace Element Chemistry at the BIF-Hosted Meliadine Gold District, Nunavut, Canada. Econ. Geol. 110, 1425-1454.

Layton-Matthews D., Peter J. M., Scott S. D., Leybourne M. I., 2008. Distribution, mineralogy, and geochemistry of selenium in felsic volcanic-hosted massive sulfide deposits of the Finlayson Lake district, Yukon Territory, Canada. Econ. Geol. 103, 61-88.

Lee, D. C., Halliday, A. N., 1995. Hafnium–tungsten chronometry and the timing of terrestrial core formation. Nature 378, 771–774.

Lepetit, P., Bente, K., Doering, T., Luckhaus, S., 2003. Crystal chemistry of Fe-containing sphalerites. Phys. Chem. Miner. 30, 185–191.

Li, C. Y., Zhang, R. Q., Ding, X., Ling, M. X., Fan, W. M., Sun, W. D., 2016. Dating cassiterite using laser ablation ICP-MS. Ore Geol. Rev. 72, 313–322.

Liu, H., Chang, L. L. Y., 1994. Phase relations in the system PbS–PbSe–PbTe. Mineral. Mag. 58, 567–578.

Liu, Z., Wu, F., Guo, C., Zhao, Z., Yang, J., Sun, J., 2011. In situ U-Pb dating of xenotime by laser ablation (LA)-ICP-MS. Chin. Sci. Bull. 56, 2948-2956.

Lockington, J., Cook, N. J., Ciobanu, C. L., Trace and minor elements in sphalerite from metamorphosed sulphide deposits. Mineral. Petrol. 108, 873-890.

Lord, C. S., 1933. A study of tetrahedrite in some British Columbia ores. Doctoral dissertation, University of British Columbia.

Lueth, V. W., Megaw, P. K. M., Pingitore, N. E., Goodell, P. C., 2000. Systematic Variation in Galena Solid-Solution Compositions at Santa Eulalia, Chihuahua, Mexico. Econ. Geol. 95, 1673–1687.

Makvandi, S., Ghasemzadeh-Barvarz, M., Beaudoin, G., Grunsky, E. C., McClenaghan, M. B., Duchesne, C., 2016a. Principal component analysis of magnetite composition from volcanogenic massive sulfide deposits: Case studies from the Izok Lake (Nunavut, Canada) and Halfmile Lake (New Brunswick, Canada) deposits. Ore Geol. Rev. 72, 60-85.

Makvandi, S., Ghasemzadeh-Barvarz, M., Beaudoin, G., Grunsky, E. C., McClenaghan, M. B., Duchesne, C., Boutroy, E., 2016b. Partial least squares-discriminant analysis of trace element compositions of magnetite from various VMS deposit subtypes: Application to mineral exploration. Ore Geol. Rev. 78, 388-408.

Marechal, C., Telouk, P., Albarede, F., 1999. Precise analysis of Cu and Zn isotopic compositions by plasma-source mass spectrometry. Chem. Geol. 156, 251–273.

Marques de Sá, C., Noronha, F., Ferreira da Silva, E., 2014. Factor analysis characterization of minor element contents in sulfides from Pb–Zn–Cu–Ag hydrothermal vein deposits in Portugal. Ore Geol. Rev. 62, 54-71.

McFarlane, C. R. M., 2016. Allanite U-Pb geochronology by 193 nm LA ICP-MS using NIST610 glass for external calibration. Chem. Geol. 438, 91-102.

McIntyre, N. S., Cabri, L. J., Chauvin, W. J., Laflamme, J. H. G., 1984. Secondary ion mass spectrometric study of dissolved silver and indium in sulfide minerals. Scanning Electron Microsc. 3, 1139-1146.

Moggi-Cecchi V., Cipriani C., Rossi P., Ceccato D., Rudello V., Somacal H., 2002. Trace element contents and distribution maps of chalcopyrite: a micro-PIXE study. Period. Mineral. 71, 101-109.

Monteiro L. V. S., Xavier R. P., Hitzman M. W., Juliani C., de Souza Filho C. R., Carvalho E. D. R., 2008. Mineral chemistry of ore and hydrothermal alteration at the Sossego iron oxide–copper–gold deposit, Carajás Mineral Province, Brazil. Ore Geol. Rev. 34, 317-336.

Morey, A. A., Tomkins, A. G., Bierlein, F. P., Weinberg, R. F., Davidson, G. J., 2008. Bimodal Distribution of Gold in Pyrite and Arsenopyrite: Examples from the Archean Boorara and Bardoc Shear Systems, Yilgarn Craton, Western Australia. Econ. Geol. 103, 599-614.

Murakami, H., Ishihara, S., 2013. Trace elements of indium-bearing sphalerite from tin-polymetallic deposits in Bolivia, China and Japan: A femto-second LA-ICPMS study. Ore Geol. Rev. 53, 223-243.

Nadoll, P., Mauk, J. L., Hayes, T. S., Koenig, A. E., Box, S. E., 2012. Geochemistry of Magnetite from Hydrothermal Ore Deposits and Host Rocks of the Mesoproterozoic Belt Supergroup, United States. Econ. Geol. 107, 1275-1292.

Nadoll, P., Angerer, T., Mauk, J. L., French, D., Walshe, J., 2014. The chemistry of hydrothermal magnetite: A review. Ore Geol. Rev. 61, 1-32.

Nakamoto, A., Urasima, Y., Sugiura, S., Nakano, H., Yachi, T., Tadokoro, K., 1969. Pyromorphite-mimetite minerals from the Otaru-Matsukura barite mine in Hokkaido, Japan. Mineral. J. 6, 85-101.

Noddack, I., Noddack, W., 1931. Die geochemie des rheniums. Z. Phys. Chem. A 154, 207-244.

Norman, M. D., Pearson, N. J., Sharma, A., Griffin, W. L., 1996. Quantitative analysis of trace elements in geological materials by laser ablation ICPMS: Instrumental operating conditions and calibration values of NIST glasses. Geostandard. Newslett. 20, 247–261.

Norman, M., Robinson, P., Clark, D., 2003. Major- and trace-element analysis of sulfide ores by laser-ablation ICP-MS, solution ICP-MS, and XRF: New data on international reference materials. Can. Mineral. 41, 293–305.

O'Brien, J. J., Spry, P. G., Teale, G. S., Jackson, S.,E., Rogers, D., 2015. Major and Trace Element Chemistry of Gahnite as an Exploration Guide to Broken Hill-Type Pb-Zn-Ag Mineralization in the Broken Hill Domain, New South Wales, Australia. Econ. Geol. 110, 1027-1057.

Oftedahl, I., 1940. Untersuchungen u¨ber die Nebenbestandteile von Erzmineralien norwegischer zinkblendfu¨hrender Vorkommen. Skrift. Norsk Vidensk. Akad. Oslo, Math. Naturv. Kl. 8, 1-103.

Pagé, P., Barnes, S. J., 2009. Using trace elements in chromites to constrain the origin of podiform chromitites in the Thetford Mines Ophiolite, Quebec, Canada. Econ. Geol. 104, 997-1018.

Pal, D. C., Chaudhuri, T., McFarlane, C., Mukherjee, A., Sarangi, A. K., 2011. Mineral Chemistry and In Situ Dating of Allanite, and Geochemistry of its Host Rocks in the Bagjata Uranium Mine, Singhbhum Shear Zone, India - Implications for the Chemical Evolution of REE Mineralization and Mobilization. Econ. Geol. 106, 1155-1171.

Park, B., 1934. Estimation of Small Amounts of Bismuth, Antimony, Tin, and Molybdenum in Copper. Industrial & Engineering Chemistry Analytical Edition 6, 189-190.

Raju, P. V. S., Hart, C. J. R., Sangurmath, P., 2016. Scheelite geochemical signatures by LA-ICP-MS and potential for rare earth elements from Hutti Gold Mines and fingerprinting ore deposits. J. Afr. Earth Sci. 114, 220–227.

Reich, M., Kesler, S. E., Utsunomiya, S., Palenik, C. S., Chryssoulis, S. L., Ewing, R.C., 2005. Solubility of gold in arsenian pyrite. Geochim. Cosmochim. Acta 69, 2781-2796.

Reich, M., Utsunomiya, S., Kesler, S.E., Wang, L., Ewing, R.C., Becker, U., 2006. Thermal behavior of metal nanoparticles in geologic materials. Geology 34, 1033-1036.

Reich M., Palacios C., Barra F., Chryssoulis S., 2013. "Invisible" silver in chalcopyrite and bornite from the Mantos Blancos Cu deposit, northern Chile. Eur. J. Mineral. 25, 453-460.

Reich, M., Simon, A. C., Deditius, A., Barra, F., Chryssoulis, S., Lagas, G., Tardani, D., Knipping, J., Bilenker, L., Sánchez-Alfaro, P., Roberts, M. P., 2016. Trace element signature of pyrite from the Los Colorados iron oxide-apatite (IOA) deposit, Chile: A missing link between Andean IOA and iron oxide copper-gold systems? Econ. Geol. 111, 743-761.

Remond, G., Cesborn, E., Traxel, K., Campbell, J. L., Cabri, L. J., 1987. Electron microprobe analysis and proton induced X-ray spectrometry applied to trace element analysis in sulfides. Problems and prospects. Scanning Microsc. 1, 1017-1037.

Renock, D., Becker, U., 2011. A first principles study of coupled substitution in galena. Ore Geol. Rev. 42, 71–83.

Russo, R. E., Mao, X. L., Gonzalez, J. J., Mao, S. S., 2002. Femtosecond laser ablation ICP-MS. J. Anal. Atom. Spectrom. 17, 1072–1075.

Sack, R. O., Ebel, D. S., 2006. Thermochemistry of sulfide mineral solutions. Rev. Mineral. Geochem. 61, 265-364.

Sadati S. N., Yazdi M., Mao J., Behzadi M., Adabi M. H., Lingang X., Zhenyu C., Mokhtari M. A. A., 2016. Sulfide mineral chemistry investigation of sediment-hosted stratiform copper deposits, Nahand-Ivand area, NW Iran. Ore Geol. Rev. 72, 760-776.

Savage K. S., Tingle T. N., O'Day P. A., Waychunas G. A., Bird D. K., 2000. Arsenic speciation in pyrite and secondary weathering phases, Mother Lode gold district, Tuolumne County, California. Appl. Geochem. 15, 1219–1244.

Scott K. M., Ashley P. M., Lawie D. C., 2001. The geochemistry, mineralogy and maturity of gossans derived from volcanogenic Zn–Pb–Cu deposits of the eastern Lachlan Fold Belt, NSW, Australia. J. Geochem. Explor. 72, 169-191.

Sebba, F., Pugh, W., 1937. 281. Gallium. Part II. The extraction of gallium and germanium from germanite. Journal of the Chemical Society (Resumed), 1371-1373.

Serranti S., Ferrini V., Masi U., Nicoletti M., Conde L. N., 2002. Geochemical features of the massive sulfide (Cu) metamorphosed deposit of Arinteiro (Galicia, Spain) and genetic implications. Period. Mineral. 71, 27-48.

Shalaby I. M., Stumpfl E., Helmy H. M., El Mahallawi M. M., Kamel O. A., 2004. Silver and silver-bearing minerals at the Um Samiuki volcanogenic massive sulphide deposit, Eastern Desert, Egypt. Mineral. Deposita 39, 608-621.

She, Y. W., Song, X. Y., Yu, S. Y., Chen, L. M., Zheng, W. Q., 2016. Apatite geochemistry of the Taihe layered intrusion, SW China: Implications for the magmatic differentiation and the origin of apatite-rich Fe-Ti oxide ores. Ore Geol. Rev. 78, 151-165.

Simon G., Huang H., Penner-Hahn J. E., Kesler S. E., Kao L. S., 1999. Oxidation state of gold and arsenic in gold-bearing arsenian pyrite. Amer. Mineral. 84, 1071–1079.

Smith, M. P., Henderson, P., Jeffries, T. E. R., Long, J., Williams, C. T., 2004. The rare earth elements and uranium in garnets from the Beinn an Dubhaich Aureole, Skye, Scotland, UK: constraints on processes in a dynamic hydrothermal system. J. Petrol. 45, 457-484.

Smith, M. P., Storey, C. D., Jeffries, T. E., Ryan, C., 2009. In Situ U-Pb and trace element analysis of accessory minerals in the Kiruna District, Norrbotten, Sweden: New constraints on the timing and origin of mineralization. J. Petrol. 50, 2063-2094.

Song, G. X., Qin, K. Z., Li, G. M., Evans, N. J., Chen, L., 2014. Scheelite elemental and isotopic signatures: Implications for the genesis of skarn-type W-Mo deposits in the Chizhou Area, Anhui Province, Eastern China. Amer. Mineral. 99, 303–317.

Stoiber, R. E., 1940. Minor elements in sphalerite. Econ. Geol. 35, 501-519.

Sugaki, A., Shima, H., Kitakaze, A., 1970. Fundamental study on the quantitative analysis of sulphide minerals by electron probe microanalyser (I). Research report, faculty of engineering, Yamaguchi University 21, 87-209.

Sung, Y. H., Brugger, J., Ciobanu, C. L., Pring, A., Skinner, W., Nugus, M., 2009. Invisible gold in arsenian pyrite and arsenopyrite from a multistage Archaean gold deposit: Sunrise Dam, Eastern Goldfields Province, Western Australia. Mineral. Deposita 44, 765-791.

Sylvester, P., Ed., 2001. Laser Ablation ICP-MS in the Earth Sciences: Principles and Applications. Mineralogical Association Canada Short Course Volume 29, 243 pp.

Sylvester, P., Ed., 2008a. Laser Ablation ICP-MS in the Earth Sciences: Current Practices and Outstanding Issues. Mineralogical Association of Canada Short Course Volume 40, 364 pp.

Sylvester, P. J., 2008b. Matrix effects in laser ablation ICP-MS. In: Sylvester, P., Ed., Laser Ablation ICP-MS in the Earth Sciences: Current Practices and Outstanding Issues. Mineralogical Association of Canada Short Course Volume 40, 67-78.

Sylvester, P. J., Jackson, S. E., 2016. A brief history of Laser Ablation Inductively Coupled Plasma Mass Spectrometry (LA-ICP-MS). Elements 12, 307-310.

Takenouchi, S., Fujiki, Y., 1968. Experimental study on Cu-Fe-S minerals (1st report) – Application of EPMA to synthetic products. Jpn. Min. J. 84, 1-6.

Thomas, R., 2013. Practical Guide to ICP-MS: A Tutorial for Beginners. CRC Press, Boca Raton, 446 pp.

Thompson, J., Meffre, S., Maas, R., Kamenetsky, V., Kamenetsky, M., Goemann, K., Ehrig, K., Danyushevsky, L., 2016. Matrix effects in Pb/U measurements during LA-ICP-MS analysis of the mineral apatite, J. Anal. Atom. Spectrom. 31, 1206-1215.

Urasima, Y., 1968. Gold-bearing ores of the Oe ore deposits in Hokkaido. Min. Geol. 17, 328-339.

Van Hook, H. J., 1960. The ternary system Ag_2S-Bi_2S_3-PbS. Econ. Geol. 55, 759–788.

Vanhaecke, F., Degryse, P., Eds., 2012. Isotopic Analysis: Fundamentals and Applications using ICP-MS. Wiley-VCH Verlag GmbH & Co, Weinheim, 550 pp.

Vaughan, D. J., Craig, J. R., 1997. Sulfide ore mineral stabilities, morphologies, and intergrowth textures. Geochemistry of hydrothermal ore deposits 3, 367-434.

Wang G., Wang Z. Q., Shi R., Zhang Y. L., Wang K. M., 2015. Mineralogy and isotope geochemical characteristics for Xiaozhen copper deposit, Langao County, Shaanxi Province and their constraint on genesis of the deposit. Geosci. J. 19, 281-294.

Warren, H. V., 1932. Relation between silver content and tetrahedrite in the ores of the North Cananea Mining Co., Cananea, Sonora, Mexico. Econ. Geol. 27, 737-743.

Warren, H. V., Loofbourow, R. W., 1932. The occurrence and distribution of silver in the silver king coalition mines, Park City, Utah. Econ. Geol. 27, 644-650.

Watson, E. B., Harrison, T. M., 2005. Zircon thermometer reveals minimum melting conditions on earliest Earth. Science 308, 841–844.

White, W. M., Albarède, F., Télouk, P., 2000. High-precision analysis of Pb isotope ratios by multi-collector ICP-MS. Chem. Geol. 167, 257-270.

Winderbaum, L., Ciobanu, C. L., Cook, N. J., Paul, M., Metcalfe, A., Gilbert, S., 2012. Multivariate Analysis of an LA-ICP-MS Trace Element Dataset for Pyrite. Math. Geosci. 44, 823-842.

Wohlgemuth-Ueberwasser, C. C., Jochum, K. P., 2015. Capability of fs-LA-ICP-MS for sulfide analysis in comparison to ns-LA-ICP-MS: reduction of laser induced matrix effects? J. Anal. Atom. Spectrom. 30, 2469-2480.

Wohlgemuth-Ueberwasser, C. C., Ballhaus, C., Berndt, J., Stotter, V., Meisel, T., 2007. Synthesis of PGE sulphide standards for laser ablation inductively coupled plasma mass spectrometry (LA-ICP-MS). Contrib. Mineral. Petrol. 154, 607-617.

Wohlgemuth-Ueberwasser, C. C., Viljoen, F., Petersen, S., Vorster, C., 2015. Distribution and solubility limits of trace elements in hydrothermal black smoker sulfides: An in-situ LA-ICP-MS study. Geochim. Cosmochim. Acta 159, 16-41.

Woodhead, J. D., Horstwood, M. S. A., Cottle, J. M., 2016. Advances in isotope ratio determination by LA-ICP-MS. Elements 12, 317-322.

Xu, J., Ciobanu, C. L., Cook, N. J., Zheng, Y., Sun, X., Wade, B. P., 2016. Skarn formation and trace elements in garnet and associated minerals from Zhibula copper deposit, Gangdese Belt, southern Tibet. Lithos 262, 213-231.

Ye, L., Cook, N. J., Ciobanu, C. L., Liu, Y. P., Zhang, Q., Gao, W., Yang, Y. L., Danyushevsky, L. V., 2011. Trace and minor elements in sphalerite from base metal deposits in South China: a LA-ICPMS study. Ore Geol. Rev. 39, 188–217.

Zack, T., Stockli, D. F., Luvizotto, G. L., Barth, M. G., Belousova, E., Wolfe, M. R., Hinton, R.W., 2011. In situ U-Pb rutile dating by LA-ICP-MS ^{208} Pb correct ion and prospects for geological applications: Contrib. Mineral. Petrol. 162, 515-530.

Zhang, J., Deng, J., Chenb, H. Y., Yang, L. Q., Cooke, D., Danyushevsky, L., Gong, Q. J., 2014. LA-ICP-MS trace element analysis of pyrite from the Chang'an gold deposit, Sanjiang region, China: Implication for ore-forming process. Gondwana Res. 26, 557-575.

Zhu, Z. Y., Jiang, S. Y., Yang, T., Ciobanu, C. L., Cook, N. J., 2017. Sulfur isotope fractionation in pyrite during laser ablation: Implications for Laser Ablation Multiple Collector Inductively Coupled Plasma Mass Spectrometry mapping. Chem. Geol. 450, 223-234.

CHAPTER 2

METHODOLOGY

CHAPTER 2: METHODOLOGY

This chapter provides a brief description of the samples used in this study, the criteria used to select them, and sample preparation. In the second part of the chapter, details of each microanalytical technique are outlined. These include Optical Microscopy, Scanning Electron Microscopy (SEM), Electron Probe Microanalysis (EPMA) and Laser Ablation Inductively-Coupled Plasma Mass Spectrometry (LA-ICP-MS).

2.1 Sample selection and preparation

A total of 115 samples from 38 deposits in 12 countries were used in this study (Table 2.1). Most samples originate from the personal collections of Prof. Nigel Cook and Dr. Cristiana Ciobanu, with additional material sourced from the South Australian Museum and the Tate Museum (The University of Adelaide) as indicated in Table 2.1. Samples were deliberately selected from a wide variety of deposit types, geological terranes and conditions of ore formation. This was to ensure that the measured trace element distributions and partitioning behaviours were sufficiently representative of an extensive range of conditions and environments. This does not imply that the sample suite is completely representative of each different deposit type (given the extraordinary variety ore deposits exhibit), only that it includes examples of as many different base metal sulphide (BMS) ores as possible. All samples contain at least one BMS (including tetrahedrite-tennantite), although most contain more than one co-existing sulphide phase.

Table 2.1. List of samples used in this study

Locality	Sample	Used in Chapter	Locality	Sample	Used in Chapter
Allihies Mine, Ireland	G13301*	6	Kochbulak, Uzbekistan	30	3
Assarel, Bulgaria	ASR 10	5		33	5
	ASR 5A	5		38	3
	ASR KB P12077	5		47	3
Baia de Aries, Romania	BdA 99-1	3	Lega Dembi, Ethiopia	7011A	3
	BdA 99-5	3	Medcritting, Australia	G6948*	6
	BdA 99-9	3	Mofjellet, Norway	Mo11	3
Baita Bihor, Romania	BB158	3		Mo16	5, 6
	BB55	3, 4, 5		Mo17A	5, 6
	BBH15-21	5		Mo2	3, 4
	BBH16AB	3		Mo5	3, 5
	BBH16B	3, 4	Mooloowatana HS, Australia	G15977*	6
	BBH20	3, 4	Mt. Camel, Australia	G10847*	6
	BBH25	3	Mt. Isa, Australia	5984B C1	3
	BBH28A	3		5984B C2	3
	BBH32	3, 4		5985 C1	4
Bleikvassli, Norway	Bv-1	3, 4, 5		5990 C1	3
	Bv-4	5	Oraparinna, Australia	G14867*	6
	Bv-97-3	3	Oravita, Romania	ORV1	5, 6
	Bv97-52	6		ORV4	5, 6
	V446	3, 6		ORV4a	5
	V538	3, 6		ORV4B	4, 5
	V57-852	3	Pulganbar, Australia	G871*	6
	V598572	4, 5		G874*	6
Bor, Serbia	BOR14	5		G882*	6
Broken Hill, Australia	BH218	3, 4, 5	Ring Valley, Australia	G879*	6
	BH221	3	S. Wheal Exmouth, England	G13289a*	6
	BH233	3		G13289b*	6
	BH73	4, 5	Siegen, Germany	G16152*	6
	G11701*	6		G6946*	6
	G14549a*	6	Sulitjelma, Norway	CV01.1	5
	G14549b*	6		CV01.2a	5
	G16396*	6		CV01.2b	5
Curtin Davis Mine, Australia	G14246*	6		CV01.3	5
Elatsite, Bulgaria	Elatsite b a	5		CV01.4	5
	ELS 157	3, 5		CV01.6b	5
Emperor Gold Mine, Fiji	VFI031**	6		NC4172	5
Evelyn Mine, Australia	EV8**	6		NC5839	5
Gortdrum Mine, Ireland	G29851*	6		NC6894	5
Great Boulder Mine, Australia	G6940*	6		Su3	5
Grosskogel Mine, Austria	G16835*	6		Sulis 1b	5
Herja, Romania	Hj13	3, 4, 5, 6		Sulis2a	5
	Hj14	3, 6	Sullivan, Canada	Sul-1	3
Kalgoorlie, Australia	G11579*	6	Tinga, Australia	G12640*	6
Kanmantoo, Australia	KTDD086(11)	5	Toroiaga, Romania	Emeric2	3, 4, 5
	KTDD086(12)	5		T1a	3, 5
	KTDD086(8)	5		TOR189	5

	KTDD086(9)	5		TOR191	4, 5
	KTDD178(12)	5		TOR197	3, 4, 5
	KTDD178(7)	5		Toroiaga R0	5
	KTDD178(8)	5	Vorta, Romania	DM3	3
	KTDD180(3)	5		DMV99-22	3, 5
	KTDD180(7)	5		ZN 99.2	3
	KTDD180S(4)	5	Webb's Ag Mine, Australia	G6949*	6
	KTDD180S(5)	5	Yerranderrie, Australia	G6951*	6
Kapp Mineral, Norway	Kmi 2a	4, 5		G873*	6
	Kmi 2b	3			
	Kmi 4	3	*Sample derives from the South Australian Museum.		
	Kmi 5	4	**Sample derives from the Tate Museum, The University of Adelaide		

Samples that displayed clear textural evidence for equilibrium co-crystallization of BMS were especially sought after (e.g., showing ~120^{o} triple-junction grain boundaries between sulphides; see Fig. 2.1), since trace element distributions in co-crystallized assemblages reveal equilibrium element partitioning resulting directly from the prevailing conditions during ore formation. While the geological histories of the deposits represented in Table 2.1 are diverse, those ores with relatively simple geological histories (i.e., single BMS deposition event, minimal to no secondary overprinting) were favoured for inclusion in the study. This was done to ensure that trace element partitioning trends related predominantly to primary events. Nevertheless, some samples, particularly those containing tetrahedrite-tennantite sourced from the South Australian Museum and the Tate Museum, come from deposits with poorly constrained, or even unknown geological histories (e.g., from historic workings or prospects). In these cases, sulphide co-crystallization may still be determined from textural evidence, and only the effects of the co-crystallized sulphide assemblage on trace element partitioning are considered. Brief descriptions of the deposits that samples were sourced from may be found in the respective chapter(s) (and their appendices) each sample was used in (see Table 2.1).

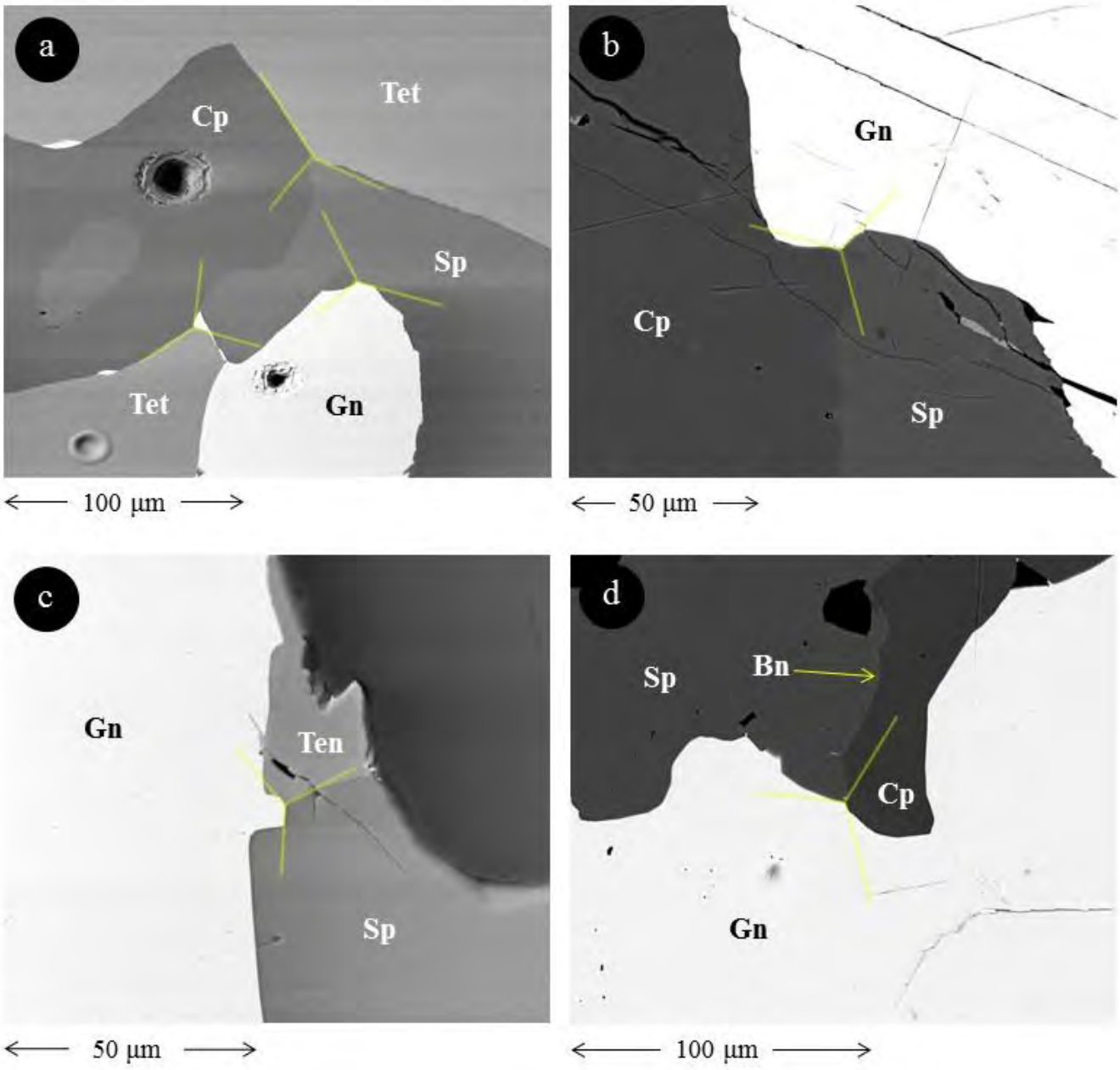

Figure 2.1. Representative back-scattered electron images illustrating textural evidence for BMS and tetrahedrite-tennantite co-crystallization. (**a**) ~120° triple-junction grain boundaries between tetrahedrite (Tet), sphalerite (Sp), galena (Gn) and chalcopyrite (Cp) from Kalgoorlie, Australia (orogenic Au deposit). (**b**) ~120° triple-junction grain boundaries between sphalerite, galena and chalcopyrite from Herja, Romania (epithermal deposit). (**c**) ~120° triple-junction grain boundaries between sphalerite, galena and tennantite (Ten) from Bleikvassli, Norway (recrystallized SEDEX deposit). (**d**) ~120° triple-junction grain boundaries between sphalerite, galena and chalcopyrite from Baita Bihor, Romania (skarn deposit). Bn = bornite. In each example note the grain boundaries curving towards the triple junction in order to approximate 120°.

Most samples were obtained as ready-prepared polished blocks, with size ranging from 1-2 inches; most were circular, although a few were rectangular. Some rock fragments were part of the material acquired from the South Australian Museum and the Tate Museum and these were sent to Adelaide Petrographic Laboratories for mounting in epoxy as 1-inch diameter polished blocks. All existing polished blocks were thoroughly re-polished and cleaned prior to use in this study. Some of the older polished blocks were professionally re-polished by Adelaide Petrographic Laboratories. All carbon coating necessary for SEM and EPMA was carried out by Adelaide Microscopy (University of Adelaide) staff where all microanalytical work was also conducted.

2.2 Optical Microscopy

Prior to any microanalytical work being conducted, all samples were thoroughly examined by reflected light optical microscopy using a Nikon Eclipse LV100 POL Petrographic Microscope. The LV100 is equipped with a high-intensity halogen light source that gives bright images with lower heat production, thus reducing heat-induced focus drift. Optical microscopy was used to classify the main sulphide phases present in each sample, categorize any textural features on the sample scale, and identify areas to be specifically investigated using scanning electron microscopy (i.e., smaller scale textural features, additional phases to be classified).

2.3 Scanning Electron Microscopy (SEM)

SEM work was conducted using a FEI Quanta 450 Field Emission Gun (FEG) Environmental Scanning Electron Microscope. The Quanta 450 is a High Resolution Field Emission SEM that may be operated in either Environmental SEM (for wet samples), Low Vacuum (for non-conductive samples) or High Vacuum modes (for high resolution imagery of conductive samples). As all samples were carbon coated prior to SEM work, imaging was carried out in High Vacuum mode. The ~15 nm thick carbon coat was produced by a Quorum Q150TE vacuum evaporator. Prior to insertion into the sample chamber, carbon-coated polished blocks were fixed to a 12 mm-diameter aluminium sample holder using double-sided carbon tape that extended to the sample surface. Operating conditions remained constant at 20 kV, 10 mm working distance, 0^{o} stage tilt and 130 Pa chamber pressure. While the Quanta 450 is equipped with both secondary electron (SE) and backscattered electron (BSE) detectors, sample characterization and imaging was primarily carried out in BSE mode. The Quanta 450 is also equipped with a SDD energy dispersive X-ray spectrometer (EDS) detector that was used for semi-quantitative compositional analysis.

The mineralogy of each sample was characterized by SEM using BSE mode at various magnifications and contrasts to highlight heterogeneities. Special attention was given to recognizing various mineral textures, including different mineral generations, overgrowths, compositional zones and replacement reactions. Such textures have direct implications for gathering and interpreting compositional data generated by EPMA or LA-ICP-MS. For the purposes of this study it was integral that compositional data for different grains of the same mineral, or different minerals, was compared only when they related to the same temporal and geological phenomena. The EDS system was used to identify, and provide semi-quantitative compositional information on the different minerals in each sample, most

importantly, the sulphide phases. Finally, the SEM was also used to locate areas of sulphide grains that were 'clean' and free of any noticeable inclusions. Such areas were noted and used for the placement of EPMA and LA-ICP-MS spots, while areas where inclusions occurred were avoided (Fig. 2.2).

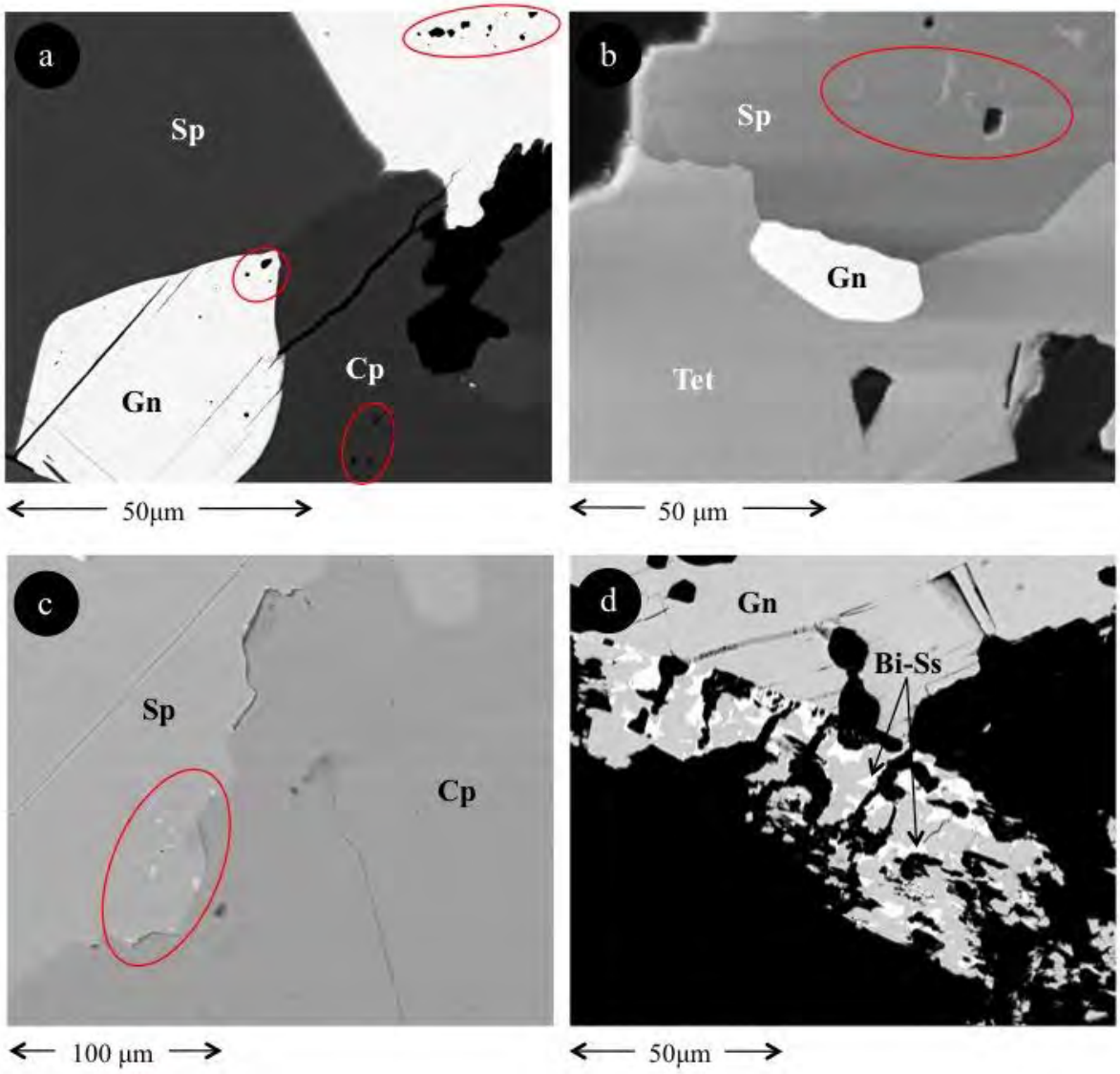

Figure 2.2. Representative back-scattered electron images illustrating areas where inclusions were recognized and thus avoided when placing EPMA and LA-ICP-MS spots. Sp = sphalerite, Gn = galena, Cp = chalcopyrite, Tet = tetrahedrite, Bi-Ss = Bi-sulphosalt. Areas containing (**a**) gangue, (**b**) tetrahedrite and (**c**) galena inclusions are circled in red. (**d**) Area containing exsolutions of a Bi-sulphosalt in galena.

2.4 Electron Probe Microanalysis (EPMA)

Quantitative microanalysis of major and minor elements in minerals of the tetrahedrite isotypic series was carried out using a Cameca SXFive Electron Probe Microanalyser running PeakSite software. The SXFive EPMA has five wavelength dispersive spectrometers (WDS) for EPMA analysis, as well as an EDS, the ability to scan the electron beam and an optical microscope. The arrangement of diffraction crystals within the WDS can be adjusted depending on the material being analysed. For this study, spectrometers 1 and 4 were large area pentaerythritol (LPET) crystals, spectrometer 2 was a thallium hydrogen phthalate (TAP) crystal, and spectrometers 3 and 5 were large area lithium fluoride (LLIF) crystals. Large area crystals increase count rate and thus improve element detection limits.

For tetrahedrite-tennantite analysis the beam operating conditions were maintained at 20 keV, 20 nA, a takeoff angle of 40^{o} and a beam size of 5 μm. The suite of elements analyzed was S, Pb, Cd, As, Se, Fe, Cu, Mn, Ag, Sn In, Hg, Zn, Ni, Co, Sb, Te, Bi, Tl and Ga. Acquisition order was set such that each spectrometer had approximately equal measurement times. Thus spectrometer 1 measured S, Pb, Cd and Bi, spectrometer 2 measured As and Se, spectrometer 3 measured Fe, Cu, Mn and Ga, spectrometer 4 measured Ag, Sn, In, Sb, Te and Tl and spectrometer 5 measured Hg, Zn, Ni and Co. Probe for EPMA software, distributed by Probe Software Inc., was used for calibration and data reduction (Donovan, 2014). Calibration was performed on certified natural and synthetic standards from Astimex Ltd. and P&H Associates. A list of X-ray lines, standards used and count times are shown in Table 2.2. Tetrahedrite-tennantite EPMA element maps were also generated using an operating voltage of 20 keV and 224 nA with a step size of 4 μm. Thus there was slight spot overlap on each line.

Table 2.2. EPMA X-ray lines, standards and count times.

Element /X-Ray Line	**Standard**	**Peak Count Time** (s)	**Background Type/Fit**	**# of Background Points Acquired** (Lo side of peak/Hi side of peak)	**Background Count Time** (Lo/Hi; s)
S Kα	P&H block Chalcopyrite	10	Multipoint	2/2	10/10
Pb Mα	P&H block Galena	30	Multipoint	4/3	7.5/40
Cd Lα	P&H block Greenockite	60	Multipoint	2/2	30/30
As Lα	Astimex Gallium Arsenide	30	Multipoint	2/2	20/5
Se Lα	P&H block Bismuth Selenide	100	Multipoint	2/3	90/60
Fe Kα	P&H block Chalcopyrite	10	Multipoint	2/2	10/10
Cu Kα	P&H block Chalcopyrite	10	Linear	-	10/10
Mn Kα	P&H block Rhodonite	30	Multipoint	2/2	20/20
Ag Lα	P&H block Silver/Silver Telluride	30	Multipoint	1/2	20/5
Sn Lα	P&H block Cassiterite	30	Multipoint	2/2	20/20
In Lα	Astimex Indium	30	Multipoint	2/1	5/20
Hg Lα	P&H block Cinnabar	100	Multipoint	3/3	90/90
Zn Kα	P&H block Sphalerite	30	Multipoint	2/2	10/10
Ni Kα	Astimex Pentlandite	30	Linear	-	10/10
Co Kα	Astimex Cobalt	30	Multipoint	2/2	10/10
Sb Lα	Astimex Stibnite	30	Multipoint	2/2	20/20
Te Lα	P&H block Silver Telluride	30	Multipoint	2/2	20/20
Bi Mα	P&H block Bismuth Selenide	30	Multipoint	2/2	20/5
Tl Mα	Astimex Thallium	20	Linear	-	10/10
Ga Kα	P&H block Gallium Arsenide	20	Linear	-	10/10

There exists a number of X-ray overlap interferences on many of the elements measured in tetrahedrite-tennantite in this study. Corrections must therefore be applied to the analyzed X-ray intensities based on the measurements of additional standards. A list of the relevant element overlap interferences and the standards used for correction are listed in Table 2.3, along with mean minimum detection limits for each analyzed element.

Table 2.3. Element overlap corrections and mean minimum detection limits (99% confidence; data in wt. %).

Element /X-Ray Line	Overlapping X-Ray Line/Diffraction Order	Overlap Standard	Mean MDL
S Kα	Co Kα1 III, Sb Lγ3 II, Hg Lγ1 I	Astimex Cobalt, Astimex Stibnite, Astimex Cinnabar	0.013
Pb Mα	Fe Kβ1 III, As Kβ1 V	P&H block Chalcopyrite, Astimex Gallium Arsenide	0.037
Cd Lα	Pb Lβ1 IV, Ag Lβ1 I, Se Kβ1 IV	Astimex Galena, P&H block Silver Telluride, Astimex Bismuth Selenide	0.031
As Lα	Sb Lβ1 III, Fe Kα1 V, Co Kβ1 VI	Astimex Stibnite, P&H block Chalcopyrite, Astimex Cobalt	0.043
Se Lα	As Lβ3 I, Te Lβ3 III, Co Kα1 V	Astimex Gallium Arsenide, P&H block Silver Telluride, Astimex Cobalt, Astimex Nickel	0.018
Fe Kα	Pb Lβ3 II	P&H block Galena	0.020
Cu Kα	-	-	0.031
Mn Kα	Hg Lβ1 II, As Kβ1 II	P&H block Cinnabar, P&H block Gallium Arsenide	0.015
Ag Lα	Hg Lβ2 IV, Cu Kβ2 III, Mn Kα1 II	P&H block Cinnabar, P&H block Chalcopyrite, P&H block Rhodonite	0.041
Sn Lα	Co Kα1 II, Hg Lγ1 IV	Astimex Cobalt, P&H block Cinnabar	0.026
In Lα	Cd Lβ1 I, Bi Lβ3 IV, Hg Lα2 III	P&H block Greenockite, P&H block Bismuth Selenide, P&H block Cinnabar	0.031
Hg Lα	-	-	0.042
Zn Kα	-	-	0.030
Ni Kα	-	-	0.022
Co Kα	Hg Lγ1 II	P&H block Cinnabar	0.018
Sb Lα	Bi Lα1 III	P&H block Bismuth Selenide	0.022
Te Lα	Sn Lβ3 I, Se Kα1 III, Ni Kα1 II	P&H block Cassiterite, P&H block Bismuth Selenide, Astimex Pentlandite	0.024
Bi Mα	Pb Mβ I	P&H block Galena	0.057
Tl Mα	Hg Mβ I	Astimex Cinnabar	0.126
Ga Kα	Pb L1 I	P&H block Galena	0.041

As many of the trace elements contained within sulphides are hosted at concentration levels below typical EPMA detection limits, EPMA was not used to determine which trace elements were present in a sulphide, nor to determine partitioning trends between sulphide phases. EPMA was used primarily to quantify major element compositions in the tetrahedrite-tennantite solid solution series. In particular, Cu concentrations in tetrahedrite-tennantite determined by EPMA were used as the internal standard for quantifying tetrahedrite-tennantite LA-ICP-MS data. In some cases EPMA was used to check the precision of LA-ICP-MS data for elements measurable by both methods (see next section) and in these cases EPMA operating conditions were maintained as above.

2.5 Laser Ablation Inductively-Coupled Plasma Mass Spectrometry (LA-ICP-MS)

2.5.1 LA-ICP-MS spot analysis

Quantitative trace element spot analyses of galena in Chapter 3 were obtained using a New Wave UP-213 nm Nd:YAG laser-ablation system coupled to an Agilent HP-7500cx inductively-coupled plasma mass spectrometer. All quantitative spot analyses in chapters 4, 5 and 6 were carried out using an ASI M-50-LR 193 nm Excimer laser attached to an Agilent 7700cx Quadrupole inductively-coupled mass spectrometer. Designed by Laurin Technic Pty., the ASI laser ablation system utilizes a two-volume small volume ablation cell, boasting superior trace element sensitivity, washout and stability (Müller et al., 2009). The sample is ablated in an atmosphere of ultra-high purity (UHP) He (0.7 L/min), and the resulting aerosol is mixed with Ar (0.93 L/min) after leaving the ablation cell. The aerosol mix passes through a pulse-homogenizing device (squid) proceeding direct introduction into the torch.

Throughout each LA-ICP-MS session, the ICP-MS was calibrated regularly by optimising the voltages that control the lens parameters. Frequent calibration maintains maximum sensitivity on the isotopes of interest, as well as minimizing the production of molecular oxide species to levels typically below 0.2 %. These are undesirable species such as $^{232}Th^{16}O$ and doubly charged ion species (i.e., $^{140}Ce^{2+}$).

Whilst analyzing galena on the New Wave laser ablation system, the laser spot size was maintained at 30 μm, at a repetition rate of 4 Hz, producing a flux at the sample surface of ~0.5 J/cm^2. Based on these settings, SEM inspection of ablation craters reveals that the approximate ablation rate for galena is ~0.6–1.0 μm/s. Since this is a high ablation rate

compared to other sulphides, while using the ASI system to analyze galena the energy output was set at 80 mJ, the repetition rate was increased to 10 Hz while the spot size was lowered significantly to 8-12 μm to ensure the sensitive ICP-MS was not oversaturated with Pb. During analysis of sphalerite, chalcopyrite and tetrahedrite-tennantite, the laser beam energy output was maintained at 100 mJ, a 26 μm spot size was used and the repetition rate was set at 10 Hz. The total acquisition time for each individual spot analysis was typically 60 s; 30 s of background measurement followed by 30 s of sample ablation. Using the New Wave laser, however, acquisition time was 80 s comprising 30 s of background measurement and 50 s of sample ablation. A 40 s delay time was allowed after each spot analysis to ensure the ablation cell was sufficiently washed-out, the gases stabilized and computer processing had finished.

During the analysis of galena outlined in chapter 3, the following suite of isotopes were measured: ^{33}S, ^{34}S, ^{53}Cr, ^{55}Mn, ^{57}Fe, ^{58}Fe, ^{59}Co, ^{60}Ni, ^{65}Cu, ^{66}Zn, ^{69}Ga, ^{75}As, ^{82}Se, ^{95}Mo, ^{107}Ag, ^{111}Cd, ^{115}In, ^{118}Sn, ^{121}Sb, ^{125}Te, ^{182}W, ^{197}Au, ^{202}Hg, ^{205}Tl, ^{204}Pb, ^{206}Pb, ^{208}Pb, and ^{209}Bi. Dwell times for all elements were set at 0.05 s, except for Ag, Sb and Bi which were set at 0.03 s, and S and Pb which were set at 0.007 s. While using the ASI LA-ICP-MS the isotopes analyzed were ^{34}S, ^{55}Mn, ^{57}Fe, ^{59}Co, ^{60}Ni, ^{65}Cu, ^{66}Zn, ^{69}Ga, ^{72}Ge, ^{75}As, ^{82}Se, ^{95}Mo, ^{107}Ag, ^{111}Cd, ^{115}In, ^{118}Sn, ^{121}Sb, ^{125}Te, ^{182}W, ^{197}Au, ^{202}Hg, ^{205}Tl, ^{206}Pb, ^{207}Pb, ^{208}Pb and ^{209}Bi. Dwell times for each isotope was set at 0.01 s, while ^{115}In, ^{197}Au and ^{205}Tl were set at 0.05 s to achieve a lower minimum detection limit.

Three analyses of the MASS-1 sulphide reference material (formerly PS-1; Wilson et al., 2002) were made before and after a maximum of 12 unknown spot analyses. Thus instrument drift was monitored and, using the bracketed MASS-1 analyses, a linear drift correction was applied to the unknown analyses. All spot data calculations were carried out using GLITTER data reduction software (Van Achterberg et al., 2001). The internal standard elements used for quantification of analyses were as follows: Zn for sphalerite, Pb for galena and Cu for

chalcopyrite and tetrahedrite-tennantite. Stoichiometric sphalerite, galena and chalcopyrite were assumed, thus values of 61 wt. % Zn in sphalerite (allowing for 4.06 wt. % Fe), 86.6 wt. % Pb in galena and 34.63 wt. % Cu in chalcopyrite were used. The maximum possible error resulting from using these values rather than actual values determined by EPMA is ~13 % for sphalerite and galena, and significantly less for chalcopyrite, and thus the maximum error was almost always less than instrumental error. The Cu wt. % value for tetrahedrite-tennantite in each sample as determined by EPMA was used as the internal standard for quantifying tetrahedrite-tennantite LA-ICP-MS data. The internal standard weight must be entered as an oxide wt. % in GLITTER, i.e., ZnO, PbO or Cu_2O. Thus element weights were converted to oxide weights based on formulas 2.1-2.4 below.

2.1 $$wt.\%\ Zn\ in\ sphalerite \times \left(\frac{Zn\ atomic\ mass + O\ atomic\ mass}{Zn\ atomic\ mass}\right)$$
$$= 61 \times \left(\frac{65.39 + 15.999}{65.39}\right) = \mathbf{75.928}$$

2.2 $$wt.\%\ Pb\ in\ galena \times \left(\frac{Pb\ atomic\ mass + O\ atomic\ mass}{Pb\ atomic\ mass}\right)$$
$$= 86.6 \times \left(\frac{207.2 + 15.999}{207.2}\right) = \mathbf{93.287}$$

2.3 $$wt.\%\ Cu\ in\ chalcopyrite \times \left(\frac{2 \times Cu\ atomic\ mass + O\ atomic\ mass}{2 \times Cu\ atomic\ mass}\right)$$
$$= 34.63 \times \left(\frac{2 \times 63.546 + 15.999}{2 \times 63.546}\right) = \mathbf{38.9895}$$

2.4 $$wt.\%\ Cu\ in\ tetrahedrite/tennantite \times \left(\frac{2 \times Cu\ atomic\ mass + O\ atomic\ mass}{2 \times Cu\ atomic\ mass}\right)$$
$$= DETERMINED\ BY\ EPMA \times \left(\frac{2 \times 63.546 + 15.999}{2 \times 63.546}\right) = \boldsymbol{X}$$

The general aim was to collect a minimum of 10 spot analyses per sulphide per sample, assuming a sample contained a sufficient number of coarse enough grains of a given sulphide to allow for this. 10 analyses was typically adequate to establish trace element variation in a sample. Nevertheless, LA-ICP-MS mapping is desirable to truly quantify variation, especially where systematic zonation is present. For elements hosted in solid solution in a mineral, LA-ICP-MS time-resolved downhole profiles will appear smooth (e.g., Fig. 2.3a), whereas sub-surface inclusions usually show as peaks on such profiles (e.g., Fig. 2.3b) if they are sufficiently large. Using GLITTER, the LA-ICP-MS downhole profile for each element in each individual unknown or MASS-1 spot analysis was carefully manually checked for peaks that may indicate an inclusion was accidentally ablated. If an inclusion was recognized, the analysis was discarded. In special cases where an inclusion was only ablated towards the end of a spot analysis, the selected time interval for integration excluded the section of the downhole ablation profile in which the inclusion was recognized (e.g., Fig. 2.3c). Ignoring analyses that are below the minimum detection limits (mdl) gives an over-estimation of the actual mean concentration of a given element in a sulphide, while treating <mdl values as 0 gives an under-estimation of the mean. As such, analyses that were below the mdl for a given element in a sulphide were generally given the artificial value mdl/2 since this normally allows for a closer estimation of the actual mean. In cases where all analyses of a certain element in a sulphide were below the mdl, these analyses were ignored and no mean was calculated.

Despite this thorough data checking process, as well as only analyzing areas of samples that are free of noticeable inclusions based on SEM imagery of the exposed surface, it is still impossible to detect all possible inclusions that may affect LA-ICP-MS data. Indeed, given a laser spot diameter in the tens of microns, only heterogeneously distributed inclusions that are in the order of tens to hundreds of nm or more could be recognized on time-resolved

downhole ablation profiles. If inclusions are smaller than that and homogenously distributed within a sample, the downhole profile will appear smooth. Similarly, spot analyses are unable to resolve chemically distinct regions (e.g., exsolution lamellae) of a sulphide mineral that are smaller than the lateral spatial resolution of the laser spot. In such a case, the resulting smooth LA-ICP-MS downhole profile would simply be an average of chemically distinct regions. In the same way, smooth time-resolved downhole profiles can also represent an averaging effect due to limited depth resolution based on rapid ablation of soft minerals (e.g., galena and, to a lesser extent, chalcopyrite), and a large list of isotopes causing a long sweep time.

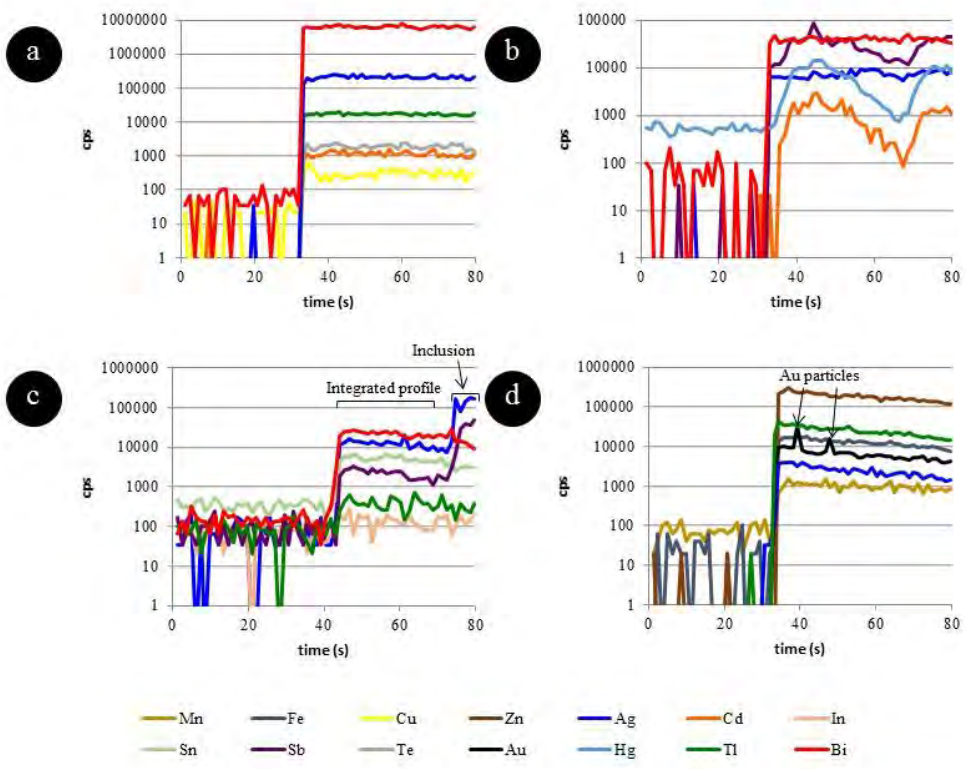

Figure 2.3. Representative LA-ICP-MS time-resolved downhole profiles for galena and the MASS-1 sulphide reference material. cps = counts per second. (**a**) Smooth profiles as evidence for Bi, Ag, Tl, Te, Cd and Cu in solid solution in galena. (**b**) Comparable peaks on Sb, Hg and Cd profiles indicate the presence of inclusions in galena. (**c**) Peaks at the end of the Ag and Sb profiles indicate the presence of an inclusion in galena. In this case quantification may still be achieved by integrating the profile before the peaks. (**d**) Smooth Zn, Tl, Fe, Ag and Mn profiles for the MASS-1 standard indicating these elements are homogeneously distributed. Small peaks on the Au profile likely indicate the presence of Au particles.

EPMA was used to check the precision of some LA-ICP-MS data, particularly for elements present in sulphides at concentrations measurable by both methods. Figure 2.4 shows representative scatter-plots displaying bi-element variation in both EPMA and LA-ICP-MS data for a given sulphide in a given sample. In each case, the LA-ICP-MS data is largely reproducible, plotting in and around EPMA data with high precision.

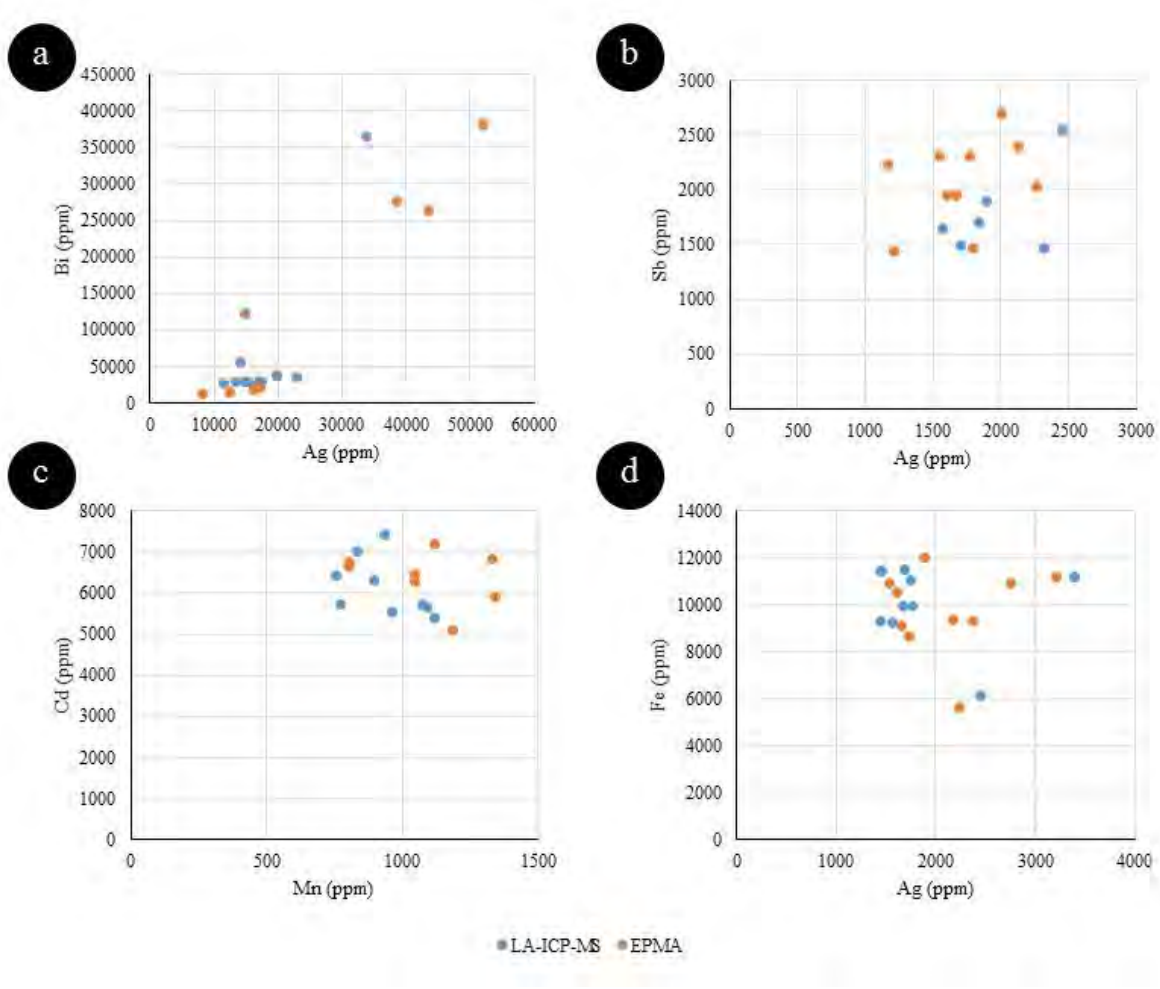

Figure 2.4. Representative scatter-plots showing the precision of LA-ICP-MS data as compared to EPMA data for elements measurable by both methods in (**a** & **b**) galena, (**c**) sphalerite and (**d**) tetrahedrite from individual samples.

As a measure of LA-ICP-MS accuracy, 1σ errors for each element from multi-sulphide analyses, as well as typical minimum detection limits (99 % confidence), are shown in Table 2.4. Errors are generally <10 % of the mean for most elements, especially those present in a sulphide at concentrations >1 ppm, and thus data accuracy may be considered good. Errors

for galena are somewhat higher due to the smaller spot size used. GLITTER calculates error based on counting statistics for ablation signal and background (i.e., internal uncertainty), as well as taking into account mass bias, the correction of unknowns to standards, laser induced elemental fractionation (LIEF) and instrument drift (i.e., external uncertainty). A 1 % relative uncertainty is assigned to the element concentrations in the standard, and 3 % relative uncertainty is given to the value of the internal standard. If a stable ablation cell is assumed, the largest contribution to analytical uncertainty is LIEF, followed by counting statistics and instrument drift. LIEF is minimized by keeping spot size, frequency and output energy constant from unknown to standard. Counting statistics are improved by setting dwell times and the method run time to as long as reasonably possible. The linear instrument drift correction is optimised by analyzing standards as often as possible.

Table 2.4. Minimum detection limits (99% confidence) and 1σ errors from multi-sulphide analyses (data in ppm).

	Sphalerite		**Galena**		**Chalcopyrite**		**Tetrahedrite-Tennantite**	
Element	**MDL**	**1σ Error**	**MDL**	**1σ Error**	**MDL**	**1σ Error**	**MDL**	**1σ Error**
^{34}S	236	32383	3141	75366	195	40775	812	90305
Mn	0.11	42	1.6	1.5	0.16	0.35	0.43	0.87
^{57}Fe	3.8	2744	35	25	3.1	25355	24	4494
Co	0.01	0.08	0.17	0.10	0.02	0.08	0.04	0.62
Ni	0.06	0.08	0.72	0.53	0.13	0.22	0.42	0.35
Cu	0.28	10	5.1	5.1	0.86	10953	0.92	11699
Zn	1.3	19290	4.8	10	0.61	42	5.5	7630
Ga	0.01	0.38	0.17	0.10	0.02	0.11	0.05	0.05
As	0.91	0.82	8.5	10	1.4	1.0	3.7	5383
Se	2.2	2.4	28	351	1.8	8.1	11	11
Mo	0.02	0.02	0.31	0.21	0.06	0.08	0.07	0.06
Ag	0.02	0.26	0.15	227	0.03	2.9	0.13	1743
Cd	0.18	289	1.5	11	0.12	0.80	0.60	113
In	<0.01	0.93	0.03	0.04	<0.01	0.56	0.01	0.13
Sn	0.08	0.17	0.66	1.5	0.09	1.6	0.37	0.47
Sb	0.04	0.10	0.29	130	0.06	0.22	0.33	46585
Te	0.08	0.06	1.2	9.4	0.17	0.26	0.25	0.30
W	0.01	<0.01	0.13	0.07	0.03	0.01	0.03	0.02
Au	0.01	0.01	0.07	0.05	0.01	0.02	0.02	0.03
Hg	0.08	4.9	0.65	0.46	0.08	0.10	0.89	15
Tl	<0.01	<0.01	0.03	0.23	<0.01	0.01	0.01	0.03
^{207}Pb	0.04	0.32	0.84	27388	0.03	0.92	0.12	4.1
Bi	<0.01	0.01	0.06	128	0.01	0.11	0.01	6.5

Data calculated by taking the mean of each spot in each sample, then taking the median of the sample means.

2.5.2 LA-ICP-MS mapping

Various LA-ICP-MS element maps of areas on selected sample surfaces, ranging in size from 0.25 – 9 mm^2, were made to give a visual representation of elemental distributions in sulphide grains, and among minerals in given assemblages. The ASI LA-ICP-MS system was used to generate all trace element maps. Mapping was achieved by ablating multiple parallel adjacent trenches in a grid across the sample surface. For all maps, the laser beam scan speed was maintained at 10 μm/s, the repetition rate was 10 Hz and energy output set at 80-100 mJ. Depending on the size of the area to be mapped, the laser spot size was varied between 7-10 μm to ensure each map provided adequate spatial resolution, and also that unnecessarily long map acquisition times were avoided. The distance between adjacent trenches was varied to match the laser spot size. The isotopes analyzed were typically those listed in section 2.5.1 above. As with spot analysis, the dwell time for each element was set at 0.01 s, while In, Au and Tl were set at 0.05 s. A 30 s background measurement was acquired before the ablation of each trench, followed by a 20 s delay to ensure the ablation cell was sufficiently washed-out, the gases stabilized and computer processing had finished. Three identical trenches were ablated on the MASS-1 standard before and after ablation on the unknown.

All LA-ICP-MS trace element maps were processed with Iolite (Paton et al., 2011), an open source software package for ICP-MS data processing developed by the Melbourne Isotope Group as an add-in for the data analysis program Igor by WaveMetrics. Since the acquisition of some larger maps took many hours, in which significant instrument drift could conceivably occur, a linear drift correction was applied to the unknown trench analyses based on the MASS-1 analyses acquired before and after a mapping run. The average background intensity for each element was then subtracted from its corresponding trench acquisition, and the resulting time-resolved linear intensities were compiled into a two dimensional image for

each element.

The resulting LA-ICP-MS images are only qualitative; they are based on the background-subtracted counts per second (cps) for each element. Since the ablation rate of different minerals may vary over orders of magnitude, and cps is directly proportional to the ablation rate, the cps measurement may vary significantly when ablating different minerals even using the same laser settings. This implies that qualitative (cps) LA-ICP-MS maps can only be used to recognize variation in a mineral (e.g., compositional zoning), but cannot be used to compare the concentration intensity of an element in different minerals, nor can quantitative concentrations be determined for a single mineral. Quantitative LA-ICP-MS maps can be generated by using an internal standard in Iolite. Imputing an internal standard value tells Iolite the concentration of one element in the mapped area, allowing the concentration of all other elements to be calculated. Nevertheless, a map consisting of multiple phases can generally not be quantified with a single internal standard if each phase contains a vastly different concentration of the internal standard. However, in the case of base metal sulphide assemblages, each mineral contains S at comparable concentrations (e.g., sphalerite = 33.06 wt. % S, galena = 13.4 wt. % S and chalcopyrite = 34.94 wt. % S). Thus semi-quantitative LA-ICP-MS maps of assemblages comprising multiple BMS were created in this study using 25 wt. % S as the internal standard. This value represents the approximate average S concentration in the assemblage. The resulting LA-ICP-MS maps display semi-quantified concentrations for all sulphides in a map on a single scale bar expressed in parts-per-million, allowing for the comparison of trace element concentrations in multiple sulphides.

Figure 2.5 shows Ag, Sb and Cd LA-ICP-MS maps of a zoned sphalerite-galena-chalcopyrite assemblage from the Herja epithermal deposit, Romania. The maps were quantified using 25 wt. % S as the internal standard. LA-ICP-MS spot analyses were also

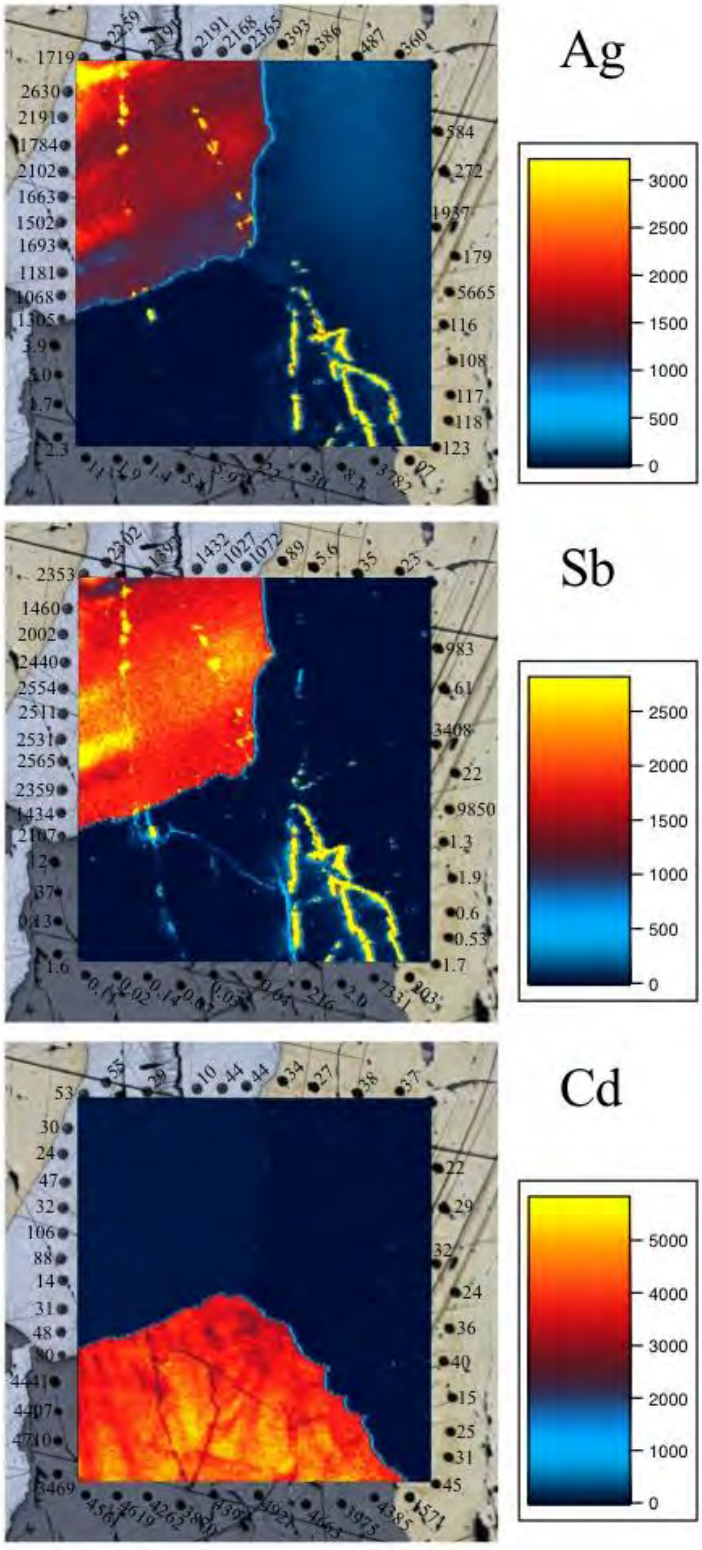

Figure 2.5. Comparison between semi-quantitative LA-ICP-MS trace element maps (Ag, Sb and Cd; ppm scales) of a galena (light grey)–sphalerite (dark grey)–chalcopyrite (yellow) assemblage from the Herja epithermal deposit (Romania) with spot analyses (in ppm) immediately adjacent to the mapped area. An average sulphur value of 25 wt. % was used as the internal standard for the maps.

obtained from around the edges of the mapped area for comparison. The concentrations defined by the spot analysis closely match those shown on the map. Discrepancies are typically less than 10 % of the spot concentrations, and are usually less than the uncertainty of assigning an exact value to a particular colour on the map. Thus this method of quantifying BMS maps is generally reliable, and provides a powerful tool in comparing and visualizing trace element distributions in multiple BMS. Such maps compliment LA-ICP-MS spot data, but should not replace such data. Where precise quantitative concentration data is required, spot data is always required.

2.5.3 The MASS-1 standard

While the analysis of galena in chapter 3 was carried out using the original MASS-1 sulphide standard certificate of analysis given in Wilson et al. (2002), the latest certificate of analysis was chosen for quantification in Chapters 4, 5 and 6. This certificate is available on the United States Geological Survey website (United States Geological Survey, 2016), and is reproduced in Table 2.5. Given subtly different concentration values in the two different MASS-1 certificates used in this study, there may be some implications for comparing the concentrations of some elements in galena between chapter 3 and the subsequent chapters. This may also be the case when comparing a sulphide analyzed here using the latest MASS-1 certificate, with the same sulphide analyzed in another study using the original MASS-1 certificate. Nevertheless, as the latest certificate was used for all analyses determining trace element partitioning trends outlined here, they will be reliable and internally consistent. The latest MASS-1 certificate contains no value for Ge, precluding quantification of Ge in sulphides analyzed in chapters 4, 5 and 6. This is despite the fact that some sulphides, particularly sphalerite (e.g., Cook et al., 2009), commonly contain Ge. In addition, and even

if the Ge value in the original MASS-1 certificate is used, Ge concentrations generally cannot be quantified with confidence (except perhaps when present at concentration >>10 ppm) given the many isotopic interferences of Ge isotopes (e.g., ^{70}Ge, ^{72}Ge, ^{73}Ge, ^{74}Ge) with molecular species such as $^{36}Ar^{34}S$, $^{40}Ar^{32}S$, $^{56}Fe^{16}O$, $^{40}Ar^{33}S$, $^{57}Fe^{16}O$, $^{56}Fe^{16}O^{1}H$, $^{40}Ar^{34}S$ and $^{58}Ni^{16}O$.

Table 2.5. MASS-1 certificate of analysis (United States Geological Survey, 2016).

Element	Concentration (ppm)	Element	Concentration (ppm)
Na	33,000	Cd	60
V	63	Sn	59
Cr	65	In	50
Fe	156,000	Sb	60
Mn	280	Ba	14
Co	60	W	20
Ni	97	Tl	50
Cu	134,000	Pb	68
Zn	210,000	Bi	60
Ga	64	S	276,000
As	65	Hg	57
Se	51	Ir	42
Mo	59	Te	15
Ag	50	Au	57

The MASS-1 standard is a poly-metal pressed pellet with an Fe-Zn-Cu-S matrix, but is not matrix matched to the structure of the sulphides analyzed in this study. It was chosen for this study since a reliable and well-circulated sulphide matrix matched standard does not exist. As such, some presently unquantifiable elemental fractionation may occur during the ablation of materials with different matrices. Nevertheless, the errors relating to such fractionation would likely be within instrument errors for most elements (typically <10 %), especially when analyzing sphalerite, chalcopyrite and tetrahedrite-tennantite since the concentration of the internal standard elements in these sulphides compared to MASS-1 are within the same order of magnitude. Similarly, any errors relating to the small amount of Pb in the MASS-1

standard compared to galena (4 orders of magnitude difference) are likely minimal since the response of the electron multiplier is linear over 9 orders of magnitude, and an electron multiplier pulse to analog calibration was performed before each LA-ICP-MS run. Therefore the counts per second/parts per million yield should not be significant when using standards with a low concentration of the internal standard element compared to the unknown, as was shown for the analogous case of molybdenite (Ciobanu et al., 2013). Danyushevsky et al. (2011) investigated the suitability of an analogous sulphide standard (STDGL2b2, containing 1,216 ppm Pb) for the analysis of galena and, using Pb as an internal standard, analyzed pressed-powder pellets by XRF and solution ICP-MS. Results showed that standard analytical errors resulting from matrix-dependent fractionation were low (<15 %) but could be as higher for W, Zn, and Cd. Nevertheless, if the quantification of some elements was slightly affected by fractionation or other errors, it would be internally consistent and would not affect any conclusions, especially those relating to the partitioning of trace elements between sulphides.

The use of the MASS-1 standard in this study also assumes the concentrations of elements in the pressed pellet are homogeneous, even though there have been reports that some elements, especially Au, may be heterogeneously distributed (e.g., Wilson et al., 2002). In some analyses, it seems inclusions of Au bearing particles (possibly large Au nanoparticles) were present in the MASS-1 standard, as the peaks on the representative LA-ICP-MS time-resolved downhole ablation profile in Figure 2.3d show. Such analyses were simply discarded, or else the integrated signal excluded any inclusion related peaks, as is the norm with the analogous case of an inclusion in an unknown analysis. No other inclusion related peak associated with any other element was ever recognized on a MASS-1 LA-ICP-MS downhole profile.

Ciobanu, C. L., Cook, N. J., Kelson, C. R., Guerin, R., Kalleske, N., Danyushevsky, L., 2013. Trace element heterogeneity in molybdenite fingerprints stages of mineralization. Chem. Geol. 347, 175–189.

Cook, N. J., Ciobanu, C. L., Pring, A., Skinner, W., Shimizu, M., Danyushevsky, L., Saini-Eidukat, B., Melcher, F., 2009. Trace and minor elements in sphalerite: A LA-ICPMS study. Geochim. Cosmochim. Acta 73, 4761–4791.

Danyushevsky, L., Robinson, P., Gilbert, S., Norman, M., Large, R., McGoldrick, P., Shelley, M., 2011. Routine quantitative multi-element analysis of sulphide minerals by laser ablation ICP-MS: Standard development and consideration of matrix effects. Geochem. Explor. Env. A. 11, 51–60.

Donovan, J. J., 2014. Probe for EPMA: Acquistion, automation and analysis. Ver. 10.3.5 Xtreme Edition, Probe Software, Inc., Oregon, United States of America.

Müller, W., Shelley, M., Miller, P., Broude, S., 2009. Initial performance metrics of a new custom-designed ArF excimer LA-ICPMS system coupled to a two-volume laser-ablation cell. J. Anal. Atom. Spectrom. 24, 209–214.

Paton, C., Hellstrom, J., Paul, B., Woodhead, J., Hergt, J., 2011. Iolite: Freeware for the visualisation and processing of mass spectrometric data. J. Anal. Atom. Spectrom. 26, 2508–2518.

United States Geological Survey, 2016. Microanalytical Reference Materials and Accessories. Available online: <http://crustal.usgs.gov/geochemical_reference_standards/microanalytical_RM.html> (accessed on 6 October 2016).

Van Achterberg, E., Ryan, C. G., Jackson, S. E., Griffin, W. L., 2001. Data reduction software for LAICP-MS. In: J.P. Sylvester, Ed., Laser-ablation-ICPMS in the Earth

Sciences; Principles and applications. Mineralogical Association of Canada, Short Course Series 29, 239-243.

Wilson, S. A., Ridley, W. I., Koenig, A. E., 2002. Development of sulfide calibration standards for the laser ablation inductively-coupled plasma mass spectrometry technique. J. Anal. Atom. Spectrom. 17, 406–409.

CHAPTER 3

TRACE AND MINOR ELEMENETS IN GALENA: A RECONNAISSANCE LA-ICP-MS STUDY

Luke L. George[1], Nigel J. Cook[2], Cristiana, L. Ciobanu[2], Benjamin P. Wade[3]

[1]*School of Physical Sciences, The University of Adelaide, Adelaide, S.A., 5005, Australia*

[2]*School of Chemical Engineering, The University of Adelaide, Adelaide, S.A., 5005, Australia*

[3]*Adelaide Microscopy, The University of Adelaide, Adelaide, S.A., 5005, Australia*

Paper published in American Mineralogist, 100, 548-569.

Statement of Authorship

Title of Paper	Trace and minor elements in galena: A reconnaissance LA-ICP-MS study
Publication Status	☒ Published ☐ Accepted for Publication ☐ Submitted for Publication ☐ Unpublished and Unsubmitted w ork w ritten in manuscript style
Publication Details	George, L., Cook, N. J., Ciobanu, C. L., Wade, B. P., 2015. Trace and minor elements in galena: A reconnaissance LA-ICP-MS study. American Mineralogist 100, 548-569.

Principal Author

Name of Principal Author (Candidate)	Luke George		
Contribution to the Paper	Performed analytical work, carried out data processing and interpretation, oversaw development of work and wrote manuscript.		
Overall percentage (%)	80		
Certification:	This paper reports on original research I conducted during the period of my honours and Higher Degree by Research candidature and is not subject to any obligations or contractual agreements with a third party that would constrain its inclusion in this thesis. I am the primary author of this paper.		
Signature		Date	28 March 2017

Co-Author Contributions

By signing the Statement of Authorship, each author certifies that:

i. the candidate's stated contribution to the publication is accurate (as detailed above);

ii. permission is granted for the candidate to include the publication in the thesis; and

iii. the sum of all co-author contributions is equal to 100% less the candidate's stated contribution.

Name of Co-Author	Nigel Cook		
Contribution to the Paper	Helped define direction of research, provided sample material, supervised development of work, assisted with data interpretation and contributed to manuscript preparation.		
Overall percentage (%)	10		
Signature		Date	20 March 2017

Name of Co-Author	Cristiana Ciobanu		
Contribution to the Paper	Provided sample material, supervised development of work, contributed to manuscript preparation.		
Overall percentage (%)	5		
Signature		Date	20 March 2017

Name of Co-Author	Benjamin Wade		
Contribution to the Paper	Assisted with data collection and manuscript evaluation.		
Overall percentage (%)	5		
Signature		Date	27 March 2017

George, L., Cook, N. J., Ciobanu, C. L. & Wade, B. P. (2015). Trace and minor elements in galena: A reconnaissance LA-ICP-MS study.
American Mineralogist, 100(2-3), 548-569.

CHAPTER 4

PARTITIONING OF TRACE ELEMENTS IN CO-CRYSTALLIZED SPHALERITE-GALENA-CHALCOPYRITE HYDROTHERMAL ORES

Luke L. George[1], Nigel J. Cook[2], Cristiana, L. Ciobanu[2]

[1]*School of Physical Sciences, The University of Adelaide, Adelaide, S.A., 5005, Australia*

[2]*School of Chemical Engineering, The University of Adelaide, Adelaide, S.A., 5005, Australia*

Paper published in Ore Geology Reviews, 77, 97-116.

Statement of Authorship

Title of Paper	Partitioning of trace elements in co-crystallized sphalerite-galena-chalcopyrite hydrothermal ores
Publication Status	☒ Published ☐ Accepted for Publication ☐ Submitted for Publication ☐ Unpublished and Unsubmitted work written in manuscript style
Publication Details	George, L. L., Cook, N. J., Ciobanu, C. L., 2016. Partitioning of trace elements in co-crystallized sphalerite–galena–chalcopyrite hydrothermal ores. Ore Geology Reviews 77, 97-116.

Principal Author

Name of Principal Author (Candidate)	Luke George		
Contribution to the Paper	Performed analytical work, developed LA-ICP-MS mapping method, carried out data processing and interpretation, oversaw development of work and wrote manuscript.		
Overall percentage (%)	85		
Certification:	This paper reports on original research I conducted during the period of my Higher Degree by Research candidature and is not subject to any obligations or contractual agreements with a third party that would constrain its inclusion in this thesis. I am the primary author of this paper.		
Signature		Date	28 March 2017

Co-Author Contributions

By signing the Statement of Authorship, each author certifies that:

i. the candidate's stated contribution to the publication is accurate (as detailed above);

ii. permission is granted for the candidate to include the publication in the thesis; and

iii. the sum of all co-author contributions is equal to 100% less the candidate's stated contribution.

Name of Co-Author	Nigel Cook		
Contribution to the Paper	Helped define direction of research, provided sample material, supervised development of work, assisted with data interpretation and contributed to manuscript preparation.		
Overall percentage (%)	10		
Signature		Date	20 March 2017

Name of Co-Author	Cristiana Ciobanu		
Contribution to the Paper	Provided sample material, supervised development of work, contributed to manuscript preparation.		
Overall percentage (%)	5		
Signature		Date	20 March 2017

Ore Geology Reviews 77 (2016) 97–116

Contents lists available at ScienceDirect

Ore Geology Reviews

journal homepage: www.elsevier.com/locate/oregeorev

Partitioning of trace elements in co-crystallized sphalerite–galena–chalcopyrite hydrothermal ores

Luke L. George [a,*], Nigel J. Cook [b], Cristiana L. Ciobanu [b]

[a] School of Physical Sciences, University of Adelaide, Adelaide, SA 5005, Australia
[b] School of Chemical Engineering, University of Adelaide, Adelaide, SA 5005, Australia

ARTICLE INFO

Article history:
Received 12 November 2015
Received in revised form 12 February 2016
Accepted 16 February 2016
Available online 18 February 2016

Keywords:
Trace element
Sphalerite
Galena
Chalcopyrite
Partitioning
Laser-ablation inductively-coupled plasma mass spectrometry

ABSTRACT

There is an abundance of published trace element data for sphalerite, galena and chalcopyrite in natural systems, yet for a co-crystallized assemblage comprising these base metal sulphides, there is no detailed understanding of the preferred host of many trace elements. Laser-ablation inductively-coupled plasma mass spectrometry trace element maps and spot analyses were generated on 17 assemblages containing co-crystallized sphalerite and/or galena and/or chalcopyrite from 9 different ore deposits. These deposits are representative of different ore types, geologic environments and physiochemical conditions of ore formation, as well as superimposed syn-metamorphic remobilisation and recrystallization. The primary factors that control the preferred base metal sulphide host of Mn, Fe, Co, Cu, Zn, Ga, As, Se, Ag, Cd, In, Sb, Te, Tl and Bi are element oxidation state, ionic radius of the substituting element, element availability and the maximum trace element budget that a given sulphide mineral can accommodate. Temperature, pressure, redox conditions at time of crystallization and metal source, do not generally appear to influence the preferred base metal sulphide host of all the trace elements. Exceptions are Ga, In and Sn recrystallized at high metamorphic grades, when the preferred host of Ga and Sn usually becomes chalcopyrite. In more typical lower temperature ores, the preferred host of Ga is sphalerite. Indium concentrations also increase in chalcopyrite during recrystallization. At lower temperatures the partitioning behaviour of Sn remains poorly constrained and shows little predictable pattern among the data here. The results obtained may be used as a tool to assess co-crystallization. If trace element distributions in a given base metal sulphide assemblage match those reported here, and assuming those distributions have not been significantly altered post (re-) crystallization, then it may be suggestive of a co-crystallized assemblage. Such information provides a foundation for novel attempts to develop trace element-in-sulphide geothermometers.

1. Introduction

Application of multi-element microanalytical techniques, e.g., micro-particle-induced X-ray emission (μ-PIXE), secondary ion mass spectrometry (SIMS), electron probe microanalysis (EPMA), or laser-ablation inductively-coupled plasma mass spectrometry (LA-ICP-MS), has become commonplace in many fields of geology, including studies relating to ore genesis. This is largely due to the accurate *in-situ* concentration data these techniques can generate, with both sub-part-per-million level precision (for μ-PIXE, SIMS and LA-ICP-MS) and micrometre-scale spatial resolution. As a result, large amounts of trace element data have been published on many common ore minerals, including the base metal sulphides (BMS), sphalerite (ZnS), galena (PbS) and chalcopyrite ($CuFeS_2$) (e.g., McIntyre et al., 1984; Cabri et al., 1985; Foord and Shawe, 1989; Cabri, 1992; Huston et al., 1995; Larocque et al., 1995; Moggi-Cecchi et al., 2002; Cook et al., 2009, 2011a; Lockington et al., 2014; George et al., 2015). As such, the diversity of trace elements and ranges of concentration that these sulphides can incorporate has been relatively well documented. However, the partitioning of trace elements between co-crystallized BMS in hydrothermal ores is not well constrained. This is in contrast to the generally well understood partitioning behaviour of trace elements, including the platinum group elements and gold, between pyrrhotite, pentlandite, pyrite and BMS in magmatic sulphide ore deposits (e.g., Holwell and McDonald, 2010; Dare et al., 2011, and references therein).

Previous work that addresses trace element concentrations within individual sulphides has demonstrated the need to understand trace element partitioning patterns in hydrothermal BMS assemblages. This study aims to identify whether trace element partitioning between co-crystallized sphalerite, galena and chalcopyrite is predictable, and if so, to determine the primary controls on this partitioning. Such information can underpin tools for assessing whether a given BMS assemblage co-crystallized, and also potentially to enable constraints to be placed on conditions of BMS co-crystallization. In this contribution, we acknowledge the role that temperature, pressure, redox conditions at

* Corresponding author.
E-mail address: luke.george@adelaide.edu.au (L.L. George).

http://dx.doi.org/10.1016/j.oregeorev.2016.02.009
0169-1368/

time of crystallization and metal source have on partitioning trends, but will emphasize the important role played by trace element oxidation state and, closely related to that, ionic radius.

2. Background

George et al. (2015) presented a reconnaissance study of trace elements in galena and showed that a range of elements are systematically hosted in solid solution within galena from SEDEX, epithermal, skarn, VMS, orogenic Au and porphyry BMS ores. A number of these elements show predictable behaviours when preferentially partitioning into galena together with other elements via coupled substitution (e.g., Bi and Sb with Ag, Tl and Cu), as well as systematic partitioning between two coexisting minerals (e.g., Tl between galena and sphalerite). It was, however, also noted that the presence or absence of other co-existing sulphides can influence the distributions of some trace elements within some deposit types (e.g., Sn distribution patterns in galena from recrystallized massive sulphide deposits containing chalcopyrite). It is thus difficult to make broad conclusions about the partitioning behaviour of trace elements when galena is largely considered in isolation. In order to gain a more accurate understanding of the partitioning behaviour of trace elements between two or more co-crystallizing BMS in a given ore system, the chemistry of any sulphide phase needs to be considered in the context of the complete BMS assemblage. In light of this, the present study sets out to answer the following question: do trace elements exhibit predictable partitioning behaviours among sphalerite, galena and chalcopyrite when the three minerals co-crystallize?

One of the outcomes of contemporary *in-situ* microanalytical investigation of sulphides is the recognition that many sulphides previously considered homogenous at the grain-scale, are in fact not always so (e.g., molybdenite; Ciobanu et al., 2013). Thus some published trace element datasets, especially those obtained before the 1980s, may simply represent averages of multiple, compositionally-distinct zones within a single grain. Recognition of elements present in solid solution, or occurring in micro-inclusions of distinct mineral phases, has been traditionally gained by carefully assessing all element concentrations and seeking combinations of elements that suggest inclusions [e.g., proton microprobe work of Cabri et al. (1985) or Huston et al. (1995)]. The LA-ICP-MS technique, however, may provide indirect evidence for the presence of micro-inclusions. If these are large enough and heterogeneously distributed, they will be recognized on time-resolved down-hole ablation profiles (e.g., George et al., 2015). The ability to distinguish a trace element in solid solution from one occurring as nano- to microscale inclusions of a distinct mineral phase is critical for interpretation of such data since it is likely that only those trace elements that are substituted into the crystal lattice of a sulphide would reveal systematic partitioning patterns. The LA-ICP-MS mapping technique allows for a visual comparison of multiple compositionally-distinct zones within a single grain or co-existing assemblage. Assuming such zoning occurs at a scale larger than the spatial resolution, even trace element heterogeneity may be recognized. LA-ICP-MS also offers advantages over SIMS in that the technique is more flexible with standards, significantly cheaper to run, and perhaps most importantly, offers simultaneous analysis of >25 elements.

Despite some of the limitations of modern microanalysis discussed, a review of the published literature provides a background to the data reported here. Table 1 summarizes the range of trace elements measured within sphalerite, galena and chalcopyrite and their typical concentrations as determined from analysis of natural specimens. The table also lists the experimentally-determined solubility limits of several of these elements.

3. Sample suite

The study covered 17 BMS-bearing samples from nine different skarn, epithermal and SEDEX deposits in Australia, Norway and Romania (Table 2 and references therein). Selected samples contain coexisting sphalerite and/or galena and/or chalcopyrite, which textural evidence suggests co-crystallized at equilibrium. SEDEX deposits metamorphosed at greenschist facies (Fig. 1A) retain primary syn-sedimentary textures while epithermal (Fig. 1B) and skarn (Fig. 1C) systems commonly display 120° triple junctions between sulphide grains. Such grain boundaries are similar to those in SEDEX deposits metamorphosed at amphibolite facies and above (Fig. 1D, E) which display a coarser grain size and characteristic 120° triple junctions developed during equilibrium recrystallization. Though the sample suite is not representative of entire mineral associations in each different deposit, the samples were selected because they represent the same co-crystallized BMS assemblage formed at different physiochemical conditions in different ore types. They are thus representative for the purposes relevant to this study.

Skarn ores are represented by 5 samples from Baita Bihor and Oravita, two deposits located ~350 km apart along the Late Cretaceous Banatitic Magmatic and Metallogenetic Belt, Romania (BMMB; e.g., Ciobanu et al., 2002). The BMMB contains a range of magmatic-hydrothermal mineralization styles relating to the same magmatic event, and formed in subduction settings during Neotethys closure. The belt is well known for exotic trace mineral signatures including a most prominent Bi-mineral signature (e.g., Ciobanu et al., 2002). The Cu–Mo–Pb–Zn skarn deposit at Baita Bihor boasts the most complex geochemical signature [Bi–Ag–W–Se–Te–Ni–Co–Sn] among the deposits considered here. Consequently, this skarn exhibits a diverse sulphide mineralogy, including As-, Sb-, and Bi-sulphosalts and Bi- and Ag-tellurides (Cioflica et al., 1995, 1997; Cook and Ciobanu, 2003; Ilinca et al., 2012; Ciobanu et al., 2014). The Antoniu orepipe is Cu-dominant and proximal to the granitoid-derived source fluids. It contains Pb–Zn ores near the marble/skarn contact and lesser amounts within the Cu zone. The distinctly Pb–Zn Marta orepipe is a distal zone, ~1.2 km ENE from Antoniu.

Oravita is one of the many Cu–Au skarns that are satellite to porphyry Cu–Mo-intrusions within the Banat region (SW Romania and Serbia), known for its rich deposits (e.g., von Cotta, 1864). As with many Cu skarns, it also contains base metal ores and minor W-mineralization (Gheorghitescu, 1975; Cioflica and Vlad, 1981; Constantinescu et al., 1988). Oravita is one of the few localities where gehlenite skarns are known along the BMMB (Katona et al., 2003; Marincea et al., 2011). Although such skarns are barren, they provide an upper temperature limit (~750 °C) for initiation of the skarn system close to intrusion contacts.

Four samples come from Herja and Toroiaga, Baia Mare District, Romania. Both deposits are polymetallic epithermal vein systems of Neogene age with a diverse mineralogy, including well-known occurrences of Pb–Ag–Sb–As or -Bi sulphosalts. Cu–Au–Pb–Zn veins at Toroiaga are located 90 km to the east of the Pb–Zn–Ag veins at Herja, but related to the same regional-scale E–W-trending Dragos Voda fault (Neubauer et al., 2005 and references therein). Toroiaga is somewhat distinct from other deposits in the Baia Mare District in that its veins are thought to have formed at higher temperatures (as much as 400 °C; Cook, 1997), i.e., unlike the typical Pb–Zn–Ag veins common in Baia Mare.

Eight samples have been selected from five SEDEX deposits (Table 2). These are divided into two groups based on metamorphic grade. Only those deposits metamorphosed at conditions above greenschist facies show clear textural evidence for recrystallization of the BMS assemblage (e.g., coarse annealed textures, commonly with 120° triple junctions between grains; Fig. 1D, E). Recrystallization allows for pervasive re-partitioning of trace elements from the primary low-temperature SEDEX distributions to the distributions preferred at high metamorphic temperatures and pressures, followed by slow cooling. Recrystallized SEDEX deposits (5 samples) can thus be distinguished from those of lower metamorphic grades (3 samples).

Those SEDEX deposits of lower metamorphic grade include Kapp Mineral and Mt. Isa. Kapp Mineral is a minor occurrence from the Hecla Hoek Complex, Svalbard Archipelago, Norway. Mineralization is of an undetermined, possibly late Precambrian age but has clearly

Table 1
Review of relevant literature relating to trace elements in sphalerite, galena and chalcopyrite.

	Sphalerite			Galena			Chalcopyrite		
Specific references	Cook et al. (2009); Johan (1988); Lockington et al. (2014); Ye et al. (2011)			Blackburn and Schwendeman (1977); Foord and Shawe (1989); George et al. (2015)			Bajwah et al. (1987); Harris et al. (1984); Moggi-Cecchi et al. (2002)		
General references	Bethke and Barton (1971); Emslie and Beukes (1981); McIntyre et al. (1984); Cabri et al. (1985); Qian (1987); Brill (1989); Cabri (1992); Huston et al. (1995)								
Trace element	Present in solid solution	Typical concentration (ppm)	Solubility limit	Present in solid solution	Typical concentration (ppm)	Solubility limit	Present in solid solution	Typical concentration (ppm)	Solubility limit
Mn	Common	Hundreds–thousands (rarely wt.%)	7 mol.% MnS at 600 °C Bethke and Barton (1971)	Uncommon	–	3.5 mol.% MnS at 850 °C Bethke and Barton (1971)	Uncommon	Few	–
Fe	Common	Thousands–wt.%	52 mol.% FeS at 700 °C Lepetit et al. (2003)	Uncommon	–	–	–	–	–
Co	Occasional	Tens–hundreds	41 mol.% CoS at 1000 °C Becker and Lutz (1978)	No/questionable	–	–	Occasional	Tens–hundreds	–
Cu	Occasional	Tens–hundreds	10.7 mol.% CuS at 800 °C Kojima and Sugaki (1984)	Uncommon	Few–tens	Extremely low below 200 °C Craig and Kullerud (1968)	–	–	–
Zn	–	–	–	Uncommon	–	–	Occasional	Tens–hundreds	0.9 at.% Zn at 500 °C Kojima and Sugaki (1985)
Ga	Occasional	Tens–hundreds	20 mol.% Ga_2S_3 below 800 °C Krämer et al. (1987)	No/questionable	–	–	No/questionable	–	–
Ge	Occasional	Tens–hundreds	–	Uncommon	–	–	Occasional	Tens–hundreds	–
As	Uncommon	–	–	Uncommon	–	–	Uncommon	Few–tens	–
Se	Occasional	Tens–hundreds	2.7 mol.% ZnSe at 600 °C Bethke and Barton (1971)	Common	Hundreds	Complete ss with PbSe below 1050 °C Liu and Chang (1994)	Occasional	Tens–hundreds	0.5 mol.% $Cu_{526}Fe_{526}Se$ at 390 °C Bethke and Barton (1971)
Ag	Occasional	Tens	–	Common	Hundreds–thousands	Complete ss with $Ag(Sb,Bi)Pb_2$ above 420 °C Chutas et al. (2008)	Common	Tens–hundreds	–
Cd	Common	Hundreds–thousands (rarely wt.%)	6 mol.% CdS at 600 °C Chen et al. (1988)	Occasional	Few–hundreds	–	Uncommon	Few	–
In	Common	Tens–hundreds (rarely thousands)	~80 mol.% $CuInS_2$ below 1000 °C Sombuthawee et al. (1978)	Uncommon	–	–	Occasional	Tens–hundreds	–
Sn	Occasional	Tens–hundreds (rarely thousands)	–	Occasional	Few–tens	–	Occasional	Few–tens	–
Sb	Uncommon	–	–	Common	Hundreds	Complete ss with $Ag(Sb,Bi)Pb_2$ above 420 °C Chutas et al. (2008)	Uncommon	–	–
Te	Uncommon	Few	–	Occasional	Few–hundreds	10 mol.% PbTe at 700 °C Liu and Chang (1994)	Uncommon	Few	–
Hg	Occasional	Tens	–	Uncommon	–	–	No/questionable	–	–
Tl	Occasional	Few–tens	–	Common	Few–tens	–	No/questionable	–	–
Bi	No/Questionable	–	–	Common	Hundreds–thousands	Complete ss with $Ag(Sb,Bi)Pb_2$ above 420 °C Chutas et al. (2008)	Uncommon	Few	–

been reworked such that it now aligns with Tertiary faults at the contact between Late Proterozoic and Palaeozoic sequences. Mt. Isa is, by contrast, a large Australian Proterozoic deposit located in the Mt. Isa Inlier, Queensland. The deposit has been metamorphosed to greenschist facies (Rubenach, 1992; Hannan et al., 1993; Large et al., 2005).

The recrystallized SEDEX deposits metamorphosed at amphibolite facies and above include Broken Hill, Bleikvassli and Mofjellet. Broken Hill is a giant Australian Proterozoic deposit located in the Curnamona Province, New South Wales (Plimer, 2007). It has experienced granulite facies metamorphism, and possible partial melting (Frost et al., 2005; Spry et al., 2008).

Bleikvassli and Mofjellet are located approximately 45 km apart in the Lower Palaeozoic Norwegian Caledonides. Mofjellet underwent amphibolite facies metamorphism whereas Bleikvassli experienced slightly higher upper amphibolite to lower granulite facies metamorphism. As a result of remobilization during regional metamorphic overprinting, the recrystallized SEDEX deposits exhibit a diverse mineralogy similar to some epithermal deposits (e.g., Cook et al., 1998).

4. Experimental methods

Each sample was prepared as a polished block of differing size. Sample characterization and selection of areas free of any noticeable inclusions for trace element analysis and element mapping was conducted using reflected light microscopy and backscattered electron (BSE) imaging.

Both LA-ICP-MS element mapping and spot analysis was carried out on a Resonetics M-50-LR 193 nm Excimer laser attached to an Agilent 7700cx Quadrupole ICP mass spectrometer (Adelaide Microscopy). The Resonetics laser uses a two-volume ablation cell designed by Laurin Technic Pty. for outstanding trace element sensitivity, washout and stability (Müller et al., 2009). Ablation takes place in an atmosphere of UHP He (0.7 L/min), creating an aerosol mixed with Ar (0.93 L/min) after leaving the ablation cell. The mix is then passed through a pulse-homogenizing device or "squid" before being directly introduced into the torch. Calibration of the ICP-MS is performed regularly in order to maximize the sensitivity on the isotopes of interest, whilst also keeping production of molecular oxide species (i.e., $^{232}Th^{16}O/^{232}Th$) and doubly charged ion species (i.e., $^{140}Ce^{2+}/^{140}Ce^{+}$) as low as possible, and usually <0.2%.

LA-ICP-MS element maps were made on selected areas to provide trace element concentrations as well as visualization of their distributions within individual sulphide grains. Mapping was performed by ablating sets of parallel line rasters in a grid across the sample. The laser spot size varied between 7–10 μm keeping the scan speed at a constant 10 μm/s. This ensured the desired sensitivity of elements of interest, as well as adequate spatial resolution depending on the size of the mapped area. The spacing between the lines was adjusted to match the laser spot size. A laser repetition of 10 Hz was selected at a constant energy output of 100 mJ. Thirty elements were analysed with the dwell time set to 0.01 s for all elements except for In, Au, and Tl which were set to 0.05 s, resulting in a total sweep time of 0.481 s. Thirty seconds of background was acquired by the ICP-MS before each raster was ablated, followed by a delay of 20 s for cell wash-out, gas stabilization, and computer processing time. At the beginning and end of each mapping run identical rasters were done on the MASS-1 (formerly PS-1) sulphide reference material (Wilson et al., 2002). Element maps were compiled and processed using the program Iolite, following the method described in George et al. (2015).

LA-ICP-MS spot analysis was carried out with the laser beam energy output set at 100 mJ at a 26 μm spot size while analysing sphalerite and chalcopyrite. When analysing galena, the energy output was set at 80 mJ and the spot size was set at 8 μm to ensure the ICP-MS was not oversaturated with Pb. A laser repetition rate of 10 Hz was used in all cases. Total acquisition time for each analysis was 60 s, comprising 30 s background measurement followed by 30 s of sample ablation. A 40 s delay was allowed after each spot analysis to ensure adequate cell wash-out, gas stabilization, and computer processing time. The following isotope suite was analysed: ^{34}S, ^{55}Mn, ^{57}Fe, ^{59}Co, ^{60}Ni, ^{65}Cu, ^{66}Zn, ^{69}Ga, ^{72}Ge, ^{75}As, ^{82}Se, ^{95}Mo, ^{107}Ag, ^{111}Cd, ^{115}In, ^{118}Sn, ^{121}Sb, ^{125}Te, ^{182}W, ^{197}Au, ^{202}Hg, ^{205}Tl, ^{207}Pb, and ^{209}Bi. Dwell times for each element were set to 0.01 s except for In, Au and Tl which were set to 0.05 s. Batches of up to 10 analyses were bracketed by repeat analyses of the MASS-1 standard. This allowed for the monitoring of, and correction for, instrumental drift by applying a linear correction based on the bracketed MASS-1 analyses. Data calculations were carried out using

Table 2
Summary of deposits and samples used in this study.

Deposit/type	Samples	Ore mineralogy	Conditions of formation or metamorphism	References
Herja, Romania Epithermal (*Neogene*)	Hj13	Gn–Cp–Py–Tet–Sp–Po–Ap–Ss–St	Formed at ~<200 °C Borcos et al. (1975)	Lang (1979) and Cook and Damian (1997)
Toroiaga, Romania Epithermal (*Neogene*)	TOR191 TOR197 Emeric2	Cp–Py–Sp–Gn Py–Sp–Cp–Gn–Ss Py–Cp–Gn–Sp	Formed at ~350 °C Cook (1997)	Szöke and Steclaci (1962) and Gotz et al. (1990)
Baita Bihor, Romania Skarn Antoniu orepipe — proximal Marta orepipe — distal (*Cretaceous*)	BBH16B (Antoniu) BBH20 (Antoniu) BB55 (Antoniu) BBH32 (Marta)	Gn–Sp–Cp Gn–Sp–Cp Gn–Sp–Cp Gn–Sp–Py	Formed at ~500 °C (proximal),~375 °C (distal)	Cioflica et al. (1971, 1977) and Shimizu et al. (1995) and Ciobanu et al. (2002)
Oravita, Romania Skarn (*Cretaceous*)	ORV4B	Gn–Cp–Py–Sp	–	Gheorghitescu (1975) and Cioflica and Vlad (1981) and Constantinescu et al. (1988)
Kapp Mineral, Norway SEDEX (*Late Precambrian*?)	Kmi2a Kmi5	Gn–Cp–Py Gn–Sp–Py	Very weakly metamorphosed	Flood (1967)
Mt. Isa, Australia SEDEX (*Proterozoic*)	5985C1	Sp–Gn–Py–Po–Ss	Greenschist facies Large et al. (2005)	Mathias and Clark (1975) and Perkins (1997) and Painter et al. (1999)
Bleikvassli, Norway Recrystallized SEDEX (*Ordovician*)	Bv-1 V598572	Py–Sp–Gn–Cp–Po Cp–Ap–Gn–Sp–Po–Ss	Upper amphibolite-lower granulite facies (570 °C, 7.5–8 kbar) Cook (1993); Rosenberg et al. (1998)	Vokes (1963, 1966) and Cook et al. (1998)
Broken Hill, Australia Recrystallized SEDEX (*Proterozoic*)	BH73 BH218	Sp–Gn–Cp–Po–Ss Gn–Sp–Po–Cp–Ss–Ac	Granulite facies (750–800 °C, 5–6 kbar)Bryndzia et al. (1990); Phillips (1981)	Haydon and McConachy (1987) and Parr and Plimer (1993) and Plimer (2007) and Spry et al. (2008)
Mofjellet, Norway Recrystallized SEDEX (*Palaeozoic*)	Mo2	Py–Gn–Sp–Cp–Po	Amphibolite facies (550 °C, 7 kbar?)Bjerkgård et al. (2001)	Saager (1967) and Cook (2001)

Mineral abbreviations: Gn = galena, Sp = sphalerite, Cp = chalcopyrite, Py = pyrite, Po = pyrrhotite, Ap = arsenopyrite, Ss = (Cu,Ag)–(Pb)–(Bi,Sb)–sulphosalts, Ac = acanthite, Tet = tetrahedrite–tennantite, St = stibnite.

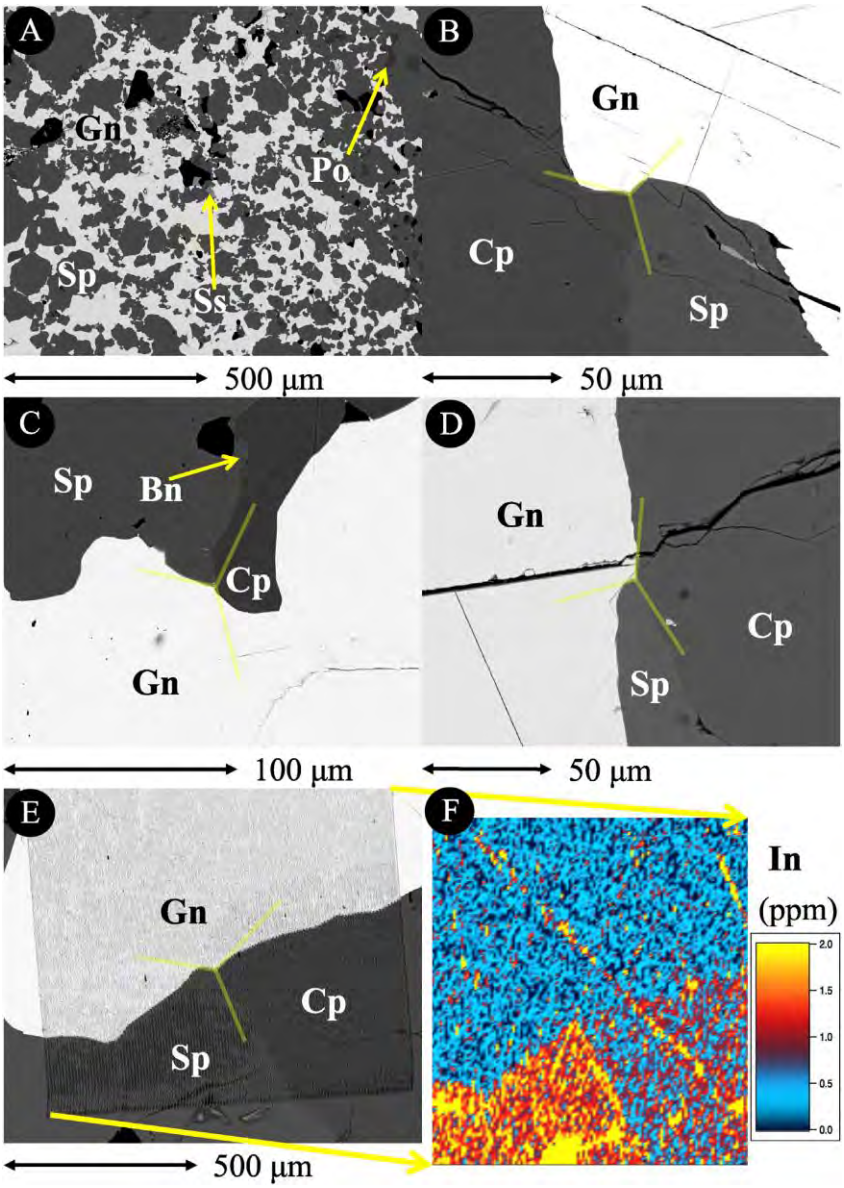

Fig. 1. Back-scattered electron images illustrating textural evidence for BMS co-crystallization. (A) Co-deposited sphalerite (Sp) and galena (Gn) in SEDEX horizon from Mt. Isa. Po = pyrrhotite, Ss = sulphosalt. (B, C, D, E) ~120° triple-junction grain boundaries between sphalerite, galena and chalcopyrite (Cp) at Herja, Baita Bihor, Bleikvassli and Broken Hill, respectively. Bn = bornite. Note grain boundaries curving towards the triple junction in order to approximate 120°. The grid in (E) has been mapped by LA-ICP-MS. (F) LA-ICP-MS element map for In corresponding to the area indicated in (E).

GLITTER data reduction software (Van Achterbergh et al., 2001). Significant effort was invested using GLITTER off-line to recognise the presence of inclusions by careful visual inspection of multi-element concentration patterns in each time-resolved depth profile. If obvious inclusions were present (e.g. by interdependencies of Ag and Te, suggestive of hessite inclusions in galena), these analyses were either discarded or the integrated time intervals restricted to inclusion-free portions of the ablation profile. We accept that our manual approach to identifying including-related analyses is imperfect and may permit the smallest inclusions to be missed. We nevertheless emphasize that very thorough examination by SEM prior to analysis and detailed mineralogical knowledge of each sample are sound preventative measures to avoid this.

The MASS-1 standard (formerly PS-1; Wilson et al., 2002) has a Fe–Zn–Cu–S matrix in which the concentrations of these elements are sufficiently close to natural sphalerite and chalcopyrite to allow for adequate calibration of sphalerite and chalcopyrite analyses. Even if Wilson et al. (2002) specifically mention that MASS-1 is not well suited for analysis of galena, we do not believe the small amount of Pb contained within MASS-1 compared to galena poses a significant problem for quantification in this study as discussed in George et al. (2015). We have chosen to consider MASS-1 homogeneous even if suggestions

of possible heterogeneity in the particle size of sulphide phases in MASS-1 have recently circulated. We have also chosen, for the purpose of the present work, to accept the trace element concentrations given in the latest MASS-1 certificate of analysis (available on the United States Geological Survey website). This may carry implications for some elements given the significant differences in concentration values compared to those given by Wilson et al. (2002) in the original paper. Irrespective of absolute concentrations, however, we have every confidence that the relative trends identified below are fully correct. As per the updated certificate of analyses for MASS-1, no value for Ge is given, precluding quantification of Ge concentrations from LA-ICP-MS analysis.

5. Results

Of the twenty-four elements analysed, seventeen were found to be present at measurable concentrations and could be quantified within sphalerite, galena or chalcopyrite (Table 3). These common 17 elements can be categorized into 3 groups based on their observed partitioning behaviours with respect to sphalerite, galena and chalcopyrite.

Group 1 elements include Mn, Fe, Zn, As, Se, Ag, Cd, Sb, Te, Tl and Bi. These elements are consistently concentrated within the same sulphide in all examined samples. Some elements also have clear secondary hosts.

Group 2 elements are Ga and In. These elements are primarily concentrated in sphalerite in samples that have not been recrystallized, whereas the concentration of these elements in chalcopyrite is high in recrystallized samples. This usually makes chalcopyrite the primary host of Ga, and occasionally of In, in recrystallized deposits.

Group 3 elements are Co, Cu and Hg. These elements display a generally predictable partitioning trend, usually preferentially incorporated within sphalerite. This trend is, however, not observed in all samples. Table 4 summarizes these trends, showing each trace element with its corresponding BMS host(s).

Tin does not fit neatly into any of the three groups. It displays behaviour similar to Group 2 elements; the concentration of Sn in chalcopyrite is higher in recrystallized samples such that chalcopyrite is usually the primary host. However, in samples that have not recrystallized, Sn may be primarily concentrated in sphalerite, galena or chalcopyrite.

Measured concentrations of Au were, in many cases, below minimum limits of detection, and are not included in our tabulated dataset. Despite this, there is published evidence for BMS hosting invisible gold, notably in seafloor sulphides (e.g., Bortnikov et al., 2000; Cabri et al., 2000).

LA-ICP-MS trace element maps representative of base metal ores formed at equilibrium in skarn, epithermal, recrystallized and primary SEDEX deposits are shown as Figs. 2–8, respectively. These visually illustrate the preferred BMS hosts for various trace elements in a range of deposits that, with the exception of skarns, are typical of base metal ores. The maps test the validity of the above-defined groups of elements for deposits of contrasting ages, spanning Neogene to Precambrian, and of different tectonic setting, varying from magmatic-hydrothermal systems in younger terranes to metamorphosed epigenetic ores in older orogens and cratons. The maps are thus relevant for the intrinsic variability in physiochemical conditions of ore formation in each specific case, and also across their representative deposit types.

Fig. 2 shows trace element distributions in a sphalerite–galena assemblage hosted by garnet skarn from the proximal Antoniu orepipe at Baita Bihor which exemplify preferential partitioning of elements in each sulphide according to the rules in Groups 1 and 3, i.e., sphalerite primarily hosts Fe, Cd, Mn, In, Co and Cu, whereas galena hosts Ag, Bi, Sb, Se, Te and Tl. The caries-like textures are indicative of the equilibrium conditions between the two sulphides. Low levels of Se are noted in sphalerite, whereas galena hosts low levels of Fe, Cd and Cu. Grain-scale zoning of Se is recognised within galena, as are Fe and Mn within sphalerite. Copper concentrations in sphalerite are sporadic, consistent with the presence of chalcopyrite disease. There also appears to be a fracture in galena highlighted by high concentrations of Cu.

A galena-sphalerite assemblage with similar carries texture but hosted within marble from the distal Marta orepipe at Baita Bihor reveals comparable trace element distributions (Fig. 3). Iron, Cd, Mn, In and Co are all primarily concentrated within sphalerite, whereas Ag, Bi, Sb, Se, Te and Tl are all primarily concentrated in galena. Moderate concentrations of Ga and Se are noted in sphalerite, and some Cd is present in galena. Both Fe and Mn display erratic distributions within sphalerite, which may be indicative of micro-inclusions, zonation or both. Fractures present in sphalerite concentrate high levels of Sb, Mn and In.

Trace element distributions in tri-component sulphide assemblages formed at equilibrium in skarn is demonstrated by sphalerite–galena–chalcopyrite association at Oravita (Fig. 4). Sphalerite primarily hosts Cd, Mn, In, Sn and Ga, with each of these elements zoned to some extent. The zonation patterns displayed by In, Sn and Ga appear to match closely, whereas Cd distributions are inversed to those for Mn. A splay of fractures near the boundary between sphalerite and chalcopyrite, concentrate Ag, Bi, Sb, Se, Te, Tl and Fe. Apart from these fractures, all these elements (excluding Fe) are primarily hosted in galena, although Sb concentrations are low and are matched closely by chalcopyrite. Low levels of Cd are also noted in galena. Notable is that, compared to sphalerite and galena, chalcopyrite is relatively barren with respect to trace elements.

Epithermal ore also comprising tri-component assemblages (sphalerite–galena–chalcopyrite) from Toroiaga shows trace element distributions that are comparable with those in the skarn at Oravita (Fig. 5). Iron, Cd, Mn, In and Ga are all primarily hosted by sphalerite and In is zoned at this spatial resolution. Silver, Bi, Sb, Se, Te and Tl are all hosted by galena, whereas moderate amounts of Cd are also noted. There is however an increase in Sb in the epithermal ore. Notable here is also that, whereas Sn is distributed quite evenly across both galena and chalcopyrite on the map, spot analysis (Table 3) reveals that galena is the primary host. Indium is also present in chalcopyrite. Galena is clearly zoned with respect to Bi, with highest concentrations at the grain rim.

Fig. 6 shows trace element distributions in a co-crystallized sphalerite–galena assemblage from Broken Hill where all elements are concentrated by their preferred host. Sphalerite primarily hosts Co, Cd, Mn, In, Ga and Cu whereas galena concentrates Ag, Bi, Sb, Se, Tl and Sn. Modest amounts of In are apparent in galena; low levels of Cd and Cu are also present. Galena displays weak zoning with respect to Ag and Sb; the absolute concentrations of both elements decrease away from what appears to be fractures.

Fig. 7 reveals the trace element distributions in a sphalerite–galena–chalcopyrite assemblage from the Bleikvassli recrystallized SEDEX deposit that are comparable to tri-component assemblages from skarn and epithermal ores. Here, however, Ga is primarily concentrated in chalcopyrite. Sphalerite concentrates Fe, Cd, Mn and In, whereas galena concentrates Ag, Bi, Sb, Se and Tl. Spot analysis (Table 3) shows that Sn concentrations are highest in galena, followed closely by chalcopyrite. Modest enrichment of Ag and In is noted in chalcopyrite, as well as Ga in sphalerite. There appears to be a poorly defined zonation in galena and chalcopyrite with respect to Sn.

Trace element distributions in a sphalerite–galena assemblage from the Kapp Mineral SEDEX deposit are shown in Fig. 8. Sphalerite primarily hosts Fe, Cd, Mn, In, Sn, Ga, Co, Hg and Cu, whereas galena hosts Ag, Bi, Sb, Se and Tl. The LA-ICP-MS mapping also shows low levels of As in galena. Modest amounts of Ag are noted in sphalerite.

Table 3
Trace element concentrations in sphalerite, galena and chalcopyrite determined by LA-ICP-MS spot analysis. Data in ppm (molar).

Locality	Sample/sulphide		Element																
Herja	Hj13		Mn	Fe	Co	Cu	Zn	Ga	As	Se	Ag	Cd	In	Sn	Sb	Te	Hg	Tl	Bi
Romania	Sphalerite (10)	Mean	2392	88022	76	585	IS	1.7	0.05	3.6	1.4	1045	4.4	38	0.32	0.02	0.60	0.00	0.00
		St. Dev.	362	8400	24	1150		0.48	0.05	3.6	1.8	139	9.1	51	0.63	0.03	0.06	0.00	0.00
	Galena (10)	Mean	9.0	50	0.09	5.0	19	0.18	1.1	258	1574	16	0.02	2.0	1509	10	0.06	0.21	179
		St. Dev.	4.1	26	0.17	8.3	10	0.23	0.50	289	254	4.4	0.01	1.3	299	14	0.03	0.06	343
	Chalcopyrite (10)	Mean	43	245967	3.3	IS	1120	0.06	0.04	5.0	71	3.1	0.69	3.9	0.53	0.00	0.04	0.01	0.00
		St. Dev.	11	14061	1.1		491	0.03	0.03	4.4	25	1.1	0.31	1.3	0.78	0.01	0.01	0.03	0.00
Toroiaga	TOR191																		
Romania	Sphalerite (10)	Mean	1035	70815	0.02	47	IS	1.4	1.7	1.0	0.54	4109	27	0.22	0.06	0.01	8.2	0.00	0.00
		St. Dev.	169	3795	0.02	36		0.49	0.89	0.77	0.32	481	31	0.30	0.09	0.02	4.7	0.00	0.00
	Galena (10)	Mean	7.9	55	0.17	5.4	4.5	0.07	27	56	2791	311	0.13	3.0	822	–	5.7	0.41	1687
		St. Dev.	5.5	44	0.19	3.9	3.4	0.05	21	58	2206	49	0.09	1.5	433	–	3.0	0.30	2185
	Chalcopyrite (10)	Mean	0.83	246711	0.03	IS	1451	0.22	0.46	0.75	54	17	14	11	0.30	0.01	39	0.00	0.00
		St. Dev.	0.34	9312	0.03		1020	0.10	0.21	0.71	53	11	8.2	7.4	0.23	0.02	14	0.00	0.00
	TOR197																		
	Sphalerite (10)	Mean	1004	75230	0.05	52	IS	1.3	1.6	0.74	0.39	4337	19	0.23	0.05	0.01	8.0	0.00	0.00
		St. Dev.	151	5397	0.09	44		0.62	1.3	0.58	0.16	407	15	0.24	0.10	0.01	7.0	0.00	0.00
	Galena (10)	Mean	7.6	344	0.33	6.8	11	0.37	118	828	1292	171	0.10	6.2	1321	14	4.7	0.35	190
		St. Dev.	6.9	940	0.29	2.7	12	0.51	102	727	328	26	0.04	1.7	291	4.9	3.5	0.20	119
	Chalcopyrite (10)	Mean	0.94	256250	0.02	IS	2213	0.08	0.73	0.80	94	24	8.2	4.2	0.53	0.04	95	0.00	0.00
		St. Dev.	1.2	9148	0.03		2971	0.06	0.58	0.69	59	27	1.8	1.7	0.49	0.04	41	0.00	0.00
	Emeric2																		
	Sphalerite (9)	Mean	831	62553	–	7207	IS	3.6	0.24	3.3	6.9	2657	89	0.35	0.88	–	2.3	0.00	0.01
		St. Dev.	121	8523	–	8088		0.82	0.26	1.9	6.8	309	79	0.23	1.3	–	0.37	0.00	0.01
	Galena (6)	Mean	5.0	31	0.04	7.8	28	0.08	1.8	–	2177	37	0.06	1.4	1756	63	0.07	0.84	863
		St. Dev.	2.5	4.1	0.04	7.1	18	0.11	1.1	–	391	4.7	0.04	0.70	391	10	0.04	0.53	536
	Chalcopyrite (9)	Mean	15	266804	–	IS	5790	1.3	0.16	11.0	41	24	13	16	4.2	–	0.39	0.00	0.05
		St. Dev.	10	16234	–		3115	0.94	0.19	7.8	25	9.4	5.2	9.5	3.5	–	0.46	0.00	0.07
Baita Bihor	BBH16B																		
Romania	Sphalerite (10)	Mean	358	1525	285	616	IS	0.62	0.04	2.4	0.25	1634	7.8	0.20	0.01	0.04	1.4	0.00	0.11
		St. Dev.	122	764	6.6	640		0.30	0.03	2.2	0.18	79	0.91	0.12	0.01	0.05	0.12	0.00	0.24
	Galena (10)	Mean	4.6	103	0.20	13	53	0.06	1.7	343	813	41	0.03	0.52	2.1	–	0.01	2.6	844
		St. Dev.	4.3	74	0.52	12	47	0.15	1.8	468	71	15	0.03	0.29	1.7	–	0.00	0.37	112
	BBH20																		
	Sphalerite (10)	Mean	3218	10333	192	27	IS	0.22	0.09	4.2	0.08	1842	3.9	0.05	0.19	0.02	1.2	0.00	0.01
		St. Dev.	525	599	10	30		0.16	0.06	3.2	0.01	118	0.42	0.02	0.38	0.04	0.19	0.00	0.01
	Galena (10)	Mean	12	110	0.17	65	39	0.06	2.7	322	3383	71	0.02	1.2	18	411	0.06	8.4	4619
		St. Dev.	6.7	96	0.29	50	17	0.10	2.5	561	368	20	0.01	0.92	9.3	65	0.04	2.0	248
	BB55																		
	Galena (10)	Mean	74	139	0.14	527	32	0.04	2.1	395	19986	156	0.21	2.4	90	–	0.02	15	38096
		St. Dev.	133	103	0.23	615	4.8	0.08	1.3	–	7159	233	0.59	1.7	245	–	0.02	2.1	60466
	Chalcopyrite (10)	Mean	31	224552	69	IS	523	0.04	0.35	4.6	22	5.1	42	47	0.28	0.05	0.02	0.02	0.36
		St. Dev.	77	11508	134		149	0.03	0.45	2.3	49	5.2	3.5	7.2	0.41	0.05	0.01	0.03	0.78
	BBH32																		
	Sphalerite (10)	Mean	1608	6558	241	15.0	IS	1.5	0.67	6.0	0.13	2834	7.0	0.20	0.20	0.02	2.4	0.00	0.01
		St. Dev.	335	1037	21	7.9		3.1	0.54	4.1	0.04	69	1.6	0.44	0.42	0.02	2.7	0.00	0.01
	Galena (10)	Mean	19	116	0.12	4.1	1.7	0.13	10	443	3694	167	0.01	0.24	33	475	11	6.4	4410
		St. Dev.	34	253	0.09	2.5	1.2	0.11	2.7	135	173	41	0.01	0.11	8.6	121	4.7	1.0	546
Oravita	ORV4B																		
Romania	Sphalerite (10)	Mean	551	1841	0.02	1490	IS	14	0.71	4.5	4.1	1409	1.6	1.3	0.04	0.06	3.3	0.00	0.37
		St. Dev.	215	314	0.04	305		11	0.44	3.1	2.2	121	3.9	2.2	0.08	0.11	2.0	0.00	0.49
	Galena (10)	Mean	2.5	17	0.07	4.4	1.6	0.07	8.6	1155	856	39	0.01	0.22	1.3	175	24	0.47	956
		St. Dev.	3.2	8.6	0.06	3.8	1.3	0.05	7.6	261	214	6.0	0.00	0.17	1.0	38	15	0.11	267
	Chalcopyrite (10)	Mean	0.12	249624	0.00	IS	6.6	0.23	0.54	8.1	0.44	0.13	0.37	0.16	0.13	0.14	2.9	0.03	1.2
		St. Dev.	0.16	7350	0.00		1.7	0.10	0.60	10	0.37	0.09	0.40	0.11	0.10	0.12	1.4	0.09	0.72
Kapp Mineral	Kmi2a																		
Norway	Galena (10)	Mean	2.4	46	0.17	7.4	4.8	0.16	8.7	300	129	39	0.02	0.41	46	–	5.7	0.07	96
		St. Dev.	1.6	34	0.08	6.4	2.7	0.14	6.0	194	38	13	0.01	0.27	14	–	5.7	0.02	53
	Chalcopyrite (10)	Mean	241	261971	0.42	IS	194	0.13	1.2	13	90	1.6	0.64	6.4	13	0.02	32	0.02	4.0
		St. Dev.	493	13155	0.87		80	0.04	1.4	29	33	1.2	0.21	1.6	7.7	0.02	40	0.01	10
	Kmi5																		
	Sphalerite (10)	Mean	5.7	10619	5.0	250	IS	2.5	0.07	2.2	18	253	0.76	8.1	0.69	0.01	7.0	0.00	0.01
		St. Dev.	1.9	1788	1.7	224		3.9	0.06	1.2	9.5	22	0.33	11	0.79	0.02	0.75	0.00	0.00
	Galena (10)	Mean	3.9	77	0.17	6.8	54	0.07	1.6	20	192	4.9	0.02	0.69	254	–	0.01	0.03	7.1
		St. Dev.	1.9	33	0.36	5.4	53	0.14	0.75	11	31	3.7	0.01	0.70	39	–	0.02	0.01	2.6
Mt. Isa	5985C1																		
Australia	Sphalerite (5)	Mean	116	38989	0.16	15	IS	2.0	3.4	0.70	3.0	1351	7.0	0.11	1.8	0.02	10	0.01	0.00
		St. Dev.	15	1062	0.04	1.5		1.2	1.3	0.54	1.1	54	0.12	0.12	0.86	0.02	5.4	0.01	0.00
	Galena (4)	Mean	5.4	224	0.25	6.4	4.3	0.13	1700	4.6	499	86	0.21	2.1	748	0.27	7.1	14	3.4
		St. Dev.	3.1	361	0.28	2.5	1.9	0.19	846	0.73	122	154	0.37	0.49	146	0.18	4.4	3.1	0.09
Bleikvassli	Bv–1																		
Norway	Sphalerite (10)	Mean	255	51984	0.05	48	IS	13	0.17	2.2	1.0	509	23	1.5	0.41	0.01	4.0	0.01	0.00
		St. Dev.	102	1134	0.04	7.4		0.75	0.19	1.5	1.1	20	0.51	1.1	0.79	0.02	0.18	0.01	0.01

(continued on next page)

Table 3 (*continued*)

Locality	Sample/sulphide		Element															
	Galena (10)	Mean	3.8	82	0.10	6.7	26	0.27	1.6	9861	1093	8.2	1.0	290	966	0.26	0.09	130	534
		St. Dev.	4.3	72	0.22	3.2	20	0.56	0.56	24503	161	6.2	0.30	87	209	0.84	0.08	6.8	41
	Chalcopyrite (5)	Mean	1.8	224617	0.01	IS	261	16	0.03	1.3	254	0.34	7.5	275	2.8	0.00	0.09	0.14	0.01
		St. Dev.	1.7	5678	0.02		46	9.1	0.01	1.1	125	0.10	1.4	221	1.6	0.01	0.07	0.15	0.01
	V598572																		
	Sphalerite (5)	Mean	1766	49536	0.35	28	IS	2.8	0.28	8.1	0.18	778	20	0.47	0.09	0.00	7.3	0.00	0.01
		St. Dev.	137	684	0.08	3.3		1.6	0.21	3.3	0.04	15	2.6	0.15	0.08	0.00	1.0	0.00	0.00
	Galena (10)	Mean	6.3	65	0.06	8.0	13	0.06	4.8	172	1042	26	0.32	98	309	–	0.04	62	1312
		St. Dev.	4.4	80	0.08	5.2	2.9	0.08	2.5	102	102	7.1	0.11	19	170	–	0.03	8.4	129
	Chalcopyrite (9)	Mean	47	221422	0.23	IS	344	1.1	0.24	7.8	5.2	2.3	10	393	1.2	0.05	0.19	0.01	0.01
		St. Dev.	10	13003	0.48		49	0.66	0.40	5.8	1.7	1.2	1.5	73	2.4	0.07	0.09	0.01	0.01
Broken Hill	BH73																		
Australia	Sphalerite (10)	Mean	16606	90076	128	71	IS	2.6	0.05	1.7	0.82	884	0.69	0.21	0.04	0.03	0.86	0.00	0.00
		St. Dev.	633	2537	10	3.2		0.12	0.04	1.0	0.27	24	0.01	0.07	0.04	0.02	0.05	0.00	0.00
	Galena (10)	Mean	36	73	0.09	2.6	16	0.09	1.3	32	249	13	0.15	39	631	0.24	0.05	0.43	4.0
		St. Dev.	17	45	0.06	1.4	8.1	0.08	0.61	20	72	3.5	0.04	5.2	615	0.33	0.04	0.11	0.77
	Chalcopyrite (5)	Mean	196	235552	1.3	IS	550	3.9	0.05	1.6	473	0.74	0.70	119	3.1	0.03	0.01	0.02	0.00
		St. Dev.	253	8084	1.1		242	0.86	0.01	0.22	110	0.68	0.10	20	3.6	0.03	0.01	0.03	0.00
	BH218																		
	Sphalerite (10)	Mean	1420	61926	47	33	IS	4.8	0.05	2.0	0.71	688	1.4	0.14	0.08	0.03	0.55	0.00	0.01
		St. Dev.	35	2316	7.8	14		0.58	0.02	1.2	0.75	30	0.05	0.13	0.10	0.05	0.06	0.00	0.02
	Galena (10)	Mean	2.3	65	0.12	3.9	30	0.05	2.2	93	237	10	0.21	72	57	–	0.05	0.09	35
		St. Dev.	1.4	44	0.11	3.4	33	0.14	2.0	167	336	5.8	0.05	8.7	107	–	0.04	0.02	2.6
Mofjellet	Mo2																		
Norway	Sphalerite (10)	Mean	460	25051	0.10	4.3	IS	0.39	0.65	2.9	0.65	1156	0.76	0.02	0.08	0.01	23	0.00	0.02
		St. Dev.	43	2452	0.05	1.0		0.09	0.46	1.1	1.2	34	0.08	0.02	0.13	0.01	8.7	0.00	0.05
	Galena (10)	Mean	2.3	33	0.12	7.5	4.6	0.14	17	319	1116	100	0.01	0.51	1750	39	333	0.33	124
		St. Dev.	1.7	10	0.07	5.6	3.0	0.07	4.6	59	348	33	0.01	0.37	325	6.0	326	0.06	24

IS: This element was used as the internal standard; Zn in sphalerite, Cu in chalcopyrite and Pb in galena.
The 17 elements displayed were commonly detected above the mdl in sphalerite, galena or chalcopyrite. S, Ni, Mo, W and Pb were measured but are not commonly detected as trace elements. Ge could not be quantified (see text). Au was measured but found to be below minimum detection limit in the majority of analysed spots. We choose not to present these data given the high levels of uncertainty and concerns about the homogeneity of Au in the MASS-1 standard (Wilson et al., 2002).
(X) = number of individual spot analyses on that sulphide in that sample. Dash = insufficient data to perform calculation (all analyses <mdl). Other <mdl values were treated as mdl/2.
*Ag concentration in galena in BH73 reduced due to secondary leaching post recrystallization (see text).

Indium, Sn and Ga all appear to be zoned in the same way within sphalerite; Bi distributions in galena are patchy.

6. Discussion

6.1. External factors on trace element partitioning

The rich exotic trace element signature of the BMMB is well documented, in particular in the Baita Bihor skarn system, where Bi, Ag, W, Se, Te, Ni, Co and Sn are all present, and are primarily concentrated within Pb-(Cu,Ag)-Sb- or Bi-sulphosalts, and as Bi- and Ag-tellurides and selenides (Cioflica et al., 1995; Cioflica et al., 1997; Ilinca et al., 2012; Ciobanu et al., 2014). It has, however, recently been shown that many of these trace elements are also present at high concentrations within common sulphides (e.g., galena; George et al., 2015). Oravita, located approximately 350 km from Baita Bihor, has a similar geochemical signature as a consequence of related ore fluids associated with Late Cretaceous calc-alkaline magmatism. From these two deposits, it is possible to directly compare the partitioning behaviour of trace elements between co-crystallizing BMS in skarns formed from similar hydrothermal fluids at high temperature (~>450 °C) conditions proximal to a porphyry granitoid-derived source of fluids (Baita Bihor, Antoniu orepipe; Fig. 2), low temperature (~<200 °C) conditions distal to a porphyry hosted in carbonate (Baita Bihor, Marta orepipe; Fig. 3), and a shallow Cu skarn satellite to a porphyry (Oravita; Fig. 4). In each case, the trace element distributions in the BMS assemblages from these systems are almost identical; all Group 1 and 2 trace elements present are primarily hosted in the same minerals (Fe, Cd, Mn, In, Sn, Ga, Co and Cu in sphalerite, Ag, Bi, Sb, Se, Te and Tl in galena).

Similar to the BMMB, both the Toroiaga and Herja epithermal systems in the Baia Mare District, Romania, boast similar geochemical signatures expressed in part by the presence of Pb–Ag–Sb–As or lesser -Bi sulphosalts. This is a result of their common association with relatively young magmatic-hydrothermal systems, which produced comparable ore fluids at both deposits. Despite the similarities however, Toroiaga is a relatively deep system, crystallizing BMS at high temperatures (~<400 °C; Cook, 1997), whereas Herja is shallow and relatively cool (~<200 °C; Borcos et al., 1975). Thus Toroiaga (Fig. 5) and Herja (see

Table 4
Base metal sulphide hosts of various trace elements as determined from LA-ICP-MS analysis.

Trace element	Mn	Fe	Co	Cu	Zn	Ga	As	Se	
Primary BMS host	Sp[1]	Sp>Gn[1]	Sp>Cp[3]	Sp>Gn[3]	Cp[1]	Sp[2]	Gn>Sp[1]	Gn[1]	
Trace element	Ag	Cd	In	Sn	Sb	Te	Hg	Tl	Bi
Primary BMS host	Gn[1]	Sp>Gn[1]	Sp>Cp[2]	?[*]	Gn>Cp[1]	Gn[1]	Sp>Cp[3]	Gn[1]	Gn[1]

Abbreviations: BMS = base metal sulphide. Sp = sphalerite, Gn = galena, Cp = chalcopyrite.
[1] Group 1 elements. Trend observed in all examined samples.
[2] Group 2 elements. Recrystallization increases element concentration in Cp and may make Cp primary host.
[3] Group 3 elements. Trend generally, yet not always, true.
[*] Recrystallization increases Sn concentration in Cp such that Cp is usually primary host in recrystallized samples. Below recrystallization conditions, no trend is observed.

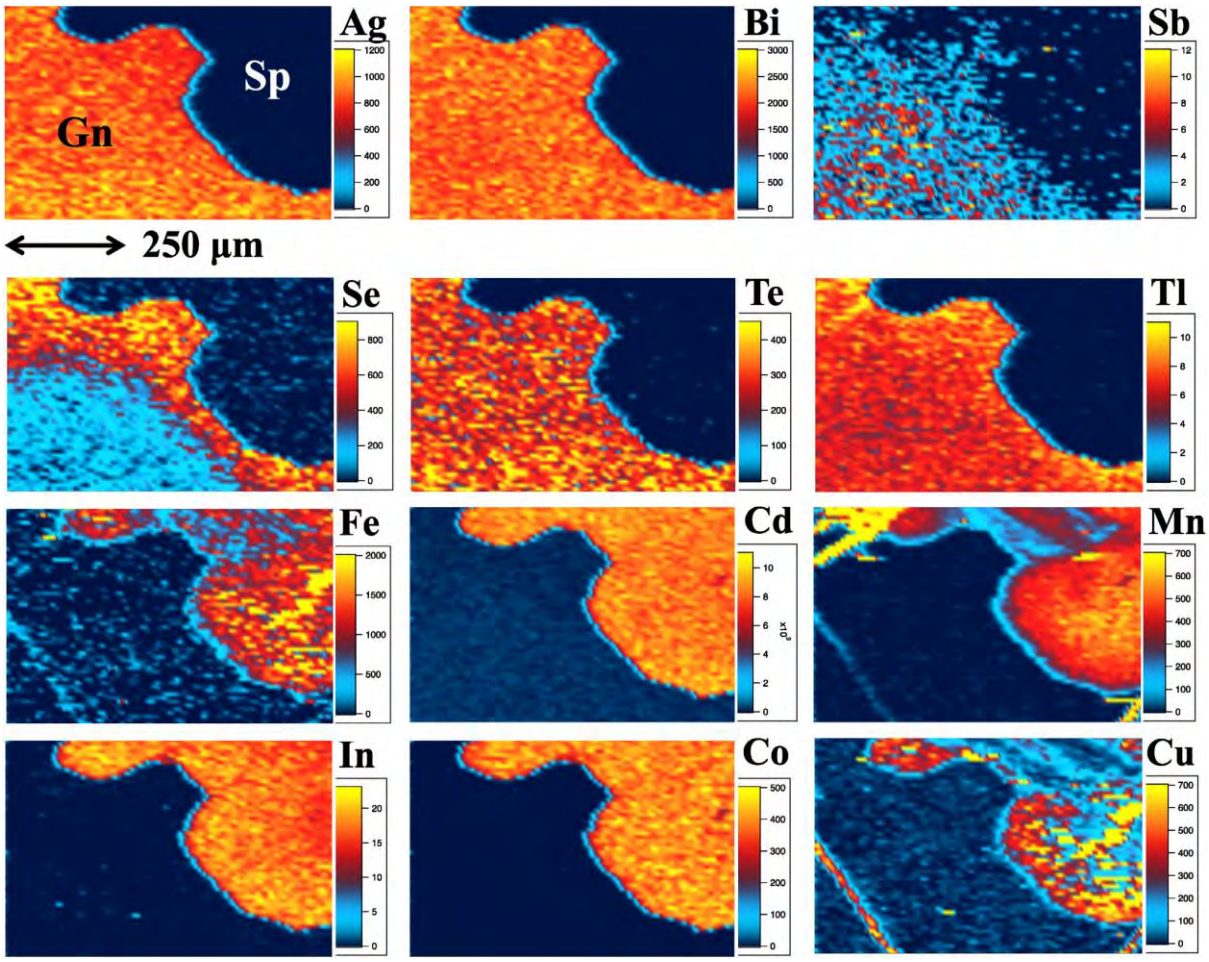

Fig. 2. LA-ICP-MS element maps (Ag, Bi, Sb, Se, Te, Tl, Fe, Cd, Mn, In, Co, Cu) of an assemblage comprising co-crystallized sphalerite (Sp) and galena (Gn) from the Antoniu orepipe, Baita Bihor skarn deposit (sample BBH16B). Note preferential concentration of Fe, Cd, Mn, In, Co and Cu in sphalerite and of Ag, Bi, Sb, Se, Te and Tl in galena. Concentration scales in parts-per-million (weight).

figure 6 in George et al., 2015) allow direct comparison of the partitioning behaviour of trace elements between two epithermal systems with similar ore fluids yet different physical conditions of ore formation. In both systems, trace element distributions in the BMS assemblages are almost identical; all Group 1 and 2 trace elements present are primarily hosted in the same BMS phase.

Even higher temperatures and pressures only slightly alter the primary BMS hosts. The recrystallized SEDEX Broken Hill deposit situated in the Curnamona Province, Australia, was regionally metamorphosed to granulite facies (750–800 °C, 5–6 kbar, Phillips, 1981; Bryndzia et al., 1990). This caused a complete recrystallization of the ore, allowing for pervasive re-partitioning of trace elements from the low temperature SEDEX distributions to the preferred distributions at these high metamorphic temperatures and pressures. Some have also argued that extensive melting of the BMS assemblage took place at peak metamorphic conditions (Mavrogenes et al., 2001; Frost et al., 2002, 2005). This too would cause a redistribution of trace elements as new sulphides crystallize from melt at high temperatures. Despite the granulite facies metamorphism however, Group 1 trace elements at Broken Hill are all hosted by the same BMS phases as the skarn and epithermal systems discussed above (Fig. 6). Only the primary hosts of Group 2 elements and Sn seem to be altered by the temperatures and/or pressures associated with upper amphibolite to granulite facies metamorphism. The preferred BMS host for Ga at lower temperatures is sphalerite, almost always becoming chalcopyrite in recrystallized assemblages. Despite In concentrations also increasing in chalcopyrite during recrystallization, sphalerite almost always remains the primary host. Tin exhibits a comparable relationship to Ga as chalcopyrite typically becomes the primary Sn host at high temperatures/pressures that cause recrystallization. Thus, as a result of recrystallization chalcopyrite usually contains more Sn than galena which, in turn, contains more Sn than sphalerite, so that $Sn_{chalcopyrite} > Sn_{galena} > Sn_{sphalerite}$.

Like Broken Hill, the Bleikvassli deposit (Norway) also underwent high-grade (upper amphibolite) metamorphism. Peak conditions reached 7.5–8 kbar, and 570 °C (Cook, 1993; Rosenberg et al., 1998). Despite a lower peak temperature than Broken Hill, these temperatures were still adequate for complete recrystallization of the BMS assemblage. The Bleikvassli system is oxidized, evidenced by large pyrite metablasts, and a distinct syn-metamorphic sulphidation–oxidation halo enclosing the ore (Rosenberg et al., 2000). In contrast, Broken Hill is a strongly reduced system, as evidenced by the stability of pyrrhotite, lack of pyrite, and the Eu enrichment of proximal exhalites

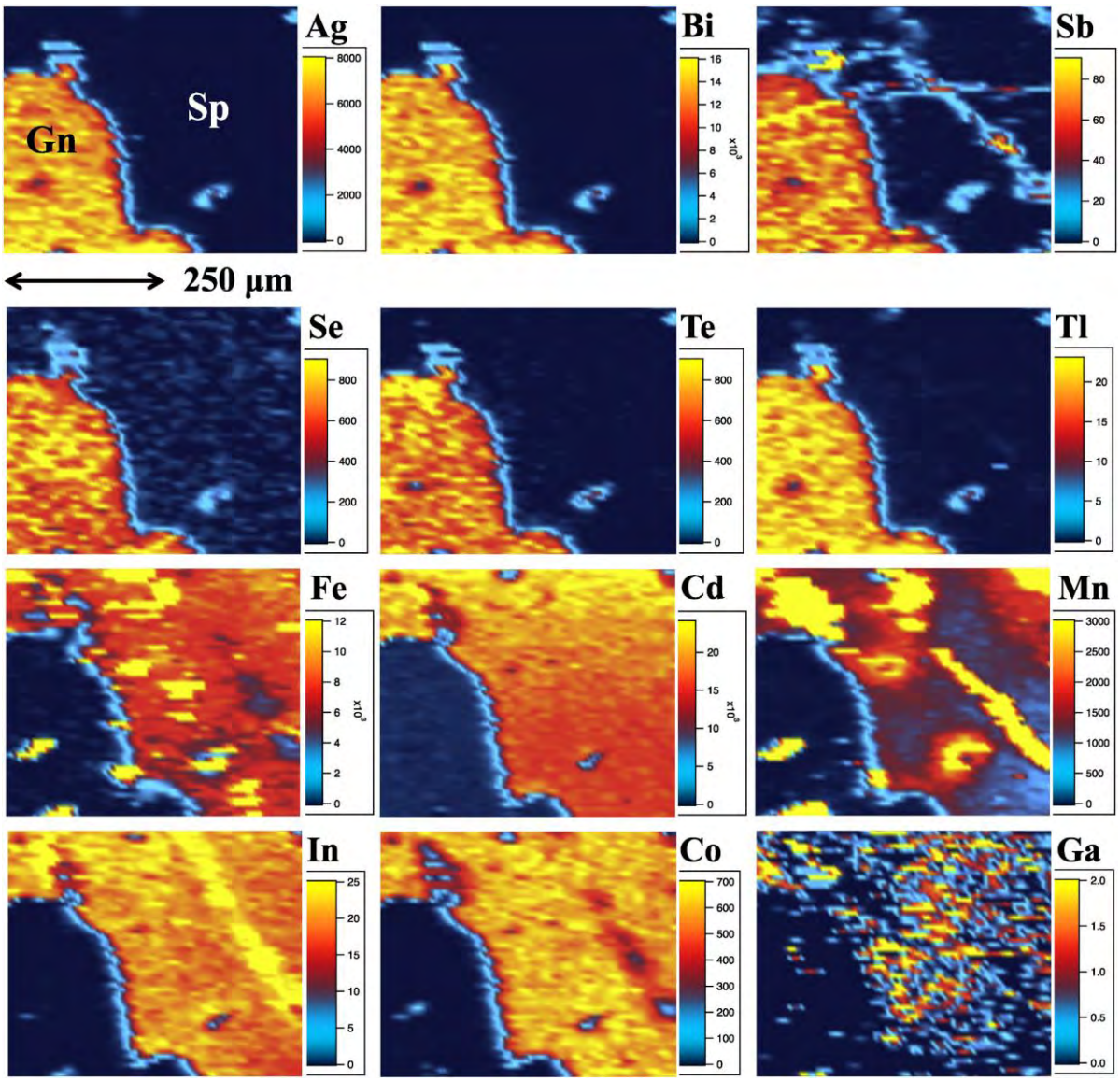

Fig. 3. LA-ICP-MS element maps (Ag, Bi, Sb, Se, Te, Tl, Fe, Cd, Mn, In, Co, Ga) of an assemblage comprising co-crystallized sphalerite (Sp) and galena (Gn) from the Marta orepipe, Baita Bihor skarn deposit (sample BBH32). Note preferential concentration of Fe, Cd, Mn, In, Co and Ga in sphalerite, and of Ag, Bi, Sb, Se, Te and Tl in galena. Concentration scales in parts-per-million (weight).

(Lottermoser, 1989; Leyh and Conor, 2000). Yet in both recrystallized SEDEX deposits, all Group 1 trace elements are hosted primarily within the same phases, galena, sphalerite and chalcopyrite (Figs. 6 and 7), strongly indicating that redox conditions have little to no effect on primary BMS hosts.

The Kapp Mineral SEDEX occurrence (Svalbard Archipelago, Norway) lacks any enhanced trace element geochemical signature such as that found in the BMMB or the Baia Mare District, and has not been significantly reworked since initial deposition. Yet despite the differences compared to deposits of more complex geochemistry and/or geological history, all Group 1 trace elements are primarily hosted by the same phases as in all other samples from all deposits, and Group 2 elements are primarily hosted by the same minerals as in all samples from non-recrystallized deposits (Fig. 8). This again strongly points to the conclusion that different ore types, deposit ages, host terrains and physiochemical conditions of ore formation do not alter the preferred host for almost all trace elements.

6.2. Intrinsic factors on trace element partitioning

The primary factors that control trace element partitioning identified in this study are intrinsic to the trace elements and BMS in question. These factors include element oxidation state, ionic radius of the substituting element, element availability and the maximum trace element budget that a given sulphide mineral can accommodate.

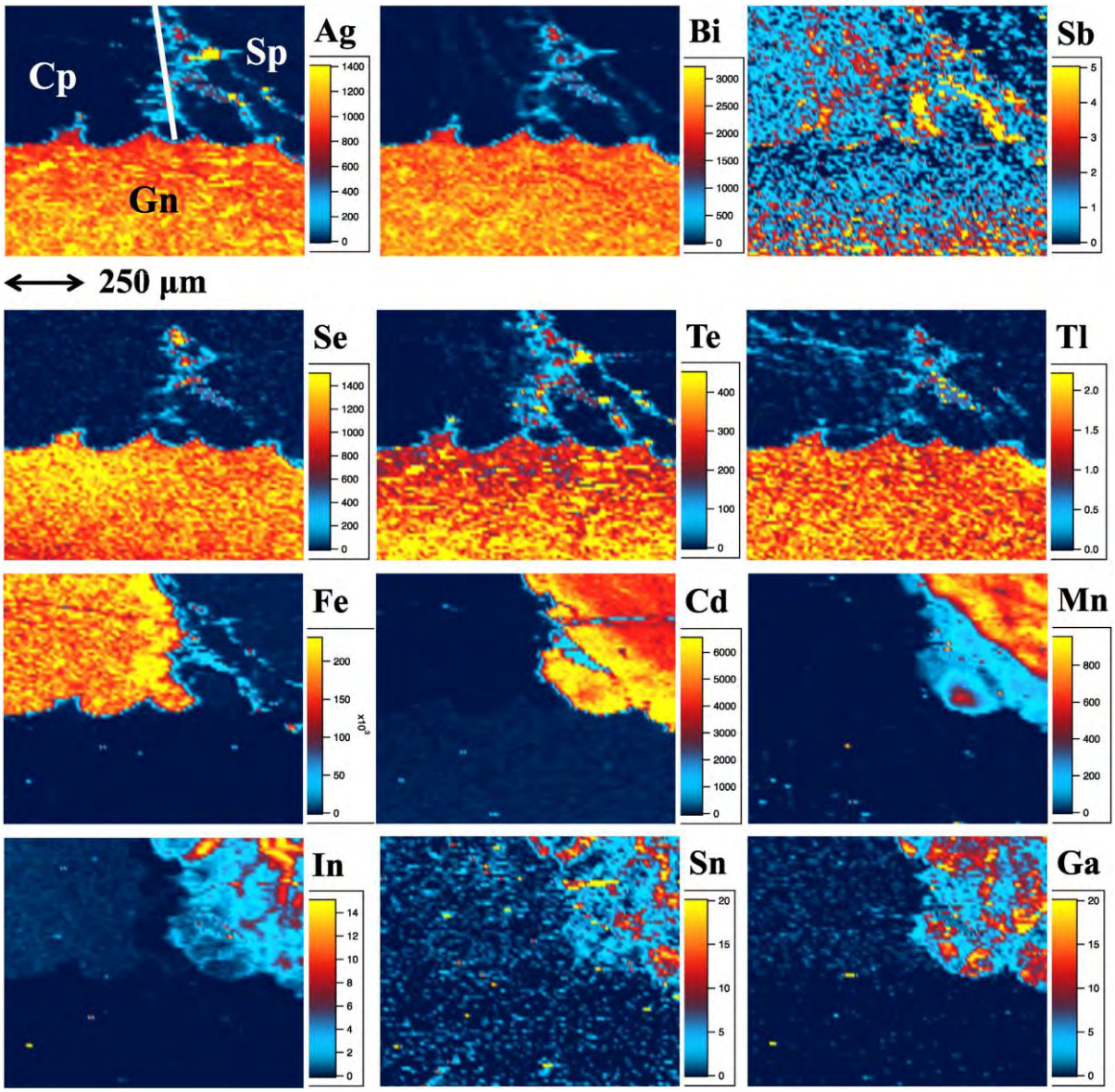

Fig. 4. LA-ICP-MS element maps (Ag, Bi, Sb, Se, Te, Tl, Fe, Cd, Mn, In, Sn, Ga) of an assemblage comprising co-crystallized sphalerite (Sp), galena (Gn) and chalcopyrite (Cp) from the Oravita skarn deposit (sample ORV4B). Note preferential concentration of Fe, Cd, Mn, In, Sn and Ga in sphalerite, of Ag, Bi, Se, Te and Tl in galena, and also the modest enrichment of Sb in galena over chalcopyrite. Concentration scales in parts-per-million (weight).

Sphalerite and galena are both ionic crystals, thus the incorporation of trace elements into them is governed by Goldschmidt's rules of substitution (Goldschmidt, 1954), and Ringwood's subsequent modifications (Ringwood, 1955). These state:

1. The ions of one element can extensively replace those of another in ionic crystals if their radii differ by less than approximately 15%.
2. Ions whose charges differ by one unit substitute readily for one another provided electrical neutrality of the crystal is maintained. If the charges differ by more than one unit, substitution is generally slight.
3. When two different ions can occupy a particular position in a crystal lattice, the ion with the higher ionic potential forms a stronger bond with the anions surrounding the site.
4. Substitutions may be limited, even when the size and charge criteria are satisfied, when the competing ions have different electronegativities and form bonds of different ionic character.

Sphalerite and galena both have simple formulae: $M^{2+}S^{2-}$, where M is Zn or Pb, respectively. All metallic trace elements considered here substitute into this M site in both minerals. Thus, as per Goldschmidt's second rule, only metals in the 1+, 2+ or 3+ oxidation state will substitute extensively into the M site. A small number of tetravalent ions may also substitute into sphalerite or galena (e.g., Ge^{4+} in sphalerite; Cook et al., 2015), although such substitutions are likely to involve the creation of lattice vacancies to maintain charge balance.

Chalcopyrite differs from sphalerite and galena in that it is not a fully ionic structure, nor is there consensus on the principal oxidation states

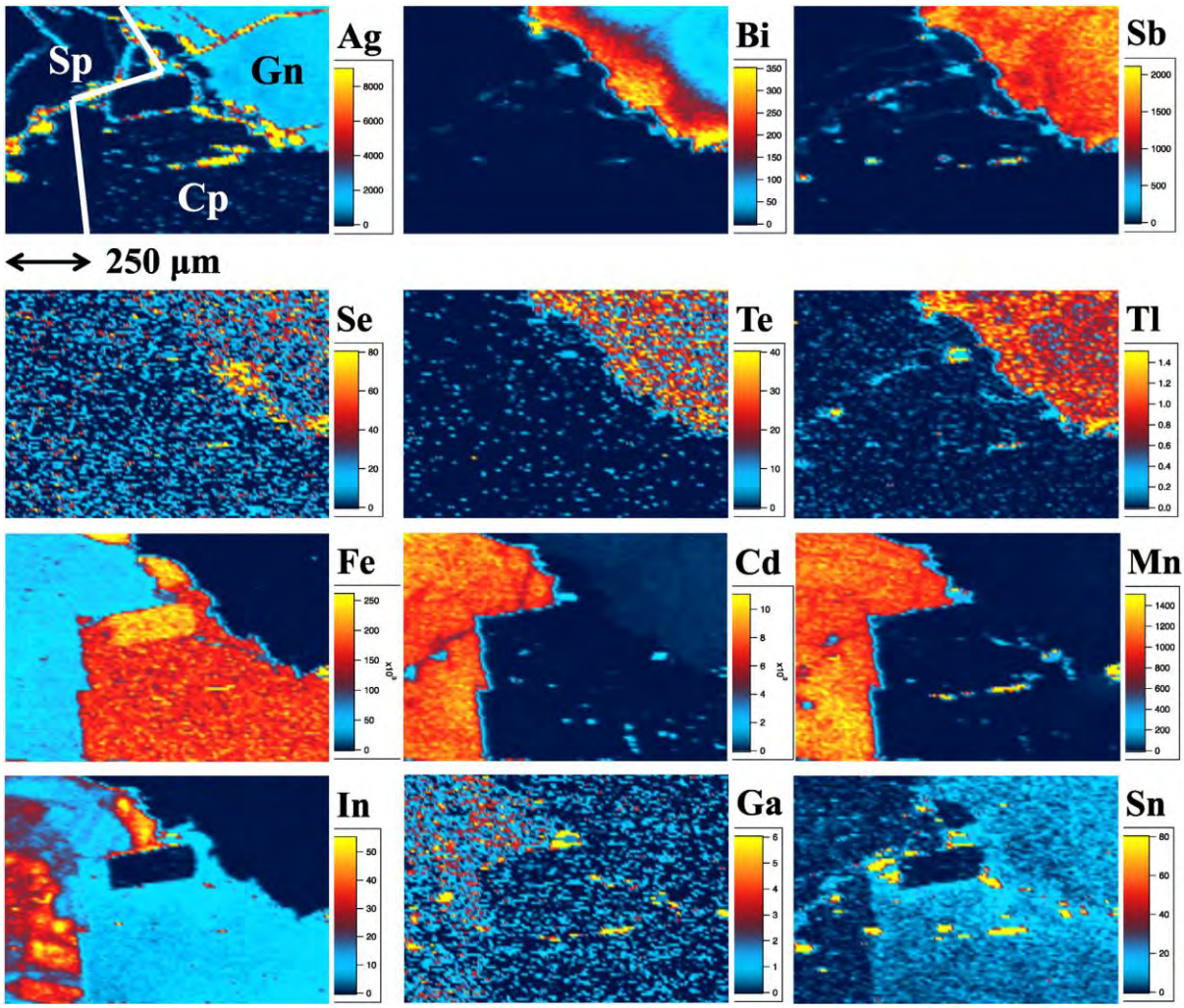

Fig. 5. LA-ICP-MS element maps (Ag, Bi, Sb, Se, Te, Tl, Fe, Cd, Mn, In, Ga, Sn) of an assemblage comprising co-crystallized sphalerite (Sp), galena (Gn) and chalcopyrite (Cp) from the Toroiaga epithermal deposit (sample TOR197). Note preferential concentration of Fe, Cd, Mn, In and Ga in sphalerite, of Ag, Bi, Sb, Se, Te and Tl in galena, and also the modest enrichment of Sn in both chalcopyrite and galena. Concentration scales in parts-per-million (weight).

of its constituents. Hall and Stewart (1973) described stereochemical evidence for a "strong covalently-bonded configuration with an effective ionic state between $Cu^{+}Fe^{3+}S^{2-}{}_{2}$ and $Cu^{2+}Fe^{2+}S^{2-}{}_{2}$". Todd and Sherman (2003), Todd et al. (2003), and Mikhlin et al. (2005) claim that the chemical structure and nominal oxidation states in chalcopyrite are $Cu^{2+}Fe^{2+}S_{2}^{2-}$. This was questioned by Pearce et al. (2006), who presented X-ray absorption spectroscopic (XAS) evidence that the Cu in chalcopyrite is nominally monovalent and that Fe is nominally trivalent; i.e., $Cu^{+}Fe^{3+}S_{2}^{2-}$. Pearce et al. (2006) also note that a nominally divalent character in copper sulphides is very rare, and energy peaks associated with Cu^{2+} can be explained by contamination by Cu^{2+} species. There is continued debate over whether the oxidation state of iron in chalcopyrite varies between Fe^{2+} and Fe^{3+}. Nevertheless, it seems trace element substitution into chalcopyrite is restricted to ions between 1+ and 4+.

For divalent metallic trace elements substituting into either sphalerite or galena, the primary factor affecting substitution is the ionic radius of the trace element and that of the corresponding Zn^{2+} or Pb^{2+} ion respectively. As per Goldschmidt's first rule, extensive substitution will take place if these ionic radii differ by less than approximately 15%. If wholly true however, this first rule seems to exclude most elements, divalent or otherwise, from substituting into either sphalerite or galena (Fig. 9A, B), despite broad evidence that many of these excluded elements are present in solid solution within these sulphides. Thus it can be assumed that at higher temperatures, elements with an ionic radius discrepancy >15% may still be substituted into an ionic lattice; indeed Goldschmidt's first rule does not take temperature into account (Philpotts, 1978).

There are several divalent transition metal ions that have ionic radii similar to Zn^{2+} (0.60 Å) in tetrahedral coordination — as in sphalerite (Fig. 9A). Iron^{2+} (0.63 Å), Mn^{2+} (0.66 Å), Co^{2+} (0.58 Å) and Cu^{2+} (0.57 Å) are within 15% of the Zn^{2+} ionic radius, whereas Cd^{2+} (0.78 Å) is slightly larger than this ±15% 'window'. This provides the basis for the exceptionally high concentrations of Fe, Mn, and Cd that are often measured in sphalerite (e.g., Cook et al., 2009; Ye et al., 2011). Divalent Cu and Co may also be significantly incorporated into sphalerite, although this is usually limited due to the relative rarity of Cu^{2+} in sulphides, and the substitution of Co into Cu-(Fe)-sulphides

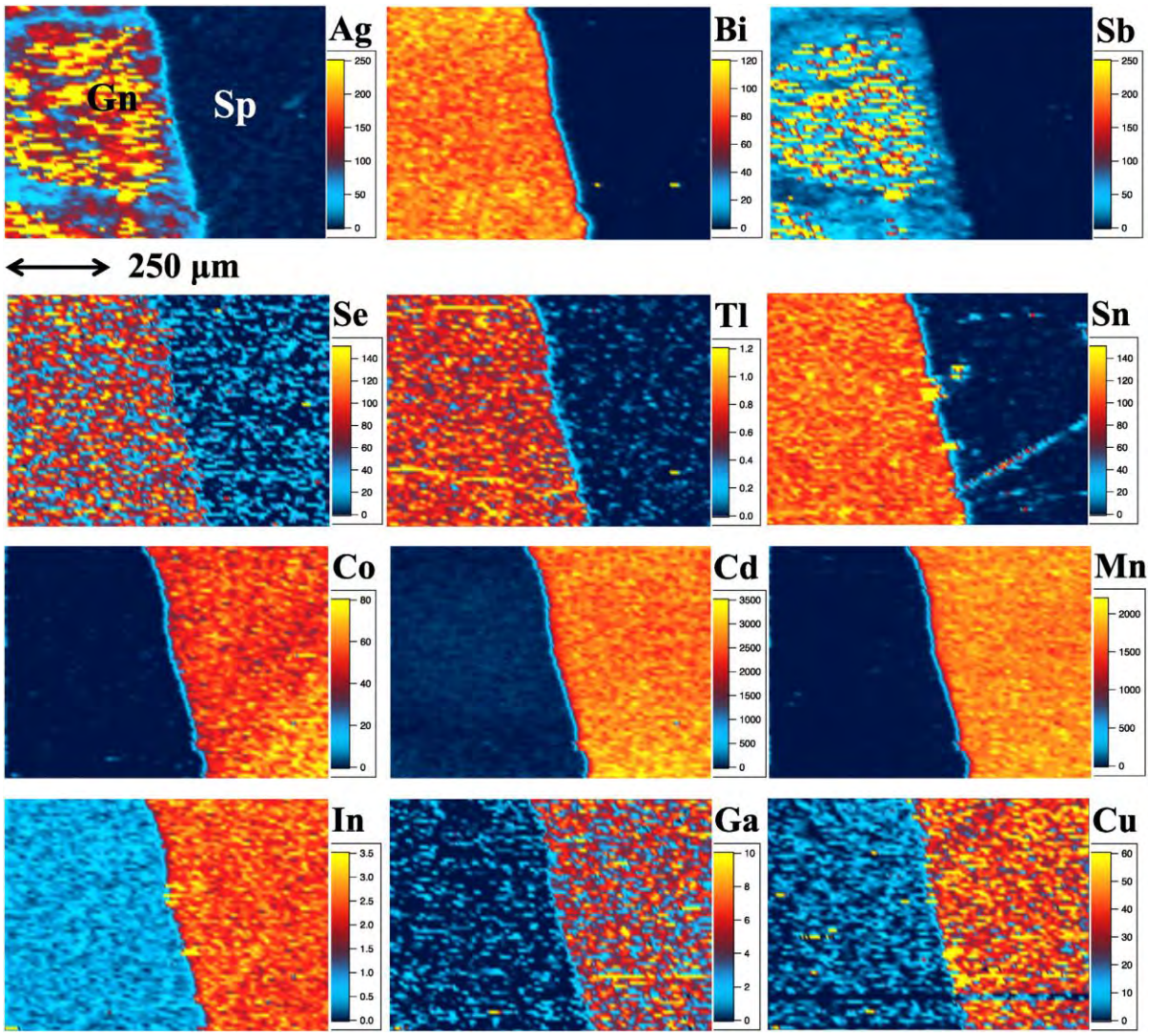

Fig. 6. LA-ICP-MS element maps (Ag, Bi, Sb, Se, Tl, Sn, Co, Cd, Mn, In, Ga, Cu) of an assemblage comprising co-crystallized sphalerite (Sp) and galena (Gn) from the Broken Hill recrystallized SEDEX deposit (sample BH218). Note preferential concentration of Co, Cd, Mn, In, Ga and Cu in sphalerite, of Ag, Bi, Sb, Se, Tl and Sn in galena, and also the modest enrichment of In in galena. Concentration scales in parts-per-million (weight).

and pyrite. Thus the presence or absence of other sulphides may significantly affect the substitution of Co into sphalerite, and this is likely the reason why Co is a Group 3 trace element; having a generally predictable partitioning trend that does not hold on all occasions. In addition, the classification of Co and Cu as a Group 3 trace elements may also reflect the tendency for these elements to be present as micro-inclusions of distinct phases in sphalerite and galena. Due to their favoured incorporation in sphalerite, galena is relatively barren of most divalent cations. However, if sphalerite is not present, or if the total number of divalent cations is greater than the trace element budget that sphalerite can accommodate, some of the surplus may substitute into galena if temperatures are high enough. This likely explains the significant amounts of Cd occasionally measured in galena (e.g., sample TOR191; Table. 3).

For metal ions that differ in charge from the 2+ oxidation state, substitution into sphalerite and galena is governed not only by ionic radius, but also the availability of other ions to participate in coupled substitutions. Fig. 9B clearly shows why galena typically hosts high concentrations of Ag and Bi, as Ag^{+} (1.15 Å) and Bi^{3+} (1.03 Å) are both within 15% of the Pb^{2+} (1.19 Å) ionic radius in octahedral coordination - as in galena. This provides the basis for the well-established coupled substitution $Ag^{+} + (Bi^{3+}, Sb^{3+}) \leftrightarrow 2Pb^{2+}$ which permits substantial incorporation of Ag and Bi into galena (Chutas et al., 2008; Renock and Becker, 2011). Due to its smaller ionic radius, substitution of Sb^{3+} (0.76 Å) tends to occur to a lesser extent than Bi^{3+}. In a similar way, ionic radius constraints restrict significant substitution of As^{3+} (0.58 Å) into galena, except perhaps at very high temperatures and in the absence of Bi and/or Sb. Incorporation of In^{3+} (0.80 Å) via the same coupled substitution together with Ag^{+} is minimal, despite the ionic radius of Pb^{2+} being closer to In^{3+} than Sb^{3+}. This is likely to be due to the preferred substitution of this ion into sphalerite, when that mineral is also present. Fig. 9A illustrates this, with the In^{3+} (0.62 Å) ion within 15% of the Zn^{2+} (0.60 Å) ionic radius in tetrahedral coordination. Similar to In^{3+}, Ga^{3+} (0.47 Å) also substitutes into sphalerite. However, in order for such substitutions to take place,

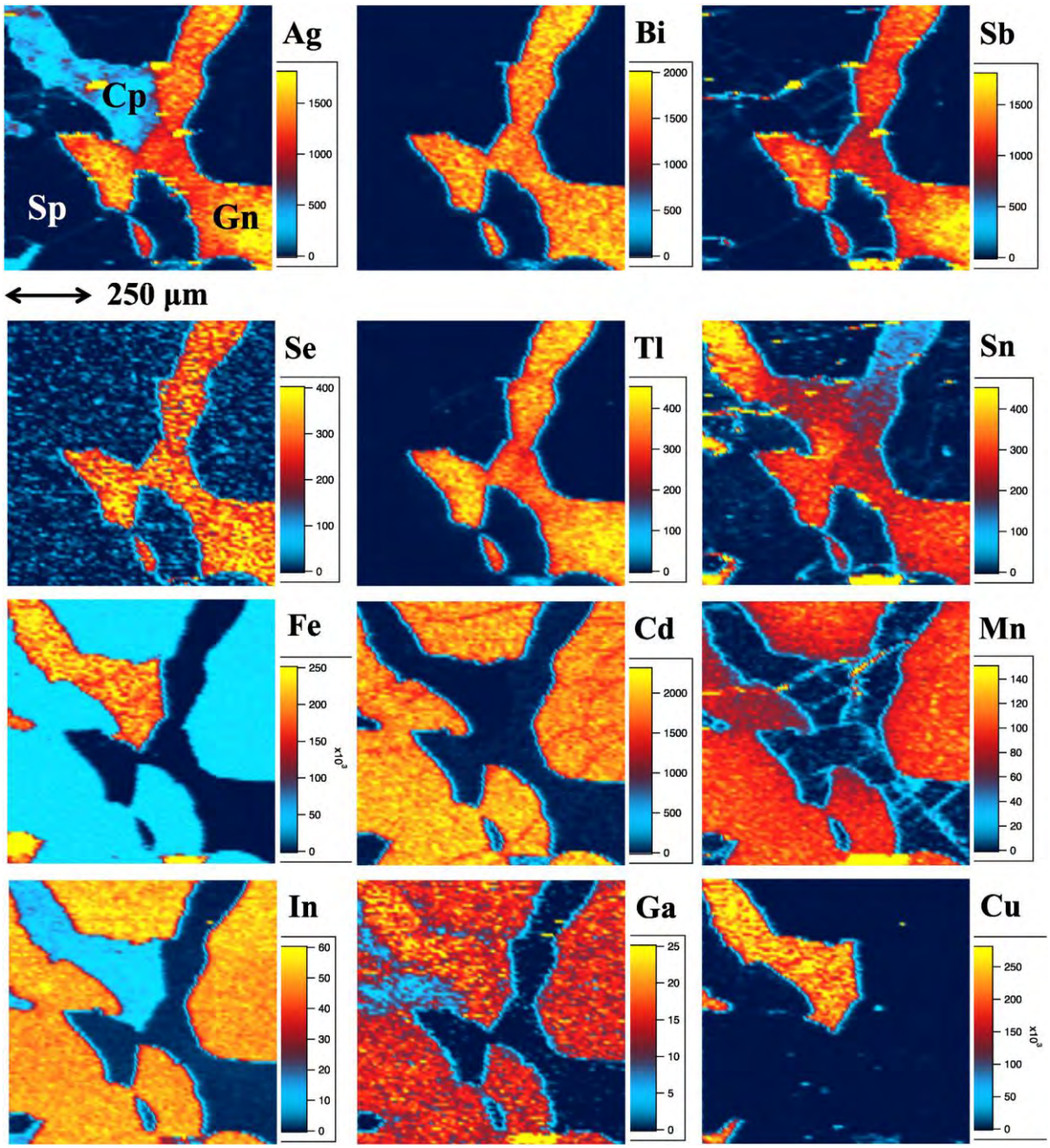

Fig. 7. LA-ICP-MS element maps (Ag, Bi, Sb, Se, Tl, Sn, Fe, Cd, Mn, In, Ga, Cu) of an assemblage comprising co-crystallized sphalerite (Sp), galena (Gn) and chalcopyrite (Cp) from the Bleikvassli recrystallized SEDEX deposit (sample Bv-1). Note preferential concentration of Fe, Cd, Mn and In in sphalerite, of Ag, Bi, Sb, Se and Tl in galena, and of Ga in chalcopyrite. Tin is distributed relatively evenly across galena and chalcopyrite. Modest amounts of Ga are noted in sphalerite, as well as Ag and In in chalcopyrite. Concentration scales in parts-per-million (weight).

a monovalent ion would be necessary to accompany these trivalent ions. Commonly, Cu^{+} (0.60 Å) plays the accompanying role (Cook et al., 2009; Cook et al., 2011b, 2012), as may Ag^{+} (1.00 Å) on rare occasions. In the absence of sphalerite, it can be assumed that In^{3+} could potentially substitute into galena, yet no supportive evidence has been found.

Small amounts of Tl^{+} and Cu^{+} may substitute into galena alongside Ag^{+} in the coupled substitution (Ag^{+}, Cu^{+}, Tl^{+}) + (Bi^{3+}, Sb^{3+}) ↔ $2Pb^{2+}$ (George et al., 2015). Fig. 9B shows that Tl^{+} (1.50 Å) is likely to be preferred over Cu^{+} (0.77 Å) in this substitution as it is closer in ionic radius to Pb^{2+} (1.19 Å) in octahedral coordination. Conversely, the Cu^{+} ion in tetrahedral coordination is much closer to the ionic radius

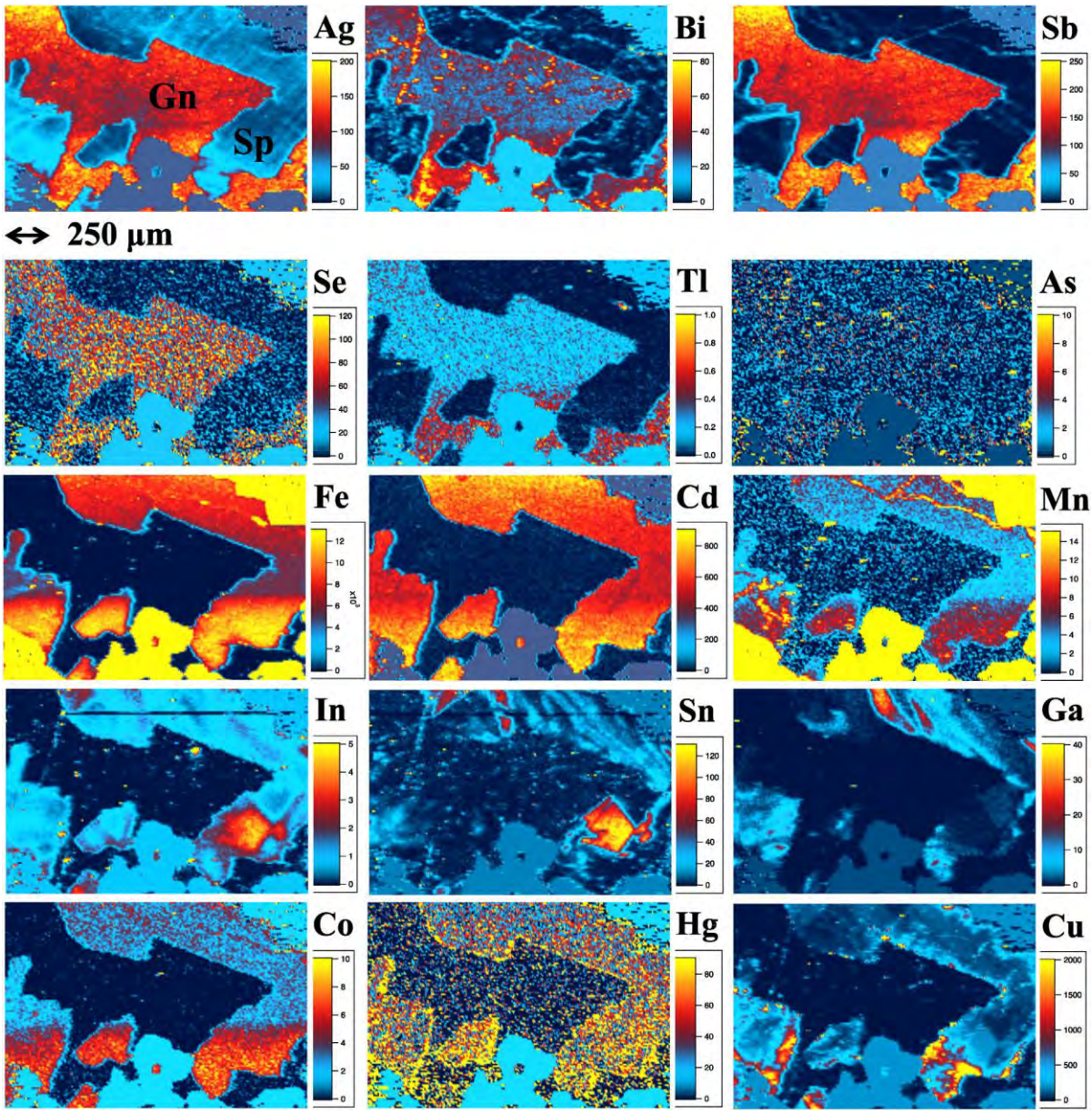

Fig. 8. LA-ICP-MS element maps (Ag, Bi, Sb, Se, Tl, As, Fe, Cd, Mn, In, Sn, Ga, Co, Hg, Cu) of an assemblage comprising co-crystallized sphalerite (Sp) and galena (Gn) from the Kapp Mineral SEDEX deposit (sample Kmi5). Note preferential concentration of Ag, Bi, Sb, Se and Tl in galena, of Fe, Cd, Mn, In, Sn, Ga, Co, Hg and Cu in sphalerite, and also a slight enrichment of As in galena. Concentration scales in parts-per-million (weight).

of Zn^{2+} (Fig. 9A), and as such, would be preferentially incorporated into sphalerite via the coupled substitution $Cu^{+} + X^{3+} \leftrightarrow 2Zn^{2+}$, where trivalent X is commonly In. Higher concentrations of Cu in galena, as occasionally reported, may therefore only occur when In or other trivalent ions are not present to facilitate coupled substitutions into sphalerite, or if sphalerite and other Cu sulphides are absent. Alternately, high Cu values in galena may be the result of substitution of Cu^{2+} directly for Pb^{2+}, however the Cu^{2+} ion would prefer sphalerite, and is generally rare; Cu^{+} is generally preferred in sulphide minerals (e.g., Goh et al., 2006). Only minor amounts of Ag^{+} can be expected in sphalerite due to its preferential incorporation into galena when present.

Since chalcopyrite is not a fully ionic structure, Goldschmidt's rules cannot be readily used to adequately predict partitioning patterns. Nevertheless, some inferences can be made from observed results and the partitioning of trace elements into sphalerite and galena. Compared to both sphalerite and galena, chalcopyrite is a relatively poor trace element carrier. Yet its ability to include trace elements is clearly increased at higher temperatures and/or pressures, where chalcopyrite can host high concentrations of Ga, In, Sn and sometimes Ag (authors as-yet

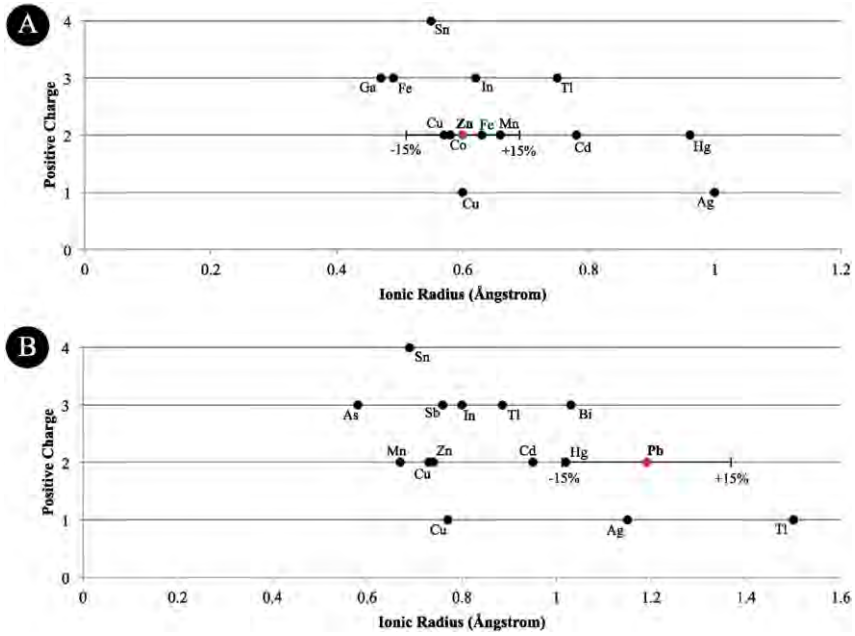

Fig. 9. Plots showing the ionic radius of various trace element ions in: (A) tetrahedral coordination (as in sphalerite) compared to Zn^{2+}; and (B) octahedral coordination (as in galena) compared to Pb^{2+} (data from Shannon, 1976).

unpublished data). Chalcopyrite may also become a more noteworthy trace element host in the absence of sphalerite and/or galena, or other carriers, notably chalcocite and bornite (e.g. chalcopyrite hosts significant Co and In in sample BB55, and Mn in sample Kmi2a in the absence of sphalerite). Despite this however, Harris et al. (1984) report analyses of high Ag-bearing chalcopyrite from two deposits (Izok Lake and Hilton), both of which contain galena.

6.3. Anomalies and exceptions

The authors are unaware of data for the ionic radius of Sn^{2+}, precluding prediction of the partitioning behaviour of this ion from Goldschmidt's rules. Indeed, Shannon (1976) states that it is impossible to define the ionic radius of Sn^{2+} since it varies depending on the degree of distortion of the host compound. In lower temperature (non-recrystallized) ores, sphalerite, galena and chalcopyrite are all primary Sn carriers in different samples. The partitioning behaviour of Sn below recrystallization conditions is thus likely to vary as a function of multiple parameters, whose relative influence differs from case to case. If Sn^{2+} is the typical cation hosted in these sulphides, then its erratic partitioning behaviour may be due to differences in sulphide crystal distortion.

The question remains why Hg is largely absent from galena, while sometimes present within co-crystallized sphalerite, considering that the Hg^{2+} ion falls within 15% of the Pb^{2+} ionic radius in octahedral coordination, while outside 15% of the Zn^{2+} ionic radius in tetrahedral coordination (Fig. 9A, B). Assuming both sphalerite and galena are present, preferential substitution of Hg^{2+} into sphalerite may be aided through direct solid solution with Hg-minerals. Metacinnabar (HgS), tiemannite (HgSe) and coloradoite (HgTe) are fully isostructural with sphalerite and complete solid solution has been reported between ZnS and HgS for example (Kremheller et al., 1960). Thus these minerals may contribute to the somewhat erratic partitioning behaviour of Hg across the sample suite, leading to its classification as a Group 3 trace element.

6.4. Implications

This study presents a tool that may be helpful in determining whether a given BMS assemblage co-crystallized. According to the factors considered here, if the BMS hosts of various trace elements in a given assemblage do not match the typical hosts described here (Table 4), it can then be suggested that the BMS did not co-crystallize. However, if the primary BMS hosts do match the typical hosts described here, then it may be suggestive of a co-crystallized assemblage. If both Ga and Sn, and possibly In, are primarily hosted in chalcopyrite in preference to either sphalerite or galena, then this may indicate that the BMS assemblage has recrystallized. Given the common association of sphalerite, galena and chalcopyrite in different ore types and geological environments (Bowles et al., 2011), the predictive understanding reached in this work has potentially wide application to a range of ore systems.

This tool may prove powerful in assessing co-crystallization of the BMS assemblage in systems with simple geological histories. However in systems that have more complex geological histories (i.e. where mobilization of trace elements occurs after BMS (re-)crystallization), it is conceivable for various trace elements to be hosted by a BMS mineral not normally preferred, even if those BMS co-crystallized. For example, in a limited number of LA-ICP-MS maps from Broken Hill, there is clear evidence that some Ag and Sb, as well as Co, has been leached out of galena and sphalerite respectively. The galena and sphalerite appear zoned as they are depleted in trace elements at grain boundaries and adjacent to fractures (Fig. 10; see also the Ag and Sb maps in Fig. 6). Growth zoning is exceptionally rare in recrystallized deposits due to high temperatures and ample time for grain-scale re-equilibration of trace elements. Thus the zoning in the Broken Hill samples is

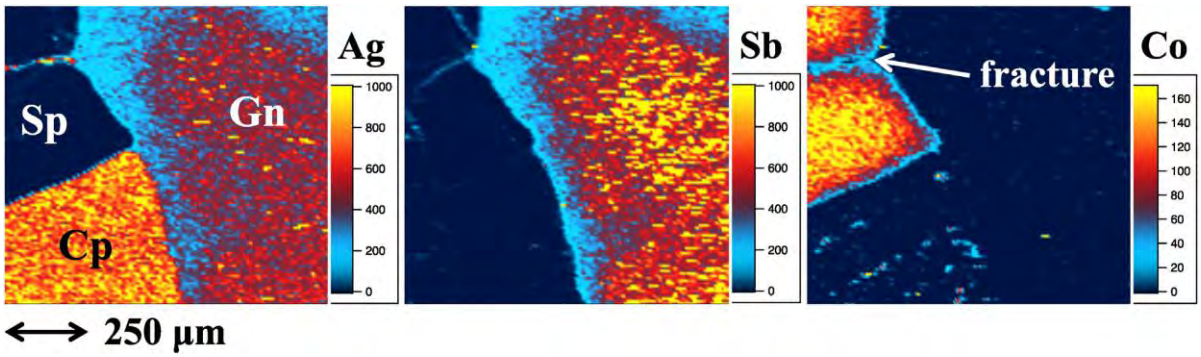

Fig. 10. LA-ICP-MS element maps (Ag, Sb, Co) of an assemblage comprising co-crystallized sphalerite (Sp), galena (Gn) and chalcopyrite (Cp) from the Broken Hill recrystallized SEDEX deposit (sample BH73). Note depletion of Ag and Sb in galena and Co in sphalerite at grain boundaries and adjacent to fracture. Concentration scales in parts-per-million (weight).

interpreted as the result of secondary sub-solidus leaching along grain boundaries and fractures as a result of fluid-rock interaction post re-crystallization. In the Broken Hill samples studied here, the apparent preferred sulphide host of Sb and Co is unchanged, whereas chalcopyrite now hosts more Ag than galena in sample BH73, contrary to what is normally preferred. It is thus apparent that such leaching, diffusion, or analogous sub-solidus processes, may markedly alter the trace element distribution patterns in a given BMS assemblage away from what is preferred during (re-) crystallization. Thus, a BMS assemblage that co-crystallized, but has since had trace elements mobilized and re-distributed within (or even outside) the assemblage, may now have a trace element distribution pattern that suggests the assemblage did not co-crystallize.

Although this work is principally concerned with the preferred BMS hosts for various trace elements rather than specific concentrations of trace elements within those sulphides, the data and interpretations provide an important foundation for future quantification of partitioning coefficients for trace elements in BMS pairs formed at equilibrium. Even if this work suggests that these ratios for many trace elements may not depend so heavily on external factors like temperature and pressure, it is nonetheless feasible that the partitioning of some trace elements between co-crystallizing BMS pairs has potential for quantitative geothermometry.

Various attempts have, in the past, been made to develop functional sulphide geothermometers utilizing trace element concentrations. Examples include using the chemical composition of Ag-rich tetrahedrite solid solutions (Sack, 2000, 2005; Gallego Hernández and Akasaka, 2010), or distributions of Cd and Mn between sphalerite/wurtzite and galena pairs to determine the temperature of ore formation (Bethke and Barton, 1971; Bortnikov et al., 1995). Analogous techniques have been established to calculate conditions of metamorphism using accessory minerals, for example using Ti in zircon or Zr in rutile or titanite (Watson et al., 2006; Ferry and Watson, 2007; Hayden et al., 2008) — methods that also have potential application in ore systems (Ismail et al., 2014).

Although encouraging results were obtained during the development of some trace element sulphide geothermometers, reliable calibration and routine application of such geothermometers was severely limited by the inability, at that time, to precisely quantify trace element concentrations at fine spatial resolutions *in-situ*. The site-specific sampling offered by modern microanalytical techniques opens the door for these approaches to be revitalized, and we would anticipate that useful BMS geothermometers will be developed in the future. Nevertheless, successful application of a geothermometer depends on analysing minerals that have co-crystallized at equilibrium. The identification of co-crystallized minerals can often be difficult and in many cases cannot be unequivocally confirmed and thus must be assumed from textural evidence; a critical problem in calibration of sulphide geothermometers, especially those based on natural samples. Trace element predictability as introduced here can be readily used for assessing co-crystallization of a BMS assemblage, and thus provides significant underpinning for future application of potential BMS geothermometers.

7. Conclusions

- The primary factors controlling the preferred BMS host for Mn, Fe, Co, Cu, Zn, Ga, As, Se, Ag, Cd, In, Sb, Te, Tl and Bi are element oxidation state, ionic radius of the substituting element, element availability and trace element budget of a given sulphide mineral.
- Temperature, pressure, redox conditions and metal source, do not appear to alter the preferred BMS host of Mn, Fe, Co, Cu, Zn, As, Se, Ag, Cd, Sb, Te, Hg, Tl and Bi.
- When sulphide recrystallization takes place at high metamorphic grades (amphibolite facies or above), the preferred BMS host for Ga and Sn usually becomes chalcopyrite. This is distinct from the favoured hosts in lower temperature regimes which, in the case of Ga, is sphalerite. During recrystallization, chalcopyrite may also become the preferred host for In, as distinct from sphalerite at lower temperatures.
- The partitioning behaviour of Sn below recrystallization conditions remains poorly constrained and shows little predictable pattern among the data presented here. Partitioning of Sn is likely to vary as a function of multiple parameters, the relative influence of which differs from case to case.
- Although general partitioning trends are identified for Co, Cu and Hg, these trends are not universally observed.
- Compared to sphalerite and galena, chalcopyrite is typically a poor trace element carrier, and generally only carries significant concentrations of trace elements in the absence of other BMS, or when formed at higher temperatures.
- Secondary leaching, diffusion, or analogous sub-solidus processes, may markedly alter the preferred trace element distribution patterns in a given sulphide assemblage post (re-) crystallization.

Acknowledgements

We are most grateful to the two reviewers, John Bowles and Louis Cabri, whose insight and expertise helped us to improve this manuscript. Laboratory assistance from Ben Wade and Aoife McFadden is also greatly appreciated.

Appendix A. Mean minimum detection limits (99% confidence). Data in ppm (molar).

Locality	Sample/sulfide	Element																
Herja	Hj13	Mn	Fe	Co	Cu	Zn	Ga	As	Se	Ag	Cd	In	Sn	Sb	Te	Hg	Tl	Bi
Romania	Sphalerite (10)	0.11	3.1	0.01	0.13	0.99	0.00	0.06	2.7	0.00	0.06	0.00	0.02	0.01	0.04	0.01	0.00	0.00
	Galena (10)	3.3	76	0.17	4.4	28	0.29	1.8	83	0.12	1.6	0.02	0.66	0.18	1.9	0.05	0.01	0.03
	Chalcopyrite (10)	0.06	1.6	0.00	0.12	0.47	0.00	0.03	1.8	0.00	0.03	0.00	0.01	0.00	–	0.00	0.00	0.00
Toroiaga	TOR191	Mn	Fe	Co	Cu	Zn	Ga	As	Se	Ag	Cd	In	Sn	Sb	Te	Hg	Tl	Bi
Romania	Sphalerite (10)	0.10	2.3	0.01	0.28	0.18	0.01	1.4	0.68	0.00	0.03	0.00	0.02	0.00	0.03	4.8	0.00	0.00
	Galena (10)	4.0	75	0.25	7.3	4.3	0.19	51	6.2	0.14	1.9	0.02	0.49	0.11	–	10	0.01	0.02
	Chalcopyrite (10)	0.07	1.6	0.00	0.27	0.09	0.00	0.84	0.49	0.00	0.02	0.00	0.01	0.00	0.03	4.3	0.00	0.00
	TOR197	Mn	Fe	Co	Cu	Zn	Ga	As	Se	Ag	Cd	In	Sn	Sb	Te	Hg	Tl	Bi
	Sphalerite (10)	0.09	2.0	0.01	0.26	0.18	0.01	1.1	0.71	0.00	0.05	0.00	0.02	0.00	0.03	7.1	0.00	0.00
	Galena (10)	6.2	114	0.43	13	7.5	0.34	–	384	0.16	2.1	0.04	0.91	0.22	0.73	6.5	0.02	0.03
	Chalcopyrite (10)	0.09	1.9	0.01	0.31	0.12	0.01	0.90	0.63	0.00	0.02	0.00	0.02	0.00	0.03	9.4	0.00	0.00
	Emeric2	Mn	Fe	Co	Cu	Zn	Ga	As	Se	Ag	Cd	In	Sn	Sb	Te	Hg	Tl	Bi
	Sphalerite (9)	0.13	3.3	–	0.19	1.8	0.01	0.07	3.5	0.00	0.12	0.00	0.03	0.01	–	0.01	0.00	0.00
	Galena (6)	2.5	63	0.15	4.0	26	0.22	1.5	–	–	1.7	0.02	0.55	0.19	–	0.04	0.01	0.02
	Chalcopyrite (9)	0.19	1.3	–	0.12	2.2	0.01	0.12	4.5	0.00	0.12	0.00	0.02	0.01	–	0.01	0.00	0.00
Baita Bihor	BBH16B	Mn	Fe	Co	Cu	Zn	Ga	As	Se	Ag	Cd	In	Sn	Sb	Te	Hg	Tl	Bi
Romania	Sphalerite (10)	0.09	2.3	0.01	0.14	1.7	0.01	0.05	2.8	0.00	0.09	0.00	0.02	0.01	0.06	0.01	0.00	0.00
	Galena (10)	5.6	136	0.33	7.3	62	0.36	2.0	65	0.16	2.6	0.04	0.72	0.23	–	0.01	0.02	0.04
	BBH20	Mn	Fe	Co	Cu	Zn	Ga	As	Se	Ag	Cd	In	Sn	Sb	Te	Hg	Tl	Bi
	Sphalerite (10)	0.09	2.4	0.01	0.13	1.6	0.01	0.05	2.3	0.00	0.10	0.00	0.02	0.01	0.06	0.01	0.00	0.00
	Galena (10)	3.9	103	0.28	5.2	51	0.21	2.0	102	0.14	2.7	0.03	0.93	0.29	–	0.06	0.02	0.06
	BB55	Mn	Fe	Co	Cu	Zn	Ga	As	Se	Ag	Cd	In	Sn	Sb	Te	Hg	Tl	Bi
	Galena (10)	7.3	178	0.52	11	65	0.37	2.4	82	0.20	2.2	0.06	1.1	0.35	–	0.02	0.02	0.06
	Chalcopyrite (10)	0.06	1.3	0.00	0.13	0.58	0.01	0.04	1.8	0.00	0.04	0.00	0.01	0.00	0.03	0.00	0.00	0.00
	BBH32	Mn	Fe	Co	Cu	Zn	Ga	As	Se	Ag	Cd	In	Sn	Sb	Te	Hg	Tl	Bi
	Sphalerite (10)	0.06	2.3	0.02	0.24	0.13	0.00	0.57	0.43	0.00	0.01	0.00	0.01	0.00	0.02	2.0	0.00	0.00
	Galena (10)	1.8	40	0.11	7.1	3.0	0.13	16	12	0.08	0.68	0.02	0.41	0.20	0.72	18	0.01	0.05
Oravita	ORV4B	Mn	Fe	Co	Cu	Zn	Ga	As	Se	Ag	Cd	In	Sn	Sb	Te	Hg	Tl	Bi
Romania	Sphalerite (10)	0.07	1.4	0.00	0.18	0.16	0.01	0.48	0.45	0.00	0.02	0.00	0.01	0.00	0.02	3.5	0.00	0.00
	Galena (10)	1.2	26	0.07	3.3	1.8	0.07	11	8.1	0.05	0.41	0.01	0.24	0.06	0.33	52	0.01	0.01
	Chalcopyrite (10)	0.08	1.5	0.00	0.28	0.13	0.00	0.52	0.51	0.00	0.02	0.00	0.02	0.00	0.02	5.3	0.00	0.00
Kapp Mineral	Kmi2a	Mn	Fe	Co	Cu	Zn	Ga	As	Se	Ag	Cd	In	Sn	Sb	Te	Hg	Tl	Bi
Norway	Galena (10)	3.9	58	0.35	10	6.9	0.19	12	15	0.10	2.7	0.03	0.50	0.08	–	5.5	0.01	0.02
	Chalcopyrite (10)	0.09	31	0.01	10	0.32	0.01	0.96	0.70	0.10	0.07	0.00	0.03	0.02	0.04	10	0.00	0.00
	Kmi5	Mn	Fe	Co	Cu	Zn	Ga	As	Se	Ag	Cd	In	Sn	Sb	Te	Hg	Tl	Bi
	Sphalerite (10)	0.10	2.1	0.01	0.17	1.8	0.01	0.08	3.3	0.00	0.07	0.00	0.02	0.01	0.05	0.01	0.00	0.00
	Galena (10)	6.6	131	0.48	7.9	60	0.27	2.6	15	0.15	1.4	0.03	0.64	0.31	–	0.01	0.01	0.04
Mt. Isa	5985C1	Mn	Fe	Co	Cu	Zn	Ga	As	Se	Ag	Cd	In	Sn	Sb	Te	Hg	Tl	Bi
Australia	Sphalerite (5)	0.11	3.3	0.01	0.29	0.17	0.01	1.5	0.88	0.00	0.03	0.00	0.03	0.01	0.03	4.6	0.00	0.00
	Galena (4)	5.2	87	0.35	8.0	6.3	0.23	2804	9.2	0.11	1.5	0.03	0.76	0.17	0.71	9.3	0.01	0.03
Bleikvassli	Bv-1	Mn	Fe	Co	Cu	Zn	Ga	As	Se	Ag	Cd	In	Sn	Sb	Te	Hg	Tl	Bi
Norway	Sphalerite (10)	0.09	2.0	0.01	0.12	0.96	0.01	0.11	1.7	0.00	0.06	0.00	0.03	0.01	0.05	0.01	0.00	0.00
	Galena (10)	3.9	80	–	5.4	35	–	3.2	1902	0.14	2.3	0.04	0.90	0.35	–	0.07	0.01	0.06
	Chalcopyrite (5)	0.06	1.2	0.00	0.09	0.52	0.00	0.06	1.0	0.00	0.03	0.00	0.02	0.01	0.03	0.00	0.00	0.00
	V598572	Mn	Fe	Co	Cu	Zn	Ga	As	Se	Ag	Cd	In	Sn	Sb	Te	Hg	Tl	Bi
	Sphalerite (5)	0.13	3.3	0.01	0.22	1.3	0.01	0.24	4.5	0.01	0.07	0.00	0.03	0.01	–	0.01	0.00	0.00
	Galena (10)	2.9	67	0.26	4.1	23	0.15	4.7	52	0.12	1.4	0.03	0.59	0.20	–	0.04	0.01	0.04
	Chalcopyrite (9)	0.06	1.6	0.00	0.14	0.55	0.00	0.09	1.8	0.00	0.03	0.00	0.02	0.01	0.02	0.00	0.00	0.00
Broken Hill	BH73	Mn	Fe	Co	Cu	Zn	Ga	As	Se	Ag	Cd	In	Sn	Sb	Te	Hg	Tl	Bi
Australia	Sphalerite (10)	0.12	3.7	0.01	0.16	1.1	0.01	0.07	2.3	0.00	0.06	0.00	0.03	0.01	0.05	0.01	0.00	0.00
	Galena (10)	3.1	90	0.13	4.2	26	0.15	1.9	34	0.09	1.1	0.03	0.81	0.29	1.2	0.05	0.02	0.07
	Chalcopyrite (5)	0.17	5.3	0.01	0.29	1.5	0.01	0.10	3.2	0.01	0.09	0.00	0.05	0.02	0.10	0.02	0.00	0.00
	BH218	Mn	Fe	Co	Cu	Zn	Ga	As	Se	Ag	Cd	In	Sn	Sb	Te	Hg	Tl	Bi
	Sphalerite (10)	0.10	2.5	0.01	0.14	1.5	0.01	0.07	3.2	0.00	0.09	0.00	0.02	0.01	–	0.01	0.00	0.00
	Galena (10)	3.4	75	0.27	3.9	38	0.24	2.5	162	0.10	2.4	0.02	0.74	0.18	–	0.05	0.01	0.04
Mofjellet	Mo2	Mn	Fe	Co	Cu	Zn	Ga	As	Se	Ag	Cd	In	Sn	Sb	Te	Hg	Tl	Bi
Norway	Sphalerite (10)	0.05	1.1	0.01	0.21	0.16	0.00	0.47	0.39	0.00	0.01	0.00	0.01	0.00	0.02	2.4	0.00	0.00
	Galena (10)	3.2	66	0.24	12	6.5	0.27	31	17	0.15	1.3	0.02	0.61	0.22	0.96	363	0.01	0.05

References

Bajwah, Z., Seccombe, P., Offler, R., 1987. Trace element distribution, Co: Ni ratios and genesis of the Big Cadia iron-copper deposit, New South Wales, Australia. Mineral. Deposita 22, 292–300.

Becker, W., Lutz, H., 1978. Phase studies in the systems CoS–MnS, CoS–ZnS, and CoS–CdS. Mater. Res. Bull. 13, 907–911.

Bethke, P.M., Barton, P.B., 1971. Distribution of some minor elements between coexisting sulphide minerals. Econ. Geol. 66, 140–163.

Bjerkgård, T., Marker, M., Sandstad, J., Cook, N., Sørdahl, T., 2001. Ore potential with emphasis on gold in the Mofjellet deposit, Rana, Nordland, Norway. NGU report.

Blackburn, W.H., Schwendeman, J.F., 1977. Trace-element substitution in galena. Can. Mineral. 15, 365–373.

Borcos, M., Lang, B., Bostinescu, S., Gheorghita, I., 1975. Neogene hydrothermal ore deposits in the volcanic Gutai Mountains, part III. Revue Roumaine de Geologie, Geophysique et Geographie, Serie de Geologie 19, pp. 21–35.

Bortnikov, N., Dobrovol'skaya, M., Genkin, A., Naumov, V., Shapenko, V., 1995. Sphalerite–galena geothermometers; distribution of cadmium, manganese, and the fractionation of sulfur isotopes. Econ. Geol. 90, 155–180.

Bortnikov, N.S., Cabri, L.J., Vikent'ev, I.V., McMahon, G., Bogdanov, Y.A., 2000. Invisible gold in sulfides from recent submarine hydrothermal vents. Dokl. Earth Sci. 373, 863–866.

Bowles, J.F.W., Howie, R.A., Vaughan, D.J., Zussman, J., 2011. Rock-forming Minerals: non-silicates: oxides, hydroxides and sulphides. Geol. Soc. Lond.

Brill, B., 1989. Trace-element contents and partitioning of elements in ore minerals from the CSA Cu–Pb–Zn deposit, Australia. Can. Mineral. 27, 263–274.

Bryndzia, L.T., Scott, S.D., Spry, P.G., 1990. Sphalerite and hexagonal pyrrhotite geobarometer; correction in calibration and application. Econ. Geol. 85, 408–411.

Cabri, L.J., 1992. The distribution of trace precious metals in minerals and mineral products. The 23rd Hallimond Lecture. Mineral. Mag. 56, 298–308.

Cabri, L.J., Campbell, J.L., Laflamme, J.G., Leigh, R.G., Maxwell, J.A., Scott, J.D., 1985. Proton-microprobe analysis of trace elements in sulphides from some massive-sulphide deposits. Can. Mineral. 23, 133–148.

Cabri, L.J., McMahon, G., Bortnikov, N.S., Vikentiev, I.V., Bogdanov, Y.A., 2000. SIMS gold analyses of sea floor sulfide minerals. In: Benninghoven, A., Bertrand, P., Migeon, H.-N., Werner, H.W. (Eds.), SIMS XII, Proceedings, 12th International Conference on Secondary Ion Mass Spectrometry, Brussels, Belgium. Elsevier, pp. 1019–1022.

Chen, W.W., Zhang, J.M., Ardell, A.J., Dunn, B., 1988. Solid-state phase equilibria in the ZnS–CdS system. Mater. Res. Bull. 23, 1667–1673.

Chutas, N.I., Kress, V.C., Ghiorso, M.S., Sack, R.O., 2008. A solution model for high-temperature PbS–$AgSbS_2$–$AgBiS_2$ galena. Am. Mineral. 93, 1630–1640.

Ciobanu, C.L., Cook, N.J., Stein, H., 2002. Regional setting and geochronology of the Late Cretaceous banatitic magmatic and metallogenetic belt. Mineral. Deposita 37, 541–567.

Ciobanu, C.L., Cook, N.J., Kelson, C.R., Guerin, R., Kalleske, N., Danyushevsky, L., 2013. Trace element heterogeneity in molybdenite fingerprints stages of mineralization. Chem. Geol. 347, 175–189.

Ciobanu, C.L., Brugger, J., Cook, N.J., Mills, S.J., Elliott, P., Damian, G., Damian, F., 2014. Graţianite, $MnBi_2S_4$, a new mineral from the Băiţa Bihor skarn, Romania. Am. Mineral. 99, 1163–1170.

Cioflica, G., Vlad, S., 1981. Cupriferous mineralization at Ciclova. An Univ Bucuresti Ser Geol 30, 1–17.

Cioflica, G., Vlad, S., Stoici, S., 1971. Repartition de la mineralisation dans les skarns de Baita Bihorului. Revue Roumaine de Geologie, Geophysique et Geographie, Serie de Geologie 15, pp. 43–58.

Cioflica, G., Vlad, S., Volanschi, E., Stoici, S., 1977. Magnesian skarns and associated mineralization at Baita Bihor. St. Cerc. Geol. Geofiz. Geogr. Ser. Geol 22, 39–57.

Cioflica, G., Jude, R., Lupulescu, M., Simon, G., Damian, G., 1995. New data on the Bi-minerals from the mineralizations related to Paleocene magmatites in Romania. Romanian J. Mineral. 76, 9–23.

Cioflica, G., Lupulescu, M., Shimizu, M., 1997. Bismuth minerals from the Baita Bihor and Valisor–Tincova mines: new compositional data. Romanian J. Mineral. 78, 13–14.

Constantinescu, E., Ilinca, G., Ilinca, A., 1988. Laramian hydrothermal alteration and ore deposition in the Oravita-Ciclova area. Southwestern Banat. DS Inst Geol Geofiz 72-73, 13–26.

Cook, N.J., 1993. Conditions of metamorphism estimated from alteration lithologies and ore at the Bleikvassli Zn–Pb–(Cu) deposit, Nordland, Norway. Nor. Geol. Tidsskr. 73, 226–233.

Cook, N.J., 1997. Bismuth and bismuth-antimony sulphosalts from Neogene vein mineralisation, Baia Borsa area, Maramures, Romania. Mineral. Mag. 61, 387–409.

Cook, N.J., 2001. Ore mineralogical investigation of the Mofjell deposit (Mo i Rana, Nordland, Norway) with emphasis on gold and silver distribution. Norges Geologiske Undersokelse Report.

Cook, N.J., Ciobanu, C.L., 2003. Cervelleite, Ag_4TeS, from three localities in Romania, substitution of Cu, and the occurrence of the associated phase, Ag_2Cu_2TeS. Neues Jahrb. Mineral. Monatshefte 321–336.

Cook, N.J., Damian, G.S., 1997. New data on "plumosite" and other sulphosalt minerals from the Herja hydrothermal vein deposit, Baia Mare district, Rumania. Geol. Carpath. 48, 387–399.

Cook, N.J., Spry, P.G., Vokes, F.M., 1998. Mineralogy and textural relationships among sulphosalts and related minerals in the Bleikvassli Zn–Pb–(Cu) deposit, Nordland, Norway. Mineral. Deposita 34, 35–56.

Cook, N.J., Ciobanu, C.L., Pring, A., Skinner, W., Shimizu, M., Danyushevsky, L., Saini-Eidukat, B., Melcher, F., 2009. Trace and minor elements in sphalerite: A LA-ICPMS study. Geochim. Cosmochim. Acta 73, 4761–4791.

Cook, N.J., Ciobanu, C.L., Danyushevsky, L.V., Gilbert, S., 2011a. Minor and trace elements in bornite and associated Cu–(Fe)-sulphides: A LA-ICP-MS study. Geochim. Cosmochim. Acta 75, 6473–6496.

Cook, N.J., Sundblad, K., Valkama, M., Nygård, R., Ciobanu, C.L., Danyushevsky, L., 2011b. Indium mineralisation in A-type granites in southeastern Finland: insights into mineralogy and partitioning between coexisting minerals. Chem. Geol. 284, 62–73.

Cook, N.J., Ciobanu, C.L., Brugger, J., Etschmann, B., Howard, D.L., de Jonge, M.D., Ryan, C., Paterson, D., 2012. Determination of the oxidation state of Cu in substituted Cu–In–Fe-bearing sphalerite via μ-XANES spectroscopy. Am. Mineral. 97, 476–479.

Cook, N.J., Etschmann, B., Ciobanu, C.L., Geraki, K., Howard, D., Williams, T., Rae, N., Pring, A., Chen, G., Johannessen, B., Brugger, J., 2015. Distribution and Substitution Mechanism of Ge in a Ge–(Fe)-Bearing Sphalerite. Minerals 5, 117–132.

Craig, J.R., Kullerud, G., 1968. Phase relations and mineral assemblages in the copper-lead-sulfur system. Am. Mineral. 53, 145–161.

Dare, S.A., Barnes, S.-J., Prichard, H.M., Fisher, P.C., 2011. Chalcophile and platinum-group element (PGE) concentrations in the sulfide minerals from the McCreedy East deposit, Sudbury, Canada, and the origin of PGE in pyrite. Mineral. Deposita 46, 381–407.

Emslie, D., Beukes, G., 1981. Minor-and trace-element distribution in sphalerite and galena from the Otavi Mountainland, South West Africa. Ann. Geol. Surv. Republic of South Africa 15, 11–28.

Ferry, J., Watson, E., 2007. New thermodynamic models and revised calibrations for the Ti-in-zircon and Zr-in-rutile thermometers. Contrib. Mineral. Petrol. 154, 429–437.

Flood, B., 1967. Sulphide mineralizations within the Hecla Hoek complex in Vestspitsbergen and Bjørnøya. Norsk Polarinstitutt Årbok, pp. 109–127.

Foord, E.E., Shawe, D.R., 1989. The Pb–Bi–Ag–Cu–(Hg) chemistry of galena and some associated sulfosalts: a review and some new data from Colorado, California and Pennsylvania. Can. Mineral. 27, 363–382.

Frost, B.R., Mavrogenes, J.A., Tomkins, A.G., 2002. Partial melting of sulphide ore deposits during medium-and high-grade metamorphism. Can. Mineral. 40, 1–18.

Frost, B.R., Swapp, S.M., Gregory, R.W., 2005. Prolonged existence of sulphide melt in the Broken Hill orebody, New South Wales, Australia. Can. Mineral. 43, 479–493.

Gallego Hernández, A.N., Akasaka, M., 2010. Ag-rich Tetrahedrite in the El Zancudo Deposit, Colombia: Occurrence, Chemical Compositions and Genetic Temperatures. Resour. Geol. 60, 218–233.

George, L., Cook, N.J., Ciobanu, C.L., Wade, B., 2015. Trace and minor elements in galena: A reconnaissance LA-ICP-MS study. Am. Mineral. 100, 548–569.

Gheorghitescu, D., 1975. Mineralogical and geochemical study of formations in the thermal, metasomatic contact at Oravita (Cosovita). DS Inst Geol Geofiz 61, 59–103.

Goh, S.W., Buckley, A.N., Lamb, R.N., Rosenberg, R.A., Moran, D., 2006. The oxidation states of copper and iron in mineral sulphides, and the oxides formed on initial exposure of chalcopyrite and bornite to air. Geochim. Cosmochim. Acta 70, 2210–2228.

Goldschmidt, V.M., 1954. Geochemistry. Soil Sci. 78, 156.

Gotz, A., Damian, G., Farbas, N., 1990. Contributii la mineralogia bournonitul associat mineralizatiilor din masivul Toroiaga-Baia Borsa. Rev. Mineral. 41, 467–471.

Hall, S.R., Stewart, J.M., 1973. The crystal structure refinement of chalcopyrite, $CuFeS_2$. Acta Crystallogr. 29, 579–585.

Hannan, K.W., Golding, S.D., Herbert, H.K., Krouse, H.R., 1993. Contrasting alteration assemblages in metabasites from Mount Isa, Queensland; implications for copper ore genesis. Econ. Geol. 88, 1135–1175.

Harris, D.C., Cabri, L.J., Nobiling, R., 1984. Silver-bearing chalcopyrite, a principal source of silver in the Izok Lake massive-sulphide deposit; confirmation by electron- and proton-microprobe analyses. Can. Mineral. 22, 493–498.

Hayden, L.A., Watson, E.B., Wark, D.A., 2008. A thermobarometer for sphene (titanite). Contrib. Mineral. Petrol. 155, 529–540.

Haydon, R.C., McConachy, G.W., 1987. The stratigraphic setting of Pb–Zn–Ag mineralization at Broken Hill. Econ. Geol. 82, 826–856.

Holwell, D., McDonald, I., 2010. A review of the behaviour of platinum group elements within natural magmatic sulphide ore systems. Platin. Met. Rev. 54, 26–36.

Huston, D.L., Sie, S.H., Suter, G.F., Cooke, D.R., Both, R.A., 1995. Trace elements in sulphide minerals from eastern Australian volcanic-hosted massive sulphide deposits; Part I, Proton microprobe analyses of pyrite, chalcopyrite, and sphalerite, and Part II, Selenium levels in pyrite; comparison with delta 34 S values and implications for the source of sulfur in volcanogenic hydrothermal systems. Econ. Geol. 90, 1167–1196.

Ilinca, G., Makovicky, E., Topa, D., Zagler, G., 2012. Cuproneyite, $Cu_7Pb_{27}Bi_{25}S_{68}$, a new mineral species from Baita Bihor, Romania. Can. Mineral. 50, 353–370.

Ismail, R., Ciobanu, C.L., Cook, N.J., Teale, G.S., Giles, D., Schmidt Mumm, A., Wade, B., 2014. Rare earths and other trace elements in minerals from skarn assemblages, Hillside iron oxide–copper–gold deposit, Yorke Peninsula, South Australia. Lithos 184, 456–477.

Johan, Z., 1988. Indium and germanium in the structure of sphalerite: an example of coupled substitution with copper. Mineral. Petrol. 39, 211–229.

Katona, I., Pascal, M.-L., Fonteilles, M., Verkaeren, J., 2003. The melilite (Gh_{50}) skarns of Oraviţa, Banat, Romania: transition to gehlenite (Gh_{85}) and to vesuvianite. Can. Mineral. 41, 1255–1270.

Kojima, S., Sugaki, A., 1984. Phase relations in the central portion of the Cu–Fe–Zn–S system between 800° and 500 °C. Mineral. J. 12, 15–28.

Kojima, S., Sugaki, A., 1985. Phase relations in the Cu–Fe–Zn–S system between 500 degrees and 300 degrees C under hydrothermal conditions. Econ. Geol. 80, 158–171.

Krämer, V., Hirth, H., Hofherr, M., Trah, H.-P., 1987. Phase studies in the systems Ag_2Te–Ga_2Te_3, ZnSe–In_2Se_3 and ZnS–Ga_2S_3. Thermochim. Acta 112, 88–94.

Kremheller, A., Levine, A.K., Gashurov, G., 1960. Hydrothermal preparation of two-component solid solutions from II–VI compounds. J. Electrochem. Soc. 107, 12–15.

Lang, B., 1979. The base metals-gold hydrothermal ore deposits of Baia Mare, Romania. Econ. Geol. 74, 1336–1351.

Large, R.R., Bull, S.W., McGoldrick, P.J., Derrick, G., Carr, G., Walters, S., 2005. Stratiform and strata-bound Zn–Pb–Ag + Cu deposits of the Proterozoic sedimentary basins of northern Australia. Economic Geology 100th Anniversary Volume, pp. 931–963.

Larocque, A.C.L., Jackman, J.A., Cabri, L.J., Hodgson, C.J., 1995. Calibration and analysis of Ag in pyrite and chalcopyrite by Secondary Ion Mass Spectrometry (SIMS) and preliminary results from the Mobrun VMS deposit, Rouyn-Noranda, Quebec. Can. Mineral. 33, 361–372.

Lepetit, P., Bente, K., Doering, T., Luckhaus, S., 2003. Crystal chemistry of Fe-containing sphalerites. Phys. Chem. Miner. 30, 185–191.

Leyh, W.R., Conor, C.H., 2000. Stratigraphically controlled metallogenic zonation associated with the regional redox boundary of the Willyama Supergroup—economic implications for the southern Curnamona Province. Mesa J. 16, 39–47.

Liu, H., Chang, L.L.Y., 1994. Phase relations in the system PbS–PbSe–PbTe. Mineral. Mag. 58, 567–578.

Lockington, J., Cook, N.J., Ciobanu, C.L., 2014. Trace and minor elements in sphalerite from metamorphosed sulphide deposits. Mineral. Petrol. 108, 873–890.

Lottermoser, B., 1989. Rare earth element study of exhalites within the Willyama Supergroup, Broken Hill Block, Australia. Mineral. Deposita 24, 92–99.

Marincea, Ş., Dumitraş, D.-G., Ghineţ, C., Fransolet, A.-M., Hatert, F., Rondeaux, M., 2011. Gehlenite from three occurrences of high-temperature skarns, Romania: new mineralogical data. Can. Mineral. 49, 1001–1014.

Mathias, B., Clark, G., 1975. Mount Isa copper and silver-lead-zinc orebodies—Isa and Hilton mines. Econ. Geol. Australia Papua New Guinea 1, 351–372.

Mavrogenes, J., MacIntosh, I., Ellis, D., 2001. Partial melting of the Broken Hill galena–sphalerite ore: experimental studies in the system PbS–FeS–ZnS–(Ag_2S). Econ. Geol. 96, 205–210.

McIntyre, N.S., Cabri, L.J., Chauvin, W.J., Laflamme, J.H.G., 1984. Secondary ion mass spectrometric study of dissolved silver and indium in sulfide minerals. Scan. Electron Microsc. 3, 1139–1146.
Mikhlin, Y., Tomashevich, Y., Tauson, V., Vyalikh, D., Molodtsov, S., Szargan, R., 2005. A comparative X-ray absorption near-edge structure study of bornite, Cu_5FeS_4, and chalcopyrite, $CuFeS_2$. J. Electron Spectrosc. Relat. Phenom. 142, 83–88.
Moggi-Cecchi, V., Cipriani, C., Rossi, P., Ceccato, D., Rudello, V., Somacal, H., 2002. Trace element contents and distribution maps of chalcopyrite: a micro-PIXE study. Periodico di Mineralogia 71, 101–109.
Müller, W., Shelley, M., Miller, P., Broude, S., 2009. Initial performance metrics of a new custom-designed ArF excimer LA-ICPMS system coupled to a two-volume laser-ablation cell. J. Anal. At. Spectrom. 24, 209–214.
Neubauer, F., Lips, A., Kouzmanov, K., Lexa, J., Ivascanu, P., 2005. Subduction, slab detachment and mineralization: the Neogene in the Apuseni Mountains and Carpathians. Ore Geol. Rev. 27, 13–44.
Painter, M.G., Golding, S.D., Hannan, K.W., Neudert, M.K., 1999. Sedimentologic, petrographic, and sulfur isotope constraints on fine-grained pyrite formation at Mount Isa Mine and environs, Northwest Queensland, Australia. Econ. Geol. 94, 883–912.
Parr, J., Plimer, I., 1993. Models for Broken Hill-type lead-zinc-silver deposits: mineral deposit modeling. Geol. Assoc. Can. Spec. Pap. 40, 253–288.
Pearce, C.I., Pattrick, R.A.D., Vaughan, D.J., Henderson, C.M.B., Van der Laan, G., 2006. Copper oxidation state in chalcopyrite: Mixed Cu d^9 d^{10} characteristics. Geochim. Cosmochim. Acta 70, 4635–4642.
Perkins, W., 1997. Mount Isa lead-zinc orebodies: replacement lodes in a zoned syndeformational copper-lead-zinc system? Ore Geol. Rev. 12, 61–110.
Phillips, G.N., 1981. Water activity changes across an amphibolite-granulite facies transition, Broken Hill, Australia. Contrib. Mineral. Petrol. 75, 377–386.
Philpotts, J.A., 1978. The law of constant rejection. Geochim. Cosmochim. Acta 42, 909–920.
Plimer, I., 2007. The world's largest Zn–Pb–Ag deposit: a re-evaluation of Broken Hill (Australia). Mineral deposits: digging deeper. Irish Association for Economic Geology, Dublin, pp. 1239–1242.
Qian, Z., 1987. Trace elements in galena and sphalerite and their geochemical significance in distinguishing the genetic types of Pb–Zn ore deposits. Chin. J. Geochem. 6, 177–190.
Renock, D., Becker, U., 2011. A first principles study of coupled substitution in galena. Ore Geol. Rev. 42, 71–83.
Ringwood, A., 1955. The principles governing trace element distribution during magmatic crystallization Part I: the influence of electronegativity. Geochim. Cosmochim. Acta 7, 189–202.
Rosenberg, J., Spry, P., Jacobson, C., Cook, N., Vokes, F., 1998. Thermobarometry of the Bleikvassli Zn–Pb–(Cu) deposit, Nordland, Norway. Mineral. Deposita 34, 19–34.
Rosenberg, J., Spry, P., Jacobson, C., Vokes, F., 2000. The effects of sulfidation and oxidation during metamorphism on compositionally varied rocks adjacent to the Bleikvassli Zn–Pb–(Cu) deposit, Nordland, Norway. Mineral. Deposita 35, 714–726.
Rubenach, M.J., 1992. Proterozoic low-pressure/high-temperature metamorphism and an anticlockwise P–T–t path for the Hazeldene area, Mount Isa Inlier, Queensland, Australia. J. Metamorph. Geol. 10, 333–346.
Saager, R., 1967. Drei Typen von Kieslagerstätten im Mofjell-Gebiet, Nordland und ein neuer Vorschlag zur Gliederung der Kaledonischen Kieslager Norwegens. Nor. Geol. Tidsskr. 8, 68–73.
Sack, R.O., 2000. Internally consistent database for sulphides and sulfosalts in the system Ag_2S–Cu_2S–ZnS–Sb_2S_3–As_2S_3. Geochim. Cosmochim. Acta 64, 3803–3812.
Sack, R.O., 2005. Internally consistent database for sulphides and sulfosalts in the system Ag_2S-Cu_2S-ZnS-FeS-Sb_2S_3-As_2S_3: update. Geochim. Cosmochim. Acta 69, 1157–1164.
Shannon, R., 1976. Revised effective ionic radii and systematic studies of interatomic distances in halides and chalcogenides. Acta Crystallogr. Sect. A: Cryst. Phys., Diffr., Theor. Gen. Crystallogr. 32, 751–767.
Shimizu, M., Cioflica, G., Lupulescu, M., 1995. Ore mineralogy of Romanian deposits. Part I. Stanija and Baita Bihor, Apuseni Mountains and Tincova-Valisor, Banat (SW Carpathians), Romania. Japanese Mag. Mineral. Petrol. Sci. 45, 280–281.
Sombuthawee, C., Bonsall, S., Hummel, F., 1978. Phase equilibria in the systems ZnS–MnS, ZnS–$CuInS_2$, and MnS–$CuInS_2$. J. Solid State Chem. 25, 391–399.
Spry, P.G., Plimer, I.R., Teale, G.S., 2008. Did the giant Broken Hill (Australia) Zn–Pb–Ag deposit melt? Ore Geol. Rev. 34, 223–241.
Szöke, A., Steclaci, L., 1962. Regiunea Toroiaga, Baia-Borsa: studiu geologic, petrografic, mineralogic si geochimic. Editura Academiei Republicii Populare Romine.
Todd, E.C., Sherman, D.M., 2003. Surface oxidation of chalcocite (Cu_2S) under aqueous (pH = 2–11) and ambient atmospheric conditions: mineralogy from Cu L-and O K-edge X-ray absorption spectroscopy. Am. Mineral. 88, 1652–1656.
Todd, E., Sherman, D., Purton, J., 2003. Surface oxidation of chalcopyrite ($CuFeS_2$) under ambient atmospheric and aqueous (pH 2–10) conditions: Cu, Fe L-and O K-edge X-ray spectroscopy. Geochim. Cosmochim. Acta 67, 2137–2146.
Van Achterbergh, E., Ryan, C., Jackson, S., Griffin, W., 2001. Data reduction software for LA-ICP-MS: Laser-Ablation-ICPMS in the earth sciences—principles and applications. Minerealogical Association of Canada (short course series) 29, pp. 239–243.
Vokes, F.M., 1963. Geological studies on the Caledonian Pyritic Zinc-Lead Orebody at Bleikvassli, Norland. Universitetsforlaget, Norway.
Vokes, F.M., 1966. On the possible modes of origin of the Caledonian sulphide ore deposit at Bleikvassli, Nordland, Norway. Econ. Geol. 61, 1130–1139.
von Cotta, B., 1864. Erzlagerstätten im Banat und in Serbien. Braumüller.
Watson, E., Wark, D., Thomas, J., 2006. Crystallization thermometers for zircon and rutile. Contrib. Mineral. Petrol. 151, 413–433.
Wilson, S., Ridley, W., Koenig, A., 2002. Development of sulphide calibration standards for the laser ablation inductively-coupled plasma mass spectrometry technique. J. Anal. At. Spectrom. 17, 406–409.
Ye, L., Cook, N.J., Ciobanu, C.L., Yuping, L., Qian, Z., Tiegeng, L., Wei, G., Yulong, Y., Danyushevskiy, L., 2011. Trace and minor elements in sphalerite from base metal deposits in South China: a LA-ICPMS study. Ore Geol. Rev. 39, 188–217.

CHAPTER 5

TRACE ELEMENTS IN HYDROTHERMAL CHALCOPYRITE

Luke L. George[1], Nigel J. Cook[2], Bryony B. P. Crowe[1], Cristiana, L. Ciobanu[2]

[1]*School of Physical Sciences, The University of Adelaide, Adelaide, S.A., 5005, Australia*

[2]*School of Chemical Engineering, The University of Adelaide, Adelaide, S.A., 5005, Australia*

Paper submitted for publication in Mineralogical Magazine 30 June 2016

Accepted 28 March 2017

Statement of Authorship

Title of Paper	Trace elements in hydrothermal chalcopyrite
Publication Status	☐ Published ☒ Accepted for Publication ☐ Submitted for Publication ☐ Unpublished and Unsubmitted w ork w ritten in manuscript style
Publication Details	George, L. L., Cook, N. J., Crowe, B. B. P., Ciobanu, C. L., 2017. Trace elements in hydrothermal chalcopyrite. Mineralogical Magazine (accepted for publication at time of thesis submission).

Principal Author

Name of Principal Author (Candidate)	Luke George		
Contribution to the Paper	Performed analytical work, carried out data processing and interpretation, oversaw development of work and wrote manuscript.		
Overall percentage (%)	85		
Certification:	This paper reports on original research I conducted during the period of my Higher Degree by Research candidature and is not subject to any obligations or contractual agreements with a third party that would constrain its inclusion in this thesis. I am the primary author of this paper.		
Signature		Date	28 March 2017

Co-Author Contributions

By signing the Statement of Authorship, each author certifies that:

i. the candidate's stated contribution to the publication is accurate (as detailed above);

ii. permission is granted for the candidate to include the publication in the thesis; and

iii. the sum of all co-author contributions is equal to 100% less the candidate's stated contribution.

Name of Co-Author	Nigel Cook		
Contribution to the Paper	Helped define direction of research, provided sample material, supervised development of work, assisted with data interpretation and contributed to manuscript preparation.		
Overall percentage (%)	5		
Signature		Date	20 March 2017

Name of Co-Author	Bryony Crowe		
Contribution to the Paper	Conducted part of the literature review, performed preliminary analysis.		
Overall percentage (%)	5		
Signature		Date	27 March 2017

Name of Co-Author	Cristiana Ciobanu		
Contribution to the Paper	Provided sample material, contributed to manuscript preparation.		
Overall percentage (%)	5		
Signature		Date	20 March 2017

ABSTRACT

Concentration data are reported for 18 trace elements in chalcopyrite from a suite of 53 samples from 15 different ore deposits obtained by laser-ablation inductively-coupled plasma-mass spectrometry. Chalcopyrite is demonstrated to host a wide range of trace elements including Mn, Co, Zn, Ga, Se, Ag, Cd, In, Sn, Sb, Hg, Tl, Pb and Bi. The concentration of some of these elements can be high (hundreds to thousands of ppm) but most are typically tens to hundreds of ppm. The ability of chalcopyrite to host trace elements generally increases in the absence of other co-crystallizing sulphides. In deposits in which the sulphide assemblage recrystallized during syn-metamorphic deformation, the concentrations of Sn and Ga in chalcopyrite will generally increase in the presence of co-recrystallizing sphalerite and/or galena, suggesting that chalcopyrite is the preferred host at higher temperatures and/or pressures. Trace element concentrations in chalcopyrite typically show little variation at the sample scale, yet there is potential for significant variation between samples from any individual deposit. The Zn:Cd ratio in chalcopyrite shows some evidence of a systematic variation across the dataset, which depends, at least in part, on temperature of crystallization. Under constant physiochemical conditions the Cd:Zn ratios in co-crystallizing chalcopyrite and sphalerite are often approximately equal. Any distinct difference in the Cd:Zn ratios in the two minerals, and/or a non-constant Cd:Zn ratio in chalcopyrite, may be an indication of varying physiochemical conditions during crystallization.

Chalcopyrite is generally a poor host for most elements considered harmful or unwanted in the smelting of Cu, suggesting it is rarely a significant contributor to the overall content of such elements in copper concentrates. The exceptions are Se and Hg which may be

sufficiently enriched in chalcopyrite to exceed statutory limits and thus incur monetary penalties from a smelter.

5.1 Introduction

Chalcopyrite is the principal ore mineral of copper (Geoscience Australia, 2015). Concentrates produced from chalcopyrite-rich ores may also be significantly enriched in other elements. Silver is one such element and is commonly extracted as an economic by-product during copper smelting and refining (Ayres et al., 2002). Other elements, including As, Sb, Hg, Bi and Se, may become enriched in copper concentrates during ore processing and can, if present at high enough concentrations, result in substantial financial penalties when sold on the world market (e.g., Fountain, 2013). Yet despite the importance of chalcopyrite in the minerals industry, there is a relative lack of understanding as to the different trace elements chalcopyrite can accommodate into its structure, as well as the ranges of concentration of these elements.

Detailed studies addressing trace element concentrations in chalcopyrite are relatively scarce when compared to other common sulphide minerals, notably pyrite (e.g., Huston et al., 1995; Large et al., 2009; Winderbaum et al., 2012; Belousov et al., 2016), or sphalerite and galena (e.g., Bethke and Barton, 1971; Blackburn and Schwendeman, 1977; Johan, 1988; Foord and Shawe, 1989; Cook et al., 2009; George et al., 2015). Much of the published data for chalcopyrite (e.g., Harris et al., 1984; Cabri et al., 1985; Kase, 1987; Brill, 1989; Huston et al., 1996; Scott et al., 2001; Moggi-Cecchi et al., 2002; Serranti et al., 2002; Shalaby et al., 2004; Demir et al., 2008; Layton-Matthews et al., 2008; Monteiro et al., 2008; Demir et al., 2013; Gena et al., 2013; Reich et al., 2013; Cioacă et al., 2014; Helmy et al., 2014; Wang et al., 2015a; Wohlgemuth-Ueberwasser et al., 2015; Sadati et al., 2016) is focused on a limited

suite of trace elements, and often the minimum detection limits of the microanalytical techniques used are too high to truly establish trace element diversity and concentration levels.

More work is thus necessary to establish the ability of chalcopyrite to host trace elements in a wide range of environments and settings. With this goal in mind, we used laser-ablation inductively-coupled plasma mass spectrometry (LA-ICP-MS) to report the concentration ranges of 18 trace elements (elements typically present at concentrations < 1 wt. %) in natural hydrothermal chalcopyrite from a diverse suite of 53 samples from different ore types, settings and environments, and physiochemical conditions of ore formation. The trace element chemistry of chalcopyrite in deposits of magmatic origin is not part of this study. A number of studies on the topic have been published, enabling a sound understanding of trace element partitioning in chalcopyrite-bearing magmatic ores (e.g., Barnes et al., 2006; Holwell and McDonald, 2007; Godel and Barnes, 2008; Dare et al., 2010; Djon and Barnes, 2012; Piña et al., 2012; Prichard et al., 2013; Chen et al., 2014; Duran et al., 2015; Barnes and Ripley, 2016; Smith et al., 2016). The LA-ICP-MS technique offers both sub-part-per-million level precision for many heavier elements and micrometer-scale spatial resolution. LA-ICP-MS may also reveal the presence of micro-inclusions within the analyzed spot since if they are large enough and heterogeneously distributed, they are recognizable on time-resolved downhole spectra (e.g., George et al., 2015). The dataset reveals chalcopyrite to be an important trace element carrier in many ore deposits. Our data carries implications for both ore genesis and mineral processing. We also show that the Cd:Zn ratio in chalcopyrite (and co-existing sphalerite) may assist in determining if physiochemical conditions remained constant during base metal sulphide crystallization.

5.2 Background

5.2.1 Chalcopyrite crystal structure

Chalcopyrite crystallizes in a body-centred tetragonal lattice system with tetrahedrally-coordinated Cu, Fe and S atoms. Both Cu and Fe are ordered into the cation sites. Pauling and Brockway (1932) regarded the bonding between atoms in the chalcopyrite structure as effectively covalent with valencies of Cu and Fe atoms fluctuating between monovalent-divalent, and divalent-trivalent, respectively. The strong covalent nature of chalcopyrite was also affirmed by Donnay et al. (1958). Hall and Stewart (1973) likewise argued for a strong covalent configuration with an effective ionic state between $Cu^{+}Fe^{3+}S_2^{2-}$ and $Cu^{2+}Fe^{2+}S_2^{2-}$. Nevertheless, for the sake of convenience, chalcopyrite is usually represented with ions of specific valencies, i.e. $Cu^{+}Fe^{3+}S_2^{2-}$.

Despite this, Todd and Sherman (2003), Todd et al. (2003) and Mikhlin et al. (2005) have argued, on the basis of X-ray absorption spectroscopy (XAS) and X-ray absorption near-edge structure (XANES) spectra, that the nominal valencies in chalcopyrite should be $Cu^{2+}Fe^{2+}S_2^{2-}$. This was rejected by Pearce et al. (2006), who affirmed that Cu in chalcopyrite is nominally monovalent, and that Fe is nominally trivalent. Nominally divalent character in copper sulphides is very rare, and energy peaks associated with Cu^{2+} can be explained by contamination by Cu^{2+} species. Li et al. (2013) confirmed that evidence for the presence of Cu^{2+} and Fe^{2+} has been largely discredited, but emphasises that the actual valence state of chalcopyrite should be understood as intermediate between $Cu^{+}Fe^{3+}S_2^{2-}$ and $Cu^{2+}Fe^{2+}S_2^{2-}$ due to covalent bonding.

5.2.2 Previous trace element data

A number of previous studies addressed the composition of natural chalcopyrite, yet most of these had purposes other than to establish if chalcopyrite is a good host for trace elements. Kase (1987), Brill (1989), Scott et al. (2001), Serranti et al. (2002), Shalaby et al. (2004), Demir et al. (2008), Layton-Matthews et al. (2008), Monteiro et al. (2008), Demir et al. (2013), Gena et al. (2013), Cioacă et al. (2014), Helmy et al. (2014), Wang et al. (2015a) and Sadati et al. (2016) report on chalcopyrite from various locations. However, in each case, only electron probe microanalysis (EPMA) is used to determine chalcopyrite composition. With minimum detection limits in the order of hundreds of ppm unless exceptionally long count times are used, EPMA is not an adequate technique for determining many trace element abundances. Harris et al. (1984), Cabri et al. (1985), Huston et al. (1996) and Moggi-Cecchi et al. (2002) used proton microprobe, Reich et al. (2013) used secondary ion mass spectrometry (SIMS) and Wohlgemuth-Ueberwasser et al. (2015) used LA-ICP-MS to investigate chalcopyrite from different localities. While these analytical techniques boast minimum detection limits significantly lower than EPMA, none of these studies reported data for more than six elements. The elements reported are typically common trace constituents, so few inferences about the presence of other trace elements could be drawn. Chalcopyrite compositions were determined by Bajwah et al. (1987), Butler and Nesbitt (1999) and Ulrich et al. (2002) by atomic absorption spectroscopy (AAS), solution ICP-MS and ICP optical emission spectrometry (OES), respectively. These techniques remain bulk methods and so are limited in their ability to determine lattice bound trace constituents with confidence. Other studies such as Subba Rao and Naqvi (1997), McClenaghan et al. (2009), Cook et al. (2011) and Maydagan et al. (2013) only measured chalcopyrite in a limited number of samples (maximum of four), as they primarily focused on characterizing the chemistry of complex

phase assemblages. The different emphasis of such studies highlights the need for a more detailed investigation of a larger, more diverse sample suite, considering a wider range of potential trace elements, and utilizing an analytical technique with low minimum detection limits. We acknowledge that the spectrum of elements analyzed in chalcopyrite has been somewhat restricted by the availability of appropriate matrix-matched standards, particularly with respect to some chalcophile semi-metals, and thus data quality remains, to this day, better for some elements than for others (e.g., Se, As, Au).

Despite their limitations, the prior studies cited above, and indeed other more thorough investigations of chalcopyrite composition (e.g., Huston et al., 1995; Maslennikov et al., 2009; Revan et al., 2014; Wang et al., 2015b; George et al., 2016), provide a valuable background for understanding chalcopyrite as a trace element carrier and serve as a broad foundation for the present study. The maximum reported concentrations of various trace elements in chalcopyrite from different deposit types is summarized in Table 5.1.

Silver is the trace element most frequently reported in chalcopyrite. Shalaby et al. (2004) described unusual green chalcopyrite from the Um Samiuki volcanogenic massive sulphide (VMS) deposit, Egypt, hosting up to 4.3 wt. % Ag. More typically, concentrations are in the tens to hundreds of ppm range, although sometimes reaching into the thousands, for example from the Izok Lake Zn-Cu-Pb deposit, N.W.T, Canada (Harris et al., 1984), the Kidd Creek mine, ON, Canada (Cabri et al., 1985), the Bottino Mine, Italy (Moggi-Cecchi et al., 2002), and Mantos Blancos, northern Chile (Reich et al., 2013).

Experiments in the Cu-Fe-Zn-S system have revealed that chalcopyrite may dissolve up to 0.9 at. % *zinc* at 500 ºC, 0.8 at. % at 400 ºC and 0.6 at. % at 300 ºC (Kojima and Sugaki, 1985). Indeed Huston et al. (1995) measured Zn in chalcopyrite from Australian volcanic-hosted massive sulphide (VHMS) deposits at concentrations from below the minimum detection limit up to as much as 5 wt. %. They concluded that concentrations up to 2,000

Table 5.1: Maximum reported trace element contents chalcopyrite by deposit type as reported in the literature

Deposit Type	Mn	Co	Ni	Zn	Ga	As	Se	Ag	Cd
Epithermal	43 ppm (George et al., 2016)	3.3 ppm (George et al., 2016)	-	1.6 wt. % (Demir et al., 2008)	1.3 ppm (George et al., 2016)	0.73 ppm (George et al., 2016)	300 ppm (Moggi-Cecchi et al., 2002)	630 ppm (Moggi-Cecchi et al., 2002)	24 ppm (George et al., 2016)
Skarn	540 ppm (Bajwah et al., 1987)	7,500 ppm (Bajwah et al., 1987)	925 ppm (Bajwah et al., 1987)	1.83 wt. % (Helmy et al., 2014)	0.23 ppm (George et al., 2016)	0.54 ppm (George et al., 2016)	538 ppm (Cook et al., 2011)	0.3 wt. % (Helmy et al., 2014)	25 ppm (Bajwah et al., 1987)
Porphyry	0.02 wt. % (Maydagan et al., 2013)	249 ppm (Cioaca et al., 2014)	9 ppm (Maydagan et al., 2013)	0.22 wt. % (Maydagan et al., 2013)	-	0.05 wt. % (Maydagan et al., 2013)	0.03 wt. % (Rubin and Kyle, 1997)	0.05 wt. % (Maydagan et al., 2013)	0.55 ppm (Maydagan et al., 2013)
Exhalative	642 ppm (Revan et al., 2014)	40 ppm (Maslennikov et al., 2009)	3.2 ppm (Maslennikov et al., 2009)	810 ppm (Huston et al., 1995)	0.13 ppm (George et al., 2016)	282 ppm (Maslennikov et al., 2009)	0.46 wt. % (Cabri et al., 1985)	0.19 wt. % (Cabri et al., 1985)	10 ppm (Huston et al., 1995)
Recrystallized Exhalative	196 ppm (George et al., 2016)	2,720 ppm (Thole, 1976)	3,300 ppm (Thole, 1976)	1.86 wt. % (Shalaby et al., 2004)	16 ppm (George et al., 2016)	2,000 ppm (Huston et al., 1995)	480 ppm (Serranti et al., 2002)	4.3 wt. % (Shalaby et al., 2004)	77 ppm (Serranti et al., 2002)

Deposit Type	In	Sn	Sb	Te	Au	Hg	Tl	Pb	Bi
Epithermal	14 ppm (George et al., 2016)	2.3 wt. % (Kase, 1987)	4.2 ppm (George et al., 2016)	0.04 ppm (George et al., 2016)	-	95 ppm (George et al., 2016)	0.01 ppm (George et al., 2016)	630 ppm (Moggi-Cecchi et al., 2002)	0.05 ppm (George et al., 2016)
Skarn	2,214 ppm (Andersen et al., 2016)	47 ppm (George et al., 2016)	0.28 ppm (George et al., 2016)	6.6 ppm (Cook et al., 2011)	0.2 ppm (Cook et al., 2011)	2.9 ppm (George et al., 2016)	0.03 ppm (Cook et al., 2011)	175 ppm (Bajwah et al., 1987)	37.9 ppm (Cook et al., 2011)
Porphyry	-	122 ppm (Maydagan et al., 2013)	0.1 wt. % (Maydagan et al., 2013)	306 ppm (Cioaca et al., 2014)	0.05 ppm (Maydagan et al., 2013)	-	-	0.17 wt. % (Maydagan et al., 2013)	0.53 ppm (Maydagan et al., 2013)
Exhalative	1,119 ppm (Cabri et al., 1985)	1,345 ppm (Cabri et al., 1985)	488 ppm (Maslennikov et al., 2009)	7,447 ppm (Maslennikov et al., 2009)	7.73 ppm (Maslennikov et al., 2009)	32 ppm (George et al., 2016)	1 ppm (Maslennikov et al., 2009)	2,943 ppm (Maslennikov et al., 2009)	1,353 ppm (Maslennikov et al., 2009)
Recrystallized Exhalative	100 ppm (Huston et al., 1995)	2,940 ppm (Huston et al., 1995)	31 ppm (McClenaghan et al., 2009)	0.05 ppm (George et al., 2016)	0.16 ppm (McClenaghan et al., 2009)	2.3 ppm (McClenaghan et al., 2009)	0.14 ppm (George et al., 2016)	287 ppm (Ulrich et al., 2002)	0.07 ppm (McClenaghan et al., 2009)

Only anomalous reports that have obviously been influenced by micro-inlusions are excluded. Other reports may still be influenced by micro-inclusions.

Literature review is thorough, though not exhaustive.

ppm probably reflect Zn in solid solution (substituted for Fe), but that concentrations exceeding 2,000 ppm Zn are likely the result of micro-inclusions of sphalerite. Moggi-Cecchi et al. (2002) also concluded that high Zn distributions in chalcopyrite from Italian and Slovak deposits are predominantly related to micro-scale inclusions of Zn-bearing phases. Nevertheless, high Zn values of 1.86 wt. %, 1.83 wt. %, 1.73 wt. % and 1.64 wt. % have been measured in chalcopyrite by Shalaby et al. (2004), Helmy et al. (2014), Serranti et al. (2002) and Wang et al. (2015a), respectively, and have not been attributed, in any case, to inclusion related Zn.

Huston et al. (1995) measured *arsenic* in chalcopyrite from Australian VHMS deposits into the thousands of ppm. These high concentrations of As could not be readily attributed to micro-inclusions of distinct As-bearing phases and so they concluded that As can substitute into the chalcopyrite lattice up to about 2,000 ppm. Scott et al. (2001) and Wang et al. (2015a) reported chalcopyrite containing up to 1,600 ppm As from Woodlawn, N.S.W., Australia, and the Xiaozhen Cu deposit, Shaanxi Province, China, respectively.

Bethke and Barton (1971) showed that chalcopyrite could accommodate as much as 0.5 mol. % eskebornite ($CuFeSe_2$) at 390 ^oC, and thus may be a significant host of *selenium*. Cabri et al. (1985) reported as much as 0.46 wt. % Se in chalcopyrite from Kidd Creek, Ontario, while Monteiro et al. (2008) and Wang et al. (2015a) each recorded over 2,000 ppm Se in chalcopyrite from Xiaozhen, China, and Sossego, Brazil, respectively.

Exceptional reports of *cobalt* and *nickel* in chalcopyrite suggest that the Cu-sulphide may, on rare occasions, be a good host for Co and Ni. Bajwah et al. (1987) documented chalcopyrite from Big Cadia, N.S.W., Australia, which hosted up to 7,500 ppm Co and 925 ppm Ni. Thole (1976) recorded up to 2,700 ppm Co and 3,300 ppm Ni in chalcopyrite from the Shamrocke mine, Zimbabwe. Wang et al. (2015a) measured up to 1,700 ppm Co and 4,100 ppm Ni in chalcopyrite from the Xiaozhen Cu deposit, Shaanxi Province, China, while

Wang et al. (2015b) also reported chalcopyrite containing 6,178 ppm Co and 2,496 ppm Ni from the Shilu Fe-Co-Cu ore district in the Hainan Province of South China.

Lead concentrations in chalcopyrite are uncommonly reported in the thousands of ppm, though such high concentrations are likely the result of micro-inclusions of Pb bearing phases, frequently galena. Among such anomalous reports are 7,054 ppm Pb in chalcopyrite from Yaman-Kasy, Russia (Maslennikov et al., 2009), and 0.34 wt. % Pb in chalcopyrite from the Xiaozhen Cu deposit, Shaanxi Province, China (Wang et al., 2015a). Maximum reported Pb concentrations in chalcopyrite are ordinarily in the hundreds of ppm (e.g., Bajwah et al., 1987; Moggi-Cecchi et al., 2002).

High levels of *bismuth* and *tellurium* are measured in chalcopyrite from active seafloor hydrothermal systems. Gena et al. (2013) recorded up to 0.32 wt. % Bi in chalcopyrite associated with bismuthinite from the Tiger sulphide chimney, Southern Okinawa Trough, Japan, while 45 ppm Te was measured in chalcopyrite from the Broken Spur vent field by Butler and Nesbitt (1999). Nevertheless, chalcopyrite is generally a poor host of both elements with reported concentrations from ore deposits rarely exceeding 10 ppm (e.g., Maydagan et al., 2013; George et al., 2016).

Chalcopyrite may contain up to a few ppm *gold* at most. Synthetic experiments carried out by Simon et al. (2000) showed that up to 16 ppm Au is soluble in chalcopyrite at 500 ^{o}C, dropping to 4 ppm at 400 ^{o}C. Reports of chalcopyrite hosting hundreds of even thousands of ppm Au are almost certainly related to Au-bearing mineral inclusions (e.g., Maslennikov et al., 2009). Nevertheless some studies have reported tens of ppm Au in chalcopyrite (e.g., Revan et al., 2014).

Although there are some rare reports of thousands of ppm *antimony* and *cadmium* in chalcopyrite (e.g., Revan et al., 2014), concentrations rarely reach into the hundreds of ppm. Monteiro et al. (2008) measured up to 330 ppm Sb in chalcopyrite from the Sossego IOCG

deposit, Brazil, and up to 77 ppm Cd have been reported from Arinteiro, Galicia, Spain (Serranti et al., 2002).

Over 2.3 wt. % *tin* has been measured in chalcopyrite from the Izumo vein, Toyoha mine, Japan (Kase, 1987), and from a sulphide chimney in an active seafloor hydrothermal system (Gena et al., 2013). Both studies attributed the Sn to solid solution. Huston et al. (1995) measured up to 2,940 ppm Sn in chalcopyrite from the Dry River South VHMS deposit, Eastern Australia, and inferred that Sn substitutes for Fe. They noted that the highest Sn concentrations occur in the more reduced and highly metamorphosed deposits, which is a reflection of the tendency of Sn to only be transported in significant quantities at reduced, high temperature conditions (Eugster, 1986). George et al. (2016) confirmed that in deposits that have recrystallized at amphibolite facies and above, chalcopyrite will typically host more Sn than co-crystallizing sphalerite or galena.

Reports of high levels of *manganese* in chalcopyrite originate from VMS deposits. Revan et al. (2014) reported chalcopyrite containing up to 958 ppm Mn from VMS deposits of the eastern Pontide orogenic belt, NE Turkey, while Maslennikov et al. (2009) measured up to 771 ppm Mn in chalcopyrite from the Yaman-Kasy VMS deposit, Southern Urals, Russia.

Chalcopyrite is isostructural with roquesite ($CuInS_2$) and thus significant concentrations of *indium* can be hosted in chalcopyrite, most likely in the Fe site (Wittmann, 1974). In the SW England ore region, chalcopyrite accounts for the majority of the In budget (locally containing up to 2,200 ppm) despite sphalerite and stannite group minerals typically hosting higher concentrations (Andersen et al., 2016). Cabri et al. (1985) reported chalcopyrite from the Kidd Creek deposit, Canada, carrying as much as 1,119 ppm In, while Kieft and Damman (1990) measured up to 0.9 wt. % In in chalcopyrite from the Gåsborn area, West Bergslagen, Sweden.

Reports of *gallium, mercury* and *thallium* in chalcopyrite are rare and concentrations are almost exclusively in the order of a few ppm (e.g., Maslennikov et al., 2009; McClenaghan et al., 2009; Cook et al., 2011). Revan et al. (2014) did, however, report chalcopyrite containing up to hundreds of ppm Tl.

5.2.3 Sample suite

Fifty-three samples were analysed from 15 different deposits in Australia, Bulgaria, Norway, Romania, Serbia and Uzbekistan (Table 5.2). The selected deposits are from a variety of different ore types including epithermal, skarn, porphyry, VMS, and sedimentary exhalative (SEDEX) systems. Some VMS and SEDEX sulphide ores have been recrystallized due to regional metamorphism and deformation.

Seven samples came from the Romanian epithermal systems Herja and Toroiaga; an additional sample was added from the Kochbulak epithermal deposit in Uzbekistan. Six samples originated from the Romanian skarn deposits, Baita Bihor and Oravita. The Bulgarian porphyry deposits of Assarel and Elatsite contributed five samples, and another porphyry sample came from Bor (Serbia). The undeformed Vorta VMS deposit, Romania, and SEDEX Kapp Mineral prospect, Norway, contributed one sample each. SEDEX deposits in which the sulphide assemblages recrystallized during regional metamorphism and deformation (recrystallized SEDEX) contributed eight samples; two from Broken Hill, Australia, and six from Bleikvassli and Mofjell in Norway. Twelve samples came from the Norwegian VMS deposit Sulitjelma, in which the sulphide assemblages also recrystallized during metamorphism and deformation (recrystallized VMS). Finally, eleven samples were added from the Kanmantoo deposit, South Australia, interpreted as a metamorphosed,

remobilised syngenetic sulphide ore. Brief descriptions of these deposits are provided as Electronic Appendix A, together with key references for each.

Table 5.2: Summary of deposits and samples used in this study

Deposit/Type	Samples	Conditions of formation or metamorphism	References
Herja, Romania Epithermal *(Neogene)*	Hj13	Formed at ~<200 °C	Lang (1979); Cook and Damian (1997)
Toroiaga, Romania Epithermal *(Neogene)*	Emeric2	Formed at ~350 °C	Szöke and Steclaci (1962); Gotz et al. (1990)
	T1a		
	TOR189		
	TOR191		
	TOR197		
	Toroiaga R0		
Kochbulak, Uzbekistan Epithermal *(Late Paleozoic)*	33	Formed at 200-400 °C	Kovalenker et al. (1997); Islamov et al. (1999); Plotinskaya et al. (2006)
Baita Bihor, Romania Skarn Antoniu orepipe - proximal Marta orepipe - distal *(Cretaceous)*	BB55 (Antoniu)	Formed at ~500 °C (proximal), ~375 °C (distal)	Cioflica et al. (1971, 1977); Shimizu et al. (1995); Ciobanu et al. (2002)
	BBH15-21 (Antoniu)		
Oravita, Romania Skarn *(Cretaceous)*	ORV1	-	Gheorghiţescu (1975); Cioflica and Vlad (1981); Constantinescu et al. (1988)
	ORV4		
	ORV4a		
	ORV4B		
Assarel, Bulgaria Porphyry *(Cretaceous)*	ASR 5A	Base metal sulphides formed at 300-150 °C	Strashimirov (1993); Popov et al. (2000); Strashimirov et al. (2002)
	ASR 10		
	ASR KB P12077		
Bor, Serbia Porphyry *(Cretaceous)*	BOR14	-	Janković (1990); Janković et al. (1998)
Elatsite, Bulgaria Porphyry *(Cretaceous)*	Elatsite b a	Various assemblages deposited at 190-575 °C	Dragov and Petrunov (1996); Georgiev (2008)
	ELS 157		

Vorta, Romania VMS *(Jurassic)*	DMV 99-22	Formed at 250-300 °C	Ciobanu et al. (2001)
Kapp Mineral, Norway SEDEX *(Late Precambrian?)*	Kmi 2a	Very weakly metamorphosed	Flood (1967)
Broken Hill, Australia Recrystallized SEDEX *(Proterozoic)*	BH73 BH218	Granulite facies (750-800 °C, 5-6 kbar)	Haydon and McConachy (1987); Parr and Plimer (1993); Plimer (2007); Spry et al. (2008)
Bleikvassli, Norway Recrystallized SEDEX *(Ordovician)*	Bv-1 Bv-4 V598572	Upper amphibolite-lower granulite facies (570 °C, 7.5-8 kbar)	Vokes (1963; 1966); Cook et al. (1998)
Mofjell, Norway Recrystallized SEDEX *(Paleozoic)*	Mo5 Mo16 Mo17A	Amphibolite facies (550 °C, 7 kbar?)	Saager (1967); Cook (2001)
Sulitjelma, Norway Recrystallized VMS *(Ordovician)*	CV01.1 CV01.2a CV01.2b CV01.3 CV01.4 CV01.6b NC4172 NC5839 NC6894 Su3 Sulis 1b Sulis2a	Lower amphibolite facies (450-500 °C)	Cook et al. (1990; 1993); Cook (1992; 1994; 1996); Barrie et al. (2010)
Kanmantoo, Australia Metamorphosed, remobilised syngenetic sulphide ore *(Cambrian)*	KTDD086(8) KTDD086(9) KTDD086(11) KTDD086(12) KTDD178(7) KTDD178(8) KTDD178(12) KTDD180(3) KTDD180(7) KTDD180S(4) KTDD180S(5)	Amphibolite facies (530-630 °C, 2.2-5.4 kbar)	Jensen and Whittle (1969); Verwoerd and Cleghorn (1975); Seccombe et al. (1985); Both et al. (1995); Spry et al. (2010)

Abbreviations: VMS = volcanogenic massive sulphide, SEDEX = sedimentary exhalative

5.3 Experimental methods

Each sample was prepared as a polished block and characterized by reflected light microscopy and backscattered electron (BSE) imaging prior to LA-ICP-MS analysis. Only areas of chalcopyrite grains free of noticeable inclusions were selected for LA-ICP-MS analysis.

LA-ICP-MS analysis was carried out using a Resonetics M-50-LR 193 nm Excimer laser attached to an Agilent 7700cx Quadrupole ICP mass spectrometer (Adelaide Microscopy, The University of Adelaide). The Resonetics laser, designed by Laurin Technic Pty., uses a two-volume ablation cell for outstanding trace element sensitivity, washout and stability (Müller et al., 2009). The ablation cell was filled with UHP He (0.7 L/min) that was mixed with Ar (0.93 L/min) after leaving the cell, and was directly introduced to the torch through a "squid" (pulse homogenizing device). The ICP-MS was calibrated regularly in order to maximize sensitivity, whilst keeping production of molecular oxide species (i.e., $^{232}Th^{16}O/^{232}Th$) and doubly-charged ion species (i.e., $^{140}Ce^{2+}/^{140}Ce^{+}$) as low as possible, and typically <0.2 %.

Laser beam energy output was set at 100 mJ at a 26 μm spot size using a repetition rate of 10 Hz. Each analysis comprised a 30 s background measurement followed by 30 s of sample ablation, while a 40 s delay was allowed after each spot analysis to ensure adequate cell wash-out, gas stabilization, and computer processing time. Analyzed isotopes include ^{34}S, ^{55}Mn, ^{57}Fe, ^{59}Co, ^{60}Ni, ^{65}Cu, ^{66}Zn, ^{69}Ga, ^{75}As, ^{82}Se, ^{95}Mo, ^{107}Ag, ^{111}Cd, ^{115}In, ^{118}Sn, ^{121}Sb, ^{125}Te, ^{182}W, ^{197}Au, ^{202}Hg, ^{205}Tl, ^{206}Pb, ^{207}Pb, ^{208}Pb and ^{209}Bi. Dwell times for In, Au and Tl were set to 0.05 s, while all other elements were set to 0.01 s. Mean errors and the minimum detection limits for common trace elements in each sample are provided as Electronic Appendix B. Typically 10 analyses were made on chalcopyrite in a given sample and as

many multiple grains were analysed as possible. Multiple analyses of the MASS-1 sulphide reference material (formerly PS-1; Wilson et al., 2002) bracketed batches of up to 10 unknown analyses. This allowed monitoring of instrument drift, and a linear correction based on the bracketed MASS-1 analyses was applied to all unknown analyses. The latest MASS-1 certificate of analysis (United States Geological Survey, 2014) was used. The stoichiometric nature of chalcopyrite was checked and confirmed by electron probe microanalysis, which also indicated that trace elements were typically present at concentrations below minimum detection limits with that method. Thus, a value of 34.63 wt. % Cu (stoichiometric chalcopyrite) was used as an internal standard. GLITTER data reduction software (Van Achterbergh et al., 2001) was used to carry out data calculations. Given poorly constrained sulphur isotopic interference on ^{66}Zn measurements (e.g., Danyushevsky et al., 2011), we accept that the concentration data for Zn reported here may be less accurate than for some other elements. We also acknowledge that there exist a number of other polyatomic interferences that may necessitate, in cases where concentrations of the interfered element are sufficiently high, correction to derive precise abundance data using LA-ICP-MS. Examples include direct mass interference from ^{115}Sn when measuring the content of In (Jenner and O'Neill, 2012), or $^{59}Co^{16}O$ interference when measuring ^{75}As (Patten et al., 2013). We have not made such corrections to the dataset, confident that although such interferences can impact on data quality when the elements concerned are present at wt. % concentration, they are negligible (well within instrumental error) for low ppm values of the order reported here. An exhaustive treatment of all potential interferences for all trace elements would be well beyond the scope of the present manuscript.

5.4 Results

Distinguishing whether a trace element is present in solid solution as opposed to microscale mineral inclusions within a given mineral is an ongoing difficulty for microanalytical research (e.g., Cook et al., 2016). In order to produce a reliable dataset, it is integral that all data is properly evaluated and great care is taken to monitor information that may suggest the presence of inclusions (for example LA-ICP-MS downhole spectra; e.g., George et al., 2015, assessing all element combinations that may indicate inclusions; e.g., proton microprobe work of Cabri et al., 1985 or Huston et al., 1995). If not, doubt may be placed on the reliability of any anomalous trace element report from the literature, especially those where wt. % levels have been measured for trace elements typically present at ppm levels. Nevertheless, one must also be cautious in attributing an anomalous trace element report from the literature to micro-inclusions of a distinct phase, simply because it is uncharacteristic. Given the right conditions, many minerals may host anomalous concentrations of trace elements not easily attributed to micro-inclusions. We have endeavoured to only analyse areas of chalcopyrite that were free of any noticeable inclusions. Nevertheless, some analyses showed anomalous results, and corresponding LA-ICP-MS downhole spectra revealed irregular profiles implying the presence of micro-inclusions beneath the chalcopyrite surface. Such analyses were discarded. The remaining LA-ICP-MS downhole spectra were relatively smooth indicating measurement of trace element concentrations in solid solution (Fig. 5.1). In some cases, where inclusions were only present at the end of an individual downhole spectrum (e.g., Fig. 5.1d), concentrations were still calculated by only integrating the signal before the inclusion-related peak. Table 5.3 summarizes the trace element data, showing 18 trace elements measured in chalcopyrite. The full dataset is provided as Electronic Appendix C. Individual spot analyses were plotted as

cumulative plots (Fig. 5.2) allowing visualization of the trace element variation within each deposit as well as within deposit types. Although the concentrations of some elements in chalcopyrite varied significantly across sample suites from individual deposits, variance was generally limited within any given sample. There was certainly no evidence of systematic grain-scale zonation as has been reported for other base metal sulphides (e.g., galena and sphalerite in low temperature epithermal ores from Herja; George et al., 2015). Chondrite-normalized spider plots (Fig. 5.3) were used to depict the mean trace element compositions of chalcopyrite (as well as the range of concentrations) in each different deposit type. Molybdenum and W were seldom present in chalcopyrite at concentrations above minimum levels of detection (see footnote to Table 5.3).

Zinc was the trace element most highly concentrated in chalcopyrite - sample Hj-13 from Herja (epithermal) contained chalcopyrite that hosted as much as 1,596 ppm Zn. Smooth LA-ICP-MS downhole spectra from Hj-13 indicated the Zn was present in solid solution (Fig. 5.1c). All chalcopyrite in samples from the epithermal deposits contained high levels of Zn; chalcopyrite from porphyry deposits hosted little Zn. Variation within samples from individual deposits was extremely low, usually only over a single order of magnitude. Chalcopyrite from the epithermal, exhalative and recrystallized exhalative deposit types all had remarkably uniform Zn compositions.

The highest *silver* concentration in chalcopyrite from any sample analysed here was 1,112 ppm (BH73, from the Broken Hill recrystallized SEDEX deposit). High concentrations of Ag appeared typical of chalcopyrite from un-recrystallized and recrystallized exhalative deposits as well as epithermal systems. Chalcopyrite in these deposit types was all similarly enriched in Ag by around 1,000 times chondritic concentrations. Chalcopyrite from the skarn at Oravita and the porphyry deposits had the lowest Ag concentrations, usually <10 ppm.

Sample variation over one or two orders of magnitude appeared normal within individual deposits (e.g. Toroiaga; epithermal, Baita Bihor; skarn, Mofjell; recrystallized SEDEX etc.).

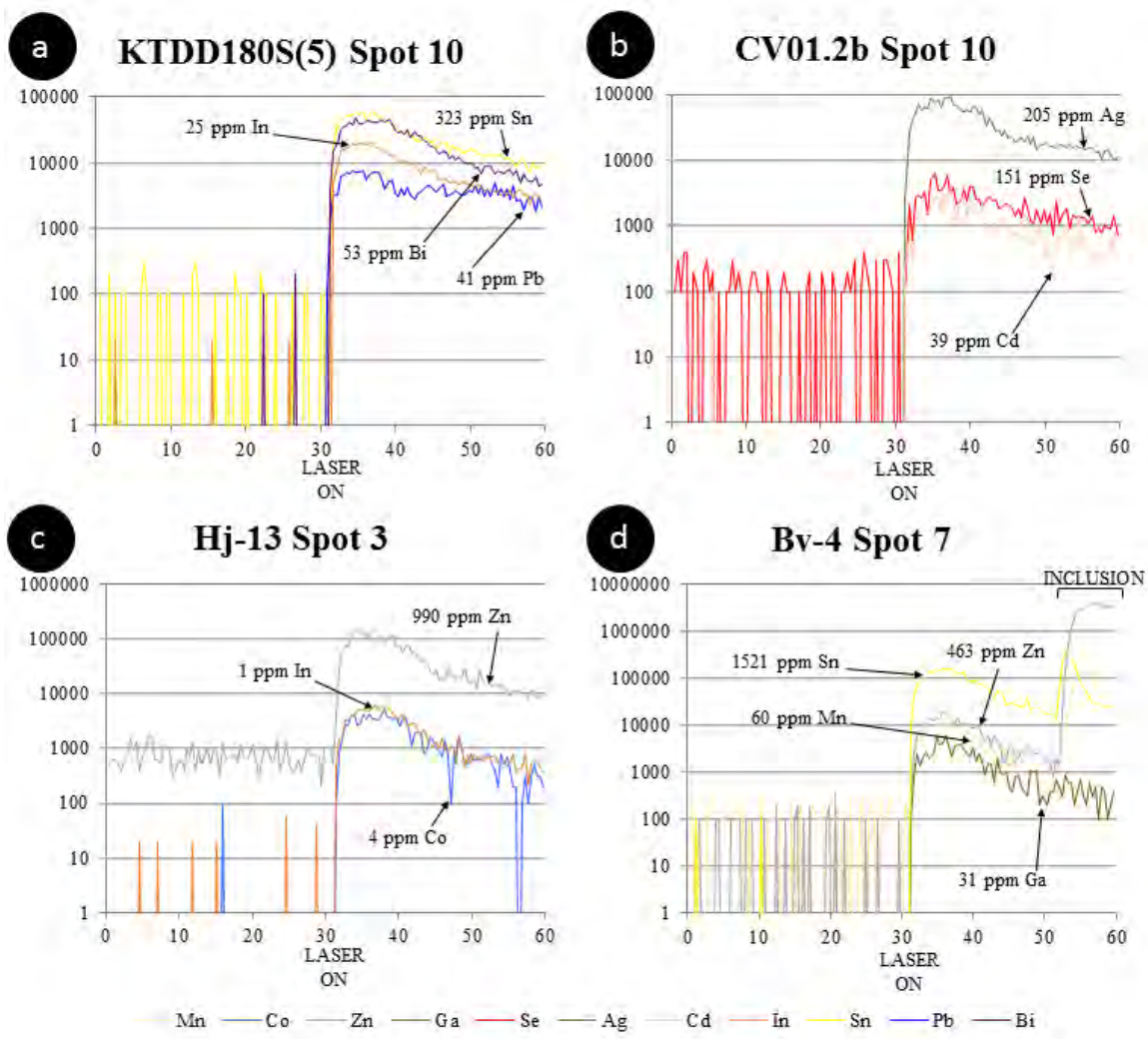

Figure 5.1. Representative time-resolved LA-ICP-MS downhole spectra for chalcopyrite. Y axis = counts per second, X axis = time (s). On each figure the point the laser is fired is indicated on the X axis. (**a-c**) Relatively flat spectra reflecting solid solution for Sn, In, Bi, Pb, Ag, Se, Cd, Zn and Co in chalcopyrite from Kanmantoo, Sulitjelma and Herja, respectively. The slight downward trajectory of the spectra indicates a lessening of ablated material over time due to gradual deepening of the ablation hole. (**d**) Relatively flat spectra for Ga (Bleikvassli). Peaks at the end of the Zn, Sn and Mn spectra (as marked on the figure) are suggestive of an inclusion of sphalerite. Concentrations are calculated by selecting and integrating only the signal before the peak.

Table 5.3: Summary of trace element concentrations in chalcopyrite determined by LA-ICP-MS (data in ppm)

Locality	**Sample** BMS		**Mn**	**Co**	**Ni**	**Zn**	**Ga**	**As**	**Se**	**Ag**	**Cd**	**In**	**Sn**	**Sb**	**Te**	**Au**	**Hg**	**Tl**	**Pb**	**Bi**
Herja	**Hj-13**	M. (10)	51	4.2	0.39	1596	0.09	0.07	8.6	167	7.6	1.7	10	0.71	-	0.001	0.17	0.002	2.0	0.005
Romania	Cp,Sp,Gn	*St. Dev.*	*14*	*1.4*	*0.57*	*699*	*0.05*	*0.04*	*7.7*	*59*	*2.7*	*0.77*	*3.4*	*0.77*	*-*	*0.001*	*0.04*	*0.002*	*1.6*	*0.003*
Epithermal			**Mn**	**Co**	**Ni**	**Zn**	**Ga**	**As**	**Se**	**Ag**	**Cd**	**In**	**Sn**	**Sb**	**Te**	**Au**	**Hg**	**Tl**	**Pb**	**Bi**
Toroiaga	**EMERIC2**	M. (9)	0.2	-	0.06	136	2.0	0.27	19	95	2	32	42	11	-	0.02	1.7	0.003	14	0.22
Romania	Cp,Sp,Gn	*St. Dev.*	*-*	*-*	*0.07*	*-*	*1.4*	*0.31*	*13*	*60*	*-*	*13*	*25*	*9.3*	*-*	*0.04*	*2.0*	*0.002*	*15*	*0.30*
Epithermal	**T1a**	M. (10)	2.4	0.03	-	533	0.60	1.1	1.7	41	10	15	20	2.5	0.25	0.004	0.23	0.001	2.4	0.03
	Cp,Sp,Gn	*St. Dev.*	*2.4*	*0.05*	*-*	*385*	*0.31*	*0.97*	*1.7*	*38*	*7.8*	*2.4*	*10*	*2.0*	*0.40*	*0.01*	*0.13*	*0.001*	*1.4*	*0.03*
	TOR189	M. (10)	0.98	13	0.28	629	0.27	0.71	78	787	10	20	18	2.2	0.45	0.02	0.46	0.01	1.2	0.9
	Cp	*St. Dev.*	*0.62*	*2.6*	*0.33*	*827*	*0.19*	*0.51*	*27*	*91*	*13.1*	*4.0*	*7.5*	*2.1*	*0.52*	*0.03*	*0.15*	*0.01*	*1.1*	*0.76*
	TOR191	M. (10)	0.8	0.04	0.02	939	0.27	-	1.4	34	19	33	27	0.91	0.02	0.01	234	0.003	1.4	0.01
	Cp,Sp,Gn	*St. Dev.*	*0.97*	*0.05*	*0.02*	*844*	*0.11*	*-*	*1.8*	*45*	*17.4*	*21*	*16*	*0.63*	*0.02*	*0.02*	*91*	*0.002*	*1.4*	*0.01*
	TOR197	M. (10)	0.9	0.02	0.02	1419	0.12	1.2	1.5	203	25	19	11	1.7	0.10	0.01	292	0.004	3.3	0.02
	Cp,Sp,Gn	*St. Dev.*	*1.4*	*0.05*	*0.03*	*857*	*0.10*	*0.86*	*1.3*	*75*	*16*	*4.7*	*4.1*	*1.6*	*0.10*	*0.01*	*214*	*0.004*	*4.5*	*0.02*
	Toroiaga R0	M. (10)	0.88	0.03	-	1192	0.44	1.6	1.6	5.4	18	18	15	0.56	-	0.002	0.28	-	1.5	0.03
	Cp,Sp,Gn	*St. Dev.*	*1.1*	*0.10*	*-*	*580*	*0.44*	*1.1*	*1.2*	*7.3*	*7.8*	*7.5*	*12*	*0.35*	*-*	*0.004*	*0.17*	*-*	*0.77*	*0.02*
			Mn	**Co**	**Ni**	**Zn**	**Ga**	**As**	**Se**	**Ag**	**Cd**	**In**	**Sn**	**Sb**	**Te**	**Au**	**Hg**	**Tl**	**Pb**	**Bi**
Kochbulak	**33**	M. (10)	0.88	0.04	0.02	915	0.17	0.86	31	11	19	2.7	11	0.30	0.39	0.02	0.05	0.26	1.5	10
Uzbekistan	Cp	*St. Dev.*	*0.89*	*-*	*0.07*	*285*	*0.15*	*0.50*	*6.2*	*5.5*	*4.7*	*1.1*	*3.6*	*0.27*	*0.39*	*0.03*	*0.05*	*0.23*	*0.69*	*2.8*
Epithermal			**Mn**	**Co**	**Ni**	**Zn**	**Ga**	**As**	**Se**	**Ag**	**Cd**	**In**	**Sn**	**Sb**	**Te**	**Au**	**Hg**	**Tl**	**Pb**	**Bi**
Baita Bihor	**BB55**	M. (10)	6.9	10	0.09	618	0.06	0.32	7.9	14	12	106	122	0.75	0.13	0.12	0.11	0.10	1.7	0.48
Romania	Cp,Gn	*St. Dev.*	*5.5*	*7.6*	*0.10*	*240*	*0.04*	*0.36*	*3.9*	*14*	*13*	*8.8*	*19*	*1.1*	*0.15*	*0.10*	*0.04*	*0.15*	*3.7*	*0.44*
Skarn	**BBH15-21**	M. (10)	2.1	11	1.3	1041	0.82	0.99	136	35	41	185	176	0.03	1.9	0.03	0.09	0.03	4.6	6.7
	Cp,Sp	*St. Dev.*	*5.3*	*5.8*	*0.91*	*153*	*0.18*	*0.91*	*23*	*7.1*	*10*	*37*	*32*	*0.03*	*1.14*	*0.06*	*0.06*	*0.04*	*2.6*	*3.2*
			Mn	**Co**	**Ni**	**Zn**	**Ga**	**As**	**Se**	**Ag**	**Cd**	**In**	**Sn**	**Sb**	**Te**	**Au**	**Hg**	**Tl**	**Pb**	**Bi**
Oravita	**ORV1**	M. (10)	0.24	0.15	-	248	0.19	1.4	43	2.9	1.1	8.6	1.1	2.4	0.27	0.01	0.12	0.01	3.3	0.15
Romania	Cp,Gn	*St. Dev.*	*0.19*	*0.10*	*-*	*120*	*0.12*	*1.0*	*14*	*1.3*	*0.96*	*2.6*	*1.0*	*3.2*	*0.30*	*0.01*	*0.13*	*0.01*	*4.6*	*0.12*
Skarn	**ORV4**	M. (10)	0.27	0.04	-	156	0.37	2.6	4.7	2.9	1.3	8.1	2.5	1.8	0.08	0.003	0.08	0.01	2.9	0.07
	Cp	*St. Dev.*	*0.17*	*0.05*	*-*	*26*	*0.43*	*1.6*	*5.5*	*2.5*	*0.71*	*1.6*	*1.5*	*2.6*	*0.17*	*0.01*	*0.08*	*0.01*	*3.9*	*0.08*
	ORV4a	M. (10)	0.17	0.01	0.03	140	0.23	1.0	10	8.0	1.3	9.2	2.0	10	0.22	0.01	0.12	0.05	4.0	0.35
	Cp	*St. Dev.*	*0.11*	*0.02*	*0.09*	*29*	*0.14*	*0.81*	*10*	*4.4*	*1.1*	*1.2*	*1.1*	*21*	*0.31*	*0.01*	*0.07*	*0.09*	*5.5*	*0.97*
	ORV4B	M. (10)	0.10	0.01	0.03	12	0.28	0.40	13	1.3	1.1	0.81	0.43	0.38	0.45	0.03	21	0.09	31	4.7
	Cp,Sp,Gn	*St. Dev.*	*0.07*	*0.03*	*0.03*	*15*	*0.12*	*0.28*	*18*	*1.8*	*1.0*	*0.89*	*0.26*	*0.33*	*0.31*	*0.02*	*14*	*0.20*	*31*	*2.8*
			Mn	**Co**	**Ni**	**Zn**	**Ga**	**As**	**Se**	**Ag**	**Cd**	**In**	**Sn**	**Sb**	**Te**	**Au**	**Hg**	**Tl**	**Pb**	**Bi**
Assarel	**ASR 5A**	M. (10)	0.53	0.01	-	24	0.52	0.50	12	2.7	2.6	0.20	0.18	0.45	0.27	0.01	35	0.01	8	3.1
Bulgaria	Cp,Sp,Gn	*St. Dev.*	*0.73*	*0.01*	*-*	*29*	*0.32*	*0.11*	*6.8*	*1.8*	*3.5*	*0.23*	*0.14*	*0.57*	*0.18*	*0.01*	*24*	*0.01*	*7.5*	*2.1*
Porphyry	**ASR 10**	M. (10)	0.24	-	0.04	11	0.51	0.82	18	2.8	0.27	7.0	0.91	0.12	0.11	0.02	0.07	0.01	5.8	1.3
	Cp	*St. Dev.*	*0.27*	*-*	*0.12*	*3.8*	*0.34*	*0.30*	*21*	*1.6*	*0.26*	*5.1*	*1.0*	*0.22*	*0.19*	*0.01*	*0.05*	*0.03*	*8.5*	*1.5*
	ASR KB P12077	M. (10)	0.36	0.02	-	8.4	0.20	1.5	226	2.1	0.73	2.8	1.0	0.07	0.54	0.02	0.08	0.02	16	20
	Cp	*St. Dev.*	*0.50*	*0.02*	*-*	*4.5*	*0.14*	*1.3*	*64*	*2.0*	*0.51*	*0.69*	*0.33*	*0.11*	*0.99*	*0.02*	*0.08*	*0.07*	*27*	*17*
			Mn	**Co**	**Ni**	**Zn**	**Ga**	**As**	**Se**	**Ag**	**Cd**	**In**	**Sn**	**Sb**	**Te**	**Au**	**Hg**	**Tl**	**Pb**	**Bi**

Bor	**BOR14**	M. (10)	2.4	0.05	-	65	0.14	1.3	2.4	12	0.77	0.69	16	0.13	0.04	0.06	0.09	0.23	12	6.2
Serbia	Cp	*St. Dev.*	*1.7*	*0.06*	-	*32*	*0.14*	*1.1*	*1.7*	*9.0*	*0.98*	*0.21*	*10*	*0.11*	*0.12*	*0.06*	*0.09*	*0.17*	*10*	*3.3*
Porphyry			**Mn**	**Co**	**Ni**	**Zn**	**Ga**	**As**	**Se**	**Ag**	**Cd**	**In**	**Sn**	**Sb**	**Te**	**Au**	**Hg**	**Tl**	**Pb**	**Bi**
Elastite	**Elastite b a**	M. (10)	0.60	0.82	-	1.2	0.34	0.78	313	2.5	0.11	2.4	2.0	0.99	0.19	0.002	0.06	0.05	10	1.0
Bulgaria	Cp	*St. Dev.*	*1.1*	*0.65*	-	*1.5*	*0.41*	*0.41*	*240*	*2.9*	*0.19*	*0.25*	*1.6*	*0.97*	*0.29*	*0.004*	*0.06*	*0.06*	*10.6*	*1.2*
Porphyry	**ELS 157**	M. (6)	0.76	0.04	-	34	0.96	1.7	2.8	14	0.59	0.35	0.12	4.4	0.23	0.03	0.11	0.01	27	0.61
	Cp,Sp,Gn	*St. Dev.*	*0.62*	*0.09*	-	*10*	*0.34*	*2.0*	*0.86*	*8.4*	*0.41*	*0.08*	*0.06*	*4.5*	*0.27*	*0.02*	*0.15*	*0.02*	*26*	*0.67*
			Mn	**Co**	**Ni**	**Zn**	**Ga**	**As**	**Se**	**Ag**	**Cd**	**In**	**Sn**	**Sb**	**Te**	**Au**	**Hg**	**Tl**	**Pb**	**Bi**
Vorta	**DMV 99-22**	M. (8)	0.27	1.5	-	258	1.0	2.8	-	44	1.2	0.10	0.30	2.4	0.02	0.01	0.72	0.07	8	0.29
Romania	Cp,Sp,Gn	*St. Dev.*	*0.29*	*4.1*	-	*235*	*0.66*	*2.3*	-	*28*	*1.2*	*0.27*	*0.31*	*2.1*	*0.05*	*0.02*	*0.81*	*0.07*	*18*	*0.79*
VMS			**Mn**	**Co**	**Ni**	**Zn**	**Ga**	**As**	**Se**	**Ag**	**Cd**	**In**	**Sn**	**Sb**	**Te**	**Au**	**Hg**	**Tl**	**Pb**	**Bi**
Kapp Mineral	**kmi 2a**	M. (9)	14	0.16	0.26	216	0.16	1.0	2.5	174	3.3	1.4	15	30	0.04	0.01	47	0.06	-	0.26
Norway	Cp,Gn	*St. Dev.*	*20*	*0.15*	*0.28*	*140*	*0.04*	*0.78*	*1.6*	*52*	*2.5*	*0.50*	*4.1*	*17*	*0.05*	*0.01*	*39*	*0.03*	-	*0.32*
SEDEX			**Mn**	**Co**	**Ni**	**Zn**	**Ga**	**As**	**Se**	**Ag**	**Cd**	**In**	**Sn**	**Sb**	**Te**	**Au**	**Hg**	**Tl**	**Pb**	**Bi**
Broken Hill	**BH73**	M. (5)	23	1.7	0.14	519	5.9	-	-	1112	1.8	1.7	307	0.7	0.05	0.01	0.05	0.10	13	0.01
Australia	Cp,Sp,Gn	*St. Dev.*	*25*	*1.4*	*0.13*	*336*	*1.3*	-	-	*259*	*1.7*	*0.24*	*53*	*0.69*	*0.08*	*0.003*	*0.04*	*0.13*	*13.2*	*0.01*
Recrystallized	**BH262**	M. (10)	2.5	0.44	0.21	460	8.6	1.2	-	138	2.2	1.3	389	0.60	-	0.002	0.09	0.002	2.5	0.004
SEDEX	Cp,Sp,Gn	*St. Dev.*	*1.4*	*0.57*	*0.44*	*128*	*4.6*	*0.86*	-	*127*	*1.4*	*0.19*	*69*	*0.52*	-	*0.003*	*0.07*	*0.003*	*2.0*	*0.01*
			Mn	**Co**	**Ni**	**Zn**	**Ga**	**As**	**Se**	**Ag**	**Cd**	**In**	**Sn**	**Sb**	**Te**	**Au**	**Hg**	**Tl**	**Pb**	**Bi**
Bleikvassli	**Bv-1**	M. (5)	2.1	0.01	0.01	371	24	-	2.3	597	0.85	19	712	7.3	-	0.24	0.41	0.64	4.1	0.03
Norway	Cp,Sp,Gn	*St. Dev.*	*2.1*	*0.02*	*0.01*	*66*	*14*	-	*1.9*	*295*	*0.25*	*3.5*	*571*	*4.2*	-	*0.35*	*0.28*	*0.65*	*3.4*	*0.03*
Recrystallized	**Bv-4**	M. (10)	34	0.24	0.10	425	22	1.2	3.5	4.3	2.0	36	1108	3.8	-	0.004	0.17	0.04	1.6	0.06
SEDEX	Cp,Sp,Gn	*St. Dev.*	*11*	*0.35*	*0.25*	*67*	*9.2*	*0.84*	*2.3*	*2.39*	*0.91*	*3.0*	*362*	*2.9*	-	*0.01*	*0.08*	*0.03*	*1.35*	*0.09*
	V598572	M. (9)	46	0.29	1.3	490	1.7	0.39	13	12	5.6	24	1017	1.0	0.14	0.01	0.85	0.03	2.7	0.02
	Cp,Sp,Gn	*St. Dev.*	*18*	*0.61*	*3.0*	*70*	*1.0*	*0.66*	*10*	*4.0*	*2.8*	*3.7*	*188*	*1.5*	*0.20*	*0.004*	*0.37*	*0.06*	*6.7*	*0.02*
			Mn	**Co**	**Ni**	**Zn**	**Ga**	**As**	**Se**	**Ag**	**Cd**	**In**	**Sn**	**Sb**	**Te**	**Au**	**Hg**	**Tl**	**Pb**	**Bi**
Mofjell	**Mo5**	M. (10)	5.3	0.01	1.3	565	0.42	-	16	26	3.1	0.87	3.0	1.1	0.60	0.004	0.16	0.12	2.6	0.01
Norway	Cp,Sp,Gn	*St. Dev.*	*3.3*	*0.02*	*0.83*	*145*	*0.17*	-	*5.4*	*1.8*	*0.75*	*0.35*	*1.3*	*1.8*	*0.70*	*0.004*	*0.09*	*0.27*	*1.5*	*0.01*
Recrystallized	**Mo16**	M. (10)	0.18	0.01	-	589	0.17	7.8	8.8	12	48	0.11	0.76	2.4	0.26	0.02	0.03	0.01	1.4	0.003
SEDEX	Cp	*St. Dev.*	*0.14*	*0.02*	-	*86*	*0.10*	*4.0*	*2.2*	*1.0*	*18*	*0.06*	*0.19*	*2.7*	*0.29*	*0.02*	*0.03*	*0.01*	*1.1*	*0.003*
	Mo17A	M. (10)	0.12	0.02	0.01	393	0.15	5.2	3.9	32	51	0.30	0.39	58	0.15	0.02	0.10	0.09	37	0.06
	Cp,Gn	*St. Dev.*	*0.18*	*0.03*	*0.03*	*101*	*0.14*	*3.0*	*2.8*	*22*	*16*	*0.09*	*0.13*	*58*	*0.22*	*0.03*	*0.05*	*0.24*	*37*	*0.10*
			Mn	**Co**	**Ni**	**Zn**	**Ga**	**As**	**Se**	**Ag**	**Cd**	**In**	**Sn**	**Sb**	**Te**	**Au**	**Hg**	**Tl**	**Pb**	**Bi**
Sulitjelma	**CV01.1**	M. (10)	0.42	5.8	0.02	699	0.06	1.8	194	248	43	0.46	0.12	-	0.74	0.003	0.16	0.003	0.85	0.22
Norway	Cp	*St. Dev.*	*0.29*	*4.7*	*0.05*	*31*	*0.04*	*1.0*	*14*	*32*	*3.2*	*0.07*	*0.09*	-	*0.64*	*0.003*	*0.09*	*0.002*	*0.54*	*0.15*
Recrystallized	**CV01.2a**	M. (10)	0.44	7.2	0.09	722	0.10	1.2	166	240	44	0.39	0.08	0.07	1.7	-	0.11	0.002	0.68	0.32
VMS	Cp	*St. Dev.*	*0.24*	*8.3*	*0.14*	*91*	*0.09*	*0.48*	*11*	*89*	*8.9*	*0.04*	*0.04*	*0.07*	*1.1*	-	*0.08*	*0.001*	*0.37*	*0.18*
	CV01.2b	M. (10)	0.27	0.91	-	586	0.04	2.0	153	163	34	0.59	0.09	0.06	1.4	0.002	0.14	0.002	1.1	0.43
	Cp	*St. Dev.*	*0.19*	*0.44*	-	*73*	*0.05*	*1.2*	*11*	*36*	*4.9*	*0.65*	*0.07*	*0.08*	*0.63*	*0.002*	*0.12*	*0.003*	*1.3*	*0.45*
	CV01.3	M. (10)	0.34	0.15	0.07	350	0.20	1.5	849	162	18	0.96	0.26	0.02	0.10	0.004	0.06	0.05	0.29	0.42
	Cp,Sp	*St. Dev.*	*0.25*	*0.12*	*0.12*	*56*	*0.11*	*0.98*	*51*	*32*	*3.8*	*0.11*	*0.17*	*0.02*	*0.16*	*0.01*	*0.04*	*0.14*	*0.18*	*0.20*
	CV01.4	M. (10)	0.23	2.1	0.09	555	0.04	1.0	212	202	27	1.3	0.55	0.14	0.03	0.003	0.22	0.03	0.89	0.62
	Cp	*St. Dev.*	*0.17*	*1.1*	*0.13*	*63*	*0.04*	*0.60*	*11*	*17*	*4.8*	*0.16*	*0.25*	*0.16*	*0.10*	*0.005*	*0.17*	*0.05*	*0.57*	*0.37*

	CV01.6b	M. (10)	0.26	0.19	0.24	394	0.14	1.0	722	196	22	0.67	0.31	0.04	0.08	0.003	0.11	0.01	0.76	0.81
	Cp,Sp	*St. Dev.*	*0.12*	*0.10*	*0.19*	*57*	*0.10*	*0.81*	*42*	*17*	*7.1*	*0.06*	*0.24*	*0.05*	*0.13*	*0.005*	*0.09*	*0.03*	*0.47*	*0.56*
	NC4172	M. (10)	6.0	3.4	0.65	282	0.63	0.97	22	41	4.0	5.4	10	10	0.60	0.01	0.10	0.85	17	4.5
	Cp	*St. Dev.*	*3.3*	*2.0*	*0.78*	*110*	*0.74*	*0.71*	*6.3*	*17*	*1.5*	*1.8*	*1.6*	*3.2*	*0.68*	*0.01*	*0.06*	*0.93*	*10.0*	*2.8*
	NC5839	M. (10)	-	1.1	0.18	471	12	0.94	46	38	2.8	6.3	66	1.5	1.1	0.02	0.13	0.01	1.4	0.25
	Cp,Sp	*St. Dev.*	-	*0.67*	*0.15*	*156*	*3.2*	*0.77*	*8.5*	*5.7*	*1.6*	*1.1*	*6.2*	*1.0*	*0.90*	*0.02*	*0.12*	*0.01*	*0.83*	*0.34*
	NC6894	M. (10)	0.24	0.02	0.02	128	0.37	2.9	68	8.4	2.1	20	53	0.13	1.2	0.05	0.39	0.002	0.46	0.07
	Cp,Sp	*St. Dev.*	*0.20*	*0.04*	*0.03*	*10*	*0.12*	*1.9*	*9.4*	*2.4*	*0.59*	*2.6*	*6.6*	*0.09*	*0.75*	*0.04*	*0.26*	*0.001*	*0.34*	*0.06*
	Su3	M. (10)	0.58	2.4	3.1	148	0.39	0.91	8.7	31	3.3	14	22	0.07	0.70	0.24	0.15	0.001	2.5	5.9
	Cp	*St. Dev.*	*0.83*	*0.60*	*1.3*	*59*	*0.14*	*0.53*	*3.3*	*12*	*0.75*	*0.64*	*7.8*	*0.08*	*0.26*	*0.23*	*0.09*	*0.001*	*2.3*	*2.6*
	Sulis 1b	M. (10)	5.3	0.25	0.11	439	9.0	1.3	53	37	2.8	6.5	58	1.7	0.72	0.01	0.32	0.01	1.3	0.74
	Cp,Sp	*St. Dev.*	*2.8*	*0.27*	*0.27*	*67*	*1.9*	*1.2*	*7.1*	*5.1*	*1.0*	*0.70*	*7.6*	*1.08*	*0.53*	*0.02*	*0.12*	*0.03*	*1.00*	*1.6*
	Sulis2a	M. (10)	16	0.41	0.23	402	2.5	2.0	67	19	5.9	1.5	3.2	1.0	0.85	0.004	0.36	0.001	3.3	0.73
	Cp,Sp	*St. Dev.*	*4.1*	*0.31*	*0.29*	*68*	*0.63*	*1.3*	*7.5*	*3.3*	*1.1*	*0.25*	*1.0*	*0.31*	*0.72*	*0.004*	*0.22*	*0.001*	*2.3*	*1.1*
			Mn	**Co**	**Ni**	**Zn**	**Ga**	**As**	**Se**	**Ag**	**Cd**	**In**	**Sn**	**Sb**	**Te**	**Au**	**Hg**	**Tl**	**Pb**	**Bi**
Kanmantoo	**KTDD086(8)**	M. (10)	1.3	0.54	1.3	350	2.4	1.1	106	83	1.5	16	80	0.18	0.14	0.12	0.07	0.01	21	2.2
Australia	Cp	*St. Dev.*	*0.39*	*0.43*	*1.04*	*145*	*0.30*	*0.81*	*11*	*115*	*0.75*	*5.4*	*13*	*0.09*	*0.16*	*0.13*	*0.05*	*0.01*	*14*	*1.03*
Metamorphosed	**KTDD086(9)**	M. (10)	0.68	0.34	0.18	427	2.2	1.4	234	19	1.5	13	58	0.22	0.12	0.07	0.09	0.003	43	2.7
remobilised	Cp	*St. Dev.*	*0.40*	*0.12*	*0.17*	*75*	*1.3*	*0.79*	*64*	*6.6*	*0.33*	*3.4*	*10*	*0.18*	*0.09*	*0.05*	*0.07*	*0.003*	*23*	*1.4*
syngenetic	**KTDD086(11)**	M. (10)	0.54	0.40	0.14	352	4.3	0.80	48	15	2.0	10	72	0.11	0.60	0.02	0.08	0.003	6.3	0.38
sulphide ore	Cp	*St. Dev.*	*0.25*	*0.12*	*0.14*	*64*	*0.65*	*0.55*	*5.8*	*6.2*	*0.57*	*2.5*	*15*	*0.11*	*0.73*	*0.02*	*0.07*	*0.003*	*2.4*	*0.15*
	KTDD086(12)	M. (10)	0.84	0.35	0.13	390	4.7	1.9	52	20	3.0	15	62	0.14	1.9	0.02	0.11	0.001	5.4	1.3
	Cp	*St. Dev.*	*0.55*	*0.10*	*0.17*	*71*	*1.2*	*1.7*	*5.9*	*9.2*	*0.36*	*3.5*	*11*	*0.09*	*0.76*	*0.02*	*0.12*	*0.001*	*2.0*	*1.2*
	KTDD178(7)	M. (10)	0.13	3.0	0.36	433	0.35	1.0	59	23	1.3	51	149	0.08	0.35	0.02	0.07	0.004	41	1.7
	Cp	*St. Dev.*	*0.09*	*1.1*	*0.21*	*65*	*0.13*	*1.1*	*5.9*	*3.8*	*0.66*	*11*	*64*	*0.06*	*0.22*	*0.02*	*0.06*	*0.003*	*30*	*0.76*
	KTDD178(8)	M. (9)	0.08	0.76	0.57	301	0.46	1.1	50	26	2.3	15	318	-	0.57	0.01	0.06	0.001	1.9	0.10
	Cp	*St. Dev.*	*0.05*	*0.57*	*0.63*	*112*	*0.20*	*1.1*	*18.9*	*11.7*	*0.98*	*6.8*	*142*	-	*0.35*	*0.004*	*0.05*	*0.001*	*1.04*	*0.06*
	KTDD178(12)	M. (10)	0.11	1.3	0.39	356	0.71	0.93	32	43	1.8	19	314	0.03	0.32	0.03	0.07	0.001	1.9	0.21
	Cp	*St. Dev.*	*0.07*	*0.58*	*0.29*	*60*	*0.28*	*0.42*	*3.2*	*8.3*	*0.57*	*9.0*	*100*	*0.01*	*0.27*	*0.02*	*0.05*	*0.001*	*1.3*	*0.14*
	KTDD180(3)	M. (7)	0.80	4.4	0.17	350	0.23	1.6	18	26	0.82	55	24	0.20	0.53	0.003	0.14	0.24	0.92	1.4
	Cp	*St. Dev.*	*0.38*	*4.2*	*0.32*	*63*	*0.13*	*1.3*	*2.5*	*30*	*0.31*	*2.5*	*4.4*	*0.13*	*0.34*	*0.003*	*0.09*	*0.46*	*0.73*	*1.2*
	KTDD180(7)	M. (10)	0.33	0.88	0.42	507	1.4	1.3	12	18	1.3	38	206	0.08	0.88	0.16	0.11	0.17	0.74	3.5
	Cp	*St. Dev.*	*0.22*	*0.35*	*0.39*	*84*	*0.38*	*1.3*	*3.5*	*6.2*	*0.43*	*11*	*47*	*0.05*	*0.58*	*0.14*	*0.07*	*0.54*	*1.2*	*2.8*
	KTDD180S(4)	M. (10)	0.44	2.1	0.06	520	0.59	2.0	54	86	2.3	49	298	0.09	0.37	0.07	0.17	0.01	44	16
	Cp	*St. Dev.*	*0.47*	*1.18*	*0.08*	*63*	*0.13*	*1.5*	*4.5*	*13*	*0.43*	*2.5*	*141*	*0.08*	*0.31*	*0.05*	*0.08*	*0.01*	*14*	*23*
	KTDD180S(5)	M. (10)	1.9	2	0.29	389	0.64	1.2	60	123	1.1	21	305	0.16	0.68	0.19	0.11	0.003	28	30
	Cp	*St. Dev.*	*1.4*	*3*	*0.39*	*155*	*0.19*	*0.94*	*9.1*	*10*	*0.64*	*3.7*	*82*	*0.11*	*0.58*	*0.09*	*0.09*	*0.002*	*24*	*20*

Abbreviations - BMS: base metal sulphides, Cp: chalcopyrite, Sp: sphalerite, Gn: galena, M.: mean, St. Dev.: standard deviation.
(X) = number of individual spot analyses in that sample. Dash = insufficient data to perform calculation (all analyses <mdl). Other <mdl values were treated as mdl/2.
The 18 elements displayed are commonly present at measurable concentrations. Mo and W were measured but are rarey present above minimum levels of detection.

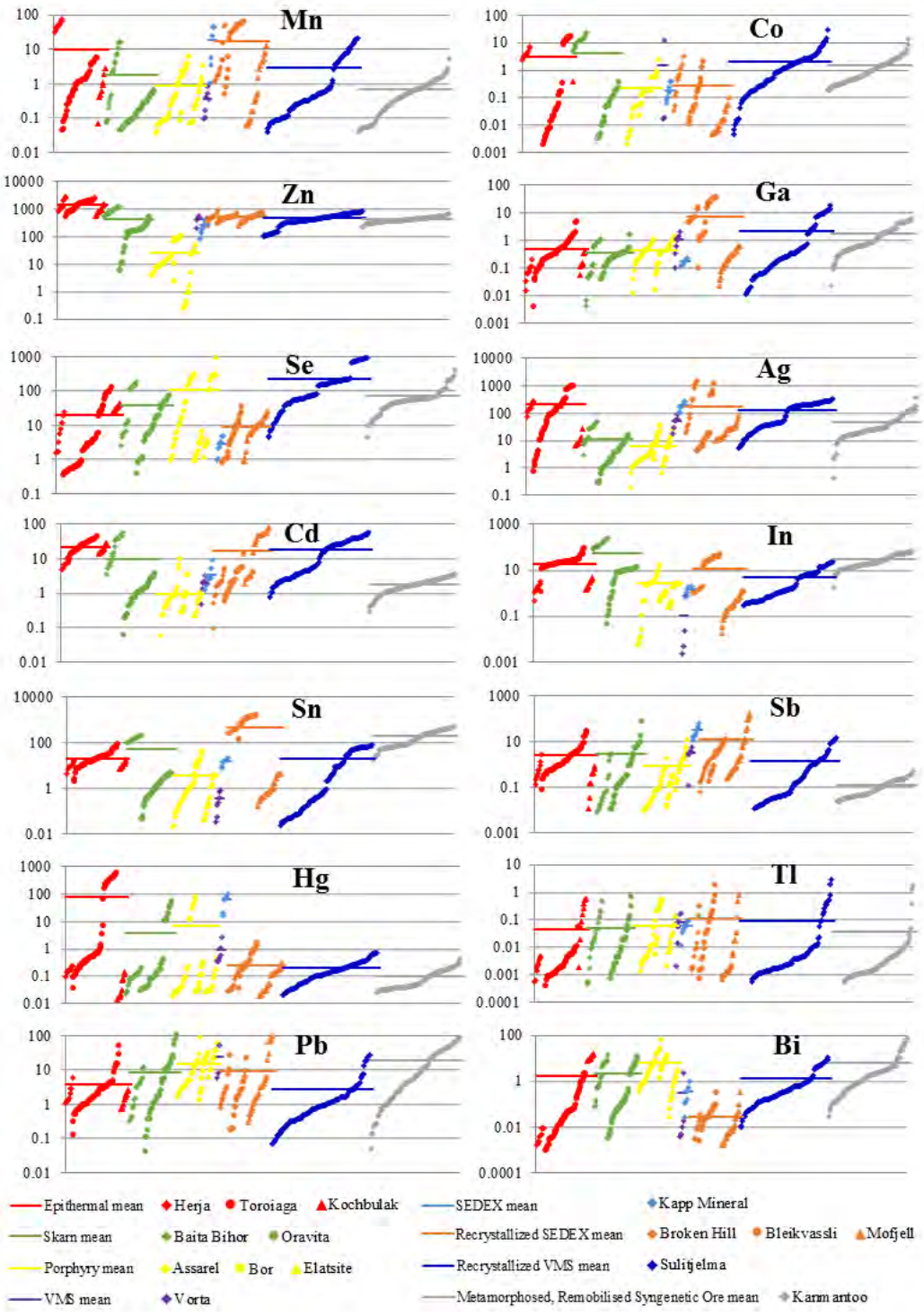

Figure 5.2. Cumulative plots showing individual spot concentrations of Mn, Co, Zn, Ga, Se, Ag, Cd, In, Sn, Sb, Hg, Tl, Pb and Bi in chalcopyrite from each deposit. Chalcopyrite concentration data for each deposit is sorted in ascending order and plotted in succession along the X axis. Y axis = concentration (parts per million). Red points are from epithermal deposits, green are from skarn deposits, yellow are from porphyry deposits, purple are from the Vorta VMS deposit, light blue are from the Kapp Mineral SEDEX prospect, orange are from recrystallized SEDEX deposits, dark blue are from the Sulitjelma recrystallized VMS deposit and grey are from the Kanmantoo deposit, interpreted as a metamorphosed, remobilised syngenetic sulphide ore. The average composition for each deposit type is given as a horizontal coloured line.

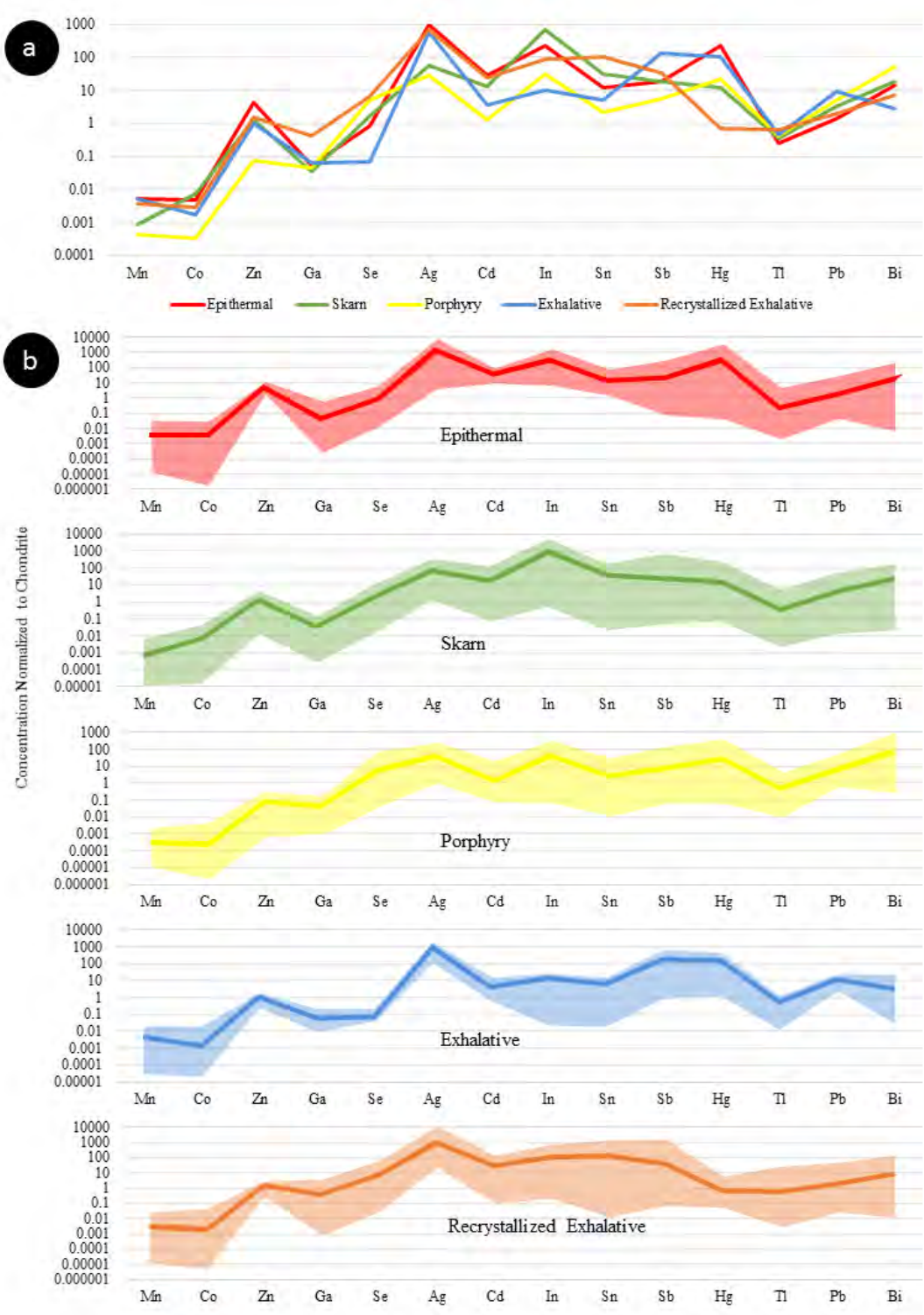

Figure 5.3. Chondrite normalized spider plots for 14 common trace elements in chalcopyrite from different deposit types. Data normalized with values from McDonough and Sun (1995). (**a**) Comparison of the mean concentration of each trace element in chalcopyrite from different deposit types. (**b**) Mean concentration and range of each trace element in chalcopyrite from epithermal, skarn, porphyry, exhalative and recrystallized exhalative deposits. Epithermal deposits consist of Herja, Toroiaga and Kochbulak, skarn deposits consist of Baita Bihor and Oravita, Porphyry deposits consist of Assarel, Bor and Elatsite, exhalative deposits consist of Vorta and Kapp Mineral and recrystallized exhalative deposits consist of Broken Hill, Bleikvassli, Mofjell and Sulitjelma.

Tin was highly concentrated in chalcopyrite from the recrystallized SEDEX deposits Broken Hill and Bleikvassli, and also at both Baita Bihor (skarn) and Kanmantoo (metamorphosed, remobilised syngenetic sulphide ore). The most Sn-rich chalcopyrite here was from sample Bv-4 (Bleikvassli; recrystallized SEDEX), which hosted an average of 1,108 ppm Sn. Smooth LA-ICP-MS downhole spectra from Bv-4 suggested the Sn was present in solid solution (Fig. 5.1d). Chalcopyrite from Oravita (skarn), Assarel (porphyry), Elatsite (porphyry) and Vorta (VMS) all hosted low levels of Sn. Variation appeared to be considerable within samples from a single deposit, for example, in the case of the Sulitjelma (recrystallized VMS) samples, Sn concentrations in chalcopyrite fluctuated over four orders of magnitude.

The highest concentration of *selenium* in chalcopyrite here was 849 ppm (from sample CV01.3, Sulitjelma; recrystallized VMS). Sample concentrations varied over three orders of magnitude at Sulitjelma, as well as in the Assarel (porphyry), Elatsite (porphyry) and Toroiaga (epithermal) samples. Typically, however, variation over two orders of magnitude was observed in samples from any deposit. Chalcopyrite from Kapp Mineral (SEDEX) and Bor (porphyry) hosted the least Se. Selenium concentrations in chalcopyrite from exhalative deposits were very uniform, although depleted relative to other deposit types. Overall, mean Se concentrations in chalcopyrite from different deposit types varied by two orders of magnitude.

Chalcopyrite in sample BBH15-21 from Baita Bihor (skarn) hosted 185 ppm *indium*, the most of any sample. Relative to other deposits, In was highly enriched in chalcopyrite at Baita Bihor, as well as Toroiaga (epithermal), Bleikvassli (recrystallized SEDEX) and, to a lesser extent, also at Kanmantoo (metamorphosed, remobilised syngenetic sulphide ore). Indium concentrations in chalcopyrite varied over one or two orders of magnitude within samples from the same deposit, although at Assarel (porphyry), sample concentrations

fluctuated over no less than four orders of magnitude. The chalcopyrite in the Vorta (VMS) sample contained the least In. Chalcopyrite from the different deposit types varied in its In content over two orders of magnitude.

We did not record more than 1 ppm *mercury* and *thallium* in chalcopyrite across the sample suite, although in a few individual samples chalcopyrite hosted high levels of Hg: samples TOR197 and TOR191 (Toroiaga; epithermal) both contained chalcopyrite hosting over 200 ppm Hg, while tens of ppm were present in chalcopyrite from kmi 2a (Kapp Mineral; SEDEX) and ASR 5A (Assarel; porphyry). Mean Tl concentrations in chalcopyrite from different deposit types varied very little, all approximately uniform with chondritic compositions. Mercury concentrations in chalcopyrite, on the other hand, varied over five orders of magnitude; the most of any element here. Chalcopyrite from recrystallized exhalative deposits was grossly depleted in Hg compared to other deposit types.

Manganese, *cadmium* and *lead* were all commonly present in chalcopyrite at concentrations between 0.1 and 50 ppm. Concentrations of Mn and Cd in chalcopyrite samples from any single deposit varied up to two orders of magnitude, although Cd concentrations varied less than that for many deposits. Lead concentrations in chalcopyrite on the other hand fluctuated over three orders of magnitude in samples from a given deposit. The highest mean concentrations in chalcopyrite for each element in any given sample were 51 ppm Mn (V598572; Bleikvassli; recrystallized SEDEX), 51 ppm Cd (Mo17A; Mofjell; recrystallized SEDEX) and 44 ppm Pb (KTDD180S(4); Kanmantoo; metamorphosed, remobilised syngenetic sulphide ore). All epithermal chalcopyrite analysed here was uniformly enriched in Cd relative to other deposit types. While Cd concentrations in recrystallized exhalative chalcopyrite were sometimes also high, the range of concentrations measured was large and extended quite low.

Concentrations of *antimony* and *bismuth* in chalcopyrite reached 58 ppm (Mo17A; Mofjell; recrystallized SEDEX) and 30 ppm (KTDD180S(5); Kanmantoo; metamorphosed, remobilised syngenetic sulphide ore), respectively. Concentrations of both elements in chalcopyrite from samples of individual deposits usually varied across two and four orders of magnitude. Kochbulak (epithermal), Baita Bihor (skarn), Assarel (porphyry) and Kanmantoo (metamorphosed, remobilised syngenetic sulphide ore) all hosted chalcopyrite containing high levels of Bi but low levels of Sb, whereas Mofjell (recrystallized SEDEX) chalcopyrite contained high levels of Sb but low levels of Bi. Overall, Sb was most enriched in chalcopyrite from exhalative deposits compared to other deposit types.

Concentrations of *cobalt* and *gallium* in chalcopyrite across the sample suite were typically between 0.001 and 10 ppm. Relative to other deposit types, chalcopyrite from the recrystallized exhalative deposits was enriched in Ga, specifically, Bleikvassli (recrystallized SEDEX) and Broken Hill (recrystallized SEDEX). Chalcopyrite concentrations in sample Bv-1 (Bleikvassli) reached 24 ppm Ga. Cobalt concentrations in chalcopyrite were highest in sample TOR189 (Toroiaga; epithermal) where 13 ppm Co was measured. Porphyry chalcopyrite was depleted in Co relative to other deposit types.

Arsenic, *nickel*, *tellurium* and *gold* were all sometimes present at measurable concentrations in chalcopyrite, however individual analyses were frequently below the minimum limit of detection. The highest concentrations of these elements in chalcopyrite was 7.8 ppm As (Mo16; Mofjell; recrystallized SEDEX), 3.1 ppm Ni (Su3; Sulitjelma; recrystallized VMS), 1.9 ppm Te (in both BBH15-21; Baita Bihor; epithermal, and KTDD086(12); Kanmantoo; metamorphosed, remobilised syngenetic sulphide ore) and 0.24 ppm Au (in both Bv-1; Bleikvassli; recrystallized SEDEX, and Su3; Sulitjelma; recrystallized VMS).

5.5 Discussion

5.5.1 Chalcopyrite as a trace element host

Chalcopyrite is generally considered to be a relatively poor host for trace elements, at least if compared to other common Cu-(Fe)-sulphides (e.g., bornite and chalcocite; Cook et al., 2011), sphalerite (Cook et al., 2009) or galena (George et al., 2015). Indeed, LA-ICP-MS element maps presented by George et al. (2016) demonstrated that chalcopyrite is generally the 'least preferred' host for a range of trace elements when chalcopyrite, sphalerite and galena are inferred to co-crystallize.

A summary of relevant literature reveals that only Ag, Zn, As, Se, Co and Pb are usually reported as trace components in solid solution within chalcopyrite, whereas Mn, In, Tl, Ga and Hg are seldom referred to, if at all. There is also a relative scarcity of empirical concentration data for natural chalcopyrite compared to other sulphides, and in cases where data are reported, often the full range of elements were not checked, or the minimum levels of detection for many trace elements were too high to gain a proper appreciation of concentration ranges (e.g., Harris et al., 1984; Cabri et al., 1985; Kase, 1987; Brill, 1989; Huston et al., 1996; Scott et al., 2001; Moggi-Cecchi et al., 2002; Serranti et al., 2002; Shalaby et al., 2004; Demir et al., 2008; Layton-Matthews et al., 2008; Monteiro et al., 2008; Demir et al., 2013; Gena et al., 2013; Reich et al., 2013; Cioacă et al., 2014; Helmy et al., 2014; Wang et al., 2015a; Wohlgemuth-Ueberwasser et al., 2015; Sadati et al., 2016). The dataset presented in this study, encompassing a wider range of trace elements, and with the generally lower minimum detection limits afforded by LA-ICP-MS, thus allow for a new evaluation of chalcopyrite as a trace element carrier.

Zinc was the most abundant trace element present in the chalcopyrite analysed here with individual spot concentrations exceeding 2,000 ppm in the Herja and Toroiaga epithermal systems. The only other trace elements commonly present at over 100 ppm were Se, Ag and Sn. As such, the trace element budget for chalcopyrite was generally lower than in other co-existing base metal sulphides for which data are available (e.g., Cook et al., 2011; George et al., 2016). Yet despite the lower overall concentrations compared to other common sulphides, particularly when they co-crystallize with chalcopyrite, it is apparent that the latter is able to incorporate a wide range of trace elements. Manganese, Co, Zn, Ga, Se, Ag, Cd, In, Sn, Sb, Hg, Tl, Pb and Bi were all commonly present at measurable levels in chalcopyrite. Generally, trace element concentrations showed little variation at the sample scale, yet most elements showed significant variation of four to five orders of magnitude across the sample suite and even from samples within individual deposits. Significantly, Mn, In, Tl, Ga and Hg were all commonly present at measurable concentrations in chalcopyrite despite rarely being reported in most previous studies. Other trace elements that were occasionally present in chalcopyrite include Ni, As, Te and Au. Thus, considering the greater abundance of chalcopyrite relative to other sulphides in many Cu-ores, in a given deposit chalcopyrite may be the main sulphide host for many of the elements listed above.

5.5.2 Trace element incorporation

The incorporation of trace elements into the chalcopyrite structure is more complex than in other common base metal sulphides, particularly sphalerite or galena. Covalent bonding in chalcopyrite means that Goldschmidt's rules (Goldschmidt, 1954) cannot be used to predict partitioning trends as for purely ionic structures (e.g., George et al., 2016). Instead, in any given ore system, the trace element content of chalcopyrite will largely depend on the

presence or absence of other co-crystallizing sulphides, particularly sphalerite and galena. All trace elements analysed here (except for Zn in the absence of sphalerite) preferentially partition into co-crystallizing sphalerite or galena if those phases are present (George et al., 2016). This is demonstrated in Figures 5.4a and b, which show the concentration of different trace elements in chalcopyrite from Toroiaga and Oravita, respectively. In the first case, Co, Se, Ag and Bi concentrations are all significantly lower in hydrothermal chalcopyrite that co-crystallized with sphalerite and galena than in chalcopyrite from assemblages in which the other base metal sulphides are absent (Fig. 5.4a). This supports observations (George et al., 2016) that Co will preferentially partition into sphalerite, and Se, Ag and Bi into galena, when those base metal sulphides co-crystallize with chalcopyrite in hydrothermal settings. At Oravita, Co, Zn, Ag, In and Sn concentrations are all significantly lower in chalcopyrite associated with sphalerite compared to chalcopyrite that has crystallized without any sphalerite in the polished section (Fig. 5.4b). Again the sphalerite has incorporated a significant proportion of the trace element budget. We thus conclude that hydrothermal chalcopyrite crystallizing without sphalerite and/or galena, is likely to host greater concentrations of Co, Zn, Se, Ag, In, Sn and Bi, whereas the concentration of these elements will be reduced when sphalerite and/or galena co-crystallize. Consequently, chalcopyrite may be thought of as a sink that will incorporate much of the 'leftover trace element budget' not taken up into other co-crystallizing sulphides (sphalerite and galena in the cases above), and efficiently explains why chalcopyrite is able to host a wide range of trace elements while measured concentrations are generally low. A similar relationship exists between chalcopyrite and pyrite, the latter well known to incorporate high levels of As, Co and Ni, and possibly also others (e.g., Large et al., 2009; Winderbaum et al., 2012). Similarly, in ores containing bornite and/or chalcocite, such as Olympic Dam, South Australia, these minerals are likely to host, and control the distribution of Ag and Bi, with chalcopyrite only an

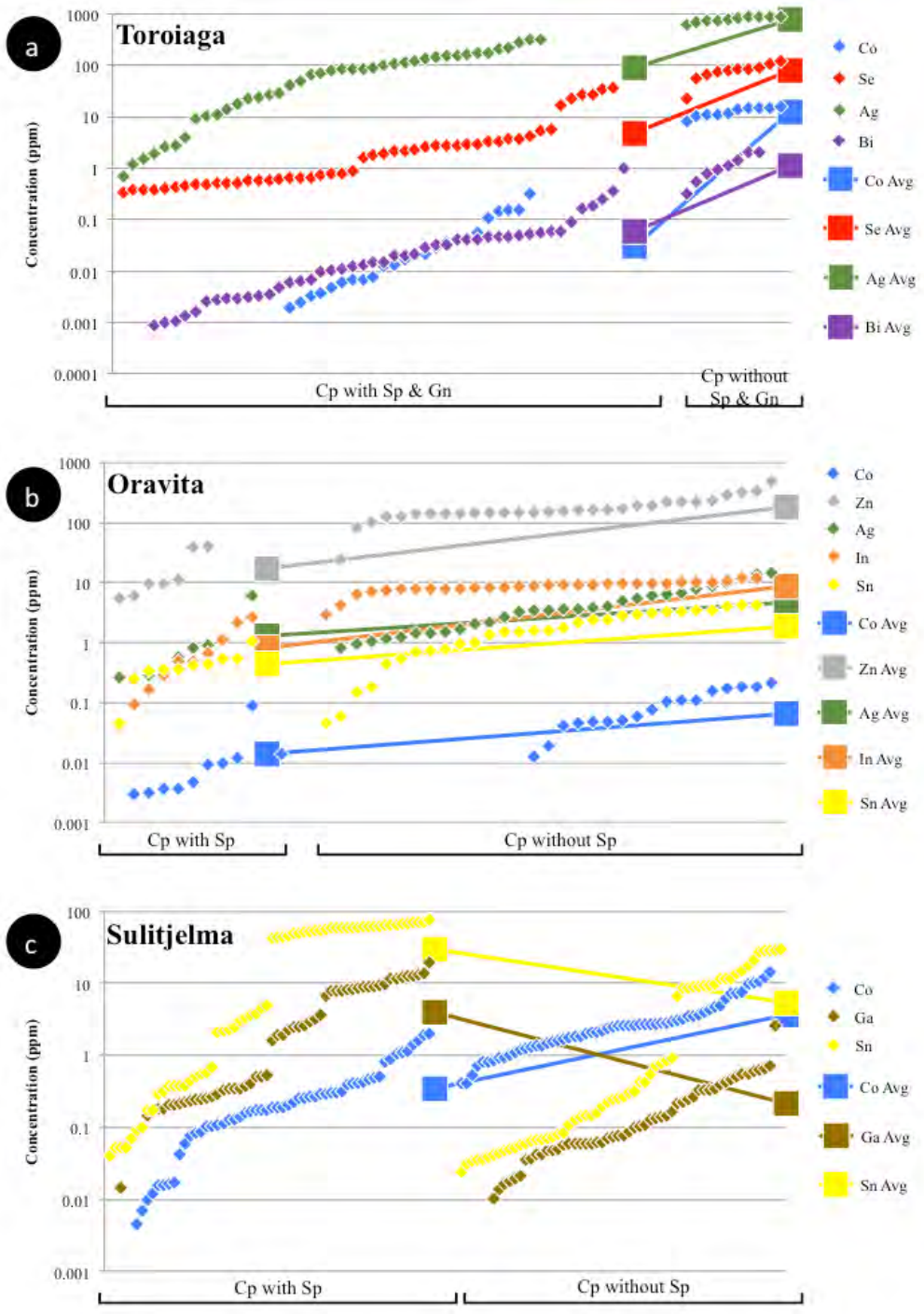

Figure 5.4. Plots showing the dependency of the trace element composition of chalcopyrite on co-crystallizing base metal sulphides (BMS). Chalcopyrite concentration data for each BMS assemblage in each deposit is sorted in ascending order and plotted in succession along the X axis. (**a**) Chalcopyrite in samples from Toroiaga. Data to the left of plot is from chalcopyrite co-crystallizing with sphalerite and galena. Data to the right of plot is from chalcopyrite crystallizing without other BMS nearby. (**b**) Chalcopyrite in samples from Oravita. Data to the left of plot is from chalcopyrite co-crystallizing with sphalerite. Data to the right of plot is from chalcopyrite crystallizing without other BMS nearby. (**c**) Chalcopyrite at Sulitjelma. Data to the left of plot is from chalcopyrite co-crystallizing with sphalerite. Data to the right of plot is from chalcopyrite without other BMS crystallized nearby.

important Ag-Bi-host when bornite and chalcocite are absent (Cook et al., 2015).

In the case of those deposits in which the sulphides recrystallized during syn-metamorphic deformation (Broken Hill, Bleikvassli, Mofjell and Sulitjelma), the presence or absence of other co-crystallizing base metal sulphides influences trace element incorporation into chalcopyrite in a different way. Under metamorphic conditions of amphibolite facies or above, both Ga and Sn will typically partition into chalcopyrite over co-crystallizing sphalerite, distinct from the preferred host of these trace elements at lower temperatures (sphalerite in the case of Ga; George et al., 2016). This is illustrated by Figure 5.4c, which shows the concentration of different trace elements in chalcopyrite from recrystallized samples from the Sulitjelma VMS deposit. Concentrations of Co are significantly lower in chalcopyrite that has recrystallized together with sphalerite if compared to chalcopyrite-only assemblages. This is the same trend depicted in Figures 5.4a and b, showing that Co is preferentially partitioned into sphalerite over chalcopyrite at all temperatures and pressures (George et al., 2016). The trends for Ga and Sn contrast, however, with those shown by Co, in that the concentrations of both Ga and Sn are significantly higher in chalcopyrite that has recrystallized with sphalerite. Our interpretation is that, during recrystallization associated with sub-solidus deformation, Ga and Sn present in pre-existing sphalerite has been remobilized and re-partitioned into chalcopyrite thus increasing the concentration of these elements in the latter more so that if it had recrystallized alone.

Other factors certainly play a contributing role in trace element incorporation into chalcopyrite however. For example, Tl is preferentially incorporated into galena over either chalcopyrite or sphalerite (George et al., 2016). However, in the absence of galena and/or sphalerite, chalcopyrite will still not host more than negligible concentrations of Tl (never more than a few ppm in the sample suite analysed here). There must therefore be factors intrinsic to the chalcopyrite crystal structure that influence trace element incorporation.

Bonding in the chalcopyrite structure is strongly covalent with an effective ionic state between $Cu^{+}Fe^{3+}S_2^{2-}$ and $Cu^{2+}Fe^{2+}S_2^{2-}$ (Li et al., 2013). Yet Goldschmidt's rules for trace element incorporation into ionic structures (Goldschmidt, 1954) may still be helpful in understanding the observed trace element trends in chalcopyrite. As per Goldschmidt's rules, the ionic radius of a substituting trace element is a major control on trace element incorporation. The ionic radii of Zn^{2+}, Sn^{4+} and In^{3+} in tetrahedral coordination all fall within a 'window' between the ionic radii of Fe^{3+} and Fe^{2+} (Fig. 5.5). Although Ag^{+} is significantly outside this 'window', is still the monovalent ion closest in size to Cu^{+} in tetrahedral coordination. These elements (plus Se which can be assumed to substitute for S) were the highest concentration trace constituents measured in chalcopyrite here. Ni^{2+} and Co^{2+} also fall within the Fe^{3+} and Fe^{2+} 'window' but were never significantly concentrated in chalcopyrite here, possibly due to their incorporation into nearly ubiquitous pyrite. Occasional studies have, however, measured high concentrations of Co and Ni in chalcopyrite (e.g., Bajwah et al., 1987; Thole, 1976; Wang et al., 2015a; Wang et al., 2015b). Despite the above observations, mechanisms of trace element incorporation into covalent structures represents a significant research gap and further study is needed to understand partitioning controls.

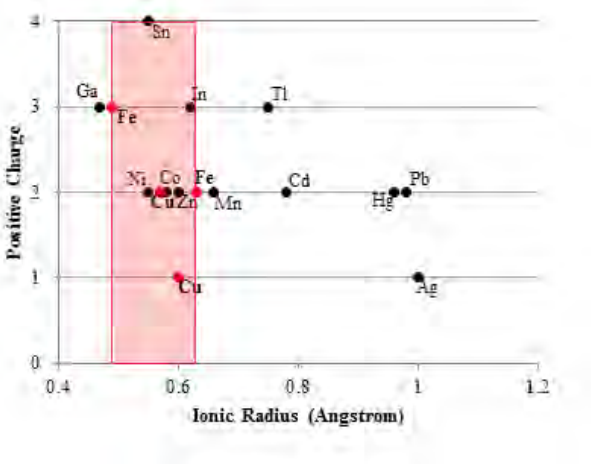

Figure 5.5. Plot showing the ionic radius of various trace element ions in tetrahedral coordination - as in chalcopyrite (data from Shannon, 1976). Red dots represent Fe^{3+}, Cu^{2+}, Cu^{+} and Fe^{2+}. Red area represents the zone in which trace elements have ideal ionic radii for incorporation into chalcopyrite.

5.5.3 Correlation between Cd and Zn

A noteworthy correlation between Cd and Zn concentrations in chalcopyrite is observed across the dataset. This strong correlation is unique as all other trace element pairs show little to no correlation. In general, higher Zn concentrations in chalcopyrite are associated with higher Cd concentrations. Concentration data from a number of individual deposits fit well to lines of differing positive slope that pass through the origin (Fig. 5.6a), such that chalcopyrite from individual deposits display relatively constant Cd:Zn ratios. This ratio increases from the VMS Vorta deposit (0.002), to the Herja epithermal system (0.003), to the SEDEX Kapp Mineral deposit (0.007), to the Toroiaga (0.010) and Kochbulak (0.012) epithermal systems, to the Baita Bihor skarn (0.017) and finally to the recrystallized VMS and SEDEX deposits Sulitjelma (0.021) and Mofjell (0.042), respectively. The Cd:Zn ratio in chalcopyrite (Cd/Zn_{cp}) increases with the inferred temperature of crystallization, thus strongly suggesting that temperature is a significant factor influencing Cd/Zn_{cp}, as illustrated by Figure 5.7. We note that this same trend is observed when chalcopyrite data are plotted for samples without any coexisting sphalerite (Fig. 5.6b). The data are thus unlikely to be influenced by sphalerite inclusions accidently (co)-analysed in the chalcopyrite, except perhaps in one population of chalcopyrite from Mofjell with low Cd but relatively high Zn.

Although crystallization temperature clearly influences Cd/Zn_{cp}, it is unlikely to be the sole factor controlling incorporation of the two elements. For instance, the Cd/Zn_{cp} for Broken Hill (0.002) and Bleikvassli (0.004) appear anomalous as they are far too low to solely reflect sulphide crystallization temperature in these high temperature deposits. Schwartz (2000) noted similar systematic variation in the Cd:Zn ratio of sphalerite (Cd/Zn_{sp}) in different deposit types, particularly among Mississippi Valley-type (MVT) and exhalative (VMS and SEDEX) deposits. Schwartz reasoned that temperature played a role in

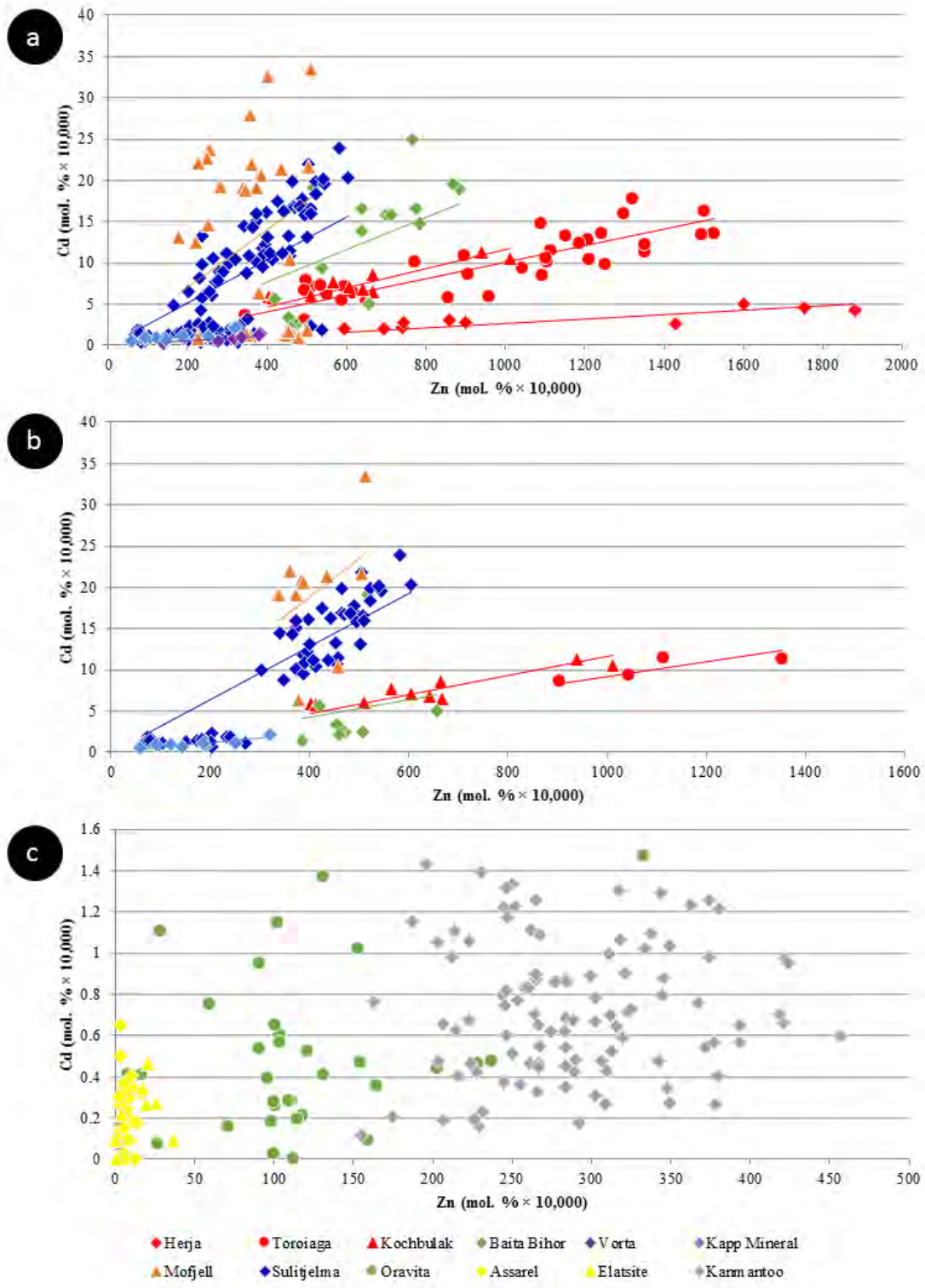

Figure 5.6. Binary plots showing correlation between Cd and Zn in chalcopyrite. (**a**) Data for Herja, Toroiaga, Kochbulak, Baita Bihor, Vorta, Kapp Mineral, Mofjell and Sulitjelma fits well to lines of positive slope that pass through the origin. (**b**) Only data from samples without any coexisting sphalerite is plotted. As general trends remain, the data are unlikely to be influenced by sphalerite inclusions accidently (co)-analysed in the chalcopyrite. (**c**) Data from Oravita, Assarel, Elatsite and Kanmantoo does not fit to lines of positive slope. See text for explanation.

determining Cd/Zn_{sp} but noted that reduced fS_2 and pH were also significant. These three factors control the stability of Cd and Zn complexes in an ore fluid, and thus the partitioning coefficients of Cd and Zn. Despite this, these influences alone cannot explain Cd:Zn ratios in natural sphalerites, prompting Schwartz (2000) to conclude that the Cd:Zn ratio in the ore-forming fluid is the most important factor in determining Cd/Zn_{sp}. A similar conclusion was reached by Gottesmann and Kampe (2007).

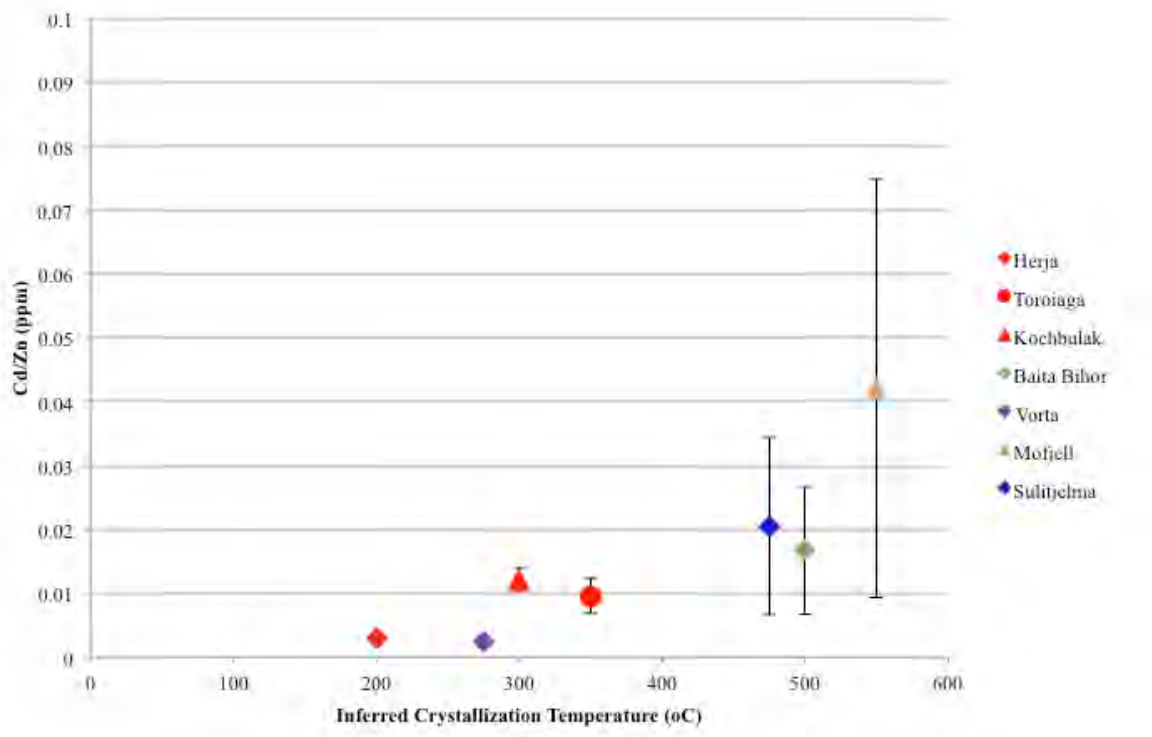

Figure 5.7. Plot showing the correlation between the Cd:Zn ratio in chalcopyrite and inferred chalcopyrite crystallization temperature. Inferred crystallization temperatures are only estimates. Deposits with no known crystallization temperatures have not been plotted, nor have those deposits whose chalcopyrite Cd versus Zn plots do not correlate well along a line of positive slope. Error bars represent one standard deviation.

It is likely that the Cd:Zn ratio in the ore-forming fluid, as well as factors controlling the stability of Cd and Zn complexes in the fluid (e.g., temperature, sulphur activity, pH), would also control Cd/Zn_{cp}. Thus specific physiochemical conditions should result in a particular Cd:Zn ratio in either sphalerite or chalcopyrite, and this ratio should remain constant if the physiochemical conditions do not change. Consequently, chalcopyrite from an individual

deposit that has a relatively constant Cd:Zn ratio likely crystallized in a system during which the physiochemical conditions remained constant. In deposits such as Oravita, Assarel, Elatsite and Kanmantoo, where the Cd versus Zn plots for chalcopyrite do not correlate well along a line of positive slope (Fig. 5.6c), chalcopyrite likely crystallized under evolving, and possibly highly localised physiochemical conditions.

Figure 5.8 shows the mean Cd:Zn ratios in chalcopyrite and co-crystallizing sphalerite. In most samples chalcopyrite and sphalerite have very similar Cd:Zn ratios. Since the Cd:Zn ratio in the ore-forming fluid is the most important factor in determining Cd/Zn_{sp}, the relationship between chalcopyrite and sphalerite is probably a reflection of co-crystallization from a common ore-forming fluid, in which case the ore fluid Cd:Zn ratio is also the most critical factor in controlling Cd/Zn_{cp}. Nevertheless, some samples do show differences in the Cd:Zn ratios of the two minerals. Typically, when a difference is present, the Cd:Zn ratio is higher in chalcopyrite than in sphalerite. Samples from Oravita, Assarel and Elatsite reveal mean chalcopyrite Cd:Zn ratios that are an order of magnitude greater than in sphalerite. Interestingly, these are the same deposits whose chalcopyrite Cd versus Zn plots do not correlate well, and where changing physiochemical conditions were invoked to explain the observed trends (Fig. 5.6c). It thus seems that evolving physiochemical conditions may affect Cd/Zn_{cp} to a greater extent than Cd/Zn_{sp}, leading to marked differences in the mean Cd:Zn ratios of the two minerals. This is intuitive since Cd and Zn concentrations in chalcopyrite may vary over three and four orders of magnitude, respectively, allowing Cd/Zn_{cp} to change over a possible seven orders of magnitude. In sphalerite, however, Cd concentrations generally vary over only one order of magnitude (Cook et al., 2009), and Zn concentrations are fixed, so limiting the Cd/Zn_{sp} to vary no more than one order of magnitude.

The Cd:Zn ratios in chalcopyrite and sphalerite may be useful in indicating whether physiochemical conditions remained constant during base metal sulphide crystallization. A

fixed Cd/Zn_{cp} approximately equal to Cd/Zn_{sp} would indicate co-crystallization of the two sulphides from the same ore-forming fluid under constant physiochemical conditions. If Cd/Zn_{cp} is constant yet distinct from Cd/Zn_{sp}, the two sulphides probably crystallized at different times and/or from different ore-forming fluids. A non-constant Cd/Zn_{cp}, especially if combined with a distinct difference in Cd/Zn_{sp} indicates varying physiochemical conditions during sulphide crystallization. A more thorough investigation is required to determine how Cd/Zn_{cp} depends on ore-forming fluid chemistry and/or other factors. The temperature dependant nature of the Cd:Zn ratio in both sphalerite and chalcopyrite may even potentially allow a geothermometer to be defined based on the partitioning of Cd and Zn among sphalerite-chalcopyrite pairs, assuming other factors affecting Cd/Zn_{cp} and Cd/Zn_{sp} can be accounted for.

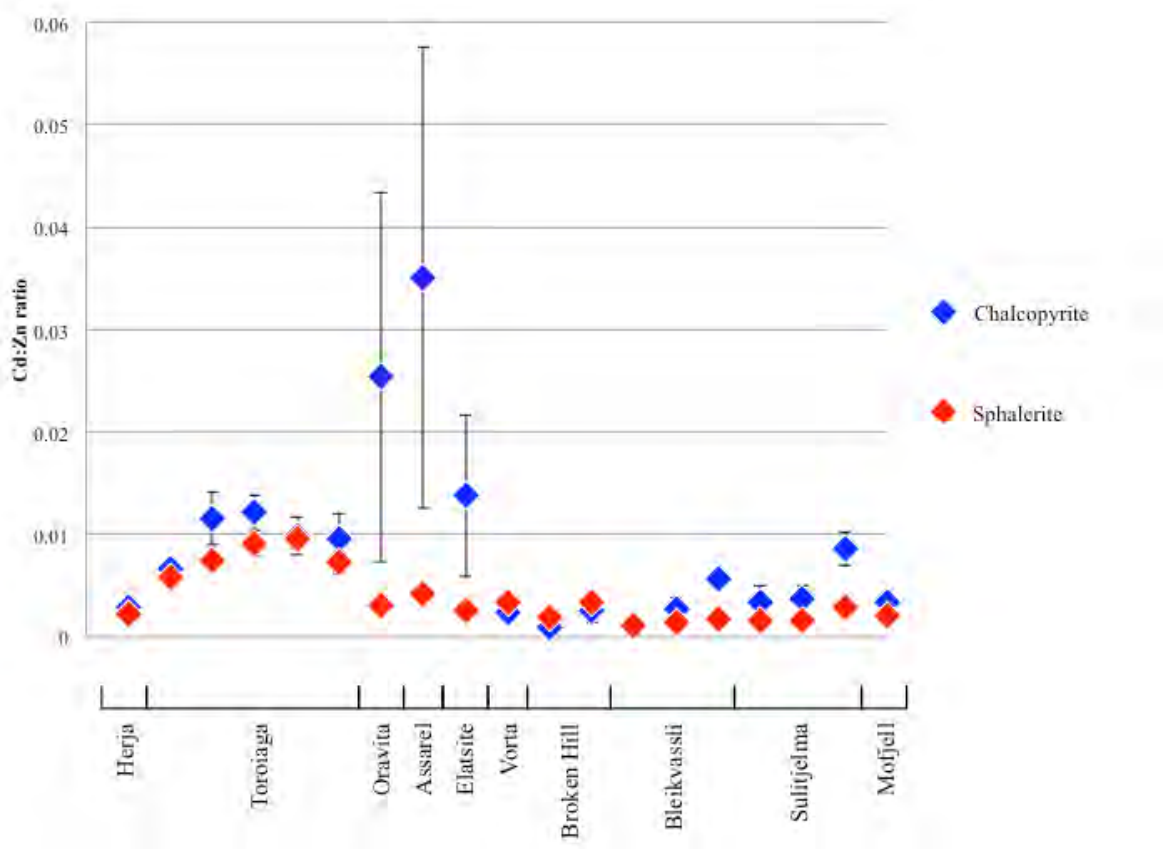

Figure 5.8. Plot showing the similarity between the Cd:Zn ratios in chalcopyrite and co-crystallizing sphalerite from various deposits. Error bars represent one standard deviation.

5.5.4 Deleterious elements

Knowledge of, or the ability to predict, the trace element chemistry of base metal sulphides carries critical economic implications. The presence of harmful or unwanted elements (deleterious elements) in sulphide copper ores is a significant concern for many mining operations selling their concentrate on the world market. If bound within the lattice of the common Cu-(Fe)-sulphides (chalcopyrite, bornite, chalcocite) or as inclusions within those minerals, elements including Co, Zn, As, Se, Cd, Sb, Hg, Pb and Bi will move to copper concentrates after froth flotation (Mular et al., 2002). Such elements reduce the overall grade of the copper concentrate and may require further, often costly treatment to remove them from final copper products. Smelters thus impose financial penalties on concentrates which contain deleterious elements at greater than certain tolerated levels. Different smelters have different lists of deleterious elements and different penalty rates for unwanted elements in a copper concentrate (e.g., Lane et al., 2016). Table 5.4 shows approximate maximum concentrations of deleterious elements that may be present in a copper concentrate before a financial penalty is incurred. Many mining operations therefore work hard to separate deleterious elements from their final saleable concentrate or seek to blend ores from different sources.

Table 5.4: Copper concentrate deleterious elements

Deleterious element	Approximate limit in concentrate before charge is incurred (ppm)
Co+Ni	5000
Zn	30,000
As	1000-2000
Se	500
Cd	200
Sb	1000
Hg	10
Pb	10,000
Bi	200-500

Data from Zanetell (2007) and Fountain (2013).

Integral to any approach to reducing the concentrations of potential penalty elements in a concentrate is an understanding of the mineralogical hosts for each element in primary ore. Since the copper minerals collected from a froth flotation circuit are usually the final saleable copper concentrate (Zanetell, 2007), the concentration of deleterious elements in a concentrate generated from a chalcopyrite-dominant ore will be directly related to the concentration of deleterious elements within chalcopyrite. Ordinarily, chalcopyrite hosts low enough concentrations of most penalty elements as to not be a significant contributor of such elements in a final copper concentrate. On the basis of the data presented here, only in exceptional circumstances could chalcopyrite itself be expected to contribute to excessive Co, Zn, As, Cd, Sb, Pb and Bi in a copper concentrate. Grains of, for example, arsenopyrite, enargite or tennantite (for As), tetrahedrite (for Sb), galena (for Pb), and Bi-chalcogenides (for Bi) could be considered the likely 'culprits', and efforts may be made to prevent flotation of these minerals.

Chalcopyrite can, however, potentially host sufficient Se or Hg to be a culpable host. Copper concentrates may incur monetary penalties from the smelter if they contain in excess of 500 ppm Se. We measure Se concentrations in chalcopyrite up to 1,000 ppm, which could potentially produce copper concentrates with high Se that is difficult to remove prior to smelting. Mercury may represent an even more serious problem in chalcopyrite-dominant copper concentrates. A number of chalcopyrite samples analysed here contain more Hg than the smelter limit of 10 ppm; we even measure hundreds of ppm Hg in chalcopyrite. Japanese smelters charge additional monetary penalties for every 1 ppm over the 10 ppm Hg limit while the Chinese government has banned the import of copper concentrates that exceed 100 ppm Hg altogether (Fountain, 2013). This renders concentrates produced from a Hg-rich chalcopyrite ore of limited value, or in the worst case, unsaleable.

5.6 Conclusions

- Chalcopyrite may host a wide range of trace elements including Mn, Co, Zn, Ga, Se, Ag, Cd, In, Sn, Sb, Hg, Tl, Pb and Bi. The readiness of chalcopyrite to host trace elements generally increases in the absence of other co-crystallizing sulphides, particularly sphalerite and galena.
- In deposits that have recrystallized sulphide assemblages, the concentration of Sn and Ga in chalcopyrite will generally increase in the presence of co-recrystallizing sphalerite and/or galena.
- Trace element concentrations in chalcopyrite typically show little variation at the sample scale, yet potential for significant variation between samples from any individual deposit.
- The Zn:Cd ratio in chalcopyrite shows systematic variation that depends, in part, on crystallization temperature.
- Under constant physiochemical conditions (e.g., temperature, fS_2, pH), the Cd:Zn ratios in co-crystallizing chalcopyrite and sphalerite are often approximately equal. A distinct difference in the Cd:Zn ratios, and/or a non-constant chalcopyrite Cd:Zn ratio, may indicate varying conditions.
- Chalcopyrite is generally a poor host of most penalty elements, Exceptions are Se and Hg, which can be sufficiently enriched in, and difficult to remove from, chalcopyrite-dominant copper concentrates.

5.7 Acknowledgements

Benjamin Wade, Aoife McFadden and Ken Neubauer (Adelaide Microscopy) are thanked for their support with analysis. We are grateful to Dominique Tanner, James Day and an additional anonymous reviewer whose insights helped improve this manuscript.

5.8 References

Andersen, J. C. Ø., Stickland, R. J., Rollinson, G. K., Shail, R. K., 2016. Indium mineralisation in SW England: Host parageneses and mineralogical relations. Ore Geol. Rev. 78, 213-238.

Ayres, R. U., Ayres, L. W., Råde, I., 2013. The life cycle of copper; Its co-products and byproducts. In: Tukker, A., Ed., Eco-Efficiency in Industry and Science, volume 13. Kluwer Academic Publishers, Dordrecht, 199 pp.

Bajwah Z., Seccombe P., Offler R., 1987. Trace element distribution, Co:Ni ratios and genesis of the Big Cadia iron-copper deposit, New South Wales, Australia. Mineral. Deposita 22, 292-300.

Barnes, S. J., Ripley, E. M., 2016. Highly Siderophile and Strongly Chalcophile Elements in Magmatic Ore Deposits. Rev. Mineral. Geochem. 81, 725-774.

Barnes, S. J., Cox, R. A., Zientek, M. L., 2006. Platinum-group element, Gold, Silver and Base Metal distribution in compositionally zoned sulfide droplets from the Medvezky Creek Mine, Noril'sk, Russia. Contrib. Mineral. Petrol. 152, 187-200.

Barrie, C. D., Boyle, A. P., Cook, N. J., Prior, D. J., 2010. Pyrite deformation textures in the massive sulfide ore deposits of the Norwegian Caledonides. Tectonophysics 483, 269-286.

Belousov, I., Large, R. R., Meffre, S., Danyushevsky, L. V., Steadman, J., Beardsmore, T., 2016. Pyrite compositions from VHMS and orogenic Au deposits in the Yilgarn Craton, Western Australia: Implications for gold and copper exploration. Ore Geol. Rev. 79, 474-499.

Bethke, P. M., Barton, P. B., 1971. Distribution of some minor elements between coexisting sulfide minerals. Econ. Geol. 66, 140-163.

Blackburn, W. H., Schwendeman, J. F., 1977. Trace element substitution in galena. Can. Mineral. 15, 365-377.

Both, R. A., McElhinney, R., Toteff, S., 1995. The Angas Zn-Pb-Ag deposit in the Kanmantoo Group, South Australia: synsedimentary or metamorphic? In: Pasava, J., Kríbek, B., Zák, K., Eds., Mineral Deposits: From their Origin to their Environmental Impacts. A. A. Balkema, Rotterdam, 847-850.

Brill B., 1989. Trace-element contents and partitioning of elements in ore minerals from the CSA Cu–Pb–Zn deposit, Australia. Can. Mineral. 27, 263-274.

Butler, I. B., Nesbitt, R. W., 1999. Trace element distributions in the chalcopyrite wall of a black smoker chimney: insights from laser ablation inductively coupled plasma mass spectrometry (LA–ICP–MS). Earth Plan. Sci. Lett. 167, 335-345.

Cabri L. J., Campbell J. L., Laflamme J. H. G., Leigh R. G., Maxwell J. A., Scott J. D., 1985. Proton-microprobe analysis of trace elements in sulfides from some massive-sulfide deposits. Can. Mineral. 23, 133-148.

Chen, L. M., Song, X. Y., Danyushevsky, L. V., Wang, Y. S., Tian, Y. L., Xiao, J. F., 2014. A laser ablation ICP-MS study of platinum-group and chalcophile elements in base metal sulfide minerals of the Jinchuan Ni-Cu sulfide deposit, NW China. Ore Geol. Rev. 65, 955-967.

Cioacă M. E., Munteanu M., Qi L., Costin G., 2014. Trace element concentrations in porphyry copper deposits from Metaliferi Mountains, Romania: A reconnaissance study. Ore Geol. Rev. 63, 22-39.

Ciobanu, C. L., Cook, N. J., Ivascanu, P., 2001. Ore deposits of the Vorţa-Dealul Mare area, South Apuseni Mts., Romania: Textures and a revised genetic model. ABCD-Geode 2001. Rom. J. Min. Depos. 79, 46-47.

Ciobanu, C. L., Cook, N. J., Stein, H., 2002. Regional setting and geochronology of the Late Cretaceous Banatitic Magmatic and Metallogenic Belt. Mineral. Deposita 37, 541-567.

Cioflica, G., Vlad, S., 1981. Cupriferous mineralization at Ciclova. An Univ. Bucuresti Ser. Geol. 30, 1-17.

Cioflica, G., Vlad, S., Stoici, S., 1971. Repartition de la mineralisation dans les skarns de Baita Bihorului. Revue Roumaine de Geologie, Geophysique et Geographie, Serie de Geologie 15, pp. 43-58.

Cioflica, G., Vlad, S., Volanschi, E., Stoici, S., 1977. Magnesian skarns and associated mineralization at Băiţa Bihor. Studii şi Cercetare Géologie Géofizică şi Géographie, Serie Géologie 22, 39-57.

Constantinescu, E., Ilinca, G., Ilinca, A., 1988. Laramian hydrothermal alteration and ore deposition in the Oravita-Ciclova area. Southwestern Banat. DS Inst. Geol. Geofiz. 72-73, 13-26.

Cook, N. J., 1992. Antimony-rich mineral parageneses and their association with Au minerals within massive sulphide deposits at Sulitjelma, Norway. Neu. Jb. Mineral. Mh. 3, 97-106.

Cook, N. J., 1994. Post-recrystallisation phenomena in metamorphosed stratabound sulphide ores: a comment. Mineral. Mag. 58, 480-484.

Cook, N. J., 1996. Mineralogy of the sulphide deposits at Sulitjelma, northern Norway. Ore Geol. Rev. 11, 303-338.

Cook, N. J., 2001. Ore mineralogical investigation of the Mofjell deposit (Mo i Rana, Nordland, Norway) with emphasis on gold and silver distribution. Norg. Geol. Unders. Report 2001.051, 31.

Cook, N. J., Damian, G. S., 1997. New data on "plumosite" and other sulphosalt minerals from the Herja hydrothermal vein deposit, Baia Mare district, Rumania. Geol. Carpath. 48, 387-399.

Cook, N. J., Halls, C., Kaspersen, P. O., 1990. The geology of the Sulitjelma ore field, Northern Norway – some new interpretations. Econ. Geol. 85, 1720-1737.

Cook, N. J., Halls, C., Boyle, A. P., 1993. Deformation and metamorphism of massive sulphides at Sulitjelma, Norway. Mineral. Mag. 57, 67-81.

Cook, N. J., Spry, P. G., Vokes, F. M., 1998. Mineralogy and textural relationships among sulphosalts and related minerals in the Bleikvassli Zn-Pb-(Cu) deposit, Nordland, Norway. Mineral. Deposita 34, 35-56.

Cook, N. J., Ciobanu, C. L., Pring, A., Skinner, W., Shimizu, M., Danyushevsky, L., Saini-Eidukat, B., Melcher, F., 2009. Trace and minor elements in sphalerite: A LA-ICPMS study. Geochim. Cosmochim. Acta 73, 4761–4791.

Cook, N. J., Ciobanu, C. L., Danyushevsky, L. V., Gilbert, S., 2011. Minor elements in bornite and associated Cu-(Fe)-sulfides: a LA-ICPMS study. Geochim. Cosmochim. Acta 73, 4761-4791.

Cook, N. J., Ciobanu, C. L., Ehrig, K., 2015. Insights into Zonation Within the Olympic Dam Cu-U-Au-Ag Deposit from Trace Element Signatures of Sulfide Minerals. Abstract, SEG 2016 Conference, Hobart, Tasmania.

Cook, N. J., Ciobanu, C. L., George, L., Zhu, Z., Wade, B., Ehrig, K., 2016. Trace element analysis of minerals in magmatic-hydrothermal ores by laser ablation inductively-coupled plasma mass spectrometry: approaches and opportunities. Minerals 6, 111.

Dare, S. A., Barnes, S. J., Prichard, H. M., Fisher, P. C., 2010. The timing and formation of platinum-group minerals from the Creighton Ni-Cuplatinum-group Element sulfide deposit, Sudbury, Canada: Early crystallization of PGE-rich sulfarsenides. Econ. Geol. 105, 1071-1096.

Demir Y., Uysal I., Burhan Sadiklar M., Sipahi F., 2008. Mineralogy, mineral chemistry, and fluid inclusion investigation of Köstere hydrothermal vein-type deposit (Gümüşhane, NE Turkey). Neu. Jb. Mineral. Abh. 185, 215-232.

Demir Y., Uysal İ., Sadıklar M. B., 2013. Mineral chemical investigation on sulphide mineralization of the Istala deposit, Gümüşhane, NE-Turkey. Ore Geol. Rev. 53, 306-317.

Djon, M. L. N., Barnes, S. J., 2012. Changes in sulfides and platinum group minerals with the degree of alteration in the Roby, Twilight, and High Grade Zones of the Lac des Iles Complex, Ontario, Canada. Mineral. Deposita 47, 875-896.

Donnay, G., Corliss, L. M., Donnay, J. D. H., Elliott, N., Hastings, J. M., 1958. Symmetry of Magnetic Structures: Magnetic Structure of Chalcopyrite. Phys. Rev. 112, 1917-1923.

Dragov, P., Petrunov, R., 1996. Elazite porphyry copper-precious metals (Au and PGE) deposit. Proceedings, Annual Meeting of IGCP Project 356, Sofia, Bulgaria, 171-175.

Duran, C. J., Barnes, S. J., Corkery, J. T., 2015. Chalcophile and platinum-group element distribution in pyrites from the sulfide-rich pods of the Lac des Iles Pd deposits, Western Ontario, Canada: Implications for post-cumulus re-equilibration of the ore and the use of pyrite compositions in exploration. J. Geochem. Explor. 158, 223-242.

Eugster, H. P., 1986. Minerals in hot water. Amer. Mineral. 71, 655-673.

Flood, B., 1967. Sulphide mineralizations within the Hecla Hoek complex in Vestspitsbergen and Bjørnøya. Norsk Polarinst. Årbok 1967, 109-127.

Foord, E. E., Shawe, D. R., 1989. The Pb-Bi-Ag-Cu-(Hg) chemistry of galena and some associated sulfosalts; a review and some new data from Colorado, California and Pennsylvania. Can. Mineral. 27, 363–382.

Fountain, C., 2013. The whys and wherefores of penalty elements in copper concentrates. In: MetPlant 2013: Metallurgical Plant Design and Operating Strategies, Volume 5. Australasian Institute of Mining and Metallurgy, Melbourne, 502-518.

Gena K., Chiba H., Kase K., Nakashima K., Ishiyama D., 2013. The Tiger Sulfide Chimney, Yonaguni Knoll IV Hydrothermal Field, Southern Okinawa Trough, Japan: The first reported occurrence of Pt–Cu–Fe-bearing bismuthinite and Sn-bearing chalcopyrite in an active seafloor hydrothermal system. Resour. Geol. 63, 360-370.

George, L., Cook, N. J., Ciobanu, C. L., Wade, B., 2015. Trace and minor elements in galena: A reconnaissance LA-ICP-MS study. Amer. Mineral. 100, 548-569.

George, L. L., Cook, N. J., Ciobanu, C. L., 2016. Partitioning of trace elements in co-crystallized sphalerite–galena–chalcopyrite hydrothermal ores. Ore Geol. Rev. 77, 97-116.

Georgiev, G., 2008. A genetic model of the Elatsite porphyry copper deposit, Bulgaria. Geochem. Miner. Petrol. 46, 143-160.

Geoscience Australia, 2015. Copper Fact Sheet. Australian atlas of minerals resources, mines and processing centres, Geoscience Australia, Commonwealth of Australia. Viewed 8 September 2016, <http://www.australianminesatlas.gov.au/education/fact_sheets/copper.html>

Gheorghitescu, D., 1975. Mineralogical and geochemical study of formations in the thermal, metasomatic contact at Oravita (Cosovita). DS Inst. Geol. Geofiz. 61, 59-103.

Godel, B., Barnes, S. J., 2008. Platinum-group elements in sulphide minerals and the whole rocks of the J-M Reef (Stillwater Complex): Implication for the formation of the reef. Chem. Geol. 248, 272-294.

Goldschmidt, V. M., 1954. Geochemistry. Soil Sci. 78, 156.

Gottesmann, W., Kampe, A., 2007. Zn/Cd ratios in calcsilicate-hosted sphalerite ores at Tumurtijn-ovoo, Mongolia. Chem. Erde-Geochem. 67, 323-328.

Gotz, A., Damian, G., Farbas, N., 1990. Contributii la mineralogia bournonitul associat mineralizatiilor din masivul Toroiaga-Baia Borsa. Rev. Mineral. 41, 467-471.

Hall, S. R., Stewart, J. M., 1973. The crystal structure refinement of chalcopyrite, $CuFeS_2$. Acta Crystallogr. 29, 579-585.

Harris D. C., Cabri L. J., Nobiling R., 1984. Silver bearing chalcopyrite, a principal source of silver in the Izok lake massive-sulfide deposit: confirmation by electron and proton-microprobe analyses. Can. Mineral. 22, 493-498.

Haydon, R. C., McConachy, G. W., 1987. The stratigraphic setting of Pb-Zn-Ag mineralization at Broken Hill. Econ. Geol. 82, 826-856.

Helmy H. M., Shalaby I. M., Rahman H. A., 2014. Large-scale metal zoning in a late-Precambrian skarn-type mineralization, Wadi Kid, SE Sinai, Egypt. J. Afr. Earth Sci. 90, 77-86.

Holwell, D. A., McDonald, I., 2007. Distribution of platinum-group elements in the Platreef at Overysel, northern Bushveld Complex: A combined PGM and LA-ICP-MS study. Contrib. Mineral. Petrol. 154, 171-190.

Huston, D. L., Sie, S. H., Suter, G. F., Cooke, D. R., Both, R. A., 1995. Trace elements in sulphide minerals from eastern Australian volcanic-hosted massive sulphide deposits; Part I, Proton microprobe analyses of pyrite, chalcopyrite, and sphalerite, and Part II, Selenium levels in pyrite; comparison with delta 34 S values and implications for the source of sulfur in volcanogenic hydrothermal systems. Econ. Geol. 90, 1167–1196.

Huston D. L., Jablonski W., Sie S. H., 1996. The distribution and mineral hosts of silver in eastern Australian volcanogenic massive sulfide deposits. Can. Mineral. 34, 529-546.

Islamov, F., Kremenetsky, E., Minzer, E., Koneev, R., 1999. The Kochbulak- Kairagach ore field. In: Shayakubov, T., Islamov, F., Kremenetshy, A., Seltmann, R., Eds., Au, Ag, and Cu deposits of Uzbekistan; Excursion Guidebook. International Field Conference of IGCP-373, Joint SGA-IAGOD symposium, Excursion B6, IGCP-SGA-IAGOD.

Janković, S., 1990. Types of copper deposits related to volcanic environment in the Bor district, Yugoslavia. Geol. Rundsch. 79, 467-478.

Janković, S., Herrington, R. J., Kozelj, D., 1998. The Bor and Majdanpek copper–gold deposits in the context of the Bor metallogenic zone (Serbia, Yugoslavia). In: Porter, T. M., Ed., Porphyry and hydrothermal copper and gold deposits; a global perspective; conference proceedings. Australian Mineral Foundation, Glenside, South Australia, 169-178.

Jenner, F. E., O'Neill, H. S. C., 2012. Major and trace analysis of basaltic glasses by laser-ablation ICP-MS. Geochem. Geophys. 13, DOI: 10.1029/2011GC003890.

Jensen, M. L., Whittle, A. W. G., 1969. Sulfur isotopes of the Nairne pyrite deposit, South Australia. Mineral. Deposita 4, 241-247.

Johan, Z., 1988. Indium and germanium in the structure of sphalerite: an example of coupled substitution with copper. Miner. Petrol. 39, 211–229.

Kase K., 1987. Tin-bearing chalcopyrite from the Izumo vein, Toyoha Mine, Hokkaido, Japan. Can. Mineral. 25, 9-13.

Kieft, K., Damman, A. H., 1990. Indium-bearing chalcopyrite and sphalerite from the Gåsborn area, West Bergslagen, central Sweden. Mineral. Mag. 54, 109-112.

Kojima, S., Sugaki, A., 1985. Phase relations in the Cu–Fe–Zn–S system between 500 degrees and 300 degrees C under hydrothermal conditions. Econ. Geol. 80, 158–171.

Kovalenker, V., Safonov, Y., Naumov, V., Rusinov, V., 1997. The epithermal gold-telluride Kochbulak deposit (Uzbekistan). Geol. Ore Depos. 39, 107-128.

Lane, D. J., Cook, N. J., Grano, S. R., Ehrig, K., 2016. Selective leaching of penalty elements from copper concentrates: a review. Miner. Eng. 98, 110-121.

Lang, B., 1979. The base metals-gold hydrothermal ore deposits of Baia Mare, Romania. Econ. Geol. 74, 1336-1351.

Large, R. R., Danyushevsky, L., Hollit, C., Maslennikov, V., Meffre, S., Gilbert, S., Bull, S., Scott, R., Emsbo, P., Thomas, H., Singh, B., 2009. Gold and trace element zonation in pyrite using a laser imaging technique: implications for the timing of gold in orogenic and Carlin-style sediment-hosted deposits. Econ. Geol. 104, 635-668.

Layton-Matthews D., Peter J. M., Scott S. D., Leybourne M. I., 2008. Distribution, mineralogy, and geochemistry of selenium in felsic volcanic-hosted massive sulfide deposits of the Finlayson Lake district, Yukon Territory, Canada. Econ. Geol. 103, 61-88.

Li, Y., Kawashima, N., Li, J., Chandra, A. P., Gerson, A. R., 2013. A review of the structure, and fundamental mechanisms and kinetics of the leaching of chalcopyrite. Adv. Colloid Interface Sci. 197, 1-32.

Maslennikov, V. V., Maslennikova, S. P., Large, R. R., Danyushevsky, L. V., 2009. Study of trace element zonation in vent chimneys from the Silurian Yaman-Kasy volcanic-hosted massive sulfide deposit (Southern Urals, Russia) using laser ablation-inductively coupled plasma mass spectrometry (LA-ICPMS). Econ. Geol. 104, 1111-1141.

Maydagán, L., Franchini, M., Lentz, D., Pons, J., McFarlane, C., 2013. Sulfide composition and isotopic signature of the Altar Cu-Au deposit, Argentina: Constraints on the evolution of the porphyry-epithermal system. Can. Mineral. 51, 813-840.

McClenaghan, S. H., Lentz, D. R., Martin, J., Diegor, W. G., 2009. Gold in the Brunswick No. 12 volcanogenic massive sulfide deposit, Bathurst Mining Camp, Canada: Evidence from bulk ore analysis and laser ablation ICP-MS data on sulfide phases. Mineral. Deposita 44, 523-557.

McDonough, W. F., Sun, S. S., 1995. The composition of the Earth. Chem. Geol. 120, 223-253.

Mikhlin, Y., Tomashevich, Y., Tauson, V., Vyalikh, D., Molodtsov, S., Szargan, R., 2005. A comparative X-ray absorption near-edge structure study of bornite, Cu_5FeS_4, and chalcopyrite, $CuFeS_2$. J. Electron Spectrosc. Relat. Phenom. 142, 83-88.

Moggi-Cecchi V., Cipriani C., Rossi P., Ceccato D., Rudello V., Somacal H., 2002. Trace element contents and distribution maps of chalcopyrite: a micro-PIXE study. Period. Mineral. 71, 101-109.

Monteiro L. V. S., Xavier R. P., Hitzman M. W., Juliani C., de Souza Filho C. R., Carvalho E. D. R., 2008. Mineral chemistry of ore and hydrothermal alteration at the Sossego iron oxide–copper–gold deposit, Carajás Mineral Province, Brazil. Ore Geol. Rev. 34, 317-336.

Mular, A. L., Halbe, D. N., Barratt, D. J., Eds., 2002. Mineral processing plant design, practice, and control. SME, 2422.

Müller, W., Shelley, M., Miller, P., Broude, S., 2009. Initial performance metrics of a new custom-designed ArF excimer LA-ICPMS system coupled to a two-volume laser-ablation cell. J. Anal. Atom. Spectrom. 24, 209–214.

Parr, J., Plimer, I., 1993. Models for Broken Hill-type lead-zinc-silver deposits. Mineral deposits modeling. Geological Association of Canada Special Paper 40, 245-288.

Patten, C., Barnes, S. J., Mathez, E. A., Jenner, F. E., 2013. Partition coefficients of chalcophile elements between sulfide and silicate melts and the early crystallization history of sulfide liquid: LA-ICP-MS analysis of MORB sulfide droplets. Chem. Geol. 358, 170-188.

Pauling, L., Brockway, L. O., 1932. The crystal structure of chalcopyrite $CuFeS_2$. Z. Kristallog.-Cryst Mater. 82, 188-194.

Pearce, C. I., Pattrick, R. A. D., Vaughan, D. J., Henderson, C. M. B., Van der Laan, G., 2006. Copper oxidation state in chalcopyrite: Mixed Cu d^9 d^{10} characteristics. Geochim. Cosmochim. Acta 70, 4635-4642.

Piña, R., Gervilla, F., Barnes, S. J., Ortega, L., Lunar, R., 2012. Distribution of platinum-group and chalcophile elements in the Aguablanca Ni-Cu sulfide deposit (SW Spain): Evidence from a LA-ICP-MS study. Chem. Geol. 302, 61-75.

Plimer, I. R., 2007. The world's largest Zn-Pb-Ag deposit: a re-evaluation of Broken Hill (Australia). In: Andrew, C. J., Ed., Mineral deposits: Digging deeper. Irish Association for Economic Geology, Dublin, 1239-1242.

Plotinskaya, O. Y., Kovalenker, V., Seltmann, R., Stanley, C., 2006. Te and Se mineralogy of the high-sulfidation Kochbulak and Kairagach epithermal gold telluride deposits (Kurama Ridge, Middle Tien Shan, Uzbekistan). Miner. Petrol. 87, 187-207.

Popov, P., Strashimirov, S., Kanazirski, M., 2000. Assarel-Medet ore field. In: Strashmirov, S., Popov, P., Eds., Geology and metallogeny of the Panagyurishte ore region. Guide to excursion A and C. ABCD–Geode 2000 Workshop, Borovets, May 2000, 19-25.

Prichard, H. M., Knight, R. D., Fisher, P. C., McDonald, I., Zhou, M. F., Wang, C. Y., 2013. Distribution of platinum-group elements in magmatic and altered ores in the Jinchuan intrusion, China: An example of selenium remobilization by postmagmatic fluids. Mineral. Deposita 48, 767-786.

Reich M., Palacios C., Barra F., Chryssoulis S., 2013. "Invisible" silver in chalcopyrite and bornite from the Mantos Blancos Cu deposit, northern Chile. Eur. J. Mineral. 25, 453-460.

Revan, M. K., Genç, Y., Maslennikov, V. V., Maslennikova, S. P., Large, R. R., Danyushevsky, L. V., 2014. Mineralogy and trace-element geochemistry of sulfide minerals in hydrothermal chimneys from the Upper-Cretaceous VMS deposits of the eastern Pontide orogenic belt (NE Turkey). Ore Geol. Rev. 63, 129-149.

Rubin, J. N., Kyle, J. R., 1997. Precious metal mineralogy in porphyry-, skarn-, and replacement-type ore deposits of the Ertsberg (Gunung Bijih) District, Irian Jaya, Indonesia. Econ. Geol. 92, 535-550.

Saager, R., 1967. Drei Typen von Kieslagerstätten im Mofjell-Gebiet, Nordland, und ein neuer Vorschlag zur Gliederung der Kaledonischen Kieslager Norwegens. Norsk Geol. Tidsskr. 47, 333-358.

Sadati, S. N., Yazdi, M., Mao, J., Behzadi, M., Adabi, M. H., Lingang, X., Zhenyu, C., Mokhtari, M. A. A., 2016. Sulfide mineral chemistry investigation of sediment-hosted stratiform copper deposits, Nahand-Ivand area, NW Iran. Ore Geol. Rev. 72, 760-776.

Schwartz, M. O., 2000. Cadmium in Zinc Deposits: Economic Geology of a Polluting Element. Int. Geol. Rev. 42, 445-469.

Scott K. M., Ashley P. M., Lawie D. C., 2001. The geochemistry, mineralogy and maturity of gossans derived from volcanogenic Zn–Pb–Cu deposits of the eastern Lachlan Fold Belt, NSW, Australia. J. Geochem. Explor. 72, 169-191.

Seccombe, P. K., Spry, P. G., Both, R. A., Jones, M. T., Schiller, J. C., 1985. Base Metal Mineralization in the Kanmantoo Group, South Australia: A Regional Sulfur Isotope Study. Econ. Geol. 80, 1824-1841.

Serranti S., Ferrini V., Masi U., Nicoletti M., Conde L. N., 2002. Geochemical features of the massive sulfide (Cu) metamorphosed deposit of Arinteiro (Galicia, Spain) and genetic implications. Period. Mineral. 71, 27-48.

Shalaby I. M., Stumpfl E., Helmy H. M., El Mahallawi M. M., Kamel O. A., 2004. Silver and silver-bearing minerals at the Um Samiuki volcanogenic massive sulphide deposit, Eastern Desert, Egypt. Mineral. Deposita 39, 608-621.

Shannon, R., 1976. Revised effective ionic radii and systematic studies of interatomic distances in halides and chalcogenides. Acta Crystallogr. Sect. A: Cryst. Phys., Diffr., Theor. Gen. Crystallogr. 32, 751–767.

Shimizu, M., Cioflica, G., Lupulescu, M., 1995. Ore mineralogy of Romanian deposits. Part I. Stanija and Baita Bihor, Apuseni Mountains and Tincova-Valisor, Banat (SW Carpathians), Romania. Japanese Mag. Mineral. Petrol. Sci. 45, 280-281.

Simon, G., Kesler, S. E., Essene, E. J., Chryssoulis, S. L., 2000. Gold in porphyry copper deposits: experimental determination of the distribution of gold in the Cu-Fe-S-Au system at 400 to 700 C. Econ. Geol. 94, 259-270.

Smith, J. W., Holwell, D. A., McDonald, I., Boyce, A. J., 2016. The application of S isotopes and S/Se ratios in determining ore-forming processes of magmatic Ni-Cu-PGE sulfide deposits: A cautionary case study from the northern Bushveld Complex. Ore Geol. Rev. 73, 148-174.

Spry, P. G., Plimer, I. R., Teale, G. S., 2008. Did the giant Broken Hill (Australia) Zn-Pb-Ag deposit melt? Ore Geol. Rev. 34, 223-241.

Spry, P. G., Both, R. A., Ogierman, J., McElhinney, R., Heimann, A., 2010. Origin of the Angas Pb-Zn-Ag deposit, Strathalbyn, South Australia. Society of Economic Geologists SEG 2010 Conference, Keystone, Colorado, Extended Abstract.

Strashimirov, S., 1993. Features in distribution of the ore minerals in the western periphery of the porphyry-copper deposit Assarel (in Bulgarian). Ann HIMG 39, 79-93.

Strashimirov, S., Petrunov, R., Kanazirski, M., 2002. Porphyry-copper mineralisation in the central Srednogorie zone, Bulgaria. Mineral. Deposita 37, 587-598.

Subba Rao, D. V., Naqvi, S. M., 1997. Geological setting, mineralogy, geochemistry and genesis of the Middle Archaean Kalyadi copper deposit, western Dharwar craton, southern India. Mineral. Deposita 32, 230-242.

Szoke, A., Steclaci, L., 1962. Regiunea Toroiaga-Baia-Borsa. Studiu Geologic, Petrografic, Mineralogic si Geochimic. Editura Academiei Republicii Populare Romine, Bucharest, 240 pp.

Thole, R. H., 1976. The geology of the Shamrocke mine, Rhodesia - a stratiform copper deposit. Econ. Geol. 71, 202-228.

Todd, E. C., Sherman, D. M., 2003. Surface oxidation of chalcocite (Cu_2S) under aqueous (pH = 2–11) and ambient atmospheric conditions: mineralogy from Cu L-and O Kedge X-ray absorption spectroscopy. Amer. Mineral. 88, 1652-1656.

Todd, E., Sherman, D., Purton, J., 2003. Surface oxidation of chalcopyrite ($CuFeS_2$) under ambient atmospheric and aqueous (pH 2–10) conditions: Cu, Fe L-and O K-edge X-ray spectroscopy. Geochim. Cosmochim. Acta 67, 2137-2146.

Ulrich, T., Golding, S. D., Kamber, B. S., Zaw, K., Taube, A., 2002. Different mineralization styles in a volcanic-hosted ore deposit: the fluid and isotopic signatures of the Mt Morgan Au–Cu deposit, Australia. Ore Geol. Rev. 22, 61-90.

United States Geological Survey, 2016. Microanalytical Reference Materials and Accessories. Available online: <http://crustal.usgs.gov/geochemical_reference_standards/microanalytical_RM.html> (accessed on 6 October 2016).

Van Achterberg, E., Ryan, C. G., Jackson, S. E., Griffin, W. L., 2001. Data reduction software for LAICP-MS. In: Sylvester, J. P., Ed., Laser-ablation-ICPMS in the Earth Sciences; Principles and applications. Mineralogical Association of Canada, Short Course Series 29, 239-243.

Verwoerd, P. J., Cleghorn, J. H., 1975. Kanmantoo copper orebody. In: Knight, C. L., Ed., Economic Geology of Australia and Papua New Guinea – I Metals. Australasian Institute of Mining and Metallurgy Monograph 5, 560-565.

Vokes, F. M., 1963. Geological studies on the Caledonian pyritic zinc-lead orebody at Bleikvassli, Norland, Norway. Norg. Geol. Unders. 222, 1-126.

Vokes, F. M., 1966. On the possible modes of origin of the Caledonian sulfide ore deposit at Bleikvassli, Nordland, Norway. Econ. Geol. 61, 1130-1139.

Wang G., Wang Z. Q., Shi R., Zhang Y. L., Wang K. M., 2015a. Mineralogy and isotope geochemical characteristics for Xiaozhen copper deposit, Langao County, Shaanxi Province and their constraint on genesis of the deposit. Geosci. J. 19, 281-294.

Wang, Z., Xu, D., Zhang, Z., Zou, F., Wang, L., Yu, L., Hu, M., 2015b. Mineralogy and trace element geochemistry of the Co-and Cu-bearing sulfides from the Shilu Fe–Co–Cu ore district in Hainan Province of South China. J. Asian Earth Sci. 113, 980-997.

Wilson, S. A., Ridley, W. I., Koenig, A. E., 2002. Development of sulfide calibration standards for the laser ablation inductively-coupled plasma mass spectrometry technique. J. Anal. Atom. Spectrom. 17, 406–409.

Winderbaum, L., Ciobanu, C. L., Cook, N. J., Paul, M., Metcalfe, A., Gilbert, S., 2012. Multivariate Analysis of an LA-ICP-MS Trace Element Dataset for Pyrite. Math. Geosci. 44, 823-842.

Wittmann, A., 1974. Indium. 49-A Crystal Chemistry. In: Wedepohl, K. H., Ed., Handbook of geochemistry: Berlin, Springer-Verlag, v. II/4, 49-A-1-49-A-8.

Wohlgemuth-Ueberwasser, C. C., Viljoen, F., Petersen, S., Vorster, C., 2015. Distribution and solubility limits of trace elements in hydrothermal black smoker sulfides: An in-situ LA-ICP-MS study. Geochim. Cosmochim. Acta 159, 16-41.

Zanetell, Z. A., 2007. Penalty element separation from copper concentrates utilizing froth flotation. Masters thesis, Colorado School of Mines, Colorado, USA.

CHAPTER 6

MINOR AND TRACE ELEMENTS IN TETRAHEDRITE-TENNANTITE: EFFECTS ON ELEMENT PARTITIONING AMONG BASE METAL SULPHIDES

Luke L. George[1], Nigel J. Cook[2], Cristiana, L. Ciobanu[2]

[1]*School of Physical Sciences, The University of Adelaide, Adelaide, S.A., 5005, Australia*

[2]*School of Chemical Engineering, The University of Adelaide, Adelaide, S.A., 5005, Australia*

Paper published in Minerals, 7, 17. doi: 10.3390/min7020017.

Statement of Authorship

Title of Paper	Minor and trace elements in tetrahedrite-tennantite: effects on element partitioning among base metal sulphides
Publication Status	☒ Published ☐ Accepted for Publication ☐ Submitted for Publication ☐ Unpublished and Unsubmitted w ork w ritten in manuscript style
Publication Details	George, L. L., Cook, N. J., Ciobanu, C. L., 2017. Minor and trace elements in natural tetrahedrite-tennantite: effects on element partitioning among base metal sulphides. Minerals 7, 17. doi: 10.3390/min7020017.

Principal Author

Name of Principal Author (Candidate)	Luke George		
Contribution to the Paper	Collected sample material, performed analytical work, carried out data processing and interpretation, oversaw development of work and wrote manuscript.		
Overall percentage (%)	90		
Certification:	This paper reports on original research I conducted during the period of my Higher Degree by Research candidature and is not subject to any obligations or contractual agreements with a third party that would constrain its inclusion in this thesis. I am the primary author of this paper.		
Signature		Date	28 March 2017

Co-Author Contributions

By signing the Statement of Authorship, each author certifies that:

i. the candidate's stated contribution to the publication is accurate (as detailed above);

ii. permission is granted for the candidate to include the publication in the thesis; and

iii. the sum of all co-author contributions is equal to 100% less the candidate's stated contribution.

Name of Co-Author	Nigel Cook		
Contribution to the Paper	Helped define direction of research, provided sample material, supervised development of work, assisted with data interpretation and contributed to manuscript preparation.		
Overall percentage (%)	5		
Signature		Date	20 March 2017

Name of Co-Author	Cristiana Ciobanu		
Contribution to the Paper	Provided sample material, contributed to manuscript preparation.		
Overall percentage (%)	5		
Signature		Date	20 March 2017

minerals

MDPI

Article

Minor and Trace Elements in Natural Tetrahedrite-Tennantite: Effects on Element Partitioning among Base Metal Sulphides

Luke L. George [1,*], Nigel J. Cook [2] and Cristiana L. Ciobanu [2]

[1] School of Physical Sciences, The University of Adelaide, Adelaide, SA 5005, Australia
[2] School of Chemical Engineering, The University of Adelaide, Adelaide, SA 5005, Australia; nigel.cook@adelaide.edu.au (N.J.C.); cristiana.ciobanu@adelaide.edu.au (C.L.C.)
* Correspondence: luke.george@adelaide.edu.au; Tel.: +61-4-3510-1187

Academic Editor: Antonio Simonetti
Received: 21 December 2016; Accepted: 23 January 2017; Published: 29 January 2017

Abstract: Minerals of the tetrahedrite isotypic series are widespread components of base metal ores, where they co-exist with common base metal sulphides (BMS) such as sphalerite, galena, and chalcopyrite. We used electron probe microanalysis and laser-ablation inductively-coupled plasma mass spectrometry to obtain quantitative multi-trace element data on tetrahedrite-tennantite in a suite of 37 samples from different deposits with the objective of understanding which trace elements can be incorporated, at what levels of concentration, and how the presence of tetrahedrite-tennantite influences patterns of trace element partitioning in base metal ores. Apart from Fe and Zn, Hg and Pb are the two most abundant divalent cations present in the analysed tetrahedrite-tennantite (up to 10.6 wt % Hg and 4 wt % Pb). Cadmium, Co and Mn are also often present at concentrations exceeding 1000 ppm. Apart from one particularly Te-rich tetrahedrite, most contained very little Te (around 1 ppm), irrespective of prevailing assemblage. Bismuth is a common minor component of tetrahedrite-tennantite (commonly > 1000 ppm). Tetrahedrite-tennantite typically hosts between 0.1 and 1000 ppm Se, while Sn concentrations are typically between 0.01 and 100 ppm. Concentrations of Ni, Ga, Mo, In, Au, and Tl are rarely, if ever, greater than 10 ppm in tetrahedrite-tennantite and measured W concentrations are consistently < 1 ppm. Taking into account the trace element concentrations in co-crystallizing BMS, the results presented allow the partitioning trends between co-crystallized sphalerite, galena, chalcopyrite, and tetrahedrite-tennantite to be defined. In co-crystallizing BMS assemblages, tetrahedrite-tennantite will always be the primary host of Ag, Fe, Cu, Zn, As, and Sb, and will be the secondary host of Cd, Hg, and Bi. In contrast, tetrahedrite-tennantite is a poor host for the critical metals Ga, In, and Sn, all of which prefer to partition to co-crystallizing BMS. This study shows that tetrahedrite-tennantite is a significant carrier of a range of trace elements at concentrations measurable using contemporary instrumentation. This should be recognized when establishing protocols for trace element analysis of tetrahedrite-tennantite, and when assessing the main hosts of trace elements in any given assemblage, e.g., for geometallurgical purposes.

Keywords: tetrahedrite-tennantite; trace elements; laser-ablation inductively-coupled plasma mass spectrometry; element partitioning

1. Introduction

The tetrahedrite isotypic series [1–4] can be expressed by the general formula $A_6(B,C)_6X_4Y_{12}Z$, where A = Cu or Ag in triangular coordination, B = Cu or Ag in tetrahedral coordination, C = Fe or Zn, or more rarely Pb, Hg, Cd or Mn also in tetrahedral coordination, X = Sb, As, or more rarely Bi or Te in trigonal pyramidal coordination, Y = S or Se in tetrahedral coordination, and Z is S or Se in a

special octahedral coordination [4], i.e., $(Cu,Ag)_6(Cu,Ag,Fe,Zn,Pb\ etc.)_6(Sb,As,Bi,Te)_4(S,Se)_{13}$. Any excess of Cu above 10 atoms per formula unit (*apfu*) ("Cu-excess tetrahedrite-tennantite"; e.g., [5,6]) is taken to indicate the presence of Cu^{2+} [7]. Divalent metals are limited to 2 *apfu* in the tetrahedrite-tennantite structure [4].

The tetrahedrite isotypic series currently comprises eight named minerals: tetrahedrite ($Cu_6[Cu_4(Fe,Zn)_2]Sb_4S_{13}$), tennantite ($Cu_6[Cu_4(Fe,Zn)_2]As_4S_{13}$), freibergite ($Ag_6[Cu_4Fe_2]Sb_4S_{13-x}$), hakite ($Cu_6[Cu_4Hg_2]Sb_4Se_{13}$), giraudite ($Cu_6[Cu_4(Fe,Zn)_2]As_4Se_{13}$), goldfieldite ($Cu_{10}Te_4S_{13}$), argentotennantite ($Ag_6[Cu_4(Fe,Zn)_2]As_4S_{13}$), and argentotetrahedrite ($Ag_{10}(Fe,Zn)_2Sb_4S_{13}$; Table 1). The series is notable among sulphides for extensive fields of solid solution and broad ranges of metals that can be incorporated within the structure (e.g., [8–10]). This diversity is borne out by the range of minor and trace elements measured in natural specimens. Perhaps most noteworthy, the tetrahedrite isotypic series is an important concentrator of silver, and may also be the main host for antimony and arsenic in many ore deposits. Research interest in tetrahedrite-tennantite has also been generated by the observation of compositional variations across an orefield that may be tied to ore-forming processes (e.g., [11–14]), and which offer insights into ore genesis as well as potential as exploration vectors in, for example, porphyry-epithermal environments.

Table 1. Named minerals in the tetrahedrite isotypic series.

Mineral	Ideal Formula	References
Tetrahedrite	$Cu_6[Cu_4(Fe,Zn)_2]Sb_4S_{13}$	[1,3,15,16]
Tennantite	$Cu_6[Cu_4(Fe,Zn)_2]As_4S_{13}$	[2,7]
Freibergite	$Ag_6[Cu_4Fe_2]Sb_4S_{13-x}$	[15,17]
Hakite	$Cu_6[Cu_4Hg_2]Sb_4Se_{13}$	[18]
Giraudite	$Cu_6[Cu_4(Fe,Zn)_2]As_4Se_{13}$	[19]
Goldfieldite	$Cu_{10}Te_4S_{13}$	[20–22]
Argentotennantite	$Ag_6[Cu_4(Fe,Zn)_2]As_4S_{13}$	[23]
Argentotetrahedrite *	$Ag_{10}(Fe,Zn)_2Sb_4S_{13}$	[24]

* Argentotetrahedrite differs from freibergite in that Ag is contained within both the A and B sites as opposed to the A site only. This endmember has only been described on the basis of electron probe microanalysis (EPMA) data. A proper definition through the IMA Commission on New Minerals, Nomenclature and Classification (CNMNC) based on X-ray powder or reflectance data is required.

The tetrahedrite isotypic series is also, undeniably, one of the most thoroughly studied among the sulphides, notably in a series of articles [10,25–29] that have explored, through experiment, how minor elements are incorporated into the tetrahedrite-tennantite (fahlore) structure.

The present contribution seeks to build on these extensive foundations, using electron probe microanalysis (EPMA) and laser-ablation inductively-coupled plasma mass spectrometry (LA-ICP-MS) on a suite of 37 samples from different locations, to address two interdependent goals. Firstly, we seek to understand the range of minor and trace elements which can be incorporated into natural tetrahedrite-tennantite, including those seldom reported in the literature for either natural or synthetic specimens. Secondly, we investigate how the preferred trace element partitioning trends among the common base metal sulphides (BMS) sphalerite, galena, and chalcopyrite outlined in George et al. (2016) [30], are modified if tetrahedrite-tennantite is present in a mineral assemblage and co-crystallizes with BMS.

2. Background

2.1. Crystal Structure

Members of the tetrahedrite isotypic series are classified as sulfosalts; a group of sulphides containing As^{3+}, Sb^{3+}, Bi^{3+} or Te^{4+}, where one or more of these metalloid cations is associated with one or more metallic cations [4]. The metalloids are not bonded to the metals; both exclusively bond to the anion S^{2-} (or more rarely Se^{2-} or Te^{2-}). They are thus distinct from sulphide minerals such as

arsenopyrite (FeAsS), löllingite ($FeAs_2$), gudmundite (FeSbS) or enargite/luzonite (Cu_3AsS_4) where trivalent metalloids bond directly to Fe or Cu.

Moëlo et al. (2008) [4] classify the tetrahedrite isotypic series as sulfosalts with an excess of small (univalent) cations (Ag,Cu) relative to (As,Sb,Bi), and further sub-group them as Cu(Ag)-rich sulfosalts. The tetrahedrite isotypic series is the most complex isostructural series among sulfosalts due to the extensive iso- and heterovalent substitutions that are possible.

In Cu pure tetrahedrite (i.e., $Cu_{12}Sb_4S_{13}$), the structure is most simply understood as linked polyhedra of metal atoms about sulphur atoms [1]. The S^{2-} anion is bonded to six Cu^{2+} cations in octahedral coordination, while each S^{-} anion is coordinated tetrahedrally to two Cu^{+} cations, one Cu^{2+} cation and one Sb^{3+} cation. The angles between bonds in the tetrahedron are significantly distorted from the ideal 109.28°. Each tetrahedron shares a corner with the octahedron, while the remaining three corners of each tetrahedron share corners with two adjacent tetrahedrons (Figure 1). Antimony cations are positioned at the tetrahedron corners closest to the octahedron. The crystal structure of tennantite is analogous to that of tetrahedrite (with As substituted for Sb), although the degree of tetrahedron distortion is generally less in tennantite [2].

Additional investigations on how the tetrahedrite-tennantite structure is changed through incorporation of major elements such as Ag, Fe, Zn or Hg have been carried out (e.g., [31–34]), as has research into the possible oxidation and coordination states of such elements (e.g., [35–37]).

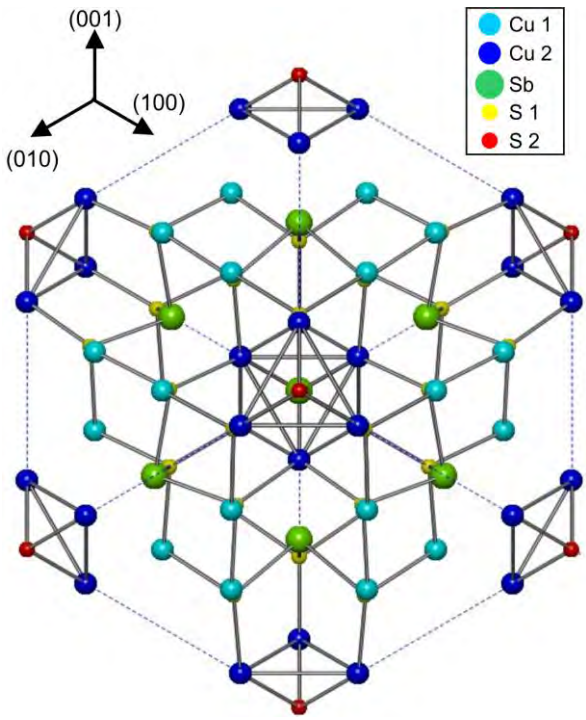

Figure 1. Crystal structure of tetrahedrite drawn from .cif file in American Mineralogist Crystal Structure Database after data in [31].

2.2. Documented Substitutions

Major metal/metalloid components of the tetrahedrite-tennantite series are copper, iron, zinc, antimony, and arsenic. Silver readily enters the tetrahedrite-tennantite structure, with argentotetrahedrite and argentotennantite the Ag end-member analogues of tetrahedrite and tennantite, respectively.

Bismuthian tetrahedrite or tennantite (the latter referred to as "*annivite*") are known from a number of localities (e.g., [38–42]), with Bi substituting into the (Sb,As) site. Staude et al. (2010) [13] document granite-hosted tetrahedrite-tennantite containing up to 22.17 wt % (1.83 *apfu*) Bi from the Schwarzwald ore district, SW Germany. Gołębiowska et al. (2012) [43] report tetrahedrite containing up to 15.86 wt % (1.36 *apfu*) Bi and tennantite containing up to 18.41 wt % (1.51 *apfu*) Bi from Rędziny, Lower Silesia, Poland. At Rędziny, Bi-poor tennantite is generally interpreted as crystallizing at lower temperatures, with the most Bi-rich varieties crystallizing between 230 and 300 °C. Bismuth incorporation in tetrahedrite-tennantite has been studied experimentally [29], with concentrations of up to 1 *apfu* attained irrespective of the Sb/As ratio, consistent with observations in natural specimens [43].

Plumbian tetrahedrite-tennantite is also commonly reported in the literature (e.g., [44–47]). Vavelidis and Melfos (1997) [48] document 1.55 wt % Pb in tennantite, and up to 12.31 wt % Pb in tetrahedrite from the Maronia area of Thrace, Greece, and advocate that Pb^{2+} is incorporated in the (Fe,Zn) site. As much as 4.64 and 5.5 wt % Pb was measured in tennantite from Sark, Channel Islands, by Bishop et al. (1977) [49] and Ixer and Stanley (1983) [50], respectively.

Mercury is frequently reported in tetrahedrite-tennantite, where it substitutes for (Fe,Zn). Mercurian giraudite and hakite containing as much as 15.32 wt % and 14.98 wt %, respectively, are documented by Förster et al. (2002) [51] from the Niederschlema-Alberoda uranium deposit, Erzgebirge, Germany. Compositions almost span the entire solid solution range between the two minerals. They infer complete miscibility between mercurian giraudite and hakite in nature, analogous to tetrahedrite and tennantite. Jurković et al. (2011a) [52] report mercurian tetrahedrite from the Duboki Vagan barite deposit, south of Kreševo, Bosnia, containing up to 3.795 wt % Hg.

Both Mn [47,53] and Cd [54] are occasionally reported as minor elements in tetrahedrite-tennantite, substituting for (Fe,Zn). Pattrick (1978; 1985) [55,56], Huiwen and Chunpei (1988) [57] and Voudouris et al. (2011) [58] each report tetrahedrite-tennantite with Cd concentrations reaching up to ~12 wt %, representing approximately 2 *apfu* Cd. Dobbe (1992) [59] reports an unusual manganoan-cadmian tetrahedrite from Tunaberg, Bergslagen, Sweden, containing up to 2.4 wt % Mn and 5 wt % Cd.

Tellurian tetrahedrite has been widely described (e.g., [6,22] and references therein). A complete solid solution exists between tetrahedrite and the telluride-bearing end-member goldfieldite [60]. Tellurium occupies the (Sb,As) site and is incorporated through the coupled substitution $(Cu,Fe,Zn)^{2+} + (As,Sb)^{3+} = Cu^{+} + Te^{4+}$ [20,61,62]. Shimizu and Stanley (1991) [63] report tetrahedrite from the Iriki mine, Japan, with compositions varying from Te-free tetrahedrite to goldfieldite containing up to 18.5 wt % Te. Similarly, Knittel (1989) [62] measure up to 17.68 wt % Te in arsenian goldfieldite from the Marian gold mine, northern Luzon, Philippines.

Hakite and giraudite are the Se-dominant analogues of tetrahedrite and tennantite, respectively. Förster et al. (2002) [51] measure up to 39.98 wt % Se (10.86 *apfu*) and 37.55 wt % Se (11.1 *apfu*) in mercurian giraudite and hakite, respectively, from the Niederschlema-Alberoda uranium deposit, Erzgebirge, Germany. Selenium-bearing goldfieldite is reported by Pohl et al. (1996) [64] suggesting extensive solid solution among the less-common members of the tetahedrite group.

Indium-bearing tetrahedrite-tennantite is occasionally recorded (e.g., [65–68]). Gaspar (2002) [69] document up to 2.7 and 0.2 wt %. In tennantite and tetrahedrite, respectively, from Neves-Corvo, Portugal.

Tin, Co and Ni have been measured in tetrahedrite-tennantite up to a few thousand ppm. Gaspar (2002) [69] report tetrahedrite and tennantite from Neves-Corvo, Portugal, carrying up to 4784 and 1300 ppm Sn, respectively. Tetrahedrite from the same deposit contains up to 4300 ppm Co. Serranti et al. (2002) [66] also measure 4784 ppm Sn in tetrahedrite from the Corvo orebody, Portugal, as well as up to 1369 ppm Ni in tennantite. Up to 3800 ppm Co was measured in tetrahedrite-tennantite in a fluorite vein from Oberwolfach, Clara, SW Germany, and up to 6900 ppm Ni was measured from nearby Urberg, Gottesehre [13].

Gold is occasionally present in tetrahedrite-tennantite, usually only at a few ppm at most. Knittel (1989) [62], however, measured up to 0.02 wt % Au in tellurian tennantite from the Marian

gold mine, northern Luzon, Philippines, while Jurković et al. (2011b) [70] record up to 39 ppm Au in mercurian tetrahedrite from the Duboki Vagan deposit, Bosnia. Wohlgemuth-Ueberwasser et al. (2015) [71] also measured up to 19.4 ppm Au in tetrahedrite-tennantite from black smokers in the Manus Basin, Papua New Guinea, and infer that tetrahedrite-tennantite may control Au distributions in a sulphide assemblage. Unique tetrahedrite from Saski Rad, Bosnia, has also been documented containing 92 ppm Tl, 20 ppm W, 7.3 ppm Mo, and 0.5 ppm Ga, elements that are rarely if ever reported as a trace component in tetrahedrite-tennantite [70].

3. Approach and Methodology

The published data above show that alongside the essential constituents Cu, Fe, Zn, Sb, As, and S, the tetrahedrite isotypic series may incorporate up to wt % levels of Ag, Mn, Cd, Bi, Pb, In, Hg, Se, and Te, thousands of ppm Ni, Co, and Sn, at least ppm-level concentrations of Au, Tl, W, and Mo, and possibly also Ga. We have sought to analyse the concentrations of these 23 elements in a suite of 37 samples (Table 2). Sample material mostly derives from collections of the South Australian Museum and the Tate Museum (The University of Adelaide; as indicated in Table 2), while some material originates from the author's personal collections. Although some samples comprise solely tetrahedrite-tennantite (i.e., without other sulphides present), most were selected because they consist of tetrahedrite-tennantite co-existing with other base metal sulphides. Textural evidence suggests that these assemblages co-crystallized at equilibrium (~120° triple-junctions between sulphides; see Figure 2). The trace element partitioning rules for BMS outlined in George et al. (2016) [30] were employed as an additional check for assessing BMS co-crystallization. Thus through trace element analysis of the sulphides in each co-crystallized assemblage, the preferred partitioning of trace elements can be determined for a BMS assemblage comprising tetrahedrite-tennantite.

Quantitative analysis on tetrahedrite-tennantite was carried out using a Cameca SX-Five EPMA (Cameca, Gennevilliers, France), which utilizes five wavelength dispersive spectrometers (WDS). The elements analysed were S, Pb, Cd, As, Se, Fe, Cu, Mn, Ag, Sn In, Hg, Zn, Ni, Co, Sb, Te, Bi, Tl, and Ga. Beam operating conditions were maintained at 20 kV and 20 A with a beam size of 5 μm. Further details on EPMA methodology, including standards, count times and typical minimum limits of detection, are given as Electronic Appendix A. EPMA element maps were generated using the same instrument. An operating voltage of 20 kV and 224 nA were applied for EPMA mapping of selected grains, with a step size of 4 μm.

LA-ICP-MS instrumentation and analytical procedures followed those given in George et al. (2016) [30] and George et al. (in press) [72]. A Resonetics M-50-LR 193 nm Excimer laser (Resonetics, Nashua, NH, USA) and an Agilent 7700cx Quadrupole ICP mass spectrometer (Agilent, Santa Clara, CA, USA) were used for the LA-ICP-MS analysis of tetrahedrite-tennantite (Adelaide Microscopy, The University of Adelaide). An atmosphere of ultra-high purity (UHP) He (0.7 L/min) was created inside the ablation cell, and Ar (0.93 L/min) was mixed with the ablated material upon exiting the cell. The mixture then passed through a pulse-homogenizing device (squid) before being directed to the torch. Regular calibration of the ICP-MS was performed so that the sensitivity on the isotopes of interest was maximized, and formation of unwanted molecular oxide species was kept at a minimum.

Laser beam energy was kept at 100 mJ with a 26 μm spot size, while the repetition rate was maintained at 10 Hz. Each analysis was a total of 60 s, consisting of a 30 s background measurement and 30 s of sample ablation. A delay of 40 s was allowed between each analysis for cell washout and gas stabilization. The following isotopes were analysed: ^{34}S, ^{55}Mn, ^{57}Fe, ^{59}Co, ^{60}Ni, ^{65}Cu, ^{66}Zn, ^{69}Ga, ^{75}As, ^{82}Se, ^{95}Mo, ^{107}Ag, ^{111}Cd, ^{115}In, ^{118}Sn, ^{121}Sb, ^{125}Te, ^{182}W, ^{197}Au, ^{202}Hg, ^{205}Tl, ^{206}Pb, ^{207}Pb, ^{208}Pb, and ^{209}Bi. The dwell time for each element was 0.01 s, while In, Au, and Tl were set to 0.05 s. Unless tetrahedrite-tennantite was fine-grained and sparse within any given sample, we aimed to make 10 spot analyses on each sample. Electronic Appendix B shows the range of minimum detection limits and mean errors for the trace elements analysed. Electronic Appendix C shows the full tetrahedrite-tennantite LA-ICP-MS dataset, as well as the data for co-existing sphalerite, galena and chalcopyrite also analysed in each sample according to methodology outlined in George et al., (2016) [30].

Table 2. Summary of samples used in this study.

Sample	Tetrahedrite-Tennantite Composition	Assemblage	Locality	Ore Type
G16396 *	$(Cu_{9},Ag_{1.2},Zn_{0.9},Fe_{0.9},Pb_{0.1})$ $(Sb_{3.8},As_{0.1})$ S_{13}	*Tet, Sp, Gn, Cp*	Broken Hill, NSW, Australia	SEDEX (recrystallized)
G11579 *	$(Cu_{9.6},Ag_{0.3},Zn_{1},Fe_{0.9})$ $(Sb_{3.7},As_{0.2})$ $S_{13.2}$	*Tet, Sp, Cp, Gn*	Kalgoorlie, WA, Australia	Orogenic Au
G13289b *	$(Cu_{10.1},Zn_{1.7},Fe_{0.3})$ $(Sb_{3.2},As_{0.8})$ $S_{12.9}$	*Tet, Gn, Cp, Sp*	S. Wheal Exmouth, Devon, England	Low temperature replacement
G6940 *	$(Cu_{9.5},Ag_{0.5},Fe_{1.2},Zn_{0.8})$ $(Sb_{3.8},As_{0.2})$ S_{13}	*Tet, Cp, Sp, Gn*	Great Boulder Mine, WA, Australia	Orogenic Au
G13289a *	$(Cu_{10.1},Zn_{1.7},Fe_{0.3})$ $(Sb_{3.2},As_{0.7})$ S_{13}	*Tet, Cp, Sp, Gn*	S. Wheal Exmouth, Devon, England	Low temperature replacement
V446	$(Cu_{8.2},Ag_{1.9},Fe_{1.7},Zn_{0.4})$ $Sb_{3.9}$ S_{13}	*Sp, Gn, Cp, Tet*	Bleikvassli, Norway	SEDEX (recrystallized)
V538	$(Cu_{7.8},Ag_{2.2},Fe_{1.7},Zn_{0.4})$ $Sb_{3.9}$ $S_{13.1}$	*Sp, Gn, Cp, Tet*	Bleikvassli, Norway	SEDEX (recrystallized)
Hj13	$(Cu_{9.2},Ag_{0.6},Fe_{1.6},Zn_{0.4})$ $Sb_{3.9}$ $S_{13.2}$	*Gn, Cp, Sp, Tet*	Herja, Romania	Epithermal
G6951 *	$(Cu_{9.4},Ag_{0.5},Zn_{1.8},Cd_{0.1})$ $(Sb_{3.5},As_{0.4})$ $S_{13.2}$	*Tet, Sp, Gn, (Cp)*	Yerranderie, NSW, Australia	Epithermal
Bv97-52	$(Cu_{9},Ag_{0.6},Fe_{1.6},Zn_{0.7},Pb_{0.2})$ $(As_{2.8},Sb_{1.5})$ $S_{13.2}$	*Ten, Sp, Gn*	Bleikvassli, Norway	SEDEX (recrystallized)
G10847 *	$(Cu_{10},Ag_{0.1},Zn_{1.7},Fe_{0.3})$ $(Sb_{2.1},As_{1.8})$ S_{13}	*Tet, Sp, Gn*	Mt. Camel, Heathcote, Vic., Australia	Greenstone hosted
EV8 **	$(Ag_{5.6},Cu_{4.6},Fe_{1.9},Zn_{0.3})$ $Sb_{3.9}$ $S_{12.6}$	*Gn, Sp, Tet*	Evelyn Mine, NT, Australia	VMS
Hj14	$(Cu_{6.8},Ag3.2,Fe_{1.8},Zn_{0.3})$ $Sb_{3.8}$ $S_{13.2}$	*Gn, Sp, Tet*	Herja, Romania	Epithermal
G6948 *	$(Cu_{9.6},Ag_{0.5},Fe_{1.4},Zn_{0.6})$ $(Sb_{3.9},As_{0.1})$ S_{13}	*Tet, Sp, Cp, (Gn)*	Medcritting, Tas., Australia	Unknown
G14549b *	$(Cu_{8.7},Ag1.8,Fe_{1.1},Zn_{0.7})$ $(Sb_{3.8},As_{2.8})$ $S_{12.8}$	*Tet, Sp, Cp*	Consols Mine, Broken Hill, NSW, Australia	SEDEX (recrystallized)
Mo17A	$(Cu_{7.2},Ag_{2.5},Fe_{1.6},Zn_{0.4},Pb_{0.4})$ $(Sb_{3.7},As_{0.1})$ $S_{13.1}$	*Cp, Gn, Tet*	Mofjell, Norway	SEDEX (recrystallized)
ORV1	$(Cu_{10.1},Ag_{0.1},Zn_{1.3},Fe_{0.4})$ $(Sb_{3.1},As_{0.8})$ $S_{13.2}$	*Cp, Gn, Tet*	Oravita, Romania	Skarn
G14549a *	$(Cu_{8.7},Ag_{2.4},Fe_{1.1},Zn_{0.7})$ $Sb_{3.7}$ $S_{12.3}$	*Tet, Gn, (Sp)*	Consols Mine, Broken Hill, NSW, Australia	SEDEX (recrystallized)
G873 *	$(Cu_{9.5},Ag_{0.7},Zn_{1.2},Fe_{0.7})$ $(Sb_{3},As_{0.9})$ $S_{12.9}$	*Tet, Gn*	Yerranderrie, NSW, Australia	Epithermal
G16152 *	$(Cu_{10},Ag_{0.1},Zn_{1.1},Fe_{0.8},Co_{0.1})$ $(Sb_{2.2},As_{1.8})$ S_{13}	*Tet, Cp, (Gn)*	Siegen, Westphalia, Germany	SEDEX?
G871 *	$(Cu_{10.1},Hg_{0.9},Fe_{0.5},Zn_{0.5})$ $(Sb_{3.2},As_{0.7})$ $S_{13.1}$	*Tet, Cp*	Pulganbar, Grafton, NSW, Australia	Vein hosted
G874 *	$(Cu_{10.3},Zn_{1},Hg_{0.5},Fe_{0.4})$ $(Sb_{3.3},As_{0.6})$ $S_{12.8}$	*Tet, Cp*	Pulganbar, Grafton, NSW, Australia	Vein hosted
G879 *	$(Cu_{9.6},Ag_{0.4},Fe_{1.6},Zn_{0.4})$ $(Sb_{3.8},As_{0.1})$ $S_{13.2}$	*Tet, Cp*	Ring Valley, Tas., Australia	Fissure fillings
G882 *	$(Cu_{10.3},Fe_{1},Zn_{0.3},Hg_{0.2})$ $(Sb_{2.5},As_{1.4})$ $S_{13.1}$	*Tet, Cp*	Pulganbar, Grafton, NSW, Australia	Vein hosted
G6946 *	$(Cu_{10},Ag_{0.1},Zn_{1.3},Fe_{0.6})$ $(Sb_{3.7},As_{0.2})$ $S_{13.1}$	*Tet, Cp*	Siegen, Westphalia, Germany	SEDEX?
G6949 *	$(Cu_{9.7},Ag_{0.2},Fe_{1.7},Zn_{0.3})$ $(Sb_{3.9},As_{0.1})$ $S_{13.1}$	*Tet, Cp*	Webb's Ag Mine, Emmaville, NSW, Australia	Veins and dissemination
G11701 *	$(Cu_{5.2},Ag_{5.1},Fe_{1.6},Zn_{0.4})$ Sb_{4} $S_{12.6}$	*Tet, Cp*	Broken Hill, NSW, Australia	SEDEX (recrystallized)
G14246 *	$(Cu_{9.8},Ag_{0.2},Fe_{1.5},Zn_{0.5})$ $(Sb_{3.8},As_{0.1})$ $S_{13.1}$	*Tet, Cp*	Curtin Davis Mine, Dundas, Tas., Australia	Intrusion related?
G14867 *	$(Cu_{10.5},Fe_{1.4},Zn_{0.2})$ $(As_{3.1},Sb_{0.8})$ S_{13}	*Ten, Cp*	Oraparinna, SA, Australia	Diapir related
Mo16	$(Cu_{7.3},Ag_{2.6},Fe_{1.8},Zn_{0.2})$ $(Sb_{3.8},As_{0.8})$ $S_{13.2}$	*Cp, Tet, (Gn)*	Mofjell, Norway	SEDEX (recrystallized)
G29851 *	$(Cu_{10.2},Fe_{1.1},Zn_{0.5},Hg_{0.2})$ $(As_{3.6},Sb_{0.3})$ S_{13}	*Cp, Ten*	Gortdrum Mine, Ireland	Carbonate hosted
ORV4	$(Cu_{10.1},Zn_{1.4},Fe_{0.4})$ $(Sb_{2.7},As_{1.2})$ $S_{13.2}$	*Cp, Tet*	Oravita, Romania	Skarn
G12640 *	$(Cu_{10.2},Zn_{1.1},Fe_{0.9})$ $(As_{2.5},Sb_{1.4})$ $S_{12.9}$	*Ten*	Tinga, NSW, Australia	Unknown
G13301 *	$(Cu_{10.2},Fe_{1.2},Zn_{0.4})$ $(Sb_{3.3},As_{0.6})$ $S_{13.3}$	*Tet*	Allihies Mine, Castletown, Cork, Ireland	Unknown
G15977 *	$(Cu_{10.1},Zn_{1.2},Fe_{0.7})$ $(Sb_{3.2},As_{0.7})$ S_{13}	*Tet*	Mooloowatana HS, SA, Australia	Unknown
G16835 *	$(Cu_{10.1},Ag_{0.1},Zn_{1},Fe_{0.7},Hg_{0.1})$ $(As_{2},Sb_{1.9})$ $S_{13.1}$	*Ten*	Grosskogel Mine, Austria	MVT?
VFI031 **	$(Cu_{8.4},Ag_{1.7},Zn_{1.9})$ $(Sb_{2.4},As_{1.4})$ $S_{13.1}$	*Tet*	Emperor Gold Mine, Fiji	Epithermal

Tet = tetrahedrite, *Ten* = tennantite, *Sp* = sphalerite, *Gn* = galena, *Cp* = chalcopyrite. Minerals in brackets are very minor phases. Tetrahedrite-tennantite composition determined by electron probe microanalysis. * Sample derives from the South Australian Museum. ** Sample derives from the Tate Museum. Other samples derive from the author's personal collection.

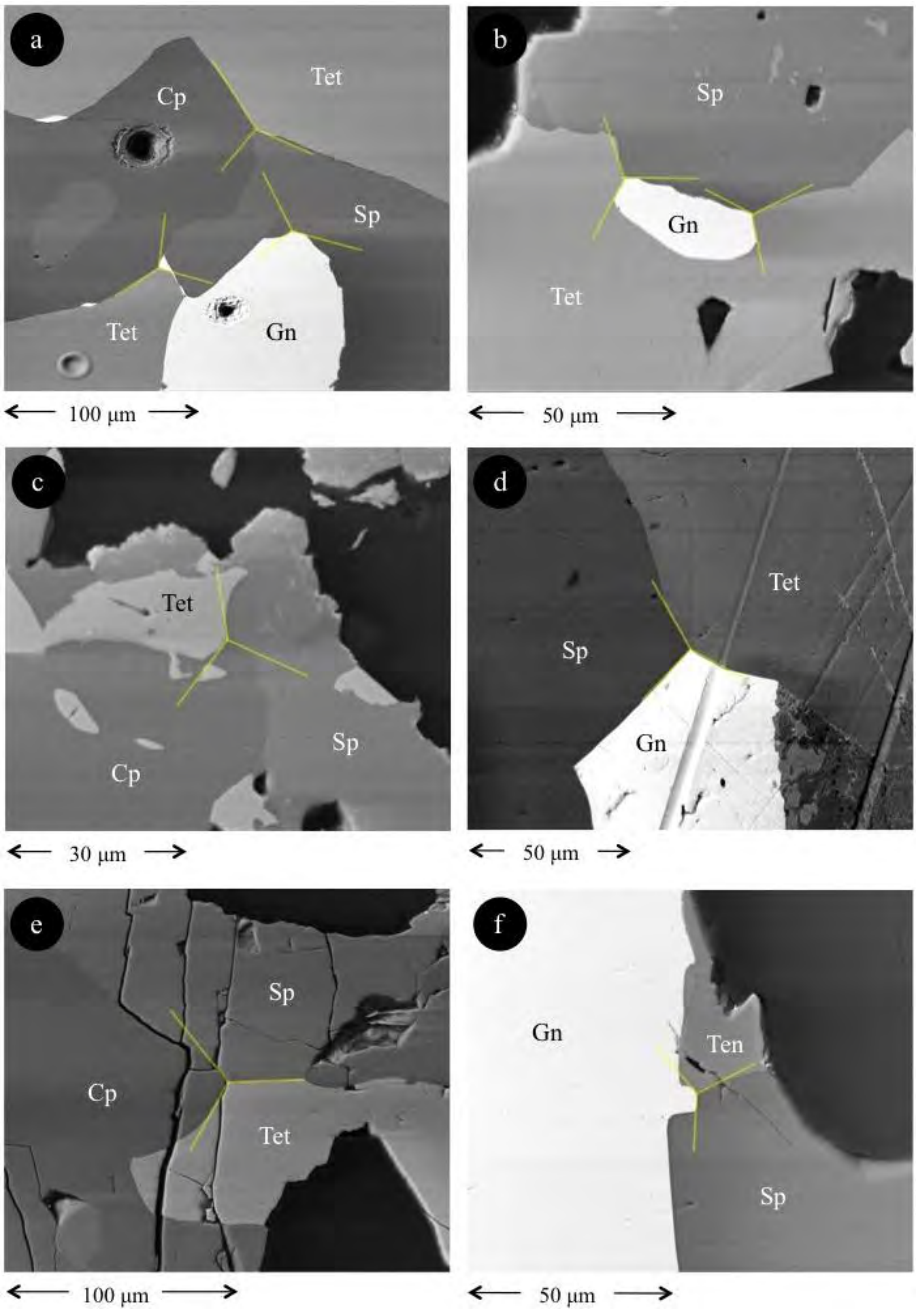

Figure 2. Representative back-scattered electron images illustrating textural evidence for tetrahedrite-tennantite and base metal sulphide (BMS) co-crystallization. (**a**) ~120° triple-junction grain boundaries as evidence for co-crystallization of tetrahedrite (Tet), sphalerite (Sp), galena (Gn) and chalcopyrite (Cp) in G11579 (Kalgoorlie, WA, Australia). Additional ~120° triple-junction grain boundaries between tetrahedrite, tennantite (Ten), sphalerite, galena, and chalcopyrite are illustrated from samples G6948 (Medcritting, Australia; (**b**,**c**), G10847 (Mt. Camel, Heathcote, Australia; (**d**), G6940 (Great Boulder Mine, WA, Australia; (**e**) and Bv97-52 (Bleikvassli, Norway; (**f**). Note grain boundaries curving towards the triple junction in order to approximate 120°.

The external standard used was MASS-1 (previously PS-1; [73]), utilizing the latest certificate of analysis [74]. Up to 10 unknown analyses were bracketed by multiple analyses of this reference material. Thus instrument drift was monitored, and a linear correction was applied to the unknown analyses. All data reduction was carried out using GLITTER [75]. Internal standardization was conducted using Cu concentration values obtained by EPMA on each individual sample. While certain interferences may have affected the reliability of some elements analysed by LA-ICP-MS (e.g., sulphur interference on ^{66}Zn; [76], or $^{59}Co^{16}O$ interference on ^{75}As; [77]), corrections were not applied as reliable measurements on these typically major elements were made by EPMA.

4. Results

As discussed in Cook et al. (2016) [78] and George et al. (in press) [72], mineral microanalysts are continually faced with the challenge of determining whether measurable concentrations of an element in any given mineral are present in solid solution, within microscale mineral inclusions hosted within the analysed mineral, or a mixture of both. Every effort has been made in the present study to report data that reflects elements in solid solution within the tetrahedrite-tennantite structure. This was done by examining all samples in back-scatter electron mode with a scanning electron microscope (SEM) prior to microanalysis so that only clean areas free of any noticeable inclusions were analysed. In addition, all downhole spectra from the LA-ICP-MS datasets were additionally checked for any peaks that suggest the presence of micro-inclusions beneath the sample surface (e.g., [72,79]). If present, such analyses were discarded. It is evident that some elements, notably Pb, are more commonly present as micro-inclusions in tetrahedrite-tennantite than others, perhaps due to the common presence of co-existing galena.

Table 3 summarizes the concentrations of 16 elements in tetrahedrite-tennantite as determined by EPMA. Nickel, Ga, In, and Tl were also measured, but analyses were consistently below the minimum limits of detection (average values of 0.022, 0.041, 0.031, and 0.126 wt %, respectively). Figure 3 shows the major element variation in the tetrahedrite-tennantite sample suite. Specimens spanning the entire tetrahedrite-tennantite solid solution range are represented (Figure 3a), as are samples ranging in composition from essentially Fe to Zn pure end-members (Figure 3b). Most tetrahedrite-tennantites here contain more Cu than Ag; only in sample EV8 (Evelyn Mine, NT, Australia) could freibergite be classified (Figure 3c; Table 3).

Concentrations of 20 trace and minor elements measured in tetrahedrite-tennantite by LA-ICP-MS are summarized in Table 4. Individual spot analyses are plotted as cumulative plots (Figures 4 and 5) that are sorted by the co-crystallized BMS assemblage. This allows a visualization of element concentrations and variation in different assemblages. In one sample (G871; Pulganbar, Grafton, NSW, Australia), clear oscillatory zoning was observed and mapped by EPMA (Figures 6 and 7). The zoning shows the inverse correlation between the trivalent cations Sb and As, such that Sb enriched zones are As depleted, and vice versa. Zones of high Cu, Fe, and Zn correlate with As enriched, Sb depleted zones, while high Hg zones correlate to Sb-enriched, As depleted zones. While such strong zoning appeared to be uncommon in the sample suite, other analysed tetrahedrite-tennantites may be considered as zoned to some degree based on variation of concentration values between spots. In general, grain-scale compositional zoning is common in tetrahedrite-tennantite, although this is more commonly observed as patchy heterogeneity (e.g., [80]). Micron-scale oscillatory zoning of the kind illustrated here is, however, well known from epithermal systems (e.g., [81]).

Table 3. Summary of element concentrations in tetrahedrite-tennantite determined by electron probe microanalysis (EPMA) (data in wt %).

Sample/Assemblage		S	Mn	Fe	Co	Cu	Zn	As	Se	Ag	Cd	Sn	Sb	Te	Hg	Pb	Bi	TOTAL
G16396 *	Mean (10)	24.4	0.016	3.07	-	33.3	3.59	0.237	0.021	7.25	0.051	-	27.3	-	0.069	0.994	-	100.1
Tet, Sp, Gn, Cp	*apfu*	*13.0*	*0.005*	*0.942*	-	*8.97*	*0.942*	*0.054*	*0.005*	*1.16*	*0.008*	-	*3.84*	-	*0.006*	*0.083*	-	*29.0*
G11579	Mean (10)	25.9	-	3.08	-	37.3	4.19	0.903	0.018	2.27	-	-	27.7	-	0.079	0.076	0.110	101.6
Tet, Sp, Cp, Gn	*apfu*	*13.2*	-	*0.902*	-	*9.59*	*1.05*	*0.197*	*0.004*	*0.344*	-	-	*3.72*	-	*0.006*	*0.006*	*0.009*	*29.0*
G13289b *	Mean (10)	25.5	-	1.06	-	39.5	6.71	3.47	-	0.243	-	-	23.6	-	0.076	0.066	-	100.1
Tet, Gn, Cp, Sp	*apfu*	*12.9*	-	*0.310*	-	*10.1*	*1.67*	*0.755*	-	*0.037*	-	-	*3.16*	-	*0.006*	*0.005*	-	*29.0*
G6940	Mean (10)	25.1	0.018	3.93	0.019	36.3	3.14	0.679	0.021	3.33	-	-	27.4	-	0.084	0.068	0.092	100.0
Tet, Cp, Sp, Gn	*apfu*	*13.0*	*0.005*	*1.18*	*0.005*	*9.55*	*0.801*	*0.151*	*0.004*	*0.516*	-	-	*3.76*	-	*0.007*	*0.005*	*0.007*	*29.0*
G13289a *	Mean (10)	25.7	-	0.976	-	39.4	6.77	3.20	0.031	0.212	-	-	24.1	-	0.073	0.079	-	100.4
Tet, Cp, Sp, Gn	*apfu*	*13.0*	-	*0.284*	-	*10.1*	*1.68*	*0.693*	*0.006*	*0.032*	-	-	*3.21*	-	*0.006*	*0.006*	-	*29.0*
V446	Mean (7)	24.1	0.031	5.36	0.022	30.0	1.69	-	-	11.6	-	-	27.5	0.032	0.098	0.108	-	100.5
Sp, Gn, Cp, Tet	*apfu*	*13.0*	*0.010*	*1.65*	*0.006*	*8.16*	*0.446*	-	-	*1.86*	-	-	*3.90*	*0.004*	*0.008*	*0.009*	-	*29.0*
V538	Mean (10)	24.2	0.020	5.42	0.023	28.7	1.33	-	0.033	13.5	-	0.029	27.3	-	0.100	0.086	-	100.6
Sp, Gn, Cp, Tet	*apfu*	*13.1*	*0.006*	*1.68*	*0.007*	*7.82*	*0.352*	-	*0.007*	*2.16*	-	*0.004*	*3.88*	-	*0.009*	*0.007*	-	*29.0*
Hj13	Mean (10)	25.4	0.021	5.39	0.025	35.2	1.76	-	0.025	3.88	-	0.053	28.7	-	0.118	0.088	-	100.5
Gn, Cp, Sp, Tet	*apfu*	*13.2*	*0.006*	*1.61*	*0.007*	*9.22*	*0.449*	-	*0.005*	*0.600*	-	*0.007*	*3.92*	-	*0.010*	*0.007*	-	*29.0*
G6951 *	Mean (10)	25.6	-	0.043	0.018	36.4	7.30	1.86	0.019	3.45	0.674	-	26.0	-	0.082	0.078	-	101.4
Tet, Sp, Gn, (Cp)	*apfu*	*13.2*	-	*0.013*	*0.005*	*9.44*	*1.84*	*0.408*	*0.004*	*0.526*	*0.099*	-	*3.51*	-	*0.007*	*0.006*	-	*29.0*
Bv97-52	Mean (10)	27.0	0.060	5.63	0.023	36.9	2.63	13.9	0.028	3.45	0.041	0.035	11.3	-	0.078	2.10	-	100.2
Ten, Sp, Gn	*apfu*	*13.2*	*0.017*	*1.58*	*0.006*	*9.01*	*0.650*	*2.80*	*0.006*	*0.568*	*0.005*	*0.004*	*1.53*	-	*0.006*	*0.199*	-	*29.0*
G10847	Mean (10)	26.8	-	1.00	-	40.7	6.98	8.43	-	0.745	-	-	16.6	-	0.230	0.076	-	101.6
Tet, Sp, Gn	*apfu*	*13.0*	-	*0.281*	-	*10.0*	*1.67*	*1.76*	-	*0.108*	-	-	*2.13*	-	*0.018*	*0.006*	-	*29.0*
EV8	Mean (10)	21.3	-	5.62	-	15.5	1.02	-	0.029	32.1	-	0.264	25.3	-	0.095	0.409	0.066	101.4
Gn, Sp, Tet	*apfu*	*12.6*	-	*1.91*	-	*4.63*	*0.294*	-	*0.007*	*5.64*	-	*0.042*	*3.94*	-	*0.009*	*0.038*	*0.006*	*29.0*
Hj14	Mean (6)	24.0	0.018	5.56	0.022	24.4	0.937	-	0.018	19.3	-	-	26.5	-	0.082	0.102	-	100.9
Gn, Sp, Tet	*apfu*	*13.2*	*0.006*	*1.76*	*0.007*	*6.77*	*0.253*	-	*0.004*	*3.15*	-	-	*3.85*	-	*0.007*	*0.009*	-	*29.0*
G6948	Mean (10)	24.9	0.047	4.60	-	36.3	2.33	0.234	0.027	3.39	-	-	28.1	-	0.086	0.071	0.091	100.0
Tet, Sp, Cp, (Gn)	*apfu*	*13.0*	*0.014*	*1.38*	-	*9.55*	*0.597*	*0.052*	*0.006*	*0.526*	-	-	*3.86*	-	*0.007*	*0.006*	*0.007*	*29.0*
G14549b	Mean (10)	24.0	-	3.73	-	32.5	2.66	0.134	0.017	11.1	0.147	-	27.3	-	0.094	0.255	0.129	101.7
Tet, Sp, Cp	*apfu*	*12.8*	-	*1.14*	-	*8.72*	*0.696*	*0.031*	*0.004*	*1.84*	*0.022*	-	*3.82*	-	*0.008*	*0.023*	*0.011*	*29.0*
Mo17A	Mean (7)	23.7	-	5.08	-	25.8	1.34	0.278	0.048	15.4	0.054	-	25.5	-	0.074	4.01	-	100.6
Cp, Gn, Tet	*apfu*	*13.1*	-	*1.62*	-	*7.21*	*0.363*	*0.065*	*0.012*	*2.54*	*0.009*	-	*3.73*	-	*0.007*	*0.390*	-	*29.0*
ORV1	Mean (10)	26.2	-	1.47	-	39.8	5.47	3.65	0.018	0.531	-	-	23.5	-	0.088	0.087	0.065	100.8
Cp, Gn, Tet	*apfu*	*13.2*	-	*0.427*	-	*10.1*	*1.34*	*0.783*	*0.004*	*0.079*	-	-	*3.11*	-	*0.007*	*0.007*	*0.005*	*29.0*
G14549a	Mean (10)	22.4	-	3.55	-	31.7	2.58	0.195	0.023	13.5	0.047	-	25.8	-	0.083	0.254	0.181	100.2
Tet, Gn, (Sp)	*apfu*	*12.3*	-	*1.12*	-	*8.74*	*0.694*	*0.045*	*0.005*	*2.36*	*0.008*	-	*3.73*	-	*0.007*	*0.021*	*0.016*	*29.0*
G873	Mean (10)	24.8	-	2.48	-	36.3	4.76	3.96	-	4.59	0.034	-	22.2	-	0.077	0.113	-	99.3
Tet, Gn	*apfu*	*12.9*	-	*0.740*	-	*9.52*	*1.21*	*0.881*	-	*0.710*	*0.005*	-	*3.04*	-	*0.006*	*0.009*	-	*29.0*
G16152	Mean (10)	26.6	-	2.82	0.362	40.7	4.38	8.48	-	0.449	-	-	16.8	-	0.185	0.066	-	100.9

Table 3. *Cont.*

Sample/Assemblage		S	Mn	Fe	Co	Cu	Zn	As	Se	Ag	Cd	Sn	Sb	Te	Hg	Pb	Bi	TOTAL
Tet, Cp, (Gn)	*apfu*	*13.0*	-	*0.792*	*0.096*	*10.0*	*1.05*	*1.77*	-	*0.065*	-	-	*2.17*	-	*0.014*	*0.005*	-	*29.0*
G871	Mean (10)	24.2	-	1.50	0.068	37.1	1.70	3.17	-	0.051	-	-	22.6	-	10.6	0.076	-	101.1
Tet, Cp	*apfu*	*13.1*	-	*0.464*	*0.020*	*10.1*	*0.449*	*0.726*	-	*0.008*	-	-	*3.23*	-	*0.922*	*0.006*	-	*29.0*
G874	Mean (10)	24.1	-	1.32	0.079	38.3	3.81	2.72	-	0.050	-	-	23.7	-	5.79	0.056	-	99.8
Tet, Cp	*apfu*	*12.8*	-	*0.404*	*0.023*	*10.3*	*1.00*	*0.621*	-	*0.008*	-	-	*3.33*	-	*0.494*	*0.005*	-	*29.0*
G879	Mean (10)	25.6	-	5.43	-	37.0	1.48	0.291	0.025	2.59	-	-	28.5	-	0.077	0.064	0.073	101.0
Tet, Cp	*apfu*	*13.2*	-	*1.60*	-	*9.58*	*0.371*	*0.064*	*0.005*	*0.395*	-	-	*3.85*	-	*0.006*	*0.005*	*0.006*	*29.0*
G882	Mean (10)	26.4	-	3.54	0.087	41.2	1.34	6.78	-	-	-	-	19.0	-	3.10	0.070	-	101.6
Tet, Cp	*apfu*	*13.1*	-	*1.01*	*0.024*	*10.3*	*0.327*	*1.44*	-	-	-	-	*2.50*	-	*0.247*	*0.005*	-	*29.0*
G6946	Mean (10)	25.7	-	2.05	-	39.0	5.14	1.04	0.023	0.600	-	-	27.5	-	0.158	0.059	-	101.3
Tet, Cp	*apfu*	*13.1*	-	*0.600*	-	*10.0*	*1.28*	*0.226*	*0.005*	*0.091*	-	-	*3.69*	-	*0.013*	*0.005*	-	*29.0*
G6949	Mean (10)	25.8	0.015	5.72	-	37.9	1.30	0.331	0.020	1.23	-	-	28.9	-	0.081	0.057	0.136	101.4
Tet, Cp	*apfu*	*13.1*	*0.004*	*1.67*	-	*9.75*	*0.326*	*0.072*	*0.004*	*0.186*	-	-	*3.87*	-	*0.007*	*0.005*	*0.011*	*29.0*
G11701	Mean (10)	21.5	-	4.72	0.026	17.6	1.48	-	0.025	29.2	-	-	26.1	-	0.081	0.055	-	100.6
Tet, Cp	*apfu*	*12.6*	-	*1.59*	*0.008*	*5.21*	*0.425*	-	*0.006*	*5.10*	-	-	*4.03*	-	*0.008*	*0.005*	-	*29.0*
G14246	Mean (10)	25.6	-	5.10	-	37.6	1.86	0.298	0.029	1.41	-	-	28.3	-	0.082	0.073	0.173	100.6
Tet, Cp	*apfu*	*13.1*	-	*1.50*	-	*9.76*	*0.470*	*0.065*	*0.006*	*0.215*	-	-	*3.83*	-	*0.007*	*0.006*	*0.014*	*29.0*
G14867	Mean (10)	28.0	-	5.06	0.023	44.7	0.765	15.5	0.020	0.049	-	-	6.40	-	0.392	0.073	0.135	101.0
Ten, Cp	*apfu*	*13.0*	-	*1.35*	*0.006*	*10.5*	*0.175*	*3.10*	*0.004*	*0.007*	-	-	*0.786*	-	*0.029*	*0.005*	*0.010*	*29.0*
Mo16	Mean (7)	24.3	-	5.62	0.024	26.5	0.933	3.60	0.024	15.9	0.054	-	26.7	-	0.089	0.088	-	100.6
Cp, Tet, (Gn)	*apfu*	*13.2*	-	*1.76*	*0.007*	*7.25*	*0.247*	*0.802*	*0.005*	*2.58*	*0.008*	-	*3.83*	-	*0.008*	*0.007*	-	*29.0*
G29851	Mean (10)	27.9	-	4.10	0.021	43.2	2.01	18.0	-	0.093	-	0.026	2.72	-	3.28	0.084	0.087	101.4
Cp, Ten	*apfu*	*13.0*	-	*1.10*	*0.005*	*10.2*	*0.461*	*3.60*	-	*0.013*	-	*0.003*	*0.337*	-	*0.246*	*0.006*	*0.006*	*29.0*
ORV4	Mean (10)	26.6	-	1.48	-	40.3	5.89	5.68	-	0.156	0.048	-	20.6	-	0.070	0.070	-	100.9
Cp, Tet	*apfu*	*13.2*	-	*0.419*	-	*10.1*	*1.43*	*1.20*	-	*0.023*	*0.007*	-	*2.70*	-	*0.006*	*0.005*	-	*29.0*
G12640	Mean (10)	27.1	0.017	3.46	-	42.3	4.53	12.1	-	0.212	-	-	11.2	-	0.122	0.072	-	101.1
Ten	*apfu*	*12.9*	*0.005*	*0.947*	-	*10.2*	*1.06*	*2.46*	-	*0.030*	-	-	*1.41*	-	*0.009*	*0.005*	-	*29.0*
G13301	Mean (10)	26.7	-	4.24	0.070	40.8	1.59	3.01	0.020	-	0.069	-	25.0	-	0.149	0.074	-	101.7
Tet	*apfu*	*13.3*	-	*1.21*	*0.019*	*10.2*	*0.387*	*0.639*	*0.004*	-	*0.010*	-	*3.27*	-	*0.012*	*0.006*	-	*29.0*
G15977	Mean (10)	26.0	-	2.53	-	39.8	5.07	3.45	-	0.102	0.243	-	24.2	-	0.117	0.083	-	101.3
Tet	*apfu*	*13.0*	-	*0.726*	-	*10.1*	*1.24*	*0.739*	-	*0.015*	*0.035*	-	*3.19*	-	*0.009*	*0.006*	-	*29.0*
G16835	Mean (10)	27.1	-	2.68	0.027	41.5	4.00	9.61	-	0.398	-	-	14.9	-	0.904	0.093	0.093	101.1
Ten	*apfu*	*13.1*	-	*0.746*	*0.007*	*10.1*	*0.952*	*1.99*	-	*0.057*	-	-	*1.90*	-	*0.070*	*0.007*	*0.007*	*29.0*
VFI031	Mean (5)	25.5	0.107	0.039	-	32.2	7.47	6.52	0.036	10.8	-	-	17.9	0.159	0.469	0.083	-	101.2
Tet	*apfu*	*13.1*	*0.032*	*0.011*	-	*8.37*	*1.89*	*1.43*	*0.008*	*1.65*	-	-	*2.43*	*0.020*	*0.039*	*0.007*	-	*29.0*

Tet = tetrahedrite, *Ten* = tennantite, *Sp* = sphalerite, *Gn* = galena, *Cp* = chalcopyrite, *apfu* = atoms per formula unit. Minerals in brackets are very minor phases. (X) = number of individual spot analyses in that sample. * Evidence suggests sulphides in sample did not co-crystallize (based on textures and partitioning trends among base metal sulphides). Dash = insufficient data to perform calculation (all analyses <mdl). Other <mdl values were ignored, thus data can be considered maximum concentrations. Totals are calculated by averaging the total for each spot in each sample. Hence each row will not add to the total.

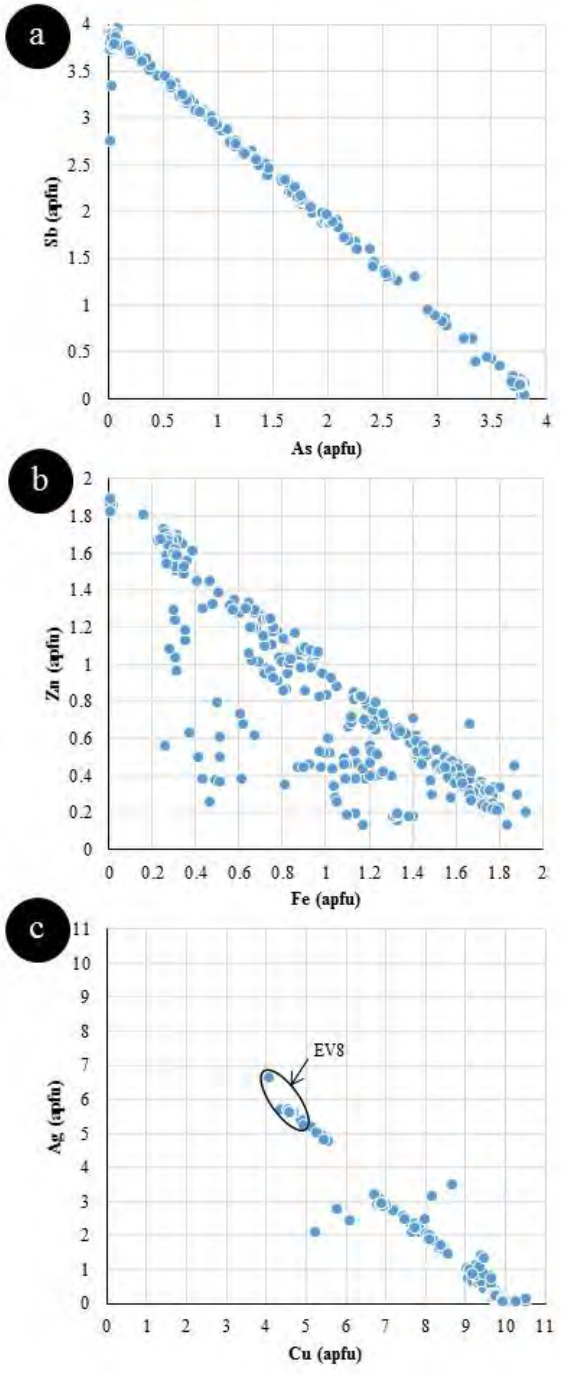

Figure 3. Scatter-plots showing the variation in major elements in the tetrahedrite-tennantite sample suite. (**a**) Sb vs. As; (**b**) Zn vs. Fe; and (**c**) Ag vs. Cu. Atoms per formula unit is calculated by normalizing mol % values to 29.

Table 4. Summary of trace element concentrations in tetrahedrite-tennantite determined by laser-ablation inductively-coupled plasma mass spectrometry (LA-ICP-MS) (data in ppm).

Sample/Assemblage		Mn	Fe	Co	Ni	Zn	Ga	As	Se	Mo	Ag	Cd	In	Sn	Te	W	Au	Hg	Tl	Pb	Bi
G16396 *	Mean (10)	1.4	ME	2.7	0.54	ME	0.09	4620	-	0.12	ME	4968	0.57	28	1.4	0.04	0.74	93	0.09	61	445
Tet, Sp, Gn, Cp	*St. Dev.*	*1.0*	*ME*	*1.1*	*0.78*	*ME*	*0.12*	*943*	*-*	*0.15*	*ME*	*751*	*0.16*	*39*	*1.1*	*0.06*	*0.53*	*20*	*0.16*	*40*	*768*
G11579	Mean (10)	32	ME	22	0.87	ME	0.06	28446	53	0.09	ME	2692	7.0	0.54	50	-	0.03	93	0.05	3.1	3007
Tet, Sp, Cp, Gn	*St. Dev.*	*2.1*	*ME*	*4.5*	*1.0*	*ME*	*0.03*	*6725*	*23*	*0.08*	*ME*	*324*	*1.1*	*0.37*	*25*	*-*	*0.02*	*31*	*0.05*	*2.2*	*595*
G13289b *	Mean (10)	0.77	ME	44	0.14	ME	0.03	ME	11	0.03	2038	2187	0.25	0.80	0.07	0.01	0.02	9.3	0.15	270	8.2
Tet, Gn, Cp, Sp	*St. Dev.*	*0.54*	*ME*	*7.8*	*0.08*	*ME*	*0.02*	*ME*	*8.6*	*0.04*	*538*	*274*	*0.34*	*0.49*	*0.16*	*0.01*	*0.04*	*3.2*	*0.22*	*257*	*8.5*
G6940	Mean (10)	43	ME	0.55	0.33	ME	0.05	12626	73	0.06	ME	1860	3.4	1.1	38	0.02	0.02	86	0.02	1.8	1539
Tet, Cp, Sp, Gn	*St. Dev.*	*7.9*	*ME*	*0.14*	*0.19*	*ME*	*0.04*	*5590*	*20*	*0.05*	*ME*	*231*	*0.92*	*0.71*	*21*	*0.03*	*0.02*	*28*	*0.02*	*0.68*	*142*
G13289a *	Mean (10)	0.83	10116	38	0.25	ME	0.03	ME	21	0.04	1866	2052	0.17	0.47	0.09	0.01	0.01	13	0.05	108	11
Tet, Cp, Sp, Gn	*St. Dev.*	*0.65*	*1653*	*11*	*0.19*	*ME*	*0.03*	*ME*	*29*	*0.05*	*615*	*262*	*0.40*	*0.35*	*0.18*	*0.01*	*0.00*	*2.9*	*0.05*	*130*	*16*
V446	Mean (4)	204	ME	0.06	0.13	ME	0.19	38	12	0.02	ME	170	1.2	16	0.06	-	0.01	10	0.16	1.9	111
Sp, Gn, Cp, Tet	*St. Dev.*	*12*	*ME*	*0.05*	*0.25*	*ME*	*0.05*	*11*	*6.1*	*0.03*	*ME*	*24*	*0.21*	*1.7*	*0.09*	*-*	*0.02*	*1.5*	*0.21*	*-*	*22*
V538	Mean (3)	122	ME	0.02	0.00	ME	0.11	92	6.0	0.00	ME	158	0.64	22	0.13	-	0.00	10	0.21	21	45
Sp, Gn, Cp, Tet	*St. Dev.*	*6.9*	*ME*	*0.03*	*0.01*	*ME*	*0.10*	*44*	*2.6*	*0.00*	*ME*	*12*	*0.08*	*0.42*	*0.17*	*-*	*0.01*	*1.3*	*0.31*	*23*	*4.2*
Hj13	Mean (9)	109	ME	0.24	-	ME	0.03	117	8.9	0.08	ME	110	0.21	0.15	0.42	0.00	0.11	0.33	0.48	3.0	3.1
Gn, Cp, Sp, Tet	*St. Dev.*	*19*	*ME*	*0.38*	*-*	*ME*	*0.02*	*24*	*4.7*	*0.07*	*ME*	*18*	*0.08*	*0.23*	*0.73*	*0.01*	*0.13*	*0.10*	*0.24*	*1.4*	*1.0*
G6951 *	Mean (10)	1.5	369	27	-	ME	0.04	ME	-	0.06	ME	29893	0.10	0.31	0.29	-	0.06	29	0.20	85	0.03
Tet, Sp, Gn, (Cp)	*St. Dev.*	*0.75*	*138*	*6.0*	*-*	*ME*	*0.02*	*ME*	*-*	*0.07*	*ME*	*7569*	*0.02*	*0.18*	*0.35*	*-*	*0.04*	*14*	*0.12*	*36*	*0.04*
Bv97-52	Mean (8)	389	ME	0.01	0.15	ME	0.32	ME	3.8	0.05	ME	682	1.9	46	-	-	0.00	46	0.00	ME	9.1
Ten, Sp, Gn	*St. Dev.*	*332*	*ME*	*0.01*	*0.37*	*ME*	*0.51*	*ME*	*1.9*	*0.05*	*ME*	*351*	*1.6*	*128*	*-*	*-*	*0.00*	*18*	*0.00*	*ME*	*5.9*
G10847	Mean (10)	18	ME	0.03	0.35	ME	0.34	ME	11	0.07	5164	1325	0.09	0.92	0.40	-	0.06	2668	0.11	13	1.3
Tet, Sp, Gn	*St. Dev.*	*4.7*	*ME*	*0.02*	*0.24*	*ME*	*0.13*	*ME*	*7.2*	*0.06*	*4579*	*169*	*0.02*	*0.78*	*0.41*	*-*	*0.09*	*493*	*0.22*	*9.3*	*0.22*
EV8	Mean (10)	7.6	ME	0.20	0.31	ME	0.21	121	19	-	ME	870	2.6	404	0.82	0.02	0.08	19	3.7	46078	1174
Gn, Sp, Tet	*St. Dev.*	*3.0*	*ME*	*0.07*	*0.41*	*ME*	*0.11*	*142*	*16*	*-*	*ME*	*418*	*2.5*	*185*	*0.82*	*0.05*	*0.13*	*8.5*	*2.1*	*29774*	*456*
Hj14	Mean (6)	80	ME	0.01	0.02	10882	0.01	310	2.7	0.08	ME	161	0.05	18	0.09	-	11	0.26	0.24	39	0.03
Gn, Sp, Tet	*St. Dev.*	*22*	*ME*	*0.03*	*0.04*	*587*	*0.01*	*135*	*2.6*	*0.12*	*ME*	*22*	*0.05*	*16*	*0.15*	*-*	*5.2*	*0.09*	*0.58*	*10*	*0.06*
G6948	Mean (10)	517	ME	0.11	0.36	ME	0.06	8222	135	0.06	ME	1033	1.4	65	0.54	-	0.02	2.4	0.02	4.6	1933
Tet, Sp, Cp, (Gn)	*St. Dev.*	*71*	*ME*	*0.10*	*0.21*	*ME*	*0.06*	*5983*	*68*	*0.06*	*ME*	*89*	*0.17*	*28*	*0.47*	*-*	*0.01*	*2.6*	*0.01*	*3.9*	*621*
G14549b	Mean (10)	2.3	ME	1.2	0.56	ME	0.12	1921	11	0.10	ME	4731	0.33	19	0.14	-	0.39	47	0.83	871	475
Tet, Sp, Cp	*St. Dev.*	*1.2*	*ME*	*1.0*	*0.61*	*ME*	*0.09*	*805*	*9.0*	*0.13*	*ME*	*1272*	*0.24*	*19*	*0.18*	*-*	*0.22*	*23*	*0.58*	*775*	*386*
Mo17A	Mean (6)	0.50	ME	0.16	0.03	ME	0.01	20439	5.8	0.03	ME	1751	0.02	0.06	0.83	-	0.06	1.9	0.12	ME	3.2
Cp, Gn, Tet	*St. Dev.*	*0.12*	*ME*	*0.20*	*0.07*	*ME*	*0.01*	*29371*	*2.1*	*0.04*	*ME*	*373*	*0.01*	*0.06*	*0.71*	*-*	*0.10*	*1.1*	*0.15*	*ME*	*0.82*
ORV1	Mean (10)	0.18	ME	23	2.9	ME	0.04	ME	21	0.12	4023	979	0.40	0.11	0.34	-	0.01	36	0.00	4.0	12
Cp, Gn, Tet	*St. Dev.*	*0.13*	*ME*	*12*	*2.3*	*ME*	*0.05*	*ME*	*16*	*0.14*	*880*	*393*	*0.26*	*0.12*	*0.46*	*-*	*0.02*	*13*	*0.01*	*3.1*	*16*
G14549a	Mean (10)	1.4	ME	0.74	0.84	ME	0.13	3988	13	0.03	ME	3104	0.82	42	0.07	0.01	0.20	25	0.30	849	2794
Tet, Gn, (Sp)	*St. Dev.*	*0.61*	*ME*	*0.36*	*1.2*	*ME*	*0.07*	*1181*	*8.7*	*0.03*	*ME*	*929*	*1.5*	*41*	*0.10*	*0.01*	*0.13*	*11*	*0.16*	*106*	*1842*
G873	Mean (10)	1.6	ME	1.4	0.35	ME	0.09	ME	13	0.33	ME	4310	10	0.70	0.19	0.03	0.08	62	0.08	23	0.11
Tet, Gn	*St. Dev.*	*1.1*	*ME*	*2.0*	*0.25*	*ME*	*0.05*	*ME*	*11*	*0.89*	*ME*	*1422*	*1.9*	*0.37*	*0.20*	*0.03*	*0.07*	*25*	*0.09*	*5.7*	*0.10*
G16152	Mean (10)	0.47	ME	2512	12	ME	0.05	ME	13	1.9	4452	683	3.0	28	-	0.01	0.02	3456	0.02	16	29

Table 4. *Cont.*

Sample/Assemblage		Mn	Fe	Co	Ni	Zn	Ga	As	Se	Mo	Ag	Cd	In	Sn	Te	W	Au	Hg	Tl	Pb	Bi
Tet, Cp, (Gn)	*St. Dev.*	*0.32*	*ME*	*880*	*7.4*	*ME*	*0.03*	*ME*	*12*	*2.2*	*634*	*70*	*1.4*	*51*	-	*0.02*	*0.02*	*921*	*0.02*	*20*	*30*
G871	Mean (10)	0.46	ME	382	0.52	ME	0.04	ME	17	0.12	372	139	0.09	0.35	0.20	0.02	0.02	ME	0.02	1.8	0.25
Tet, Cp	*St. Dev.*	*0.45*	*ME*	*220*	*0.42*	*ME*	*0.03*	*ME*	*9.5*	*0.17*	*48*	*71*	*0.13*	*0.32*	*0.29*	*0.03*	*0.02*	*ME*	*0.01*	*1.4*	*0.21*
G874	Mean (10)	0.46	ME	557	0.20	ME	0.03	ME	14	0.11	206	263	1.8	0.47	0.17	0.02	0.01	ME	0.01	5.9	0.47
Tet, Cp	*St. Dev.*	*0.41*	*ME*	*397*	*0.12*	*ME*	*0.02*	*ME*	*15*	*0.07*	*40*	*157*	*1.2*	*0.35*	*0.16*	*0.02*	*0.01*	*ME*	*0.01*	*3.5*	*0.54*
G879	Mean (10)	7.1	ME	3.6	1.9	ME	0.14	8555	-	-	ME	380	15	1.4	0.29	0.04	0.09	20	0.11	18	1229
Tet, Cp	*St. Dev.*	*3.7*	*ME*	*2.6*	*2.9*	*ME*	*0.16*	*9952*	*-*	*-*	*ME*	*57*	*4.5*	*1.5*	*0.35*	*0.04*	*0.12*	*10*	*0.12*	*28*	*549*
G882	Mean (10)	0.70	ME	613	0.56	ME	0.13	ME	56	0.36	303	328	2.3	0.68	0.69	0.04	0.05	ME	0.03	37	4.8
Tet, Cp	*St. Dev.*	*0.62*	*ME*	*475*	*0.30*	*ME*	*0.10*	*ME*	*69*	*0.36*	*90*	*283*	*2.2*	*0.56*	*0.79*	*0.04*	*0.04*	*ME*	*0.04*	*40*	*3.3*
G6946	Mean (10)	1.4	ME	53	28	ME	0.14	ME	63	0.08	6202	1268	1.4	2.3	0.35	0.01	0.03	1917	0.01	7.3	98
Tet, Cp	*St. Dev.*	*1.2*	*ME*	*40*	*9.1*	*ME*	*0.09*	*ME*	*28*	*0.05*	*420*	*163*	*0.61*	*2.2*	*0.36*	*0.02*	*0.02*	*710*	*0.01*	*8.2*	*147*
G6949	Mean (10)	11	ME	0.32	2.6	ME	0.09	8922	16	0.09	ME	283	15	3.0	0.12	-	0.10	13	0.65	19	2821
Tet, Cp	*St. Dev.*	*7.9*	*ME*	*0.31*	*2.8*	*ME*	*0.07*	*2833*	*11*	*0.12*	*ME*	*47*	*5.9*	*2.5*	*0.13*	-	*0.08*	*4.5*	*0.39*	*15*	*1101*
G11701	Mean (10)	1.1	ME	78	0.55	ME	0.05	134	13	0.07	ME	1124	0.14	5.1	0.12	0.02	0.04	192	0.02	6.1	23
Tet, Cp	*St. Dev.*	*0.64*	*ME*	*21*	*0.56*	*ME*	*0.05*	*36*	*14*	*0.07*	*ME*	*902*	*0.05*	*7.5*	*0.22*	*0.02*	*0.06*	*91*	*0.04*	*3.0*	*23*
G14246	Mean (10)	18	ME	3.0	0.23	ME	0.06	5264	-	0.06	ME	365	7.3	1.5	0.22	0.01	0.02	58	0.08	3.2	2269
Tet, Cp	*St. Dev.*	*13*	*ME*	*1.4*	*0.13*	*ME*	*0.05*	*3493*	*-*	*0.06*	*ME*	*63*	*4.5*	*1.0*	*0.26*	*0.01*	*0.01*	*29*	*0.08*	*3.2*	*1035*
G14867	Mean (10)	0.36	ME	146	0.54	16696	0.07	ME	376	0.15	70	183	3.0	0.68	0.34	-	0.02	5310	0.14	3.0	3768
Ten, Cp	*St. Dev.*	*0.15*	*ME*	*3.6*	*0.49*	*903*	*0.05*	*ME*	*293*	*0.12*	*20*	*19*	*0.35*	*0.44*	*0.53*	*-*	*0.01*	*3594*	*0.18*	*0.91*	*1038*
Mo16	Mean (3)	15	ME	7.0	1.7	8795	0.06	ME	11	0.01	ME	1213	0.03	0.10	2.0	-	0.02	31	0.03	2.2	2.7
Cp, Tet, (Gn)	*St. Dev.*	*6.6*	*ME*	*12*	*2.9*	*6021*	*0.09*	*ME*	*3.4*	*0.02*	*ME*	*599*	*0.01*	*0.04*	*1.2*	*-*	*0.02*	*10*	*0.06*	*1.0*	*1.0*
G29851	Mean (10)	0.88	ME	78	1.1	ME	0.10	ME	33	1.0	909	535	0.31	0.91	1.7	0.07	0.11	ME	0.12	108	1361
Cp, Ten	*St. Dev.*	*0.79*	*ME*	*28*	*0.75*	*ME*	*0.10*	*ME*	*22*	*1.0*	*382*	*97*	*0.12*	*0.77*	*1.3*	*0.07*	*0.22*	*ME*	*0.21*	*89*	*1471*
ORV4	Mean (10)	29	ME	3.3	1.9	ME	0.02	ME	12	0.19	1409	1269	4.5	0.07	3.0	-	-	37	0.01	2.9	140
Cp, Tet	*St. Dev.*	*29*	*ME*	*2.7*	*1.6*	*ME*	*0.04*	*ME*	*4.5*	*0.31*	*274*	*395*	*2.3*	*0.06*	*4.9*	*-*	*-*	*21*	*0.02*	*2.1*	*136*
G12640	Mean (10)	79	ME	3.1	0.62	ME	0.08	ME	107	0.15	1301	658	0.34	2.6	7.1	0.03	0.03	1654	0.14	7.3	54
Ten	*St. Dev.*	*13*	*ME*	*0.49*	*0.47*	*ME*	*0.06*	*ME*	*22*	*0.18*	*185*	*39*	*0.05*	*1.2*	*2.7*	*0.03*	*0.03*	*329*	*0.22*	*2.3*	*12*
G13301	Mean (10)	1.0	ME	633	31	ME	0.27	ME	127	-	158	7005	2.7	0.66	3.4	0.03	0.02	1747	0.02	11	100
Tet	*St. Dev.*	*2.2*	*ME*	*18*	*26*	*ME*	*0.20*	*ME*	*43*	*-*	*27*	*991*	*0.79*	*0.60*	*2.7*	*0.03*	*0.02*	*322*	*0.02*	*6.1*	*49*
G15977	Mean (10)	9.2	ME	19	0.28	ME	0.11	ME	32	0.06	630	1488	0.04	0.77	1.0	-	0.18	321	0.01	3.9	10.9
Tet	*St. Dev.*	*2.0*	*ME*	*2.7*	*0.16*	*ME*	*0.11*	*ME*	*15*	*0.08*	*181*	*114*	*0.03*	*0.42*	*0.73*	*-*	*0.05*	*129*	*0.02*	*2.4*	*1.0*
G16835	Mean (10)	2.0	ME	85	0.88	ME	0.11	ME	12	0.14	3942	331	1.1	0.70	1.1	0.05	0.18	14761	0.06	61	2385
Ten	*St. Dev.*	*2.8*	*ME*	*8.4*	*0.76*	*ME*	*0.10*	*ME*	*11*	*0.13*	*314*	*45*	*0.19*	*0.65*	*1.3*	*0.12*	*0.13*	*2281*	*0.08*	*24*	*770*
VFI031	Mean (10)	1019	153	-	0.16	ME	1.2	ME	624	0.17	ME	1095	6.9	6.1	3648	0.01	2.2	8965	0.22	67	1.7
Tet	*St. Dev.*	*236*	*57*	*-*	*0.10*	*ME*	*0.42*	*ME*	*213*	*0.34*	*ME*	*129*	*2.1*	*11*	*3185*	*0.01*	*1.1*	*3439*	*0.13*	*76*	*0.11*

Tet = tetrahedrite, *Ten* = tennantite, *Sp* = sphalerite, *Gn* = galena, *Cp* = chalcopyrite, *St. Dev.* = standard deviation. Minerals in brackets are very minor phases. (X) = number of individual spot analyses in that sample. Dash = insufficient data to perform calculation (all analyses <mdl). Other <mdl values were treated as mdl/2. ME = major/minor element (concentration from EPMA > 1 wt %). * Evidence suggests sulphides in sample did not co-crystallize (based on textures and partitioning trends among base metal sulphides).

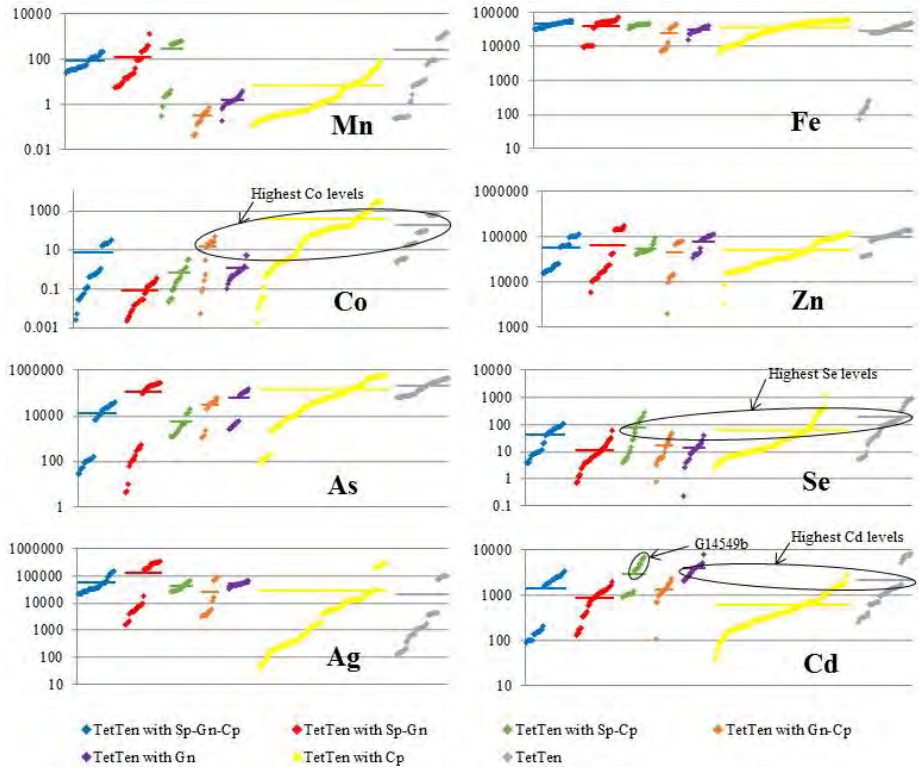

Figure 4. Cumulative plots showing individual spot concentrations of Mn, Fe, Co, Zn, As, Se, Ag and Cd in tetrahedrite-tennantite from different assemblages. Tetrahedrite-tennantite concentration data for each assemblage is sorted in ascending order and plotted in succession along the X axis. Y axis = concentration (parts per million). The average composition for each assemblage is given as a horizontal coloured line. TetTen = tetrahedrite-tennantite, Sp = sphalerite, Gn = galena, Cp = chalcopyrite.

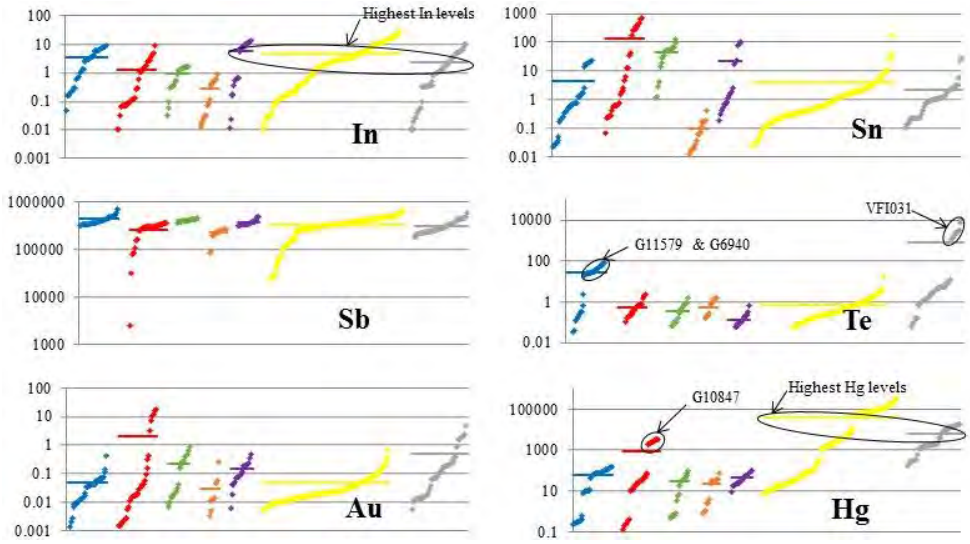

Figure 5. *Cont.*

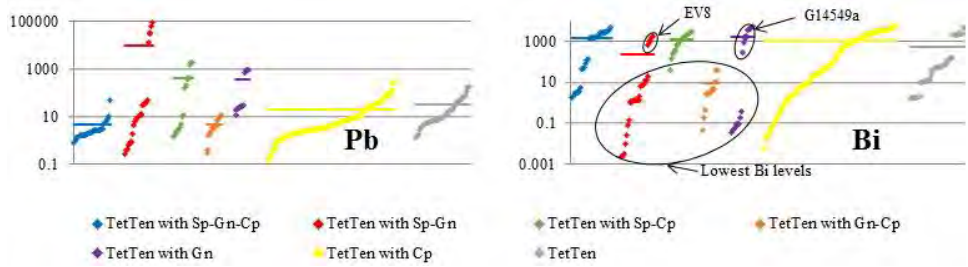

Figure 5. Cumulative plots showing individual spot concentrations of In, Sn, Sb, Te, Au, Hg, Pb, and Bi in tetrahedrite-tennantite from different assemblages. Tetrahedrite-tennantite concentration data for each assemblage is sorted in ascending order and plotted in succession along the X axis. Y axis = concentration (parts per million). The average composition for each assemblage is given as a horizontal coloured line.

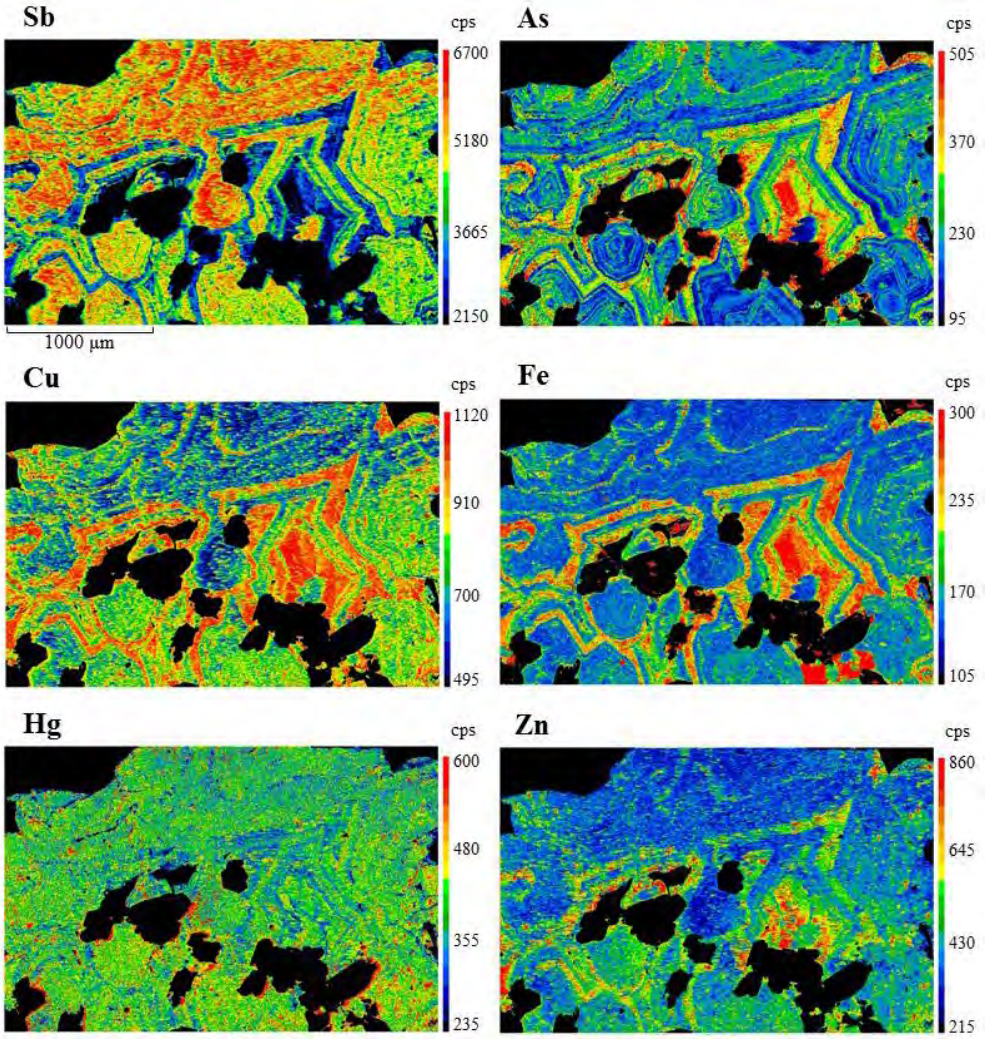

Figure 6. Electron probe microanalysis element maps showing chemical zoning of Sb, As, Cu, Fe, Hg, and Zn in tetrahedrite from sample G871 (Pulganbar, Grafton, NSW, Australia). Scales are in counts per second (cps).

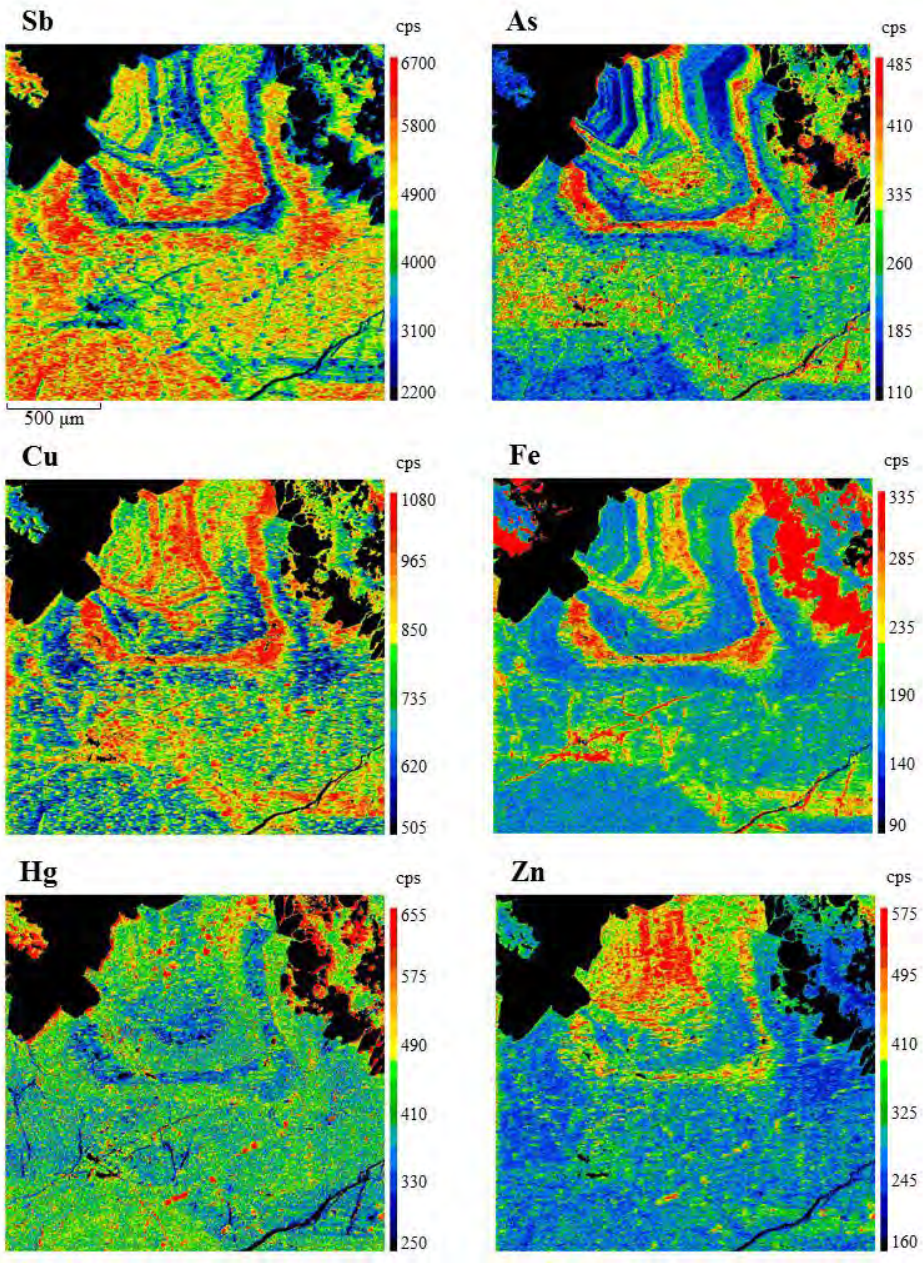

Figure 7. Electron probe microanalysis element maps showing chemical zoning of Sb, As, Cu, Fe, Hg, and Zn in tetrahedrite from sample G871 (Pulganbar, Grafton, NSW, Australia). Scales are in counts per second (cps).

Apart from Fe and Zn, Hg and Pb are the two most common divalent cations determined as present in tetrahedrite-tennantite. 10.6 wt % Hg and 4 wt % Pb are the highest measured levels of the two elements in tetrahedrite-tennantite, measured in samples G871 (Pulganbar, Grafton, NSW, Australia) and Mo17A (Mofjell, Norway), respectively. Tetrahedrite-tennantite (TetTen) crystallizing in isolation, or with chalcopyrite (Cp; i.e., TetTen-Cp assemblages), hosts the most Hg (see Hg plot in

Figure 5). While those tetrahedrite-tennantites crystallizing with sphalerite (Sp) and galena (Gn; TetTen-Sp-Gn assemblages) also host high levels of Hg, this trend is swayed by one population of Hg-rich tetrahedrites from sample G10847 (Mt. Camel, Heathcote, Australia; see Hg plot in Figure 5). The tetrahedrite in this sample co-crystallized with the most Hg-rich sphalerite of any sample here, implying a particularly Hg-rich crystallization environment. Thus, excluding this one sample, the highest Hg concentrations are present in tetrahedrite-tennantite, crystallizing without sphalerite or galena, which is in close agreement with Hg partitioning trends outlined in George et al. (2016) [30], where sphalerite is the preferred Hg host in BMS assemblages.

Cadmium, cobalt, and manganese are the other common divalent cations in tetrahedrite-tennantite. All may be present at concentrations greater than 1000 ppm. Whereas the EPMA data shows 0.674 wt % Cd in sample G6951 (Yerranderie, NSW, Australia), the LA-ICP-MS data shows almost 30,000 ppm in the same sample, hinting at heterogeneity from area to area of the sample. The highest Co and Mn in tetrahedrite-tennantite here is 0.362 wt % and 0.107 wt %, in samples G16152 (Siegen, Westphalia, Germany) and VF1031 (Emperor Gold Mine, Fiji), respectively. The LA-ICP-MS data for these samples is in close agreement. Cadmium concentrations are highest in tetrahedrite-tennantite that has not crystallized with sphalerite or chalcopyrite (see Cd plot in Figure 4). This is anticipated since Cd displays a strong preference for the sphalerite structure in BMS systems [30]. The only exception is the tetrahedrite from sample G14549b (Consols Mine, Broken Hill, NSW, Australia), which co-crystalized with sphalerite hosting up to 10,000 ppm Cd (see Cd plot in Figure 4). The exceptionally Cd-rich environment this assemblage formed in explains the high Cd concentrations in tetrahedrite, even though sphalerite co-crystallized. In a similar way, Co concentrations are also highest in those tetrahedrite-tennantites that have not crystallized with sphalerite (see Co plot in Figure 4), in line with findings reported by George et al. (2016) [30].

Tetrahedrite in sample VFI031 (Emperor Gold Mine, Fiji) contains as much as 3648 ppm Te, the highest concentration measured in this study. Apart from this sample, and two samples from the Kalgoorlie ore district, Western Australia (G11579 and G6940 with tetrahedrites containing 50 and 38 ppm Te, respectively), the mean Te concentrations in all tetrahedrite-tennantites from all assemblages are remarkably constant around the 1 ppm level (see Te plot in Figure 5).

Bismuth concentrations exceed 1000 ppm in tetrahedrite-tennantites from all assemblages except those co-crystallizing with galena and chalcopyrite, where concentrations only exceed 10 ppm in two spots. Bismuth concentrations in tetrahedrite-tennantite from TetTen-Sp-Gn and TetTen-Gn assemblages are also very low if samples EV8 (Evelyn Mine, NT, Australia) and G14549a (Consols Mine, Broken Hill, NSW, Australia) are excluded, both of which contain galena with up to 10,000 ppm Bi (see Bi plot in Figure 5). The Bi-rich galena co-crystallizing with high Bi tetrahedrite points at particularly Bi-rich crystallization environments for these samples. Such samples are anomalous for the otherwise Bi-depleted tetrahedrite-tennantites in TetTen-Sp-Gn and TetTen-Gn assemblages (see Bi plot in Figure 5). As shown in George et al. (2016) [30], the presence of galena can be considered the cause of this Bi depletion in tetrahedrite-tennantite since it is the preferred host of Bi in BMS assemblages.

Tetrahedrite-tennantite typically hosts between 0.1 and 1000 ppm Se. The most Se-rich tetrahedrite is recorded in sample VFI031 (Emperor Gold Mine, Fiji; 624 ppm). In general, the highest levels of Se in tetrahedrite-tennantite are reached when galena does not co-crystallize; i.e., from TetTen, TetTen-Sp-Cp, and TetTen-Cp assemblages (see Se plot in Figure 4). This is to be expected since galena is always the preferred host of Se in BMS assemblages [30].

Tin concentrations in tetrahedrite-tennantite are usually an order of magnitude lower than those of Se (typically between 0.01 and 100 ppm); they are the highest in EV8 (Evelyn Mine, NT, Australia; 404 ppm). Interestingly, the EPMA data records up to 0.264 wt % Sn in the tetrahedrite from EV8, though this may be due to inclusions of a Sn-rich phase (possibly stannite), since some were recognized on LA-ICP-MS downhole spectra from this sample.

The concentrations of Ni, In, Au, Tl, Mo and Ga are rarely, if ever, greater than 10 ppm in tetrahedrite-tennantite. The highest mean concentrations for these elements in tetrahedrite-tennantite are 31 ppm Ni (G13301; Allihies Mine, Castletown, Cork, Ireland), 15 ppm In

(G879; Ring Valley, Tas., Australia, and G6949; Webb's Ag Mine, Emmaville, NSW, Australia), 11 ppm Au (Hj14; Herja, Romania), 3.7 ppm Tl (EV8; Evelyn Mine, NT, Australia), 1.9 ppm Mo (G16152; Siegen, Westphalia, Germany) and 1.2 ppm Ga (VFI031; Emperor Gold Mine, Fiji). Measured W concentrations never exceeded 1 ppm. The highest In concentrations are recorded in tetrahedrite-tennantites that crystallize without any sphalerite observed nearby (excluding 4-component assemblages); i.e., in TetTen-Gn, TetTen-Cp and TetTen assemblages (see In plot in Figure 5). This is concordant with George et al. (2016) [30] where sphalerite was shown to be the typical preferred host of In.

5. Discussion

5.1. Element Partitioning Between Tetrahedrite-Tennantite, Sphalerite, Galena, and Chalcopyrite

Figure 8 is a series of tri-plots that show where various elements are hosted in co-crystallized three-component assemblages in which one component is tetrahedrite-tennantite. Each individual point is a sample average, and where it plots shows how much of a given element is contained within the sulphides of that assemblage as a fraction of the overall amount of that element in the assemblage (using molar percentages for comparisons between sulphides). For example, in TetTen-Sp-Gn assemblages, sphalerite always concentrates more than 60% of the Mn budget, no more than 40% is ever contained in tetrahedrite-tennantite, and co-crystallizing galena essentially contains none of the available Mn. In the TetTen-Sp-Cp assemblage, sphalerite again always concentrates >50% of the Mn budget. We can thus say that whenever sphalerite is present, it is always the primary Mn host.

Apart from cases where chalcopyrite (or other Fe-sulphides such as pyrite and pyrrhotite) co-crystallizes, Fe is always hosted in either tetrahedrite-tennantite or sphalerite. In most cases tetrahedrite-tennantite is the primary host, but in four TetTen-Sp-Gn assemblages, sphalerite hosts > 50% of the Fe budget. Cobalt does not have a strong affiliation with any of the four sulphides, although it is never primarily hosted in chalcopyrite. In the absence of sphalerite, Zn always partitions to tetrahedrite-tennantite. Gallium seems to be most affiliated with sphalerite, although in TetTen-Sp-Cp assemblages, chalcopyrite hosts the larger share of Ga in four samples. Two of these samples (V446 and V538) come from the Bleikvassli deposit, Norway, a sedimentary-exhalative deposit which is interpreted to have recrystallized at conditions of granulite facies [82,83]. The other two (G6940 and G11579) come from Kalgoorlie, Western Australia, where Boulter et al. (1987) [84] describe recrystallization of pyrite during deformation associated with regional metamorphism. Thus, those assemblages in which chalcopyrite hosts more Ga than sphalerite, both come from environments where sulphides have recrystallized under regional metamorphism. Such conditions result in chalcopyrite becoming the primary Ga host, distinct from lower temperature/pressure environments where sphalerite is the preferred host [30,72].

Selenium is always concentrated in galena whenever that mineral is present, and tetrahedrite-tennantite seems to be the secondary host in most cases. Tetrahedrite-tennantite typically hosts > 90% of the Ag budget whenever it co-crystallizes with any combination of BMS. In all but one sample, Cd is principally hosted in sphalerite when present. In the single exception (sample G10847; Mt. Camel, Heathcote, Australia), tetrahedrite-tennantite is the preferred host. The same is true in assemblages in which sphalerite is absent.

As is the case in the three-component Sp-Gn-Cp assemblage, Sn does not have a strong affiliation with any sulphide [30]. It is concentrated in different phases in different samples. In most cases, however, Sn seems to prefer the BMS over tetrahedrite-tennantite. Tellurium has a strong affiliation with galena, while Hg appears to be preferentially incorporated into either sphalerite or tetrahedrite-tennantite in different samples. Galena will concentrate Bi whenever it is present, and in its absence tetrahedrite-tennantite always becomes the primary host.

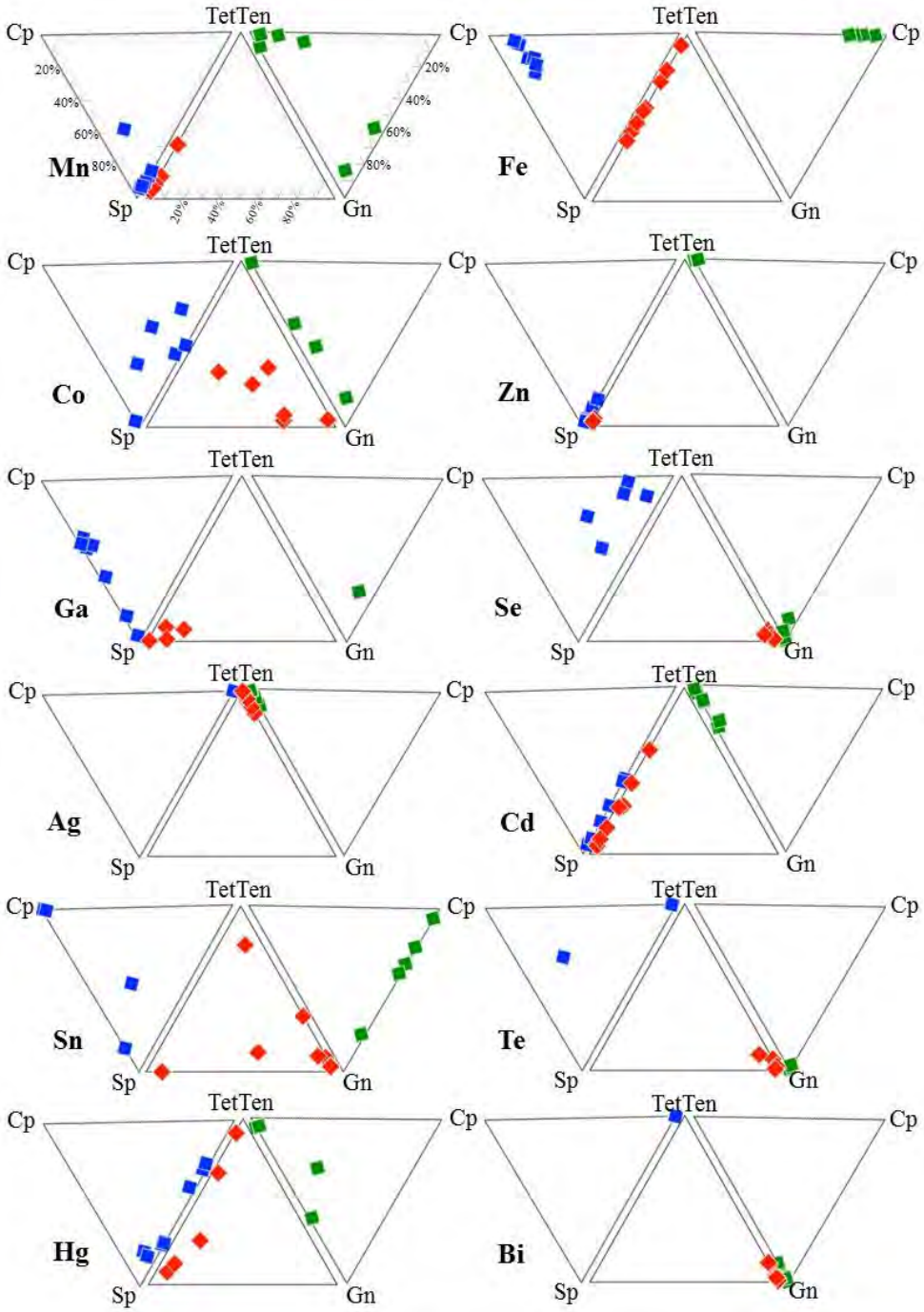

Figure 8. Series of tri-plots that show where the Mn, Fe, Co, Zn, Ga, Se, Ag, Cd, Sn, Te, Hg, and Bi budget is hosted in co-crystallized three-component assemblages comprising tetrahedrite-tennantite. Each individual point is a sample, and where it plots shows how much of a given element is contained within the sulphides of that assemblage as a fraction of the overall amount of that element in the assemblage (using molar percentages for comparisons between sulphides). TetTen = tetrahedrite-tennantite, Sp = sphalerite, Gn = galena, Cp = chalcopyrite.

5.2. Controls on Fe and Hg Partitioning

Both tetrahedrite-tennantite and sphalerite may be the primary host phase for Fe and Hg in different samples (excluding, of course, samples containing Fe-sulphides). Which mineral will host a greater molar percentage of Fe or Hg in a given system seems to depend on the amount of that element available in the system. In systems with lesser Fe, tetahedrite-tennantite is the primary Fe host, indicating that Fe prefers to partition into tetrahedrite-tennantite relative to sphalerite (Figure 9a). Sphalerite is the primary host of Fe only in those systems where Fe concentrations in tetrahedrite-tennantite approach 2 *apfu*, i.e., the maximum concentration of Fe allowed in the tetrahedrite-tennantite structure ([4]; Figure 9b). Thus, in assemblages free of Fe-sulphides, if there is more Fe than can be incorporated by tetrahedrite-tennantite, then the excess will partition to sphalerite such that sphalerite may host more Fe than tetrahedrite-tennantite.

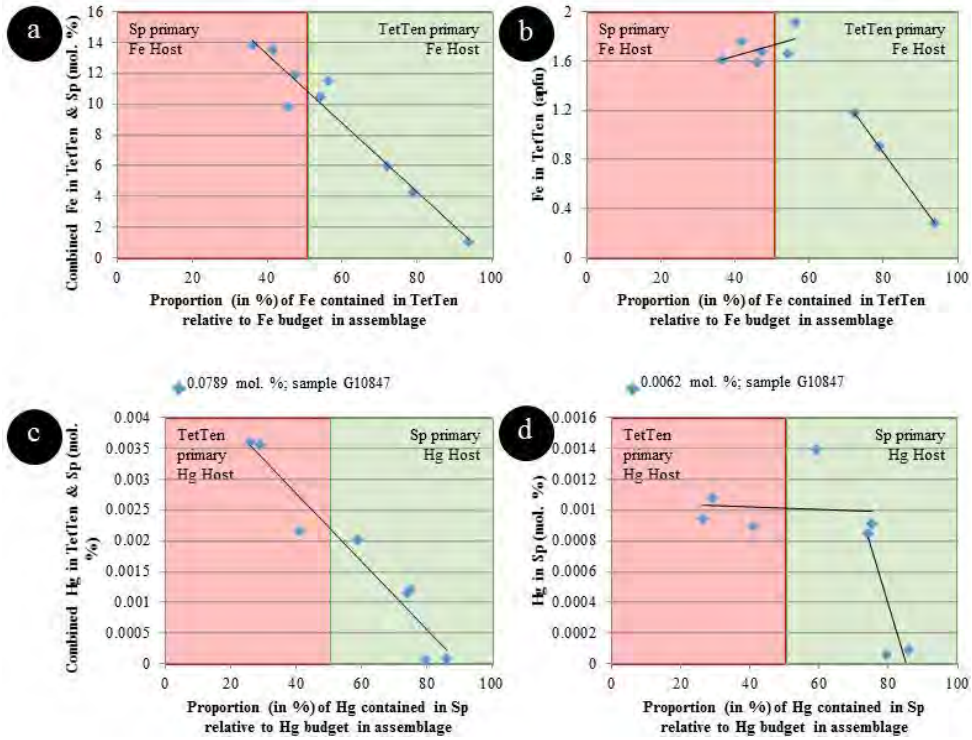

Figure 9. Scatter-plots that show the primary host of Fe and Hg depends on the concentration of Fe and Hg in tetrahedrite-tennantite and sphalerite. (**a**) Fe in tetrahedrite-tennantite and sphalerite vs. Fe in tetrahedrite-tennantite as a % of the assemblage Fe budget. (**b**) Fe in tetrahedrite-tennantite vs. Fe in tetrahedrite-tennantite as a % of the assemblage Fe budget. (**c**) Hg in tetrahedrite-tennantite and sphalerite vs. Hg in sphalerite as a % of the assemblage Hg budget. (**d**) Hg in sphalerite vs. Hg in sphalerite as a % of the assemblage Hg budget. TetTen = tetrahedrite-tennantite, Sp = sphalerite.

Similar patterns are observed for Hg. In systems with lesser Hg, sphalerite is the primary Hg host, indicating that Hg preferentially partitions into sphalerite (Figure 9c). Tetrahedrite-tennantite is the primary host of Hg only in those systems where Hg concentrations in sphalerite are ~0.001 mol% (Figure 9d). The present dataset may thus indicate that this is an approximate upper limit to Hg concentrations in sphalerite, at least when co-crystallizing with tetrahedrite-tennantite. Only in one sample is the concentration of Hg in sphalerite significantly higher than this; sample G10847 (Mt. Camel, Heathcote, Vic., Australia) which concentrates 0.0062 mol% Hg in sphalerite (equivalent to ~250 ppm Hg), and where co-crystallizing tetrahedrite hosts more than 0.07 mol% Hg (>2500 ppm Hg equivalent). This is the most Hg in any tetrahedrite-tennantite co-crystallizing with

sphalerite analysed here. This particularly Hg-rich system seems to allow for exceptional Hg concentrations in sphalerite. In any case, if a given system contains more Hg than can be incorporated by sphalerite, then the excess will partition to tetrahedrite such that tetrahedrite may host more Hg than sphalerite.

6. Implications and Conclusions

This study shows that tetrahedrite-tennantite is a significant carrier of a range of trace elements at concentrations measurable using contemporary instrumentation. This should be recognized when establishing protocols for trace element analysis of tetrahedrite-tennantite, and when assessing the primary hosts for trace elements of interest in any given assemblage, e.g., for geometallurgical purposes. Most noteworthy, tetrahedrite-tennantite will always be the primary host of Ag in co-crystallizing BMS assemblages. Iron, Cu, Zn, As, Cd, Sb, Hg, and Bi are the additional elements that are controlled to some degree by the presence of tetrahedrite-tennantite. In contrast, tetrahedrite-tennantite does not appear, from the data here, to be a very good host for the critical metals Ga, In, and Sn, all of which prefer to partition to co-crystallizing BMS.

As an extension of arguments put forward by George et al. (2016) [30], the partitioning trends outlined here may be used as a tool to assess co-crystallization of a given TetTen ± Sp ± Gn ± Cp assemblage. If the hosts of various trace elements in such an assemblage do not match the preferred hosts outlined in Table 5, then it strongly suggests that assemblage did not co-crystallize. On the other hand, if the primary hosts do match those given here, that is typically suggestive of a co-crystallized assemblage.

Table 5. Preferred hosts of various trace elements in a co-crystallizing TetTen-Sp-Gn-Cp assemblage

Trace Element	**Mn**	**Fe**	**Cu**	**Zn**
Preferred Host	Sp [1]	TetTen >Sp [3]	TetTen >Sp [3]	TetTen [1]
Trace Element	**Ga**	**As**	**Se**	**Ag**
Preferred Host	Sp [2]	TetTen >Gn [1]	Gn [1]	TetTen >Gn [1]
Trace Element	**Cd**	**In**	**Sn**	**Sb**
Preferred Host	Sp >TetTen [3]	Sp > Cp [2]	? *	TetTen >Gn [1]
Trace Element	**Te**	**Hg**	**Tl**	**Bi**
Preferred Host	Gn [1]	Sp >TetTen [3]	Gn [1]	Gn >TetTen [1]

Abbreviations: TetTen = tetrahedrite-tennantite, Sp = sphalerite, Gn = galena, Cp = chalcopyrite. [1] Trend observed in all examined samples. [2] Recrystallization increases element concentration in Cp and may make Cp primary host. [3] Trend generally, yet not always, true. * Recrystallization increases Sn concentration in Cp such that Cp is usually primary host in recrystallized samples. Below recrystallization conditions, no trend is observed.

Supplementary Materials: The following are available online at www.mdpi.com/2075-163X/7/2/17/s1.

Acknowledgements: We are deeply grateful to Ben Grguric and Ben McHenry for providing relevant sample material from the South Australian Museum. Similarly, Anthony Milnes is thanked for providing access to Tate Museum collections. We are also appreciative of microanalysis support from Ben Wade and Aoife McFadden.

Author Contributions: Nigel J. Cook conceived the research within the framework of Luke L. George's Ph.D. project. Luke L. George acquired the samples, performed all analytical work reported here, and interpreted the data. Luke L. George, and Nigel J. Cook wrote the paper with contributions from Cristiana L. Ciobanu.

Conflicts of Interest: The authors declare no conflict of interest.

References

1. Wuensch, B.J. The crystal structure of tetrahedrite, $Cu_{12}Sb_4S_{13}$. *Zeitschrift Krist. Cryst. Mater.* **1964**, *119*, 437–453.
2. Wuensch, B.J.; Tackeuchi, Y.; Nowacki, W. Refinement of the crystal structure of binnite, $Cu_{12}As_4S_{13}$. *Zeitschrift Krist. Cryst. Mater.* **1966**, *123*, 1–20.

3. Makovicky, E.; Skinner, B. Studies of the sulfosalts of copper. VII. Crystal structures of the exsolution products $Cu_{12.3}Sb_4S_{13}$ and $Cu_{13.8}Sb_4S_{13}$ of unsubstituted synthetic tetrahedrite. *Can. Mineral.* **1979**, *17*, 619–634.
4. Moëlo, Y.; Makovicky, E.; Mozgova, N.N.; Jambor, J.L.; Cook, N.J.; Pring, A.; Paar, W.; Nickel, E.H.; Graeser, G.; Karup-Møller, S.; et al. Sulfosalt systematics: A review. Report of the sulfosalt sub-committee of the IMA commission on ore mineralogy. *Eur. J. Mineral.* **2008**, *20*, 7–46.
5. Repstock, A.; Voudouris, P.; Kolitsch, U. New occurrences of watanabeite, colusite, "arsenosulvanite" and "Cu-excess" tetrahedrite-tennantite at the Pefka high-sulfidation epithermal deposit, northeastern Greece. *Neues Jahrb. Miner. Abh. J. Miner. Geochem.* **2015**, *192*, 135–149.
6. Repstock, A.; Voudouris, P.; Zeug, M.; Melfos, V.; Zhai, M.; Li, H.; Kartal, T.; Matuszczak, J. Chemical composition and varieties of fahlore-group minerals from Oligocene mineralization in the Rhodope area, Southern Bulgaria and Northern Greece. *Mineral. Petrol.* **2016**, *110*, 103–123.
7. Makovicky, E.; Karanović, L.; Poleti, D.; Balić-Žunić, T.; Paar, W.H. Crystal structure of copper-rich unsubstituted tennantite, $Cu_{12.5}As_4S_{13}$. *Can. Mineral.* **2005**, *43*, 679–688.
8. Sack, R.O.; Loucks, R.R. Thermodynamic properties of tetrahedrite-tennantites: Constraints on the interdependence of the Ag ↔ Cu, Fe ↔ Zn, Cu ↔ Fe, and As ↔ Sb exchange reactions. *Am. Mineral.* **1985**, *70*, 1270–1289.
9. Johnson, N.E.; Craig, J.R.; Rimstidt, J.D. Compositional trends in tetrahedrite. *Can. Mineral.* **1986**, *24*, 385–397.
10. Makovicky, E.; Karup-Möller, S. Exploratory studies on substitution of minor elements in synthetic tetrahedrite. Part I. Substitution by Fe, Zn, Co, Ni, Mn, Cr, V and Pb. Unit-cell parameter changes on substitution and the structural role of "Cu^{2+}". *Neues Jahrb. Miner. Abh.* **1994**, *167*, 89–123.
11. Hackbarth, C.J.; Petersen, U. A fractional crystallization model for the deposition of argentian tetrahedrite. *Econ. Geol.* **1984**, *79*, 448–460.
12. Kovalenker, V.A.; Bortnikov, N.S. Chemical composition and mineral associations of sulphosalts in the precious metal deposits from different geological environment. *Geol. Carpathica* **1985**, *36*, 283–291.
13. Staude, S.; Mordhorst, T.; Neumann, R.; Prebeck, W.; Markl, G. Compositional variation of the tennantite-tetrahedrite solid-solution series in the Schwarzwald ore district (SW Germany): The role of mineralization processes and fluid source. *Mineral. Mag.* **2010**, *74*, 309–339.
14. Apopei, A.I.; Damian, G.; Buzgar, N.; Buzatu, A. Mineralogy and geochemistry of Pb-Sb/As-sulfosalts from Coranda-Hondol ore deposit (Romania)—Conditions of telluride deposition. *Ore Geol. Rev.* **2016**, *72*, 857–873.
15. Peterson, R.C.; Miller, I. Crystal structure and cation distribution in freibergite and tetrahedrite. *Mineral. Mag.* **1986**, *50*, 717–721.
16. Pfitzner, A.; Evain, M.; Petricek, V. $Cu_{12}Sb_4S_{13}$: A temperature-dependent structure investigation. *Acta Cryst.* **1997**, *B53*, 337–345.
17. Rozhdestvenskaya, I.V.; Zayakina, N.V.; Samusikov, V.P. Crystal structure features of minerals from the tetrahedrite-freibergite series. *Mineral. Zhurnal* **1993**, *15*, 9–17. (In Russian)
18. Johan, Z.; Kvaček, M. La hakite, un nouveau minéral du groupe de la tétraédrite. *Bull. Soc. Fr. Minéral.* **1971**, *94*, 45–48. (In French)
19. Johan, Z.; Picot, P.; Ruhlmann, F. Evolution paragénétique de la minéralisation uranifère de Chaméane (Puy-de-Dôme) France: Chaméanite, geffroyite et giraudite, trois séléniures nouveaux de Cu, Fe, Ag, and As. *Tscher. Miner. Petrog. Mitt.* **1982**, *29*, 151–167. (In French)
20. Kalbskopf, R. Synthese und Kristallstruktur von $Cu_{12-x}Te_4S_{13}$, dem Tellur-Endglied der Fahlerze. *Tscher. Miner. Petrog. Mitt.* **1974**, *21*, 1–10. (In German)
21. Dmitrieva, M.T.; Bojik, G.B. The crystallochemical mechanism of formation of vacancies in goldfieldite structure. *Zeitschrift Krist.* **1988**, *185*, 601.
22. Trudu, A.G.; Knittel, U. Crystallography, mineral chemistry and chemical nomenclature of goldfeldite, the tellurian member of the tetrahedrite solid-solution series. *Can. Mineral.* **1998**, *36*, 1115–1137.
23. Spiridonov, E.M.; Sokolova, N.F.; Gapeyev, A.K.; Dashevskaya, D.M.; Yevstigneyeva, T.L.; Chvileva, T.N.; Demidov, V.G.; Balashov, Y.P.; Shul'ga, V.I. The new mineral argentotennantite. *Dokl. Akad. Nauk SSSR* **1986**, *290*, 206–210. (In Russian)
24. Zhdanov, Y.Y.; Amuzinskii, V.A.; Andrianov, N.G. Discovery of a natural Ag-rich fahlore with the highest parameter of the unit cell. *Dokl. Akad. Nauk SSSR* **1992**, *326*, 337–340. (In Russian)

25. Karup-Møller, S. Exploratory studies on element substitutions in synthetic tetrahedrite. Part V. Mercurian tetrahedrite. *Neues Jahrb. Miner. Abh.* **2003**, *179*, 73–83.
26. Karup-Møller, S.; Makovicky, E. Exploratory studies of element substitutions in synthetic tetrahedrite. Part II. Selenium and tellurium as anions in Zn-Fe tetrahedrites. *Neues Jahrb. Miner. Abh.* **1999**, *9*, 385–399.
27. Karup-Møller, S.; Makovicky, E. Exploratory studies of the solubility of minor elements in tetrahedrite: VI. Zinc and the combined zinc-mercury and iron-mercury substitutions. *Neues Jahrb. Miner. Mon.* **2004**, *11*, 508–524.
28. Hansen, M.K.; Makovicky, E.; Karup-Møller, S. Exploratory studies on substitutions in tennantite-tetrahedrite solid solution. Part IV. Substitution of germanium and tin. *Neues Jahrb. Miner. Abh. J. Miner. Geochem.* **2003**, *179*, 43–71.
29. Klünder, M.H.; Karup-Møller, S.; Makovicky, E. Exploratory studies on substitutions in the tetrahedrite-tennantite solid solution series Part III. The solubility of bismuth in tetrahedrite-tennantite containing iron and zinc. *Neues Jahrb. Miner. Mon.* **2003**, *2003*, 153–175.
30. George, L.L.; Cook, N.J.; Ciobanu, C.L. Partitioning of trace elements in co-crystallized sphalerite–galena–chalcopyrite hydrothermal ores. *Ore Geol. Rev.* **2016**, *77*, 97–116.
31. Foit, F.F., Jr.; Hughes, M.J. Structural variations in mercurian tetrahedrite. *Am. Mineral.* **2004**, *89*, 159–163.
32. Johnson, M.L.; Burnham, C.W. Crystal structure refinement of an arsenic-bearing argentian tetrahedrite. *Am. Mineral.* **1985**, *70*, 165–170.
33. Johnson, N.E.; Craig, J.R.; Rimstidt, J.D. Crystal chemistry of tetrahedrite. *Am. Mineral.* **1988**, *73*, 389–397.
34. Pattrick, R.A.D.; Hall, A.J. Silver substitution into synthetic zinc, cadmium and iron tetrahedrites. *Mineral. Mag.* **1983**, *47*, 441–451.
35. Charnock, J.M.; Garner, C.D.; Pattrick, R.A.D.; Vaughan, D.J. Co-ordination sites of metals in tetrahedrite minerals determined by EXAFS. *J. Solid State Chem.* **1989**, *82*, 279–289.
36. Charnock, J.M.; Garner, C.D.; Pattrick, R.A.D.; Vaughan, D.J. EXAFS and Mössbauer spectroscopic study of Fe-bearing tetrahedrites. *Mineral. Mag.* **1989**, *53*, 193–199.
37. Pattrick, R.A.D.; van der Lann, G.; Vaughan, D.J.; Henderson, C.M.B. Oxidation state and electronic configuration determination of copper in tetrahedrite group minerals by L-edge X-ray absorption spectroscopy. *Phys. Chem. Miner.* **1993**, *20*, 395–401.
38. Oen, I.S.; Kieft, C. Bismuth-rich tennantite and tetrahedrite in the Mangualde pegmatite, Viseu district, Portugal. *Neues Jahrb. Miner. Mon.* **1976**, *2*, 94–96.
39. Bortnikov, N.S.; Kudryavtsev, A.S.; Troneva, N.V. Bi-rich tetrahedrite from the Tary-Ekan deposit (East Karamazar, central Asia). *Mineral. Zhurnal* **1979**, *198*, 61–64. (In Russian)
40. Kieft, K.; Eriksson, G. Regional zoning and metamorphic evolution of the Vindfall Pb-Zn ore, east central Sweden. *GFF* **1984**, *106*, 305–317.
41. Spiridonov, E.M.; Chvileva, T.N.; Borodaev, Y.S.; Vinogradova, R.A.; Kononov, O.V. The influence of bismuth on optical properties of gray copper. *Dokl. Akad. Nauk SSSR* **1986**, *290*, 1475–1478. (In Russian)
42. Breskovska, V.V.; Tarkian, M. Compositional variation in Bi-bearing fahlores. *Neues Jahrb. Miner. Mon.* **1994**, *5*, 230–240.
43. Gołębiowska, B.; Pieczka, A.; Parafiniuk, J. Substitution of Bi for Sb and As in minerals of the tetrahedrite series from Rędziny, Lower Silesia, southwestern Poland. *Can. Mineral.* **2012**, *50*, 267–279.
44. Nash, J.T. Geochemical studies in the Park City District; II, Sulfide mineralogy and minor-element chemistry, Mayflower Mine. *Econ. Geol.* **1975**, *70*, 1038–1049.
45. Basu, K.; Bortnykov, N.; Mookherjee, A.; Mozgova, N.; Tsepin, A.I. Rare minerals from Rajpura-Dariba, Rajasthan, India III: Plumbian tetrahedrite. *Neues Jahrb. Miner. Abh.* **1981**, *141*, 280–289.
46. Mozgova, N.N.; Tsepin, A.I. *Fahlore (Features of Chemical Composition and Properties)*; Nauka: Moscow, Russia, 1983; p. 279. (In Russian)
47. Moh, G.H. Sulfosalts: Observations and mineral descriptions, experiments and applications. *Neues Jahrb. Miner. Abh.* **1984**, *150*, 25–64.
48. Vavelidis, M.; Melfos, V. Two plumbian tetrahedrite-tennantite occurrences from Maronia area (Thrace) and Milos island (Aegean sea), Greece. *Eur. J. Mineral.* **1997**, *9*, 653–658.
49. Bishop, A.C.; Criddle, A.J.; Clark, A.M. Plumbian tennantite from Sark, Channel Islands. *Mineral. Mag.* **1977**, *41*, 59–63.
50. Ixer, R.A.; Stanley, C.J. Silver mineralization at Sark's Hope mine, Sark, Channel Islands. *Mineral. Mag.* **1983**, *47*, 539–545.

51. Förster, H.J.; Rhede, D.; Tischendorf, G. Continuous solid-solution between mercurian giraudite and hakite. *Can. Mineral.* **2002**, *40*, 1161–1170.
52. Jurković, I.B.; Garašić, V.; Jurković, I.M. Geochemical characteristics of mercurian tetrahedrite, barite and fluorite from the Duboki Vagan, Glumac and Dubrave-Dugi Dol barite deposits, south of Kreševo, Mid-Bosnian Schist Mts. *Geol. Croat.* **2011**, *64*, 49–59.
53. Basu, K.; Bortnykov, N.; Mookherjee, A.; Mozgova, N.; Sivtsov, A.V.; Tsepin, A.I.; Vrublevskaja, Z.V. Rare minerals from Rajpura-Dariba, Rajasthan, India V: The first recorded occurrence of a manganoan fahlore. *Neues Jahrb. Miner. Abh.* **1984**, *149*, 105–112.
54. Voropayev, A.V.; Spiridonov, E.M.; Shchibrik, V.I. Cd-Tetrahedrite, first find in the USSR. *Dokl. Acad. Sci. USSR.* **1988**, *300,* 1446–1468.
55. Pattrick, R.A. Microprobe analyses of cadmium-rich tetrahedrites from Tyndrum, Perthshire, Scotland. *Mineral. Mag.* **1978**, *42*, 286–288.
56. Pattrick, R.A. Pb-Zn and minor U mineralization at Tyndrum, Scotland. *Mineral. Mag.* **1985**, *49*, 671–681.
57. Huiwen, J.D.F.Z.Z.; Chunpei, Z. The first Discovery of Cd-Freibergite in China. *Acta Mineral. Sin.* **1988**, *2*, 005.
58. Voudouris, P.C.; Spry, P.G.; Sakellaris, G.A.; Mavrogonatos, C. A cervelleite-like mineral and other Ag-Cu-Te-S minerals [Ag_2CuTeS and $(Ag, Cu)_2TeS$] in gold-bearing veins in metamorphic rocks of the Cycladic Blueschist Unit, Kallianou, Evia Island, Greece. *Mineral. Petrol.* **2011**, *101*, 169–183.
59. Dobbe, R.T. Manganoan-cadmian tetrahedrite from the Tunaberg Cu-Co deposit, Bergslagen, central Sweden. *Mineral. Mag.* **1992**, *56*, 113–115.
60. Kovalenker, V.A.; Rusinov, V.L. Goldfieldite: Chemical composition, parageneses and conditions of formation. *Mineral. Zhurnal* **1986**, *8*, 57–70. (In Russian)
61. Kase, K. Tellurian tennantite from the Besshitype deposits in the Sambagawa metamorphic belt, Japan. *Can. Mineral.* **1986**, *24*, 399–404.
62. Knittel, U. Composition and association of arsenian goldfieldite from the Marian gold deposit, northern Luzon, Philippines. *Mineral. Petrol.* **1989**, *40*, 145–154.
63. Shimizu, M.; Stanley, C.J. Coupled Substitutions in Goldfieldite-Tetrahedrite Minerals from the Iriki Mine, Japan. *Mineral. Mag.* **1991**, *55*, 515–551.
64. Pohl, D.; Liessmann, W.; Okrugin, V.M. Rietveld analysis of selenium-bearing goldfieldites. *Neues Jahrb. Miner. Mon.* **1996**, *1996,* 1–8.
65. Pinto, A.; Ferreira, A.; Bowles, J.F.W.; Gaspar, O.C. Mineralogical and textural characterization of the Neves-Corvo ores. Metallogenetic implications. In *Geology and VMS Deposits of the Lberian Pyrite Belt*; Ser. 27; Baniga, F.J.A.S., Carvalho, D., Eds.; SEG Neves Corvo Field Conference: Lisbon, Portugal, 1997; p. 90.
66. Serranti, S.; Ferrini, V.; Masi, U.; Cabri, L.J. Trace-element distribution in cassiterite and sulfides from rubané and massive ores of the Corvo deposit, Portugal. *Can. Mineral.* **2002**, *40*, 815–835.
67. Figueiredo, M.O.; Silva, T.P.; de Oliveira, D.P.S.; Rosa, D.R.N. Searching for In-carrier minerals in polymetallic sulphide deposits: Digging deeper into the crystal chemistry of indium chalcogenides. In *Digging Deeper, Proceedings of the 9th Biennial SGA Meeting, Ferrara, Italy, 29–31 August 2007*; Andrew, C.J., Ed.; Irish Association Economic Geologists: Dublin, Ireland, 2007; pp. 1355–1358.
68. McClenaghan, S.H.; Lentz, D.R.; Martin, J.; Diegor, W.G. Gold in the Brunswick No. 12 volcanogenic massive sulfide deposit, Bathurst Mining Camp, Canada: Evidence from bulk ore analysis and laser ablation ICP-MS data on sulfide phases. *Miner. Depos.* **2009,** *44*, 523–557.
69. Gaspar, O.C. Mineralogy and sulfide mineral chemistry of the Neves-Corvo ores, Portugal: Insight into their genesis. *Can. Mineral.* **2002**, *40*, 611–636.
70. Jurković, I.B.; Garašić, V.; Jurković, I.M. Cobalt, nickel, wolfram, cadmium, selenium, silver and gold-bearing mercurian tetrahedrite from the Saski Rad barite-siderite deposit in the Mid-Bosnian Schist Mts. *Geol. Croat.* **2011**, *64*, 223–237.
71. Wohlgemuth-Ueberwasser, C.C.; Viljoen, F.; Petersen, S.; Vorster, C. Distribution and solubility limits of trace elements in hydrothermal black smoker sulfides: An in-situ LA-ICP-MS study. *Geochim. Cosmochim. Acta* **2015**, *159*, 16–41.
72. George, L.L.; Cook, N.J.; Crowe, B.B.P.; Ciobanu, C.L. Trace elements in hydrothermal chalcopyrite. *Mineral. Mag.* **2017**, in press.
73. Wilson, S.; Ridley, W.; Koenig, A. Development of sulphide calibration standards for the laser ablation inductively-coupled plasma mass spectrometry technique. *J. Anal. At. Spectrom.* **2002**, *17*, 406–409.

74. United States Geological Survey. Microanalytical Reference Materials and Accessories. Available online: http://crustal.usgs.gov/geochemical_reference_standards/microanalytical_RM.html (accessed on 6 October 2016).
75. Van Achterbergh, E.; Ryan, C.; Jackson, S.; Griffin, W. Data reduction software for LA-ICP-MS: Laser-Ablation-ICPMS in the earth sciences—Principles and applications. *Mineral. Ass. Can.* **2001**, *29*, 239–243.
76. Danyushevsky, L.; Robinson, P.; Gilbert, S.; Norman, M.; Large, R.; McGoldrick, P.; Shelley, M. Routine quantitative multi-element analysis of sulphide minerals by laser ablation ICP-MS: Standard development and consideration of matrix effects. *Geochem. Explor. Environ. Anal.* **2011**, *11*, 51–60.
77. Patten, C.; Barnes, S.J.; Mathez, E.A.; Jenner, F.E. Partition coefficients of chalcophile elements between sulfide and silicate melts and the early crystallization history of sulfide liquid: LA-ICP-MS analysis of MORB sulfide droplets. *Chem. Geol.* **2013**, *358*, 170–188.
78. Cook, N.; Ciobanu, C.L.; George, L.; Zhu, Z.Y.; Wade, B.; Ehrig, K. Trace element analysis of minerals in magmatic-hydrothermal ores by laser ablation inductively-coupled plasma mass spectrometry: Approaches and opportunities. *Minerals* **2016**, *6*, 111.
79. George, L.; Cook, N.J.; Cristiana, L.; Wade, B.P. Trace and minor elements in galena: A reconnaissance LA-ICP-MS study. *Am. Mineral.* **2015**, *100*, 548–569.
80. Plotinskaya, O.Y.; Grabezhev, A.I.; Seltmann, R. Fahlores compositional zoning in a porphyry-epithermal system: Biksizak occurrence, South Urals, Russia as an example. *Geol. Ore Depos.* **2015**, *57*, 42–63.
81. Buzatu, A.; Damian, G.; Dill, H.G.; Buzgar, N.; Apopei, A.I. Mineralogy and geochemistry of sulfosalts from Baia Sprie ore deposit (Romania)—New bismuth minerals occurrence. *Ore Geol. Rev.* **2015**, *65*, 132–147.
82. Vokes, F.M. Geological studies on the Caledonian pyritic zinc-lead orebody at Bleikvassli, Norland, Norway. *Nor. Geol. Unders.* **1963**, *222*, 1–126.
83. Vokes, F.M. On the possible modes of origin of the Caledonian sulfide ore deposit at Bleikvassli, Nordland, Norway. *Econ. Geol.* **1966**, *61*, 1130–1139.
84. Boulter, C.A.; Fotios, M.G.; Phillips, G.N. The Golden Mile, Kalgoorlie; a giant gold deposit localized in ductile shear zones by structurally induced infiltration of an auriferous metamorphic fluid. *Econ. Geol.* **1987**, *82*, 1661–1678.

CHAPTER 7

SUMMARY AND RECOMMENDATIONS

7.1 Summary

7.1.1 Trace element distributions in base metal sulphides and tetrahedrite-tennantite

Of the sulphides considered here, tetrahedrite-tennantite has the greatest potential to host a wide range of minor and trace elements at the highest concentrations, owing to extensive fields of solid solution (e.g., Moëlo et al., 2008). Major components of the tetrahedrite-tennantite series including Cu, Fe, Zn, Sb, As, and in some cases Ag, as well as minor components Hg and Pb, may all be present at concentrations exceeding 1 wt. %. In addition, Cd, Co, Mn, Bi and Te may all be present above 1,000 ppm, while Se and Sn are occasionally concentrated above 100 ppm. This potential trace element diversity should be recognized when analyzing tetrahedrite-tennantite for trace elements, as well as when establishing the primary hosts of economic elements for metallurgical purposes. Compositional zoning seems to be common in tetrahedrite-tennantite, especially in epithermal systems. These results are likely also applicable to other sulphosalt series with extensive solid solutions. There are currently few published trace element datasets for other sulphosalts, even though they may be carriers of elements of value. For example, significant concentrations of Au have been documented in various bismuth sulphosalts, as well as the tetradymite group and aleksite series of Bi and Bi-Pb-chalcogenides (Ciobanu et al., 2009; 2016).

Although to a lesser extent, sphalerite may also be a significant host for a range of minor and trace elements (e.g., Cook et al., 2009). Iron is most abundant, normally present above 1 wt. % and frequently as high as 8 – 10 wt. %. Furthermore, Mn, Cd, and less commonly, In, Sn and Hg, may also be concentrated above 1 wt. %. More typical concentrations for these

elements are hundreds to thousands of ppm. Cobalt, Cu and Ga may also be concentrated above 100 ppm.

Galena commonly hosts Bi, Ag and Sb at concentrations which range from hundreds to thousands of ppm. Apart from these three common trace components, Se, Cd, Sn and Te are the only additional elements that may be routinely expected to be present above 100 ppm. Trace element sector and oscillatory zoning has been recognized in epithermal galena for the first time, and it is inferred that this relates to slow crystal growth in a closed, local system.

Compared with the other sulphides considered in this study, chalcopyrite generally hosts trace elements at low levels. Measured concentrations of Zn, Ag and Sn, the three most common trace components in chalcopyrite, only exceed 1,000 ppm in rare cases. Selenium, In and Hg are the only additional elements measured at concentrations above 100 ppm. Nevertheless, given its abundance in many Cu ores, chalcopyrite may be the most significant host for a wide range of trace elements (e.g., Mn, Cd, Pb, Sb, In and Bi), despite their low absolute concentrations (e.g., chalcopyrite accounts for the majority of the In budget in the SW England ore region despite sphalerite and stannite-group minerals typically hosting higher concentrations; Andersen et al., 2016). Interestingly, no grain-scale zonation has been observed in any of the chalcopyrite samples studied in Chapter 5, even in low temperature epithermal environments where co-crystallized sphalerite and galena display extensive grain-scale zoning (e.g., Herja). The fine scale repetitive zoning observed in galena in such systems, and to a lesser extent sphalerite, support an intrinsic mechanism for oscillatory zoning formation (Shore and Fowler, 1996). A number of different intrinsic mechanisms have been suggested to produce oscillatory zoning, e.g., resulting from differing endmember phase solubilities controlling the supersaturation threshold for nucleation (e.g., Putnis et al., 1992), or based on pH controlled adsorption and desorption changing the electrical charge on crystal surfaces (e.g., Wang and Merino, 1992). Whatever the mechanism, the absence of

such oscillatory zoning in chalcopyrite may be due to the preference of all trace elements to partition to sphalerite or galena (oscillatory zoning is only noted for trace elements in sulphides that are their preferred host). Any intrinsic mechanism for oscillatory zonation formation may only act on trace elements that are actively partitioning into a mineral, not passively partitioning for lack of a better host, as is the typical case for chalcopyrite. More work, including compositional mapping, may yet reveal inhomogeneous trace element distributions in chalcopyrite, especially in systems where co-crystallizing sulphides are absent.

In general, there is little evidence, at least among the samples studied here, or in the existing literature, to suggest that the distribution and concentration of trace elements in base metal sulphides or tetrahedrite-tennantite is markedly distinct in genetically different deposit types. Characterization of deposit type based purely on sulphide trace element analysis appears to be an over-simplification of the wide variation present in most types of deposits. It seems rather that local factors inherent to individual deposits play the crucial role of determining the trace element signature of that deposit. For example, one skarn deposit may be anomalously enriched in Bi (e.g., Baita Bihor analyzed here), while another may not be. This primarily depends on the geological environment which the deposits form in, and the source of ore-forming fluids, not simply the fact that they are both 'skarns'. Although the source of ore-forming fluids in any given deposit type may be analogous, and thus the concentrations of metals in the fluids may be somewhat comparable (e.g., sourced from a magma in the case of an epithermal deposit as opposed to sediments for SEDEX deposits), this distinction should not be overstated. For example, Chapter 5 showed that chalcopyrite from Bleikvassli and Mofjell has vastly different Cd, In and Sn signatures, despite the fact that both are recrystallized SEDEX deposits within regionally metamorphosed rock packages in the Scandinavian Caledonides. Distinct Sn, Se and As signatures are also noted in

chalcopyrite from Balcooma and Dry River South, two VMS deposits hosted within the same lower amphibolite facies metamorphosed lithologies, Queensland, Australia (Huston et al., 1995).

Although not commonly observed, there is evidence that post-crystallization element mobilization at the grain-scale does occur in some assemblages. For example, in some base metal sulphide assemblages from the recrystallized Broken Hill deposit, N.S.W., Australia, galena and sphalerite are zoned in that they show a depletion in trace elements at grain boundaries and adjacent to fractures (Fig. 7.1). This is likely the result of secondary sub-solidus leaching of Ag and Sb from galena, and Co from sphalerite, along grain boundaries and fractures following fluid-rock interaction post recrystallization. Such secondary trace element mobilization may even appear to alter the preferred host of some trace elements (e.g., in Figure 7.1 chalcopyrite now hosts more Ag than galena, contrary to what is normally observed). Further evidence for post-crystallization element diffusion in sulphides is seen in the depletion of Ag and other trace elements towards the margins of bornite grains in the Olympic Dam iron-oxide copper gold ore (Ciobanu, pers. comm.). This is an area in which additional research is needed.

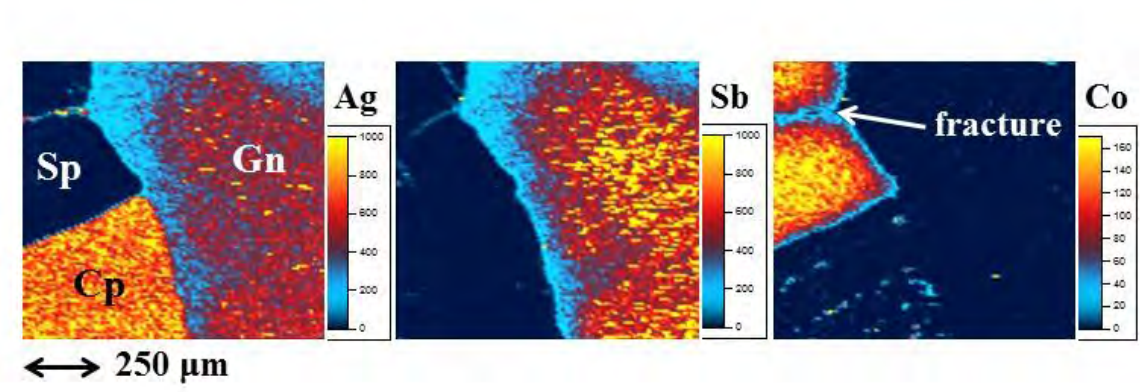

Figure 7.1. LA-ICP-MS trace element maps (Ag, Sb, Co; ppm scales) of an assemblage comprising co-crystallized sphalerite (Sp), galena (Gn) and chalcopyrite (Cp) from the Broken Hill recrystallized SEDEX deposit. Note depletion of Ag and Sb in galena and Co in sphalerite at grain boundaries and adjacent to fracture. Depleted boundaries are much wider than the beam diameter and are thus are not edge effects due to poor resolution.

7.1.2 Trace element partitioning in base metal sulphide ores

In hydrothermal base metal sulphide ores comprising co-crystallized sphalerite, galena and chalcopyrite, almost all trace elements will be primarily concentrated in either sphalerite or galena. Sphalerite will be the primary host of Fe, Cd and Mn, and in most cases, also the chief host for Co, Cu and Hg (Fig. 7.2). Galena will host the major proportion of the Ag, Bi, Sb, Se, Tl, Te and As budgets. Zinc is the only trace element that prefers to partition to chalcopyrite (in the absence of sphalerite). Chalcopyrite will generally only host high trace element concentrations in the absence of either sphalerite or galena (or other Cu-(Fe)-sulphides such as bornite or chalcocite; Cook et al., 2011; 2015a). The only exception is in ores that undergo syn-metamorphic sulphide recrystallization. Under such conditions, the concentration of Ga, In and Sn increases in chalcopyrite due to repartitioning from sphalerite and galena such that in recrystallized ores, chalcopyrite is typically the main host of Ga and Sn, and occasionally the main host of In. Similar compositional changes may occur in feldspars that undergo recrystallization (Passchier and Trouw, 2005). In ores that have not recrystallized, Sn may be hosted in either sphalerite, galena or chalcopyrite.

Synthetic experiments have shown that grain-boundary and lattice diffusion of Fe and Mg between diopside and ferrosalite is essentially nonexistent at 900 ^{o}C and 15 kbar without any intergranular H_2O present (Watson and Lupulescu, 1993). When ~2.4 wt. % fluid is added, diffusion is observed on the scale of a few millimeters during experiments lasting 21 days. These experiments highlight the importance of fluids in re-partitioning elements from one mineral to another. Thus, the re-partitioning of Ga, In and Sn during recrystallization associated with regional metamorphism is likely driven by metamorphic fluids present, and the heating and subsequent cooling over long time scales likely allows for chemical transport

over longer distances (on the scale of metres or tens of metres) and homogenization of recrystallized phases.

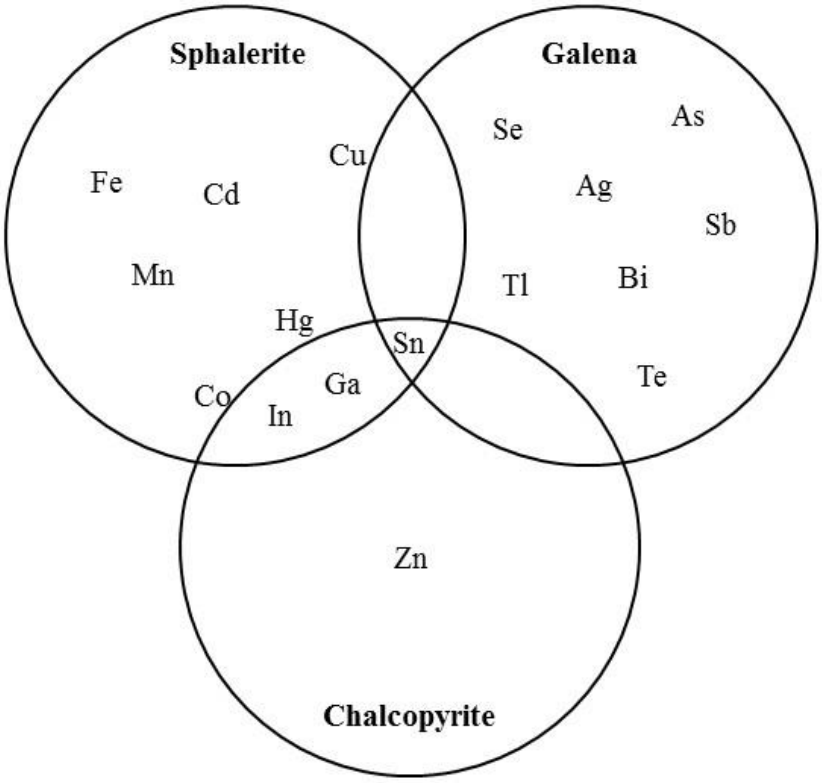

Figure 7.2. Schematic diagram showing the main hosts of various trace elements in a hydrothermal ore in which sphalerite, galena and chalcopyrite have co-crystallized.

If tetrahedrite-tennantite is also present in a hydrothermal base metal sulphide ore and co-crystallizes with sphalerite, galena and chalcopyrite, many trace elements will preferentially partition to tetrahedrite-tennantite. In such an assemblage, tetrahedrite-tennantite will be the primary host of Cu, Sb, As, Zn, Ag, and typically also Fe (Fig. 7.3). On rare occasions, it may also host the most Hg and Cd.

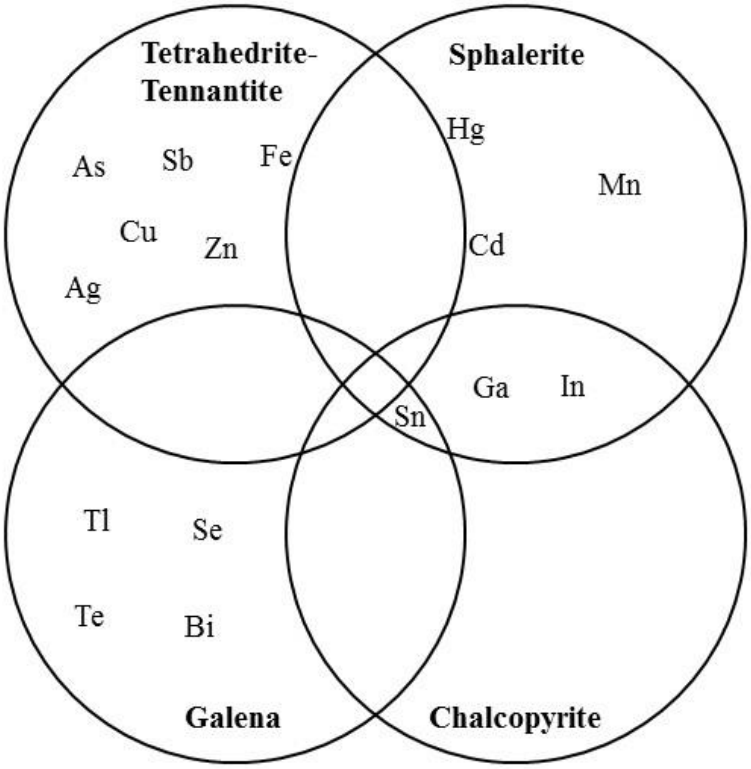

Figure 7.3. Schematic diagram showing the main hosts of various trace elements in a hydrothermal ore in which tetrahedrite-tennantite, sphalerite, galena and chalcopyrite have co-crystallized.

The preferred partitioning of all trace elements (except for Sn) is governed primarily by the sulphides present in the co-crystallizing assemblage. Even during sulphide crystallization under vastly different physiochemical conditions (e.g., temperature, pressure, redox conditions), preferred partitioning patterns for most elements will not be altered. The only exceptions are Ga, In and Sn under conditions of syn-metamorphic recrystallization. The observed consistency of trace element partitioning is due to the fact that the primary factors controlling partitioning are intrinsic to the substituting trace elements and their sulphide hosts. Such factors include trace element oxidation state, ionic radius of the substituting trace element, element availability in the ore forming environment (e.g., for some trace elements to be incorporated in sulphides, they need other elements of certain oxidation state and ionic

radius present in the system to participate in coupled substitutions) and the maximum trace element budget that a sulphide mineral can accommodate (e.g., in the case of Fe and Hg partitioning between sphalerite and tetrahedrite-tennantite).

Many ore deposits also contain other minerals that may be the primary hosts of various trace elements listed above. For example, pyrite (and arsenopyrite) is typically a good host of Co, Ni and As (Cabri et al., 1985; Bajwah et al., 1987; Huston et al., 1995; Reich et al., 2005; Large et al., 2009; Deditius et al., 2014). Bornite and chalcocite may concentrate significant amounts of Ag and Bi (Cook et al., 2011), certainly more than coexisting chalcopyrite. Although textural observations often suggest that pyrite and arsenopyrite did not crystallize in equilibrium with sphalerite, galena, chalcopyrite and tetrahedrite-tennantite, in cases where they do co-crystalize, this would undoubtedly affect the partitioning preferences for some trace elements (e.g., Cook et al., 2015a). Some oxide minerals may be stable with sulphides at certain physiochemical conditions and therefore crystallize in an ore deposit at the same time. For example, cassiterite is stable with both sphalerite and galena over quite extensive Eh and pH ranges (Fig. 7.4). Tin would obviously preferentially partition to cassiterite when the oxide co-crystallizes with the sulphide assemblage.

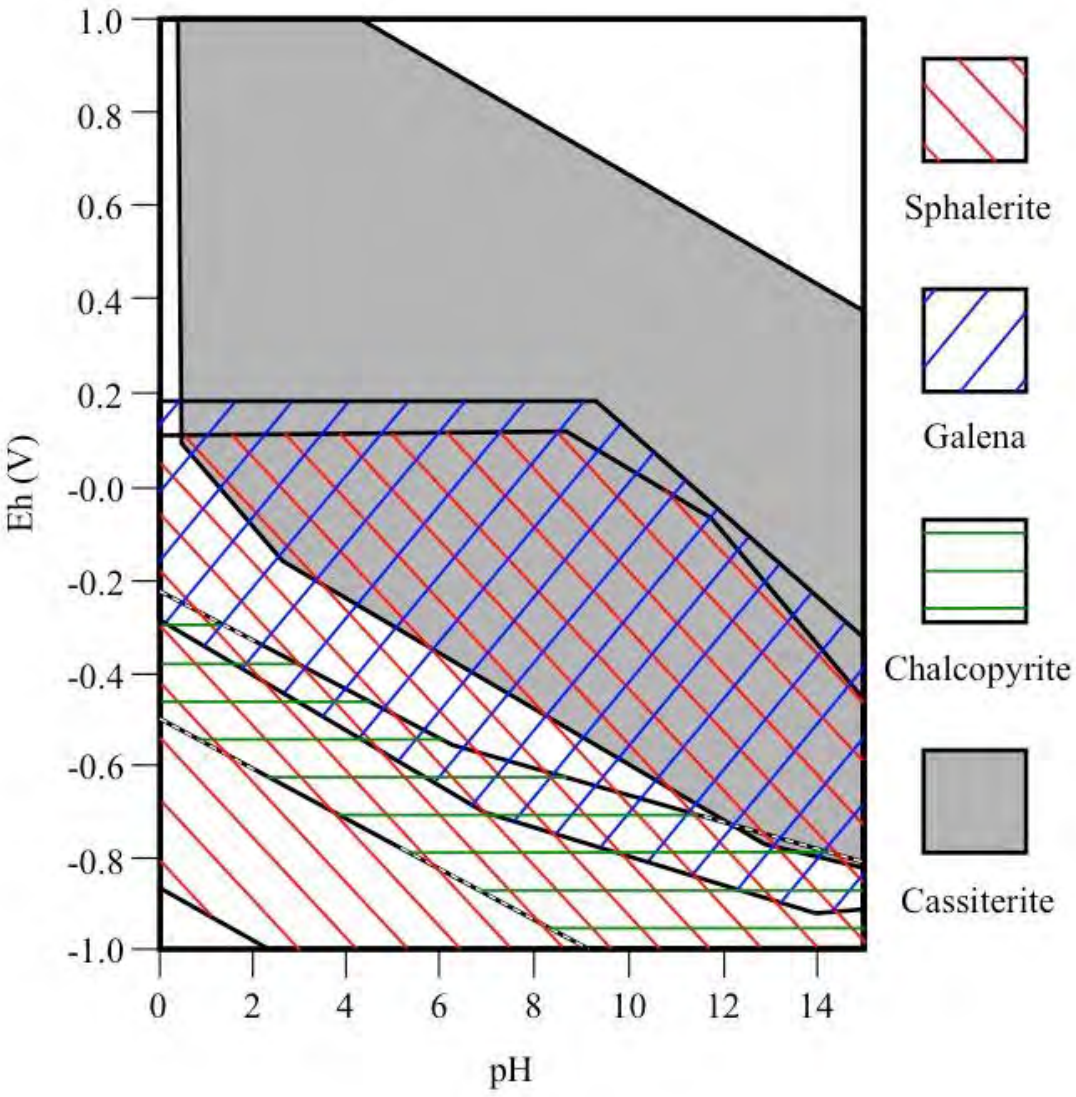

Figure 7.4. Simplified Eh-pH stability field diagrams for sphalerite, galena, chalcopyrite and cassiterite at 25 ^{o}C and 1 atm. Figure modified from Sato (1992) and Giaccherini et al. (2016).

7.2 Research gaps and recommendations

7.2.1 Partitioning coefficients and geothermobarometry

Although the preferred host of almost all trace elements does not change under varying physiochemical conditions, this does not imply that the absolute concentration of trace elements in a given sulphide or multi-phase assemblage will not be altered by factors such as pressure and temperature (analogous to other systems, e.g., Sr and Ba partitioning into plagioclase; Blundy and Wood, 1991, or rare earth element partitioning into hydrothermal minerals; Morgan and Wandless, 1980). It has been shown in Chapter 5 that the ratio of certain trace elements in co-crystalizing sulphides does depend to some degree on physiochemical conditions such as temperature (e.g., Cd:Zn ratio in chalcopyrite). Thus, the next step in understanding trace element partitioning in hydrothermal base metal sulphide ores is an attempt at quantifying partitioning coefficients (e.g., $X_{sphalerite}/X_{galena}$, $X_{sphalerite}/X_{chalcopyrite}$ and $X_{galena}/X_{chalcopyrite}$) under different physiochemical conditions.

In magmatic sulphide ore deposits, the distribution and partitioning of trace elements, including the platinum group elements (PGE; Ru, Rh, Pd, Os, Ir, Pt) and gold, between pentlandite, pyrrhotite, chalcopyrite/cubanite and pyrite, has been the subject of extensive study in recent years (e.g., Barnes et al., 2006; Holwell and McDonald, 2007; 2010; Godel and Barnes, 2008; Dare et al., 2010; 2011; Djon and Barnes, 2012; Piña et al., 2012; Prichard et al., 2013; Chen et al., 2014; Duran et al., 2015; Barnes and Ripley, 2016; Smith et al., 2016). This work has shown that most PGE, particularly Pd, have a strong affiliation with pentlandite, while Ru, Rh, Os, Ir are also primarily concentrated in pyrrhotite on occasions. Chalcopyrite is typically relatively barren of PGE (as has been shown for other trace elements in Chapter 5). In addition to these trends, the partitioning coefficients for many

trace elements between sulphide liquid, silicate melts and mono-sulphide solid solution have been quantified (e.g., Campbell and Barnes, 1984; Peach et al., 1990; 1994; Barnes and Picard, 1993; Fleet et al., 1993; 1999; Li et al., 1996; Barnes et al., 1997; Jugo et al., 1999; Ripley et al., 2002; Mungall et al., 2005; Helmy et al., 2010). Although much work has focused on natural specimens, quantification has typically involved synthetic crystallization of sulphides from melts using experimental approaches (e.g., evacuated silica capsules, piston-cylinder apparatus).

As has been the case for magmatic sulphide ore deposits, attempts at quantifying trace element partitioning coefficients in hydrothermal base metal sulphide ores would almost certainly necessitate an experimental approach in which natural conditions are reproduced in the laboratory. Using natural assemblages to quantify partitioning coefficients introduces too many variables that are difficult to constrain with any confidence. For example, the physiochemical conditions during primary base metal sulphide crystallization must be precisely known, sulphides must co-crystallize at equilibrium and subsequently must preserve their trace element composition throughout their post-depositional history. Analogously, in magmatic sulphide ores, the work focused on determining chalcophile element partitioning coefficients between silicate melts and sulphides from natural specimens (e.g., Keays and Campbell, 1981; Sharpe, 1982; Barnes and Naldrett, 1985; Klöck and Palme, 1988; Prendergast and Keays, 1989) has also been fundamentally limited. Variables include poorly constrained initial magma conditions, the fact that the partitioning of some elements may be controlled by the presence or absence of certain magmatic phases, and that measured element concentrations may be a product of post-magmatic processes or metamorphism (e.g., Boudreau et al., 1986; Naldrett and Lehmann, 1988; Peach et al., 1990). Experimental apparatus allows each unknown variable to be constrained, and thus partitioning coefficients to be accurately determined.

Experiments involving hydrothermal fluids have been carried out to investigate element diffusion and partitioning in various silicates and oxides (see Table 7.1). This reveals the potential of using similar experiments to investigate trace element partitioning among base metal sulphides. Nevertheless, such hydrothermal experimental approaches would almost inevitably include difficulties, as has been the case for the hydrothermal experimental work on silicates and oxides. Simple assemblages typically used in experiments are rare in nature, and therefore results may have limited applicability to real world examples where more complex assemblages exist (e.g., assemblages comprising clinopyroxene used by Watson and Lupulescu (1993) would typically also include other minerals such as feldspar, olivine, quartz etc.). Phases used as starting products may be poorly soluble in experimental fluids (e.g., zircon; Ayers and Watson, 1991). Chemical starting products may unfavorably oxidize or reduce (e.g., reduction of PbO and PbO_2 to Pb^0 by hydrogen influx; Watson et al., 1997). Minerals of interest may fail to crystallise from fluid when required (e.g., the inability to effectively crystallize zircon below 1000 ^oC; Watson et al., 2006). Alternatively, too many unwanted or accessory minerals may crystallize in place of minerals of interest (e.g., baddeleyite crystallizing instead of zircon; Ayers and Watson, 1991). The grain size of synthesised sulphides may be too small for microanalysis (e.g., hydrothermally grown zircon; Watson et al., 1997). Additionally, designing an experiment that takes into account the large number of variables potentially effecting trace element partitioning is difficult. All these potential problems stem from the fact that it can often be extremely difficult to accurately reproduce natural hydrothermal conditions in synthetic experiments, especially crystallization and cooling times. This is highlighted by the results shown in Chapters 4 and 5 that trace element partitioning is affected to the greatest extent during conditions of recrystallization during metamorphism. This is likely not exclusively due to the prevailing physiochemical

conditions during such metamorphism, but related to the long time-scales such recrystallization occurs over, and slow cooling post recrystallization.

Table 7.1 Examples of hydrothermal fluid experiments on various minerals either through element partitioning between existing grains, or partitioning into newly crystallizing grains

Mineral	**Reference**
Diopside	Zielinski and Frey, 1974
Quartz	Matsuhisa et al., 1978
Phlogopite	Bos, 1990
Olivine	Watson, 1991
Clinopyroxene	Watson and Lupulescu, 1993
Zircon	Watson et al., 1997; 2006
Rutile	Watson et al., 2006
Tourmaline	See references in London, 2011

Nevertheless, if a suitable method could be developed that allowed for either co-crystallization of base metal sulphides from a hydrothermal solution, or partitioning of trace elements between existing base metal sulphides at equilibrium, then the partitioning trends outlined in Chapters 4 and 6 could be elucidated, and partitioning coefficients between sulphides could be calculated for various physiochemical conditions. This would inevitably lead to the possibility of developing geothermobarometers for hydrothermal base metal sulphide ores.

Over the years, a number of efforts have been made to develop geothermometers using trace elements in sulphides. For example, Sack (2000; 2005) and Gallego Hernández and Akasaka (2010) have sought to derive crystallization temperatures using the compositions of Ag-rich tetrahedrite solid solutions, and Bethke and Barton (1971) and Bortnikov et al. (1995) have tried using the partitioning of Cd and Mn between sphalerite/wurtzite and galena

to determine the temperature of ore formation. Such attempts have been mirrored by the development of analogous approaches for the determination of metamorphic conditions using the accessory minerals zircon, rutile and titanate (Watson et al., 2006; Ferry and Watson, 2007; Hayden et al., 2008). Titanium in zircon and zirconium-in-rutile geothermometry has also been successfully applied to ore systems (e.g., Ismail et al., 2014; Sharrad et al., 2014). Although establishing a reliable, well-calibrated sulphide geothermometer useful for routine application has eluded researchers, it is hoped that hydrothermal synthetic experiments on base metal sulphides could allow for such a geothermometer to be defined in future.

7.2.2 The oxidation state of tin in sulphides

While partitioning trends for most trace elements have been shown to be consistent, Sn is an element displaying erratic partitioning in lower temperature (non-recrystallized) hydrothermal base metal ores. Sphalerite, galena and chalcopyrite have all been observed to be the main Sn host in such assemblages (Fig. 7.5). Yet despite the erratic partitioning of Sn in these systems, Sn partitioning is observed to be consistent in deposits where the base metal sulphide assemblage has undergone syn-metamorphic recrystallization. Under such conditions, chalcopyrite is always observed to be the preferred Sn host. Various explanations may be advanced for the unique partitioning behaviour of Sn, three of which are briefly outlined here that are based on either Sn partitioning in the 2+ oxidation state, the 4+ oxidation state, or a combination of both.

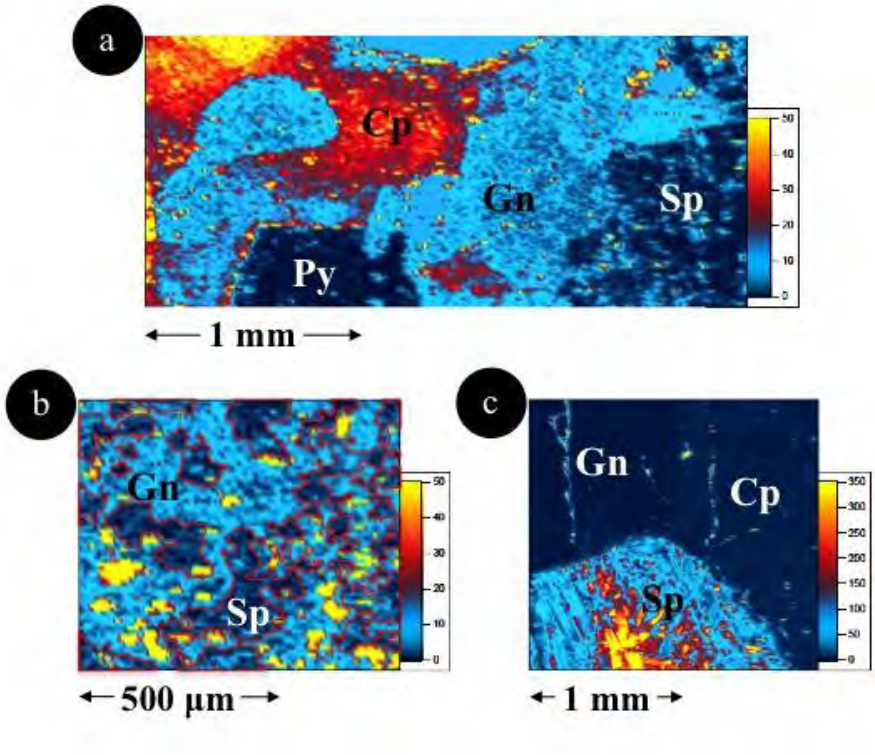

Figure 7.5. LA-ICP-MS trace element maps for tin (ppm scales) in non-recrystallized assemblages comprising co-crystallized sphalerite (Sp), galena (Gn) and chalcopyrite (Cp) from (**a**) the Toroiaga epithermal deposit, Romania, (**b**) the Mt. Isa SEDEX deposit, Australia and (**c**) the Herja epithermal deposit, Romania. Note how Sn is primarily hosted in different base metal sulphides in each assemblage.

Firstly, the erratic partitioning of Sn may be due to it being present in different oxidation states in different hydrothermal environments (e.g., as Sn^{2+} or Sn^{4+}), and the comparative preference of these oxidation states for one sulphide species over the others. In phases of the SnS-In_2S_3-SnS_2 system (where Sn_2S_3 is part of this system), Sn is present as both Sn^{2+} and Sn^{4+}, i.e., $Sn^{2+}S$ and $Sn^{4+}S_2$ (Lefebvre et al., 1991). As such, Sn_2S_3 is a mixed valence Sn compound, comprising both Sn^{2+} and Sn^{4+} (Jiang and Ozin, 1998). It is thus possible that Sn may be present in different oxidation states when hosted by different minerals, and even that both Sn oxidation states may coexist in the same phase. The different stabilities of these Sn oxidation states in different environments may explain the observed trends.

Among other deposits, consistent Sn partitioning in recrystallized assemblages has been noted in both Broken Hill, Australia, and Bleikvassli, Norway, two recrystallized SEDEX ores. Interestingly, the Bleikvassli system is oxidized, evidenced by large pyrite metablasts, and a distinct syn-metamorphic sulphidation–oxidation halo enclosing the ore (Rosenberg et al., 2000). In contrast, Broken Hill is strongly reduced, as evidenced by the stability of pyrrhotite, a lack of pyrite, and the Eu enrichment of proximal exhalites (Lottermoser, 1989; Leyh and Conor, 2000). Thus, it may seem somewhat unlikely that erratic Sn partitioning is due solely to differing Sn oxidation states, since erratic Sn partitioning is not observed in Broken Hill and Bleikvassli assemblages where different Sn oxidation states might be expected, i.e., reduced Sn^{2+} at Broken Hill and oxidised Sn^{4+} at Bleikvassli. Yet pH also has a strong control on the oxidation state of Sn, with acidic conditions favouring Sn^{4+} and alkali conditions favouring Sn^{2+} (Brookins, 1988). Without more detailed data on the stability of Sn oxidation states as a function of, for example, Eh and temperature, it is difficult to draw general conclusions about the likely oxidation state of Sn in different environments.

Shannon (1976) does not define the ionic radius of Sn^{2+} in any coordination and asserts that it is impossible to do so, since Sn^{2+} distorts the host compound such that the ionic radius differs depending on the host. Similarly, Lefebvre et al. (1991) show that, in contrast to Sn^{4+}, Sn^{2+} is concentrated in strongly distorted sites in phases of the SnS-In_2S_3-SnS_2 system. The partitioning behaviour of the Sn^{2+} cation between ionic base metal sulphides (and to a lesser extent covalent chalcopyrite) cannot, therefore, be predicted from Goldschmidt's rules (Goldschmidt, 1954) as can be done for most trace elements.

Assuming Sn^{2+} is the form of tin hosted in base metal sulphides, and since incorporation of Sn^{2+} into a compound is accompanied by significant distortion of that compound, then Sn^{2+} incorporation may be limited, or aided, by lattice distortion induced in the host compound by external factors. For example, the incorporation of other minor and trace elements into a host

compound also typically causes lattice distortion to some degree (e.g., distortion of the goethite lattice caused by substitution of Co, Ni, Cu, Zn, Cd and Pb; Gerth, 1990, or Ag and Sb substitution into galena; Sharp et al., 1990). In such a scenario, Sn^{2+} incorporation may be limited if the host lattice cannot be distorted more than it already has been by incorporation of other minor and trace elements. On the contrary, an already distorted host lattice may provide the ideal environment for a substituting Sn^{2+} cation. Lattice distortion is also produced during deformation associated with regional metamorphism (Passchier and Trouw, 2005). The consistent partitioning of Sn to chalcopyrite during syn-metamorphic recrystallization may, therefore, be a product of somewhat-consistent sulphide deformation as a result of regional metamorphism, at least in the recrystallized deposits studied here, whereas lesser amounts of distortion in the absence of regional metamorphism often allow either sphalerite or galena to be the primary Sn host.

According to Goldschmidt's rules (Goldschmidt, 1954), it should be difficult to incorporate Sn^{4+} into the lattice of either ionic sphalerite or galena since the charges on the bivalent cations in these sulphides differ by more than one unit with Sn^{4+}. Thus, complex coupled substitutions, such as those proposed by Johan (1988) for sphalerite, would be necessary for incorporation of Sn^{4+} into ionic sulphides. Such substitutions are entirely dependent on there being other bivalent and monovalent cations present to facilitate Sn^{4+} incorporation. Thus the erratic partitioning of Sn in lower temperature (non-recrystallized) base metal ores may be a result of Sn^{4+} substitution being driven by the partitioning preferences of the available 1+ and 2+ cations (assuming Sn^{4+} incorporation into sulphides). Since the 4+ oxidation state of Sn is more stable than 2+ (Harrison, 1989), this explanation does seem favorable, at least in part. In this scenario, the preference of Sn for chalcopyrite, especially in base metal sulphide assemblages that have undergone syn-metamorphic

recrystallization, may be due to the covalent nature of chalcopyrite 'tolerating', at least to some degree, charge imbalance.

It is desirable that further studies be undertaken to determine the oxidation state of Sn (and potentially other trace elements of interest) when hosted in different base metal sulphides using various X-ray Absorption Spectroscopy (XAS) methods at synchrotron radiation sources, i.e., X-ray Absorption Near-Edge Structure (XANES), Extended X-ray Absorption Fine Structure (EXAFS), or even X-ray Photoelectron Spectroscopy (XPS). Such methods have successfully determined the oxidation states of important elements in such base metal sulphides before (e.g., Cu and Ge in sphalerite; Cook et al., 2012; 2015b, Ag in galena; Giuli et al., 2005). Tin may be hosted in sphalerite, galena and chalcopyrite at high enough concentrations to allow such analyses to be possible using synchrotron radiation. For example, sphalerite from Toyoha, Japan, contains between 1000 ppm to >1 wt. % Sn (Cook et al., 2009). Some galena specimens from Bleikvassli, Norway, contain more than 700 ppm Sn, and chalcopyrite from the same deposit may host more than 1000 ppm Sn. XAS investigation that determines whether Sn is typically hosted as Sn^{2+}, as Sn^{4+}, or a mixture of both (when Sn is present at high concentrations in base metal sulphides), will allow inference to be made on the controls of Sn partitioning. The most likely explanation, however, may be that the partitioning of Sn between base metal sulphides, especially in lower temperature (non-recrystallized) ores, is a function of multiple parameters whose relative influence differs from case to case.

7.3 Practical economic implications

The data and interpretations outlined in this study have direct implications for the minerals industry, and economic geology in general. First and foremost, the LA-ICP-MS datasets for

sphalerite, galena, chalcopyrite and tetrahedrite-tennantite presented here offer a fundamental understanding of which trace elements may be expected within these hydrothermal sulphides, and at roughly what levels of concentration. This provides guidelines for future LA-ICP-MS researchers as to which elements should be measured (and which elements should have lower priority, or need not be measured at all) when analysing different sulphides.

As this work has endeavoured to report elements present in solid solution in the investigated sulphides, the datasets presented here may also be used to help recognise anomalous analyses affected by micro-inclusions in new LA-ICP-MS datasets. Nevertheless, one should be cautious in attributing an anomalous analysis as 'inclusion-related' simply because it is anomalous. Chapters 3, 5 and 6 have shown, as have other studies, that many sulphides can host anomalous concentrations of trace elements not easily attributed to micro-inclusions given the right conditions (e.g., Co and Ni in chalcopyrite; Bajwah et al., 1987, Mo in sphalerite; Orberger et al., 2003).

The knowledge of what trace elements may be expected within the investigated sulphides, and at what levels of concentration, is also directly applicable to understanding the hosts of economic elements in hydrothermal base metal sulphide ores. This especially relates to elements that can be recovered and exploited as by-products of the primary ore if valuable and present at high enough concentrations. For example, galena has long been noted as a potential economic carrier for the precious metal Ag, yet it has been shown in Chapter 6 that when tetrahedrite-tennantite co-crystallizes with galena, Ag will always prefer to partition to tetrahedrite-tennantite. This implies that tetrahedrite-tennantite is commonly the primary Ag host in an ore if it is present at a high enough volume. The critical metals In, Ga and Sn generally do not form discrete economically exploitable minerals, and therefore must be extracted from ores primarily concentrating other metals. Chapters 4, 5 and 6 have helped identify the primary hosts of these elements in hydrothermal base metal sulphide ores

(typically sphalerite), how these hosts change during syn-metamorphic recrystallization (i.e., repartitioning to chalcopyrite), as well as identifying which sulphides will not typically host these elements in significant amounts (e.g., tetrahedrite-tennantite).

In contrast to economically valuable elements, some elements can become impurities in concentrates, making such concentrates liable to financial penalties or difficult to market, and sometimes causing them to become an environmental hazard (e.g., Lane et al., 2016). This study allows researchers and metallurgists to identify which sulphide may be the culpable host of deleterious elements in a base metal concentrate, and thus assist in the processing of the corresponding ore. For example, it has been recognized that chalcopyrite may potentially host enough Se and Hg to cause a produced Cu-concentrate to incur a monetary penalty from a smelter, or in the worst case, cause such a concentrate to be unsaleable.

In recent years, much research has focused on vector approaches to mineral exploration based on there being systematic trace element variation in a specific mineral or mineral group in different rock types across an ore deposit and alteration envelope (e.g., Nadoll et al., 2012; Boutroy et al., 2014; Acosta-Góngora et al., 2015; O'Brien et al., 2015; Canil et al., 2016; Makvandi et al., 2016a; 2016b). Despite this, no trace element exploration vector has been applied generally outside its immediate context of a single well-explored deposit or orefield. This is partly due to the failure of exploration vectors defined in one environment to be representative of another environment, especially given the wide variation in individual deposits, even deposits of the same type. In addition, the necessity for large sample volumes, the high level of analytical noise in such samples, and the fact that vector techniques are expensive and time consuming, has also hindered their applicability (e.g., Cook et al., 2016). Nevertheless, as research continues, it is hoped that a reliable and widely applicable trace element exploration vector could be defined. While subtle physiochemical changes in the ore environment as a function of distance to mineralization are typically reflected in the absolute

concentration of trace elements in minerals, Chapters 4 and 6 have shown that the co-crystallizing mineral assemblage has the greatest control on trace element partitioning into minerals. Thus, it is recommended that future research aimed at investigating potential trace element exploration vectors should not focus on absolute trace element concentrations in a single mineral without considering the assemblage such a mineral co-crystallized in. Rather, a holistic approach is necessary, taking into account the partitioning of trace elements as determined by the co-crystallizing assemblage, as well as physiochemical controls on trace element incorporation.

Several tools have been identified in this study that may help in the characterization of hydrothermal base metal sulphide ores, as well as aiding the understanding of their genesis. Firstly, Chapters 4 and 6 have established the preferred hosts of various trace elements when base metal sulphides and tetrahedrite-tennantite co-crystallize, an understanding that may be used to help determine whether any other analogous assemblage has co-crystallized. Specifically, if the sulphide hosts of various trace elements in a given base metal sulphide assemblage do not correlate to the typical hosts described in Chapters 4 and 6 (see Tables 7.2 and 7.3), then it is likely that such an assemblage did not co-crystallize. On the other hand, if the primary sulphide hosts do correlate to the preferred hosts described in Chapters 4 and 6, then it may be suggestive of a co-crystallized assemblage. If both Ga and Sn, and possibly In, are more highly concentrated in chalcopyrite compared with sphalerite or galena, then this likely indicates that the sulphide assemblage has recrystallized. It has also been shown in Chapter 5 that the Cd:Zn ratios in co-existing chalcopyrite (Cd/Zn_{cp}) and sphalerite (Cd/Zn_{sp}) may be useful in indicating whether physiochemical conditions varied during base metal sulphide crystallization. A constant Cd/Zn_{cp} approximately equal to Cd/Zn_{sp} indicates that both sulphides have co-crystallized under constant physiochemical conditions from the same ore-forming fluid. If Cd/Zn_{cp} is constant yet markedly distinct from Cd/Zn_{sp}, the two

sulphides likely crystallized from distinct ore-forming fluids and/or at different times. A variable Cd/Zn_{cp}, especially coupled with a distinct difference in Cd/Zn_{sp}, likely indicates varying physiochemical conditions during sulphide crystallization. It would be helpful for these tools to be tested in additional ore deposits to determine their reliabilities and outline their exceptions. Nevertheless, given the common association of sphalerite, galena, chalcopyrite and tetrahedrite-tennantite in different ore types and geological environments (e.g., Bowles et al., 2011), the tools outlined in this study have potential to be widely applicable in a range of ore systems.

Table 7.2 Preferred hosts for various trace elements in a co-crystallizing Sp-Gn-Cp assemblage

Trace Element	**Mn**	**Fe**	**Co**	**Cu**	**Zn**	**Ga**	**As**	**Se**
Preferred Host	Sp[1]	Sp>Gn[1]	Sp>Cp[3]	Sp>Gn[3]	Cp[1]	Sp[2]	Gn>Sp[1]	Gn[1]

Trace Element	**Ag**	**Cd**	**In**	**Sn**	**Sb**	**Te**	**Hg**	**Tl**	**Bi**
Preferred Host	Gn[1]	Sp>Gn[1]	Sp>Cp[2]	?*	Gn>Cp[1]	Gn[1]	Sp>Cp[3]	Gn[1]	Gn[1]

Abbreviations: Sp = sphalerite, Gn = galena, Cp = chalcopyrite.

[1]Trend observed in all examined samples.

[2]Recrystallization increases element concentration in Cp and may make Cp primary host.

[3]Trend generally, yet not always, true.

*Recrystallization increases Sn concentration in Cp such that Cp is usually primary host in recrystallized samples. Below recrystallization conditions, no trend is observed.

Table 7.3 Preferred hosts for various trace elements in a co-crystallizing TetTen-Sp-Gn-Cp assemblage

Trace Element	**Mn**	**Fe**	**Cu**	**Zn**	**Ga**	**As**	**Se**	**Ag**
Preferred Host	Sp[1]	TetTen>Sp[3]	TetTen >Sp[3]	TetTen[1]	Sp[2]	TetTen>Gn[1]	Gn[1]	TetTen>Gn[1]

Trace Element	**Cd**	**In**	**Sn**	**Sb**	**Te**	**Hg**	**Tl**	**Bi**
Preferred Host	Sp> TetTen[3]	Sp>Cp[2]	?*	TetTen>Gn[1]	Gn[1]	Sp>TetTen[3]	Gn[1]	Gn>TetTen[1]

Abbreviations: TetTen = tetrahedrite-tennantite, Sp = sphalerite, Gn = galena, Cp = chalcopyrite.

[1]Trend observed in all examined samples.

[2]Recrystallization increases element concentration in Cp and may make Cp primary host.

[3]Trend generally, yet not always, true.

*Recrystallization increases Sn concentration in Cp such that Cp is usually primary host in recrystallized samples. Below recrystallization conditions, no trend is observed.

Acosta-Góngora, P., Gleeson, S. A., Samson, I. M., Ootes, L., Corriveau, L., 2015. Trace Element Geochemistry of Magnetite and Its Relationship to Cu-Bi-Co-Au-Ag-U-W Mineralization in the Great Bear Magmatic Zone, NWT, Canada. Econ. Geol. 109, 1901-1928.

Andersen, J. C. Ø., Stickland, R. J., Rollinson, G. K., Shail, R. K., 2016. Indium mineralisation in SW England: Host parageneses and mineralogical relations. Ore Geol. Rev. 78, 213-238.

Ayers, J. C., Watson, E. B., 1991. Solubility of apatite, monazite, zircon, and rutile in supercritical aqueous fluids with implications for subduction zone geochemistry. Phil. Trans. R. Soc. A: Math. Phys. Eng. Sci. 335, 365-375.

Bajwah Z., Seccombe P., Offler R., 1987. Trace element distribution, Co:Ni ratios and genesis of the Big Cadia iron-copper deposit, New South Wales, Australia. Mineral. Deposits 22, 292-300.

Barnes, S. J., Naldrett, A. J., 1985. Geochemistry of the J-M (Howland) Reef of the Stillwater Complex, Minneapolis adit area. 1. Sulfide chemistry and sulfide-olivine equilibrium. Econ. Geol. 80, 627-645.

Barnes, S. J., Picard, C. P., 1993. The behaviour of platinum-group elements during partial melting, crystal fractionation, and sulphide segregation: an example from the Cape Smith Fold Belt, northern Quebec. Geochim. Cosmochim. Acta 57, 79-87.

Barnes, S. J., Ripley, E. M., 2016. Highly Siderophile and Strongly Chalcophile Elements in Magmatic Ore Deposits. Rev. Mineral. Geochem. 81, 725-774.

Barnes, S. J., Makovicky, E., Makovicky, M., Rose-Hansen, J., Karup-Moller, S., 1997. Partition coefficients for Ni, Cu, Pd, Pt, Rh, and Ir between monosulfide solid solution and sulfide liquid and the formation of compositionally zoned Ni–Cu sulfide bodies by fractional crystallization of sulfide liquid. Can. J. Earth Sci. 34, 366-374.

Barnes, S. J., Cox, R. A., Zientek, M. L., 2006. Platinum-group element, Gold, Silver and Base Metal distribution in compositionally zoned sulfide droplets from the Medvezky Creek Mine, Noril'sk, Russia. Contrib. Mineral. Petrol. 152, 187-200.

Baruah, M. K., Kotoky, P., Borah, G. C., 2014. Geochemical Association of Ni^{2+}, Zn^{2+}, Pb^{2+}, Ag^{+}, Cu^{2+}, and Co^{2+} Ions in Natural Pyrite. J. Geochem. 2014. doi: 10.1155/2014/161850.

Bethke, P. M., Barton, P. B., 1971. Distribution of some minor elements between coexisting sulphide minerals. Econ. Geol. 66, 140–163.

Blundy, J. D., Wood, B. J., 1991. Crystal-chemical controls on the partitioning of Sr and Ba between plagioclase feldspar, silicate melts, and hydrothermal solutions. Geochim. Cosmochim. Acta 55, 193-209.

Bortnikov, N., Dobrovol'skaya, M., Genkin, A., Naumov, V., Shapenko, V., 1995. Sphalerite–galena geothermometers; distribution of cadmium, manganese, and the fractionation of sulfur isotopes. Econ. Geol. 90, 155–180.

Bos, A., 1990. Hydrothermal element distributions at high temperatures: an experimental study on the partitioning of major and trace elements between phlogopite, haplogranitic melt and vapour. Ph.D. thesis, University of Utrecht.

Boudreau, A. E., Mathez, E. A., McCallum, I. S., 1986. Halogen geochemistry of the Stillwater and Bushveld Complexes: Evidence for transport of the platinum-group elements by Cl-rich fluids. J. Petrol. 27, 967-986.

Boutroy, E., Dare, S. A. S., Beaudoin, G., Barnes, S. J., Lightfoot, P. C., 2014. Magnetite composition in Ni-Cu-PGE deposits worldwide: application to mineral exploration. J. Geochem. Explor. 145, 64-81.

Bowles, J. F. W., Howie, R. A., Vaughan, D. J., Zussman, J., 2011. Rock-forming Minerals: non-silicates: oxides, hydroxides and sulphides. Geol. Soc. London, 920 pp

Brookins, D. G., 1988. Eh-pH Diagrams for Geochemistry. Springer-Verlag Berlin

Heidelberg.

Cabri, L. J., Campbell, J. L., Laflamme, J. G., Leigh, R. G., Maxwell, J. A., Scott, J. D., 1985. Proton-microprobe analysis of trace elements in sulphides from some massive-sulphide deposits. Can. Mineral. 23, 133–148.

Campbell, I. H., Barnes, S. J., 1984. A model for the geochemistry of the platinum-group elements in magmatic sulfide deposits. Can. Mineral. 22, 151-160.

Canil, D., Grondahl, C., Lacourse, T., Pisiak, L. K., 2016. Trace elements in magnetite from porphyry Cu–Mo–Au deposits in British Columbia, Canada. Ore Geol. Rev. 72, 1116-1128.

Chen, L. M., Song, X. Y., Danyushevsky, L. V., Wang, Y. S., Tian, Y. L., Xiao, J. F., 2014. A laser ablation ICP-MS study of platinum-group and chalcophile elements in base metal sulfide minerals of the Jinchuan Ni-Cu sulfide deposit, NW China. Ore Geol. Rev. 65, 955-967.

Ciobanu, C. L., Cook, N. J., Pring, A., Brugger, J., Danyushevsky, L. V., Shimizu, M., 2009. 'Invisible gold'in bismuth chalcogenides. Geochim. Cosmochim. Acta 73, 1970-1999.

Ciobanu, C. L., Cook, N. J., Maunders, C., Wade, B. P., Ehrig, K., 2016. Focused ion beam and advanced electron microscopy for minerals: Insights and outlook from bismuth sulphosalts. Minerals 6, 112. doi:10.3390/min6040112.

Cook, N. J., Ciobanu, C. L., Pring, A., Skinner, W., Shimizu, M., Danyushevsky, L., Saini-Eidukat, B., Melcher, F., 2009. Trace and minor elements in sphalerite: A LA-ICPMS study. Geochim. Cosmochim. Acta 73, 4761-4791.

Cook, N. J., Ciobanu, C. L., Danyushevsky, L. V., Gilbert, S., 2011. Minor and trace elements in bornite and associated Cu–(Fe)-sulfides: A LA-ICP-MS study. Geochim. Cosmochim. Acta 75, 6473-6496.

Cook, N. J., Ciobanu, C. L., Brugger, J., Etschmann, B., Howard, D. L., de Jonge, M. D., Ryan, C., Paterson, D., 2012. Determination of the oxidation state of Cu in substituted Cu–In–Fe-bearing sphalerite via μ-XANES spectroscopy. Amer. Mineral. 97, 476–479.

Cook, N. J., Ciobanu, C. L., Ehrig, K., 2015a. Insights into Zonation Within the Olympic Dam Cu-U-Au-Ag Deposit from Trace Element Signatures of Sulfide Minerals. Abstract, SEG 2016 Conference, Hobart, Tasmania.

Cook, N. J., Etschmann, B., Ciobanu, C. L., Geraki, K., Howard, D. L., Williams, T., Rae, N., Pring, A., Chen, G., Johannessen, B., Brugger, J., 2015b. Distribution and substitution mechanism of Ge in a Ge-(Fe)-bearing sphalerite. Minerals 5, 117-132.

Cook, N. J., Ciobanu, C. L., George, L., Zhu, Z., Wade, B., Ehrig, K., 2016. Trace element analysis of minerals in magmatic-hydrothermal ores by laser ablation inductively-coupled plasma mass spectrometry: approaches and opportunities. Minerals 6, 111.

Dare, S. A., Barnes, S. J., Prichard, H. M., Fisher, P. C., 2010. The timing and formation of platinum-group minerals from the Creighton Ni-Cuplatinum-group Element sulfide deposit, Sudbury, Canada: Early crystallization of PGE-rich sulfarsenides. Econ. Geol. 105, 1071-1096.

Dare, S. A., Barnes, S. J., Prichard, H. M., Fisher, P. C., 2011. Chalcophile and platinum group element (PGE) concentrations in the sulfide minerals from the McCreedy East deposit, Sudbury, Canada, and the origin of PGE in pyrite. Mineral. Deposita 46, 381-407.

Deditius, A. P., Reich, M., Kesler, S. E., Utsunomiya, S., Chryssoulis, S. L., Walshe, J., Ewing, R. C., 2014. The coupled geochemistry of Au and As in pyrite from hydrothermal ore deposits. Geochim. Cosmochim. Acta 140, 644-670.

Djon, M. L. N., Barnes, S. J., 2012. Changes in sulfides and platinum group minerals with the degree of alteration in the Roby, Twilight, and High Grade Zones of the Lac des Iles Complex, Ontario, Canada. Mineral. Deposita 47, 875-896.

Duran, C. J., Barnes, S. J., Corkery, J. T., 2015. Chalcophile and platinum-group element distribution in pyrites from the sulfide-rich pods of the Lac des Iles Pd deposits, Western Ontario, Canada: Implications for post-cumulus re-equilibration of the ore and the use of pyrite compositions in exploration. J. Geochem. Explor. 158, 223-242.

Ferry, J., Watson, E., 2007. New thermodynamic models and revised calibrations for the Ti-in-zircon and Zr-in-rutile thermometers. Contrib. Mineral. Petrol. 154, 429–437.

Fleet, M. E., Chryssoulis, S. L., Stone, W. E., Weisener, C. G., 1993. Partitioning of platinum-group elements and Au in the Fe− Ni− Cu− S system: experiments on the fractional crystallization of sulfide melt. Contrib. Mineral. Petrol. 115, 36-44.

Fleet, M. E., Crocket, J. H., Liu, M., Stone, W. E., 1999. Laboratory partitioning of platinum-group elements (PGE) and gold with application to magmatic sulfide–PGE deposits. Lithos 47, 127-142.

Gallego Hernández, A. N., Akasaka, M., 2010. Ag-rich Tetrahedrite in the El Zancudo Deposit, Colombia: Occurrence, Chemical Compositions and Genetic Temperatures. Resour. Geol. 60, 218–233.

Gerth, J., 1990. Unit-cell dimensions of pure and trace metal-associated goethites. Geochim. Cosmochim. Acta 54, 363-371.

Giaccherini, A., Montegrossi, G., Di Benedetto, F., 2016. Stability of Naturally Relevant Ternary Phases in the Cu–Sn–S System in Contact with an Aqueous Solution. Minerals 6, 79.

Giuli, G., Paris, E., Wu, Z., De Panfilis, S., Pratesi, G., Cipriani, C., 2005. The structural role of Ag in galena (PbS). A XANES study. Phys. Scripta T115, 387–389.

Godel, B., Barnes, S. J., 2008. Platinum-group elements in sulphide minerals and the whole rocks of the J-M Reef (Stillwater Complex): Implication for the formation of the reef. Chem. Geol. 248, 272-294.

Goldschmidt, V. M., 1954. Geochemistry. Soil Sci. 78, 156.

Harrison, P. G., 1989. Chemistry of Tin. Blackie & Son Limited.

Hayden, L. A., Watson, E. B., Wark, D. A., 2008. A thermobarometer for sphene (titanite). Contrib. Mineral. Petrol. 155, 529–540.

Helmy, H. M., Ballhaus, C., Wohlgemuth-Ueberwasser, C., Fonseca, R. O., Laurenz, V., 2010. Partitioning of Se, As, Sb, Te and Bi between monosulfide solid solution and sulfide melt–application to magmatic sulfide deposits. Geochim. Cosmochim. Acta 74, 6174-6179.

Holwell, D. A., McDonald, I., 2007. Distribution of platinum-group elements in the Platreef at Overysel, northern Bushveld Complex: A combined PGM and LA-ICP-MS study. Contrib. Mineral. Petrol. 154, 171-190.

Holwell, D., McDonald, I., 2010. A review of the behaviour of platinum group elements within natural magmatic sulphide ore systems. Platin. Met. Rev. 54, 26–36.

Huston, D. L., Sie, S. H., Suter, G. F., Cooke, D. R., Both, R. A., 1995. Trace elements in sulfide minerals from eastern Australian volcanic-hosted massive sulfide deposits; Part I, Proton microprobe analyses of pyrite, chalcopyrite, and sphalerite, and Part II, Selenium levels in pyrite; comparison with delta 34 S values and implications for the source of sulfur in volcanogenic hydrothermal systems. Econ. Geol. 90, 1167-1196.

Ismail, R., Ciobanu, C. L., Cook, N. J., Teale, G. S., Giles, D., Schmidt Mumm, A., Wade, B., 2014. Rare earths and other trace elements in minerals from skarn assemblages, Hillside iron oxide–copper–gold deposit, Yorke Peninsula, South Australia. Lithos 184, 456–477.

Jiang, T., Ozin, G. A., 1998. New directions in tin sulfide materials chemistry. J. Mater. Chem. 8, 1099-1108.

Johan, Z., 1988. Indium and germanium in the structure of sphalerite: an example of coupled substitution with copper. Mineral. Petrol. 39, 211-229.

Jugo, P. J., Candela, P. A., Piccoli, P. M., 1999. Magmatic sulfides and Au: Cu ratios in porphyry deposits: an experimental study of copper and gold partitioning at 850 C, 100 MPa in a haplogranitic melt–pyrrhotite–intermediate solid solution–gold metal assemblage, at gas saturation. Lithos 46, 573-589.

Keays, R. R., Campbell, I. H., 1981. Precious metals in the Jimberlana Intrusion, Western Australia: Implications for the genesis of platiniferous ores in layered intrusions. Econ. Geol. 76, 1118-1141.

Klock, W., Palme, H., 1988. Partitioning of siderophile and chalcophile elements between sulfide, olivine, and glass in a naturally reduced basalt from Disko Island, Greenland. Proc. Lunar Planet. Sci. Conf. 18th, 471-483.

Kołodziejczyk, J., Prsek, J., Asllani, B., Maliqi, F., 2016. The paragenesis of silver minerals in the Pb-Zn Stan Terg deposit, Kosovo: an example of precious metal epithermal mineralization. Geol. Geophys. Env. 42, 19-29.

Kornicker, W. A., Morse, J. W., 1991. Interactions of divalent cations with the surface of pyrite. Geochim. Cosmochim. Acta 55, 2159-2171.

Lane, D. J., Cook, N. J., Grano, S. R., Ehrig, K., 2016. Selective leaching of penalty elements from copper concentrates: a review. Miner. Eng. 98, 110-121.

Large, R. R., Danyushevsky, L., Hollit, C., Maslennikov, V., Meffre, S., Gilbert, S., Bull, S., Scott, R., Emsbo, P., Thomas, H., Singh, B., 2009. Gold and trace element zonation in pyrite using a laser imaging technique: implications for the timing of gold in orogenic and Carlin-style sediment-hosted deposits. Econ. Geol. 104, 635-668.

Lefebvre, I., Lannoo, M., Olivier-Fourcade, J., Jumas, J. C., 1991. Tin oxidation number and the electronic structure of SnS-In_2S_3-SnS_2 systems. Phys. Rev. B 44, 1004.

Leyh, W. R., Conor, C. H., 2000. Stratigraphically controlled metallogenic zonation associated with the regional redox boundary of the Willyama Supergroup—economic implications for the southern Curnamona Province. Mesa J. 16, 39–47.

Li, C., Barnes, S. J., Makovicky, E., Rose-Hansen, J., Makovicky, M., 1996. Partitioning of nickel, copper, iridium, rhenium, platinum, and palladium between monosulfide solid solution and sulfide liquid: effects of composition and temperature. Geochim. Cosmochim. Acta 60, 1231-1238.

London, D., 2011. Experimental synthesis and stability of tourmaline: a historical overview. Can. Mineral. 49, 117-136.

Lottermoser, B., 1989. Rare earth element study of exhalites within the Willyama Supergroup, Broken Hill Block, Australia. Mineral. Deposita 24, 92–99.

Makvandi, S., Ghasemzadeh-Barvarz, M., Beaudoin, G., Grunsky, E. C., McClenaghan, M. B., Duchesne, C., 2016a. Principal component analysis of magnetite composition from volcanogenic massive sulfide deposits: Case studies from the Izok Lake (Nunavut, Canada) and Halfmile Lake (New Brunswick, Canada) deposits. Ore Geol. Rev. 72, 60-85.

Makvandi, S., Ghasemzadeh-Barvarz, M., Beaudoin, G., Grunsky, E. C., McClenaghan, M. B., Duchesne, C., Boutroy, E., 2016b. Partial least squares-discriminant analysis of trace element compositions of magnetite from various VMS deposit subtypes: Application to mineral exploration. Ore Geol. Rev. 78, 388-408.

Matsuhisa, Y., Goldsmith, J. R., Clayton, R. N., 1978. Mechanisms of hydrothermal crystallization of quartz at 250 C and 15 kbar. Geochim. Cosmochim. Acta 42, 173-182.

Moëlo, Y., Makovicky, E., Mozgova, N. N., Jambor, J. L., Cook, N., Pring, A., Paar, W., Nickel, E. H., Graeser, S., Karup-Møller, S., Balic-Žunic, T., 2008. Sulfosalt systematics: A review. Report of the sulfosalt sub-committee of the IMA commission on ore mineralogy. Eur. J. Mineral. 20, 7–46.

Morgan, J. W., Wandless, G. A., 1980. Rare earth element distribution in some hydrothermal minerals: evidence for crystallographic control. Geochim. Cosmochim. Acta 44, 973-980.

Mungall, J. E., Andrews, D. R., Cabri, L. J., Sylvester, P. J., Tubrett, M., 2005. Partitioning of Cu, Ni, Au, and platinum-group elements between monosulfide solid solution and sulfide melt under controlled oxygen and sulfur fugacities. Geochim. Cosmochim. Acta 69, 4349-4360.

Nadoll, P., Mauk, J. L., Hayes, T. S., Koenig, A. E., Box, S. E., 2012. Geochemistry of Magnetite from Hydrothermal Ore Deposits and Host Rocks of the Mesoproterozoic Belt Supergroup, United States. Econ. Geol. 107, 1275-1292.

Naldrett, A. J., Lehmann, J., 1988. Spinel non-stoichiometry as the explanation for Ni-, Cu- and PGE-enriched sulphides in chromitites. In: Geo-platinum 87, 93-109. Springer, Netherlands.

O'Brien, J. J., Spry, P. G., Teale, G. S., Jackson, S.,E., Rogers, D., 2015. Major and Trace Element Chemistry of Gahnite as an Exploration Guide to Broken Hill-Type Pb-Zn-Ag Mineralization in the Broken Hill Domain, New South Wales, Australia. Econ. Geol. 110, 1027-1057.

Orberger, B., Pasava, J., Gallien, J. P., Daudin, L., Trocellier, P., 2003. Se, As, Mo, Ag, Cd, In, Sb, Pt, Au, Tl, Re traces in biogenic and abiogenic sulfides from Black Shales (Selwyn Basin, Yukon territories, Canada): a nuclear microprobe study. Nucl. Instr. Meth. Phys. Res. B210, 441–448.

Passchier, C. W., Trouw, R. A. J., 2005. Microtectonics. 2nd edition. Springer-Verlag Berlin Heidelberg.

Peach, C. L., Mathez, E. A., Keays, R. R., 1990. Sulfide melt-silicate melt distribution coefficients for noble metals and other chalcophile elements as deduced from MORB: Implications for partial melting. Geochim. Cosmochim. Acta 54, 3379-3389.

Peach, C. L., Mathez, E. A., Keays, R. R., Reeves, S. J., 1994. Experimentally determined sulfide melt-silicate melt partition coefficients for iridium and palladium. Chem. Geol. 117, 361-377.

Piña, R., Gervilla, F., Barnes, S. J., Ortega, L., Lunar, R., 2012. Distribution of platinum-group and chalcophile elements in the Aguablanca Ni-Cu sulfide deposit (SW Spain): Evidence from a LA-ICP-MS study. Chem. Geol. 302, 61-75.

Prendergast, M. D., Keays, R. R., 1989. Controls of platinum group element mineralization and the origin of the PGE-rich Main Sulphide Zone in the Wedza Subchamber of the Great Dike, Zimbabwe: implications for the genesis of, and exploration for, stratiform PGE mineralization in layered intrusions. In: Prendergast, M. D., Jones, M. J., Eds., Magmatic Sulphides-the Zimbabwe Volume 43-69. Inst. M. M., London.

Prichard, H. M., Knight, R. D., Fisher, P. C., McDonald, I., Zhou, M. F., Wang, C. Y., 2013. Distribution of platinum-group elements in magmatic and altered ores in the Jinchuan intrusion, China: An example of selenium remobilization by postmagmatic fluids. Mineral. Deposita 48, 767-786.

Putnis, A., Fernandez-Diaz, L., Prieto, M., 1992. Experimentally produced oscillatory zoning in the (Ba,Sr)SO_4 solid solution. Nature 358, 743-745.

Reich, M., Kesler, S. E., Utsunomiya, S., Palenik, C. S., Chryssoulis, S. L., Ewing, R. C., 2005. Solubility of gold in arsenian pyrite. Geochim. Cosmochim. Acta 69, 2781-2796.

Sack, R. O., 2000. Internally consistent database for sulphides and sulfosalts in the system Ag_2S–Cu_2S–ZnS–Sb_2S_3–As_2S_3. Geochim. Cosmochim. Acta 64, 3803–3812.

Sack, R. O., 2005. Internally consistent database for sulphides and sulfosalts in the system Ag_2S-Cu_2S-ZnS-FeS-Sb_2S_3-As_2S_3: update. Geochim. Cosmochim. Acta 69, 1157–1164.

Sato, M., 1992. Persistency-field Eh-pH diagrams for sulfides and their application to supergene oxidation and enrichment of sulfide ore bodies. Geochim. Cosmochim. Acta 56, 3133-3156.

Shannon, R., 1976. Revised effective ionic radii and systematic studies of interatomic distances in halides and chalcogenides. Acta Crystallogr. Sect. A: Cryst. Phys., Diffr., Theor. Gen. Crystallogr. 32, 751–767.

Sharp, T. G., Zheng, N. J., Tsong, I. S., Buseck, P. R., 1990. Scanning tunneling microscopy of defects in Ag-and Sb-bearing galena. Amer. Mineral. 75, 1438–1442.

Sharpe, M. R., 1982. Noble metals in the marginal rocks of the Bushveld Complex. Econ. Geol. 77, 1286-1295.

Sharrad, K. A., McKinnon-Matthews, J., Cook, N. J., Ciobanu, C. L., Hand, M., 2014. The Basil Cu–Co deposit, Eastern Arunta Region, Northern Territory, Australia: A metamorphosed volcanic-hosted massive sulphide deposit. Ore Geol. Rev. 56, 141-158.

Shore, M., Fowler, A. D., 1996. Oscillatory zoning in minerals; a common phenomenon. Can. Mineral. 34, 1111-1126.

Smith, J. W., Holwell, D. A., McDonald, I., Boyce, A. J., 2016. The application of S isotopes and S/Se ratios in determining ore-forming processes of magmatic Ni-Cu-PGE sulfide deposits: A cautionary case study from the northern Bushveld Complex. Ore Geol. Rev. 73, 148-174.

Ripley, E. M., Brophy, J. G., Li, C., 2002. Copper solubility in a basaltic melt and sulfide liquid/silicate melt partition coefficients of Cu and Fe. Geochim. Cosmochim. Acta 66, 2791-2800.

Rosenberg, J., Spry, P., Jacobson, C., Vokes, F., 2000. The effects of sulfidation and oxidation during metamorphism on compositionally varied rocks adjacent to the Bleikvassli Zn–Pb–(Cu) deposit, Nordland, Norway. Mineral. Deposita 35, 714–726.

Wang, Y., Merino, E., 1992. Dynamic model of oscillatory zoning of trace elements in calcite: double layer, inhibition, and self-organization. Geochim. Cosmochim. Acta 56, 587-596.

Watson, E. B., 1991. Diffusion in fluid-bearing and slightly-melted rocks: experimental and numerical approaches illustrated by iron transport in dunite. Contrib. Mineral. Petrol. 107, 417-434.

Watson, E. B., Lupulescu, A., 1993. Aqueous fluid connectivity and chemical transport in clinopyroxene-rich rocks. Earth Planet. Sci. Lett. 117, 279-294.

Watson, E. B., Chemiak, D. J., Hanchar, J. M., Harrison, T. M., Wark, D. A., 1997. The incorporation of Pb into zircon. Chem. Geol. 141, 19-31.

Watson, E., Wark, D., Thomas, J., 2006. Crystallization thermometers for zircon and rutile. Contrib. Mineral. Petrol. 151, 413–433.

Zielinski, R. A., Frey, F. A., 1974. An experimental study of the partitioning of a rare earth element (Gd) in the system diopside—aqueous vapour. Geochim. Cosmochim. Acta 38, 545-565.

CHAPTER 8

ADDITIONAL MATERIAL

ADDITIONAL MATERIAL A

FOR CHAPTER 3

ELECTRONIC APPENDIX A FOR CHAPTER 3

American Mineralogist: Feb-March 2015 Deposit AM-15-24862

George et al.: Trace and minor elements in galena

Electronic Appendix. Mean minimum detection limits and precision values for each sample (99% confidence, ppm)

MINIMUM DETECTION LIMITS

SAMPLE	^{65}Cu	^{82}Se*	^{107}Ag	^{111}Cd	^{115}In	^{118}Sn	^{121}Sb	^{125}Te	^{197}Au	^{202}Hg	^{205}Tl	^{209}Bi
BH218 (n=24)	1.4	71	0.35	1.9	0.10	0.86	0.51	3.9	0.36	0.28	0.10	0.17
BH221 (n=23)	1.4	57	0.35	1.8	0.10	0.83	0.51	3.8	0.36	0.33	0.10	0.18
BH233 (n=24)	72	171	0.54	2.7	0.10	2.1	0.38	3.0	0.09	0.39	0.03	0.10
Bv-1 (n-24)	340	215	1.9	7.5	0.22	3.2	0.96	9.7	0.18	1.0	0.04	0.16
Bv-97-3 (n=24)	521	1534	2.5	10	0.30	5.3	1.1	9.6	0.22	1.3	0.06	0.22
V446 (n=12)	1.9	31.0	0.48	2.4	0.11	0.86	0.60	4.2	0.45	0.40	0.12	0.21
V538 (n=12)	2.1	38.0	0.51	2.7	0.13	1.1	0.69	4.9	0.52	0.52	0.13	0.23
V57-852 (n=12)	30	64.0	0.18	0.74	0.03	0.71	0.17	0.78	0.02	0.20	0.01	0.04
Mo 2 (n=23)	1.5	103	0.36	2.1	0.10	0.89	0.53	3.3	0.32	0.30	0.08	0.16
Mo 5 (n=12)	1.6	-	0.38	2.0	0.10	0.77	0.48	3.2	0.40	0.28	0.10	0.16
Mo 11 (n=24)	12	-	0.18	0.54	0.03	0.75	0.19	0.74	0.03	0.27	0.01	0.04
BB55 (n=11)	187	-	1.3	5.5	0.16	2.9	0.70	5.9	0.10	0.52	0.04	0.16
BB158 (n=12)	190	669	1.1	4.4	0.16	2.8	0.71	3.8	0.12	0.57	0.03	0.14
BBH16AB (n=24)	34	72.0	0.19	0.73	0.04	0.82	0.14	0.87	0.03	0.31	0.01	0.05
BBH16B (n=24)	158	172	1.1	3.8	0.16	3.0	0.64	5.3	0.13	0.84	0.04	0.13
BBH20 (n=24)	9.2	45	0.07	0.35	0.02	0.82	0.08	0.49	0.02	0.12	0.01	0.04
BBH25 (n=12)	19	76.2	0.13	0.50	0.03	0.68	0.12	0.88	0.02	0.17	0.01	0.04
BBH28A (n=24)	247	-	1.3	6.4	0.23	3.4	0.72	6.5	0.14	0.87	0.04	0.15
BBH32 (n=12)	24	-	0.17	0.57	0.03	0.65	0.90	0.78	0.03	0.18	0.01	0.05
ELS-157 (n=24)	315	155	1.6	7.3	0.27	3.9	0.85	6.9	0.17	0.84	0.05	0.16
7011 A (n=24)	48	146	0.32	1.8	0.07	1.9	0.37	1.7	0.06	0.62	0.02	0.09
BdA 99-1 (n=11)	208	-	1.3	7.3	0.20	5.2	0.90	8.3	0.20	1.1	0.05	0.20
BdA 99-5 (n=24)	39	97	0.47	1.8	0.08	2.4	0.36	2.9	0.08	0.43	0.03	0.11
BdA 99-9 (n=12)	85	289	0.64	3.1	0.12	3.0	0.49	4.3	0.15	0.50	0.03	0.17
Hj13 (n=24)	76	655	0.62	2.8	0.10	4.2	0.40	3.3	0.09	0.62	0.03	0.10
Hj14 (n=24)	214	-	1.5	6.2	0.23	4.2	0.90	3.3	0.17	1.0	0.05	0.17
Emeric2 (n=23)	224	116	1.3	4.8	0.17	3.1	0.68	5.2	0.14	0.84	0.03	0.14
T1a (n=24)	167	112	1.1	4.2	0.16	3.6	0.67	5.0	0.15	0.69	0.04	0.19
TOR197 (n=12)	126	208	0.86	4.2	0.15	3.3	0.63	4.9	0.15	0.57	0.04	0.16
30 (n=23)	38	146	0.19	0.78	0.03	0.72	0.16	1.1	0.02	0.19	0.01	0.04
38 (n=12)	56	-	0.28	0.97	0.04	0.80	0.20	0.83	0.02	0.17	0.01	0.04
47 (n=24)	71	366	0.35	1.5	0.05	0.83	0.22	1.7	0.03	0.26	0.01	0.05
DM3 (n=24)	34	133	0.22	0.74	0.04	0.82	0.14	0.99	0.03	0.24	0.01	0.05
DMV99-22 (n=24)	166	216	1.1	4.6	0.14	2.9	0.51	4.9	0.10	0.53	0.03	0.12
Sullivan (n=24)	25	133	0.17	0.75	0.03	0.86	0.15	0.71	0.03	0.35	0.01	0.04
ZN 99.2 (n=24)	14	175	0.21	0.87	0.05	1.5	0.28	1.3	0.05	0.43	0.02	0.07

5984B C1 (n=12)	1.7	109	0.43	2.3	0.12	0.93	0.57	4.4	0.40	0.41	0.12	0.16
5984B C2 (n=11)	1.1	84.0	0.31	1.8	0.10	1.0	0.50	2.7	0.33	0.30	0.07	0.13
5990 C1 (n=24)	120	564	0.69	3.1	0.11	2.5	0.51	3.5	0.10	0.48	0.03	0.12
Kmi 2b (n=24)	188	167	0.98	3.4	0.14	2.8	0.58	4.5	0.27	0.76	0.07	0.14
Kmi 4 (n=24)	119	641	0.97	4.1	0.17	4.0	0.72	5.5	0.15	0.83	0.04	0.18

Minimum detection limits are unique for each spot analysis and vary from run to run. The dataset was collected over a six-month period

Minimum detection limits can be influenced by factors including the element concentrations in the previous sample

*Median values are shown for Se.

RELATIVE PRECISION (%)

SAMPLE	^{65}Cu	^{82}Se	^{107}Ag	^{111}Cd	^{115}In	^{118}Sn	^{121}Sb	^{125}Te	^{197}Au	^{202}Hg	^{205}Tl	^{209}Bi
BH218 (n=24)	37.3	-	10.1	13.0	28.9	17.0	16.4	66.2	40.9	52.8	16.8	11.9
BH221 (n=23)	42.4	-	17.9	24.4	28.2	17.9	25.0	65.9	82.2	71.4	13.1	14.2
BH233 (n=24)	-	-	32.3	40.1	49.4	16.3	21.0	137	129	62.9	12.7	28.9
Bv-1 (n-24)	-	-	32.5	74.4	29.7	17.2	18.1	149	129	-	12.3	15.7
Bv-97-3 (n=24)	-	-	39.0	60.7	29.3	22.2	24.5	148	132	-	14.9	24.5
V446 (n=12)	33.7	-	18.1	31.5	20.2	11.9	11.0	52.3	55.3	37.7	18.6	33.9
V538 (n=12)	63.0	-	62.3	54.0	20.6	36.4	32.8	109	-	-	28.6	48.9
V57-852 (n=12)	369	-	17.8	22.5	18.7	14.5	15.6	52.1	93.3	38.7	17.4	8.4
Mo 2 (n=23)	49.5	-	32.5	33.5	51.5	48.4	35.4	59.8	70.4	58.3	23.7	27.6
Mo 5 (n=12)	29.3	-	16.1	25.9	-	46.6	17.3	46.8	-	32.6	27.5	21.8
Mo 11 (n=24)	178	-	16.7	20.6	36.7	37.7	18.3	29.7	84.3	20.2	15.9	10.6
BB55 (n=11)	667	-	33.7	37.5	102	37.1	39.1	63.0	51.1	61.4	6.3	20.7
BB158 (n=12)	711	-	24.5	50.5	112	-	44.3	20.1	57.4	60.9	13.4	14.5
BBH16AB (n=24)	208	-	20.5	25.2	83.7	32.8	14.0	18.0	65.6	44.8	14.9	9.2
BBH16B (n=24)	-	-	31.9	33.5	111	-	41.6	52.6	102	-	14.6	20.9
BBH20 (n=24)	147	-	16.0	13.2	66.2	29.1	15.0	30.1	80.0	46.0	5.6	7.2
BBH25 (n=12)	246	-	18.6	18.4	91.4	-	13.6	21.1	102	43.0	8.4	10.2
BBH28A (n=24)	-	-	32.5	40.8	76.1	48.8	27.9	38.4	133	38.9	19.7	20.0
BBH32 (n=12)	-	-	18.7	22.3	92.3	36.5	12.1	34.7	53.8	42.7	13.0	11.9
ELS-157 (n=24)	-	-	34.8	48.4	131	-	26.6	45.7	131	-	21.3	20.4
7011 A (n=24)	242	-	57.2	54.4	100	-	48.2	52.2	136	61.1	39.3	47.0
BdA 99-1 (n=11)	-	-	31.4	31.8	113	-	25.4	98.3	65.2	-	29.9	22.4
BdA 99-5 (n=24)	-	-	31.0	30.5	49.2	-	18.1	50.9	127	43.4	14.7	12.0
BdA 99-9 (n=12)	-	-	30.3	29.4	66.7	-	26.4	68.2	75.7	49.1	34.3	10.9
Hj13 (n=24)	288	-	17.9	27.4	92.9	42.8	25.5	48.3	127	-	16.5	14.4
Hj14 (n=24)	-	-	30.1	55.9	93.5	41.4	28.5	107	127	-	14.3	22.7
Emeric2 (n=23)	-	-	38.7	28.4	92.6	39.6	23.9	52.7	120	44.2	21.1	16.7
T1a (n=24)	460	-	31.4	30.5	56.4	44.6	25.3	44.1	95.5	38.8	19.9	15.1
TOR197 (n=12)	372	-	45.5	36.0	60.6	40.9	35.4	63.3	137	39.2	41.4	16.6
30 (n=23)	594	-	36.1	35.4	66.7	65.3	21.9	36.0	42.2	46.9	12.6	16.9
38 (n=12)	661	-	20.2	31.2	49.2	22.0	14.4	43.0	44.9	37.0	7.3	10.5
47 (n=24)	718	-	24.5	34.4	25.4	33.8	22.0	35.2	44.9	34.8	15.5	21.4

DM3 (n=24)	374	-	16.3	29.0	90.9	-	12.9	45.3	54.3	43.3	16.6	38.9
DMV99-22 (n=24)	707	-	38.1	64.0	94.7	53.1	27.0	108	115	40.0	10.7	40.3
Sullivan (n=24)	351	-	15.0	25.1	10.2	10.0	13.2	128	131	58.5	14.3	9.5
ZN 99.2 (n=24)	-	-	14.4	24.7	65.7	26.0	17.6	130	136	-	12.7	11.5
5984B C1 (n=12)	45.9	-	32.9	-	33.9	28.9	23.8	-	-	60.5	41.6	19.1
5984B C2 (n=11)	51.7	-	35.5	29.0	-	27.0	23.8	-	-	55.3	32.1	23.0
5990 C1 (n=24)	-	-	27.4	52.0	91.7	36.7	23.1	116	131	49.2	13.3	16.7
Kmi 2b (n=24)	42.9	-	29.2	26.3	87.3	39.3	32.0	148	133	57.5	29.2	25.0
Kmi 4 (n=24)	-	-	20.7	41.5	93.6	47.3	20.7	133	129	49.0	22.4	24.3

Precision values for Se exceed 100% in all cases.

ADDITIONAL MATERIAL B

FOR CHAPTER 5

ELECTRONIC APPENDIX A FOR CHAPTER 5

APPENDIX A: BRIEF DESCRIPTIONS OF SAMPLED DEPOSITS

HERJA

The epithermal vein system at Herja, consisting of more than 180 veins, is located in the metallogenic district around Baia Mare, northern Romania. Veins are hosted by Samartian-Pannonian volcanics and Neogene and Paleogene sediments. Herja is one of a number of major polymetallic ores of epithermal type of Neogene age in the Carpathians and Apuseni Mts. associated with subduction and slab-detachment (Neubauer et al., 2005).

The Herja veins follow fractures orientated along a ENE-WSW trend which are associated with a subvolcanic body of pyroxene andesite and porphyritic quartz microdiorite (Cook and Damian, 1997). Veins are classified in two sets, the southern and northern. The southern vein set are surrounded by porphyritic quartz microdiorite while the northern veins are enclosed by altered sediments (Cook and Damian, 1997). Hydrothermal activity associated with andesitic volcanism has been dated via the K-Ar method between 11.5 and 8 Ma, with mineralisation occurring at 8.8 ± 0.6 Ma (Edelstein et al., 1992; Lang et al., 1994). As a whole, the system extends to more than 1000 m at a width of 1200 m. Pb and Zn are relatively evenly distributed throughout; little evidence exists for any vertical zonation (Borcos et al., 1975).

The ore is massive, often drusy without abundant vugs, and consists of sphalerite, galena with lesser chalcopyrite, pyrite, pyrrhotite, marcasite, tetrahedrite and various sulphosalts. Gangue minerals are quartz and calcite. Mineralisation is interpreted as being single phase, with pyrite and pyrrhotite deposited first followed by sphalerite and galena. Idiomorphic chalcopyrite, galena and marcasite were deposited last at temperatures probably well below 200 oC, often coating other minerals (Borcos et al., 1975).

TOROIAGA

The Toroiaga epithermal Cu-Pb-Zn-Ag-Au system is part of the Neogene Toroiaga-Tiganul sub-volcanic Massif, Maramures Mountains, northwest Romania (100 km east of Herja). The deposit is comprised of a number of polymetallic hydrothermal veins, some of which are several hundred meters long, which plunge sharply to the southwest (Cook, 1997). These polymetallic veins are interpreted as healing fractures associated with the last of five injections of magma into the epithermal system (Borcos, 1967).

The epithermal system is vertically zoned with chalcopyrite increasing downwards while sphalerite, galena, a rich variety of sulphosalts and gold increase upwards (Borcos et al., 1982). The primary ore minerals at Toroiaga are Au-bearing pyrite and pyrrhotite (at lower levels), chalcopyrite, marcasite, arsenopyrite, sphalerite and galena. The presence of porphyry copper mineralisation beneath the epithermal vein system was proposed by Socolescu (1954) and supported by Chioreanu et al. (1993) but not confirmed. The mine was closed in 2003; additional exploration was carried out in 2006-2008 but failed to establish significant additional reserves.

KOCHBULAK

The Kochbulak deposit is located in the Kochbulak-Kairagach caldera in the Chatkel-Kurama ore district, Uzbekistan. The caldera is located at the intersection of the Southern Angren and Lashkerek-Dukent fault zones and is filled with andesites, dacites and minor volcanics (Akcha and Nadak formations), rhyolite (Oyasai and Kyzylnura formations) and other subvolcanic intrusions (Islamov et al., 1999). Mineralisation is primarily concentrated within volcanics of the Nadak formation. Volcanic rocks have been mildly affected by a propylitic alteration while faults and ore zones concentrate more intense chlorite-epidote and

silica alteration (Islamov et al., 1999). These ore zones are controlled by structures resulting in three types of ore; steeply dipping veins, flat lenticular lodes and ore pipes.

Mineralisation is classified in three groups; gold-pyrite, gold-polysulphide and gold-telluride (Islamov et al., 1999). The gold-pyrite mineralisation is most prominent at depth and is typified by low grades of finely dispersed gold in pyrite. The gold-polysulphide group is most prominent at upper levels with gold associated with a complex assemblage of Cu-Pb-Zn-Bi and –Sb minerals (Plotinskaya et al., 2006). The gold-telluride group has gold associated with tellurides such as calaverite, petzite, sylvanite, hessite, stützite and empessite and is most prominent close to surface. Developed reserves at Kochbulak are 5.6 Mt of ore at 13.4 g/t Au and 120 g/t Ag (Islamov et al., 1999).

BAITA BIHOR

Baita Bihor is a Cu-Au-Pb-Zn-Mo skarn deposit located in the northernmost district of the Upper Cretaceous Banatitic Magmatic and Metallogenetic Belt (Ciobanu et al., 2002). This belt extends for 1500 km through Romania, Serbia and Bulgaria, and hosts many intrusion-related ore deposits. The host rocks at Baita Bihor are sedimentary and metamorphic rocks of Permo-Mesozoic and Paleozoic ages, respectively. The skarn system at Baita Bihor (Cioflica et al., 1971; 1977) consists of around 10 orepipes controlled by major faults in the area. A large granite pluton some 1-1.2 km below the surface is responsible for the mineralisation. Ages for intrusion and mineralisation coincide at ~ 74 Ma (Ciobanu et al., 2002; Zimmerman et al., 2008).

The mine closed in 2007. Commodities exploited included Cu, Mo, Zn, Pb and Mo; the main ore minerals are bornite, chalcopyrite, molybdenite, sphalerite and galena. Lesser pyrrhotite, pyrite and magnetite are also present. More than 100 different minerals have been reported, making it well known among mineralogists. The deposit is particularly noted for the unusual enrichment in Bi, which is hosted primarily by a wide range of rare Bi-sulphosalts,

many of which are only known from this single locality (e.g. cuproneyite; Ilinca et al. 2012). The abundance of Bi and intimate association of Bi-minerals in the Cu-ores presented a significant problem in ore processing, and was one reason for closure of the operation.

Ores are contained in skarns varying from magnesian (spinel – forsterite – chondrodite – phlogopite) to calcic (scapolite – diopside – wollastonite – vesuvianite) in composition. There is a marked west-to-east metal zonation (Mo-Cu-Pb/Zn) across the orefield, but each orepipe also features similar zonation trends from the core of each orepipe to the skarn-marble contact, sometimes with superposition of discrete zones due to telescoping (Cook et al. 2009, unpubl. consultancy report).

ORAVITA

The Oravita deposit is located ~350 km away from Baita Bihor along the Late Cretaceous Banatitic Magmatic and Metallogenetic Belt, Romania (BMMB; e.g., Ciobanu et al., 2002). The BMMB contains a range of magmatic-hydrothermal mineralization styles relating to the same magmatic event, and formed in subduction settings during Neotethys closure. Oravita is one of the many Cu–Au skarns that are satellite to porphyry Cu–Mo-intrusions within the Banat region (SW Romania and Serbia), known for its rich deposits (e.g., von Cotta, 1864). As with many Cu skarns, it also contains base metal ores and minor W-mineralization (Gheorghitescu, 1975; Cioflica and Vlad, 1981; Constantinescu et al., 1988). Oravita is one of the few localities where gehlenite skarns are known along the BMMB (Katona et al., 2003; Marincea et al., 2011). Although such skarns are barren, they provide an upper temperature limit (~750 °C) for initiation of the skarn system close to intrusion contacts.

ASSAREL

The Assarel Cu-Au deposit (130 Mt reserves @ 0.44% Cu, 0.2 g/t Au) is situated in the Panagyurishte ore district of the central Srednogorie zone, Bulgaria, an ore district featuring a

pairing of large porphyry systems with epithermal 'massive sulphide' deposits (von Quadt et al., 2005). The Panagyurishte district follows a NNW-SSE orientated structural corridor within the Banatitic Magmatic and Metallogenic Belt (BMMB; Ciobanu et al., 2002), a belt of Late Cretaceous calc-alkaline magmatism. The deposit consists of stockwork-style porphyry mineralization within volcanic host rocks (Angelkov and Parvanov, 1980; Bogdanov, 1987). Geochronology points to multiple generations of intrusion in the Medet-Assarel orefield in the 85-70 Ma period (e.g., Zimmerman et al., 2008). The dominant hypogene quartz + chalcopyrite ± pyrite assemblage is associated with sericitic and sericitic-propylitic alteration. Galena and sphalerite are found mostly in veins at depth, and in the upper part of the deposit where high-sulphidation mineralization overprints porphyry style ore (Strashimirov et al., 2002). Ore mineralogy studies have been carried out by Bogdanov (1987), Petrunov et al. (1991), Strashimirov (1993) and Popov et al. (2000).

BOR

Also hosted in the BMMB is the Bor porphyry system, Serbia. Similar to Panagyurishte, the Bor district is also characterised by hypabyssal intrusions within contemporary volcanic host rocks. However, mineralization within the Bor district occurs over a greater vertical extent and exposed porphyritic intrusions close to mineralization are less common and sometimes only inferred at depth. Ore occurs as stockworks below a high-sulphidation epithermal system; massive sulphide mineralization grades down to porphyry style some 800 m below the current surface (Janković, 1990; Janković et al., 1998). A feature of the district is the large vertical extent of mineralisation exposed across the district. Porphyry-style mineralisation occurs in a variety of styles and at various locations as stockworks in plutonic cupolas (Valja Strz), at the same level as dyke swarms above intrusions (Veliki Krivelj), and as stockworks above intrusions, but below high-sulphidation epithermal ores (Bor; Janković, 1990).

ELATSITE

The >300 Mt Elatsite porphyry copper system is located in the Panagyurishte metallogenetic district in central Bulgaria. This district contains hypabyssal intrusions with approximately coeval volcanic rocks that host the ore. At Elatsite, the porphyritic intrusion is either monzonite or diorite, and is exposed adjacent to the mineralisation (Strashimirov and Popov, 2000). Coupled with the porphyry system is high-sulphidation epithermal-style massive sulphide mineralisation at Chelopech (Kouzmanov et al., 2002). Porphyry ore stockworks are concentrated along the boundary between the porphyry intrusion and the schist/granite basement. The system has a strong potassic alteration and lesser argillic alteration. Mineralisation has been dated at ~92-90 Ma (Von Quadt et al., 2005; Zimmerman et al., 2008), placing it within the same upper Cretaceous metallogenic belt as Baita Bihor (Ciobanu et al., 2002).

The Elatsite deposit is moderately gold-rich, contains a number of rare polymetallic minerals and, notably in the massive magnetite-bornite core, also platinum group metals (Dragov and Petrunov, 1996; Kouzmanov et al., 2000; Strashimirov et al., 2002). Galena-sphalerite-chalcopyrite assemblages are found in distal cm-scale veins at the perimeters of the porphyry mineralisation.

VORTA

Vorta is a massive and disseminated Zn-Pb-(Cu)-(Ag)-(Au) deposit located in the Vorta-Dealul Mare-Barbura belt, Barasti Formation, Romania. Mineralisation is ophiolite hosted and Middle to Late Jurassic in age. The deposit is composed of lenses of variable grade that are discontinuous along an east-west alignment (Ciobanu et al., 2001). Mineralisation comes in two types, the first being massive but compact lenticular and spheroidal bodies with the second being disseminations and veinlets which surround and overprint the massive

mineralisation. The fine-grained ore is contained in a reworked, remobilised quartz rich breccia hosted within alkali basalt lavas altered to a calcite-quartz-chlorite-albite assemblage (Ciobanu et al., 2001). The deposit is non-metamorphosed and it is believed to closely resemble VMS-style mineralization formed at the ocean floor.

KAPP MINERAL

The small Kapp Mineral prospect is located 2.5 km east of Isfjorden Radio in the Hecla Hoek Complex, which extends along the entire west coast of Spitsbergen, Svalbard Archipelago. The basement rocks of the archipelago are Precambrian and to a lesser extent lowermost Paleozoic. These rocks, comprising a wide range of metamorphosed sedimentary and igneous lithologies, outcrop widely on Western Spitsbergen. Beginning in the Silurian, around 400 million years ago, these rocks were involved in the formation of the Caledonide mountain chain. Erosion of the mountain chain and development of a central basin began in the Devonian after the end of mountain building, enabling the deposition of thick volumes of sedimentary rocks. This was followed by continued sedimentation throughout the Carboniferous and Permian, and into the Mesozoic as Svalbard moved northwards. The complex is a thick metamorphosed sequence consisting of latest Precambrian, Eocambrian and lower Paleozoic rocks of both igneous and sedimentary origin.

Lead-Zn ores at Kapp Mineral were worked on a small scale in the 1920's. Sphalerite and galena occur within a brecciated carbonate phyllite (Flood, 1967). The breccia zone, from which the bulk of the ore was exploited is several metres wide and contains a mass of crosscutting calcite veins. Many of these are barren, but some contain veinlets of sphalerite and galena a few cm in thickness.

BROKEN HILL

The giant (>300 Mt) Broken Hill Pb-Zn-Ag orebody lies in the south-eastern part of the Curnamona Craton, South-eastern Australia, within Early to Middle Proterozoic meta-sedimentary and meta-volcanic rocks of the Willyama Supergroup (Haydon and McConachy, 1987). These rocks encompass a range of metamorphic lithologies including pelitic, quartzofeldspathic and mafic rocks (Pidgeon, 1967; Haydon and McConachy, 1987). They were deposited in a continental back-arc environment between ca. 1710-1640 Ma, and were subsequently deformed during the Olarian Orogeny ca. 1600-1580 Ma (Clarke et al., 1986; Stevens, 1986; Stevens et al., 1988; Stüwe and Ehlers, 1997). There is a regional progressive increase in metamorphic grade from northwest to southeast, ranging from andalusite grade to granulite grade (Binns, 1964). Sedimentary rocks of the Adelaidian sequence (ca. 820-750 Ma) were unconformably deposited onto the metamorphic rocks during break-up of the Rodinia supercontinent. Both the Adelaidian and Willyama Supergroups then underwent deformation during the Delamerian Orogeny (520-500 Ma).

There is a substantial literature on the genesis of the Broken Hill orebody (Greenfield et al., 2003; Webster, 2006; Spry et al., 2008). Phillips et al. (1985), Plimer (1986) and Parr and Plimer (1993) argued that deposition of the Broken Hill ore deposit was coeval with bimodal felsic–mafic volcanism and pre-metamorphic alteration. The most commonly accepted (sedimentary-exhalative) genetic model therefore encompasses formation by hydrothermal processes and subsequent multi-phase high-grade metamorphism and deformation. This has been favoured by many authors (Stanton and Russell, 1959; Both and Rutland, 1976; Laing et al., 1978; Plimer, 1979; 1984; 2007; Parr and Plimer, 1993; Marshall and Spry, 2000; Spry et al., 2007).

Overprinting of the Broken Hill deposit during high-temperature metamorphism led to substantial recrystallization of both ore and host rock assemblage. An alternative model

involving syntectonic introduction of metals during peak metamorphism or post-tectonic replacement has been proposed (Stillwell and Edwards, 1956; Stillwell, 1959; Lewis et al., 1965; Nutman and Ehlers, 1998; Rothery, 2001; Gibson and Nutman, 2004). A second alternative model considers metamorphic melting of a primary sediment-hosted mineralization (Lawrence, 1967; Mavrogenes et al., 2001). Some researchers (Mavrogenes et al., 2001; Frost et al., 2002; 2005) have argued that extensive melting of the sulphide assemblages may have occurred. Others (e.g. Spry et al., 2008) suggest that although there may have been localised partial melting of minor parts of the ore, there was no substantial liquidation of the sulphides during the metamorphic event.

BLEIKVASSLI

The Bleikvassli deposit is located ~45 km southeast of Mo i Ranan north-central Norway. Mining between 1957 and 1997 produced about 5.0 Mt of ore grading 4.0% Zn, 2% Pb, 0.15% Cu and 25 g/t Ag. The main orebody is made up of interlayered lenses of massive sulphide ore hosted within amphibolites, quartzites, mica schists and quartzofeldspathic gneisses of the Uppermost Allochthon, Scandinavian Caledonides (Ramberg, 1967; Stephens et al., 1985; Bjerkgard et al., 1997). The deposit is believed by most researchers to be of SEDEX-type (Vokes, 1963; 1966; Skauli, 1990; 1992; 1993; Skauli et al., 1992a; 1992b; Moralev et al., 1995; Cook et al., 1998).

The deposit underwent Caledonian metamorphism at peak conditions of roughly 570 °C and 7.5-8 kbar (Cook, 1993; Rosenberg et al., 1998). At least five phases of syn-metamorphic deformation are recognised (Bjerkgard et al., 1995). Spry et al. (1995) identified a syn-metamorphic sulphidation-oxidation halo enclosing the ores. Ore petrography is comprehensively described by (Vokes, 1963). Massive ores are medium-grained (mm-scale) and comprise assemblages of pyrite-sphalerite-galena ore with lesser amounts of pyrrhotite and chalcopyrite. Pyrrhotite and base-metal sulphides occupy the matrix between the pyrite

metablasts. A distinct pyrrhotite-rich ore, usually with greater chalcopyrite content and often displaying a brecciated texture, with numerous, generally rounded, clasts of wall-rock schists and vein quartz occurs close to the footwall in the southern part of the deposit. Remobilisation of ore components is abundant, with a characteristic 'wall rock mineralization' that includes abundant, coarse Pb-As-(Sb)-sulphosalt-dominant assemblages emplaced in crosscutting veins within wallrock adjacent to massive ore (Vokes, 1963; Cook et al., 1998).

MOFJELL

The Mofjell deposit, located roughly 1 km south of the city of Mo i Rana, north-central Norway, is hosted within metapelitic quartz-mica-feldspar gneisses and amphibolites of the Mofjellet Group in the Rødjngsfjellet Nappe complex of the Uppermost Allochthon of the Scandinavian Caledonides (Saager, 1967; Bjerkgard et al., 2001). Bjerkgard et al. (1997) proposed that the Mofjellet Group was formed in a volcanic arc or a back-arc basin. The Mofjell deposit was under exploitation between 1926 and 1987, producing 4.3 Mt of ore grading 3.61% Zn, 0.71% Pb, 0.31% Cu, as well as sulphuric acid from pyrite. The presence of gold was confirmed during exploration work carried out since 1990; a remaining resource of ~4 Mt is indicated.

The deposit consists of three massive, stratiform lenses and has been metamorphosed at lower amphibolite facies conditions of approximately 550°C and 7 kbar (Bjerkgard et al., 2001). The ores and host rocks have experienced at least one stage of deformation and folding. Like Bleikvassli, the Mofjell deposit is interpreted to be of SEDEX-type (Bjerkgard et al., 2001). Sulphide recrystallization and mobilization of minor elements, including gold, is widespread with sulphosalt-rich remobilizate assemblages noted within thin veinlets, up to 3 cm in width, located in host rocks immediately adjacent to massive pyrite ore (Cook, 2001).

SULITJELMA

The Sulitjelma Cu-Zn orefield (Cook et al., 1990, 1993; Cook, 1996), central-north Norway, hosts over 20 sulphide bodies totalling around 35 Mt of massive sulphide. The sulphide bodies are dominantly, though not exclusively, located at the contact between the Otervatn Volcanic Formation, a dominantly basaltic sequence, and the overlying metasedimentary Furulund Group. Geology and metamorphism of the district are discussed by Boyle et al. (1985), Burton et al. (1989) and Boyle and Westhead (1992). The stratiform and stratabound sulphides are interpreted to have formed as a single stratigraphic interval via chemical exhalative precipitation of hydrothermal fluids onto the seafloor from hydrothermal vents (Cook et al., 1990). Deposit geochemistry is consistent with convective circulation of heated seawater and leaching of subjacent mafic volcanic rocks. Amphibolite facies regional metamorphism and accompanying deformation significantly modified the geometry of individual sulphide lenses and their spatial relationships with associated alteration (Cook et al. 1990). Isoclinal folding led to stacking of mineralized horizons within the stratigraphy; multiple sulphide bodies are arranged *en-echelon* within each horizon (Cook et al., 1993).

Sulitjelma ores are widely cited as spectacular examples of the effects of deformation on sulphide assemblages. These include *durchbewegt* textures, involving milling of refractory sulphides such as pyrite within matrices of ductile sulphides, plastic deformation of giant pyrite porphyroblasts and shearing along the ore horizons producing sulphide mylonites (Cook et al., 1990, 1993; Cook, 1996). There is evidence for sulphide recrystallization, remobilization, and local redistribution of trace elements, including precious metals, within the sulphide bodies (Cook, 1992, 1994, 1996). Chalcopyrite typically occurs, together with lesser sphalerite and pyrrhotite, in the sulphide matrix between coarse pyrite. Remobilized chalcopyrite is also observed filling fractures in refractory pyrite (Cook, 1994). Peak metamorphic conditions have been estimated at ca. 450-500 °C; see also Barrie et al. (2010).

KANMANTOO

The Kanmantoo Cu deposit (http://www.hillgroveresources.com.au/section/Projects/Kanmantoo) is hosted within metasedimentary rocks of the Cambrian Kanmantoo Group, Adelaide Fold Belt, South Australia; predominately psammitic schists with lesser aluminous pelites, black shales and calc-silicates (Oliver et al., 1998). Deposition occurred in the Kanmantoo trough about 520 Ma and rocks were deformed and metamorphosed at (~530-630 ^{o}C and 2.2-5.4 kbar during the ~500 Ma Delamerian Orogeny (Offler and Fleming, 1968; Sandiford et al., 1992; 1995). Although Thomson (1975), and several more recent authors attributed much of the mineralization to late-stage regional metamorphism, Jensen and Whittle (1969), Verwoerd and Cleghorn (1975), Seccombe et al. (1985), Both et al. (1995) and Spry et al. (2010) regarded the deposit, and others in the same belt, as having a syn-sedimentary (possibly VMS-style) genesis, albeit with substantial evidence for syn-metamorohic deformation and associated remobilization. The most common mineral assemblage in the Kanmantoo ore is quartz-chlorite-garnet ± pyrrhotite ± chalcopyrite. Mineralization is pipe-like and stratabound within a garnet-andalusite-biotite schist (Seccombe et al., 1985). At least three deformation events are recognised (e.g., Toteff, 1999).

ELECTRONIC APPENDIX B FOR CHAPTER 5

APPENDIX B: Mean errors and minimum detection limits determined by LA-ICP-MS (data in ppm)

Locality	Sample		Mn	Co	Ni	Zn	Ga	As	Se	Ag	Cd	In	Sn	Sb	Te	Au	Hg	Tl	Pb	Bi
Herja	**Hj-13**	1σ error	3.3	0.28	0.24	93	0.01	0.03	3.3	11	0.64	0.08	0.67	0.09	0.05	0.001	0.02	0.003	0.51	0.002
Romania		MDL	0.07	0.003	0.02	0.67	0.01	0.05	3.0	0.004	0.07	0.001	0.03	0.01	<0.001	0.002	0.02	0.001	0.01	0.002
			Mn	**Co**	**Ni**	**Zn**	**Ga**	**As**	**Se**	**Ag**	**Cd**	**In**	**Sn**	**Sb**	**Te**	**Au**	**Hg**	**Tl**	**Pb**	**Bi**
Toroiaga	**EMERIC2**	1σ error	39	-	0.31	19413	5.3	0.57	46	63	119	40	46	20	-	0.89	5.3	0.01	31	0.75
Romania		MDL	0.23	<0.001	0.16	3.2	0.02	0.19	7.7	0.01	0.29	0.003	0.05	0.02	<0.001	0.005	0.06	0.003	0.07	0.01
	T1a	1σ error	0.87	0.03	0.04	111	0.13	0.90	2.5	4.5	3.7	0.84	1.6	0.26	0.38	0.01	0.07	0.002	0.28	0.01
		MDL	0.15	0.03	0.11	0.42	0.03	1.1	1.5	0.03	0.12	0.004	0.08	0.03	<0.001	0.01	0.05	0.003	0.04	0.01
	TOR189	1σ error	0.18	1.3	0.23	159	0.08	1.0	11	35	3.1	0.92	1.1	0.42	0.26	0.02	0.09	0.005	0.48	0.19
		MDL	0.14	0.02	0.12	0.44	0.02	1.2	1.2	0.02	0.09	0.004	0.07	0.02	0.12	0.005	0.06	0.002	0.02	0.004
	TOR191	1σ error	0.15	0.01	0.02	267	0.04	0.90	0.59	5.4	6.2	2.5	1.9	0.10	0.03	0.01	427	0.001	0.88	0.003
		MDL	0.08	0.005	0.03	0.13	0.01	1.4	0.84	0.01	0.04	0.002	0.04	0.01	0.07	0.004	19	0.001	0.03	0.003
	TOR197	1σ error	0.15	0.01	0.03	329	0.02	0.88	0.72	10.0	5.3	0.74	0.47	0.11	0.06	0.01	1784	0.002	0.85	0.003
		MDL	0.10	0.01	0.04	0.17	0.01	1.5	1.1	0.01	0.05	0.002	0.05	0.01	0.07	0.01	41	0.001	0.03	0.002
	Toroiaga R0	1σ error	0.21	0.07	-	112	0.12	1.2	1.0	3.7	2.3	1.5	3.1	0.10	0.06	0.01	0.08	0.001	0.21	0.01
		MDL	0.16	<0.001	<0.001	0.46	0.02	1.4	1.1	0.02	0.08	0.003	0.09	0.02	0.18	0.01	0.07	0.002	0.02	0.01
			Mn	**Co**	**Ni**	**Zn**	**Ga**	**As**	**Se**	**Ag**	**Cd**	**In**	**Sn**	**Sb**	**Te**	**Au**	**Hg**	**Tl**	**Pb**	**Bi**
Kochbulak	**33**	1σ error	0.35	1.7	0.18	58	0.07	1.0	3.7	1.1	2.2	0.19	1.5	0.10	0.34	0.02	0.05	0.04	0.21	0.64
Uzbekistan		MDL	0.16	0.03	0.14	0.48	0.03	1.4	1.6	0.02	<0.001	0.004	0.08	0.04	0.22	0.01	0.04	0.003	0.03	0.01
			Mn	**Co**	**Ni**	**Zn**	**Ga**	**As**	**Se**	**Ag**	**Cd**	**In**	**Sn**	**Sb**	**Te**	**Au**	**Hg**	**Tl**	**Pb**	**Bi**
Baita Bihor	**BB55**	1σ error	4.9	11	2.8	79	0.01	0.10	3.2	2.8	0.92	3.8	9.3	0.07	0.10	0.02	0.03	0.01	19	0.10
Romania		MDL	0.07	0.004	0.03	0.83	0.01	0.06	3.1	0.004	0.09	0.002	0.03	0.01	0.09	0.001	0.02	0.001	0.02	0.003
	BBH15-21	1σ error	0.47	7.6	1.2	105	0.14	0.69	40	3.2	3.0	14	19	0.02	0.60	0.02	0.05	0.01	0.45	0.46
		MDL	0.16	0.03	0.13	0.49	0.03	1.0	1.6	0.03	0.16	0.01	0.08	0.03	<0.001	0.01	0.05	0.003	0.03	0.01
			Mn	**Co**	**Ni**	**Zn**	**Ga**	**As**	**Se**	**Ag**	**Cd**	**In**	**Sn**	**Sb**	**Te**	**Au**	**Hg**	**Tl**	**Pb**	**Bi**
Oravita	**ORV1**	1σ error	0.13	0.05	0.06	12	0.06	1.1	6.4	0.25	0.31	0.72	0.19	0.21	0.27	0.01	0.07	0.004	0.35	0.03
Romania		MDL	0.17	0.03	0.19	0.51	0.02	1.5	1.5	0.02	0.12	0.004	0.11	0.03	0.14	0.01	0.09	0.002	0.02	0.005
	ORV4	1σ error	0.12	0.03	0.05	13	0.10	1.1	1.9	0.29	0.38	0.77	0.43	0.18	0.25	0.01	0.05	0.01	0.35	0.02
		MDL	0.15	<0.001	0.15	0.44	0.03	1.4	1.7	0.04	0.13	0.004	0.08	0.03	<0.001	0.01	0.07	0.003	0.03	0.01
	ORV4a	1σ error	0.12	0.02	0.16	13	0.07	0.96	4.3	0.52	0.39	0.84	0.25	0.88	0.31	0.01	0.06	0.02	0.44	0.04
		MDL	0.17	0.04	<0.001	0.44	0.04	1.4	2.0	0.03	0.14	0.004	0.10	0.03	<0.001	0.01	0.06	0.004	<0.001	0.01

	ORV4B	1σ error	0.06	0.01	0.02	4.2	0.03	1.1	2.1	0.10	0.14	0.04	0.05	0.04	0.13	0.02	46	0.01	2.2	0.21
		MDL	0.09	0.01	0.03	0.19	0.01	0.85	0.88	0.01	0.06	0.001	0.04	0.01	0.06	0.01	23	0.001	0.05	0.004
			Mn	**Co**	**Ni**	**Zn**	**Ga**	**As**	**Se**	**Ag**	**Cd**	**In**	**Sn**	**Sb**	**Te**	**Au**	**Hg**	**Tl**	**Pb**	**Bi**
Asarel	**ASR 5A**	1σ error	0.10	0.01	0.02	19	0.06	0.63	1.8	0.20	0.49	0.02	0.04	0.05	0.11	0.01	60	0.004	11	0.19
Bulgaria		MDL	0.11	0.01	0.05	0.18	0.01	0.99	1.1	0.01	0.07	0.002	0.04	0.01	0.10	0.01	20	0.001	0.05	0.003
	ASR 10	1σ error	0.12	0.01	0.36	1.2	0.10	0.87	5.5	0.25	0.17	0.49	0.16	0.04	0.29	0.02	0.04	0.01	0.57	0.10
		MDL	0.16	0.03	<0.001	0.43	0.03	1.3	1.8	0.03	0.14	0.01	0.10	0.03	0.23	<0.001	0.05	0.003	0.03	0.01
	ASR KB P12077	1σ error	0.16	0.03	0.05	1.4	0.09	1.3	47	0.29	0.33	0.38	0.24	0.03	0.66	0.02	0.07	0.01	1.8	2.2
		MDL	0.16	<0.001	0.16	0.46	0.02	1.6	1.7	0.03	<0.001	0.004	0.08	0.03	<0.001	0.01	0.08	0.003	<0.001	0.01
			Mn	**Co**	**Ni**	**Zn**	**Ga**	**As**	**Se**	**Ag**	**Cd**	**In**	**Sn**	**Sb**	**Te**	**Au**	**Hg**	**Tl**	**Pb**	**Bi**
Bor	**BOR14**	1σ error	0.25	0.04	0.07	3.2	0.06	0.98	1.6	0.89	0.28	0.08	1.4	0.05	0.22	0.04	0.05	0.03	1.3	0.35
Serbia		MDL	0.20	0.05	0.24	0.68	0.04	1.5	1.9	0.04	0.19	0.01	0.11	0.03	<0.001	0.01	0.06	0.003	0.03	0.01
			Mn	**Co**	**Ni**	**Zn**	**Ga**	**As**	**Se**	**Ag**	**Cd**	**In**	**Sn**	**Sb**	**Te**	**Au**	**Hg**	**Tl**	**Pb**	**Bi**
Elastite	**Elastite b a**	1σ error	0.15	0.13	-	0.55	0.14	0.95	42	0.55	0.10	0.19	0.26	0.14	1.8	0.05	0.05	0.02	64	0.11
Bulgaria		MDL	0.16	<0.001	<0.001	0.63	0.03	1.3	1.6	0.03	0.12	0.004	0.08	0.03	0.20	0.01	0.06	0.004	0.04	0.01
	ELS 157	1σ error	0.19	0.07	-	2.7	0.17	1.2	1.8	1.1	0.38	0.06	0.08	0.44	0.32	0.02	0.06	0.01	4.9	0.24
		MDL	0.18	<0.001	<0.001	0.68	0.04	1.5	1.9	0.03	0.12	0.005	0.10	0.03	<0.001	<0.001	0.07	<0.001	<0.001	0.01
			Mn	**Co**	**Ni**	**Zn**	**Ga**	**As**	**Se**	**Ag**	**Cd**	**In**	**Sn**	**Sb**	**Te**	**Au**	**Hg**	**Tl**	**Pb**	**Bi**
Vorta	**DMV 99-22**	1σ error	0.27	0.01	-	186	0.17	7.8	1.0	3.1	2.8	0.01	0.11	0.38	0.10	0.07	0.12	0.02	19	0.01
Romania		MDL	0.17	0.04	<0.001	0.60	<0.001	1.5	1.8	0.04	0.19	0.005	0.08	0.04	0.29	0.01	0.06	0.004	0.14	0.01
			Mn	**Co**	**Ni**	**Zn**	**Ga**	**As**	**Se**	**Ag**	**Cd**	**In**	**Sn**	**Sb**	**Te**	**Au**	**Hg**	**Tl**	**Pb**	**Bi**
Kapp Mineral	**kmi 2a**	1σ error	9.5	0.04	0.12	20	0.02	0.68	0.93	8.3	0.39	0.07	0.55	1.0	0.04	0.01	337	0.01	-	0.07
Norway		MDL	0.08	0.01	0.03	0.12	0.01	1.1	0.82	0.01	0.04	0.001	0.04	0.01	0.05	0.004	30	0.001	0.09	0.002
			Mn	**Co**	**Ni**	**Zn**	**Ga**	**As**	**Se**	**Ag**	**Cd**	**In**	**Sn**	**Sb**	**Te**	**Au**	**Hg**	**Tl**	**Pb**	**Bi**
Broken Hill	**BH73**	1σ error	31	0.22	0.08	82	0.75	0.09	2.9	82	0.31	0.23	27	1.4	0.13	0.005	0.04	0.01	12	0.01
Australia		MDL	0.21	0.01	0.05	2.2	0.02	0.17	5.5	0.01	0.21	0.005	0.13	0.05	0.27	0.01	0.07	0.01	0.04	0.02
	BH262	1σ error	0.29	0.10	0.22	42	1.1	0.83	0.92	14	0.48	0.14	42	0.12	0.07	0.005	0.06	0.003	0.37	0.01
		MDL	0.17	0.02	0.13	0.53	<0.001	1.2	1.5	0.03	0.13	0.01	0.10	0.03	0.21	0.01	0.07	0.004	0.03	0.01
			Mn	**Co**	**Ni**	**Zn**	**Ga**	**As**	**Se**	**Ag**	**Cd**	**In**	**Sn**	**Sb**	**Te**	**Au**	**Hg**	**Tl**	**Pb**	**Bi**
Bleikvassli	**Bv-1**	1σ error	0.19	0.01	0.03	29	1.7	0.05	1.4	51	0.12	1.4	57	0.60	0.03	0.04	0.06	0.05	0.96	0.005
Norway		MDL	0.07	0.004	0.03	0.74	0.01	0.09	1.8	0.004	0.08	0.001	0.04	0.02	0.09	0.001	0.02	0.001	0.02	0.004
	Bv-4	1σ error	4.6	0.10	0.20	57	1.7	0.94	1.6	0.48	0.48	1.6	82	0.55	-	0.02	0.06	0.05	0.61	0.03
		MDL	0.17	0.02	<0.001	0.64	<0.001	1.2	1.5	0.03	0.10	0.004	0.07	0.03	<0.001	0.01	0.06	0.002	0.06	0.01
	V598572	1σ error	6.7	0.03	0.33	40	0.17	0.14	3.6	1.1	0.92	2.0	124	0.33	0.10	0.004	0.13	0.004	0.27	0.01
		MDL	0.07	0.003	0.04	0.78	0.01	0.15	3.1	0.004	0.07	0.001	0.04	0.01	0.07	0.001	0.02	0.001	0.02	0.005
			Mn	**Co**	**Ni**	**Zn**	**Ga**	**As**	**Se**	**Ag**	**Cd**	**In**	**Sn**	**Sb**	**Te**	**Au**	**Hg**	**Tl**	**Pb**	**Bi**
Mofjell	**Mo5**	1σ error	0.65	0.01	0.38	63	0.11	0.73	5.6	2.8	0.70	0.13	0.41	0.19	0.49	0.01	0.05	0.02	0.37	0.01

Norway		MDL	0.17	0.03	0.14	0.69	<0.001	1.1	1.3	0.03	0.13	0.01	0.09	0.03	<0.001	0.01	0.06	0.003	0.05	0.01
	Mo16	1σ error	0.11	0.01	0.02	85	0.05	2.0	2.6	1.0	4.1	0.02	0.18	0.31	0.13	0.01	0.09	0.003	0.33	0.003
		MDL	0.14	0.01	0.05	0.34	0.01	2.2	2.1	0.02	0.10	0.003	0.08	0.06	0.11	0.01	0.05	0.002	0.05	0.004
	Mo17A	1σ error	2.2	0.01	0.04	38	0.04	1.5	1.6	2.5	8.0	0.05	0.10	4.6	0.21	0.01	0.12	0.03	3.9	0.02
		MDL	0.13	0.01	0.05	0.27	0.02	1.7	1.9	0.02	0.08	0.003	0.07	0.06	0.12	0.01	0.09	0.002	0.02	0.004
			Mn	**Co**	**Ni**	**Zn**	**Ga**	**As**	**Se**	**Ag**	**Cd**	**In**	**Sn**	**Sb**	**Te**	**Au**	**Hg**	**Tl**	**Pb**	**Bi**
Sulitjelma	**CV01.1**	1σ error	0.10	0.53	0.05	50	0.02	1.2	19	9.7	4.2	0.04	0.08	0.07	0.21	0.01	0.10	0.002	0.13	0.02
Norway		MDL	0.18	0.02	0.06	0.74	0.02	2.2	2.6	0.03	0.12	0.004	0.14	0.14	0.21	0.01	0.11	0.003	0.03	0.01
	CV01.2a	1σ error	0.09	0.59	0.06	50	0.03	1.0	25	19	2.3	0.05	0.07	0.05	0.32	0.003	0.09	0.002	0.49	0.03
		MDL	0.13	0.01	0.04	0.47	0.01	1.7	1.7	0.01	0.08	0.003	0.11	0.09	0.13	0.01	0.09	0.002	0.02	0.01
	CV01.2b	1σ error	0.08	0.10	0.01	69	0.02	0.78	26	17	2.8	0.07	0.05	0.04	0.40	0.004	0.06	0.002	0.13	0.04
		MDL	0.11	0.01	0.04	0.33	0.01	1.1	1.4	0.02	0.07	0.003	0.07	0.06	0.11	0.01	0.07	0.002	0.02	0.004
	CV01.3	1σ error	0.15	0.05	0.10	68	0.08	1.0	205	26	2.6	0.21	0.11	0.02	0.21	0.01	0.04	0.02	1.1	0.10
		MDL	0.20	0.03	0.13	0.57	0.04	1.5	1.7	0.03	0.16	0.005	0.10	0.04	0.00	0.01	0.04	0.003	0.03	0.01
	CV01.4	1σ error	1.2	0.23	0.14	42	0.07	0.82	46	11	3.2	0.11	0.14	0.05	0.21	0.01	0.06	0.01	0.15	0.06
		MDL	0.19	<0.001	0.22	0.54	<0.001	1.2	2.0	0.03	0.14	0.01	0.11	0.03	0.00	0.01	0.07	0.004	0.03	0.01
	CV01.6b	1σ error	0.12	0.06	0.19	25	0.05	0.78	230	13	3.1	0.08	0.11	0.03	0.13	0.01	0.05	0.01	0.13	0.07
		MDL	0.17	0.03	0.15	0.63	0.03	1.2	1.5	0.03	0.16	0.004	0.09	0.04	0.26	0.01	0.07	0.003	0.05	0.01
	NC4172	1σ error	1.1	0.45	0.28	17	0.11	0.95	6.1	2.8	0.84	0.49	1.2	0.76	0.54	0.02	0.05	0.09	11	0.51
		MDL	0.15	0.02	<0.001	0.54	0.03	1.3	1.6	0.03	0.13	0.004	0.08	0.03	0.00	<0.001	0.06	<0.001	0.02	0.01
	NC5839	1σ error	1.0	0.11	0.07	30	1.8	1.0	3.7	2.4	0.63	0.52	5.1	0.22	0.56	0.02	0.12	0.01	0.28	0.05
		MDL	1.4	0.01	0.03	0.97	0.08	1.5	0.72	0.03	0.19	0.01	0.14	0.06	0.30	0.02	0.15	0.01	0.08	0.02
	NC6894	1σ error	0.12	0.01	0.05	15	0.09	1.5	16	0.70	0.47	3.2	8.0	0.08	0.38	0.02	0.32	0.002	0.11	0.02
		MDL	0.15	0.02	0.13	0.75	0.02	1.9	1.9	0.02	0.11	0.003	0.12	0.10	0.16	0.01	0.09	0.003	0.02	0.01
	Su3	1σ error	0.14	0.26	0.68	7.3	0.09	0.88	2.9	1.3	0.62	0.56	1.1	0.06	0.39	0.08	0.10	0.002	0.28	0.36
		MDL	0.17	0.04	<0.001	0.61	0.03	1.3	1.4	0.03	0.15	0.01	0.09	0.04	0.000	0.01	0.06	0.003	0.03	0.01
	Sulis 1b	1σ error	0.55	0.07	0.22	31	0.99	0.88	16	1.5	0.55	0.51	7.4	0.27	0.41	0.01	0.07	0.01	0.21	0.06
		MDL	0.18	0.03	<0.001	0.45	0.03	1.3	1.7	0.02	0.15	0.004	0.08	0.03	0.25	0.01	0.06	0.003	0.03	0.01
	Sulis2a	1σ error	2.3	0.08	0.11	46	0.46	1.3	12	1.5	1.1	0.16	0.49	0.19	0.29	0.004	0.50	0.002	0.41	0.08
		MDL	0.13	0.01	0.04	0.89	0.01	1.7	1.5	0.01	0.09	0.003	0.11	0.08	0.11	0.01	0.07	0.002	0.02	0.01
			Mn	**Co**	**Ni**	**Zn**	**Ga**	**As**	**Se**	**Ag**	**Cd**	**In**	**Sn**	**Sb**	**Te**	**Au**	**Hg**	**Tl**	**Pb**	**Bi**
Kanmantoo	**KTDD086(8)**	1σ error	0.19	0.43	0.26	105	0.32	0.84	7.7	5.7	0.60	1.2	6.4	0.07	0.12	0.03	0.06	0.003	1.9	0.35
Australia		MDL	0.12	0.01	0.05	0.40	0.02	1.3	1.9	0.02	0.09	0.003	0.08	0.08	0.15	0.01	0.08	0.002	0.02	0.004
	KTDD086(9)	1σ error	0.12	0.05	0.08	37	0.30	1.1	33	1.1	0.28	1.4	6.3	0.08	0.09	0.02	0.11	0.003	4.9	0.25
		MDL	0.16	0.01	0.10	0.77	0.02	1.8	2.1	0.01	0.12	0.003	0.11	0.11	0.17	0.01	0.09	0.003	0.02	0.01
	KTDD086(11)	1σ error	0.12	0.06	0.07	30	0.62	1.1	12	1.3	0.40	1.2	9.2	0.07	0.30	0.01	0.12	0.003	0.88	0.06
		MDL	0.12	0.01	0.04	0.50	0.02	1.5	1.7	0.01	0.09	0.003	0.09	0.09	0.14	0.01	0.08	0.003	0.02	0.005

KTDD086(12)	1σ error	0.13	0.05	0.08	20	0.50	1.2	6.0	2.2	0.44	1.4	6.0	0.07	0.56	0.01	0.07	0.002	0.58	0.15
	MDL	0.13	0.01	0.05	0.40	0.02	1.6	1.7	0.01	0.08	0.003	0.10	0.08	0.12	0.01	0.08	0.003	0.02	0.01
KTDD178(7)	1σ error	0.07	0.20	0.10	17	0.06	0.85	8.5	2.1	0.28	3.6	13	0.05	0.15	0.02	0.05	0.003	5.5	0.13
	MDL	0.10	0.01	0.03	0.30	0.01	1.2	1.4	0.01	0.07	0.002	0.08	0.07	0.11	0.01	0.07	0.002	0.02	0.005
KTDD178(8)	1σ error	0.07	0.11	0.14	25	0.08	0.88	6.5	3.7	0.39	1.4	30	0.05	0.29	0.01	0.07	0.001	0.23	0.02
	MDL	0.11	0.01	0.04	0.35	0.02	1.3	1.6	0.02	0.08	0.002	0.08	0.07	0.07	0.005	0.07	0.002	0.02	0.01
KTDD178(12)	1σ error	0.07	0.28	0.13	56	0.13	0.69	3.6	4.8	0.31	1.9	42	0.04	0.19	0.01	0.05	0.001	0.23	0.04
	MDL	0.10	0.01	<0.001	0.29	0.01	1.0	1.4	0.01	0.07	0.002	0.06	0.06	0.11	0.01	0.07	0.002	0.02	0.003
KTDD180(3)	1σ error	0.11	1.8	0.95	31	0.05	0.73	3.1	3.2	0.17	2.9	2.9	0.06	0.35	0.005	0.06	0.02	0.13	0.12
	MDL	0.11	0.01	0.05	0.34	0.01	1.1	1.6	0.01	0.07	0.003	0.07	0.07	0.10	0.01	0.08	0.002	0.01	0.004
KTDD180(7)	1σ error	0.09	0.12	0.15	49	0.14	0.86	1.9	1.1	0.25	2.2	25	0.05	0.28	0.03	0.13	0.05	0.10	0.27
	MDL	0.12	0.01	<0.001	0.36	0.01	1.3	1.6	0.01	0.07	0.003	0.08	0.08	0.13	0.01	0.06	0.002	0.02	0.005
KTDD180S(4)	1σ error	0.19	3.5	3.5	212	0.26	1.4	8.9	22	0.80	19	127	0.07	0.19	0.03	0.12	0.005	16	4.6
	MDL	0.11	0.01	0.05	0.34	0.01	1.3	1.5	0.01	0.09	0.002	0.08	0.08	0.14	0.01	0.08	0.002	0.03	0.005
KTDD180S(5)	1σ error	0.23	2.0	8.3	46	0.11	1.3	8.7	6.0	0.34	1.6	15	0.08	0.30	0.06	0.29	0.003	2.7	2.6
	MDL	0.12	0.01	0.06	0.42	0.01	1.5	1.6	0.01	0.08	0.003	0.09	0.08	0.12	0.01	0.07	0.002	0.02	0.01

MDL = minimum detection limit (99% confidence). Dash = insufficient data to perform calculation.

Error is calculated from internal (counting statistic noise) and external signal uncertainties (mass bias, correction of unknowns to standards, laser induced elemental fractionation [LIEF] and instrument drift).

ELECTRONIC APPENDIX C FOR CHAPTER 5

APPENDIX C: Complete chalcopyrite trace element dataset determined by LA-ICP-MS (data in ppm)

Herja	**Mn55**	**Co59**	**Ni60**	**Zn66**	**Ga69**	**As75**	**Se82**	**Ag107**	**Cd111**	**In115**	**Sn118**	**Sb121**	**Te125**	**Au197**	**Hg202**	**Tl205**	**Pb207**	**Bi209**
Hj-13	65.61	6.85	0.488	1281.95	0.067	0.072	3.13	150.33	6.82	1.899	9.52	0.599	<0.00	0.0039	0.238	0.0045	1.375	0.0047
	30.27	4.47	<0.0166	2037.62	0.0338	0.065	11.31	73.02	6.55	2.223	13.88	0.883	<0.00	<0.0018	0.144	0.00132	2.09	0.0044
	36.41	3.62	1.23	989.95	0.015	<0.0276	7.52	148.97	4.76	1.42	4.45	0.603	<0.00	<0.0020	0.225	0.00236	2.9	0.009
	73.38	3.57	Inc	2497.46	0.114	0.088	18.31	111.99	11	1.512	11.54	1.347	Inc	<0.0020	0.165	0.0043	2.82	0.0088
	49.01	3.18	0.585	1056.17	0.07	<0.056	23.8	134.28	5.34	3.12	16.63	0.325	<0.00	0.001	0.168	<0.00110	1.496	0.0024
	52.67	4.92	1.53	1061.9	0.074	0.143	11.67	263.35	6.82	2.6	7.38	0.216	<0.00	<0.00126	0.156	<0.00117	1.252	0.0022
	67.13	6.36	Inc	2283.27	0.206	<0.049	<3.21	195.26	12.3	0.44	7.97	2.6	<0.00	<0.0026	0.161	Inc	1.299	<0.0033
	47.62	2.43	0.026	2681.61	0.102	0.078	5.71	144.93	10.36	1.368	9.2	Inc	<0.00	<0.00156	0.166	0.00179	Inc	0.0084
	48.45	3.89	Inc	1224.69	0.106	0.13	<3.33	219.4	7.4	1.477	9.58	0.141	<0.00	<0.00205	0.135	0.0024	1.044	0.0038
	43.18	3.15	Inc	845.25	0.063	<0.060	<3.32	232.38	4.88	1.12	9.87	0.379	<0.00	<0.0030	0.098	0.0034	6.05	<0.0035
Toroiaga	**Mn55**	**Co59**	**Ni60**	**Zn66**	**Ga69**	**As75**	**Se82**	**Ag107**	**Cd111**	**In115**	**Sn118**	**Sb121**	**Te125**	**Au197**	**Hg202**	**Tl205**	**Pb207**	**Bi209**
EMERIC2	Inc	-	<0.29	Inc	4.68	<0.49	36.55	23.76	Inc	47.85	65.01	20.75	-	Inc	6.63	<0.010	27.04	0.97
	Inc	-	<0.15	Inc	4.07	<0.00	17.03	10.76	Inc	44.35	57.48	15.02	-	Inc	3.14	0.006	14.17	0.36
	Inc	-	0.2	Inc	1.94	0.31	26.38	147.17	Inc	43.87	34.95	8.39	-	<0.0059	1.02	<0.0033	11.04	0.25
	Inc	-	0.07	Inc	1.11	<0.22	26.85	109.11	Inc	42.68	53.1	3.03	-	0.09	1.36	<0.0032	4.77	0.013
	Inc	-	<0.00	Inc	1.47	1.06	22.41	72.12	Inc	26.29	18.87	16.97	-	<0.0023	0.82	0.0047	13.95	0.16
	Inc	-	<0.00	Inc	1.61	0.25	33.34	48.07	Inc	20.91	13.29	1.72	-	0.009	0.66	<0.0017	3.01	0.006
	1.78	-	0.045	1219.6	1.27	<0.13	<5.79	177.36	13.97	28.16	49.43	4.33	-	0.09	0.79	<0.0016	3.64	0.015
	Inc	-	<0.00	Inc	0.47	0.19	<5.32	154.91	Inc	12.5	7.14	27.27	-	0.0033	0.39	0.0032	47.25	0.19
	Inc	-	<0.028	Inc	1.22	0.19	<5.41	114.75	Inc	21.06	77.25	1.84	-	0.0053	0.43	<0.0016	2.65	0.059
Toroiaga	**Mn55**	**Co59**	**Ni60**	**Zn66**	**Ga69**	**As75**	**Se82**	**Ag107**	**Cd111**	**In115**	**Sn118**	**Sb121**	**Te125**	**Au197**	**Hg202**	**Tl205**	**Pb207**	**Bi209**
T1a	Inc	0.041	<0.00	836.28	0.81	<1.24	Inc	Inc	13.42	14.26	4.36	0.51	0.5	0.019	0.201	0.0028	0.64	0.041
	5.29	0.036	<0.00	490.72	1.02	<1.13	<1.53	18.14	9.08	17.38	21.23	3.04	0.33	0.012	0.228	0.0037	3.07	0.0207
	3.86	0.156	<0.00	784.67	0.31	2.82	2.31	29.28	15.17	14.49	14.71	4.45	<0.00	<0.00	0.45	<0.0039	4.07	0.042
	Inc	<0.00	<0.00	Inc	0.78	<1.02	2.14	87.98	Inc	14.14	14.81	0.87	<0.00	<0.00	0.108	<0.00	1.48	<0.0051
	1.35	<0.00	<0.00	927.82	0.96	2.96	<1.19	86.27	13.09	17.54	30.09	6.43	1.22	<0.0081	0.188	<0.00255	4.05	0.032

	5.27	<0.00	<0.111	846.46	0.33	<1.03	<1.28	Inc	17.51	10.66	13.05	1.92	<0.00	<0.00	0.083	<0.00233	0.93	<0.00
	3.86	<0.00	<0.00	730.59	0.211	<1.17	5.59	79.46	17.28	13.33	23.63	2.54	<0.00	<0.00	0.137	<0.00	3.76	0.089
	4.65	<0.00	<0.00	709.09	0.228	<1.26	<1.57	82.87	19.41	18.45	41.93	0.294	<0.00	<0.00	0.44	<0.00292	0.485	0.032
	Inc	<0.0252	<0.00	Inc	0.73	1.37	3.73	26.43	Inc	12.53	14.76	0.99	0.44	<0.00	0.155	<0.00	2.58	0.046
	Inc	<0.041	<0.00	Inc	0.67	<1.14	<1.78	1.16	Inc	15.23	17.07	3.55	<0.00	<0.00	0.293	<0.00274	3.36	0.0197
Toroiaga	**Mn55**	**Co59**	**Ni60**	**Zn66**	**Ga69**	**As75**	**Se82**	**Ag107**	**Cd111**	**In115**	**Sn118**	**Sb121**	**Te125**	**Au197**	**Hg202**	**Tl205**	**Pb207**	**Bi209**
TOR189	0.41	10.12	1	Inc	0.508	<1.21	54.76	848.01	Inc	24.16	19.17	2.45	0.31	0.049	0.353	<0.00168	3.12	2.09
	2.13	10.79	0.48	Inc	0.445	<1.08	86.72	873.69	Inc	14.6	22.28	3.88	0.58	<0.0049	0.564	0.0064	1.84	1.411
	1.2	11.37	0.18	1926.1	0.507	<1.12	89.47	871.4	27.65	15.11	9.67	1.45	<0.119	<0.00	0.433	<0.0017	1.68	1.114
	0.52	7.89	<0.00	1588.34	0.416	<1.06	80.25	840.32	28.2	16.05	6.81	0.573	0.3	<0.00	0.474	0.0015	0.99	0.762
	0.15	14.64	0.53	Inc	0.098	<0.99	64.34	878.15	Inc	19.87	24	2.67	<0.00	0.093	0.64	<0.00	1.24	0.928
	1.26	15.08	<0.089	Inc	0.25	<1.02	85.09	671.48	Inc	21.79	27.55	6.95	1.44	0.016	0.51	0.009	Inc	Inc
	1.16	13.84	<0.151	Inc	<0.00	Inc	105.53	626.94	Inc	21.7	20.42	Inc	1.34	0.015	0.176	0.049	Inc	Inc
	0.35	14.45	0.49	1486.98	0.072	1.72	22.67	794.85	22.97	24.7	24.85	0.88	<0.00	0.013	0.64	<0.00197	0.68	0.538
	1.53	11.15	<0.00	Inc	0.152	1.5	119.17	715.92	Inc	22.35	12.41	3.02	0.23	0.0104	0.475	0.0025	2.64	2.08
	1.04	15.73	Inc	1289.12	0.268	<1.34	74.24	749.05	21.1	15.06	8.99	0.358	0.29	<0.00	0.291	0.0019	0.121	0.312
Toroiaga	**Mn55**	**Co59**	**Ni60**	**Zn66**	**Ga69**	**As75**	**Se82**	**Ag107**	**Cd111**	**In115**	**Sn118**	**Sb121**	**Te125**	**Au197**	**Hg202**	**Tl205**	**Pb207**	**Bi209**
TOR191	3.25	0.055	<0.00	1881.32	0.522	<1.26	<0.78	10.06	43.35	17.97	18.96	0.481	<0.00	0.067	246.65	0.0073	0.55	0.0034
	1.04	<0.00	<0.00	Inc	0.269	<1.63	<1.00	118.1	Inc	63.76	53.38	1.39	<0.00	0.0184	228.63	<0.0020	3.85	<0.0057
	1.04	0.0069	0.068	1643.07	0.236	<1.30	<0.78	100.13	32.47	18.6	26.39	0.686	<0.00	<0.0041	241.62	<0.00072	0.63	0.0127
	Inc	0.0062	<0.00	Inc	0.235	<1.41	<0.87	3.85	Inc	21.01	16.5	0.791	0.066	<0.0056	176	0.0056	1.83	0.0418
	0.546	<0.0038	<0.044	1551.22	0.183	<1.12	<0.69	0.681	36.25	23.38	58.12	0.51	<0.070	0.0195	243.38	0.0013	0.95	0.0032
	Inc	0.11	<0.0241	Inc	0.232	<1.23	<0.78	Inc	Inc	20.39	17.41	1.35	<0.00	0.0108	307.76	0.002	0.89	<0.0021
	0.277	0.154	<0.0273	1928.34	0.395	<1.37	4.11	Inc	30.01	31.33	26.51	0.99	<0.050	0.0073	321.01	<0.00211	Inc	0.0066
	Inc	0.0133	0.046	Inc	0.118	<1.45	1.64	66.32	Inc	79.84	20.55	2.29	<0.092	<0.0026	371.86	0.0053	3.93	<0.00
	1.07	0.0297	<0.00	1101.59	0.263	<1.46	5.41	40.55	24.8	24.67	7.23	0.363	<0.00	0.0064	57.93	0.0019	0.78	<0.00182
	0.646	0.0169	<0.0307	1279.57	0.288	<1.49	<1.00	Inc	26.66	28.12	25.59	0.209	<0.00	0.0073	150.1	<0.00117	0.75	<0.0027
Toroiaga	**Mn55**	**Co59**	**Ni60**	**Zn66**	**Ga69**	**As75**	**Se82**	**Ag107**	**Cd111**	**In115**	**Sn118**	**Sb121**	**Te125**	**Au197**	**Hg202**	**Tl205**	**Pb207**	**Bi209**
TOR197	1.88	<0.0133	<0.00	1851.67	0.041	<1.67	<1.18	219.63	39.07	11.82	6.13	0.567	0.089	<0.0063	313.33	0.0052	0.92	0.0601
	Inc	<0.0096	0.05	Inc	0.09	<1.74	<1.21	168.03	Inc	25.63	9.75	3.65	<0.077	<0.0075	Inc	<0.0018	14.2	0.0151
	Inc	<0.0068	<0.041	Inc	0.032	<1.67	<1.30	313.96	Inc	26.21	9.15	3.07	<0.078	0.0124	Inc	<0.0018	2.86	0.0048
	<0.087	<0.00	<0.055	1722.68	0.199	<1.33	<1.01	271.86	31.29	20.92	12.18	0.44	<0.00	0.0213	448.59	<0.00118	0.5	0.0029

	0.398	<0.0074	<0.00	1772.9	0.184	3.37	<0.98	157.3	33.36	16.88	7.58	0.524	0.064	0.0041	553.89	<0.00	1.27	0.003
	0.243	<0.0049	0.093	2175.55	0.079	<1.21	<0.97	162.87	33.14	18.55	9.4	0.688	0.181	0.0019	499.54	<0.00	1.01	0.0104
	<0.095	0.149	<0.00	704.24	0.301	<1.40	1.9	83.67	7.47	13.87	20.27	4.94	0.105	0.0052	362.83	0.0093	8.29	<0.00205
	4.28	0.0075	<0.037	2140.61	0.058	<1.56	3.4	208.92	39.82	15.22	10.3	1.371	0.35	<0.0035	322.54	0.0107	1.46	<0.0032
	0.237	0.021	<0.00	2130.61	<0.0069	1.39	2.87	138.63	32.86	17.37	7.01	0.824	<0.00	0.033	414.46	0.0041	1.27	0.0572
	1.38	0.04	<0.00	1690.97	0.187	1.86	3.36	305.87	30.27	20.34	13.42	0.862	0.104	<0.0061	Inc	0.0041	0.75	0.0096
Toroiaga	**Mn55**	**Co59**	**Ni60**	**Zn66**	**Ga69**	**As75**	**Se82**	**Ag107**	**Cd111**	**In115**	**Sn118**	**Sb121**	**Te125**	**Au197**	**Hg202**	**Tl205**	**Pb207**	**Bi209**
Toroiaga R0	0.88	<0.00	<0.00	1782.7	0.248	<1.24	2.84	2.58	23.92	23.94	11.95	0.77	<0.00	<0.0050	<0.070	<0.00	1.61	0.0215
	0.66	<0.00	<0.00	1724.7	0.29	2.58	<1.14	1.51	25.46	20.62	12.26	0.224	<0.178	<0.00	0.096	<0.00161	1.03	0.0111
	1.25	<0.00	<0.00	1573.81	0.5	4	3.71	2.77	24.6	18.6	25.03	1.32	<0.00	<0.00	0.12	<0.00299	2.66	0.046
	0.88	<0.00	<0.00	1558.11	<0.00	1.92	2.73	Inc	20.87	11.15	2.27	0.62	<0.00	<0.00	0.236	<0.00267	1.14	<0.00
	<0.18	0.318	<0.00	703.69	1.54	1.73	<1.33	1.96	16.14	1.03	1.96	0.534	<0.00	0.0048	0.495	<0.00203	0.296	<0.0070
	<0.22	<0.00	<0.00	1570.89	0.51	<1.98	<1.49	Inc	25.97	21.1	28.5	0.425	<0.00	<0.0078	0.35	<0.00248	1.69	0.047
	Inc	<0.00	<0.00	Inc	0.089	<1.33	2.21	Inc	Inc	19.27	35	0.8	<0.00	0.012	0.57	<0.00	1.48	0.051
	<0.145	<0.00	<0.00	878.46	0.119	2	1.84	9.27	15.52	28.27	Inc	0.074	<0.00	<0.00	0.3	<0.00232	0.65	0.0068
	1.24	<0.00	<0.00	1367.25	0.64	<1.19	<0.94	21.89	14.5	15.99	24.63	0.31	<0.00	<0.00	0.26	<0.00	2.14	0.054
	3.6	<0.00	<0.00	763.87	0.42	<1.27	<0.83	13.75	17.61	19.89	12.32	0.56	<0.00	<0.00	0.35	<0.00235	2.52	0.029
Kochbulak	**Mn55**	**Co59**	**Ni60**	**Zn66**	**Ga69**	**As75**	**Se82**	**Ag107**	**Cd111**	**In115**	**Sn118**	**Sb121**	**Te125**	**Au197**	**Hg202**	**Tl205**	**Pb207**	**Bi209**
33	2.88	0.404	<0.00	1440.78	0.052	<1.43	31.59	8.59	25.92	2.93	13.88	0.63	0.24	<0.00	0.117	0.38	2.38	7.4
	0.49	Inc	<0.00	1338.76	0.386	<1.58	34.41	10.43	27.57	3.99	12.62	0.143	<0.239	0.016	<0.064	0.51	1.84	12.29
	0.59	Inc	<0.00	949.28	0.109	<1.54	32.95	11.67	16.08	1.63	8.55	0.381	0.71	0.023	0.14	0.0179	1.85	10.04
	1.88	Inc	<0.00	575.06	<0.00	<1.17	22.61	12.76	14.6	1.99	8.19	Inc	0.72	0.015	<0.037	0.161	1.57	15.7
	1.07	Inc	<0.00	806.22	<0.00	<1.41	40.66	7.38	18.97	3.75	11.48	0.147	Inc	<0.014	<0.042	0.05	0.71	12.1
	0.47	Inc	0.23	948.11	0.131	<1.30	25.35	8.11	21.06	1.79	10.19	0.463	1.18	0.009	0.068	0.262	1.02	13.64
	<0.14	Inc	<0.00	588.71	0.35	2.27	35.7	7.48	14.15	2.93	11.04	0.39	<0.00	<0.0106	<0.027	0.53	0.84	8.22
	Inc	Inc	<0.00	915.25	0.39	<1.49	27.2	25.09	16.64	1.64	6.76	0.78	<0.00	0.086	<0.035	0.58	0.71	7.49
	0.89	Inc	<0.00	726.48	0.152	<1.29	24.91	6.98	14.83	4.48	18.59	<0.0228	0.43	0.019	<0.033	0.086	2.64	9.82
	0.42	Inc	<0.00	863.54	0.12	<1.45	38.81	6.52	17.55	1.39	7.12	0.034	0.51	<0.00	0.081	0.0018	1.36	8.29
Baita Bihor	**Mn55**	**Co59**	**Ni60**	**Zn66**	**Ga69**	**As75**	**Se82**	**Ag107**	**Cd111**	**In115**	**Sn118**	**Sb121**	**Te125**	**Au197**	**Hg202**	**Tl205**	**Pb207**	**Bi209**
BB55	14.74	24.26	Inc	597.73	0.06	0.82	6.04	Inc	13.88	88.43	133.98	0.037	0.121	0.0028	0.119	0.0433	0.95	0.528
	1.98	8.9	0.087	549.45	0.0063	0.276	4.42	12.82	3.59	100.12	109.34	0.365	<0.00	0.0112	0.088	0.023	0.35	0.0763
	10.59	Inc	Inc	935.73	<0.0078	0.494	6.75	12.33	12.09	107.49	157.57	2.96	0.119	0.13	0.12	0.206	1.41	0.592

	4.5	14.89	0.253	724.33	0.054	0.046	11.87	2.73	6.19	98.92	105.01	0.058	0.24	0.0409	0.048	0.0017	0.77	0.461
	7.34	10.12	0.025	672.95	0.046	0.5	12.53	9.25	6.16	113.4	125.86	0.233	0.135	0.109	0.092	0.12	12.21	1.439
	2.52	4.7	0.218	659.16	0.067	<0.038	10.85	9.53	7.19	98.31	96.19	0.074	<0.00	0.096	0.136	<0.00107	0.46	0.624
	Inc	Inc	Inc	737.05	0.117	Inc	<5.22	26.11	46.87	116.61	111.33	1.43	<0.00	0.321	0.177	0.452	Inc	Inc
	16.54	11.12	0.046	Inc	0.043	0.97	5.5	10.08	14.88	110.68	112.16	2.32	<0.00	0.083	0.111	0.183	Inc	0.844
	6.75	18.21	0.206	647.44	0.139	<0.079	5.01	50.1	8.38	109.84	139.77	0.008	0.25	0.252	0.101	<0.00088	0.31	0.0887
	3.89	11.65	0.104	655.67	0.044	0.078	13.62	7.35	5.36	111.82	129.08	0.025	0.46	0.11	0.06	<0.00113	0.41	0.147
Baita Bihor	**Mn55**	**Co59**	**Ni60**	**Zn66**	**Ga69**	**As75**	**Se82**	**Ag107**	**Cd111**	**In115**	**Sn118**	**Sb121**	**Te125**	**Au197**	**Hg202**	**Tl205**	**Pb207**	**Bi209**
BBH15-21	<0.148	11.43	0.94	907.98	0.92	<0.89	112.55	32.97	33.75	162.65	168.56	<0.00	3.9	0.011	<0.055	0.04	4.63	14.12
	0.2	10.63	0.4	910.05	0.81	<1.05	184.19	49.46	40.46	206.32	175.63	0.058	1.19	0.0056	0.08	0.128	11.07	4.89
	0.37	6.02	1.91	768.55	0.87	<0.98	117.69	32.45	22.76	224.16	184.64	0.034	2.84	0.202	0.084	0.0133	3.93	6.51
	17	11.54	1.54	1261.17	0.6	1.85	159.71	29.51	46.52	166.85	200.11	0.077	2.93	0.025	0.139	0.079	5.63	7.74
	Inc	13.17	1.77	996.97	0.7	<1.17	111.36	32.37	38.81	186.53	187.57	<0.034	1.3	0.012	<0.058	0.008	1.48	5.8
	2.12	14.52	2.57	1104.41	0.92	<1.04	125.02	27.98	40.5	221.43	212.79	<0.0202	2.19	0.01	<0.047	0.0147	3.15	7.76
	0.48	13.33	2.48	1118.47	1.04	<1.12	145.91	25.73	36.13	245.27	208.97	<0.0238	1.53	<0.0086	0.082	0.0179	3.26	7.86
	0.28	21.88	1.33	1092.48	0.73	1.15	128.88	39.24	61.1	154.24	157.84	<0.035	2.23	0.016	0.154	0.0043	3.62	4.16
	<0.152	6.89	0.21	1017.91	0.56	3.26	136.16	40.01	38.71	140.94	103.49	<0.00	Inc	0.0059	0.21	0.0102	5.33	1.68
	<0.171	Inc	Inc	1236.25	1.09	<1.00	141.71	38.87	48	144.24	155.44	0.056	0.94	0.037	0.082	0.0303	3.82	5.99
Oravita	**Mn55**	**Co59**	**Ni60**	**Zn66**	**Ga69**	**As75**	**Se82**	**Ag107**	**Cd111**	**In115**	**Sn118**	**Sb121**	**Te125**	**Au197**	**Hg202**	**Tl205**	**Pb207**	**Bi209**
ORV1	<0.14	<0.00	<0.00	220.62	0.061	1.47	44.95	2.7	1.15	8.14	0.73	0.301	0.72	<0.0063	<0.080	<0.00255	0.98	0.043
	<0.104	0.35	<0.00	474.7	0.412	<0.94	52.85	4.97	3.6	12.16	3.52	0.037	<0.00	<0.00	0.086	<0.00140	1.22	0.108
	<0.126	0.109	<0.00	337.34	0.188	2.65	38.64	3.88	1.17	7.91	0.55	4.83	0.41	0.008	<0.067	0.0094	3.85	0.129
	0.26	0.106	<0.00	288.7	0.201	<1.32	40.11	3.73	1.08	9.46	0.71	0.084	0.44	<0.00	<0.072	<0.00	1.59	0.276
	0.47	0.177	<0.00	186.54	0.101	<1.80	49.23	3.21	1.01	10.58	0.15	9.58	0.66	0.0065	0.334	0.0175	4.9	0.04
	0.3	0.184	<0.188	24.11	0.042	<2.12	27.78	3.65	1.01	6.24	1.59	4.76	<0.00	0.027	0.15	0.017	15.67	0.423
	0.6	0.214	<0.00	226.55	0.292	<2.41	66.87	1.45	0.23	8.73	1.61	2.8	<0.00	<0.00	0.38	0.0043	2.45	0.089
	0.34	<0.0261	<0.00	234.55	0.294	<1.64	50.07	3.38	0.88	10.21	1.54	<0.0203	0.48	<0.00	<0.090	<0.00	0.353	0.173
	0.15	0.11	<0.00	160.44	0.235	<1.41	17.31	1.45	<0.00	2.89	<0.090	1.53	<0.00	0.023	<0.075	<0.00199	0.69	0.07
	<0.138	0.189	<0.00	325.48	0.114	3.77	44.23	1.07	1.14	9.74	0.97	<0.0250	<0.00	<0.00	0.076	<0.00	1.71	0.152
Oravita	**Mn55**	**Co59**	**Ni60**	**Zn66**	**Ga69**	**As75**	**Se82**	**Ag107**	**Cd111**	**In115**	**Sn118**	**Sb121**	**Te125**	**Au197**	**Hg202**	**Tl205**	**Pb207**	**Bi209**
ORV4	<0.155	0.075	<0.00	136.6	0.405	6.06	<1.86	1.17	0.96	4.22	4.2	5.26	<0.00	0.019	<0.082	0.04	9.82	0.029
	0.32	<0.00	<0.00	167.41	0.171	<1.52	17.58	2.15	0.52	9.02	<0.116	0.86	<0.00	<0.00	<0.071	0.0023	5.33	0.249

	0.28	<0.00	<0.00	143.72	1.53	2.29	3.15	2.02	0.64	8.82	4.05	0.157	0.45	<0.00	0.103	<0.00	0.361	0.0135
	<0.16	0.049	<0.00	172.71	<0.00	2.74	9.31	4	1.28	9.5	2.12	0.185	0.37	<0.00	<0.063	<0.00	0.101	0.0196
	0.25	0.061	<0.00	142.38	0.292	2.57	<1.92	1.64	0.68	7.24	2.84	5.33	<0.00	<0.0088	<0.069	0.0173	1.55	0.025
	0.15	<0.00	<0.00	158.05	0.162	3.81	5	6.76	0.69	7.47	2.94	<0.0206	<0.00	<0.00	<0.060	<0.00	9.67	0.028
	<0.16	0.159	<0.00	147.44	0.127	3.54	<1.55	1.51	1.47	7.82	4.2	<0.037	<0.00	<0.00	0.074	<0.00252	0.7	0.191
	0.55	<0.00	<0.146	129.36	0.356	1.48	<1.60	7.8	2.32	8.97	1.53	0.092	<0.00	<0.00	0.112	<0.00	0.105	0.067
	0.39	0.048	<0.00	143.61	0.285	<1.48	7.53	1.26	1.6	9.8	0.187	6.16	<0.00	<0.00	0.082	0.0198	1.82	0.053
	0.49	0.041	<0.00	218.12	0.339	2.1	<2.15	0.97	2.5	7.76	3.23	0.117	<0.00	<0.0096	0.281	<0.00	0.041	<0.0061
Oravita	**Mn55**	**Co59**	**Ni60**	**Zn66**	**Ga69**	**As75**	**Se82**	**Ag107**	**Cd111**	**In115**	**Sn118**	**Sb121**	**Te125**	**Au197**	**Hg202**	**Tl205**	**Pb207**	**Bi209**
ORV4a	<0.17	<0.00	<0.00	129.36	0.52	2.83	<1.74	0.83	1.32	7.81	3.32	<0.037	<0.00	<0.00	0.068	<0.00	0.174	<0.013
	0.19	0.046	<0.00	148.1	0.057	<1.38	14.38	6.25	1.38	11.66	2.47	16.97	<0.00	<0.0093	0.091	0.118	0.508	0.057
	0.18	<0.00	<0.00	142.39	0.327	<1.18	4.31	11.5	<0.118	7.78	3.51	2.24	0.41	0.007	0.08	0.0043	10.25	3.12
	<0.21	<0.00	<0.00	100.96	0.276	<1.54	<2.32	6.07	0.39	9.39	3.12	1.01	0.88	<0.00	0.18	<0.00	0.99	0.066
	0.42	<0.00	<0.00	84.28	0.268	1.8	13.52	13.61	1.84	10	2.39	0.3	<0.00	<0.0109	<0.057	0.0026	11.63	<0.0100
	0.26	<0.00	0.27	139.98	0.233	<1.28	<1.87	14.36	0.45	8.1	1	0.286	<0.00	<0.009	0.255	<0.00	0.355	0.116
	<0.18	<0.039	<0.00	186.87	0.044	<1.31	18.72	9.67	3.35	9.53	0.77	68.04	0.44	<0.00	0.13	0.281	13.66	0.103
	<0.19	<0.00	<0.00	145.64	0.22	Inc	4.67	8.73	2.81	10.1	1.36	6.45	<0.00	0.028	<0.065	0.058	1.26	0.054
	<0.134	<0.00	<0.00	162.94	0.248	<1.30	6.82	5.35	0.47	8.42	1.81	0.045	0.43	0.008	0.175	<0.00	<0.00	<0.0079
	0.17	0.05	<0.00	155.43	0.122	1.46	32.61	3.5	0.69	9.19	0.44	8.34	<0.00	<0.0102	0.14	0.0077	1.04	<0.00
Oravita	**Mn55**	**Co59**	**Ni60**	**Zn66**	**Ga69**	**As75**	**Se82**	**Ag107**	**Cd111**	**In115**	**Sn118**	**Sb121**	**Te125**	**Au197**	**Hg202**	**Tl205**	**Pb207**	**Bi209**
ORV4B	0.244	<0.0074	<0.00	11.35	0.035	<0.74	<0.74	0.302	1	0.0415	0.426	0.103	0.21	0.0141	<21.33	0.0065	24.58	2.62
	<0.098	0.0096	0.036	Inc	0.2	1.01	6.04	0.292	1.84	0.0958	0.444	0.169	0.69	0.028	35.52	0.0043	Inc	1.823
	0.09	<0.0062	<0.0258	Inc	0.203	<0.84	16.77	0.26	1.34	2.62	0.54	0.133	0.228	0.028	<20.12	0.0016	11.45	3.2
	<0.087	<0.0073	<0.0249	5.61	0.329	<0.80	5.23	0.262	0.173	0.493	0.362	0.22	0.151	0.021	<21.61	0.0025	11.99	3.78
	0.12	0.09	0.036	40.19	0.486	Inc	3.44	6.2	2.71	0.297	0.247	0.929	0.41	0.047	28.52	0.13	96.1	5.16
	<0.113	<0.0096	<0.00	9.54	0.323	<1.06	6.54	0.825	0.213	1.088	0.339	0.131	0.64	0.0195	<34.67	0.098	19.08	5.77
	0.167	<0.00	<0.0265	38.23	0.298	<0.85	10.06	0.9	0.179	0.5	0.531	0.838	1.13	0.026	48.8	0.0169	69.55	4.11
	<0.086	<0.0059	0.082	9.82	0.384	Inc	15.7	2.09	0.223	0.664	0.361	0.775	0.53	0.052	<21.21	0.0206	52.79	11.12
	0.136	0.0092	<0.0271	6.03	0.238	<0.87	61.5	1.166	0.418	2.16	1.038	0.254	0.278	0.052	<24.48	0.0042	21.94	7.21
	<0.089	0.0123	0.058	Inc	0.284	<0.82	5.42	0.561	2.53	0.163	0.046	0.227	0.205	Inc	30.3	0.648	5.04	1.875
Asarel	**Mn55**	**Co59**	**Ni60**	**Zn66**	**Ga69**	**As75**	**Se82**	**Ag107**	**Cd111**	**In115**	**Sn118**	**Sb121**	**Te125**	**Au197**	**Hg202**	**Tl205**	**Pb207**	**Bi209**
ASR 5A	0.115	0.0071	<0.051	12.1	0.446	<0.80	9.67	0.623	0.22	0.0053	0.213	0.085	0.22	<0.0061	80.71	0.0046	3.68	0.711

	<0.073	0.0188	<0.00	Inc	0.684	<0.65	10.75	2.36	6.49	0.012	0.394	0.079	0.073	0.0148	29.78	0.0073	13.41	1.458
	1.09	<0.0070	<0.00	7.8	0.206	<0.93	6.89	2.82	0.88	0.0102	<0.041	0.508	0.202	0.051	<23.67	0.0115	17.41	2.23
	0.487	<0.0087	<0.036	87.46	0.281	<1.16	6.08	3.53	10.25	0.0258	0.054	0.761	0.131	0.019	48.24	0.0509	Inc	7.27
	0.145	<0.00	<0.039	15.56	0.397	<1.26	26.26	1.51	0.84	0.11	0.403	0.14	0.45	0.01	<25.55	0.0029	3.77	2.52
	0.415	0.043	<0.00	67.02	0.364	<1.06	13.34	7.23	5.22	0.49	<0.049	0.069	0.4	<0.0063	<24.46	0.0272	Inc	2.42
	2.42	<0.0116	<0.00	Inc	0.658	<1.25	15.8	2.58	Inc	0.427	0.088	0.622	0.33	<0.0095	40.57	0.0069	12.32	3.45
	0.349	0.022	<0.071	10.89	1.15	<1.14	2.29	1.89	0.51	0.442	0.136	1.91	0.119	0.0079	<22.69	0.0132	Inc	4.88
	0.226	<0.0069	<0.040	22.79	0.162	<0.90	17.32	1.43	0.79	0.477	0.262	0.035	0.164	0.0072	64.93	0.0036	8.6	5.46
	<0.082	<0.0041	<0.00	20.44	0.891	<0.75	10.22	2.77	0.431	0.0066	0.254	0.286	0.64	0.0193	39.01	0.0117	19.7	1.087
Asarel	**Mn55**	**Co59**	**Ni60**	**Zn66**	**Ga69**	**As75**	**Se82**	**Ag107**	**Cd111**	**In115**	**Sn118**	**Sb121**	**Te125**	**Au197**	**Hg202**	**Tl205**	**Pb207**	**Bi209**
ASR 10	<0.17	<0.00	<0.00	12.03	0.54	<1.38	<1.95	1.85	0.72	3.19	0.192	0.078	<0.00	0.016	0.178	<0.00	7.22	0.884
	0.39	<0.00	<0.00	16.74	0.393	<1.33	46.64	1.45	0.45	16.6	3.13	0.042	<0.00	<0.00	<0.053	<0.00	2.45	0.643
	<0.15	<0.00	<0.00	10.01	0.306	<1.35	25.64	1.43	<0.00	8.75	1.87	<0.0248	0.3	0.016	0.084	<0.00	3.21	1.67
	<0.17	<0.00	<0.00	9.77	0.469	<1.33	4.18	2.67	0.39	3.13	0.54	<0.034	<0.00	0.019	<0.051	<0.00	1.62	0.476
	<0.17	<0.00	<0.00	13.31	0.46	1.45	48.8	2.45	0.23	14.01	1.77	0.043	<0.00	<0.00	<0.050	0.0048	2.42	0.705
	0.88	<0.00	<0.00	3.88	0.039	<1.20	44.75	6.54	<0.00	9.53	0.31	0.75	<0.00	0.029	0.097	0.093	29.58	5.47
	<0.134	<0.00	<0.00	8.19	1.13	1.31	3.93	2.14	<0.118	2.27	0.87	0.086	0.39	<0.00	<0.039	0.0022	2.86	0.354
	<0.22	<0.034	0.38	16.28	0.085	<1.74	<2.64	3.34	<0.00	6.04	<0.18	<0.046	<0.00	0.033	0.073	0.0036	2.92	0.857
	0.51	<0.0225	Inc	10.7	0.89	<1.17	2.79	4.26	0.6	3.57	0.187	0.033	<0.00	0.023	0.099	<0.00	2.95	0.809
	<0.18	<0.00	<0.00	10.39	0.75	<1.46	<2.01	2.12	0.24	3.22	0.109	0.091	0.45	0.031	<0.049	0.0115	3.25	0.818
Asarel	**Mn55**	**Co59**	**Ni60**	**Zn66**	**Ga69**	**As75**	**Se82**	**Ag107**	**Cd111**	**In115**	**Sn118**	**Sb121**	**Te125**	**Au197**	**Hg202**	**Tl205**	**Pb207**	**Bi209**
ASR KB P12077	<0.19	0.038	<0.00	4.99	0.138	3.04	253.54	2.83	0.64	2.31	0.81	0.079	1.65	0.038	<0.093	<0.00285	5.11	16.45
	<0.17	<0.00	<0.00	18.25	0.49	<1.60	292.4	1.04	<0.00	2.68	1.51	<0.0208	<0.00	<0.00	<0.077	<0.00	12.86	29.99
	0.31	0.049	<0.00	8.16	0.292	<1.78	288.62	1.96	0.81	2.39	0.47	<0.047	<0.00	0.008	<0.083	<0.00	4.93	8.66
	<0.13	0.054	<0.163	7.7	<0.0242	<1.36	232.86	1.67	0.9	2.23	0.71	0.195	0.46	0.018	<0.061	0.0027	5	15.89
	<0.14	<0.00	<0.00	8.43	0.245	<1.41	136.01	1.11	0.38	3.56	1.27	<0.0191	<0.00	<0.00	<0.067	0.0034	2.02	5.57
	1.08	<0.00	<0.00	5.02	0.209	<1.74	164.75	7.49	1.6	2.52	1.34	0.354	<0.00	0.059	0.244	0.209	90.48	63.51
	<0.134	0.045	<0.00	5.22	<0.00	1.49	148.48	2.52	1.23	2.99	1.03	<0.032	0.37	0.015	<0.053	0.0045	17.65	19.36
	0.25	<0.00	<0.00	8.17	0.225	<1.41	217.37	1.07	<0.00	2.53	1.13	<0.0290	<0.00	0.014	<0.068	<0.00	5.07	15.49
	<0.17	<0.00	<0.00	3.93	0.162	4.62	205.64	1.27	0.74	2.53	1.19	<0.0220	<0.00	0.008	<0.078	0.0045	7.83	23.17
	1.46	<0.00	<0.00	14.3	0.22	<2.24	324.96	0.19	0.99	4.45	0.71	<0.033	2.95	<0.00	0.22	<0.00	4.84	3.85

Bor	**Mn55**	**Co59**	**Ni60**	**Zn66**	**Ga69**	**As75**	**Se82**	**Ag107**	**Cd111**	**In115**	**Sn118**	**Sb121**	**Te125**	**Au197**	**Hg202**	**Tl205**	**Pb207**	**Bi209**
BOR14	3.48	0.111	<0.238	82.17	0.274	<2.01	<3.40	7.02	0.38	0.583	13.53	0.279	<0.00	0.012	<0.101	0.019	16.25	5.83
	3.39	<0.00	<0.00	96.37	<0.00	<1.46	2.92	6.44	0.79	0.419	16.76	<0.0274	<0.00	0.019	0.291	0.011	5.24	3.51
	2.28	<0.00	<0.00	75.53	<0.00	2.45	3.95	13.17	0.94	0.862	16.16	0.275	<0.00	0.086	<0.071	0.251	22.49	6.29
	2.41	<0.042	<0.00	76.97	0.076	<1.37	2.98	3.29	0.93	0.668	12.43	0.1	<0.00	<0.00	<0.052	0.196	19.52	4.75
	<0.26	0.134	<0.00	9.4	0.054	<1.93	<2.68	31.23	<0.00	0.678	4.07	0.041	<0.00	0.067	0.207	0.366	2.61	8.66
	<0.16	<0.00	<0.00	2.11	<0.0303	<1.13	6.08	20.25	<0.00	0.915	8.31	0.293	0.37	0.149	<0.052	0.28	1.24	8.71
	5.75	0.05	<0.00	72.03	0.119	<1.49	<1.80	17.09	3.36	1.059	37.48	<0.029	<0.00	0.037	<0.056	0.46	30.19	12.62
	2.48	0.055	<0.00	69.95	0.389	<1.41	2.72	8.67	0.26	0.694	30.88	0.13	<0.00	0.12	<0.061	0.216	9.09	7.02
	1.65	<0.00	<0.00	78.96	0.13	4.16	<2.05	8.19	0.26	0.411	14.51	0.131	<0.00	0.136	0.103	0.466	14.06	2.97
	2.03	0.162	<0.00	85.63	0.32	<1.51	<1.71	1.96	0.77	0.628	7.73	0.033	<0.00	0.023	0.108	0.0052	2.1	1.3
Elastite	**Mn55**	**Co59**	**Ni60**	**Zn66**	**Ga69**	**As75**	**Se82**	**Ag107**	**Cd111**	**In115**	**Sn118**	**Sb121**	**Te125**	**Au197**	**Hg202**	**Tl205**	**Pb207**	**Bi209**
Elastite b a	0.25	0.92	<0.00	<0.98	0.75	<1.30	211.08	1.42	<0.00	2.55	3.77	0.492	<0.191	<0.00	<0.061	0.0088	10.99	0.229
	0.59	0.88	<0.00	<0.68	0.487	<1.13	285.5	2.52	<0.00	1.92	3.76	0.251	0.64	0.012	<0.058	<0.00	6.47	0.07
	0.69	0.64	<0.00	<0.77	<0.00	<1.37	964.25	9.31	<0.00	2.82	1.31	0.71	Inc	<0.00	0.131	0.007	Inc	3.31
	<0.157	0.194	<0.00	1	<0.00	<1.27	291.31	Inc	0.31	2.68	0.255	2.23	Inc	Inc	<0.058	0.146	Inc	Inc
	<0.18	0.6	<0.00	0.97	<0.00	1.93	114.95	0.71	<0.126	2.54	0.46	2	0.37	<0.00	<0.063	0.064	23.16	1.82
	<0.146	0.59	<0.00	1.12	0.62	<1.15	275.27	2.19	<0.108	2.51	3.12	0.178	0.74	<0.00	<0.054	0.0109	23.38	0.165
	0.28	2.6	<0.00	5.28	0.452	<1.40	321.12	2.1	0.53	2.33	4.31	0.187	<0.206	<0.00	0.098	0.0022	10.5	0.028
	3.69	0.61	<0.00	<0.58	1.13	<1.13	117.82	5.96	<0.106	2.21	1.69	2.68	<0.00	<0.00	0.048	0.136	25.7	0.98
	0.2	0.604	<0.00	<0.54	<0.00	<1.53	283.33	1.24	0.22	2.43	1.26	0.085	Inc	<0.011	<0.064	0.0167	Inc	0.363
	<0.18	0.57	<0.00	1.86	<0.00	<1.38	261.44	Inc	<0.00	2.47	<0.088	1.11	Inc	Inc	0.19	0.07	Inc	2.85
Elastite	**Mn55**	**Co59**	**Ni60**	**Zn66**	**Ga69**	**As75**	**Se82**	**Ag107**	**Cd111**	**In115**	**Sn118**	**Sb121**	**Te125**	**Au197**	**Hg202**	**Tl205**	**Pb207**	**Bi209**
ELS 157	<0.15	<0.00	<0.00	36.92	1.51	<1.25	3.64	13.76	0.67	0.276	0.185	3.77	0.38	0.021	<0.072	0.0072	65.5	1.64
	0.26	<0.00	<0.00	52.2	0.7	<1.36	2.81	6.45	0.23	0.346	0.186	0.71	0.39	0.014	<0.063	<0.00	16.98	0.191
	1.02	<0.00	<0.00	29.32	0.61	<1.21	2.59	10.15	1.14	0.394	0.16	1.32	<0.00	0.06	<0.061	<0.00	41.67	1.13
	1.29	<0.00	<0.00	27.94	0.99	<1.42	2.95	8.81	0.65	0.467	<0.111	1.88	<0.00	<0.00	0.41	<0.00	38.78	0.71
	1.58	<0.00	<0.00	25.18	0.77	1.89	<2.47	18.07	0.85	0.249	<0.098	6.25	<0.00	0.034	0.096	0.036	Inc	Inc
	0.36	0.217	<0.00	30.23	1.2	5.55	3.5	29.57	Inc	0.383	<0.178	12.76	0.62	0.06	<0.092	0.029	Inc	Inc
Vorta	**Mn55**	**Co59**	**Ni60**	**Zn66**	**Ga69**	**As75**	**Se82**	**Ag107**	**Cd111**	**In115**	**Sn118**	**Sb121**	**Te125**	**Au197**	**Hg202**	**Tl205**	**Pb207**	**Bi209**
DMV 99-22	0.17	<0.00	<0.00	451.08	0.35	3.19	<1.43	29.73	2.07	0.0049	<0.073	3.23	<0.00	0.032	0.465	0.0138	8.22	0.0102
	<15.21	11.71	<0.00	Inc	<2.75	Inc	<120.95	Inc	Inc	0.76	Inc	Inc	Inc	Inc	Inc	Inc	Inc	2.24

	<0.19	<0.00	<0.00	198.61	0.98	2.82	<1.89	51.63	0.48	<0.0045	0.73	2.63	<0.00	0.022	0.403	0.167	52.59	<0.00
	Inc	<0.00	<0.00	Inc	2.15	5.78	<2.09	92.43	Inc	<0.00	0.23	3.88	<0.00	Inc	2.6	0.059	Inc	<0.0099
	0.83	<0.00	<0.00	Inc	1.29	4.5	<1.39	53.3	Inc	<0.00	0.37	5.59	<0.00	<0.00	1.04	0.081	Inc	<0.0100
	0.42	<0.00	<0.00	395.46	0.105	<1.46	<1.68	56.49	1.3	<0.00	0.192	0.112	<0.00	Inc	0.339	<0.0042	6.05	0.0188
	<0.20	<0.036	<0.00	479.09	0.63	Inc	<1.94	18.18	2.23	0.023	0.79	Inc	<0.294	0.008	0.35	0.058	Inc	<0.0074
	0.51	<0.034	<0.00	538.33	1.44	5.21	<2.09	51.43	3.19	<0.00	<0.116	3.51	<0.00	0.034	0.59	0.161	Inc	<0.00
Kapp Mineral	**Mn55**	**Co59**	**Ni60**	**Zn66**	**Ga69**	**As75**	**Se82**	**Ag107**	**Cd111**	**In115**	**Sn118**	**Sb121**	**Te125**	**Au197**	**Hg202**	**Tl205**	**Pb207**	**Bi209**
kmi 2a	Inc	0.393	Inc	268.65	0.124	<1.18	4.61	169.52	1.88	1.863	16.39	20.19	<0.00	0.014	<37.36	0.0117	Inc	0.526
	43.12	0.083	0.233	Inc	0.233	<1.26	4.77	197.57	9.11	1.846	19.01	17.26	<0.00	<0.0029	84.49	0.0426	Inc	0.42
	0.336	0.062	0.304	457.96	0.119	<1.03	3.2	230.23	5.35	1.023	16.09	45.01	0.106	0.0056	<31.36	0.0707	Inc	Inc
	1.033	<0.00	0.039	172.81	0.13	2.37	1.03	169.19	2.51	1.67	14.52	41.26	<0.049	0.0106	75.72	0.0717	Inc	0.96
	24.14	0.386	0.723	264.58	0.108	<1.01	2.4	97.98	2.85	1.92	15.42	29.06	<0.00	0.0034	61.92	0.089	Inc	0.152
	48.27	Inc	Inc	130.91	0.153	Inc	Inc	185.41	2.47	0.638	9.21	64.02	0.11	0.0047	102.72	0.098	Inc	Inc
	5.56	0.104	0.312	358.42	0.204	1.34	0.99	257.72	2.85	1.64	20.67	21.04	<0.00	0.031	Inc	0.0502	Inc	0.0253
	Inc	0.228	0.688	85.06	0.179	1.77	2.1	104.22	1.28	0.747	7.89	17.41	<0.051	0.0113	67.84	0.0481	Inc	0.131
	3.52	0.158	<0.035	206.15	0.196	1.69	3.09	155.74	1.74	1.67	14.87	11.77	0.073	0.0117	Inc	0.0353	Inc	0.114
Broken Hill	**Mn55**	**Co59**	**Ni60**	**Zn66**	**Ga69**	**As75**	**Se82**	**Ag107**	**Cd111**	**In115**	**Sn118**	**Sb121**	**Te125**	**Au197**	**Hg202**	**Tl205**	**Pb207**	**Bi209**
BH73	Inc	0.431	0.177	897.89	7.6	<0.150	<6.61	1286.9	1.7	1.46	268.73	Inc	Inc	<0.0139	<0.087	0.305	Inc	<0.022
	48.17	1.09	0.164	Inc	4.95	<0.199	<5.90	1060.2	4.53	1.72	288.1	0.8	<0.22	<0.0113	<0.071	0.0135	25.97	<0.0176
	15.56	0.556	<0.047	474.65	4.58	<0.177	<4.68	1450.34	<0.19	1.94	364.55	1.15	<0.00	<0.0075	0.116	0.0348	11.58	0.0176
	49.34	3.09	0.312	707.89	7.03	<0.159	<5.07	963.15	1.84	1.57	252.85	1.53	<0.00	<0.0093	<0.058	0.0082	26.91	0.026
	Inc	3.23	Inc	516.97	5.58	<0.157	<5.23	798.03	0.93	2.04	362.66	Inc	<0.32	0.0109	<0.063	0.134	Inc	<0.0152
Broken Hill	**Mn55**	**Co59**	**Ni60**	**Zn66**	**Ga69**	**As75**	**Se82**	**Ag107**	**Cd111**	**In115**	**Sn118**	**Sb121**	**Te125**	**Au197**	**Hg202**	**Tl205**	**Pb207**	**Bi209**
BH262	2.59	0.054	<0.00	588.4	14.47	<1.37	<1.61	89.47	2.25	1.65	498.91	0.53	<0.00	<0.00	0.234	<0.00	2.78	<0.00
	1.34	1.24	<0.00	337.74	16.89	<1.33	<1.41	337.04	0.8	0.97	274.65	1.76	<0.00	<0.00	0.107	0.0093	3.29	0.035
	1.85	0.73	0.85	532.38	6.75	2.29	<1.35	24.1	2.15	1.26	342.44	0.172	<0.181	0.008	0.08	<0.00	0.96	<0.00
	4.73	0.035	<0.00	529.09	5.81	<1.13	<1.44	182.63	1.68	1.22	367.99	0.062	<0.00	<0.00	0.112	0.0047	1.47	<0.00
	5.1	<0.00	<0.131	690.16	4.61	<1.09	<1.33	39.81	5.42	1.19	383.64	0.73	<0.00	<0.0081	0.159	<0.0037	7.74	<0.0055
	1.17	1.6	1.23	432.5	7.77	2.84	<1.15	32.95	2.34	1.23	421.71	0.319	<0.236	<0.00	<0.070	<0.00311	1.3	<0.0066
	3.02	0.155	<0.00	410.41	4.56	<1.23	<1.54	281.4	1.86	1.29	399.7	1.09	<0.00	<0.00	<0.066	<0.00	2.88	<0.00
	1.68	<0.00	<0.00	242.79	5.56	1.95	<1.38	18.63	0.5	1.05	346.58	0.3	<0.00	<0.0075	0.103	<0.00	1.97	<0.00
	1.92	0.119	<0.00	407.08	6.1	<1.62	<2.05	66.55	3.34	1.3	360.18	0.86	<0.00	<0.00	<0.091	0.0046	2.21	<0.00

	1.75	0.5	<0.00	432.57	13.57	<1.14	<1.58	304.32	1.59	1.44	494.8	0.216	<0.00	<0.00	<0.061	<0.0039	0.81	<0.00
Bleikvassli	**Mn55**	**Co59**	**Ni60**	**Zn66**	**Ga69**	**As75**	**Se82**	**Ag107**	**Cd111**	**In115**	**Sn118**	**Sb121**	**Te125**	**Au197**	**Hg202**	**Tl205**	**Pb207**	**Bi209**
Bv-1	2.29	0.051	Inc	359.23	33.72	<0.078	<1.77	614.23	0.84	19.81	787.14	12.33	<0.00	0.075	0.284	0.68	Inc	0.0624
	1.4	<0.00	0.035	463.58	32.94	<0.082	3.23	425.6	1	21.94	1226.33	7.14	<0.00	0.0363	0.262	0.197	5.85	0.0536
	0.469	0.0143	<0.034	366.67	25.64	<0.104	<1.88	443.85	1.16	21.9	1296.75	2.55	<0.00	0.103	0.346	0.159	1.74	0.0065
	5.59	<0.00	<0.0246	387.96	0.094	<0.069	<2.06	400.85	0.69	14.35	123.63	3.96	<0.00	0.111	0.259	0.442	4.27	0.0064
	0.746	<0.00	<0.00	279.95	28.15	<0.127	5.24	1102.3	0.535	15.82	125.04	10.73	<0.086	0.86	0.92	1.74	8.79	0.0404
Bleikvassli	**Mn55**	**Co59**	**Ni60**	**Zn66**	**Ga69**	**As75**	**Se82**	**Ag107**	**Cd111**	**In115**	**Sn118**	**Sb121**	**Te125**	**Au197**	**Hg202**	**Tl205**	**Pb207**	**Bi209**
Bv-4	38.77	0.255	<0.00	472.53	24.02	2.76	6.51	6.99	1.82	43.79	1482.03	7.18	<0.00	<0.00	0.169	0.103	4.08	0.046
	39.03	0.044	<0.00	470.22	25.55	<1.15	4.34	4.31	1.28	37.98	1265.91	3.72	<0.00	<0.0080	<0.067	0.034	2.44	0.0266
	27.89	0.045	0.77	394.5	30.82	2.52	<1.46	5.19	1.91	35.49	1020.7	3.61	<0.00	<0.00	0.158	0.028	1.72	0.023
	18.59	0.22	<0.00	294.04	23.7	<1.30	<1.87	4.69	1.9	34.79	622.12	9.31	<0.00	0.034	0.3	0.039	Inc	Inc
	32.69	<0.00	<0.00	441.88	21.54	1.24	2.46	5.85	0.87	38.18	1202.82	4.73	<0.00	<0.00	0.182	0.08	1.64	0.072
	26.23	0.49	<0.00	352.7	29.92	<1.06	7.4	5.85	2.17	33.8	601.88	3.35	<0.00	<0.00	0.095	0.039	2.59	0.081
	60.48	<0.00	<0.00	462.76	30.73	1.32	3.72	4.39	2.36	35.65	1521.38	2.4	<0.00	<0.00	0.159	0.0146	2.44	0.0238
	35.96	1.14	<0.00	380.85	1.43	<1.05	4.85	Inc	2.17	34.19	668.87	Inc	<0.00	<0.00	0.171	Inc	Inc	0.298
	32.19	0.158	0.22	465.28	15.22	<1.34	<1.85	Inc	1.47	34.48	1227.06	Inc	<0.00	0.0061	0.171	Inc	Inc	0.0217
	31.72	0.028	<0.00	514.7	14.11	<1.42	3.25	5.47	4.26	35.6	1468.32	3.52	<0.00	<0.00	0.271	0.032	1.29	0.039
Bleikvassli	**Mn55**	**Co59**	**Ni60**	**Zn66**	**Ga69**	**As75**	**Se82**	**Ag107**	**Cd111**	**In115**	**Sn118**	**Sb121**	**Te125**	**Au197**	**Hg202**	**Tl205**	**Pb207**	**Bi209**
V598572	46.81	0.0099	0.272	464.43	0.927	0.96	32.87	11.18	4.75	26.51	1025.58	0.168	<0.00	0.007	0.89	0.0014	0.174	0.032
	48.55	0.096	0.305	441.3	1.41	<0.18	19.15	13.46	3.73	24.48	1088.52	1.87	0.35	0.0062	0.7	0.186	0.452	0.0202
	48.65	0.339	0.82	489.73	1.92	<0.15	21.3	17.24	5.31	23.36	1073.57	4.84	<0.00	0.0082	1.6	<0.00132	0.187	<0.0048
	57.93	<0.00	<0.00	475.93	1.64	0.16	14.23	9.3	4.39	23.52	1202.99	0.412	<0.00	0.0062	0.71	0.00139	0.182	0.011
	55.3	0.035	<0.00	479.86	1.54	<0.14	10.17	12.89	4.09	22.17	840.08	0.319	0.31	0.0153	0.93	0.0035	0.176	0.0176
	49.06	1.9	9.17	487.25	1.18	1.96	9.74	15.5	5.48	26.06	1190.48	Inc	<0.00	0.0032	1.24	0.091	20.51	0.0264
	57.29	0.0176	0.095	618.1	1.26	<0.124	<2.34	11	5.29	16.07	965.39	0.423	<0.058	0.0094	0.63	0.0015	0.78	0.0084
	52.65	0.0273	1.34	376.06	1.51	<0.128	10.1	15.49	4	26.61	1149.67	0.5	0.51	0.014	0.6	0.0043	0.456	0.0197
	Inc	0.178	<0.00	573.49	4.33	<0.17	<3.09	3.85	12.96	29.31	619.82	0.79	<0.080	0.0066	0.355	0.0085	1.5	0.084
Mofjell	**Mn55**	**Co59**	**Ni60**	**Zn66**	**Ga69**	**As75**	**Se82**	**Ag107**	**Cd111**	**In115**	**Sn118**	**Sb121**	**Te125**	**Au197**	**Hg202**	**Tl205**	**Pb207**	**Bi209**
Mo5	13.03	0.059	3.18	324.76	0.128	<1.01	7.69	27.59	2.98	0.49	0.63	0.7	<0.00	<0.0095	0.132	<0.00	0.55	<0.0112
	7.35	<0.00	1.2	509.5	0.38	<1.06	10.91	27.63	2.79	1.27	4.4	0.247	<0.00	<0.0103	0.183	0.002	0.98	0.0097
	7.68	<0.0298	1.05	666.67	0.62	<1.19	12.71	26.79	2.97	1.35	4.26	0.419	1.17	<0.00	0.167	<0.00	1.5	<0.0093

	4.3	<0.0291	1.08	497.56	0.59	<1.24	15.91	25.12	3.09	1.14	3.85	0.359	<0.00	<0.00	0.13	<0.0029	1.98	<0.0064
	1.5	<0.0303	0.27	321.07	0.58	<1.16	22.61	28.75	1.87	0.567	2.78	0.369	<0.00	<0.0115	<0.080	0.0065	3.02	0.0071
	4.55	<0.00	1.34	653.03	0.43	<1.19	18.74	24.46	3.37	1.15	4.39	0.26	0.75	0.008	0.125	<0.00287	1.59	0.0072
	5.14	<0.00	1.13	682.21	0.226	<1.12	18.57	26.12	2.49	0.512	2.58	0.58	0.78	0.009	0.271	<0.0047	3.26	0.0224
	3.19	<0.0280	1.81	712.24	0.57	<1.14	16.5	29.11	4.4	0.537	1.6	6.05	1.4	0.008	0.331	0.748	5.13	0.0069
	2.56	<0.00	1.69	631.99	0.283	Inc	12.13	25.5	3.26	0.67	1.59	1.42	1.88	<0.00	0.174	0.48	4.36	<0.00
	4.16	<0.00	0.27	648.31	0.37	<1.19	25.16	23.78	4.24	0.99	3.64	0.85	<0.00	<0.00	<0.055	<0.00	3.76	<0.0092
Mofjell	**Mn55**	**Co59**	**Ni60**	**Zn66**	**Ga69**	**As75**	**Se82**	**Ag107**	**Cd111**	**In115**	**Sn118**	**Sb121**	**Te125**	**Au197**	**Hg202**	**Tl205**	**Pb207**	**Bi209**
Mo16	<0.19	0.038	<0.00	728.85	0.157	10.35	9.94	13.08	82.11	0.067	0.95	8.83	<0.00	<0.00	<0.06	0.017	Inc	<0.0059
	<0.145	<0.019	<0.00	547.03	0.289	9.94	5.16	11.02	50.66	0.12	0.57	0.448	0.55	0.023	<0.039	<0.0024	0.309	<0.00
	0.157	<0.0182	<0.053	514.67	0.301	11.86	10.16	11.03	53.85	0.198	0.67	1.42	0.31	<0.00	<0.041	0.0049	1.2	<0.0040
	<0.142	<0.00	<0.00	551	0.176	13.55	10.47	11.94	50.53	0.2	0.91	1.31	<0.115	<0.0060	<0.041	<0.00234	0.81	0.006
	0.151	0.017	<0.041	621.97	0.104	8.42	6.72	13.13	52.31	0.152	0.43	2.02	<0.126	0.07	<0.036	<0.00183	1.97	<0.00
	0.3	<0.0105	<0.00	540.17	0.13	6.37	9.14	12.18	15.58	0.031	0.78	0.528	0.158	0.045	<0.057	<0.0019	1.97	0.0086
	<0.12	<0.0104	<0.00	650.89	<0.00	5.45	7.47	10.16	25.43	0.0174	0.58	0.59	<0.090	0.017	<0.043	<0.00236	3.11	<0.00318
	0.46	0.05	<0.00	482.02	0.036	<1.86	11.53	10.72	46.69	0.107	0.75	2.47	0.3	0.0072	<0.055	0.035	1.41	<0.0039
	0.36	<0.0132	<0.00	719.12	0.219	2.83	6.2	12.58	52.87	0.152	1.04	5.35	0.95	0.008	<0.058	<0.00141	3.26	<0.0032
	<0.17	<0.0110	<0.00	532.58	0.266	8.54	10.84	10.97	46.74	0.1	0.87	0.78	0.168	0.0042	0.11	<0.00204	0.382	0.0061
Mofjell	**Mn55**	**Co59**	**Ni60**	**Zn66**	**Ga69**	**As75**	**Se82**	**Ag107**	**Cd111**	**In115**	**Sn118**	**Sb121**	**Te125**	**Au197**	**Hg202**	**Tl205**	**Pb207**	**Bi209**
Mo17A	Inc	<0.00	<0.00	250.1	0.236	5.48	<1.79	24.45	32.22	0.248	0.412	29.41	<0.00	0.031	<0.089	0.0175	19.39	0.0332
	Inc	<0.00	0.101	311.82	0.209	10.37	8.49	24.62	30.79	0.239	0.303	40.51	<0.00	0.04	0.12	<0.00193	28.46	0.0305
	Inc	<0.0093	<0.055	361.68	0.393	7.08	7.56	78.52	58.28	0.232	0.28	134.99	0.65	0.084	<0.102	0.0195	69.1	0.342
	Inc	0.032	<0.00	493.46	0.043	5.23	3.84	58.11	45.93	0.279	0.37	157.93	Inc	0.009	0.15	0.124	98.38	0.095
	0.34	<0.0097	<0.00	401.77	0.087	7.78	<2.27	16.14	47.08	0.298	0.429	10.89	0.21	<0.00	<0.101	0.0012	6.4	<0.0042
	Inc	0.013	<0.00	352.22	0.117	7.2	1.71	41.79	55.72	0.242	0.46	94.57	0.29	0.0075	0.18	0.76	77.49	0.048
	<0.13	<0.0122	<0.00	322.62	<0.00	<1.67	<1.72	35.09	54.29	0.442	0.17	95.88	<0.00	<0.00	0.1	<0.00	63.13	0.032
	0.53	<0.00	<0.00	356.95	0.022	2.26	5.19	17.12	35.87	0.229	0.361	12.41	0.34	0.017	0.14	<0.00	6.04	0.0125
	0.15	0.102	<0.00	571.78	0.077	2.64	5.5	16.52	79.88	0.353	0.579	0.639	<0.114	0.0065	<0.10	0.0019	0.517	<0.00
	<0.130	<0.0117	<0.00	510.04	0.349	3.38	3.36	9.51	68.57	0.472	0.58	1.41	<0.00	<0.0074	0.11	<0.00	0.65	<0.00
Sulitjelma	**Mn55**	**Co59**	**Ni60**	**Zn66**	**Ga69**	**As75**	**Se82**	**Ag107**	**Cd111**	**In115**	**Sn118**	**Sb121**	**Te125**	**Au197**	**Hg202**	**Tl205**	**Pb207**	**Bi209**
CV01.1	0.45	10.36	0.063	710.06	0.035	<2.38	191.27	239.53	40.62	0.347	<0.163	<0.144	0.25	0.0058	0.29	<0.00258	1.04	0.155
	0.6	9.92	<0.00	744.19	0.088	<2.86	215.93	270.4	48.76	0.387	<0.166	<0.173	<0.29	<0.0095	<0.151	<0.0045	0.9	0.236

	<0.192	12.19	<0.00	662.54	0.077	2.45	185.48	248.25	48.56	0.452	<0.148	<0.135	0.152	<0.00	0.16	0.0032	1.09	0.381
	0.32	7.35	<0.00	745.22	0.061	3.73	214.18	266.76	44.94	0.471	<0.142	<0.137	0.54	<0.0075	0.22	0.0044	1.72	0.3
	0.255	2.88	0.151	696.7	0.057	2.88	187.71	255.98	43.38	0.459	0.243	<0.132	1.09	<0.00	0.167	<0.0031	1.3	0.515
	0.26	0.91	<0.00	664.12	0.0165	2.7	187.83	212.33	41.39	0.49	0.303	<0.160	0.29	<0.0124	0.26	0.0066	0.343	0.127
	1.08	10.67	<0.00	668.8	0.149	<1.55	175.95	238.36	41.02	0.54	<0.096	<0.087	1.97	<0.00	0.22	0.0036	0.53	0.049
	<0.157	1.58	<0.060	687.05	0.042	<1.90	199.43	289.2	40.97	0.506	<0.131	<0.114	0.33	<0.0092	<0.096	<0.0022	1.32	0.239
	0.53	1.32	<0.00	686.12	<0.021	<2.31	204.32	182.93	41.28	0.565	<0.135	<0.138	1.42	<0.0080	<0.116	<0.0047	0.211	0.088
	0.51	1.21	<0.00	724.8	0.106	<2.21	181.91	273.48	40.36	0.403	0.163	<0.147	1.17	<0.0110	<0.113	<0.0037	0.091	0.064
Sulitjelma	**Mn55**	**Co59**	**Ni60**	**Zn66**	**Ga69**	**As75**	**Se82**	**Ag107**	**Cd111**	**In115**	**Sn118**	**Sb121**	**Te125**	**Au197**	**Hg202**	**Tl205**	**Pb207**	**Bi209**
CV01.2a	0.62	14.19	<0.045	719.39	0.348	<1.77	155.76	272.65	53.57	0.391	0.132	<0.091	4.23	<0.0048	0.15	0.0039	0.48	0.124
	0.837	28.32	0.424	828.35	0.138	1.61	154.8	331.28	58.38	0.368	<0.089	0.269	2.22	<0.0037	0.127	<0.0013	1.39	0.608
	0.73	7.26	0.197	775.93	0.131	<1.90	159.94	269.27	47.88	0.369	<0.118	<0.095	2.38	<0.0054	<0.100	<0.0033	0.19	0.12
	0.318	1.86	<0.00	714.52	0.02	<1.97	156.36	229.89	32.03	0.404	0.144	<0.090	1.56	<0.0078	0.16	0.0035	0.8	0.271
	0.451	2.21	<0.00	861	0.049	<2.03	184.24	267.32	49.8	0.394	0.147	<0.108	1.44	<0.0056	0.29	0.0023	0.74	0.362
	0.453	2.05	0.138	647.94	0.078	2.23	167.08	237.91	32.6	0.452	<0.137	<0.099	1.39	<0.0055	<0.102	<0.00	0.3	0.161
	0.457	6.04	0.118	565.95	0.059	<1.65	167.32	282.05	39.37	0.388	<0.104	<0.081	0.59	<0.0067	0.15	0.0036	0.87	0.427
	0.122	3.45	<0.00	770.9	0.059	<1.35	173.09	Inc	49.41	0.463	<0.086	<0.068	0.8	<0.0038	<0.067	<0.0023	0.71	0.576
	0.171	4.67	<0.00	704.98	0.101	1.55	155.83	258.67	38.63	0.301	<0.099	<0.066	0.67	<0.0037	<0.065	0.0021	1	0.375
	0.201	1.83	<0.00	630.79	0.042	<1.80	183.5	254.64	39.83	0.39	<0.114	<0.099	1.82	<0.0103	<0.091	<0.0026	0.33	0.164
Sulitjelma	**Mn55**	**Co59**	**Ni60**	**Zn66**	**Ga69**	**As75**	**Se82**	**Ag107**	**Cd111**	**In115**	**Sn118**	**Sb121**	**Te125**	**Au197**	**Hg202**	**Tl205**	**Pb207**	**Bi209**
CV01.2b	0.419	0.418	<0.045	532.32	0.021	2.12	180.38	195.46	36.84	2.44	<0.077	<0.075	2.09	<0.0050	0.384	<0.0015	0.073	0.041
	0.222	0.863	<0.00	650.14	0.062	3.5	150.77	157.33	26.4	0.354	<0.069	<0.071	1.68	<0.00	0.112	<0.00219	0.324	0.157
	0.199	0.529	<0.00	553.38	0.037	3.38	155.2	82.5	28.91	0.43	<0.073	<0.069	0.12	<0.00	0.114	0.0048	1.76	0.8
	0.53	1.39	<0.00	646.55	0.07	1.15	150.21	175.93	32.5	0.344	0.221	<0.054	1.08	0.0031	0.076	<0.00	0.679	0.318
	0.168	0.417	<0.044	484.99	0.165	1.75	160.93	144.4	35.37	0.398	0.195	0.283	0.63	<0.0068	<0.068	0.0102	3.63	1.36
	0.197	0.708	<0.00	564.26	0.075	3.62	140.88	176.66	29.81	0.365	0.11	<0.075	1.54	<0.0074	0.208	0.0022	0.132	0.0444
	<0.078	0.91	<0.00	519.46	<0.00	<0.85	141.83	130.78	34.94	0.405	<0.048	<0.050	1.19	<0.00	<0.050	<0.00	2.93	0.849
	0.58	1.78	<0.00	607.47	<0.00	<1.11	144.58	176.1	42.69	0.385	<0.072	<0.062	1.74	<0.0065	0.194	0.0024	0.95	0.566
	0.271	0.99	<0.00	571.71	<0.00	1.55	152.47	189.45	32.16	0.407	0.139	<0.075	1.93	<0.00	<0.074	<0.0016	0.374	0.128
	<0.108	1.12	<0.00	728.11	0.018	2.23	150.92	204.67	39.16	0.325	<0.063	<0.062	1.88	<0.00	0.263	<0.00	0.071	0.051
Sulitjelma	**Mn55**	**Co59**	**Ni60**	**Zn66**	**Ga69**	**As75**	**Se82**	**Ag107**	**Cd111**	**In115**	**Sn118**	**Sb121**	**Te125**	**Au197**	**Hg202**	**Tl205**	**Pb207**	**Bi209**
CV01.3	0.69	0.159	<0.00	385.59	0.212	3.45	926.37	194.54	18.89	0.9	0.38	<0.00	<0.00	<0.00	<0.058	<0.00	0.36	0.56

	0.74	0.116	<0.00	384.94	0.34	1.8	849.8	218.09	19.03	1.03	0.38	<0.048	<0.00	<0.00	<0.053	<0.00	0.08	0.161
	0.25	0.43	<0.144	286.35	0.34	<1.56	871.79	133.4	16.02	0.84	<0.103	<0.046	0.31	<0.0093	0.083	0.004	0.4	0.61
	<0.22	0.188	<0.00	397.11	0.17	<1.56	818.69	148.81	21.97	0.88	0.178	<0.0256	<0.00	<0.00	0.121	0.0046	0.325	0.61
	0.35	0.186	<0.129	336.11	0.21	<1.38	730.36	160.51	24.13	0.95	0.37	<0.033	<0.00	<0.0118	0.085	<0.00	0.33	0.382
	<0.20	0.107	0.36	326.75	0.208	2.84	857.15	192.83	20.09	0.88	0.098	0.054	0.32	<0.00	<0.041	<0.0028	0.098	0.181
	0.4	0.042	<0.00	232.64	<0.00	1.68	866.45	148.89	11.95	0.94	0.175	0.041	<0.00	0.027	<0.041	<0.00	Inc	0.08
	0.55	0.078	<0.00	373.86	0.051	<1.56	834.51	156.88	14.67	0.91	0.37	<0.00	<0.00	<0.00	<0.047	0.0021	0.48	0.56
	<0.21	<0.034	0.19	358.98	0.227	<1.34	842.02	109.91	16.03	1.11	0.55	<0.040	<0.00	<0.00	0.13	0.452	0.256	0.57
	<0.18	0.186	<0.00	413.09	0.239	1.62	890.34	158.94	21.87	1.17	<0.144	<0.0229	0.37	<0.00	0.062	0.0024	0.56	0.47
Sulitjelma	**Mn55**	**Co59**	**Ni60**	**Zn66**	**Ga69**	**As75**	**Se82**	**Ag107**	**Cd111**	**In115**	**Sn118**	**Sb121**	**Te125**	**Au197**	**Hg202**	**Tl205**	**Pb207**	**Bi209**
CV01.4	<0.17	2.55	<0.00	531.36	0.06	<1.17	215.72	208.94	24.6	1.24	0.55	0.034	<0.00	<0.00	0.639	<0.0028	1.63	0.964
	Inc	3.98	0.26	432.74	Inc	1.39	231.91	226.86	24.21	1.053	0.73	0.373	<0.00	<0.00	0.344	0.096	0.84	1.106
	<0.19	2.57	<0.00	552.43	<0.00	<1.20	211.25	205.81	23.38	1.103	0.26	<0.034	<0.00	<0.00	0.16	<0.00302	0.253	0.179
	0.25	1.59	<0.00	651.89	0.06	2.12	226.73	210.03	28	1.15	0.86	0.183	<0.00	<0.00	0.1	<0.00	0.39	0.279
	<0.153	1.23	<0.00	556.45	0.062	<1.04	208.11	192.96	26.77	1.47	0.78	0.472	<0.00	<0.00	0.271	0.055	1.67	0.405
	0.42	0.83	0.32	496.16	0.134	1.43	210.76	170.37	21.48	1.44	0.43	0.157	<0.00	<0.0119	0.177	0.149	1.59	0.643
	0.24	0.82	<0.00	588.66	<0.00	<1.03	196.8	206.75	25.56	1.29	0.43	<0.00	<0.00	<0.00	0.17	<0.0039	1.04	0.843
	0.54	2.73	<0.224	531.93	<0.00	<1.76	201.37	189.92	39.21	1.3	0.27	0.096	<0.00	<0.00	0.18	0.02	0.7	1.12
	0.3	1.36	0.24	581.34	0.05	<1.00	201.49	191.03	27.17	1.13	0.32	<0.0274	0.32	0.0067	<0.056	0.0021	0.52	0.429
	0.26	2.99	<0.00	624.1	0.049	1.74	214.16	220.62	27.3	1.52	0.91	0.06	<0.00	0.013	0.124	<0.00	0.263	0.183
Sulitjelma	**Mn55**	**Co59**	**Ni60**	**Zn66**	**Ga69**	**As75**	**Se82**	**Ag107**	**Cd111**	**In115**	**Sn118**	**Sb121**	**Te125**	**Au197**	**Hg202**	**Tl205**	**Pb207**	**Bi209**
CV01.6b	0.34	0.085	<0.00	335.14	<0.00	<1.16	682.11	170.49	14.18	0.683	<0.103	0.082	<0.00	<0.00	<0.075	0.011	1.36	1.64
	<0.23	0.254	0.3	331.71	0.244	<1.31	732.12	205.71	10.47	0.554	<0.106	<0.064	0.39	<0.00	0.108	0.084	0.92	0.969
	0.33	0.171	0.24	360.93	0.144	<1.10	702.39	186.42	15.85	0.63	0.44	<0.032	<0.194	<0.00	0.114	0.0111	1.27	1.76
	0.33	<0.00	0.25	392.52	0.248	<1.09	679.42	201.65	19.18	0.68	0.289	0.037	<0.00	<0.00	0.19	<0.00	0.66	0.443
	0.41	0.105	0.59	336.51	0.179	<1.37	746.12	223.1	32.59	0.751	0.59	<0.05	<0.241	0.014	0.256	<0.0032	0.5	0.567
	0.2	0.303	0.29	375.28	0.286	1.96	792.58	197.67	25.73	0.708	0.69	<0.00	<0.00	0.008	<0.069	<0.00	0.121	0.316
	<0.20	0.176	<0.00	420.55	0.067	1.42	770.67	169.25	27.38	0.666	0.32	<0.0283	<0.35	<0.00	0.233	0.0095	0.87	1.164
	0.37	0.318	<0.00	503.09	0.087	2.9	746.53	210.13	26.55	0.654	0.091	<0.00	<0.00	<0.0095	<0.050	0.004	0.373	0.219
	0.31	0.176	0.33	425.51	0.101	<1.14	709.82	199.08	27.16	0.63	0.5	<0.039	<0.00	<0.00	<0.067	<0.00263	0.166	0.258
	<0.164	0.27	0.39	454.68	<0.0290	<1.10	662.22	196.88	25.4	0.754	<0.081	0.162	<0.00	<0.00	<0.063	0.0144	1.32	0.757
Sulitjelma	**Mn55**	**Co59**	**Ni60**	**Zn66**	**Ga69**	**As75**	**Se82**	**Ag107**	**Cd111**	**In115**	**Sn118**	**Sb121**	**Te125**	**Au197**	**Hg202**	**Tl205**	**Pb207**	**Bi209**

NC4172	Inc	2.45	<0.00	214.61	0.25	<1.24	34.79	Inc	3	1.9	11.86	10.9	1.66	0.013	<0.076	2.03	Inc	Inc
	Inc	2.6	0.46	Inc	0.27	1.69	12.21	70.36	6.57	4.35	6.65	13.51	<0.00	<0.00	0.14	3.03	Inc	Inc
	6.54	Inc	2.46	342.27	2.62	<1.27	26.24	39.88	3.71	5.71	9.51	4.27	Inc	<0.00	<0.060	0.19	13.01	3.38
	7.42	3.68	1.01	337.87	0.72	2.74	16.17	43.28	4.12	5.38	8.96	10.08	0.37	0.025	0.163	0.25	20.36	5.46
	7.66	2.65	0.24	290.54	<0.0280	<1.34	19.96	48.61	5.75	5.19	8.56	9.81	<0.00	<0.00	0.188	0.519	28.1	6.28
	9.85	2.62	<0.00	333.08	0.6	<1.04	24.53	42.89	4.72	6.89	9.82	9.32	0.59	<0.00	0.051	0.781	22.54	4.89
	5.67	7.6	1.29	289.13	0.334	<1.43	26.49	38.39	1.71	7.56	11.43	13.51	0.64	0.014	0.191	0.365	26.53	5.66
	8.1	4.3	0.79	344.77	0.62	<1.24	21.87	49.42	4.38	8.2	11.37	15.23	1.78	0.013	0.092	0.416	23.95	8.15
	7.4	3.53	0.24	284.97	0.218	<1.54	17.77	42.8	2.92	4.18	8.57	7.82	<0.00	0.025	<0.068	0.548	17.95	7.36
	7.57	4.87	<0.00	384.78	0.67	<1.42	22.19	38.84	2.77	5.06	9.21	7.94	0.97	0.0072	0.106	0.34	18.32	4.18
Sulitjelma	**Mn55**	**Co59**	**Ni60**	**Zn66**	**Ga69**	**As75**	**Se82**	**Ag107**	**Cd111**	**In115**	**Sn118**	**Sb121**	**Te125**	**Au197**	**Hg202**	**Tl205**	**Pb207**	**Bi209**
NC5839	<1.56	0.3	0.208	370.5	13.99	<1.63	42.14	36.2	2.6	7.14	75.38	2.69	0.44	0.088	<0.19	<0.019	2.54	0.16
	<1.62	1.093	0.295	414.43	13	<1.65	41.1	34.96	2.62	6.48	64.21	1.36	1.16	<0.0304	<0.18	<0.023	0.7	0.066
	<2.08	0.23	0.119	726.12	9.16	<2.10	51.83	34.85	5.71	7.81	71.46	1.33	2.02	<0.032	0.34	<0.021	1.18	0.96
	<1.29	0.392	<0.042	521.45	8.26	<1.31	65.2	37	3.47	4.87	55.08	3.37	<0.00	<0.014	<0.135	0.022	2.33	0.319
	<1.34	1.17	0.229	346.53	11.67	<1.37	48.91	44.7	4.03	6.08	65.76	1.98	2.62	<0.0201	<0.14	<0.009	1.63	0.065
	<1.87	1.42	0.51	768.43	9.58	3.1	52.51	51.04	4.62	6.4	67.68	2.31	<0.37	0.031	<0.20	<0.022	1.64	0.78
	<1.12	0.506	0.243	462.82	8.85	<1.11	43.79	35.16	0.79	4.29	59.07	0.65	0.93	<0.0292	<0.122	<0.0094	0.12	<0.0222
	2.19	1.59	<0.041	381.35	19.1	<1.27	38.4	36.45	1.52	6.79	70.38	1.08	0.46	<0.027	<0.124	<0.012	0.95	0.059
	<1.07	1.99	0.125	388.66	11.92	<1.08	42.89	40.9	1.7	5.78	61.37	0.5	1.1	<0.016	<0.106	<0.0158	2.1	0.028
	<1.15	1.88	0.049	333.03	12.72	<1.15	36.43	31.69	1.02	7.17	70.45	0.222	2.23	<0.017	0.36	<0.0084	0.39	<0.0198
Sulitjelma	**Mn55**	**Co59**	**Ni60**	**Zn66**	**Ga69**	**As75**	**Se82**	**Ag107**	**Cd111**	**In115**	**Sn118**	**Sb121**	**Te125**	**Au197**	**Hg202**	**Tl205**	**Pb207**	**Bi209**
NC6894	<0.10	0.131	<0.00	119.08	0.5	5.33	62.01	6.76	1.06	18.72	49.32	<0.076	2.63	0.105	0.72	<0.00240	0.171	0.024
	<0.20	0.016	<0.130	146.6	0.352	<2.51	74.92	5.05	2.49	18.85	51.32	0.151	1.38	0.029	0.74	<0.00242	0.135	0.029
	<0.132	<0.0093	<0.00	127	0.415	2.25	60.18	6.72	2.58	18.31	57.97	<0.090	1.84	<0.0079	0.32	<0.0034	0.321	0.054
	0.32	0.016	<0.00	137.89	0.385	5.04	74.83	7.42	2.21	17.28	52.99	0.125	0.7	0.056	0.44	<0.00202	0.63	0.051
	0.5	<0.014	<0.00	124.28	0.184	5.24	77.85	11.64	2.4	25.84	44.02	0.3	0.48	0.074	0.13	0.0016	1.19	0.198
	<0.155	<0.020	<0.00	119.5	0.258	3.04	77.88	11.04	2.2	22.88	59.06	0.179	0.29	<0.0106	0.1	<0.0018	0.386	0.073
	0.33	<0.0247	0.094	114.85	0.264	<2.40	72.06	10.26	2.53	19.49	59.26	<0.120	0.63	0.127	0.55	0.0056	0.49	0.0187
	<0.133	<0.00	<0.00	129.91	0.53	4.11	54.66	9.1	1.42	18.05	42.83	0.201	0.66	0.034	0.13	<0.0033	0.285	0.106
	0.58	<0.00	<0.00	126.88	0.51	<1.59	53.15	10.58	2.84	21.2	50.64	0.191	1.21	0.013	0.14	<0.00214	0.8	0.147
	0.29	0.0164	<0.00	134.75	0.332	<1.84	69.39	5.91	1.49	21.39	62.04	<0.109	1.81	0.031	0.62	<0.0036	0.143	0.029

Sulitjelma	**Mn55**	**Co59**	**Ni60**	**Zn66**	**Ga69**	**As75**	**Se82**	**Ag107**	**Cd111**	**In115**	**Sn118**	**Sb121**	**Te125**	**Au197**	**Hg202**	**Tl205**	**Pb207**	**Bi209**
Su3	<0.170	1.71	2.55	148.44	0.227	<1.33	10.5	27.56	2.51	13.49	29.09	<0.036	0.75	0.202	0.29	<0.00	0.201	3.09
	1.21	3.25	1.37	105.97	0.329	<1.47	11.98	29.65	4.44	13.24	14.88	0.115	0.72	0.077	0.085	<0.00	3.33	7.71
	<0.17	1.49	1.19	105.28	0.333	<1.22	8.43	45.26	3.11	12.89	30.27	0.025	1.24	0.123	0.17	0.0019	2.56	4.51
	2.66	3.12	5.05	138.24	0.394	<1.21	6.5	26.28	2.22	13.11	28.83	0.257	0.36	0.76	0.136	<0.00264	1.58	6.98
	0.83	1.97	4.31	97.46	0.46	<1.52	4.4	40.76	3.11	14.71	13.67	Inc	0.62	0.54	0.32	0.0037	5.74	7.71
	<0.15	2.66	3.55	113.29	0.55	<1.13	4.71	15.65	4.29	14.47	8.94	<0.0311	0.91	0.112	0.1	<0.0034	0.54	3.63
	<0.171	2.88	3.99	147.12	0.107	2.05	10.34	25.05	2.58	14.23	21.32	<0.033	0.39	0.098	0.062	<0.00	4.1	11.44
	<0.17	2.37	2.42	247.17	0.55	<1.38	7.22	15.92	3.49	13.29	27.26	0.047	0.77	0.062	0.06	0.0023	0.319	3.9
	<0.22	2.67	3.93	262.59	0.5	1.72	7.91	28.76	3.87	13.97	29	<0.054	0.45	0.106	0.16	<0.0049	6.24	4.48
	0.59	2.08	2.45	112.18	0.43	<1.31	14.92	52.74	3.62	13.09	17.63	0.142	0.76	0.27	0.107	<0.00265	0.2	5.35
Sulitjelma	**Mn55**	**Co59**	**Ni60**	**Zn66**	**Ga69**	**As75**	**Se82**	**Ag107**	**Cd111**	**In115**	**Sn118**	**Sb121**	**Te125**	**Au197**	**Hg202**	**Tl205**	**Pb207**	**Bi209**
Sulis 1b	3.58	<0.00	<0.00	407.41	6.58	1.59	55.06	30.34	1.98	5.27	43.06	0.87	0.58	<0.00	0.369	0.0057	0.584	0.121
	3.77	0.104	<0.00	546.37	7.92	<1.05	56.94	34.53	3.6	6.93	60.18	1.78	0.9	<0.00	0.329	0.0039	0.87	0.06
	4.27	0.88	0.85	487.8	7.73	<1.26	50.45	31.37	3.67	7.14	63.94	1.68	0.45	0.025	0.324	<0.0026	1.19	0.159
	4.2	0.479	<0.00	425.53	8.89	<1.26	52.74	34.31	1.53	6.32	61.53	Inc	1.13	0.0054	0.157	0.094	Inc	0.516
	12.84	0.088	0.24	365.9	9.47	<1.25	60.84	45.09	2.07	7.94	67.23	1.69	0.38	0.044	0.216	0.0073	3.47	0.333
	3.66	0.407	<0.00	443.69	8.63	<1.64	60.28	42.71	3.79	6.35	56.72	4.11	1.47	0.031	0.267	0.0082	2.56	0.318
	5.99	<0.00	<0.00	315	7.9	<1.30	56.33	32.58	2.52	6.48	46.42	1.95	0.87	0.0056	0.374	0.0018	1.51	0.231
	5.6	0.129	<0.00	503.22	11.73	2.74	58.2	41.87	2.27	6.63	61.95	2.41	Inc	0.0062	0.61	0.004	0.84	5.33
	4.96	0.141	<0.00	431.71	12.73	3.89	44.12	38.06	4.47	6.26	55.12	0.99	<0.00	<0.00	0.251	0.0038	1.15	0.211
	4.42	0.265	<0.00	459.21	8.14	<1.25	38.76	36.24	1.94	6.16	59	1.84	1.43	0.021	0.341	0.0036	1.07	0.138
Sulitjelma	**Mn55**	**Co59**	**Ni60**	**Zn66**	**Ga69**	**As75**	**Se82**	**Ag107**	**Cd111**	**In115**	**Sn118**	**Sb121**	**Te125**	**Au197**	**Hg202**	**Tl205**	**Pb207**	**Bi209**
Sulis2a	19.2	0.297	0.21	391.91	1.88	3.79	69.36	15.72	4.63	1.33	3.65	0.86	0.87	<0.00	0.34	<0.00166	1.02	0.096
	21.44	1.06	<0.00	487.32	2.95	<1.86	78.87	20.31	7.09	1.58	3.35	1.23	2.24	<0.0054	0.71	0.0024	7.22	0.621
	19.8	0.417	0.157	452.42	3.18	2.22	59.45	20.75	5.31	1.81	3.82	0.94	<0.084	0.015	0.48	<0.0019	3.94	0.303
	16.88	0.253	0.11	324.48	2.48	<2.02	69.36	24.97	4.57	1.3	3.14	0.59	<0.16	<0.0118	0.25	<0.00306	2.48	0.134
	19.54	0.83	0.118	499.23	2.52	<2.02	71.97	18.23	7.87	1.93	4.46	1.72	0.74	<0.0085	0.56	<0.0035	7.52	0.795
	15.44	0.167	<0.00	323.7	2.54	2.16	53.64	15.21	6.42	1.5	2.48	0.72	1.46	<0.0037	0.23	<0.00108	3.31	0.149
	13.48	0.208	0.179	464.29	2.29	<1.75	73.24	19.27	5.26	1.38	2.19	1.23	1.02	<0.0095	0.62	<0.0032	1.6	0.212
	10.34	0.061	0.35	361.02	1.61	3.43	66.21	17.88	6.84	1.59	2.26	1.01	<0.00	<0.0058	0.24	<0.00265	0.92	3.89
	10.2	0.47	1	340.69	3.63	<1.35	59.98	13.59	5.2	1.75	4.98	0.95	1.37	<0.0060	0.1	<0.00173	2.8	0.86

	12.36	0.293	0.13	376.4	1.9	3.89	68.42	20.57	5.52	1.16	2.12	0.99	0.69	<0.0054	0.1	<0.0022	2.53	0.197
Kanmantoo	**Mn55**	**Co59**	**Ni60**	**Zn66**	**Ga69**	**As75**	**Se82**	**Ag107**	**Cd111**	**In115**	**Sn118**	**Sb121**	**Te125**	**Au197**	**Hg202**	**Tl205**	**Pb207**	**Bi209**
KTDD086(8)	0.64	Inc	Inc	307.98	2.5	<1.30	88.17	173	0.99	6.5	59.43	0.167	<0.00	0.436	0.172	0.0137	0.481	2.65
	1.88	1.49	0.092	404.04	2.57	1.64	94.45	130.44	1.68	26.16	76.68	<0.087	0.15	0.07	<0.085	<0.0019	11.6	3.91
	1.33	0.468	0.73	318.28	2.27	<1.37	105.02	29.34	1.65	12.5	104.11	0.266	<0.00	0.023	<0.085	0.0031	26.43	2.09
	0.9	0.418	0.42	290.34	2.66	<1.18	104.04	370.07	1.17	19.84	74.58	0.174	<0.172	0.224	<0.063	0.0106	42.85	3.18
	1.55	0.95	0.85	402.87	2.18	2.09	110.82	25.28	1.52	12.65	71.19	<0.096	<0.185	0.054	<0.093	<0.00214	11.37	1.98
	1.06	Inc	1.69	Inc	2.77	<1.20	107.52	30.42	Inc	15.09	88.37	0.255	<0.00	0.134	<0.069	0.046	25.66	Inc
	1.83	0.558	2.86	449.4	1.73	<1.04	101.29	8	1.58	19.43	79.71	0.219	0.29	0.008	0.167	<0.00244	43.48	2.21
	1.38	0.39	1.78	351.06	2.18	2.88	100.69	15.01	1.47	18.35	70	0.191	0.162	0.037	<0.080	<0.00166	12	1.46
	1.34	0.604	1.52	542.13	2.39	<1.55	122.21	27.3	2.98	14.44	82.39	0.281	0.52	0.075	<0.089	0.0025	20.23	2.19
	1.35	0.515	2.85	431.49	2.58	<1.30	124.89	17.17	1.91	19.15	96.71	0.116	<0.21	0.119	<0.084	0.0122	12.45	1.92
Kanmantoo	**Mn55**	**Co59**	**Ni60**	**Zn66**	**Ga69**	**As75**	**Se82**	**Ag107**	**Cd111**	**In115**	**Sn118**	**Sb121**	**Te125**	**Au197**	**Hg202**	**Tl205**	**Pb207**	**Bi209**
KTDD086(9)	<0.122	0.297	0.239	319.34	0.022	1.8	222.36	33.58	1.14	4.88	31.55	0.469	<0.168	0.049	<0.099	0.0037	2.15	3.08
	1.26	0.613	<0.00	561.07	2.03	<1.79	208.68	23.13	1.39	14.67	63	0.51	<0.141	0.039	<0.105	<0.0029	62.14	4.74
	0.361	0.253	0.088	410.75	1.98	<1.40	190.35	15.02	1.65	13.7	59.39	<0.097	<0.113	0.017	<0.074	<0.0016	46.42	3.99
	0.409	0.277	0.46	404.27	1.67	<1.68	207.83	16.75	1.11	13.93	56	<0.106	<0.135	0.047	<0.087	0.0084	42.05	2.08
	0.93	0.433	0.086	523.58	1.79	<2.12	223.16	19.79	1.86	16.44	59.63	0.369	0.32	0.149	<0.11	<0.0024	65.79	2.62
	1.27	0.434	0.182	454.94	1.31	<1.89	209	20.02	1.44	13.54	60.06	0.13	<0.27	0.134	<0.090	<0.00311	42.24	4.51
	0.499	0.277	0.48	356.38	1.78	3.06	177.53	8.59	1.25	17.35	56.94	0.083	0.163	0.0169	0.14	0.0041	32.13	0.759
	0.7	0.188	0.084	368.15	2.39	<2.08	239.84	14.02	2.03	13.98	60.85	0.181	<0.00	0.094	0.26	0.0013	80.78	1.96
	0.38	0.346	0.191	460.26	4	2.46	259.63	17.93	1.76	13.02	61.02	<0.141	0.21	0.082	<0.096	0.0068	31.07	2.29
	0.89	0.275	<0.00	413.49	4.64	<2.13	402.37	17.18	1.18	10.74	67.72	0.243	<0.18	0.113	0.14	<0.0034	22.1	0.98
Kanmantoo	**Mn55**	**Co59**	**Ni60**	**Zn66**	**Ga69**	**As75**	**Se82**	**Ag107**	**Cd111**	**In115**	**Sn118**	**Sb121**	**Te125**	**Au197**	**Hg202**	**Tl205**	**Pb207**	**Bi209**
KTDD086(11)	0.297	0.369	0.168	396.58	5.17	<1.48	55.65	12.4	2.1	12.19	84.65	0.125	<0.00	0.0086	<0.084	0.0012	7.2	0.387
	0.79	0.357	<0.00	232.77	4.36	<1.15	40.54	10.81	1.87	9.17	80.65	0.329	<0.00	0.014	0.064	0.0033	4.98	0.559
	0.249	0.497	0.197	377.08	5.06	<1.47	47.21	11.49	1.73	10.36	80.8	<0.089	0.39	<0.0062	<0.080	<0.00	5.48	0.206
	0.38	0.59	<0.00	381.05	2.78	Inc	47.46	15.12	1.35	9.54	47.02	<0.092	<0.00	<0.014	<0.07	0.0044	9.76	0.421
	0.374	0.464	0.076	443.66	4.41	<1.78	48.04	20.36	2.45	11.92	80.64	<0.118	0.61	0.018	<0.094	0.0041	2.5	0.155
	0.39	0.345	<0.046	318.12	4.39	<1.26	44.48	7.06	2.59	11.18	69.26	<0.079	0.33	0.01	0.073	<0.0046	8.28	0.401
	0.73	0.537	0.237	347.46	4.53	<1.54	40.77	22.69	1.95	7.24	48.53	<0.107	0.98	0.017	0.12	<0.00187	4.5	0.278
	0.54	0.197	0.28	266.63	4.16	<1.04	44.17	25.25	2.83	11.28	83.12	<0.069	2.45	0.007	<0.06	0.009	6.81	0.251

	0.61	0.363	<0.00	348.47	4.02	2.18	49.6	19	0.91	6.53	58.91	0.292	0.38	0.072	0.1	<0.00207	3.92	0.588
	1.03	0.33	0.39	404.14	4.4	<1.91	58.15	8.47	2.13	15.05	81.52	<0.103	0.82	0.019	0.25	0.0012	9.31	0.522
Kanmantoo	**Mn55**	**Co59**	**Ni60**	**Zn66**	**Ga69**	**As75**	**Se82**	**Ag107**	**Cd111**	**In115**	**Sn118**	**Sb121**	**Te125**	**Au197**	**Hg202**	**Tl205**	**Pb207**	**Bi209**
KTDD086(12)	2.24	0.224	0.261	489.38	1.77	<2.14	57.7	43.25	3.17	12.28	48.66	<0.109	2.65	<0.0078	<0.100	0.0024	4.66	4.65
	0.56	0.273	<0.00	304.23	4.53	<1.36	43.22	13.15	2.71	18.15	59.35	0.24	1.51	<0.0035	0.103	<0.00	6.9	0.88
	0.34	0.243	0.117	328.89	5.99	<1.37	51.56	24.31	3.42	19.26	77.75	0.151	0.54	0.017	0.151	<0.00	5.76	0.607
	0.53	0.274	0.21	377.91	5.45	4.99	56.1	20.57	2.14	18.08	76.43	0.227	3	0.011	<0.091	<0.00280	4.07	0.569
	0.8	0.431	0.057	356.91	5.23	<1.90	56.55	20.87	3.27	14.97	52.91	<0.085	2.25	0.041	0.44	<0.0033	6.72	0.9
	0.79	0.497	<0.045	350.56	5.66	4.53	55.56	11.78	3.22	18.22	71.29	<0.087	1.7	0.0108	0.091	<0.0041	4.83	0.719
	0.72	0.359	0.121	378.09	4.27	<1.72	52.31	12.44	3.08	16.09	65.56	0.23	1.72	0.0053	<0.080	0.0044	8.37	0.88
	0.493	0.492	<0.00	452.58	4.79	3.6	59.38	16.65	3.19	11.39	67.6	0.104	1.61	0.017	<0.076	0.0028	6.19	0.76
	1.26	0.425	0.53	516.95	3.99	1.21	42.13	16.49	3.02	9.82	48.38	0.226	1.16	0.018	0.14	<0.00	1.16	1.68
	0.62	0.31	<0.00	348.51	4.89	<1.28	49.49	16.58	2.99	11.18	55.93	<0.069	2.71	0.074	<0.063	<0.00	4.91	1.01
Kanmantoo	**Mn55**	**Co59**	**Ni60**	**Zn66**	**Ga69**	**As75**	**Se82**	**Ag107**	**Cd111**	**In115**	**Sn118**	**Sb121**	**Te125**	**Au197**	**Hg202**	**Tl205**	**Pb207**	**Bi209**
KTDD178(7)	0.308	3.98	0.088	498.12	0.272	4.13	58.59	17.78	2.54	36.05	92.38	<0.074	0.47	<0.0076	0.121	<0.0016	15.9	1.212
	<0.116	1.59	0.307	446.02	0.281	<1.48	66.89	24.55	1.28	57.75	102.21	0.092	0.169	0.027	<0.088	0.005	13.27	2.59
	<0.103	2.66	0.195	457.43	0.62	<1.28	55.69	23.21	2.21	51.26	116.91	0.205	0.39	0.011	<0.077	0.0078	23.11	1.115
	<0.092	2.46	0.303	363.04	0.484	<1.13	63.61	26.06	0.89	52.11	55.18	0.077	0.79	0.02	<0.063	0.0043	12.67	1.77
	<0.108	2.99	0.44	412.5	0.393	<1.18	58.64	23.82	1.04	57.05	254.82	<0.063	0.6	0.039	0.123	0.0014	53.98	1.029
	<0.085	3.45	0.53	326.84	0.135	<1.04	55.78	23.87	0.39	54.6	232.16	<0.047	0.2	0.027	<0.059	0.0078	71.41	0.879
	0.197	2.89	0.78	440.3	0.347	<1.34	53.99	22.41	0.66	44.59	206.76	<0.086	0.37	Inc	<0.071	0.0021	87.1	1.48
	0.164	5.44	0.336	530.08	0.267	<1.14	66.48	26.5	1.33	55.64	139.52	<0.066	0.123	0.017	<0.062	0.0071	20.44	3.08
	0.237	2.27	0.471	487.67	0.366	<1.45	61.88	28.54	1.17	70.13	156.41	0.128	<0.19	0.076	0.203	0.005	29.42	2.58
	0.13	1.92	0.139	372.15	0.363	1.31	47.91	16.26	1.14	32.34	135.34	0.091	0.34	0.02	<0.052	<0.00111	84.7	1.73
Kanmantoo	**Mn55**	**Co59**	**Ni60**	**Zn66**	**Ga69**	**As75**	**Se82**	**Ag107**	**Cd111**	**In115**	**Sn118**	**Sb121**	**Te125**	**Au197**	**Hg202**	**Tl205**	**Pb207**	**Bi209**
KTDD178(8)	<0.136	1.46	0.317	359.15	0.637	2.68	59.01	23.97	3.01	19.76	363.44	<0.100	0.92	<0.0060	<0.107	0.0023	3.07	0.118
	<0.079	1.48	0.8	305.27	0.61	3.51	45.01	26.45	1.54	18.94	434.1	<0.053	1.15	0.008	0.119	0.0026	3.33	0.111
	<0.125	0.618	0.059	380.64	0.451	<1.44	57.76	26.05	2.67	16.38	415.94	<0.076	0.74	<0.0050	<0.074	<0.00228	0.89	0.0305
	<0.109	0.758	0.314	373.71	0.324	<1.28	54.58	48.31	2.72	16.61	317.62	<0.068	0.48	0.0104	<0.067	<0.0025	2.4	0.118
	0.105	0.574	0.21	302.72	0.395	<1.24	43.66	23.4	2.4	13.51	242.07	<0.067	0.54	<0.0043	<0.060	<0.00198	1.22	0.101
	0.176	1.63	1.71	371.32	0.597	<1.59	61.87	24.08	2.04	20.45	234.62	<0.090	0.83	0.0069	<0.077	<0.0026	1.99	0.206
	<0.115	0.347	0.28	290.2	0.382	<1.33	57.37	30.49	2.57	10.37	410.57	<0.075	0.16	0.013	0.07	<0.00	1.38	0.061

	0.156	0.577	0.322	351.83	0.71	<1.16	65.81	30.21	2.87	23.54	495.14	<0.048	0.44	<0.0054	<0.057	<0.00181	2.7	0.176
	0.122	0.185	1.66	279.24	0.489	<1.15	55.37	27.28	3.5	10.66	266.2	<0.056	0.41	<0.0039	0.16	<0.00130	1.72	0.091
Kanmantoo	**Mn55**	**Co59**	**Ni60**	**Zn66**	**Ga69**	**As75**	**Se82**	**Ag107**	**Cd111**	**In115**	**Sn118**	**Sb121**	**Te125**	**Au197**	**Hg202**	**Tl205**	**Pb207**	**Bi209**
KTDD178(12)	0.11	0.75	0.237	351.36	0.513	1.35	28.02	46.45	2.01	26.88	271.19	<0.050	0.139	0.039	<0.074	<0.00128	1.01	0.152
	<0.097	1.02	0.139	294.68	1.18	<1.02	32.12	46.32	1.61	17.06	217.53	<0.060	<0.12	0.018	<0.076	<0.00233	1.45	0.131
	0.236	1.15	0.5	380.23	0.83	<0.98	32.54	51.59	1.59	27.27	389.11	0.071	0.63	0.048	0.202	<0.0030	3.67	0.507
	0.137	2.63	0.33	394.13	0.63	1.32	29.51	39.69	2.11	19.1	376.27	<0.055	0.62	0.0136	<0.076	0.0011	1.04	0.127
	0.232	0.86	0.89	405.77	0.81	1.54	31.45	44.53	2.1	12.74	391.95	<0.052	0.52	0.041	<0.076	<0.00	1.42	0.189
	0.102	1.64	0.1	360.7	0.68	1.1	33.56	45.72	1.88	10.01	358.83	<0.047	0.39	0.069	<0.063	0.0014	2.4	0.364
	<0.112	0.92	0.42	426.36	0.75	<1.19	32.45	46.18	2.18	19.87	446.29	<0.061	0.65	0.0107	0.082	0.001	4.67	0.295
	<0.104	0.99	0.58	349.62	0.7	<1.11	30.14	45.65	1.83	26.15	274.83	<0.076	0.133	0.0063	<0.079	<0.00	1.97	0.107
	<0.102	1.83	<0.00	220.81	0.089	<1.13	39.79	21.16	0.282	1.66	111	<0.070	<0.00	0.003	<0.075	<0.00	0.606	0.169
	<0.104	1.31	0.72	377.35	0.92	1.25	29.98	47.15	2.2	30.17	300.12	<0.062	<0.16	0.0066	0.108	<0.00150	0.66	0.051
Kanmantoo	**Mn55**	**Co59**	**Ni60**	**Zn66**	**Ga69**	**As75**	**Se82**	**Ag107**	**Cd111**	**In115**	**Sn118**	**Sb121**	**Te125**	**Au197**	**Hg202**	**Tl205**	**Pb207**	**Bi209**
KTDD180(3)	0.85	13.25	0.89	379.21	0.442	<1.27	17.9	51.75	0.8	56.68	27.71	0.195	0.57	<0.0092	0.24	1.24	0.92	0.789
	1.59	Inc	Inc	248.44	0.128	<1.05	19.03	54.26	0.51	50.43	17.83	0.371	0.87	<0.00	0.169	0.0295	2.44	3.68
	0.476	2.94	<0.00	294.75	0.204	<1.04	13.83	2.52	0.46	54.58	19.17	0.06	0.24	<0.00	<0.073	<0.0020	0.272	0.492
	0.69	3.1	0.093	380.28	0.137	2.8	18.84	2.04	1.14	53.5	29.52	0.212	0.81	<0.00	0.218	<0.0024	0.93	1.21
	0.55	4.06	<0.00	380.2	0.236	<0.95	18.52	0.404	1.09	56.57	27.48	<0.061	0.86	0.0079	0.215	0.0031	0.273	0.621
	0.9	2.55	0.095	329.49	0.101	3.61	22.01	3.12	0.56	55.89	23.62	0.144	0.38	<0.0052	<0.084	0.394	0.79	0.495
	0.57	5.14	0.119	436.28	0.394	2.48	16.94	64.84	1.16	57.7	25.3	0.356	Inc	0.0065	<0.087	0.002	0.84	2.47
Kanmantoo	**Mn55**	**Co59**	**Ni60**	**Zn66**	**Ga69**	**As75**	**Se82**	**Ag107**	**Cd111**	**In115**	**Sn118**	**Sb121**	**Te125**	**Au197**	**Hg202**	**Tl205**	**Pb207**	**Bi209**
KTDD180(7)	0.64	0.783	0.256	541.05	1.02	<1.31	11.94	19.14	0.99	28.96	152.16	0.121	Inc	0.304	0.071	0.001	4	7.87
	0.234	0.617	0.96	430.75	1.38	2.08	4.36	15.33	1.63	42.41	224.05	0.168	1.99	0.157	0.051	<0.00	0.457	3.91
	<0.159	1.25	0.084	651.43	1.44	<1.67	10.75	17.51	1.46	36.26	215.71	<0.107	1.49	0.044	0.098	<0.00	0.256	1.69
	0.7	1.08	0.74	560.59	1.18	4.74	15.39	16.9	1.6	26.92	143.8	0.135	0.58	0.157	0.18	<0.0023	0.052	2.68
	0.297	0.9	0.5	491.43	1.17	<1.45	15.68	28.22	1.95	29.32	222.25	0.092	0.89	0.064	<0.063	<0.00168	0.285	1.51
	0.166	0.76	<0.00	599.3	1.68	<1.29	14.64	17.21	1.62	34.57	283.09	<0.079	0.61	0.054	0.14	<0.0015	0.219	1.146
	0.435	0.332	Inc	404.36	1.84	1.61	9.77	30.51	1.33	35.48	192.2	<0.089	0.72	0.191	0.16	<0.00	0.143	2.36
	<0.121	1.13	0.48	538.1	1.94	<1.34	14.81	10.64	1.38	47.91	270.95	<0.085	0.76	0.036	<0.067	<0.00	0.132	1.84
	0.276	0.492	1.05	440.54	1.15	<1.12	11.97	14.56	1.05	38.59	163.63	0.068	0.44	0.149	0.1	<0.00	0.465	2.69
	0.445	1.45	0.15	416.08	0.75	<1.01	9.87	14.58	0.43	64.56	190.96	<0.072	1.33	0.466	0.23	1.72	1.43	9.17

Kanmantoo	**Mn55**	**Co59**	**Ni60**	**Zn66**	**Ga69**	**As75**	**Se82**	**Ag107**	**Cd111**	**In115**	**Sn118**	**Sb121**	**Te125**	**Au197**	**Hg202**	**Tl205**	**Pb207**	**Bi209**
KTDD180S(4)	1.46	Inc	Inc	533.65	0.59	<1.29	47.86	90.65	3.07	48.3	462.83	<0.082	0.68	0.073	0.119	0.0016	60.77	73.29
	0.177	2.1	<0.00	492.28	0.53	<1.36	53.04	68.45	2.15	49.69	239.31	<0.080	0.3	0.066	0.2	0.0117	47.01	4.37
	0.96	3.77	<0.00	596.15	0.4	3.36	47.32	63.84	1.72	48.77	365.62	0.24	0.93	0.139	<0.061	<0.0013	63.21	36.59
	<0.108	2.13	0.074	601.34	0.78	2.67	58.57	84.3	2.38	49.64	58.39	0.22	<0.094	0.065	0.21	0.0203	36.74	10.5
	0.34	1.25	<0.00	444.01	0.53	3.27	57.9	95.95	1.71	53.8	163.21	<0.089	<0.18	<0.0097	0.17	0.0146	33.54	2.81
	0.73	4.2	0.23	604.51	0.53	<1.25	60.98	94.56	2.32	50.6	432.4	<0.082	0.58	0.125	0.19	0.0066	56.8	19.11
	<0.133	1.97	0.072	475.71	0.79	4.6	55.24	77.05	2.5	48.72	357.81	<0.094	<0.12	0.0039	0.19	0.0112	22.82	2.93
	0.36	1.98	<0.00	452.93	0.46	<1.32	53.11	109.08	2.61	43.86	304.22	<0.072	0.16	0.114	<0.076	0.0085	51.87	3.49
	0.23	2.19	0.19	533.6	0.63	2.79	50.81	85.48	2.4	48.93	451.55	0.149	0.27	0.03	0.26	<0.0020	29.21	1.95
	<0.114	1.59	<0.062	463.26	0.63	<1.29	53.63	86.24	1.79	50.29	148.83	<0.078	0.63	0.057	0.28	0.0065	36.64	3.03
Kanmantoo	**Mn55**	**Co59**	**Ni60**	**Zn66**	**Ga69**	**As75**	**Se82**	**Ag107**	**Cd111**	**In115**	**Sn118**	**Sb121**	**Te125**	**Au197**	**Hg202**	**Tl205**	**Pb207**	**Bi209**
KTDD180S(5)	2.52	1.73	Inc	321.95	0.469	<1.18	45.43	107.86	0.47	21.18	131.2	0.07	0.27	0.198	0.08	0.0036	29.27	66.73
	0.64	8.91	0.83	430.71	0.63	1.46	62.69	133.03	0.75	29	355.63	0.08	1.13	0.142	<0.065	<0.00205	78.1	21.3
	5.49	1.43	0.57	538.35	0.825	<1.32	57.97	117.86	0.65	22	396.02	0.218	0.66	0.2	<0.064	<0.00	33.62	37.14
	2.6	0.26	Inc	495.68	0.67	<1.42	58.3	133.17	0.85	23.75	393.32	<0.070	2.06	0.044	<0.07	<0.00	44.93	45.98
	1.43	Inc	Inc	324.44	0.52	<1.39	58.21	137.14	1.03	17.96	251.53	0.073	0.37	0.124	<0.069	0.0059	11.95	30.16
	0.97	3.86	0.56	391.57	0.8	3.41	64.13	128.23	1.52	17.43	292.23	0.211	0.38	0.215	0.14	0.0053	0.9	4.51
	1.48	Inc	Inc	497.13	0.768	<1.47	63.29	114.52	0.67	20.84	342.46	0.185	0.36	0.259	0.09	<0.0023	3.98	10.47
	1.28	2.67	0.92	404.25	0.265	<1.43	74.47	112.62	0.86	19.16	337.53	0.28	0.62	0.108	0.14	0.0045	3.21	10.86
	0.54	Inc	Inc	481.56	0.87	2.38	46.42	127.09	2.68	17.52	226.49	0.102	<0.104	0.205	0.15	<0.00220	35.19	22.56
	2.03	Inc	Inc	Inc	0.582	<2.19	69.39	116.93	1.3	24.66	322.6	0.386	0.88	0.369	0.33	0.0026	41.38	53.45

Inc = data influenced by micro-inclusion. - = data could not be determined.

ADDITIONAL MATERIAL C

FOR CHAPTER 6

ELECTRONIC APPENDIX A FOR CHAPTER 6

Electronic Appendix A. EPMA methodology

Element	**Standard**	**X-ray Line**	**On Peak Time** (s)	**Background Time** (s)	**Average MDL** (wt. %)
S	Chalcopyrite	S Kα	10	20	0.013
Pb	Galena	Pb Mα	30	47.5	0.037
Cd	Greenockite	Cd Lα	60	60	0.031
As	Gallium Arsenide	As Lα	30	25	0.043
Se	Bismuth Selenide	Se Lα	100	150	0.018
Fe	Chalcopyrite	Fe Kα	10	20	0.020
Cu	Chalcopyrite	Cu Kα	10	20	0.031
Mn	Rhodonite	Mn Kα	30	40	0.015
Ag	Silver/Silver Telluride	Ag Lα	30	25	0.041
Sn	Cassiterite	Sn Lα	30	40	0.026
In	Indium	In Lα	30	25	0.031
Hg	Cinnabar	Hg Lα	100	180	0.042
Zn	Sphalerite	Zn Kα	30	20	0.030
Ni	Pentlandite	Ni Kα	30	20	0.022
Co	Cobalt	Co Kα	30	20	0.018
Sb	Stibnite	Sb Lα	30	40	0.022
Te	Silver Telluride	Te Lα	30	40	0.024
Bi	Bismuth Selenide	Bi Mα	30	25	0.057
Tl	Thallium	Tl Mα	20	20	0.126
Ga	Gallium Arsenide	Ga Kα	20	20	0.041

ELECTRONIC APPENDIX B FOR CHAPTER 6

Electronic Appendix B. Mean errors and minimum detection limits determined by LA-ICP-MS (data in ppm)

Sample		Mn	Fe	Co	Ni	Zn	Ga	As	Se	Mo	Ag	Cd	In	Sn	Te	W	Au	Hg	Tl	Pb	Bi
G16396	1σ error	0.55	6311	0.71	0.39	16461	0.05	1099	11	0.08	16470	941	0.09	3.9	0.68	0.03	0.43	29	0.03	8.4	62
	MDL	0.39	19	0.04	0.37	5.2	0.04	2.4	11	0.06	0.13	0.74	0.01	0.34	0.25	0.02	0.02	0.72	0.01	0.09	0.01
G11579	1σ error	5.8	6087	3.7	0.64	14185	0.07	4276	38	0.07	2472	322	1.3	0.52	19	0.04	0.04	11	0.03	0.64	500
	MDL	0.93	44	0.08	0.94	9.1	0.11	11	22	0.12	0.24	1.6	0.02	0.75	0.45	0.06	0.04	1.3	0.03	0.24	0.03
G13289b	1σ error	0.77	12143	44	0.29	134074	0.06	72892	19	0.09	2038	2187	0.31	0.97	0.53	0.03	0.05	9.3	0.15	270	41
	MDL	0.40	4415	14	0.20	37580	0.03	28051	7.9	0.03	399	619	0.06	0.37	0.11	0.01	0.02	3.5	0.05	52	8.7
G6940	1σ error	6.0	3584	0.10	0.31	9409	0.04	1781	28	0.04	2797	117	0.74	0.37	6.0	0.01	0.03	16	0.02	0.44	118
	MDL	0.46	24	0.04	0.42	5.1	0.05	2.1	12	0.06	0.15	0.54	0.01	0.42	0.18	0.03	0.02	0.92	0.02	0.16	0.02
G13289a	1σ error	0.30	1185	4.4	0.24	11051	0.03	14576	10	0.04	396	242	0.03	0.26	0.12	0.01	0.01	2.4	0.02	15	1.2
	MDL	0.34	17	0.03	0.32	3.3	0.04	3.7	8.5	0.05	0.06	0.42	0.01	0.30	0.20	0.02	0.02	0.60	0.01	0.06	0.01
V446	1σ error	23	5890	0.03	0.11	1687	0.07	6.5	4.9	0.04	20196	45	0.13	2.1	0.07	-	0.01	10	0.04	0.32	5.8
	MDL	0.09	1.9	0.01	0.05	0.19	0.01	1.0	1.3	-	0.02	0.06	0.002	0.05	0.08	-	0.004	0.07	0.002	0.01	0.004
V538	1σ error	6.0	4665	0.01	0.01	975	0.05	12	1.5	-	9484	20	0.06	1.8	0.06	-	0.01	1.9	0.03	3.6	2.5
	MDL	0.07	1.3	0.00	0.03	0.23	-	0.80	1.1	-	0.02	0.08	0.002	0.04	0.07	-	0.01	0.06	0.001	0.09	0.003
Hj13	1σ error	14	4872	0.04	-	1610	0.02	17	1.3	0.05	5135	14	0.03	0.09	0.23	0.01	0.36	0.07	0.07	25	0.37
	MDL	0.09	1.4	0.01	-	0.24	0.01	0.79	0.81	-	0.02	0.09	0.002	0.05	0.12	-	0.004	0.03	0.001	0.01	0.004
G6951	1σ error	0.86	135	8.8	0.55	51815	0.05	12230	11	0.06	4932	5047	0.04	0.45	0.35	0.01	0.06	9.0	0.09	20	0.02
	MDL	0.61	30	0.05	0.62	6.2	0.07	4.3	13	0.09	0.19	0.95	0.02	0.53	0.33	0.03	0.03	0.94	0.02	0.17	0.01
Bv97-52	1σ error	29	2459	0.00	0.04	1539	0.04	19809	1.3	0.03	482	59	0.23	5.2	0.03	0.003	0.002	11	0.003	0.12	0.61
	MDL	0.07	1.5	0.01	0.03	0.16	0.01	1.7	1.2	0.02	0.01	0.04	0.001	0.05	0.07	0.01	0.004	0.07	0.001	0.04	0.003
G10847	1σ error	3.7	3093	0.03	0.34	34906	0.10	47886	12	0.06	1097	265	0.04	0.42	0.30	0.02	0.03	889	0.04	2.9	0.23
	MDL	0.59	29	0.04	0.50	7.2	0.06	8.7	16	0.08	0.12	0.78	0.01	0.52	0.43	0.04	0.03	0.80	0.02	0.12	0.01
EV8	1σ error	0.83	5897	0.05	0.22	1883	0.06	14	10	0.02	38907	88	0.25	41	0.42	0.02	0.03	2.6	0.43	5472	137

	MDL	0.26	13	0.02	0.24	2.7	0.03	1.5	7.8	0.04	0.14	0.24	0.01	0.24	0.16	0.02	0.01	0.64	0.01	0.11	0.01
	1σ																				
Hj14	error	7.0	3914	0.01	0.05	791	0.01	20	1.4	0.08	19580	33	0.02	2.4	0.15	0.01	2.0	0.09	0.04	4.2	0.01
	MDL	0.13	2.9	0.01	-	0.34	0.02	1.2	1.2	0.07	0.09	0.08	0.002	0.07	-	0.02	0.01	0.03	0.003	0.03	0.01
	1σ																				
G6948	error	62	4405	0.05	0.39	5554	0.05	1092	27	0.05	3563	67	0.13	8.3	0.42	0.01	0.02	1.1	0.01	0.55	248
	MDL	0.53	26	0.04	0.50	5.5	0.07	3.1	13	0.08	0.15	0.61	0.01	0.48	0.31	0.03	0.03	1.1	0.02	0.16	0.02
	1σ																				
G14549b	error	0.62	9084	0.30	0.40	10356	0.07	626	10	0.08	7170	1706	0.08	4.4	0.16	0.01	0.25	15	0.22	2593	112
	MDL	0.41	20	0.04	0.37	4.6	0.04	2.6	10	0.05	0.12	0.50	0.01	0.32	0.19	0.03	0.02	0.61	0.01	0.09	0.01
	1σ																				
Mo17A	error	0.08	3603	0.03	0.05	1145	0.01	1254	1.3	0.02	5963	140	0.01	0.03	0.20	0.002	0.02	1.1	0.02	0.62	0.33
	MDL	0.06	1.0	0.01	0.02	0.12	0.01	0.92	0.9	0.02	0.01	0.04	0.001	0.03	0.06	0.01	0.003	0.05	0.001	0.01	0.002
	1σ																				
ORV1	error	0.10	1660	2.7	0.55	6714	0.04	4653	5.7	0.09	486	85	0.06	0.05	0.30	-	0.01	8.3	0.005	0.46	1.1
	MDL	0.11	2.1	0.02	0.09	0.31	0.03	1.3	1.1	-	0.02	0.07	0.004	0.05	-	-	0.01	0.05	0.002	0.09	-
	1σ																				
G14549a	error	0.36	5221	0.17	0.31	8762	0.05	808	6.0	0.02	4457	495	0.11	8.0	0.09	0.01	0.06	5.9	0.05	84	262
	MDL	0.28	14	0.02	0.22	3.0	0.03	1.9	6.9	0.04	0.07	0.26	0.01	0.25	0.18	0.02	0.02	0.61	0.01	0.05	0.01
	1σ																				
G873	error	0.49	5224	0.28	0.36	13513	0.05	17027	11	0.10	7027	499	1.7	0.36	0.18	0.03	0.04	10	0.03	4.9	0.03
	MDL	0.56	28	0.05	0.53	6.4	0.06	4.7	15	0.08	0.16	0.74	0.01	0.51	0.26	0.04	0.03	1.4	0.02	0.21	0.02
	1σ																				
G16152	error	0.33	2490	292	1.1	9075	0.04	24871	10	0.28	660	35	0.41	2.8	0.14	0.02	0.02	604	0.01	1.4	2.5
	MDL	0.49	24	0.04	0.46	5.1	0.05	7.1	15	0.07	0.09	0.60	0.01	0.42	0.29	0.04	0.02	1.0	0.02	0.16	0.01
	1σ																				
G871	error	0.34	3757	96	0.31	4651	0.04	15639	12	0.08	35	27	0.02	0.27	0.22	0.02	0.02	66848	0.01	0.47	0.05
	MDL	0.43	21	0.04	0.35	7.5	0.05	5.0	12	0.06	0.19	0.62	0.01	0.37	0.25	0.03	0.02	1.4	0.01	0.09	0.01
	1σ																				
G874	error	0.27	1470	67	0.21	8291	0.03	6570	8.1	0.06	26	21	0.21	0.22	0.15	0.02	0.01	35714	0.01	0.76	0.05
	MDL	0.36	18	0.03	0.29	5.5	0.04	2.4	8.5	0.05	0.02	0.40	0.01	0.28	0.19	0.02	0.02	1.2	0.01	0.05	0.01
	1σ																				
G879	error	1.7	11235	0.82	0.87	5465	0.09	2600	20	0.06	3419	68	3.4	0.76	0.32	0.05	0.07	6.0	0.04	3.7	221
	MDL	0.88	42	0.08	0.88	8.7	0.09	6.4	21	0.14	0.26	1.2	0.02	0.74	0.62	0.08	0.04	1.4	0.02	0.27	0.02
	1σ																				
G882	error	0.53	2879	104	0.52	3280	0.07	26355	29	0.13	23	45	0.38	0.47	0.37	0.03	0.04	33702	0.02	5.2	0.68
	MDL	0.82	41	0.07	0.83	9.2	0.08	8.8	25	0.13	0.30	1.2	0.02	0.73	0.46	0.05	0.05	2.0	0.02	0.50	0.02
	1σ																				
G6946	error	0.62	4021	8.2	5.2	13070	0.07	4024	22	0.06	942	183	0.28	0.59	0.36	0.03	0.04	447	0.01	1.5	17
	MDL	0.73	37	0.06	0.63	9.4	0.08	5.9	19	0.09	0.14	0.96	0.02	0.62	0.49	0.05	0.03	0.92	0.02	0.23	0.02
	1σ																				
G6949	error	2.0	8470	0.11	0.77	3348	0.07	1266	18	0.05	1808	65	3.7	0.79	0.14	0.01	0.07	4.0	0.17	5.4	505

	MDL 1σ	0.62	32	0.05	0.53	8.9	0.07	5.1	17	0.07	0.16	0.85	0.01	0.53	0.28	0.03	0.03	0.82	0.02	0.13	0.01
G11701	error	0.42	7954	19	0.42	3048	0.04	17	13	0.07	25776	156	0.04	0.93	0.30	0.03	0.04	65	0.01	1.5	3.4
	MDL 1σ	0.50	25	0.04	0.48	6.9	0.06	2.9	14	0.06	0.25	0.80	0.01	0.46	0.32	0.04	0.03	1.0	0.01	0.17	0.01
G14246	error	1.8	6518	0.35	0.27	1953	0.04	484	6.9	0.05	1582	45	0.85	0.37	0.21	0.01	0.02	15	0.03	0.59	252
	MDL 1σ	0.40	20	0.03	0.35	4.6	0.04	3.7	8.5	0.06	0.04	0.39	0.01	0.33	0.24	0.02	0.02	0.83	0.01	0.07	0.01
G14867	error	0.37	4494	11	0.33	1925	0.05	60186	66	0.08	4.7	19	0.43	0.30	0.23	0.02	0.02	982	0.03	0.53	437
	MDL 1σ	0.55	26	0.04	0.45	6.5	0.06	8.9	12	0.08	0.03	0.51	0.01	0.42	0.29	0.03	0.03	1.9	0.02	0.09	0.02
Mo16	error	4.1	5726	1.6	1.5	1608	0.08	9437	2.0	0.02	1743	223	0.01	0.04	0.71	-	0.01	35	0.01	0.43	0.37
	MDL 1σ	0.06	1.0	0.00	-	0.12	0.01	0.82	0.77	-	0.01	0.03	0.001	0.03	0.06	-	0.002	0.03	-	0.01	0.003
G29851	error	0.68	17398	31	0.87	13465	0.09	103447	20	0.43	228	136	0.08	0.51	1.1	0.05	0.07	37159	0.06	45	319
	MDL 1σ	0.85	43	0.08	0.88	9.1	0.10	14	23	0.11	0.18	1.4	0.02	0.67	0.52	0.05	0.04	2.1	0.02	0.21	0.02
ORV4	error	1.7	1018	0.24	0.42	4801	0.03	5383	4.0	0.12	91	113	0.64	0.05	1.0	-	-	7.0	0.01	0.38	7.5
	MDL 1σ	0.12	2.1	0.02	0.13	0.32	0.03	1.6	1.0	-	0.02	0.11	0.003	0.06	0.15	-	-	0.05	0.002	0.03	0.01
G12640	error	15	7330	0.62	0.62	21215	0.07	91213	55	0.11	236	98	0.08	0.70	3.1	0.02	0.04	407	0.05	1.5	6.5
	MDL 1σ	0.68	34	0.05	0.78	7.7	0.08	11	15	0.10	0.17	1.3	0.02	0.56	0.35	0.04	0.03	1.1	0.02	0.22	0.01
G13301	error	0.60	11654	177	7.6	7397	0.14	26979	70	0.04	40	895	0.62	0.46	1.2	0.03	0.02	681	0.02	3.3	25
	MDL 1σ	0.53	26	0.05	0.56	5.2	0.06	4.8	13	0.09	0.15	0.76	0.01	0.45	0.31	0.03	0.03	0.85	0.01	0.21	0.01
G15977	error	3.1	6462	5.4	0.32	24410	0.06	21116	12	0.04	122	325	0.02	0.36	0.36	0.01	0.08	156	0.01	1.0	2.6
	MDL 1σ	0.41	21	0.04	0.39	4.6	0.05	3.4	12	0.06	0.08	0.54	0.01	0.36	0.18	0.03	0.02	0.97	0.01	0.09	0.01
G16835	error	0.87	4402	25	0.63	23381	0.07	86436	14	0.11	967	34	0.17	0.44	0.70	0.06	0.20	5419	0.03	8.9	371
	MDL 1σ	0.55	25	0.05	0.60	5.0	0.06	8.5	11	0.09	0.10	0.75	0.01	0.45	0.36	0.03	0.02	0.99	0.01	0.12	0.02
VFI031	error	142	29	0.02	0.18	12202	0.16	21645	245	0.06	4986	124	1.4	0.91	792	0.01	0.59	1784	0.05	7.7	0.22
	MDL	0.35	16	0.03	0.27	8.1	0.04	4.2	10	0.04	0.13	0.55	0.01	0.28	0.22	0.02	0.02	0.69	0.01	0.08	0.01

MDL = minimum detection limit (99% confidence). Dash = insufficient data to perform calculation.

Error is calculated from internal (counting statistic noise) and external signal uncertainties (mass bias, correction of unknowns to standards, laser induced elemental fractionation [LIEF] and instrument drift).

ELECTRONIC APPENDIX C FOR CHAPTER 6

Electronic Appendix C. Complete trace element datasets for tetrahedrite-tennantite, sphalerite, galena and chalcopyrite determined by LA-ICP-MS (data in ppm).

Tetrahedrite-tennantite

Sample	Mn	Fe	Co	Ni	Cu	Zn	Ga	As	Se	Mo	Ag	Cd	In	Sn	Sb	Te	W	Au	Hg	Tl	Pb	Bi
G16396*	1.2	31666	2.1	0.35	I.S.	71229	0.02	3607	-	0.15	52313	6381	0.54	92	403970	1.6	<0.001	0.57	91	0.02	Inc.	16
	0.18	32232	2.2	0.21	I.S.	56656	0.02	4685	-	0.03	38003	4385	0.47	1.0	414757	0.69	0.01	1.3	110	0.05	Inc.	1.1
	1.3	35925	1.8	0.20	I.S.	88051	0.04	6411	-	0.03	129323	5137	0.45	1.2	459984	3.4	<0.001	1.1	117	0.55	81	1321
	2.1	26829	5.4	2.7	I.S.	73561	0.41	5906	-	0.49	26821	5064	0.28	1.7	414580	2.7	0.01	0.96	104	0.02	Inc.	365
	0.19	34188	2.8	0.68	I.S.	89780	0.04	3764	-	0.03	130532	4693	0.64	32	463333	0.95	<0.001	0.37	73	0.005	87	6.9
	2.1	23409	3.4	0.17	I.S.	105129	0.08	4179	-	0.28	93069	4711	0.47	40	453995	2.3	0.18	1.6	85	0.05	Inc.	16
	1.8	26424	2.3	0.18	I.S.	103384	0.10	3945	Inc.	0.04	104085	3878	0.71	2.5	439138	1.7	0.01	0.36	49	0.05	Inc.	2311
	3.1	33111	1.6	0.18	I.S.	85478	0.02	5256	-	0.03	123162	4272	0.83	0.15	429298	0.09	0.01	1.1	106	0.05	Inc.	169
	1.3	40601	3.5	0.23	I.S.	69797	0.09	4297	-	0.03	129172	5303	0.66	7.3	437146	0.55	0.06	0.06	106	0.05	16	206
	0.24	33050	1.9	0.49	I.S.	54174	0.03	4152	-	0.13	14792	5852	0.71	102	400897	0.48	0.08	0.07	93	0.04	Inc.	36
G11579	36	33277	26	0.31	I.S.	96558	0.03	30443	80	0.04	20899	2494	5.6	0.23	461342	67	-	0.04	77	0.01	0.85	3022
	33	34110	21	0.27	I.S.	96178	0.04	31176	40	0.04	22142	2570	6.0	0.20	466437	28	-	0.04	75	0.02	2.9	2596
	32	33192	19	0.69	I.S.	105753	0.08	39211	44	0.07	25208	2948	7.3	0.51	571280	40	-	0.03	125	0.02	2.5	3657
	31	30583	22	0.29	I.S.	100466	0.03	20379	83	0.04	21772	2447	8.3	0.24	475959	60	-	0.07	43	0.19	8.1	2591
	30	31437	16	0.29	I.S.	99155	0.09	21154	51	0.05	21656	2348	7.5	0.79	468965	51	-	0.01	69	0.04	1.5	2754
	31	33730	24	0.32	I.S.	97790	0.04	21280	41	0.05	25169	2456	8.3	0.57	488952	24	-	0.01	78	0.05	2.7	2616
	34	33976	22	0.42	I.S.	97603	0.04	23854	9.4	0.06	27335	2689	6.2	0.34	516280	63	-	0.01	91	0.04	1.8	2620
	33	34722	32	1.8	I.S.	98475	0.05	31050	70	0.31	25095	2540	6.1	0.37	525158	39	-	0.02	111	0.03	2.0	3155
	35	32728	18	3.5	I.S.	114107	0.11	28405	57	0.09	25147	3311	8.8	1.4	681930	105	-	0.04	147	0.03	2.7	4392
	30	34496	22	0.81	I.S.	108667	0.11	37512	Inc.	0.13	24528	3122	6.3	0.75	674626	26	-	0.04	111	0.08	5.8	2670
G13289b*	2.0	13813	49	0.13	I.S.	144259	0.02	60855	Inc.	0.02	2656	2224	1.0	1.5	429191	<0.001	<0.001	0.01	8.5	0.13	44	Inc.
	0.51	11870	44	0.11	I.S.	139044	0.05	74550	22	0.02	2403	2092	0.13	0.66	393684	0.06	0.01	0.01	11	0.01	143	0.03
	0.65	14473	53	0.29	I.S.	134729	0.02	77043	3.7	0.03	3046	1874	0.30	0.14	385364	<0.001	0.01	0.15	2.1	0.07	221	0.41
	1.5	10205	38	0.15	I.S.	150589	0.08	62578	4.9	0.02	1862	2649	0.01	0.90	451060	<0.001	0.01	0.01	15	0.72	43	12
	0.62	11494	40	0.09	I.S.	132369	0.02	79307	15	0.02	2018	2325	0.02	1.0	365259	<0.001	0.01	0.01	9.9	0.03	203	4.1
	0.75	13897	56	0.07	I.S.	125410	0.01	79480	24	0.02	1547	1958	0.03	1.4	335627	0.04	0.01	0.01	9.5	0.03	713	18
	0.57	11054	32	0.08	I.S.	129818	0.02	80492	13	0.01	1650	2392	0.02	0.41	341739	<0.001	0.03	0.01	7.6	0.03	724	19
	0.33	11618	45	0.12	I.S.	125435	0.01	79956	3.9	0.01	1555	2110	0.004	0.14	335060	<0.001	0.01	0.02	9.3	0.05	354	0.03
	0.48	13609	48	0.13	I.S.	126682	0.02	83829	Inc.	0.04	1422	1786	0.71	1.2	352450	0.53	<0.001	0.01	9.6	0.14	226	19

	0.31	9401	35	0.29	I.S.	132404	0.04	50832	3.6	0.13	2226	2456	0.26	0.65	386750	0.05	0.01	0.02	11	0.28	26	1.9
G6940	41	39540	0.52	0.40	I.S.	61476	0.08	12597	52	0.03	31995	1723	2.9	1.7	396331	27	0.01	0.01	63	0.03	1.8	1438
	41	40226	0.84	0.30	I.S.	56711	0.13	12690	74	0.11	31947	1596	2.4	0.65	370334	65	<0.001	0.01	56	0.02	1.3	1480
	51	40742	0.40	0.18	I.S.	60641	0.02	8922	72	0.11	35594	1791	3.4	0.75	402062	28	0.01	0.04	86	0.01	1.7	1398
	45	42378	0.49	0.13	I.S.	57541	0.02	18264	80	0.03	33804	1541	3.0	1.3	379608	30	0.01	0.01	65	0.02	1.6	1660
	41	39593	0.65	0.14	I.S.	62570	0.02	6457	72	0.02	32134	1774	3.1	0.55	401086	30	0.01	0.01	72	0.02	2.1	1364
	24	41136	0.55	0.15	I.S.	60068	0.07	6723	51	0.02	31930	2233	3.5	0.17	393356	83	0.01	0.01	73	0.01	0.93	1509
	40	41133	0.50	0.60	I.S.	61308	0.02	10473	42	0.03	33314	2133	2.7	1.7	414570	45	0.01	0.07	83	0.01	1.7	1510
	47	43454	0.72	0.43	I.S.	64190	0.06	8237	96	0.17	35113	2107	3.7	1.2	487216	25	0.12	0.02	147	0.07	3.2	1542
	50	44020	0.43	0.29	I.S.	60541	0.09	21345	103	0.05	34574	1802	3.9	2.6	428667	26	0.02	0.02	112	0.01	1.4	1837
	52	43172	0.45	0.67	I.S.	63807	0.04	20556	90	0.04	32853	1899	5.7	0.70	438708	20	0.02	0.06	106	0.01	2.8	1649
G13289a*	0.94	11510	35	0.42	I.S.	118233	0.02	86377	4.4	0.02	1689	2205	0.01	0.51	324857	0.09	<0.001	0.01	14	0.02	369	2.0
	0.13	6164	14	0.12	I.S.	127472	0.02	76868	3.3	0.02	2455	1873	0.08	0.80	307273	0.06	0.01	0.01	8.2	0.19	18	24
	2.2	11195	37	0.12	I.S.	124913	0.02	50583	7.3	0.16	3402	2640	0.13	1.2	353685	<0.001	0.01	0.01	15	0.08	10	0.67
	1.2	9289	40	0.35	I.S.	123306	0.01	51540	11	0.02	1448	2030	0.01	0.45	345033	0.09	<0.001	0.01	9.0	0.04	4.6	0.18
	0.99	11422	46	0.12	I.S.	119236	0.11	60326	99	0.08	1445	1869	1.3	0.32	343951	<0.001	<0.001	0.01	10	0.04	119	49
	0.71	9957	32	0.16	I.S.	122074	0.01	77626	14	<0.001	1680	2276	0.005	0.15	322584	<0.001	0.01	0.01	13	0.07	304	1.1
	0.17	11037	51	0.15	I.S.	117968	0.02	49257	35	0.02	1756	1764	0.08	0.15	345284	0.08	0.04	0.01	15	0.05	16	Inc.
	1.2	11444	53	0.22	I.S.	117422	0.08	69699	14	<0.001	1453	1884	0.02	0.20	346663	<0.001	<0.001	0.01	17	0.01	130	6.1
	0.29	9928	37	0.72	I.S.	123466	0.03	88783	7.2	0.04	1763	2065	0.02	0.74	356879	0.58	0.02	0.01	14	0.03	83	5.2
	0.37	9217	31	0.17	I.S.	113559	0.02	58186	15	0.03	1571	1915	0.01	0.15	308215	<0.001	0.01	0.01	11	0.01	22	9.0
V446	211	52797	0.03	<0.001	I.S.	17063	0.18	47	8.5	0.07	123534	156	1.4	18	334830	0.18	-	0.001	10	0.004	1.9	118
	211	54518	0.01	0.50	I.S.	18113	0.14	48	11	<0.001	131463	172	1.3	16	362716	0.04	-	0.04	11	0.07	Inc.	127
	186	49521	0.10	<0.001	I.S.	18109	0.26	29	8.9	<0.001	87734	149	1.0	16	324423	<0.001	-	0.002	10	0.47	Inc.	79
	210	54915	0.11	0.02	I.S.	17223	0.20	29	21	<0.001	102220	203	0.95	14	367485	<0.001	-	<0.001	7.9	0.09	Inc.	120
V538	126	54637	0.002	<0.001	I.S.	15080	0.21	140	8.9	<0.001	144634	172	0.57	22	339894	0.03	-	0.003	11	0.03	4.8	42
	126	53177	<0.001	0.01	I.S.	14911	0.13	53	5.4	<0.001	144809	151	0.61	21	344349	0.32	-	<0.001	11	0.56	48	43
	114	48945	0.06	<0.001	I.S.	17095	<0.001	84	3.7	<0.001	132288	152	0.73	21	328362	0.03	-	0.01	8.4	0.02	11	49
Hj13	117	50147	0.13	-	I.S.	24225	0.06	156	7.5	0.19	55916	102	0.28	0.03	361858	0.13	<0.001	0.08	0.30	0.39	2.7	3.5
	114	53457	0.67	-	I.S.	17073	0.03	101	20	<0.001	53319	133	0.17	0.61	360036	2.3	<0.001	0.44	0.26	0.16	2.4	2.1
	86	48173	0.10	-	I.S.	23434	<0.001	108	3.9	<0.001	63590	98	0.22	0.03	352067	<0.001	<0.001	0.06	0.31	0.50	2.2	2.4
	122	51273	0.03	-	I.S.	19165	0.04	95	9.3	0.13	48009	136	0.17	0.41	361914	0.26	<0.001	0.11	0.24	0.32	2.9	5.3
	126	47254	0.03	-	I.S.	22002	0.06	117	7.5	<0.001	50425	100	0.25	0.02	341750	0.62	<0.001	0.06	0.26	0.56	6.5	3.1
	80	46996	0.05	-	I.S.	24682	0.04	105	7.4	0.07	59395	100	0.23	0.03	340166	<0.001	0.02	0.07	0.37	0.29	3.0	3.5
	135	48835	0.03	-	I.S.	18632	<0.001	88	12	0.06	51635	134	0.20	Inc.	335632	0.34	<0.001	0.14	0.37	1.0	2.2	3.2
	106	45366	0.04	-	I.S.	22710	<0.001	151	3.9	0.09	38911	102	0.05	0.04	339022	<0.001	<0.001	0.04	0.57	0.56	3.0	2.9
	94	45163	1.1	-	I.S.	23772	0.04	128	9.2	0.18	37790	88	0.30	0.05	324531	0.13	<0.001	0.04	0.33	0.54	1.8	1.8

G6951*	1.0	173	21	-	I.S.	151039	0.04	30432	-	0.03	35395	21464	0.09	0.27	389821	<0.001	-	0.05	20	0.05	44	0.01
	0.24	183	21	-	I.S.	136419	0.03	30584	-	0.04	29511	21606	0.10	0.21	345842	0.73	-	0.01	19	0.04	56	0.01
	1.1	396	22	-	I.S.	160797	0.01	40128	-	0.04	32040	26402	0.08	0.15	379921	0.98	-	0.12	20	0.35	Inc.	0.02
	1.4	411	27	-	I.S.	168827	0.05	39005	-	0.24	37034	29919	0.07	0.40	457188	0.24	-	0.02	65	0.39	91	0.13
	0.97	476	25	-	I.S.	173027	0.04	39772	Inc.	0.05	37436	27239	0.12	0.78	447330	<0.001	-	0.10	24	0.16	64	0.04
	1.8	Inc.	25	-	I.S.	167538	0.03	70677	-	0.04	34056	48401	0.14	0.26	426159	0.56	-	0.08	38	0.27	117	0.01
	1.9	306	23	-	I.S.	204984	0.03	32241	-	0.03	39718	29239	0.13	0.17	491496	<0.001	Inc.	0.10	17	0.24	127	0.06
	2.2	562	30	-	I.S.	179254	0.04	50884	-	0.04	35547	33298	0.10	0.29	465558	<0.001	-	0.10	28	0.21	Inc.	0.04
	2.9	510	36	-	I.S.	197578	0.08	55729	-	0.07	35097	31331	0.11	0.26	477786	0.15	-	0.05	26	0.21	132	0.01
	1.3	300	38	-	I.S.	191539	0.05	56469	Inc.	<0.001	38141	30028	0.10	0.35	484994	0.21	-	0.02	32	0.09	52	0.01
Bv97-52	270	47461	0.02	0.02	I.S.	20840	0.16	141400	5.8	0.04	7409	896	2.5	0.22	104071	-	-	0.002	31	0.004	0.41	20
	1193	52367	0.03	1.1	I.S.	12219	1.6	211377	4.7	<0.001	3971	1052	4.3	363	2575	-	-	0.002	Inc.	Inc.	0.88	0.08
	364	47969	0.004	<0.001	I.S.	22034	0.13	103140	3.7	<0.001	7537	1018	2.7	0.07	156392	-	-	0.002	32	0.002	0.79	12
	196	35471	0.004	0.02	I.S.	40841	0.02	161916	1.3	0.10	4590	329	0.29	0.54	81861	Inc.	-	0.002	49	<0.001	0.44	7.0
	212	35832	0.003	<0.001	I.S.	42308	0.12	163216	4.6	0.05	4535	340	0.30	0.59	80811	-	-	0.003	51	<0.001	0.63	8.3
	235	59980	<0.001	0.10	I.S.	5862	0.16	185559	2.6	0.01	9617	396	1.4	2.1	31713	-	-	0.003	73	0.01	0.29	5.8
	381	48749	0.01	0.01	I.S.	23615	0.17	98387	6.5	0.05	7925	1062	3.5	0.28	162687	-	-	0.002	25	0.01	0.79	13
	258	38382	0.002	<0.001	I.S.	41009	0.19	161361	1.4	0.16	5742	365	0.26	0.60	85267	-	-	0.002	63	0.01	1.8	6.9
G10847	15	10350	0.06	0.29	I.S.	143706	0.47	243107	21	0.17	6116	1174	0.12	0.71	271488	0.25	-	0.02	2313	0.07	8.5	1.3
	9.5	9928	0.03	0.91	I.S.	146696	0.62	278285	12	0.18	4568	1421	0.11	0.41	328375	0.33	-	0.03	3095	0.06	36	1.9
	15	9728	0.02	0.18	I.S.	144937	0.30	229879	5.5	0.04	5101	1098	0.07	0.64	252690	0.11	-	0.10	1793	0.06	12	1.3
	18	9232	0.02	0.15	I.S.	142087	0.22	184679	4.2	<0.001	4477	1218	0.08	2.5	241192	0.62	-	0.30	2043	0.74	Inc.	1.2
	14	10331	0.01	0.23	I.S.	137905	0.24	234076	7.1	0.07	1608	1220	0.09	1.6	269257	0.20	-	0.01	2935	0.10	14	1.1
	18	10307	0.03	0.67	I.S.	146139	0.36	245469	7.5	0.06	7166	1288	0.10	0.27	280380	0.21	-	0.03	2535	0.01	6.5	1.3
	20	9864	0.02	0.27	I.S.	144752	0.28	230923	27	0.03	1857	1312	0.08	1.8	297890	1.4	-	0.02	2868	0.02	10	1.1
	24	10109	0.09	0.26	I.S.	147052	0.37	236352	8.3	0.03	1752	1348	0.07	0.26	294628	<0.001	-	0.02	2669	0.02	11	1.2
	21	9996	0.02	0.30	I.S.	166803	0.29	293894	10	0.08	2070	1663	0.12	0.79	347368	0.62	-	0.02	3215	0.05	9.8	1.3
	24	10200	0.02	0.25	I.S.	148884	0.22	229573	8.4	0.07	16920	1513	0.07	0.26	308602	0.22	-	0.02	3213	0.01	4.6	1.1
EV8	6.4	53796	0.21	0.15	I.S.	15628	0.18	87	4.4	-	255545	419	1.9	431	293212	0.78	0.03	0.01	10	2.2	31921	984
	6.1	54378	0.13	0.58	I.S.	16567	0.18	4.0	31	-	311069	590	0.57	180	348007	0.40	<0.001	0.04	10	5.1	Inc.	Inc.
	Inc.	68549	0.34	1.4	I.S.	144525	Inc.	117	18	-	294398	1896	8.7	259	306312	0.79	<0.001	0.03	28	4.5	87892	1774
	5.8	53853	0.15	0.11	I.S.	14703	0.29	102	15	-	273644	632	1.1	285	303631	0.54	0.01	0.15	12	1.8	33633	1009
	8.3	52082	0.19	0.10	I.S.	16881	0.31	168	13	-	271552	715	2.6	720	306846	0.52	0.01	0.06	22	2.5	64226	1489
	8.7	49508	0.27	0.11	I.S.	22402	0.33	493	25	-	296578	908	2.4	668	331074	0.64	0.01	0.43	27	6.1	Inc.	Inc.
	6.8	50051	0.22	0.10	I.S.	16590	0.18	93	3.0	-	260151	773	1.2	335	292667	<0.001	<0.001	0.04	17	0.61	12719	616
	15.04	50700	0.14	0.12	I.S.	22758	0.31	127	10	-	294259	1219	4.7	Inc.	322645	<0.001	<0.001	0.02	18	5.7	Inc.	Inc.
	5.7	57850	0.21	0.32	I.S.	15413	0.04	4.9	15	-	339112	824	1.6	461	354411	2.5	0.15	0.01	34	2.3	Inc.	Inc.

	5.4	54384	0.13	0.12	I.S.	17263	0.07	9.3	56	-	300979	723	1.1	300	330730	2.0	0.01	0.01	12	6.6	Inc.	Inc.
Hj14	36	51776	0.01	<0.001	I.S.	9975	<0.001	58	3.8	0.31	167180	131	0.07	12	293653	0.36	-	3.3	0.38	1.4	Inc.	0.01
	86	48435	0.01	<0.001	I.S.	10693	0.03	294	2.4	0.10	173005	145	0.03	12	279682	<0.001	-	7.1	0.26	0.01	Inc.	0.15
	88	52222	<0.001	<0.001	I.S.	11137	0.01	369	7.3	<0.001	182311	169	0.01	4.4	293599	<0.001	-	15	0.36	0.01	29	0.003
	84	50133	<0.001	<0.001	I.S.	10646	<0.001	446	0.79	<0.001	188588	149	0.01	6.0	295929	<0.001	-	17	0.20	<0.001	34	0.002
	94	51173	0.07	0.09	I.S.	11706	0.02	383	1.1	0.09	186483	190	0.13	43	293094	0.16	-	11	0.14	0.01	41	0.002
	95	52493	<0.001	<0.001	I.S.	11136	<0.001	309	0.72	<0.001	198797	179	0.06	33	308603	<0.001	-	11	0.24	0.01	52	0.03
G6948	552	43041	0.09	0.23	I.S.	42397	0.03	11488	187	0.05	26551	968	1.2	73	402035	<0.001	-	0.01	0.49	0.01	3.2	1594
	477	43948	0.03	0.33	I.S.	46194	0.06	1900	103	0.07	29794	1220	1.6	57	456198	0.17	-	0.03	0.77	0.01	1.5	2485
	465	44237	0.02	0.30	I.S.	42525	0.21	20517	134	0.03	26478	988	1.6	53	418457	0.82	-	0.02	0.62	0.01	3.0	2288
	419	42571	0.09	0.85	I.S.	40761	0.02	4617	123	0.03	27681	886	1.7	19	376142	0.74	-	0.01	6.2	0.02	3.7	2089
	443	43676	0.03	0.30	I.S.	46845	0.03	14202	170	0.08	26919	1051	1.4	62	434544	<0.001	-	0.02	0.63	0.01	2.6	3016
	512	45685	0.03	0.29	I.S.	44406	0.04	11672	276	<0.001	29724	1019	1.6	52	453027	0.53	-	0.02	0.65	0.02	1.7	2318
	550	42937	0.21	0.29	I.S.	47274	0.15	4791	68	0.03	29154	1087	1.3	124	436845	0.29	-	0.02	Inc.	0.01	11	1485
	614	42985	0.13	0.26	I.S.	49753	0.04	3153	167	0.03	30838	1080	1.4	93	435529	1.5	-	0.02	Inc.	0.04	4.9	1757
	499	43061	0.27	0.63	I.S.	47372	0.03	4378	50	0.06	27535	1050	1.2	61	413303	0.88	-	0.01	6.6	0.02	2.3	1389
	636	42539	0.25	0.14	I.S.	46071	0.01	5497	77	0.20	31586	980	1.3	53	373290	0.46	-	0.04	3.5	0.02	12	909
G14549b	2.5	36716	0.32	0.86	I.S.	65969	0.21	2255	4.2	0.03	44759	6192	0.10	14	405268	<0.001	-	0.85	36	0.40	Inc.	1187
	4.5	35231	0.39	2.0	I.S.	95168	0.18	1950	29	0.29	42035	3617	0.84	52	398781	<0.001	-	0.38	43	1.2	1926	344
	Inc.	44137	1.1	0.17	I.S.	44081	0.23	3411	11	<0.001	35349	3644	0.36	29	388056	0.07	-	0.22	27	2.0	402	271
	3.1	38255	0.87	0.41	I.S.	75910	0.21	1623	5.2	0.03	Inc.	4902	0.46	Inc.	431676	<0.001	-	0.27	33	0.24	448	130
	2.0	44077	0.88	Inc.	I.S.	40637	0.19	1378	26	0.26	58691	3989	0.32	34	403104	0.10	-	0.63	91	1.0	169	39
	2.9	45311	2.7	0.21	I.S.	48890	0.09	1213	5.2	<0.001	44370	3439	0.28	4.1	412835	0.33	-	0.41	19	1.5	213	254
	0.32	40089	3.1	0.32	I.S.	43457	0.05	1234	8.4	0.03	41662	4721	0.32	1.3	429886	0.58	-	0.49	75	0.57	1928	612
	2.1	32321	1.3	0.13	I.S.	67264	0.02	Inc.	14	0.29	57887	5978	0.51	32	401587	0.07	-	0.29	45	0.51	Inc.	601
	2.8	40528	0.68	0.79	I.S.	51676	0.02	2956	6.2	0.02	63071	3791	0.03	1.1	409639	0.10	-	0.16	Inc.	0.22	374	1054
	0.81	33665	0.67	0.13	I.S.	50654	0.02	1274	3.9	0.02	50831	7036	0.06	2.9	349410	0.11	-	0.20	52	0.63	1509	258
Mo17A	Inc.	33606	0.005	0.17	I.S.	10099	<0.001	59632	3.1	<0.001	11511	1443	0.02	0.16	83708	1.6	-	<0.001	3.6	0.002	3.7	4.4
	0.69	36316	<0.001	<0.001	I.S.	11688	0.003	57046	9.2	0.01	16503	1256	0.01	0.01	96058	1.5	-	0.27	0.85	0.001	8.1	3.9
	0.41	44542	0.10	<0.001	I.S.	14151	0.003	1270	6.4	0.12	91483	2310	0.02	0.02	212140	1.3	-	0.01	2.6	0.23	2.4	2.5
	0.39	43583	0.07	<0.001	I.S.	13707	0.03	1403	6.1	0.04	83013	1953	0.03	0.06	211961	0.20	-	0.01	2.3	<0.001	0.40	2.7
	0.48	41403	0.51	<0.001	I.S.	14225	0.003	2163	4.4	<0.001	65796	1767	0.03	0.02	200882	0.15	-	0.01	0.90	0.35	12	3.0
	0.51	40009	0.27	0.01	I.S.	13079	0.01	1120	5.5	0.04	69372	1775	0.03	0.12	199834	0.22	-	0.05	1.0	0.12	4.5	2.5
ORV1	0.34	8163	20	3.2	I.S.	72335	<0.001	41486	26	0.14	3394	1191	0.39	0.18	227560	0.90	-	0.004	33	<0.001	7.2	Inc.
	0.40	8178	22	2.8	I.S.	73955	0.14	42114	0.77	<0.001	3357	1042	0.43	0.03	237564	<0.001	-	<0.001	24	<0.001	4.7	0.18
	0.16	8228	23	1.7	I.S.	70362	0.01	35926	15	<0.001	3384	1070	0.90	0.08	245674	<0.001	-	<0.001	38	<0.001	9.7	11
	0.04	33437	2.9	6.9	I.S.	1997	0.09	20741	5.7	0.14	5630	108	0.07	0.02	258020	0.30	Inc.	0.01	25	0.02	Inc.	0.05

	0.05	30660	13	6.9	I.S.	9157	0.06	20882	51	0.48	5163	682	0.09	0.17	263172	1.3	-	0.05	69	0.01	Inc.	4.6
	0.12	7161	23	2.8	I.S.	76801	<0.001	35247	22	0.11	3131	954	0.35	0.02	244792	0.73	-	<0.001	36	<0.001	1.8	Inc.
	0.18	6742	25	0.87	I.S.	78404	0.06	29179	5.1	0.18	3739	1293	0.53	0.17	257401	<0.001	-	<0.001	29	0.005	3.4	2.9
	0.17	9760	27	0.80	I.S.	74391	<0.001	38090	33	<0.001	3555	1331	0.51	0.04	235996	<0.001	-	0.01	33	0.002	3.4	37
	0.28	9164	25	1.8	I.S.	71749	<0.001	30933	17	0.11	3996	1414	0.58	0.39	247532	<0.001	-	<0.001	33	<0.001	1.9	0.42
	0.05	12846	50	0.62	I.S.	65594	0.06	31149	40	0.10	4883	707	0.11	0.06	240187	0.21	-	<0.001	Inc.	<0.001	0.32	39
G14549a	1.1	29362	0.28	0.14	I.S.	53372	0.02	2523	4.2	0.02	61232	2506	0.02	1.9	329615	0.32	0.01	0.08	24	0.29	861	281
	2.9	33659	1.5	4.3	I.S.	40046	0.14	4139	17	0.12	62819	3186	0.37	2.4	315541	0.10	0.02	0.36	24	0.36	Inc.	5336
	1.8	15481	0.83	0.46	I.S.	102544	0.07	5472	18	0.03	53031	3795	0.01	1.7	368223	<0.001	0.01	0.19	24	0.16	Inc.	1656
	1.2	36529	0.30	1.1	I.S.	40439	0.11	2876	2.7	0.01	39740	2425	0.16	22	355981	<0.001	<0.001	0.20	17	0.54	689	826
	0.91	38173	0.78	0.81	I.S.	34348	0.09	5825	12	0.02	43820	2102	0.61	102	343816	0.09	<0.001	0.11	19	0.46	957	1636
	1.5	39048	0.45	0.14	I.S.	84213	0.16	2948	26	0.03	40725	4472	5.1	24	342205	0.09	<0.001	0.24	33	0.38	Inc.	4866
	1.4	34346	0.59	0.09	I.S.	45033	0.15	3252	8.4	0.02	46559	2386	0.17	17	340651	0.08	0.01	0.49	21	0.12	Inc.	3668
	1.3	36198	0.79	0.35	I.S.	41816	0.08	5311	0.24	0.01	33540	2103	0.51	79	312188	<0.001	0.05	0.09	8.4	0.47	810	1285
	1.5	34995	1.0	0.65	I.S.	40418	0.25	4001	14	0.02	50036	3618	0.62	93	311011	<0.001	0.01	0.15	30	0.19	Inc.	4193
	0.62	35231	0.81	0.42	I.S.	40953	0.21	3534	24	0.01	39030	4449	0.66	82	336306	<0.001	0.01	0.09	51	0.07	929	4194
G873	1.1	28825	0.60	0.31	I.S.	93856	0.17	119007	9.6	0.13	48136	4042	8.1	1.1	409557	0.70	0.03	0.22	73	0.03	30	0.19
	2.5	25912	0.17	0.37	I.S.	102707	0.04	119275	9.3	0.06	46933	3087	10	0.32	402930	0.15	0.03	0.07	57	0.07	22	0.09
	1.3	26263	0.47	0.49	I.S.	115321	0.07	156752	15	0.05	50736	4828	11	0.50	494590	0.23	0.03	0.08	88	0.08	27	0.09
	1.6	30034	5.4	0.40	I.S.	101813	0.13	117266	12	0.05	63925	5223	8.2	1.4	476415	0.19	0.03	0.02	92	0.05	25	0.35
	1.3	30338	5.2	0.28	I.S.	88921	0.09	114694	40	0.05	52253	4345	7.8	0.79	380403	0.20	0.02	0.05	94	0.04	26	0.05
	0.77	27312	0.47	0.18	I.S.	101701	0.08	93092	4.9	2.9	51396	7664	12	0.87	381658	<0.001	0.01	Inc.	64	0.33	Inc.	0.06
	4.0	26677	1.1	0.21	I.S.	90434	0.02	94597	20	0.04	49685	3919	7.3	0.19	361713	0.09	<0.001	0.19	52	0.07	Inc.	0.03
	0.19	26546	0.50	0.18	I.S.	87712	0.13	100298	5.1	0.03	44795	4247	9.5	0.42	331473	0.23	0.12	0.04	46	0.01	19	0.05
	2.4	23851	0.10	0.98	I.S.	96496	0.02	85400	3.9	0.03	45197	2835	10	0.71	336158	0.06	<0.001	0.04	21	0.06	24	0.09
	1.0	22494	0.33	0.15	I.S.	98155	0.13	77970	8.0	0.02	44774	2913	13	0.71	342780	0.06	0.05	0.01	36	0.06	12	0.08
G16152	0.98	26401	3005	17	I.S.	84799	0.03	179370	6.5	0.11	4224	656	4.0	2.6	274713	-	0.02	0.01	3145	0.02	3.0	38
	0.32	26596	3042	9.3	I.S.	86671	0.12	233465	9.2	1.8	4377	678	4.0	38	290133	-	0.03	0.01	4872	0.02	Inc.	94
	0.34	28911	2733	15	I.S.	87701	0.04	312625	38	3.6	3803	551	3.6	167	256933	-	0.02	0.02	2352	0.03	55	7.3
	0.16	19365	2769	9.5	I.S.	97498	0.02	88635	4.4	0.25	5868	677	5.0	1.4	320734	-	<0.001	0.01	3977	0.07	4.2	Inc.
	0.27	24707	3088	11	I.S.	86615	0.07	176640	7.7	0.88	4518	692	1.8	3.7	310184	-	0.01	0.01	4273	0.01	4.1	22
	0.42	24560	2800	5.9	I.S.	83268	0.01	145921	7.6	2.5	3791	601	2.6	9.7	245887	-	<0.001	0.08	1949	0.03	37	7.5
	0.75	26822	2821	4.4	I.S.	77978	0.03	202577	32	0.80	4292	717	4.9	35	248094	-	<0.001	0.02	3984	0.01	Inc.	29
	0.26	27166	2163	15	I.S.	81539	0.05	218215	8.1	1.4	3903	709	1.6	11	265606	-	0.06	0.02	2718	0.01	3.4	6.1
	1.0	26862	2577	27	I.S.	80129	0.03	222436	9.5	7.5	4793	801	1.6	7.9	300080	-	<0.001	0.02	3324	0.02	5.4	2.7
	0.24	12364	126	0.97	I.S.	113744	0.08	117552	7.6	0.46	4956	745	1.4	0.52	324755	-	<0.001	0.01	3963	0.02	17	55
G871	0.58	19847	470	1.5	I.S.	19043	0.03	32093	16	0.06	322	71	0.01	0.21	375093	0.81	0.02	0.02	189602	0.04	0.20	0.11

	0.35	16636	361	0.27	I.S.	25532	0.04	13554	9.5	<0.001	320	102	0.04	0.30	427876	<0.001	0.02	0.02	252741	0.01	3.9	0.26
	0.22	11291	566	0.45	I.S.	26275	0.08	56126	29	0.11	400	164	0.10	0.20	335621	0.23	0.02	0.02	199870	0.01	0.34	0.35
	0.26	12451	611	0.21	I.S.	33978	0.08	91346	7.4	0.18	407	213	0.02	1.2	333815	<0.001	0.07	0.04	170873	0.01	2.3	0.18
	0.90	20398	145	0.21	I.S.	17236	0.03	160177	31	0.03	298	55	0.43	0.20	265324	0.64	0.02	0.02	110684	0.02	1.8	0.46
	0.24	12776	135	0.22	I.S.	17892	0.03	69862	7.0	0.03	400	89	0.03	0.21	333813	<0.001	<0.001	0.08	171082	0.01	0.66	0.06
	1.6	11621	Inc.	0.85	I.S.	35014	0.01	83441	16	0.22	334	208	0.10	0.11	282146	0.09	<0.001	0.01	80323	0.004	3.6	0.22
	0.22	10503	197	0.21	I.S.	19795	0.02	61098	6.4	0.03	425	136	0.04	0.57	323076	<0.001	0.01	0.02	154442	0.01	0.44	0.06
	0.11	13176	229	0.59	I.S.	29500	0.01	40633	21	0.01	404	89	0.16	0.33	301971	<0.001	0.07	0.01	66921	0.04	1.9	0.71
	0.18	9581	727	0.67	I.S.	33601	0.11	65944	27	0.55	412	268	0.01	0.16	302144	0.19	<0.001	0.01	95804	0.01	3.1	0.07
G874	0.13	31143	440	0.11	I.S.	18837	0.09	90487	16	0.03	167	40	3.3	0.50	270609	0.33	0.01	0.01	51135	0.01	4.6	1.2
	0.19	9414	317	0.52	I.S.	74668	0.02	64328	4.5	0.12	196	256	0.51	0.15	331700	0.11	0.02	0.01	123817	0.01	7.6	0.02
	0.71	18981	1306	0.15	I.S.	47243	0.02	78753	50	0.13	223	111	2.9	0.14	318690	0.31	0.04	0.01	103980	0.02	6.4	1.4
	0.14	12486	568	0.23	I.S.	75477	0.02	44565	28	0.10	176	159	0.58	0.12	328259	<0.001	0.03	0.01	55954	0.004	2.7	0.01
	0.41	9487	181	0.15	I.S.	85319	0.03	69449	4.7	0.26	189	309	0.88	0.57	336530	0.13	<0.001	0.01	76309	0.01	6.4	0.03
	0.21	10787	169	0.18	I.S.	88950	0.03	80486	11	0.17	153	186	3.0	1.2	334090	<0.001	0.02	0.04	62355	0.01	8.7	0.02
	0.54	8189	682	0.10	I.S.	62623	0.01	34091	2.6	0.10	266	590	1.2	0.46	339391	0.51	0.01	0.01	92937	0.01	6.8	0.54
	0.17	10273	715	0.14	I.S.	68534	0.05	51657	4.0	0.02	211	407	3.2	0.56	337872	0.07	0.01	0.02	94192	0.01	2.6	0.95
	0.62	9397	122	0.16	I.S.	84265	0.02	62012	16	0.15	199	301	0.35	0.16	348833	0.17	0.06	0.01	69100	0.02	0.39	0.02
	1.5	18417	1071	0.25	I.S.	39771	0.03	96639	7.0	0.05	277	274	2.1	0.86	392516	0.12	<0.001	0.01	131952	0.03	13	0.51
G879	11	60379	1.4	0.99	I.S.	32979	0.24	3353	-	-	27498	357	17	0.40	577874	0.26	0.03	0.06	19	0.10	8.2	1196
	Inc.	55658	Inc.	Inc.	I.S.	39533	0.03	4499	-	-	22851	431	23	0.58	476823	0.13	<0.001	0.40	24	0.36	91	1344
	12	56776	2.6	0.48	I.S.	32644	0.23	2036	-	-	27942	362	16	0.44	563315	0.26	0.05	0.08	9.8	0.08	3.2	1059
	7.6	57337	1.9	0.30	I.S.	32054	0.04	4251	-	-	25411	284	15	0.28	494550	<0.001	<0.001	0.06	8.7	0.02	2.4	624
	6.5	56408	4.2	9.3	I.S.	41733	0.16	9538	-	-	31518	496	19	3.7	672341	0.59	0.06	0.03	39	0.20	37	1228
	1.6	52942	9.6	0.37	I.S.	44244	0.04	3300	Inc.	-	23398	406	11	1.8	498860	<0.001	0.03	0.02	31	0.01	2.1	1100
	5.6	55623	2.6	0.47	I.S.	33504	0.06	7464	-	-	23037	345	13	0.40	505839	0.35	0.03	0.12	11	0.05	2.8	1051
	12	52774	2.5	1.1	I.S.	35319	0.52	2328	-	-	24291	395	19	4.5	479191	0.16	0.15	0.13	14	0.21	28	1225
	3.3	54001	2.2	0.47	I.S.	32815	0.05	13984	-	-	22527	375	8.6	2.0	500881	1.1	<0.001	0.02	25	0.01	1.5	2668
	5.5	54156	5.8	3.3	I.S.	31000	0.04	34800	-	-	20638	349	10	0.36	463099	<0.001	0.03	0.01	21	0.01	5.3	796
G882	0.38	33234	1246	0.39	I.S.	19620	0.11	225825	54	0.73	234	194	5.6	0.33	288425	0.22	0.02	0.09	79492	0.01	24	6.6
	2.1	33341	1090	1.2	I.S.	18815	0.20	242130	11	1.1	226	160	0.32	0.37	323348	1.6	0.02	0.14	73554	0.05	128	6.8
	0.40	30600	976	0.47	I.S.	36154	0.04	180662	27	0.20	213	106	3.2	1.6	354014	0.31	0.02	0.03	64653	0.01	40	1.9
	0.46	34967	211	0.48	I.S.	19259	0.23	154997	62	0.12	284	126	2.9	1.8	402352	0.51	0.08	0.03	45776	0.06	8.4	7.3
	0.42	32265	165	0.43	I.S.	29407	0.05	109532	13	0.33	293	541	0.19	0.37	432078	0.22	0.02	0.03	66763	0.01	38	9.0
	0.40	31993	1190	0.99	I.S.	22723	0.29	229050	220	0.06	231	184	5.8	0.36	325212	0.55	0.06	0.02	70068	0.01	35	8.2
	0.52	31768	290	0.54	I.S.	39165	0.23	163180	16	0.27	268	131	1.7	0.48	449131	2.6	0.06	0.03	46722	0.02	16	2.9
	1.7	25661	702	0.38	I.S.	37233	0.04	118049	130	0.63	427	213	3.4	0.35	424295	0.19	<0.001	0.02	119006	0.12	78	4.9

	0.31	6506	106	0.29	I.S.	24693	0.04	92024	10	0.04	449	805	0.08	0.30	349695	0.23	0.02	0.05	321170	0.01	0.16	0.05
	0.43	8096	157	0.45	I.S.	20913	0.11	144649	14	0.06	403	816	0.11	0.84	346574	0.45	0.11	0.02	348698	0.01	0.24	0.09
G6946	0.36	21741	39	15	I.S.	109448	0.04	29118	102	0.16	6386	1237	1.8	0.30	456856	<0.001	<0.001	0.02	2615	0.01	2.5	68
	0.36	23844	29	22	I.S.	102458	0.23	25145	30	0.06	6452	1091	1.5	0.31	458643	0.84	<0.001	0.04	1523	0.01	3.7	46
	0.52	25611	22	21	I.S.	105561	0.05	40632	60	0.05	7077	1661	0.79	3.1	524278	0.25	<0.001	0.06	3494	0.01	27	19
	1.3	24455	24	20	I.S.	102094	0.04	26061	32	0.08	6365	1175	0.78	1.2	458701	<0.001	0.03	0.02	1335	0.01	1.0	17
	1.7	17738	126	19	I.S.	112987	0.22	22152	49	0.12	5933	1173	0.85	0.71	405648	<0.001	<0.001	0.01	1896	0.01	1.4	39
	1.1	24993	13	34	I.S.	96603	0.14	18097	39	0.03	6332	1141	0.63	1.1	455560	0.62	0.02	0.01	1132	0.01	4.2	25
	1.7	20152	116	35	I.S.	118667	0.04	24706	104	0.05	6012	1248	1.2	4.1	490330	0.27	<0.001	0.02	1509	0.01	6.6	502
	4.4	17739	77	40	I.S.	120207	0.16	32744	79	0.04	5531	1399	1.9	7.2	474152	0.29	<0.001	0.08	2322	0.01	Inc.	147
	1.3	21795	45	36	I.S.	107532	0.28	21040	81	0.03	6051	1283	2.2	3.6	466161	1.0	0.03	0.02	1708	0.03	9.2	66
	1.3	21848	42	35	I.S.	109075	0.15	26069	50	0.14	5884	1275	2.2	1.9	474394	0.27	0.07	0.02	1641	0.01	10	55
G6949	7.7	54438	0.04	0.33	I.S.	31734	0.04	6430	10	0.06	12747	306	19	1.6	488225	<0.001	-	0.02	13	0.60	18	2079
	8.1	57377	0.51	0.37	I.S.	32551	0.06	6847	28	0.06	10969	259	29	8.4	486756	Inc.	Inc.	0.25	18	1.2	52	2341
	5.9	54909	0.02	1.4	I.S.	25677	0.15	8861	16	0.02	12397	237	11	0.57	418388	0.40	-	0.09	11	1.1	29	2700
	32	55487	0.75	Inc.	I.S.	29965	0.17	16439	8.3	0.04	11392	213	15	4.9	460376	<0.001	-	Inc.	9.5	0.34	15	3684
	9.1	56484	0.03	0.22	I.S.	26248	0.07	8437	24	0.02	11564	251	9.4	0.54	426552	0.11	-	0.01	6.3	0.08	1.7	3266
	8.8	55657	0.12	6.7	I.S.	29109	0.04	8419	40	0.18	12799	294	13	3.1	460980	0.14	-	0.18	10	1.1	26	1261
	11	55621	0.54	7.3	I.S.	28174	0.02	7737	4.5	0.02	12431	311	12	2.5	427218	0.08	-	0.12	11	0.47	27	2222
	16	56442	0.01	3.3	I.S.	26032	0.25	7639	5.9	0.02	11598	269	9.3	1.5	418326	0.16	-	0.05	19	0.93	11	2080
	8.3	57910	0.75	0.39	I.S.	35942	0.06	8334	12	0.05	14518	376	19	1.8	594767	0.22	-	0.07	18	0.22	1.9	5164
	5.9	53095	0.40	3.2	I.S.	33139	0.05	10073	12	0.41	11737	312	18	5.2	531971	<0.001	-	0.10	19	0.56	7.3	3411
G11701	0.29	50615	77	0.27	I.S.	25475	0.04	148	8.7	0.11	301902	483	0.06	0.83	370762	<0.001	0.02	0.02	282	0.13	3.6	24
	0.26	43795	60	0.23	I.S.	22184	0.03	130	38	0.04	226723	714	0.12	2.0	328429	0.23	<0.001	0.01	164	0.01	3.0	80
	1.7	41475	72	1.9	I.S.	23280	0.03	127	7.5	0.03	214605	1706	0.19	0.24	320655	0.17	<0.001	0.02	219	0.02	2.3	21
	2.4	49444	67	0.22	I.S.	23519	0.02	132	5.7	0.25	270378	303	0.20	9.3	336723	<0.001	0.02	0.01	77	0.01	11	38
	1.1	49919	68	0.33	I.S.	26385	0.03	164	8.4	0.05	282370	435	0.16	0.28	372828	<0.001	<0.001	0.02	137	0.01	6.6	23
	1.4	45703	79	1.1	I.S.	24095	0.03	138	41	<0.001	238149	1621	0.20	2.5	346840	<0.001	<0.001	0.03	257	0.01	3.6	24
	0.61	26309	55	0.14	I.S.	56852	0.01	86	3.3	0.08	210048	2536	0.16	1.6	288463	0.08	0.07	0.03	215	0.003	6.5	12
	1.1	42757	106	0.88	I.S.	22918	0.04	112	6.9	0.03	205438	550	0.09	2.1	334038	<0.001	0.03	0.05	104	0.01	9.8	4.3
	0.93	44627	121	0.25	I.S.	24090	0.03	88	6.7	0.12	219621	331	0.14	25	336465	0.71	<0.001	0.20	104	0.01	9.1	2.3
	1.3	45306	73	0.26	I.S.	31393	0.18	210	6.9	0.03	245633	2559	0.13	7.4	348983	<0.001	0.02	0.02	361	0.02	5.8	2.3
G14246	Inc.	49883	5.0	0.16	I.S.	38865	0.15	4544	-	0.02	12860	428	2.1	0.98	398745	0.52	0.01	0.01	18	0.01	1.1	3075
	36	50059	5.2	0.45	I.S.	36883	0.16	11959	-	0.12	12736	436	2.2	0.73	390849	0.08	<0.001	0.02	18	0.03	1.0	1263
	19	51217	0.61	0.13	I.S.	35923	0.07	4069	-	<0.001	12197	431	4.2	3.3	385601	<0.001	0.01	0.01	34	0.26	8.4	2185
	6.7	54006	3.3	0.25	I.S.	30369	0.03	3392	Inc.	0.04	12439	411	5.1	2.0	433938	<0.001	0.01	0.02	61	0.07	2.8	3488
	6.4	56695	1.8	0.20	I.S.	23564	0.10	2025	-	0.03	13386	338	14	2.6	397864	0.08	<0.001	0.03	78	0.10	2.1	3488

	35	59576	2.7	0.47	I.S.	18171	0.02	2536	-	0.02	14608	283	11	1.2	403100	0.65	0.03	0.01	91	0.08	1.6	873
	12	58672	1.9	0.15	I.S.	16411	0.02	9359	-	0.06	12274	308	10	0.87	374784	<0.001	<0.001	0.01	69	0.09	2.8	1623
	34	52332	2.7	0.12	I.S.	28226	0.02	8951	-	0.02	13371	408	2.3	0.61	383770	0.05	0.01	0.04	39	0.16	9.8	3295
	5.6	58359	3.6	0.20	I.S.	17146	0.03	2660	-	0.19	14772	301	9.6	2.2	397867	0.57	0.01	0.05	94	0.04	1.1	2389
	11	58918	3.4	0.21	I.S.	16307	0.05	3144	-	0.07	14553	308	12	0.24	409492	0.29	0.01	0.02	81	0.01	1.0	1014
G14867	0.28	56754	151	0.19	I.S.	17904	0.10	552799	338	0.05	66	194	3.0	0.21	98170	0.10	-	0.03	1234	0.05	2.4	3758
	Inc.	52379	148	0.18	I.S.	16011	0.04	529296	300	0.02	58	169	3.0	0.70	66246	0.13	-	0.01	1294	0.49	Inc.	3505
	0.70	50621	141	1.1	I.S.	15174	0.02	530265	257	0.02	85	146	2.8	0.98	62603	<0.001	-	0.05	1408	0.45	Inc.	3293
	0.37	49175	150	0.34	I.S.	17303	0.05	498297	350	0.35	109	198	3.2	1.5	158469	0.34	-	0.02	11036	0.08	4.0	5937
	0.36	51786	142	0.31	I.S.	15572	0.01	370539	301	0.30	66	174	3.0	0.42	108947	<0.001	-	0.02	2622	0.24	Inc.	2677
	0.16	49445	145	0.13	I.S.	16594	0.10	410102	124	0.17	93	164	3.0	1.3	123147	0.06	-	0.01	7091	0.01	3.2	3130
	0.36	50566	149	0.91	I.S.	17012	0.13	535019	429	0.23	53	179	2.7	0.30	143414	0.25	-	0.02	8673	0.01	2.9	4586
	0.41	50694	148	0.36	I.S.	17839	0.14	549079	1175	0.04	44	202	2.9	0.68	159738	1.7	-	0.02	8999	0.05	4.3	2724
	0.24	50947	145	1.6	I.S.	16647	0.04	476369	186	0.13	52	201	4.0	0.42	120218	0.84	-	0.01	5684	0.05	2.3	3263
	0.38	49624	143	0.32	I.S.	16904	0.04	535705	296	0.24	73	201	2.8	0.30	145757	<0.001	-	0.02	5060	0.01	1.9	4806
Mo16	14	34434	0.002	<0.001	I.S.	15116	0.02	30592	15	0.03	19270	1866	0.02	0.06	119768	1.5	-	0.01	27	0.001	2.9	3.8
	9.1	37210	21	5.0	I.S.	8144	0.17	84476	8.9	<0.001	10799	1086	0.03	0.14	58367	3.4	-	0.05	43	0.10	Inc.	1.9
	22	37118	0.04	<0.001	I.S.	3125	<0.001	81385	8.8	<0.001	7618	688	0.03	0.12	49820	1.2	-	0.01	23	0.001	1.6	2.4
G29851	2.6	42398	75	0.45	I.S.	47180	0.05	584483	37	0.21	747	577	0.21	1.3	30080	1.2	0.02	0.02	74368	0.08	82	529
	0.49	41167	72	0.51	I.S.	42074	0.04	492228	12	0.20	663	485	0.22	0.38	27604	0.23	0.17	0.03	73872	0.04	32	322
	0.48	41066	93	1.0	I.S.	51287	0.06	456357	77	2.5	1064	560	0.36	1.8	114627	0.32	0.03	0.02	80459	0.01	65	859
	0.51	37436	103	2.1	I.S.	54333	0.07	458896	55	0.42	1512	729	0.39	0.40	161189	3.5	0.04	0.03	107978	0.01	42	4745
	0.64	37817	131	1.4	I.S.	71298	0.36	585677	48	2.1	1662	633	0.50	2.0	191550	2.0	0.03	0.03	102337	0.04	110	693
	0.39	45235	63	0.95	I.S.	48526	0.05	594945	26	0.08	660	505	0.27	0.30	40011	4.4	0.23	0.02	71154	0.02	105	310
	0.35	42168	98	0.40	I.S.	45208	0.20	565908	9.8	0.40	583	433	0.20	0.28	25369	0.72	0.06	0.03	74343	0.02	27	653
	0.93	37111	53	0.85	I.S.	44820	0.04	559474	24	0.50	648	409	0.15	0.27	23769	1.2	0.03	0.02	72212	0.09	236	556
	2.0	48881	43	2.6	I.S.	37919	0.04	497179	9.8	2.8	741	466	0.41	2.0	26127	1.8	0.02	0.73	95588	0.68	295	1835
	0.39	43990	51	0.45	I.S.	49453	0.04	565084	33	1.0	807	552	0.41	0.32	75105	1.5	0.06	0.15	56308	0.23	84	3110
ORV4	60	9115	2.6	0.87	I.S.	94207	0.03	42323	16	0.11	1662	1576	5.8	0.03	266862	3.6	-	-	22	0.002	2.6	398
	30	10508	0.87	2.1	I.S.	87850	<0.001	59294	12	0.19	1436	1465	6.4	0.02	242188	2.3	-	-	26	0.001	1.6	83
	25	10416	2.8	2.8	I.S.	89264	<0.001	48058	11	0.15	1576	1557	6.3	0.07	260251	1.0	-	-	30	<0.001	Inc.	301
	49	13773	1.9	0.56	I.S.	87215	<0.001	110832	12	0.16	832	1184	2.6	0.04	131496	17	-	-	12	<0.001	1.2	Inc.
	0.38	33243	Inc.	1.5	I.S.	31854	<0.001	46230	4.2	<0.001	1832	658	0.16	0.03	245803	<0.001	-	-	78	0.04	2.3	1.3
	0.34	14723	8.1	1.1	I.S.	83122	0.01	57027	4.8	0.26	1294	694	4.3	0.21	255710	0.90	-	-	49	0.01	7.8	8.6
	85	10426	1.4	2.4	I.S.	95007	<0.001	59050	16	1.0	1337	1332	4.7	0.13	262609	2.8	-	-	19	0.02	4.1	203
	38	9796	1.3	0.95	I.S.	94909	<0.001	41986	11	<0.001	1360	1614	5.8	0.04	287424	1.8	-	-	31	<0.001	2.4	109
	0.86	19912	7.5	0.71	I.S.	79547	0.10	41084	11	<0.001	1534	884	1.7	0.09	289018	0.66	-	-	66	0.04	0.76	120

	3.8	8828	3.2	6.1	I.S.	99578	0.07	59258	18	<0.001	1225	1725	7.4	0.03	263965	0.46	-	-	37	0.01	3.0	38
G12640	86	38169	2.9	0.93	I.S.	108446	0.17	401110	124	0.04	1267	635	0.34	2.6	228726	5.7	0.02	0.02	1665	0.04	9.7	62
	91	37803	3.6	0.48	I.S.	112812	0.05	413475	91	0.04	1306	640	0.36	2.0	228565	5.5	<0.001	0.01	1737	0.02	8.4	59
	86	37394	3.3	0.48	I.S.	109756	0.05	426326	138	0.08	1246	622	0.32	2.0	228479	13	0.02	0.02	1807	0.01	8.1	50
	58	36752	3.2	0.40	I.S.	108277	0.11	395135	121	0.20	1093	609	0.32	3.1	213923	4.8	0.11	0.02	1580	0.03	3.9	53
	69	35354	2.8	0.24	I.S.	111317	0.21	329379	99	0.15	1209	611	0.32	2.6	202632	8.8	<0.001	0.01	1241	0.32	6.7	52
	91	36864	2.2	0.53	I.S.	115205	0.06	423460	116	0.14	1438	695	0.34	1.2	249020	4.7	0.02	0.06	1874	0.01	5.7	68
	83	35087	3.3	0.22	I.S.	112662	0.02	337115	100	0.65	1133	676	0.31	1.9	206576	5.5	0.01	0.11	1233	0.70	5.4	55
	57	33844	2.6	1.7	I.S.	122114	0.05	372837	92	0.07	1717	704	0.36	5.7	318188	7.8	0.02	0.02	2268	0.01	6.0	66
	82	37948	3.1	0.95	I.S.	119710	0.04	459051	123	0.08	1426	708	0.31	3.1	248277	9.7	0.03	0.01	1840	0.13	7.6	54
	88	34863	4.0	0.24	I.S.	117213	0.03	393371	63	0.05	1173	678	0.46	2.2	188997	5.6	0.01	0.01	1292	0.12	12	23
G13301	0.24	44236	608	63	I.S.	36058	0.34	71235	48	-	182	7284	2.1	1.3	429054	1.1	0.07	0.01	1752	0.01	9.7	48
	0.25	43416	611	50	I.S.	35994	0.21	73458	95	-	154	7249	1.8	0.97	438218	<0.001	0.08	0.01	1889	0.01	6.6	37
	0.24	42063	627	85	I.S.	36508	0.03	73108	107	-	123	6224	1.7	0.20	438218	5.3	0.02	0.04	1558	0.01	6.9	75
	0.27	46456	617	28	I.S.	38817	0.36	77357	179	-	172	7574	3.5	0.23	465107	8.7	0.01	0.01	2010	0.03	9.1	166
	0.30	44307	643	1.1	I.S.	38130	0.04	79206	132	-	128	5117	2.0	1.2	472401	2.7	0.07	0.03	1249	0.05	18	91
	7.3	46319	635	25	I.S.	Inc.	0.04	104063	116	Inc.	209	Inc.	3.4	0.32	582320	Inc.	0.02	0.02	Inc.	0.05	19	159
	0.26	46817	665	16	I.S.	37879	0.33	74455	168	-	172	7445	3.8	0.22	446860	3.3	0.02	0.02	1602	0.02	6.9	143
	0.28	43496	638	18	I.S.	38434	0.44	83947	168	-	130	7484	2.5	0.24	450778	0.91	0.01	0.01	1903	0.01	5.2	46
	0.27	45404	649	20	I.S.	39244	0.65	80374	168	-	154	8469	3.1	1.8	445931	4.5	<0.001	0.01	2315	0.02	4.4	138
	1.1	38313	636	6.5	I.S.	36224	0.23	67042	93	-	155	6196	3.3	0.18	433140	3.9	<0.001	0.07	1445	0.04	21	99
G15977	9.0	24624	17	0.21	I.S.	94834	0.26	77369	64	0.28	662	1417	0.01	1.1	344274	0.10	-	0.12	297	0.01	1.8	11
	7.4	24690	20	0.20	I.S.	94993	0.06	70574	17	0.02	671	1419	0.02	0.79	336204	0.62	-	0.23	321	0.01	5.5	11
	9.9	24487	22	0.16	I.S.	91013	0.02	66492	32	0.03	716	1362	0.03	1.1	320719	1.5	-	0.19	165	0.004	1.3	9.3
	11	25011	18	0.33	I.S.	96684	0.11	91276	38	0.05	679	1635	0.03	1.0	395386	1.8	-	0.19	269	0.01	6.9	12
	9.4	24337	19	0.44	I.S.	97295	0.02	70263	38	0.02	620	1524	0.10	0.14	340670	1.3	-	0.20	347	0.07	7.7	11
	13	24931	22	0.66	I.S.	92673	0.17	65842	36	0.02	338	1377	0.04	0.83	332545	0.06	-	0.18	333	0.004	5.5	9.9
	6.0	25423	15	0.14	I.S.	90596	0.02	67242	26	0.03	558	1417	0.05	0.43	323235	0.10	-	0.11	191	0.01	1.5	10
	7.5	25089	17	0.20	I.S.	96064	0.10	79086	43	0.07	585	1563	0.06	0.80	355561	0.97	-	0.25	319	0.01	2.9	12
	9.8	24296	19	0.14	I.S.	94060	0.02	67580	22	0.03	1024	1469	0.05	0.14	330586	2.1	-	0.21	320	0.02	1.9	10
	9.1	25065	24	0.31	I.S.	99857	0.34	91016	10	0.03	442	1700	0.01	1.4	408369	1.2	-	0.13	644	0.01	3.7	12
G16835	0.26	25932	102	2.3	I.S.	103357	0.14	225837	5.3	0.13	3886	360	0.83	0.22	281458	3.6	0.02	0.40	14480	0.05	70	2113
	0.28	28064	88	0.31	I.S.	98429	0.04	239247	32	<0.001	4223	367	1.2	0.23	282948	2.7	<0.001	0.38	17394	0.02	73	2213
	0.28	27595	94	1.6	I.S.	97400	0.03	257841	5.7	0.05	3876	361	1.1	0.23	273828	0.16	<0.001	0.06	15128	0.04	36	1932
	2.7	26691	83	0.25	I.S.	102678	0.16	279051	28	0.02	3810	412	1.5	0.91	280882	<0.001	<0.001	0.07	17066	0.04	53	1953
	0.26	29044	84	0.28	I.S.	88294	0.24	263820	5.2	0.05	3568	318	1.3	0.22	258783	1.9	0.08	0.19	14436	0.04	59	1931
	7.8	28267	81	0.24	I.S.	90053	0.03	271683	21	0.33	4130	291	0.90	0.22	258457	1.2	<0.001	0.31	14106	0.04	110	4526

	6.2	29924	81	0.84	I.S.	85724	0.03	284697	5.8	0.10	3499	307	1.0	2.3	254102	0.77	0.39	0.18	13537	0.04	83	2235
	0.28	27933	75	0.33	I.S.	90281	0.14	303187	5.7	0.31	3700	252	1.0	0.98	278578	0.16	<0.001	0.08	9541	0.28	43	2381
	1.5	30207	91	0.85	I.S.	79991	0.003	304943	7.0	0.30	4373	320	1.2	0.96	260538	<0.001	0.02	0.07	17014	0.03	35	2321
	0.31	30785	77	1.9	I.S.	78420	0.28	295683	6.3	0.06	4352	324	0.95	0.78	253229	0.17	<0.001	0.10	14912	0.02	46	2243
VFI031	802	189	-	0.12	I.S.	130689	1.0	183080	430	0.14	75411	1005	10	1.0	189087	7695	0.03	0.82	6147	0.14	46	1.8
	1435	68	-	0.11	I.S.	133409	1.7	124982	598	0.06	100135	924	5.5	0.11	238299	2328	<0.001	2.2	10124	0.09	12	1.6
	1015	162	-	0.11	I.S.	135953	1.5	128726	791	0.01	98845	1093	5.7	0.40	238936	1283	0.01	2.0	9897	0.09	12	1.8
	1177	104	-	0.12	I.S.	133674	1.5	146163	656	<0.001	96282	1039	5.8	0.15	237145	2569	0.01	4.9	9402	0.25	12	1.7
	911	233	-	0.12	I.S.	136847	0.53	152634	571	0.09	93278	1304	7.2	24	221951	1207	0.01	1.8	8216	0.40	167	1.7
	744	245	Inc.	0.15	I.S.	135990	1.1	191568	313	1.1	72576	1079	9.4	3.2	206900	11055	<0.001	2.2	4005	0.24	163	1.7
	967	143	-	0.13	I.S.	129468	0.78	147238	334	0.16	85166	961	9.7	29	223342	3211	0.01	1.6	3967	0.42	198	1.6
	860	117	-	0.19	I.S.	134587	1.3	197957	844	0.10	81225	1243	5.0	1.1	221766	2447	0.01	1.6	13846	0.15	17	1.9
	1374	112	-	0.15	I.S.	133228	1.9	150362	793	0.02	96889	1056	4.8	1.3	251686	1822	0.01	2.4	10713	0.08	18	1.9
	900	161	-	0.43	I.S.	129716	1.1	170674	907	0.02	88345	1248	5.5	0.53	228393	2862	<0.001	Inc.	13331	0.37	28	1.6

Sphalerite

Sample	**Mn**	**Fe**	**Co**	**Ni**	**Cu**	**Zn**	**Ga**	**As**	**Se**	**Mo**	**Ag**	**Cd**	**In**	**Sn**	**Sb**	**Te**	**W**	**Au**	**Hg**	**Tl**	**Pb**	**Bi**
G16396*	3.2	6560	2.0	0.05	22	I.S.	0.71	1.0	-	<0.001	29	2086	2.0	0.24	3.2	0.13	0.01	0.08	32	0.001	14	0.02
	1.3	2002	0.43	0.04	1220	I.S.	6.7	210	-	0.01	209	4646	0.52	4.3	410	0.54	0.003	0.05	29	0.02	315	0.63
	0.75	2730	2.4	0.05	323	I.S.	29	1.1	-	0.01	19	2441	3.2	40	21	0.03	0.01	0.02	26	0.004	16	0.04
	5.4	8536	7.5	0.17	73	I.S.	16	2.8	-	0.004	26	3166	0.20	1.2	29	<0.001	0.003	0.28	27	0.02	67	0.09
	0.92	2062	0.40	0.05	215	I.S.	15	1.8	-	0.02	17	3038	6.9	78	5.4	0.03	<0.001	0.05	36	0.005	12	0.01
	0.62	1996	0.54	0.37	49	I.S.	0.82	1.6	-	0.004	23	3739	2.3	4.3	22	0.26	0.002	0.45	36	0.003	50	0.05
	1.3	2368	0.48	0.06	1084	I.S.	8.2	123	-	0.01	227	6346	1.8	24	357	0.28	<0.001	0.03	37	0.03	369	0.04
	1.3	2765	0.54	0.04	369	I.S.	6.4	13	-	0.01	36	3171	3.0	41	47	0.46	<0.001	0.21	33	0.11	93	0.06
	0.76	1826	0.58	0.05	511	I.S.	11	1.5	-	0.01	20	3135	0.23	3.0	22	0.05	0.003	0.03	36	0.01	18	0.01
	1.8	2199	8.7	0.32	147	I.S.	6.6	0.34	-	0.02	35	2969	3.0	110	4.0	0.25	0.01	0.05	35	0.002	13	0.01
G11579	149	10498	23	0.67	Inc.	I.S.	0.51	2.6	14	0.01	Inc.	4294	85	0.78	Inc.	<0.001	-	0.05	44	0.02	Inc.	0.58
	234	11492	35	0.30	Inc.	I.S.	Inc.	0.44	17	0.03	Inc.	4539	114	0.41	Inc.	<0.001	-	0.03	42	0.30	Inc.	0.32
	201	9880	26	0.08	Inc.	I.S.	0.75	2.6	2.1	0.01	2.3	4455	118	0.59	0.43	0.06	-	0.01	48	0.002	0.48	0.09
	229	10523	30	0.05	159	I.S.	0.54	3.1	12	0.01	2.9	4294	116	0.36	3.5	<0.001	-	0.02	36	0.01	1.5	0.09
	279	10788	36	0.16	130	I.S.	0.60	0.43	6.9	0.03	1.8	4400	119	0.17	2.6	0.03	-	0.003	37	0.02	1.9	0.21
	295	11064	35	0.06	136	I.S.	0.56	2.2	1.4	0.07	1.8	4250	122	0.38	2.1	0.04	-	0.01	35	0.001	1.7	0.18
	131	8941	23	0.33	149	I.S.	0.71	0.52	6.7	0.01	3.6	3963	114	0.12	0.78	0.11	-	0.01	37	0.002	2.3	0.32
	236	9665	7.0	0.07	111	I.S.	0.62	0.54	12	0.01	0.83	4232	136	0.31	0.17	0.30	-	0.003	46	0.002	0.25	0.03
	148	10910	31	0.45	Inc.	I.S.	0.87	0.40	15	0.01	2.0	3921	132	0.29	0.36	0.05	-	0.01	29	0.001	0.52	0.003
	90	10023	21	0.10	Inc.	I.S.	0.65	0.65	10	0.03	3.2	3730	133	0.21	0.04	0.44	-	0.01	35	0.002	0.60	0.04

G13289b*	0.73	504	0.56	0.22	Inc.	I.S.	3.1	6.7	2.0	0.17	25	8279	0.75	1.4	67	<0.001	0.003	0.002	37	0.13	Inc.	0.33
	0.84	2098	0.70	0.03	96	I.S.	22	0.25	0.97	0.13	5.4	2423	Inc.	2.6	7.0	<0.001	<0.001	0.002	31	0.02	16	0.03
	3.8	1082	Inc.	0.03	Inc.	I.S.	11	6.0	Inc.	1.7	Inc.	6222	0.05	0.42	Inc.	<0.001	<0.001	0.01	54	3.0	Inc.	Inc.
	0.11	49	3.0	0.03	30	I.S.	0.56	0.22	7.1	1.3	2.3	6189	0.07	0.50	2.4	0.03	0.02	0.002	28	0.05	13	0.02
	2.1	2465	9.8	0.38	Inc.	I.S.	9.5	Inc.	Inc.	0.31	82	7897	Inc.	1.5	Inc.	0.01	<0.001	0.02	47	2.7	Inc.	Inc.
	1.2	2416	1.6	0.04	276	I.S.	14	4.0	5.6	1.9	12	2934	Inc.	Inc.	48	Inc.	0.002	0.001	37	0.14	25	0.75
	0.44	299	0.80	0.12	182	I.S.	6.0	2.4	5.6	0.01	3.5	10480	0.09	0.38	9.2	<0.001	0.002	0.002	29	0.15	Inc.	0.61
	1.1	3036	0.70	0.03	368	I.S.	35	4.5	1.0	0.82	3.5	2085	0.90	0.39	69	0.03	0.01	0.004	34	0.02	3.7	0.01
	0.72	1731	Inc.	Inc.	Inc.	I.S.	1.1	Inc.	5.1	0.04	30	9470	0.001	0.13	Inc.	<0.001	0.003	0.01	19	0.65	Inc.	1.3
	1.9	1040	Inc.	1.3	Inc.	I.S.	6.0	13	11	1.6	59	4676	Inc.	Inc.	Inc.	<0.001	0.02	0.05	35	Inc.	Inc.	Inc.
G6940	213	16855	0.22	0.04	Inc.	I.S.	1.3	0.17	Inc.	-	3.6	5351	99	0.44	1.8	<0.001	-	0.003	53	0.01	1.4	0.08
	196	16851	0.94	0.21	342	I.S.	1.4	0.37	3.0	-	4.4	5546	83	0.91	3.1	<0.001	-	0.02	43	0.04	3.9	0.15
	312	21806	1.0	0.44	295	I.S.	0.63	1.6	1.6	-	2.8	5448	84	0.63	2.1	0.03	-	0.05	50	0.002	5.6	0.62
	452	20716	0.93	0.40	192	I.S.	0.95	2.2	7.0	-	3.8	5568	87	0.47	3.1	<0.001	-	0.002	40	0.02	3.3	0.15
	452	20721	1.4	0.51	270	I.S.	0.77	2.4	2.1	-	5.4	5511	91	0.61	4.1	<0.001	-	0.04	36	0.03	5.9	0.40
	274	17413	0.81	0.55	193	I.S.	1.0	1.2	4.9	-	1.9	5259	81	0.36	1.0	<0.001	-	0.003	43	0.002	2.1	0.18
G13289a*	0.06	Inc.	0.60	0.07	Inc.	I.S.	1.3	Inc.	1.6	0.13	12	9251	0.01	0.67	Inc.	0.03	-	0.003	Inc.	0.47	29	0.33
	0.36	101	0.46	0.04	38	I.S.	2.6	11	2.6	0.31	2.7	6129	0.26	0.33	2.7	<0.001	-	0.002	73	0.16	71	0.04
	0.87	223	0.35	0.04	260	I.S.	0.64	12	Inc.	0.06	12	9660	0.001	0.60	85	<0.001	-	0.004	72	0.47	53	0.69
	Inc.	Inc.	Inc.	0.04	Inc.	I.S.	3.3	5.8	5.6	0.84	21	7453	0.87	0.40	86	0.03	-	0.002	31	0.99	Inc.	1.8
	0.36	207	0.75	0.03	197	I.S.	6.6	4.5	1.0	0.01	8.7	9652	0.06	0.37	46	0.03	-	0.002	25	0.47	Inc.	0.33
	0.60	272	1.4	0.36	Inc.	I.S.	2.0	7.3	3.7	0.88	11	6042	0.29	0.40	37	0.02	-	0.004	25	0.30	Inc.	1.1
V446	2358	50609	0.04	0.06	83	I.S.	1.4	-	2.3	Inc.	1.2	2043	116	0.64	1.8	0.09	-	0.002	34	0.002	0.51	0.02
	2526	55731	0.03	<0.001	100	I.S.	1.5	-	0.68	<0.001	Inc.	2007	130	0.84	4.4	0.31	-	<0.001	35	0.04	Inc.	0.03
	2466	55998	0.09	<0.001	85	I.S.	1.6	Inc.	3.8	<0.001	1.5	2024	108	1.4	3.7	<0.001	-	0.01	35	0.004	1.1	0.004
	2556	55654	0.003	<0.001	105	I.S.	1.7	-	4.3	<0.001	2.9	2165	137	2.0	3.8	<0.001	-	0.01	40	0.01	1.7	0.04
	2661	56022	0.02	0.05	150	I.S.	0.97	-	0.81	<0.001	4.9	2203	188	1.8	4.7	<0.001	-	0.01	43	0.02	3.0	0.05
V538	2145	66133	0.16	-	93	I.S.	6.5	2.0	5.8	<0.001	0.49	2006	48	5.0	2.7	-	-	Inc.	34	0.002	0.85	0.01
	2288	70031	0.05	Inc.	Inc.	I.S.	6.8	0.48	8.2	<0.001	0.93	1977	46	7.6	1.2	-	Inc.	-	34	0.001	0.93	0.01
	1989	75422	<0.001	-	45	I.S.	6.5	0.53	5.7	Inc.	0.96	1894	52	2.8	0.14	-	-	-	34	0.001	0.04	0.01
	2142	71736	0.12	-	Inc.	I.S.	6.4	0.50	10	<0.001	1.0	1847	49	4.8	0.69	-	-	-	39	0.01	0.89	<0.001
	2091	75577	0.07	-	46	I.S.	6.0	1.7	9.4	<0.001	1.0	1842	52	3.0	0.10	-	-	-	35	<0.001	0.38	0.002
Hj13	3033	102490	108	0.64	Inc.	I.S.	2.1	0.31	2.3	<0.001	Inc.	2753	0.16	45	Inc.	0.05	-	-	2.8	0.003	Inc.	0.002
	2783	100681	106	0.82	90	I.S.	1.9	0.04	2.1	<0.001	0.60	2484	0.24	70	0.01	<0.001	-	-	2.7	0.001	0.76	0.004
	2937	109905	121	0.72	455	I.S.	2.8	0.05	2.2	<0.001	Inc.	2667	1.7	Inc.	0.36	<0.001	-	-	2.7	0.002	Inc.	0.002
	3179	117794	119	0.13	132	I.S.	2.3	0.05	5.6	<0.001	0.82	2945	0.50	123	0.15	<0.001	-	-	2.7	0.004	1.5	0.01
	2615	93406	97	0.73	87	I.S.	4.1	0.05	2.2	0.02	0.69	2250	0.24	73	0.03	<0.001	-	Inc.	2.3	0.001	1.3	0.002

	2013	96597	48	0.42	61	I.S.	2.1	0.08	17	<0.001	0.88	2153	58	5.4	0.06	0.18	-	-	2.5	0.001	1.8	0.02
	2896	101084	105	0.32	328	I.S.	2.1	0.07	6.7	0.02	1.2	2409	0.34	103	0.17	0.15	-	-	2.4	0.001	3.7	0.02
	2997	108334	115	0.23	113	I.S.	2.1	0.05	2.0	0.05	0.55	2468	0.23	70	0.12	0.05	-	-	2.2	0.001	3.6	0.01
	2033	95016	47	0.51	44	I.S.	1.8	0.04	16	<0.001	1.1	2013	44	3.1	0.01	0.05	-	-	2.2	0.002	4.2	0.01
	2480	83565	59	0.39	Inc.	I.S.	2.5	0.05	2.2	<0.001	Inc.	1961	0.30	3.6	Inc.	<0.001	-	-	2.1	0.001	4.0	0.02
G6951*	0.81	1691	10.0	0.05	1051	I.S.	0.11	2.4	0.97	0.01	30	8399	1.3	0.14	13	0.02	-	0.05	26	0.003	21	0.001
	4.6	5185	9.5	0.06	481	I.S.	0.12	2.9	1.3	0.01	13	10080	0.08	0.76	14	<0.001	-	0.03	31	0.01	21	0.001
	2.8	3390	8.0	0.04	1105	I.S.	0.98	4.0	0.99	0.01	32	8908	1.9	0.11	22	0.02	-	Inc.	21	0.01	42	0.001
	0.98	803	6.5	0.07	763	I.S.	0.32	4.1	0.11	0.70	89	11279	3.7	0.64	26	0.03	-	0.07	28	0.01	Inc.	0.002
	2.3	2496	7.6	0.33	481	I.S.	0.10	8.9	1.0	0.005	49	9329	1.1	0.25	37	<0.001	-	0.07	24	0.01	64	0.02
	1.7	1613	6.9	0.07	1169	I.S.	0.17	0.45	1.6	0.01	43	9155	0.98	0.24	20	0.05	-	0.01	30	0.002	33	0.01
	5.1	2267	5.8	0.06	1985	I.S.	0.40	0.34	4.1	0.01	43	9373	1.1	0.29	21	0.04	-	0.57	31	0.001	17	0.005
	2.5	1741	15	0.23	1530	I.S.	0.33	4.8	7.9	0.005	51	9086	1.8	0.45	37	0.03	-	0.02	20	0.001	41	0.001
	7.3	6882	11	0.22	1802	I.S.	Inc.	0.81	1.2	<0.001	24	8167	3.5	0.55	6.6	<0.001	-	0.08	24	0.002	52	0.001
	3.6	2008	15	0.12	1329	I.S.	0.13	0.32	6.5	0.01	69	8122	1.0	0.48	44	<0.001	-	0.52	29	0.01	53	0.001
Bv97-52	932	68754	0.12	0.03	18	I.S.	3.9	7.0	7.3	-	1.5	1800	13	5.2	0.14	<0.001	<0.001	0.004	46	0.001	0.30	0.01
	941	65166	0.09	<0.001	21	I.S.	3.7	4.4	5.9	-	0.98	1768	13	7.2	0.12	<0.001	<0.001	0.004	43	0.001	0.04	0.003
	898	64932	0.06	<0.001	17	I.S.	3.9	1.1	3.4	-	1.2	1768	13	1.3	0.23	0.11	0.01	0.003	40	0.01	0.54	0.03
	901	65213	0.08	<0.001	17	I.S.	3.4	1.1	3.6	-	1.0	1802	13	3.3	0.17	<0.001	<0.001	0.004	39	0.002	0.36	0.004
	899	57622	0.004	0.51	22	I.S.	3.2	3.8	4.9	-	2.0	1754	14	11	4.2	0.05	0.01	0.005	39	0.14	Inc.	0.003
	954	67259	0.07	<0.001	14	I.S.	3.8	2.2	5.1	-	0.75	1788	14	1.1	0.02	0.04	<0.001	0.01	35	<0.001	0.26	<0.001
	916	65462	0.11	0.04	17	I.S.	3.3	3.2	0.94	-	1.3	1828	13	0.83	0.33	0.09	0.01	0.004	35	0.001	0.21	0.003
	881	54907	0.03	0.04	16	I.S.	3.5	3.9	4.6	-	1.6	1778	14	0.43	0.66	<0.001	<0.001	0.002	31	0.004	0.59	<0.001
	840	48508	0.01	<0.001	36	I.S.	3.4	3.2	4.4	-	Inc.	1743	13	4.6	30	0.04	<0.001	0.05	29	0.59	Inc.	0.02
	895	52025	0.01	<0.001	17	I.S.	3.3	0.91	4.3	-	1.1	1910	13	3.4	0.25	<0.001	<0.001	0.003	30	0.001	0.46	0.01
G10847	22	645	0.01	0.16	102	I.S.	2.9	8.6	-	<0.001	Inc.	809	0.32	3.4	5.9	0.05	0.01	0.29	217	0.04	Inc.	0.05
	26	767	0.004	0.04	131	I.S.	4.4	10	-	0.76	69	901	0.31	4.8	Inc.	0.02	0.04	0.002	241	0.01	8.0	0.01
	29	817	0.004	0.04	59	I.S.	4.1	4.2	-	0.02	28	890	0.40	0.75	0.34	0.02	0.002	0.08	260	0.01	1.0	0.03
	26	744	0.004	0.15	50	I.S.	1.8	1.5	-	0.05	32	907	0.48	0.67	0.27	0.03	0.002	0.11	266	0.01	1.1	0.03
	24	702	0.004	0.04	83	I.S.	3.6	3.5	-	0.60	25	873	0.35	0.88	0.93	0.02	<0.001	0.02	266	0.02	2.5	0.05
	30	788	0.11	0.51	Inc.	I.S.	5.7	11	-	Inc.	Inc.	893	0.35	1.7	Inc.	0.21	0.14	0.06	242	0.01	Inc.	0.06
	30	550	0.01	0.04	60	I.S.	2.9	5.4	-	<0.001	45	778	0.33	7.9	6.0	<0.001	0.003	0.25	230	0.08	Inc.	0.01
	34	765	0.004	0.12	71	I.S.	1.7	2.6	-	0.01	34	952	0.50	3.7	2.3	0.04	0.01	0.09	296	0.01	1.5	0.04
	26	763	0.003	0.04	64	I.S.	6.6	1.7	-	0.01	34	881	0.31	1.2	1.1	<0.001	<0.001	0.12	272	0.01	4.3	0.04
	24	725	0.003	0.04	84	I.S.	5.6	1.8	Inc.	Inc.	24	886	0.40	5.0	0.73	0.07	0.06	0.02	276	0.02	3.9	0.04
EV8	175	52131	0.40	0.08	86	I.S.	47	0.50	2.4	0.01	18	6584	45	5.1	0.30	<0.001	<0.001	0.01	73	-	4.2	0.10
	184	60032	0.48	0.17	120	I.S.	47	1.5	4.4	0.01	15	6500	50	Inc.	0.13	0.03	0.005	0.01	26	-	6.0	0.12

	166	57301	0.52	0.37	80	I.S.	47	0.42	2.1	0.01	7.8	6406	47	2.1	0.03	0.03	0.02	0.005	47	-	8.5	0.02
	171	58725	0.21	0.05	73	I.S.	47	0.28	1.4	0.11	15	6473	50	2.2	1.3	0.04	0.03	0.003	23	-	4.9	0.13
	159	57291	0.27	0.16	75	I.S.	48	1.4	7.4	0.01	6.9	6059	57	5.5	0.03	0.04	<0.001	0.004	79	-	0.84	0.02
	166	60000	0.16	0.06	92	I.S.	45	0.40	2.0	0.01	14	6011	61	1.7	0.79	<0.001	<0.001	0.003	47	-	3.4	0.28
	165	56722	0.26	0.08	72	I.S.	44	0.44	6.1	0.01	9.7	5981	58	5.5	0.03	0.04	0.01	0.004	94	-	1.9	0.05
	167	57057	0.27	0.07	69	I.S.	45	0.43	2.2	0.01	9.1	6072	54	3.1	0.03	Inc.	0.01	0.003	45	-	5.5	0.04
	149	56666	0.40	0.21	74	I.S.	52	0.42	2.1	0.01	11	5842	52	1.9	0.93	0.03	0.004	0.004	69	-	3.2	0.21
	166	58371	0.27	0.40	80	I.S.	57	1.4	1.4	0.04	9.0	5591	46	2.8	0.03	0.02	<0.001	0.002	69	-	1.9	0.03
Hj14	1930	103692	0.02	-	19	I.S.	4.8	0.82	1.0	<0.001	0.56	3691	0.16	1.4	0.03	<0.001	-	-	2.5	<0.001	0.43	<0.001
	2308	95290	0.84	-	8.4	I.S.	4.2	1.0	1.1	<0.001	0.23	3473	0.08	0.12	0.14	0.33	-	-	3.7	<0.001	0.38	<0.001
	1733	92452	0.04	-	27	I.S.	6.4	1.1	1.2	<0.001	Inc.	3005	0.10	4.6	Inc.	<0.001	-	-	3.8	0.005	Inc.	0.02
	1606	81414	0.81	-	17	I.S.	5.3	4.3	1.1	<0.001	0.22	2727	0.02	7.4	0.19	<0.001	-	-	4.1	0.002	1.1	0.01
	2869	77675	0.33	-	11	I.S.	2.7	1.0	1.4	<0.001	2.2	2530	0.34	0.24	3.1	<0.001	-	-	3.4	<0.001	3.2	<0.001
	2372	97706	0.98	-	37	I.S.	2.7	2.5	1.5	<0.001	1.0	3164	1.2	Inc.	3.1	<0.001	-	-	2.9	0.01	Inc.	0.01
	1553	79297	0.65	-	8.4	I.S.	4.6	4.9	5.8	Inc.	0.32	2783	<0.001	1.7	0.05	<0.001	-	-	4.2	0.003	0.50	0.01
	1701	91220	0.71	-	30	I.S.	3.3	0.96	0.99	<0.001	0.77	3569	0.08	Inc.	0.14	<0.001	-	-	3.1	0.003	1.1	0.01
	1595	86183	0.67	Inc.	8.6	I.S.	2.2	3.9	5.2	<0.001	0.55	2993	0.01	1.8	0.06	0.35	-	-	3.9	<0.001	2.0	0.01
	1991	98553	0.62	-	32	I.S.	4.8	2.7	5.6	<0.001	0.99	3744	0.02	5.3	0.41	<0.001	-	-	4.4	<0.001	0.37	0.01
G6948	5827	55793	0.08	-	59	I.S.	0.75	0.46	28	0.12	1.3	5784	88	3.8	0.16	<0.001	0.01	-	17	0.003	1.2	0.19
	5049	54721	0.11	-	59	I.S.	0.85	0.45	27	0.08	1.4	5518	89	2.6	1.7	<0.001	0.01	-	17	0.002	0.94	0.22
	5136	56445	0.20	-	61	I.S.	1.2	0.46	20	0.04	1.3	5545	92	3.0	1.9	<0.001	0.01	-	19	0.003	1.1	0.12
	5372	54603	0.05	-	75	I.S.	0.72	0.42	21	0.14	2.2	5530	92	12	3.8	0.03	<0.001	-	11	0.01	4.2	0.46
	4954	53297	0.05	-	64	I.S.	1.5	0.85	26	0.14	1.7	4691	86	1.7	3.9	0.02	0.02	-	12	0.002	2.1	0.35
	4474	51155	0.01	Inc.	59	I.S.	1.6	0.42	33	0.01	1.7	4203	89	2.3	3.3	0.04	<0.001	-	15	0.002	2.3	0.29
	5418	59282	0.01	-	84	I.S.	0.73	0.28	30	0.24	1.4	4556	87	18	3.1	0.02	0.003	-	6.8	0.01	2.4	0.31
	5602	58017	0.73	-	74	I.S.	3.3	0.97	17	0.10	3.7	5327	95	13	0.92	0.04	<0.001	-	46	0.003	0.23	0.003
	5243	45044	0.12	-	Inc.	I.S.	1.8	Inc.	15	0.10	Inc.	4859	88	2.2	Inc.	0.02	0.002	-	21	0.02	5.8	0.29
	5746	57005	0.04	-	62	I.S.	0.72	0.66	21	0.24	3.9	5113	88	2.7	2.0	0.04	<0.001	-	13	0.002	0.89	0.08
G14549b	13	22228	0.54	-	200	I.S.	4.1	0.79	-	0.005	161	4979	49	4.8	30	0.09	-	0.003	35	0.01	19	0.25
	16	23569	0.52	-	514	I.S.	2.6	7.5	-	0.01	548	5017	26	9.3	99	0.02	-	0.002	25	0.07	33	0.57
	14	22237	0.55	-	240	I.S.	2.5	0.37	-	0.04	128	4628	37	2.8	6.8	0.03	-	0.01	29	0.01	34	0.19
	11	21143	0.34	-	Inc.	I.S.	2.8	0.99	Inc.	0.01	88	4763	36	5.6	81	0.04	-	0.01	45	0.11	101	3.0
	1.1	4591	0.30	-	589	I.S.	16	Inc.	-	0.01	Inc.	7303	0.85	116	107	<0.001	Inc.	0.01	32	0.001	27	1.3
	19	19923	1.3	-	107	I.S.	3.0	2.2	-	0.005	115	12973	1.8	4.2	43	0.02	-	0.003	45	0.03	11	0.38
	2.2	5967	0.22	-	98	I.S.	9.9	1.6	-	0.02	73	4291	2.2	46	37	<0.001	-	0.003	37	0.02	7.4	0.42
	2.4	6362	0.14	-	148	I.S.	16	1.3	Inc.	<0.001	163	4038	2.3	37	48	0.03	-	0.02	87	0.06	18	2.1
	16	24419	1.9	Inc.	Inc.	I.S.	4.4	Inc.	-	0.01	Inc.	11790	2.6	25	Inc.	0.02	-	0.01	32	0.03	19	Inc.

	17	19230	1.7	-	324	I.S.	5.6	0.86	-	<0.001	104	11840	3.2	207	114	0.09	-	0.01	48	0.03	10	0.42
Galena																						
Sample	**Mn**	**Fe**	**Co**	**Ni**	**Cu**	**Zn**	**Ga**	**As**	**Se**	**Mo**	**Ag**	**Cd**	**In**	**Sn**	**Sb**	**Te**	**W**	**Au**	**Hg**	**Tl**	**Pb**	**Bi**
G16396*	6.7	-	0.11	0.97	43	-	-	-	-	0.11	356	51	0.03	-	601	<0.001	-	0.12	4.7	1.5	I.S.	398
	1.4	Inc.	0.11	1.1	26	-	-	Inc.	-	0.11	288	63	0.03	-	607	6.0	Inc.	0.08	4.0	1.7	I.S.	88
	1.5	-	0.31	1.1	21	-	-	-	-	0.18	296	32	0.03	-	493	0.68	-	0.09	14	1.4	I.S.	452
	3.3	-	0.33	2.4	22	-	-	-	-	0.68	338	42	0.09	-	516	0.72	-	0.11	4.1	1.7	I.S.	648
	7.6	Inc.	0.77	1.5	36	-	-	-	-	0.15	301	27	0.21	-	557	0.59	-	0.07	4.1	1.7	I.S.	373
	1.9	-	0.13	1.7	13	-	-	-	-	<0.001	265	84	0.04	-	639	3.1	-	0.06	12	2.2	I.S.	275
	2.1	Inc.	0.17	1.7	14	-	-	-	Inc.	0.66	307	37	0.04	-	364	0.72	-	0.11	2.4	1.6	I.S.	904
	12	-	0.17	6.2	26	-	-	-	Inc.	0.17	298	36	0.04	-	593	2.3	-	0.10	6.6	1.9	I.S.	402
	5.0	-	0.19	1.5	22	-	-	Inc.	Inc.	<0.001	287	48	0.04	Inc.	645	<0.001	-	0.21	15	1.7	I.S.	135
	2.8	-	0.33	2.2	34	-	-	-	Inc.	0.60	254	39	0.05	-	571	1.00	-	0.17	8.5	1.8	I.S.	360
G11579	-	-	-	-	16	Inc.	Inc.	-	705	-	1211	16	-	-	59	Inc.	-	-	Inc.	29	I.S.	10046
	-	-	-	-	18	-	-	-	406	-	1415	38	-	-	54	Inc.	-	Inc.	-	28	I.S.	10712
	-	Inc.	-	-	16	-	-	-	485	-	1332	39	-	-	43	Inc.	-	-	-	28	I.S.	11509
G13289b*	1.1	-	0.07	0.69	32	Inc.	0.09	3.6	-	0.13	120	24	0.02	0.71	772	-	-	-	3.3	0.25	I.S.	0.05
	4.7	-	0.30	0.77	32	-	0.09	4.3	-	0.12	54	2.7	0.06	0.85	3513	-	Inc.	Inc.	1.7	0.22	I.S.	0.11
	1.1	-	0.07	0.74	23	-	0.10	8.7	-	0.54	104	23	0.02	0.73	808	-	-	-	0.48	0.10	I.S.	1.5
	4.3	Inc.	0.12	0.83	90	-	0.24	4.4	Inc.	0.14	105	2.5	0.03	1.8	Inc.	-	-	-	0.58	1.4	I.S.	0.86
	1.3	-	0.10	0.91	45	Inc.	0.11	33	Inc.	0.85	9.7	19	0.03	0.86	173	-	-	-	1.7	0.10	I.S.	Inc.
	1.2	-	0.08	0.81	45	-	0.10	4.0	-	0.13	54	16	0.02	0.85	3230	-	-	-	1.8	0.32	I.S.	0.57
	1.3	-	0.11	0.96	28	Inc.	0.12	4.5	-	0.20	11	19	0.03	0.96	34	-	-	-	0.55	0.14	I.S.	Inc.
	1.3	-	0.08	3.6	40	-	0.39	3.9	-	0.16	9.6	13	0.03	1.8	15	-	-	-	0.53	0.20	I.S.	0.28
	3.6	-	0.11	0.96	32	-	0.11	24	-	<0.001	86	10	0.03	2.8	446	-	-	-	2.7	0.17	I.S.	0.61
	1.3	Inc.	0.11	1.0	41	-	0.12	4.1	Inc.	0.18	101	19	0.07	0.97	703	-	-	-	1.3	0.25	I.S.	0.02
G6940	3.9	-	0.10	2.0	1.7	-	-	4.3	Inc.	0.13	1012	38	-	6.9	152	1625	0.07	0.08	1.3	23	I.S.	7253
	0.97	-	0.28	0.82	1.7	-	-	Inc.	Inc.	0.15	1057	25	-	7.2	140	1552	0.04	0.06	1.2	26	I.S.	7307
	0.92	-	0.07	4.4	4.0	Inc.	-	3.6	Inc.	0.17	965	43	-	4.7	102	1589	<0.001	0.14	3.5	33	I.S.	7922
	3.0	-	0.38	0.96	11	-	-	3.9	Inc.	2.6	994	35	-	5.7	160	658	<0.001	0.07	2.7	43	I.S.	5950
	2.2	-	0.08	5.8	5.5	-	-	3.7	2014	0.12	1009	63	-	3.4	221	1034	0.08	0.08	1.2	26	I.S.	5664
	1.00	-	0.09	0.88	6.3	-	-	3.7	1550	0.17	1013	58	-	4.0	175	998	0.33	0.06	1.1	28	I.S.	5626
	2.5	Inc.	0.38	0.91	8.5	-	-	15	1878	0.13	480	25	-	0.85	72	379	0.06	0.21	1.2	41	I.S.	3206
	0.99	-	0.10	0.80	6.2	-	-	3.7	1315	0.97	764	37	-	2.3	78	826	0.04	0.08	1.1	42	I.S.	5073
	2.2	Inc.	0.09	8.5	2.1	Inc.	Inc.	3.6	859	0.46	956	53	-	8.9	126	824	<0.001	0.04	6.0	31	I.S.	5371
G13289a*	-	-	0.57	Inc.	16	Inc.	0.41	6.9	-	-	9.6	23	-	2.7	16	-	-	-	1.3	0.11	I.S.	13

	-	-	0.12	-	8.6	-	0.43	25	-	-	18	33	-	1.2	15	-	-	-	3.9	0.14	I.S.	49
V446	0.50	Inc.	0.07	-	2.3	1.3	Inc.	-	457	-	718	10	0.68	215	298	4.4	-	-	-	59	I.S.	1474
	3.6	-	0.03	-	8.6	6.6	-	-	440	-	689	8.2	0.64	219	344	3.2	-	-	Inc.	59	I.S.	1518
	0.50	-	<0.001	-	10	1.1	-	Inc.	435	-	835	12	0.68	270	600	<0.001	-	-	-	60	I.S.	1414
	1.9	-	0.10	-	2.2	1.0	-	-	432	-	754	9.9	0.49	181	336	1.6	-	-	-	61	I.S.	1745
	2.3	-	<0.001	-	2.6	4.1	-	-	396	-	571	6.4	0.42	130	218	1.9	-	-	-	55	I.S.	1659
V538	1.3	-	0.14	-	-	11	-	-	72	-	819	12	0.83	272	667	-	-	-	-	79	I.S.	899
	0.49	Inc.	0.06	-	-	19	-	Inc.	66	-	755	4.4	0.73	254	547	-	-	-	Inc.	83	I.S.	1026
	1.2	-	0.14	-	-	4.8	-	-	71	Inc.	726	6.3	0.69	248	581	-	-	-	-	80	I.S.	739
	1.4	Inc.	0.04	-	-	1.8	-	-	64	-	501	9.9	0.35	141	335	Inc.	-	-	-	75	I.S.	855
	2.3	Inc.	0.09	-	Inc.	1.7	-	-	70	-	922	Inc.	1.4	575	Inc.	-	-	-	-	110	I.S.	574
Hj13	2.9	-	-	-	1.4	-	0.36	0.38	Inc.	-	1294	10.0	0.02	0.89	1734	1.0	-	0.05	0.06	0.36	I.S.	18
	3.8	Inc.	Inc.	-	1.1	-	0.05	0.52	Inc.	-	1485	23	0.04	0.33	1686	2.0	-	0.03	0.11	0.23	I.S.	343
	0.79	Inc.	-	-	Inc.	-	0.11	0.65	Inc.	-	955	18	0.03	1.8	1081	0.91	-	0.03	0.04	0.46	I.S.	5.7
	5.9	-	-	-	1.3	-	<0.001	1.2	Inc.	-	1648	14	0.01	2.6	1989	<0.001	-	0.03	0.05	0.33	I.S.	6.8
	7.5	-	-	-	1.2	Inc.	<0.001	0.54	Inc.	-	1446	15	0.04	1.9	1668	3.4	-	0.05	0.10	0.27	I.S.	3.4
	5.9	-	-	-	1.5	-	0.13	0.83	Inc.	-	1755	16	0.01	2.1	1249	28	-	0.01	0.12	0.58	I.S.	Inc.
	4.4	-	-	-	1.2	-	0.33	1.2	Inc.	-	1353	15	0.02	5.0	1626	<0.001	-	0.03	0.16	0.33	I.S.	29
	3.6	-	-	-	1.0	Inc.	<0.001	0.40	48	-	1258	17	0.03	1.3	1477	13	-	0.04	0.15	0.31	I.S.	49
	2.9	-	-	-	1.7	-	<0.001	0.31	390	-	1380	8.9	0.01	1.7	1090	Inc.	-	0.01	0.14	0.37	I.S.	771
	3.7	-	-	-	1.2	-	0.07	0.61	73	-	1615	12	0.01	2.5	1757	18	Inc.	0.04	0.04	0.30	I.S.	40
G6951*	8.4	-	0.13	-	4.2	Inc.	-	5.3	-	Inc.	25	53	Inc.	-	14	Inc.	-	0.08	5.3	0.11	I.S.	0.10
	1.3	-	0.13	-	3.5	Inc.	-	Inc.	Inc.	-	45	111	-	-	Inc.	Inc.	-	0.09	1.2	0.03	I.S.	0.28
	1.5	-	0.16	-	21	-	-	79	-	-	34	62	-	-	116	Inc.	-	0.24	7.0	0.08	I.S.	0.62
	4.2	-	0.47	-	4.9	-	-	93	-	-	12	91	-	-	203	Inc.	-	0.10	1.6	0.04	I.S.	0.03
	1.9	-	1.2	Inc.	Inc.	Inc.	-	Inc.	-	-	Inc.	Inc.	-	-	Inc.	Inc.	-	0.46	1.6	0.03	I.S.	0.03
	2.4	Inc.	0.30	-	15	-	-	23	-	-	8.8	62	-	-	12	Inc.	-	0.14	2.2	0.05	I.S.	0.14
	2.6	-	0.19	-	6.3	-	-	7.9	-	-	14	67	-	-	12	Inc.	-	0.11	2.3	0.06	I.S.	0.10
	2.7	-	0.23	-	20	Inc.	-	8.3	-	-	19	64	-	-	26	Inc.	-	0.98	2.4	0.04	I.S.	0.15
	3.0	-	0.30	-	6.9	-	Inc.	17	-	-	7.0	93	-	-	20	Inc.	-	0.12	2.5	0.10	I.S.	0.16
Bv97-52	3.7	-	0.06	-	Inc.	1.9	0.05	8.3	72	0.22	174	96	0.90	300	745	2.4	-	0.02	-	150	I.S.	220
	2.6	-	0.05	-	Inc.	1.6	0.04	7.4	76	<0.001	166	104	1.1	314	1103	0.62	-	<0.001	-	161	I.S.	192
	1.5	-	<0.001	-	Inc.	1.8	0.07	22	59	0.33	228	89	0.85	336	880	<0.001	-	0.03	-	150	I.S.	202
	1.8	-	0.10	-	Inc.	3.5	0.08	36	77	0.25	519	24	0.37	112	833	<0.001	-	0.02	-	171	I.S.	252
	2.1	Inc.	0.04	Inc.	6.2	1.9	0.09	9.3	153	<0.001	679	11	0.77	247	985	0.76	-	0.02	-	158	I.S.	141
	0.66	-	0.05	-	5.8	1.7	0.19	8.8	146	0.20	394	2.9	0.52	180	636	<0.001	Inc.	0.02	-	98	I.S.	147
	2.1	Inc.	0.04	-	5.4	1.6	0.09	26	142	<0.001	497	9.0	0.67	175	690	0.39	-	0.02	-	99	I.S.	138

	2.1	Inc.	0.22	-	29	1.9	0.06	11	170	<0.001	656	3.6	0.65	212	944	<0.001	-	<0.001	-	139	I.S.	154
	0.79	-	0.05	-	7.4	1.9	0.23	11	207	<0.001	558	6.5	0.32	151	808	0.75	-	<0.001	-	119	I.S.	151
	2.8	-	0.04	-	18	1.6	0.05	25	215	<0.001	895	5.9	1.1	231	1275	0.66	-	0.04	-	155	I.S.	148
G10847	Inc.	-	0.21	-	3.4	-	0.17	8.7	228	-	120	2.5	0.03	1.2	297	-	0.14	0.19	1.9	0.86	I.S.	13
	-	-	0.15	-	3.2	-	0.16	7.8	223	-	215	9.8	0.03	1.1	646	-	<0.001	0.09	17	1.2	I.S.	12
	-	Inc.	0.17	-	3.2	-	0.83	Inc.	280	-	94	2.2	0.05	1.1	267	-	0.10	0.08	9.2	0.27	I.S.	12
	-	Inc.	0.18	-	3.6	-	0.21	8.1	49	-	198	15	0.03	1.2	537	-	<0.001	0.11	14	1.1	I.S.	12
	-	-	0.66	Inc.	3.7	-	0.21	27	43	-	122	2.2	0.04	4.2	299	-	0.30	0.29	1.8	0.53	I.S.	13
	-	-	0.16	-	Inc.	-	0.15	5.5	191	-	322	1.7	0.03	0.90	469	Inc.	0.06	0.08	20	1.3	I.S.	11
	-	Inc.	0.20	-	3.3	-	1.01	6.2	30	-	143	16	0.03	1.0	423	-	0.12	0.06	9.2	0.58	I.S.	12
	Inc.	-	0.84	-	4.0	-	0.19	6.7	88	Inc.	185	2.8	0.04	1.1	494	-	<0.001	0.12	3.8	0.89	I.S.	19
	-	-	0.14	-	14	-	0.20	13	117	-	94	1.6	0.15	5.6	299	-	0.07	0.10	9.4	0.90	I.S.	15
	-	Inc.	0.16	-	15	-	0.22	6.7	79	-	135	5.2	0.04	1.2	333	-	0.27	0.11	1.6	0.89	I.S.	12
EV8	Inc.	-	0.39	-	Inc.	-	0.08	Inc.	228	-	4100	33	2.1	717	538	5.2	-	-	1.3	13	I.S.	16679
	-	Inc.	0.14	-	-	-	0.30	-	183	-	4420	25	0.47	159	113	1.1	-	-	2.3	23	I.S.	15735
	-	-	0.12	-	-	-	0.35	-	190	-	4070	28	0.24	120	96	3.2	-	-	2.0	27	I.S.	15101
	-	-	0.16	-	-	-	0.11	-	108	-	3817	19	1.4	467	230	6.8	Inc.	-	13	18	I.S.	13805
	-	-	0.10	-	-	-	0.14	-	89	-	3911	22	0.36	116	102	2.5	-	-	6.8	16	I.S.	14851
	-	-	0.21	-	-	-	0.10	-	102	-	3822	30	0.32	101	29	5.5	-	-	9.3	19	I.S.	14432
	-	-	0.15	-	-	-	0.18	-	181	-	3939	45	2.4	877	293	12	-	-	2.4	2.3	I.S.	14062
	-	-	0.34	-	-	-	0.14	-	97	-	4101	67	2.5	836	396	21	-	-	3.7	17	I.S.	14743
	-	-	0.12	-	-	-	0.13	-	92	-	3859	33	1.1	384	130	<0.001	-	-	9.5	31	I.S.	14920
	-	-	0.11	-	-	-	0.16	-	131	-	3993	39	2.0	651	293	4.4	-	-	5.5	18	I.S.	14395
Hj14	3.1	-	-	-	0.69	-	-	2.3	53	-	1469	5.3	0.01	1.4	1982	0.70	-	<0.001	0.06	1.5	I.S.	1.6
	0.96	-	-	-	0.81	-	-	2.4	51	-	1621	13	<0.001	1.2	2166	<0.001	-	<0.001	0.06	1.6	I.S.	0.54
	0.44	Inc.	-	-	0.95	-	-	2.4	Inc.	-	1226	8.9	0.01	1.1	1754	1.2	-	<0.001	0.14	2.5	I.S.	Inc.
	0.49	Inc.	Inc.	-	0.73	-	-	7.9	15	-	1532	11	0.01	1.7	1990	<0.001	-	0.02	0.06	1.2	I.S.	0.57
	2.6	-	-	-	0.81	-	-	2.3	Inc.	-	1135	11	<0.001	1.3	1442	0.37	-	<0.001	0.17	1.1	I.S.	Inc.
	0.95	-	-	-	2.0	Inc.	-	2.3	57	-	1357	14	<0.001	2.6	1776	<0.001	-	<0.001	0.05	1.4	I.S.	3.7
	2.6	Inc.	-	-	5.4	-	-	2.5	70	-	1180	9.2	<0.001	0.30	1480	0.74	-	0.04	0.07	1.2	I.S.	Inc.
	0.76	-	-	-	2.4	-	-	6.8	19	-	1351	9.8	0.01	3.9	1868	0.98	-	<0.001	0.34	1.6	I.S.	0.77
	4.3	-	-	Inc.	0.85	-	-	2.6	37	-	1084	9.7	0.01	1.3	1480	<0.001	-	0.02	0.05	1.1	I.S.	6.4
	1.3	Inc.	-	-	0.86	-	-	6.3	15	-	1552	9.7	0.02	2.6	1782	<0.001	-	0.02	0.06	1.5	I.S.	0.41
Mo17A	3.5	-	-	-	-	2.3	Inc.	8.3	602	-	523	151	-	-	736	50	-	<0.001	0.61	0.29	I.S.	239
	1.0	Inc.	-	-	-	1.9	-	8.0	729	-	725	224	Inc.	-	863	66	-	0.07	2.5	0.28	I.S.	229
	0.96	-	-	-	Inc.	3.9	-	16	424	-	402	213	-	-	725	65	-	0.14	2.2	0.09	I.S.	222
	4.0	-	-	-	-	1.9	-	7.3	482	-	458	201	-	-	613	78	-	0.06	2.1	0.09	I.S.	231

	2.9	-	-	-	-	2.0	-	8.1	479	-	446	195	-	-	782	94	-	<0.001	0.60	0.12	I.S.	218
	1.0	-	-	-	-	1.8	-	Inc.	428	-	1043	538	-	-	2322	142	-	<0.001	0.64	0.16	I.S.	242
	1.2	-	-	-	Inc.	2.8	-	Inc.	461	-	744	450	-	Inc.	1254	115	-	0.17	2.8	0.21	I.S.	239
	4.1	-	-	-	-	2.5	-	10	486	-	901	357	-	-	2003	133	-	0.08	0.77	0.23	I.S.	272
	1.2	-	-	-	-	6.1	-	Inc.	447	-	1089	320	-	-	1643	146	-	0.05	1.4	0.14	I.S.	225
	5.3	-	-	-	-	Inc.	-	8.6	297	-	1113	489	-	-	1666	162	-	<0.001	1.8	0.37	I.S.	221
ORV1	0.46	-	<0.001	-	Inc.	2.2	-	2.8	173	-	260	6.5	0.02	0.20	1807	Inc.	-	0.42	1.7	0.19	I.S.	Inc.
	0.54	Inc.	0.15	-	Inc.	1.1	-	19	170	-	81	0.78	0.01	0.26	316	Inc.	-	<0.001	0.13	0.06	I.S.	57
	2.0	Inc.	0.53	-	Inc.	Inc.	-	Inc.	182	-	522	40	0.03	0.23	16746	Inc.	-	0.24	2.0	0.10	I.S.	74
	0.68	-	0.09	-	Inc.	1.7	-	9.4	58	-	97	4.7	<0.001	0.33	2379	Inc.	-	<0.001	0.17	0.19	I.S.	12
	1.5	Inc.	<0.001	-	Inc.	3.4	-	23	62	-	130	31	0.02	0.26	988	-	-	0.03	0.44	0.07	I.S.	40
	0.55	Inc.	<0.001	-	Inc.	1.1	Inc.	4.4	162	-	315	83	<0.001	0.71	3545	Inc.	-	0.70	0.90	0.83	I.S.	1.3
	0.64	-	<0.001	-	Inc.	1.4	-	4.7	306	-	134	<0.001	<0.001	0.88	1075	Inc.	-	0.16	0.07	0.11	I.S.	88
	0.57	-	<0.001	-	Inc.	1.3	-	5.2	295	-	285	19	0.02	10	2525	Inc.	-	0.05	2.1	0.43	I.S.	119
G14549a	1.3	-	0.11	1.2	Inc.	-	-	19	17	0.09	1052	43	0.03	1.1	Inc.	-	-	0.08	1.2	4.6	I.S.	3481
	3.8	-	0.10	2.9	Inc.	-	Inc.	73	15	0.14	699	38	0.07	5.4	1510	-	-	0.06	1.0	2.4	I.S.	2163
	4.9	-	0.13	6.9	Inc.	Inc.	-	5.1	18	0.09	662	48	0.02	6.7	885	Inc.	Inc.	0.10	1.1	3.8	I.S.	1925
	1.0	Inc.	0.09	0.82	Inc.	-	-	30	Inc.	0.11	2274	48	0.02	0.84	393	-	-	0.36	3.6	7.0	I.S.	4993
	2.2	-	0.47	0.98	Inc.	Inc.	-	4.3	18	0.08	1891	44	0.02	0.82	90	-	-	0.07	Inc.	4.4	I.S.	5965
	1.3	-	0.10	3.3	Inc.	-	-	5.5	68	0.17	2587	48	0.02	3.5	107	-	-	0.06	3.1	16	I.S.	10029
	1.3	-	0.27	1.2	Inc.	-	-	5.4	Inc.	0.75	2900	35	0.06	0.99	63	-	-	0.05	4.5	11	I.S.	10753
	6.6	-	0.16	6.2	Inc.	-	-	7.3	37	0.19	2627	32	0.12	1.3	235	-	-	0.11	1.6	5.0	I.S.	3850
G873	-	Inc.	0.18	1.4	4.8	-	Inc.	13	82	-	145	1.8	-	-	346	4.3	-	0.51	4.6	0.05	I.S.	0.06
	-	-	0.11	1.4	13	-	-	12	60	-	117	2.2	-	-	262	<0.001	Inc.	0.26	8.4	0.11	I.S.	0.06
	-	Inc.	0.26	3.5	8.6	-	-	40	51	-	66	8.7	-	Inc.	141	1.2	-	2.8	2.3	0.16	I.S.	0.45
	Inc.	-	0.16	3.1	9.0	-	-	Inc.	Inc.	-	Inc.	4.9	-	-	Inc.	3.3	-	0.10	7.7	0.20	I.S.	0.05
	-	-	0.15	1.6	2.8	-	-	11	71	-	311	2.3	-	-	693	0.88	-	0.10	6.5	0.18	I.S.	0.15
	-	Inc.	1.7	Inc.	Inc.	Inc.	-	Inc.	25	Inc.	104	Inc.	-	-	581	0.77	-	2.1	4.5	0.30	I.S.	0.24

Chalcopyrite

Sample	**Mn**	**Fe**	**Co**	**Ni**	**Cu**	**Zn**	**Ga**	**As**	**Se**	**Mo**	**Ag**	**Cd**	**In**	**Sn**	**Sb**	**Te**	**W**	**Au**	**Hg**	**Tl**	**Pb**	**Bi**
G16396*	4.8	297451	0.12	-	I.S.	588	5.3	24	20	0.34	291	11	2.5	35	286	8.1	-	5.4	0.54	0.06	Inc.	0.88
	0.29	310493	0.02	-	I.S.	355	1.1	20	7.3	0.03	474	15	0.52	46	113	2.3	-	0.12	2.1	0.03	Inc.	0.10
	1.0	302635	0.08	-	I.S.	Inc.	5.9	15	6.9	0.04	905	Inc.	2.7	65	216	1.5	-	0.53	9.5	0.22	Inc.	0.51
	9.4	298283	0.03	-	I.S.	847	4.5	25	28	0.48	Inc.	12	0.48	52	403	6.4	-	2.5	2.2	0.40	Inc.	Inc.
G11579	1.7	308056	0.09	0.70	I.S.	193	0.59	-	Inc.	Inc.	4.9	6.3	65	64	9.5	-	-	0.19	0.89	0.02	9.3	3.2
	0.65	302378	0.04	3.5	I.S.	218	1.6	-	-	-	3.7	1.2	63	72	5.9	-	-	0.35	3.0	0.02	6.8	1.7

	0.71	287692	0.07	0.68	I.S.	209	1.6	-	-	-	3.0	4.8	64	65	7.7	Inc.	-	0.29	3.1	0.05	5.5	2.6
	0.68	280144	0.25	0.78	I.S.	214	1.0	Inc.	-	-	5.2	10	41	40	1.6	-	-	0.24	6.0	0.06	5.5	2.3
G13289b*	0.19	333186	0.05	0.15	I.S.	36	0.02	32	21	0.03	13	1.8	0.75	1.2	477	-	-	0.02	1.8	0.84	104	11
	0.19	324193	0.01	0.16	I.S.	31	0.02	17	59	0.21	5.7	1.6	0.44	0.90	272	-	-	0.01	0.99	0.33	41	7.2
	0.44	315206	0.01	0.12	I.S.	45	0.02	32	104	0.02	5.7	0.26	0.64	3.2	373	Inc.	-	0.01	1.7	0.35	109	7.7
	0.37	297609	0.06	0.32	I.S.	126	0.10	36	90	0.23	Inc.	Inc.	0.69	3.8	514	-	-	0.01	3.7	0.65	Inc.	1.9
	0.20	303505	0.06	1.7	I.S.	12	0.02	20	118	0.04	12	1.7	0.39	0.18	284	-	Inc.	0.01	1.3	1.3	Inc.	Inc.
	0.26	317877	0.02	0.21	I.S.	176	0.03	54	37	0.05	18	1.8	0.20	0.24	781	-	-	0.01	1.7	0.95	73	Inc.
	1.4	313665	2.2	0.14	I.S.	319	0.02	Inc.	5.0	0.02	88	1.8	0.01	0.52	Inc.	-	-	0.01	6.7	0.42	Inc.	0.11
	0.84	306334	0.47	0.53	I.S.	44	0.13	Inc.	19	7.2	Inc.	0.29	0.01	0.24	9.7	-	-	0.01	2.0	8.9	76	0.01
	0.21	317692	0.28	0.18	I.S.	Inc.	0.08	50	4.6	0.24	Inc.	Inc.	0.01	1.6	Inc.	-	-	0.01	5.3	1.1	Inc.	1.2
G6940	0.45	314260	0.15	0.34	I.S.	298	1.3	8.4	12	-	13	16	24	247	8.4	1.4	0.02	0.10	0.93	0.05	5.0	0.70
	0.65	299974	0.07	0.58	I.S.	486	1.2	2.8	75	-	14	14	27	322	5.1	1.5	0.03	0.15	1.4	0.02	6.4	0.65
	0.92	321334	0.03	1.6	I.S.	369	1.1	1.8	45	-	7.8	11	23	172	10	0.68	0.02	0.38	5.9	0.03	7.5	0.99
	1.0	320405	0.03	0.31	I.S.	392	2.0	1.6	10.0	-	4.6	5.0	30	208	9.0	0.16	0.09	2.2	4.9	0.02	5.4	5.2
	0.75	305942	0.11	0.59	I.S.	350	1.7	13	81	-	7.2	16	39	258	6.2	<0.001	0.04	0.28	3.7	0.03	9.8	1.1
	0.24	327322	0.02	0.20	I.S.	309	0.51	3.7	6.3	-	14	5.7	29	144	3.0	4.5	0.01	0.26	0.52	0.05	4.7	0.95
	0.25	329718	0.02	0.22	I.S.	193	1.4	1.0	14	-	4.7	7.7	28	127	5.4	0.15	0.02	0.07	1.2	0.07	4.1	0.59
	0.20	323050	0.01	0.84	I.S.	345	1.4	0.86	4.9	-	9.9	16	23	145	20	1.4	0.02	0.01	0.40	0.18	6.3	1.4
	0.94	318489	0.02	0.22	I.S.	255	2.2	1.1	6.9	-	4.0	12	34	146	10	0.61	0.01	0.30	0.50	0.04	4.8	2.2
	1.6	321013	0.07	0.30	I.S.	341	1.4	2.9	18	-	2.9	10	32	276	4.5	0.15	<0.001	0.18	5.4	0.01	2.0	2.0
G13289a*	Inc.	269766	0.02	Inc.	I.S.	110	0.10	31	20	-	Inc.	5.1	0.01	0.84	365	-	-	-	5.7	0.98	Inc.	7.5
	1.4	276516	0.13	0.62	I.S.	38	0.16	12	5.7	-	13	2.4	0.02	0.19	268	-	-	-	4.2	0.30	50	2.3
	Inc.	287778	0.22	0.21	I.S.	147	0.06	26	5.7	-	28	11	0.01	0.19	627	-	-	-	0.36	1.0	Inc.	2.4
	Inc.	289332	0.02	0.59	I.S.	59	0.21	19	61	-	9.1	0.83	0.16	1.5	143	-	-	-	3.3	0.29	30	3.4
	9.6	266314	0.09	0.40	I.S.	41	0.04	30	10.0	-	1.6	2.1	0.12	2.0	47	-	-	-	0.65	0.03	7.1	0.08
V446	3.9	280995	0.05	0.31	I.S.	336	2.4	2.9	5.1	<0.001	25	2.7	67	1315	5.7	<0.001	-	-	0.41	0.13	4.0	0.10
	13	275577	0.01	<0.001	I.S.	391	0.99	0.64	6.8	<0.001	14	3.2	42	616	Inc.	0.14	-	-	0.15	0.66	8.6	0.34
	23	295078	<0.001	0.33	I.S.	473	2.0	0.51	0.70	<0.001	12	7.3	41	3630	3.8	0.06	-	-	0.20	0.05	2.2	0.17
	6.5	284989	0.01	0.32	I.S.	341	2.1	1.4	6.9	<0.001	10	2.0	30	1447	1.4	0.17	-	-	0.16	0.05	1.5	0.01
	22	289686	0.02	0.15	I.S.	433	2.7	0.70	4.7	0.11	17	2.9	63	1522	4.3	0.24	-	-	0.38	0.16	2.7	0.09
V538	25	296281	0.05	0.15	I.S.	502	12	-	2.5	0.07	4.2	3.7	35	1358	3.4	0.08	-	-	0.05	0.10	1.3	0.02
	31	288201	0.06	0.19	I.S.	427	12	-	0.94	<0.001	7.5	4.0	22	1429	Inc.	<0.001	Inc.	-	0.29	0.03	1.0	0.03
	19	270844	0.01	0.02	I.S.	380	11	-	2.1	<0.001	9.7	1.8	22	1166	Inc.	0.13	-	-	0.21	0.24	0.62	0.01
	32	289306	0.01	0.21	I.S.	371	8.7	-	3.2	<0.001	5.5	2.0	26	888	1.3	0.16	-	-	0.04	0.04	1.1	0.02
	25	274094	0.02	<0.001	I.S.	325	9.3	-	6.8	<0.001	15	2.5	23	973	0.66	<0.001	-	Inc.	0.09	0.03	0.44	0.004
Hj13	66	323308	6.9	0.49	I.S.	1282	0.07	0.07	3.1	<0.001	150	6.8	1.9	9.5	0.60	-	-	0.004	0.24	0.005	1.4	0.005

	30	285136	4.5	0.01	I.S.	2038	0.03	0.07	11	<0.001	73	6.6	2.2	14	0.88	-	Inc.	0.001	0.14	0.001	2.1	0.004
	36	290374	3.6	1.2	I.S.	990	0.02	0.01	7.5	<0.001	149	4.8	1.4	4.5	0.60	-	-	0.001	0.23	0.002	2.9	0.01
	73	298771	3.6	14	I.S.	2497	0.11	0.09	18	0.01	112	11	1.5	12	1.3	Inc.	-	0.001	0.17	0.004	2.8	0.01
	49	285887	3.2	0.59	I.S.	1056	0.07	0.03	24	<0.001	134	5.3	3.1	17	0.33	-	-	0.001	0.17	0.001	1.5	0.002
	53	285730	4.9	1.5	I.S.	1062	0.07	0.14	12	<0.001	263	6.8	2.6	7.4	0.22	-	-	0.001	0.16	0.001	1.3	0.002
	67	314607	6.4	8.2	I.S.	2283	0.21	0.02	1.6	0.03	195	12	0.44	8.0	2.6	-	-	0.001	0.16	0.37	1.3	0.002
	48	317391	2.4	0.03	I.S.	2682	0.10	0.08	5.7	<0.001	145	10	1.4	9.2	Inc.	-	-	0.001	0.17	0.002	Inc.	0.01
	48	275894	3.9	4.1	I.S.	1225	0.11	0.13	1.7	0.005	219	7.4	1.5	9.6	0.14	-	-	0.001	0.14	0.002	1.0	0.004
	43	316792	3.2	5.8	I.S.	845	0.06	0.03	1.7	<0.001	232	4.9	1.1	9.9	0.38	-	-	0.002	0.10	0.003	6.1	0.002
G6948	0.19	296662	0.15	0.17	I.S.	397	0.53	1.2	5.1	0.03	5.1	2.9	31	2167	23	-	-	-	0.40	0.04	9.6	0.26
	0.51	292976	0.04	0.51	I.S.	868	1.0	3.2	13	0.18	4.4	9.4	23	3965	6.8	Inc.	-	-	1.1	0.02	1.5	0.08
	0.22	291976	0.06	0.23	I.S.	571	0.71	5.7	6.0	0.14	7.7	3.5	16	2246	11	-	-	-	1.2	0.01	2.0	0.20
	0.28	294278	0.12	1.9	I.S.	811	0.30	11	47	0.03	24	22	32	4709	15	-	-	-	4.2	0.01	4.7	1.4
	1.8	304996	0.03	1.9	I.S.	548	1.0	11	28	0.05	12	11	21	2731	9.9	-	-	-	2.4	0.03	1.6	0.48
	0.95	291271	0.17	0.26	I.S.	533	0.92	7.5	7.0	0.04	11	0.44	18	2134	9.6	-	-	-	0.53	0.04	0.74	0.01
	0.34	288835	0.03	0.36	I.S.	705	0.73	2.0	9.5	0.03	19	10	19	2828	6.2	-	-	-	6.3	0.01	0.68	0.17
	0.46	277009	0.24	2.8	I.S.	766	0.86	2.5	30	<0.001	10	3.4	18	3203	12	-	-	Inc.	0.91	0.01	1.8	0.23
	1.5	289622	0.04	1.4	I.S.	526	1.1	2.9	14	0.32	18	2.2	8.5	2614	40	-	-	-	3.1	0.01	1.5	0.12
	0.20	302120	0.02	0.60	I.S.	507	1.6	5.6	5.4	0.03	34	6.7	18	2229	20	-	Inc.	-	0.47	0.01	2.8	1.5
G14549b	0.46	319996	Inc.	0.43	I.S.	419	0.56	20	-	-	361	15	0.12	7.8	35	-	-	-	0.78	0.04	15	1.5
	21	323367	-	3.5	I.S.	292	0.86	24	Inc.	-	169	5.0	0.18	25	Inc.	-	-	-	3.9	0.07	59	1.1
	0.48	313322	-	0.48	I.S.	435	0.71	10	-	-	251	6.9	0.36	24	96	-	-	-	4.6	0.05	25	1.8
	Inc.	325805	-	1.1	I.S.	249	3.4	5.9	-	-	261	10	0.10	3.0	50	-	-	-	6.2	0.03	11	2.1
	0.33	318762	-	0.34	I.S.	334	0.86	6.1	-	-	465	18	0.36	97	102	Inc.	-	-	5.1	0.03	48	5.6
Mo17A	2.9	273166	<0.001	-	I.S.	250	0.24	5.5	0.90	0.26	24	32	0.25	0.41	29	<0.001	-	0.03	0.04	0.02	19	0.03
	5.0	289740	<0.001	Inc.	I.S.	312	0.21	10	8.5	<0.001	25	31	0.24	0.30	41	<0.001	-	0.04	0.12	0.001	28	0.03
	12	283707	0.005	-	I.S.	362	0.39	7.1	7.6	<0.001	79	58	0.23	0.28	135	0.65	-	0.08	0.05	0.02	69	0.34
	16	285402	0.03	-	I.S.	493	0.04	5.2	3.8	<0.001	58	46	0.28	0.37	158	2.4	-	0.01	0.15	0.12	98	0.10
	0.34	300560	0.005	-	I.S.	402	0.09	7.8	1.1	<0.001	16	47	0.30	0.43	11	0.21	-	<0.001	0.05	0.001	6.4	0.002
	Inc.	259091	0.01	-	I.S.	352	0.12	7.2	1.7	<0.001	42	56	0.24	0.46	95	0.29	-	0.01	0.18	0.76	77	0.05
	0.07	301015	0.01	-	I.S.	323	<0.001	0.84	0.86	<0.001	35	54	0.44	0.17	96	<0.001	-	<0.001	0.10	<0.001	63	0.03
	0.53	275177	<0.001	-	I.S.	357	0.02	2.3	5.2	0.20	17	36	0.23	0.36	12	0.34	-	0.02	0.14	<0.001	6.0	0.01
	0.15	282139	0.10	-	I.S.	572	0.08	2.6	5.5	<0.001	17	80	0.35	0.58	0.64	0.06	-	0.01	0.05	0.002	0.52	<0.001
	0.07	275328	0.01	-	I.S.	510	0.35	3.4	3.4	0.09	9.5	69	0.47	0.58	1.4	<0.001	-	0.004	0.11	<0.001	0.65	<0.001
ORV1	0.07	240111	<0.001	-	I.S.	221	0.06	1.5	45	-	2.7	1.2	8.1	0.73	0.30	0.72	-	0.003	0.04	0.001	0.98	0.04
	0.05	257728	0.35	-	I.S.	475	0.41	0.47	53	Inc.	5.0	3.6	12	3.5	0.04	<0.001	-	<0.001	0.09	0.001	1.2	0.11
	0.06	245741	0.11	-	I.S.	337	0.19	2.7	39	-	3.9	1.2	7.9	0.55	4.8	0.41	-	0.01	0.03	0.01	3.9	0.13

	0.26	259213	0.11	-	I.S.	289	0.20	0.66	40	-	3.7	1.1	9.5	0.71	0.08	0.44	-	<0.001	0.04	<0.001	1.6	0.28
	0.47	278394	0.18	-	I.S.	187	0.10	0.90	49	-	3.2	1.0	11	0.15	Inc.	0.66	-	0.01	0.33	0.02	4.9	0.04
	0.30	272101	0.18	-	I.S.	24	0.04	1.1	28	-	3.7	1.0	6.2	1.6	4.8	<0.001	-	0.03	0.15	0.02	Inc.	0.42
	0.60	281751	0.21	-	I.S.	227	0.29	1.2	67	-	1.5	0.23	8.7	1.6	2.8	<0.001	-	<0.001	0.38	0.004	2.5	0.09
	0.34	250314	0.01	-	I.S.	235	0.29	0.82	50	-	3.4	0.88	10	1.5	0.01	0.48	-	<0.001	0.05	<0.001	0.35	0.17
	0.15	248526	0.11	-	I.S.	160	0.24	0.71	17	-	1.5	<0.001	2.9	0.05	1.5	<0.001	-	0.02	0.04	0.001	0.69	0.07
	0.07	260803	0.19	-	I.S.	325	0.11	3.8	44	-	1.1	1.1	9.7	0.97	0.01	<0.001	-	<0.001	0.08	<0.001	1.7	0.15
G16152	0.24	260967	0.18	0.25	I.S.	15	0.31	15	7.8	0.04	0.53	0.30	3.7	37	10	0.12	0.02	0.01	2.8	0.01	0.79	0.03
	0.24	264271	0.23	0.66	I.S.	2.5	0.41	17	25	1.6	1.2	0.35	1.3	10	21	0.52	0.01	0.01	4.7	0.01	1.3	0.12
	0.22	272364	0.02	0.98	I.S.	19	0.33	40	34	0.52	0.88	0.24	1.3	6.3	24	<0.001	0.01	0.02	4.5	0.02	1.8	0.49
	0.23	271603	0.75	0.24	I.S.	24	0.28	Inc.	35	0.22	0.29	2.3	2.1	57	Inc.	0.73	0.15	0.02	2.5	0.02	9.4	1.3
	0.21	269386	0.22	0.19	I.S.	8.6	0.10	27	6.3	0.08	1.5	0.86	1.4	27	5.1	0.10	<0.001	0.11	4.0	0.01	2.1	0.03
	0.22	269202	0.39	0.20	I.S.	7.9	0.23	68	6.5	0.62	2.0	0.26	1.0	58	20	0.15	0.01	0.17	10	0.01	3.2	0.21
	0.22	266647	1.3	1.0	I.S.	17	0.07	124	6.2	0.21	4.9	0.29	1.7	Inc.	87	0.11	0.01	0.01	4.2	0.01	1.7	0.57
	0.27	268464	0.41	Inc.	I.S.	11	0.31	43	7.5	2.1	2.0	0.34	1.7	24	28	0.19	0.02	0.02	0.82	0.01	2.7	0.14
	0.76	272437	0.20	0.75	I.S.	29	0.19	Inc.	6.0	1.3	8.0	0.25	4.1	60	Inc.	0.15	0.02	0.06	4.7	0.02	9.2	1.2
G871	1.5	248855	0.13	-	I.S.	17	0.09	71	-	0.44	35	-	0.03	2.2	350	-	0.10	0.27	11	0.12	Inc.	2.3
	4.9	243278	0.85	-	I.S.	61	0.24	Inc.	-	Inc.	52	-	0.04	6.0	Inc.	-	0.02	0.07	Inc.	0.62	Inc.	2.6
G874	0.55	300222	0.05	0.41	I.S.	7.8	0.73	3.1	14	0.07	0.65	0.64	1.1	0.41	7.5	1.6	-	0.06	2.9	0.02	Inc.	0.14
	6.5	289736	0.57	3.8	I.S.	11	0.13	4.6	20	0.20	0.65	6.0	1.6	3.8	Inc.	1.2	-	0.05	20	0.26	Inc.	1.8
	0.20	310084	0.15	0.14	I.S.	2.7	0.26	3.5	5.0	0.02	0.34	1.1	0.52	0.36	Inc.	2.7	-	0.02	4.1	0.01	Inc.	0.35
	0.22	314936	0.02	1.2	I.S.	3.0	0.34	4.8	11	0.02	0.42	0.22	0.94	1.1	2.2	0.13	-	0.01	1.9	0.02	43	0.30
	0.38	307730	0.35	0.32	I.S.	11	0.10	1.9	8.9	0.04	0.41	0.36	1.2	0.29	2.4	1.0	-	0.02	3.0	0.01	45	0.88
	1.4	322891	0.10	0.19	I.S.	6.2	0.14	1.1	27	0.02	0.25	0.19	1.3	0.69	3.5	2.0	-	0.01	4.3	0.01	1.8	0.12
	0.33	319045	0.03	0.26	I.S.	4.1	0.11	7.0	50	0.05	0.25	0.23	4.5	0.73	2.1	<0.001	-	0.02	5.3	0.01	3.5	0.01
	0.25	315419	0.08	0.21	I.S.	15	0.03	2.8	19	<0.001	0.47	0.49	1.1	1.0	7.1	0.54	-	0.02	6.6	0.02	6.8	0.11
	0.21	321571	0.02	2.1	I.S.	2.6	0.10	2.9	16	0.03	2.4	0.24	0.22	0.93	8.1	0.83	-	0.01	7.7	0.04	47	0.17
	3.7	309611	0.02	0.24	I.S.	3.1	0.06	8.8	31	<0.001	0.18	0.25	0.82	0.75	5.7	-	-	0.01	2.7	0.03	21	0.21
G879	1.5	252916	0.24	0.94	I.S.	Inc.	0.26	67	Inc.	0.05	Inc.	13	31	63	Inc.	0.24	<0.001	0.09	1.9	0.41	25	Inc.
	0.32	273915	0.03	0.87	I.S.	71	0.54	36	-	<0.001	80	0.47	18	99	Inc.	0.24	<0.001	0.02	2.6	0.01	6.9	12
	0.59	269876	0.04	1.2	I.S.	6.1	0.11	3.8	-	0.19	32	2.8	98	162	12	2.4	0.03	0.02	1.00	0.02	4.7	4.1
	0.45	263004	0.03	2.0	I.S.	27	0.65	15	-	0.05	29	0.59	77	134	29	1.0	0.10	0.02	0.79	0.04	5.5	9.7
	0.45	260518	0.04	0.42	I.S.	25	0.06	11	-	<0.001	39	5.1	224	73	Inc.	0.34	<0.001	0.02	0.79	0.01	9.8	7.4
	5.4	261263	0.06	0.73	I.S.	7.5	0.08	16	-	0.13	35	6.6	175	105	18	0.67	<0.001	0.04	1.2	0.02	3.5	1.6
	11	288633	0.08	2.5	I.S.	30	0.10	21	-	0.71	26	7.2	100	105	30	3.6	0.04	0.06	1.4	0.04	4.5	3.8
	4.1	262027	0.15	0.41	I.S.	17	1.7	2.5	-	0.07	58	0.54	51	95	67	1.3	0.13	0.87	0.63	0.89	Inc.	Inc.
	2.0	266649	0.07	2.3	I.S.	Inc.	0.78	25	-	0.09	Inc.	0.66	54	149	Inc.	<0.001	0.03	0.03	2.1	0.12	29	24

	Inc.	271465	0.43	0.71	I.S.	7.4	1.9	4.7	-	0.13	23	0.89	138	94	74	0.37	<0.001	0.03	1.1	0.54	21	19
G882	-	260352	0.30	0.46	I.S.	4.8	0.14	4.0	12	0.23	0.38	0.65	0.28	1.7	9.6	1.5	0.03	0.01	0.95	0.01	6.3	0.07
	-	258669	1.3	0.60	I.S.	Inc.	0.15	Inc.	17	0.10	5.6	0.87	2.0	0.53	Inc.	1.4	0.32	0.03	Inc.	0.02	21	1.7
	-	264852	0.04	0.44	I.S.	5.2	0.30	12	64	0.10	1.4	0.64	0.11	1.7	14	<0.001	0.19	0.03	5.3	0.03	13	0.17
	-	255491	0.04	0.42	I.S.	11	0.28	Inc.	99	0.06	Inc.	0.59	0.04	3.4	Inc.	0.28	<0.001	1.2	Inc.	0.20	Inc.	0.38
	-	272901	0.03	0.30	I.S.	2.8	0.02	23	76	<0.001	2.0	1.9	0.44	0.57	15	0.13	0.01	0.02	5.4	0.04	13	0.36
	-	284099	0.20	1.5	I.S.	3.5	0.04	8.1	9.3	0.05	0.32	0.41	0.12	1.5	7.5	0.27	0.12	0.06	8.1	0.05	13	0.19
	-	290069	0.02	0.25	I.S.	31	0.11	16	7.0	0.04	4.6	4.3	0.15	0.79	17	0.12	0.01	0.01	6.3	0.05	41	0.04
	-	303414	0.04	0.65	I.S.	7.7	0.04	6.9	9.4	0.35	1.3	0.57	0.22	1.2	11	0.16	0.03	0.02	0.75	0.01	12	0.06
	-	306914	0.32	0.29	I.S.	21	0.13	14	54	<0.001	1.4	0.47	0.10	0.23	37	<0.001	0.01	0.01	11	0.16	15	0.14
	-	299663	1.3	1.1	I.S.	Inc.	0.19	Inc.	59	0.04	2.7	0.51	0.25	0.34	Inc.	2.0	<0.001	0.01	Inc.	0.08	19	1.0
G6946	0.32	299507	0.91	1.8	I.S.	4.3	0.46	19	6.7	<0.001	2.9	0.32	4.0	530	41	-	-	0.02	5.3	0.04	Inc.	0.13
	0.27	309238	0.41	1.5	I.S.	3.4	0.25	32	5.9	0.05	5.7	0.36	2.0	526	46	-	-	0.14	2.6	0.01	9.2	0.33
	4.8	336463	0.59	1.9	I.S.	7.7	0.07	377	13	0.47	19	0.89	12	177	625	-	-	0.35	0.76	0.63	Inc.	3.1
	1.4	310441	2.9	0.95	I.S.	22	0.03	Inc.	5.4	0.02	30	0.26	7.2	150	817	-	-	0.93	8.9	0.64	Inc.	1.3
	0.58	292544	1.4	4.5	I.S.	Inc.	0.03	366	5.9	2.8	72	Inc.	11	211	677	-	-	6.3	7.0	1.1	Inc.	8.6
	0.26	295789	1.0	0.24	I.S.	31	0.47	567	48	1.0	Inc.	1.7	22	254	620	-	-	0.08	4.5	0.26	Inc.	0.91
	0.28	318479	1.2	0.26	I.S.	78	0.03	587	6.4	0.25	31	3.5	4.6	124	674	-	-	2.0	2.1	0.38	Inc.	5.9
	7.0	157297	Inc.	2.8	I.S.	Inc.	0.20	Inc.	48	0.24	Inc.	Inc.	7.9	259	Inc.	-	-	0.35	Inc.	0.43	179	Inc.
	5.9	290677	3.2	5.6	I.S.	Inc.	0.04	Inc.	Inc.	Inc.	Inc.	6.2	13	265	1064	-	-	0.10	Inc.	0.93	Inc.	6.1
	3.3	297135	0.46	0.51	I.S.	139	0.13	109	155	4.6	14	0.53	2.3	537	971	-	-	0.72	5.4	0.01	72	1.4
G6949	4.6	291789	0.02	0.21	I.S.	414	1.2	1.6	16	0.04	13	5.8	179	1048	31	1.6	-	0.01	1.4	0.17	3.0	1.1
	0.48	286459	0.03	0.41	I.S.	535	0.98	3.4	12	0.58	7.8	4.3	160	550	Inc.	<0.001	-	0.02	0.62	0.27	Inc.	Inc.
	1.4	286763	0.03	0.27	I.S.	454	0.66	2.5	9.2	0.03	6.3	0.44	178	688	42	0.16	-	0.02	3.6	0.19	3.2	2.0
	12	296574	0.05	0.20	I.S.	359	2.0	6.9	6.7	<0.001	13	4.1	153	553	66	1.8	-	0.01	3.1	0.46	11	2.0
	4.5	288194	0.03	2.7	I.S.	364	0.84	32	27	0.05	17	7.7	161	298	101	0.31	-	0.02	8.9	0.21	26	12
	0.54	281340	0.04	0.46	I.S.	488	1.4	19	15	0.09	2.0	2.4	238	992	29	0.37	Inc.	0.03	3.9	0.19	3.7	4.2
	7.1	275520	0.33	0.52	I.S.	514	0.62	18	15	0.10	13	11	180	1299	Inc.	0.39	-	0.03	8.2	0.14	12	8.3
	10	277764	0.15	0.32	I.S.	496	0.26	3.5	13	0.50	7.0	4.1	176	342	60	<0.001	-	0.03	4.7	0.70	6.0	1.4
	2.7	262341	0.04	5.0	I.S.	496	1.4	15	15	0.08	5.6	8.3	229	1282	67	<0.001	-	0.08	4.6	0.66	7.0	2.9
	11	281270	0.05	0.22	I.S.	449	0.32	1.6	16	0.73	13	5.0	178	476	64	<0.001	-	0.03	3.6	0.40	5.3	3.4
G11701	0.28	287822	0.25	0.28	I.S.	71	0.01	5.1	-	0.03	Inc.	5.3	0.01	0.91	919	-	0.20	0.01	9.0	9.4	63	1.6
	0.52	291545	0.04	0.54	I.S.	114	0.06	11	-	0.07	623	3.2	0.03	0.45	848	-	0.13	0.03	12	1.1	104	0.98
	0.38	294122	0.14	0.37	I.S.	84	0.17	17	-	0.36	450	4.1	0.06	1.8	663	-	0.03	0.02	6.5	5.2	69	3.0
	0.54	291607	0.04	2.1	I.S.	72	0.07	7.8	-	<0.001	308	3.1	0.01	0.47	226	-	<0.001	0.02	11	0.75	31	0.35
	0.54	280270	0.57	0.58	I.S.	128	0.07	15	-	0.12	422	2.8	0.02	0.47	916	-	0.03	0.07	11	8.1	80	2.4
	0.61	281795	0.14	0.50	I.S.	135	0.07	12	-	<0.001	Inc.	1.0	0.01	2.8	866	-	<0.001	0.04	12	2.3	75	1.9

	2.7	285128	0.05	0.92	I.S.	94	0.32	2.8	-	0.05	437	8.4	0.01	1.1	217	-	<0.001	0.02	15	0.57	18	0.17
	0.50	280368	0.12	0.53	I.S.	118	0.18	2.7	-	0.20	489	3.4	0.03	1.2	517	-	<0.001	0.02	13	2.9	63	4.7
	0.43	271485	0.03	0.37	I.S.	90	0.06	2.2	-	0.07	339	2.4	0.01	0.38	1035	-	0.03	0.02	4.7	6.0	116	7.4
	1.4	276540	0.03	0.23	I.S.	110	0.30	6.4	-	0.04	Inc.	2.0	0.11	0.23	540	-	<0.001	0.01	1.2	3.4	86	0.40
G14246	0.18	288880	0.16	0.93	I.S.	353	1.6	21	4.2	0.10	2.2	5.3	101	637	24	-	-	0.03	0.44	0.14	15	6.9
	0.59	292725	0.02	0.15	I.S.	362	2.0	9.2	19	0.03	3.0	3.8	90	425	65	-	-	0.02	3.6	0.24	16	11
	0.19	282768	0.08	0.14	I.S.	430	1.3	15	4.4	0.11	2.9	4.7	88	586	42	-	-	0.03	3.1	0.25	13	11
	0.79	288142	0.13	2.1	I.S.	402	1.2	17	4.2	0.16	3.1	2.4	90	1016	25	-	-	0.01	4.3	0.18	20	7.1
	1.1	287784	0.03	0.18	I.S.	257	1.1	15	5.4	0.03	0.75	2.2	99	477	14	-	-	0.01	2.6	0.03	12	4.1
	0.20	287233	0.10	0.91	I.S.	509	2.4	1.6	24	0.03	5.3	3.7	141	406	38	-	-	0.01	3.8	0.23	13	10
	3.2	285782	0.30	0.14	I.S.	338	0.73	14	11	0.11	3.2	4.7	64	692	34	-	-	0.01	9.0	0.55	14	13
	1.6	284596	0.02	0.57	I.S.	589	1.4	15	4.7	0.04	1.2	7.1	83	639	17	-	-	0.01	7.8	0.08	16	14
	1.2	283034	0.01	0.33	I.S.	376	0.74	13	4.0	<0.001	2.3	2.1	88	225	28	-	-	0.01	4.0	0.17	14	13
	0.18	282395	0.14	0.37	I.S.	Inc.	1.9	Inc.	4.7	0.02	0.92	5.2	147	219	12	Inc.	-	0.01	4.3	0.04	15	14
G14867	0.84	293267	0.02	1.6	I.S.	2.2	0.18	82	100	0.10	26	0.20	0.03	3.4	8.1	-	-	0.13	20	0.09	20	6.2
	0.16	314568	0.01	0.15	I.S.	1.9	0.08	80	Inc.	0.16	29	1.1	0.04	1.4	13	-	-	0.17	89	0.05	14	4.2
	0.99	269372	0.26	1.1	I.S.	2.1	0.04	Inc.	53	0.25	Inc.	0.20	0.07	7.1	67	-	-	0.23	Inc.	0.16	34	9.7
	0.72	259818	0.02	0.15	I.S.	2.2	0.07	79	25	0.03	42	0.19	0.03	3.1	12	-	-	0.27	104	0.03	7.5	3.3
	0.20	293796	0.02	0.16	I.S.	9.1	0.03	52	106	0.02	14	0.22	0.05	2.7	6.6	-	-	0.03	47	0.06	8.5	5.2
	2.1	243143	0.16	1.2	I.S.	Inc.	0.02	Inc.	Inc.	1.0	88	0.54	0.07	0.61	77	-	-	0.17	128	0.08	9.2	19
	1.2	294979	0.02	0.23	I.S.	2.7	0.05	26	47	0.04	11	0.25	0.05	4.2	4.6	-	-	0.09	8.9	0.01	10	3.8
	0.20	283178	0.02	1.1	I.S.	2.2	0.02	40	65	<0.001	22	0.21	0.08	3.7	19	-	-	0.18	13	0.12	14	2.5
	0.60	291302	0.02	0.36	I.S.	10.0	0.03	75	67	<0.001	9.1	0.25	0.07	4.2	13	-	-	0.06	90	0.03	17	15
	0.74	291563	0.01	0.16	I.S.	5.1	0.03	54	Inc.	0.74	14	2.7	0.04	1.6	7.9	-	-	0.20	51	0.06	14	5.0
Mo16	0.10	279846	0.04	-	I.S.	729	0.16	10	9.9	<0.001	13	82	0.07	0.95	8.8	<0.001	-	<0.001	0.03	0.02	11	0.003
	0.07	279031	0.01	-	I.S.	547	0.29	9.9	5.2	<0.001	11	51	0.12	0.57	0.45	0.55	-	0.02	0.02	0.001	0.31	<0.001
	0.16	258379	0.01	-	I.S.	515	0.30	12	10	0.10	11	54	0.20	0.67	1.4	0.31	-	<0.001	0.02	0.005	1.2	0.002
	0.07	276326	<0.001	-	I.S.	551	0.18	14	10	0.12	12	51	0.20	0.91	1.3	0.06	-	0.003	0.02	0.001	0.81	0.01
	0.15	293286	0.02	-	I.S.	622	0.10	8.4	6.7	0.43	13	52	0.15	0.43	2.0	0.06	-	0.07	0.02	0.001	2.0	<0.001
	0.30	285367	0.01	-	I.S.	540	0.13	6.4	9.1	<0.001	12	16	0.03	0.78	0.53	0.16	-	0.05	0.03	0.001	2.0	0.01
	0.06	288811	0.01	-	I.S.	651	<0.001	5.5	7.5	0.02	10	25	0.02	0.58	0.59	0.05	-	0.02	0.02	0.001	3.1	0.002
	0.46	259398	0.05	-	I.S.	482	0.04	0.93	12	<0.001	11	47	0.11	0.75	2.5	0.30	-	0.01	0.03	0.04	1.4	0.002
	0.36	269392	0.01	-	I.S.	719	0.22	2.8	6.2	<0.001	13	53	0.15	1.0	5.4	0.95	-	0.01	0.03	0.001	3.3	0.002
	0.09	285128	0.01	-	I.S.	533	0.27	8.5	11	0.02	11	47	0.10	0.87	0.78	0.17	-	0.004	0.11	0.001	0.38	0.01
G29851	-	323117	0.04	0.68	I.S.	19	0.06	Inc.	-	0.17	9.4	0.80	0.11	2.3	Inc.	0.45	0.04	0.22	Inc.	0.02	86	3.2
	-	313079	0.05	0.62	I.S.	6.4	0.20	24	Inc.	0.11	30	0.89	0.14	1.5	13	1.6	0.05	0.16	9.7	0.01	124	1.3
	-	295608	0.06	0.83	I.S.	7.3	0.11	11	-	0.07	66	2.4	0.08	0.56	13	0.78	0.11	0.04	23	0.21	139	1.6

	-	312881	0.06	2.2	I.S.	12	0.06	32	-	0.35	10	2.9	0.12	0.45	17	4.3	0.03	0.68	9.9	0.03	121	0.28
	-	297033	0.20	0.59	I.S.	5.7	0.07	37	-	0.09	54	0.86	0.06	2.9	11	1.6	0.04	0.02	17	0.01	91	0.56
	-	312092	0.05	0.64	I.S.	22	0.17	50	-	0.07	70	0.75	0.06	2.4	6.1	0.31	0.11	0.03	15	0.05	31	0.34
	-	292322	0.08	1.3	I.S.	6.0	0.08	35	-	0.08	35	0.81	0.12	4.2	4.6	1.6	0.03	0.03	12	0.02	19	0.08
	-	300512	0.14	0.62	I.S.	5.7	0.07	7.3	-	0.09	11	0.73	0.10	1.9	8.3	0.33	0.03	0.07	12	0.03	47	0.22
	-	301672	0.06	2.0	I.S.	5.4	0.07	18	-	0.08	6.1	0.92	0.10	0.49	12	0.78	0.03	0.34	9.7	0.01	59	0.29
	Inc.	292372	0.06	0.69	I.S.	5.5	0.07	6.8	Inc.	0.08	14	0.92	0.12	0.45	8.5	3.1	<0.001	0.03	12	0.01	50	0.32
ORV4	0.08	243555	0.08	-	I.S.	137	0.41	6.1	0.93	<0.001	1.2	0.96	4.2	4.2	5.3	<0.001	-	Inc.	0.04	0.04	9.8	0.03
	0.32	231188	<0.001	-	I.S.	167	0.17	0.76	Inc.	0.36	2.2	0.52	9.0	0.06	0.86	<0.001	-	-	0.04	0.002	5.3	0.25
	0.28	240866	<0.001	-	I.S.	144	1.5	2.3	3.2	<0.001	2.0	0.64	8.8	4.1	0.16	0.45	-	-	0.10	<0.001	0.36	0.01
	0.08	232848	0.05	-	I.S.	173	<0.001	2.7	9.3	0.36	4.0	1.3	9.5	2.1	0.19	0.37	-	-	0.03	<0.001	0.10	0.02
	0.25	239708	0.06	-	I.S.	142	0.29	2.6	0.96	0.67	1.6	0.68	7.2	2.8	5.3	<0.001	-	-	0.03	0.02	1.6	0.03
	0.15	232801	<0.001	-	I.S.	158	0.16	3.8	5.0	<0.001	6.8	0.69	7.5	2.9	0.01	<0.001	-	-	0.03	<0.001	9.7	0.03
	0.08	226757	0.16	-	I.S.	147	0.13	3.5	0.78	<0.001	1.5	1.5	7.8	4.2	0.02	<0.001	-	-	0.07	0.001	0.70	0.19
	0.55	231795	<0.001	-	I.S.	129	0.36	1.5	0.80	0.18	7.8	2.3	9.0	1.5	0.09	<0.001	-	-	0.11	<0.001	0.11	0.07
	0.39	238211	0.05	-	I.S.	144	0.29	0.74	7.5	<0.001	1.3	1.6	9.8	0.19	6.2	<0.001	Inc.	-	0.08	0.02	1.8	0.05
	0.49	240699	0.04	-	I.S.	218	0.34	2.1	1.1	<0.001	0.97	2.5	7.8	3.2	0.12	<0.001	-	-	0.28	<0.001	0.04	0.003

Dash indicates all analyses <mdl. Other <mdl values were treated as mdl/2. I.S. = Internal standard. Inc. = Inclusion detected.

*Evidence suggests sulphides in sample did not co-crystallize (based on textures and partitioning trends among base metal sulphides).

ADDITIONAL MATERIAL D

TRACE ELEMENT ANALYSIS OF MINERALS IN MAGMATIC-HYDROTHERMAL ORES BY LASER ABLATION INDUCTIVELY-COUPLED PLASMA MASS SPECTROMETRY: APPROACHES AND OPPORTUNITIES

Nigel J. Cook[1], Cristiana L. Ciobanu[1], **Luke L. George**[2], Zhi-Yong Zhu[1,3], Benjamin Wade[4], Kathy Ehrig[5]

[1]*School of Chemical Engineering, The University of Adelaide, Adelaide, S.A., 5005, Australia*

[2]*School of Physical Sciences, The University of Adelaide, Adelaide, S.A., 5005, Australia*

[3]*State Key Laboratory for Mineral Deposits Research, Department of Earth Sciences, Nanjing University, Nanjing 210093, China*

[4]*Adelaide Microscopy, The University of Adelaide, Adelaide, S.A., 5005, Australia*

[5]*BHP Billiton Olympic Dam Operations, Adelaide, S.A., 5000, Australia*

Paper published in Minerals, 6, 111. doi: 10.3390/min6040111.

minerals

MDPI

Review

Trace Element Analysis of Minerals in Magmatic-Hydrothermal Ores by Laser Ablation Inductively-Coupled Plasma Mass Spectrometry: Approaches and Opportunities

Nigel Cook [1,*], Cristiana L. Ciobanu [1], Luke George [2], Zhi-Yong Zhu [1,3], Benjamin Wade [4] and Kathy Ehrig [5]

1 School of Chemical Engineering, University of Adelaide, Adelaide, SA 5005, Australia; cristiana.ciobanu@adelaide.edu.au (C.L.C.); zhiyong.zhu@adelaide.edu.au (Z.-Y.Z.)
2 School of Physical Sciences, University of Adelaide, Adelaide, SA 5005, Australia; luke.george@adelaide.edu.au
3 State Key Laboratory for Mineral Deposits Research, Department of Earth Sciences, Nanjing University, Nanjing 210093, China
4 Adelaide Microscopy, University of Adelaide, Adelaide, SA 5005, Australia; benjamin.wade@adelaide.edu.au
5 BHP Billiton Olympic Dam Operations, Adelaide, SA 5000, Australia; Kathy.J.Ehrig@bhpbilliton.com
* Correspondence: nigel.cook@adelaide.edu.au; Tel.: +61-8-8313-1096

Academic Editor: Antonio Simonetti
Received: 31 July 2016; Accepted: 16 August 2016; Published: 20 October 2016

Abstract: Laser ablation inductively-coupled plasma mass spectrometry (LA-ICP-MS) has rapidly established itself as the method of choice for generation of multi-element datasets for specific minerals, with broad applications in Earth science. Variation in absolute concentrations of different trace elements within common, widely distributed phases, such as pyrite, iron-oxides (magnetite and hematite), and key accessory minerals, such as apatite and titanite, can be particularly valuable for understanding processes of ore formation, and when trace element distributions vary systematically within a mineral system, for a vector approach in mineral exploration. LA-ICP-MS trace element data can assist in element deportment and geometallurgical studies, providing proof of which minerals host key elements of economic relevance, or elements that are deleterious to various metallurgical processes. This contribution reviews recent advances in LA-ICP-MS methodology, reference standards, the application of the method to new mineral matrices, outstanding analytical uncertainties that impact on the quality and usefulness of trace element data, and future applications of the technique. We illustrate how data interpretation is highly dependent on an adequate understanding of prevailing mineral textures, geological history, and in some cases, crystal structure.

Keywords: laser ablation inductively coupled plasma mass spectrometry; trace element data; ore genesis; sulphide minerals

1. Introduction

Significant advances have taken place in laser ablation inductively-coupled plasma mass spectrometry (LA-ICP-MS) over the past two decades ([1] and references therein). Instruments have become widely available in laboratories worldwide and the number of applications in Earth science has been greatly expanded by ongoing technological development, particularly with respect to analysis speed, resolution and sensitivity, and by the availability of reliable reference materials designed for specific purposes. The LA-ICP-MS method is also cost-effective compared to other techniques, such as secondary ion mass spectrometry (SIMS). For these reasons, LA-ICP-MS has rapidly established itself

as the method of choice for generation of multi-element datasets for specific minerals. Applications have expanded from trace element 'spot' analysis to mapping of areas within a sample, greatly assisted by the widespread availability of software, such as iolite [2]. The LA-ICP-MS platform has also been developed to undertake stable (e.g., [3]) and radiogenic isotope analysis (e.g., [4,5]), and is also widely applied in geochronology to obtain U–Pb ages for zircon (e.g., [6]). LA-ICP-MS-based geochronology is rapidly being extended to other dateable minerals, including hematite [7,8], apatite [9], cassiterite [10], and epidote-group minerals [11].

This contribution reviews a number of recent advances both from a technological method-development and scientific problem-solving perspective. The focus of this contribution is on multi-trace element analysis for mineral characterisation and petrogenetic interpretation of magmatic-hydrothermal ore deposits. We highlight, drawing in part on our own published and previously unpublished data, the wide range of different mineral matrices that have been studied and the diversity of geological problems that can be addressed by accurate, reproducible trace element microanalysis. Secondly, this contribution discusses good analytical practice, stressing the need to have a detailed understanding of what has been analyzed and the potential limitations that area selection will have on data quality. We speculate on future developments and new applications. Recent advances in geochronology using LA-ICP-MS, Pb isotope analysis, and mapping of sulphur isotopes are covered elsewhere in this Special Issue ([8,12,13], respectively). Due to space limitations, LA-ICP-MS analysis of fluid inclusions (e.g., [14]), melt inclusions (e.g., [15]), and LA-ICP-MS trace element geothermobarometery (e.g., Ti-in-zircon [16], or Zr-in-titanite [17]), are also not covered here despite their great relevance to understanding the genesis of hydrothermal ore deposits.

2. LA-ICP-MS Trace Element Microanalysis

LA-ICP-MS applications in the Earth sciences are described in an extensive volume of literature. The reader is referred to Sylvester (2008) [1] for authoritative chapters on LA-ICP-MS hardware, the underlying principles of analysis, and outstanding issues. Although the overwhelming majority of LA-ICP-MS facilities (as is our own) are based around nanosecond LA-ICP-MS systems, one significant development over the past decade has been the emergence of femtosecond (fs) laser systems [18,19]. This has prompted concerns about the comparative performance of the two instrument types for geological materials (e.g., [20]).

For example, in a study of four glass reference materials, Ohata et al. (2014) [21] established that femto- and nanosecond LA-ICP-MS systems provide comparable results if Ca was used as an internal standard but significant deviations if Si-normalized fractionation was applied with fs laser ablation at 795 nm. These deviations were attributed to the composition and/or particle size distribution of aerosols formed over the sampling interval and could be corrected for by modifying fluence and spot size. Wohlgemuth-Ueberwasser and Jochum (2015) [22] compared the performance of nanosecond solid state and excimer lasers with a 200 nm femtosecond laser for analysis of common sulphide minerals. They report significant differences in the degrees of melting, with no melting observed utilizing the femtosecond laser.

2.1. Melts, Aerosols, Vapours and Mineral Decomposition

The many recent technical developments in mass spectrometry that have enabled greater accuracies and sensitivity have also focused interest on matrix effects and the physical state of the ablated material. One factor considered to potentially influence data quality is heating and generation of melts or particles precipitated from aerosols and vaporized products of ablation (e.g., [23]) during laser ablation. If melts are generated, and these are inherently different, chemically to the reference material used for calibration, fractionation may be introduced that could lead to a reduction in precision [22].

An additional topic of concern is the potential for fractionation during transport of ablated material from sample to plasma to mass spectrometer, e.g., between iron and sulfur [24]. Fractionation

can be caused at various stages, including chemical reaction processes (mineral decomposition, etc.) at the site of laser ablation, differential particle transport from the site of ablation as a function of particle size, preferential redeposition of particles of different size at the site of ablation or within the instrument, and selective ionization of some minerals in the ICP-MS. Each of these issues may be influenced by, and corrected for, by adjusting operating parameters of the LA-ICP-MS system (e.g., [23]), and judicious use of appropriate matrix-matched standards. There is also the issue of downhole fractionation, when operating in 'spot' mode, with fractionation increasing as a function of the aspect ratio of the crater.

2.2. Reference Materials and Matrix Effects

Use of appropriate matrix-matched reference standards is critical to enable correction for laser-induced fractionation during ablation, and thus reliable and reproducible quantitative outcomes (e.g., [25–32]). Table 1 lists reference materials commonly employed for LA-ICP-MS trace element analysis, matrices for which they have been applied, and key references regarding their suitability. The reader is referred to Reference [33] for a more extensive list of LA-ICP-MS reference materials. Although there are, to our knowledge, few published examples of comparative cross-laboratory or cross-standard testing (e.g., [34]), several publications have offered insights into the relative analytical accuracy that can be achieved. The use of multiple reference materials is encouraged [35]. New, alternative methods are also being sought to prepare suitable reference materials for analysis of elements not present in the more commonly used standards (e.g., [36]).

Table 1. Reference materials (RM) commonly employed for laser ablation inductively-coupled plasma mass spectrometry (LA-ICP-MS) trace element analysis of minerals in hydrothermal settings.

Standard	Matrix Type	Suitability	Comments	References
NIST-610, -612	Synthetic glass	Silicates	Widely used for silicates; have been used as secondary RM for Fe-oxides (low Fe content but some trace elements (e.g., As) not present in primary RM such as BHVO	Norman et al. (1996) [29], Jochum et al. (2011) [37], Nadoll and Koenig [38]
BCR-2G	Columbia River basalt glass	-	Secondary RM for some silicates	Wilson (1997) [39]
GSE-1G, GSD-1G	Synthetic glasses	Fe-oxides	Doped with most elements found in Fe-oxides	Jochum et al. (2005) [40]
BHVO-1	Hawaiian basalt glass	-	Suitable RM for Fe-oxides	Flanagan (1976) [41]
MASS-1	Cold-pressed pellet	Sulphides	Commercially available RM for sulphides; widely applied	Wilson et al. (2002) [42], Yuan et al. (2012) [43]
$(Fe,Ni)_{1-x}S$ and $(Fe,Cu)_{1-x}S$	Synthetic sulphides	Sulphides	-	Wohlgemuth-Ueberwasser et al. (2007) [31]
STDGL2b-2	Fused glass disk (25% Zn concentrate and 75% pyrrhotite), mixture of CANMET international reference materials RTS-4 and CZN-1 doped with a range of trace elements	Sulphides	Wide range of chalcophile, siderophile and lithophile elements	Danyushevsky et al. (2011) [32]
NiS-3	-	Sulphides	-	Gilbert et al. (2013) [34]
IMER-1	Chalcogenide glass ($Ge_{28}Sb_{12}S_{60}$)	Sulphides	4 minor elements, 34 trace elements	Ding et al. (2012) [44]

In some cases, it may be advantageous to use two or more reference materials with different concentrations of the element to be used for internal calibration. For example, when analyzing trace elements in iron oxides, we prefer to use National Institute of Standards and Technology (NIST)-610 and

one of the basalt glass standards (BHVO—basalt, Hawaiian volcano observatory or BCR-2G—basalt Columbia River glass; Table 1) since Fe, the only element that can be used as an internal standard for Fe-oxides, is much lower in NIST-610 (<1 wt %) relative to the natural basalt glasses. We also encourage users to compare LA-ICP-MS data for elements at concentrations of hundreds to thousands of ppm with electron probe microanalysis (EPMA) data on the same material as a further check on the validity of results.

It is clear, for example, that better quality analyses will be systematically obtainable for some elements than for others. In our experience with trace element analysis of sulphides, As, Se and Hg are among the more problematic elements, and can be difficult to completely remove from the ablation system, leading to high background counts for these elements. Samples suspected to contain high concentrations of these elements should only be run after others with lower concentrations. Lead can also be a problematic element. Higher background signals are encountered after analysis of galena or other Pb-bearing minerals, compromising the detection of Pb in other minerals where the element is only a trace component. Similarly, arsenopyrite, a mineral that may be a source of valuable trace element data, should never be run before other sulphides containing only ppm concentrations of As. Thorough cleaning of the LA-ICP-MS system is in any case essential when switching between analysis of different minerals.

An appreciation of potential interferences remains an important issue associated with LA-ICP-MS analysis. This includes: (i) poly-atomic interferences such as the generation of argides if using Ar as the plasma gas (e.g., argides of Cu and Ni (e.g., [45])) that may interfere with Pd, Rh, and Ru (^{101}Ru with ^{61}Ni^{40}Ar, and so on); (ii) isobaric interferences between elements which have the same isotopic masses (e.g., ^{108}Pd with ^{108}Cd, ^{115}In with ^{115}Sn); and (iii) multiple ionization interferences (generally less significant for trace element analysis). An understanding of potential interferences and isotopic proportions is necessary to know whether or not corrections need to be applied (for instance, correction of ^{101}Ru for ^{61}Ni^{40}Ar when analyzing pentlandite, or ^{115}In for ^{115}Sn in stannite, Ni and Sn being major components of the two sulphides). Other potential interferences may not necessitate correction. For example, ^{92}Zr measurement in magnetite need not be corrected for ^{52}Cr^{40}Ar since Cr is a minor component of magnetite and interference is thus negligible. The same would apply to analysis of In and Sn in sphalerite, since both elements are only minor components of that mineral, and any interference would be small, within the precision of the method. Interferences can be corrected for by careful analysis of blanks of known composition without the interfering element present. The list of potential interferences is large and, thus, beyond the scope of the present contribution.

When reporting trace element data, all users should provide full information on analytical methodology, including details of isotopes measured (with interference corrections as necessary), dwell times, external standard(s), internal calibration routines and precision and reproducibility of concentration data. It is also critical to report how the data were processed, both in terms of integrating segments of LA-ICP-MS depth profiles, and in terms of treatment of outliers and values below minimum detection limit to derive statistically meaningful data.

2.3. What Is Being Analyzed?

Compared to other techniques, notably electron probe microanalysis (EPMA) or SIMS, the volume of analyzed material by LA-ICP-MS is relatively large. Even with a small spot size of 15 μm, an ablation crater for a moderately hard mineral such as pyrite can be 20 μm deep, giving an ablated volume of several thousand μm^3. Softer minerals, such as galena or chalcopyrite, ablate far more rapidly. It is always prudent to ensure the ablated surface is free of inclusions prior to analysis but knowledge about the presence or absence of inclusions does not extend to depth within the section. Following guidelines to only analyze inclusion-free materials will, by and large, give reliable information on contained trace elements in a range of matrices. Nevertheless, by analyzing only 'clean' areas of a mineral, typically in its center, significant bias can be introduced into the dataset if that mineral is

compositionally zoned (Figure 1). Problems associated with representative analysis of zoned grains are particularly accentuated when the grains are so small they do not accommodate multiple spot analyses.

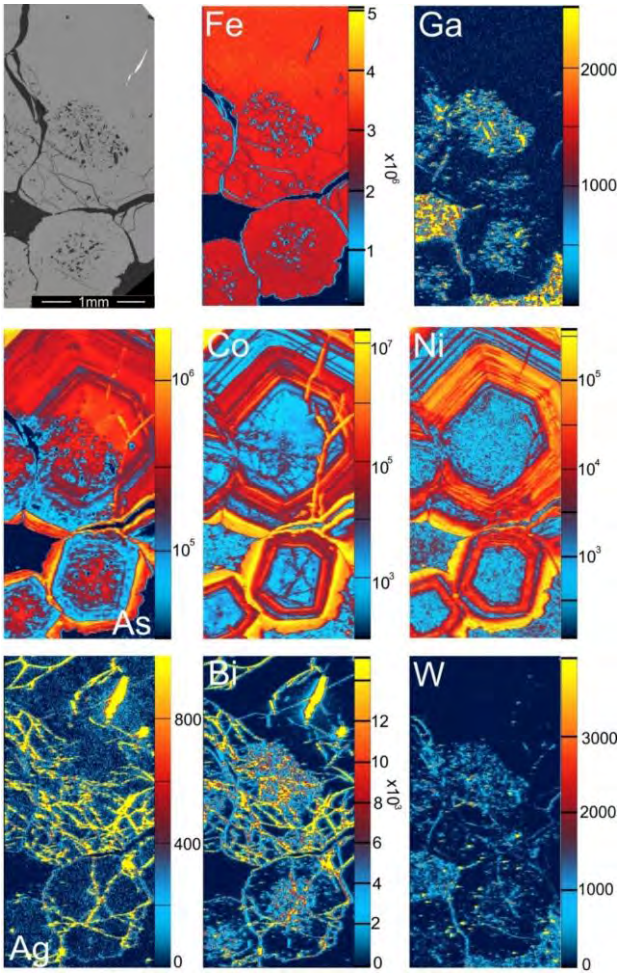

Figure 1. LA-ICP-MS maps of mm-sized pyrite grains displaying micron-scale oscillatory zoning. Note that, whereas As, Co and Ni occur in solid solution, within the pyrite grains and display concentric zoning, the map for Ga shows that element associated with microscopic silicate inclusions in the pyrite cores, and the maps for Ag, Bi and W show these elements are distributed not within the zones but in crosscutting microfractures. The mapped area is shown as a backscatter electron image at upper left. Scales in counts-per-second. Measured isotopes: ^{56}Fe, ^{69}Ga, ^{75}As, ^{59}Co, ^{60}Ni, ^{109}Ag, ^{2095}Bi, ^{182}W.

A second, related problem, commonly observed but not restricted to studies of gold-bearing pyrite and arsenopyrite, is that areas of a grain with abundant microfractures, pores and non-sulphide inclusions, can contain significantly more Au than 'clean' areas without inclusions and/or pore-rich domains in pyrite and arsenopyrite (e.g., [46–48]). An assessment should therefore be made of whether grain-scale compositional heterogeneity (including chemical zoning) is present—either by creating a LA-ICP-MS map, or if simply by comparing absolute concentrations from a number of randomly positioned spot analyses. This assumes, however, that the micro-fractures or pores are visible. In some cases, the micro-fractures in particular will not be visible. Similarly, trace elements may

be strongly concentrated along cleavage planes not visible under the SEM, and often only revealed by element mapping.

We also encourage LA-ICP-MS users to visually inspect laser craters after analysis—indications of possible inclusions can be seen in debris around the crater edge. In some cases, we have followed up LA-ICP-MS spot analysis by in-situ extraction of slices adjacent to the crater by focused ion beam (SEM) methods [49]. Subsequent investigation by transmission electron microscopy (TEM) allows the identity of what has been analyzed to be confirmed. A combined FIB-TEM approach can also be a powerful method to distinguish between nanoparticle-hosted and lattice-bound trace elements [50].

2.4. Trace Element Mineral Signatures—TESIM

A persistent question is whether analyzed elements are present in solid solution or as fine particle or nanoparticle mineral inclusions. Provided the particles are sufficiently large (roughly a few hundred nm in size), their presence will be recognized—and in many cases, their identity confirmed, on the down-hole laser ablation profiles. If the nanoparticles are fine enough and homogeneously distributed, however, it is impossible to recognize them on the downhole profiles, which will typically be smooth. Further investigation by transmission electron microscopy, as for example, done by Junge et al. (2015) [51], may help to understand if these elements are in the lattice, or occur as nanoparticle inclusions. Valuable information can nonetheless be obtained from analysis of areas within ore minerals that are known to include gangue or sub-µm to nanoscale inclusions of discrete minerals. We illustrate this with examples of chondrite-normalized REE + Y (REY) fractionation trends in hematite where the LA-ICP-MS spot size is significantly larger than the individual grains in the analyzed specimen (Figures 2 and 3).

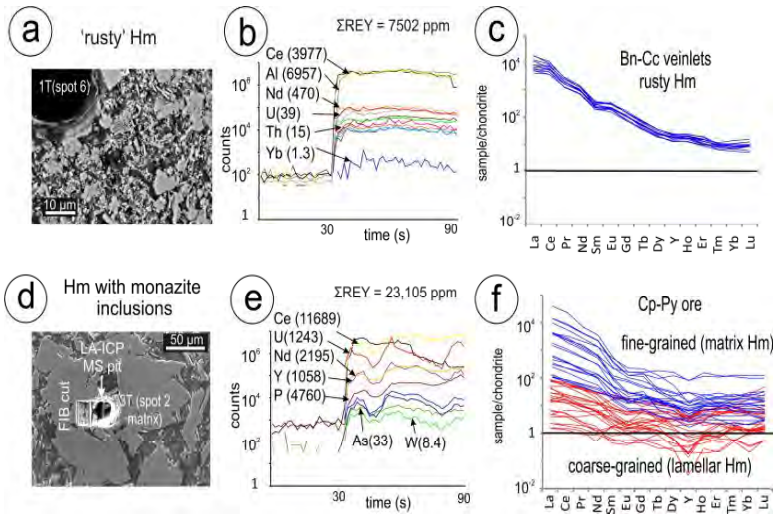

Figure 2. (**a**) Secondary electron (SE) image of fine-grained rusty hematite (Olympic Dam; OD). Note size of laser spot relative to grain size; (**b**) time-resolved depth profile showing 'flat' signals for most elements interpreted to he hosted in the hematite lattice; (**c**) chondrite-normalized REY fractionation trends for this type of hematite; note coherent, readily interpretable trends; (**d**) SE image of coarser hematite aggregate containing inclusions of monazite (see Figure 3a–d; OD); (**e**) time-resolved depth profile for spot in (d) showing rough signals indicative of inclusions during ablation. This hematite is not zoned with respect to trace elements; (**f**) chondrite-normalized REY fractionation trends for the hematite in the same sample shown in (d,e) separated by grain size. There is an increase in ΣREY with the fine-grained hematite in the matrix, which shows similar REY profiles with the rusty hematite. Note however their wider range relatively to the finest, rusty hematite in (c).

In Figure 2, we contrast LA-ICP-MS analyses of (i) rusty, finest-grained hematite (Figure 2a–c) and (ii) analysis of coarser hematite containing inclusions of monazite and at grain boundaries (Figure 2d–f). Both cases show high ΣREY (thousands of ppm, and >2 wt % for the rusty and coarser hematite, respectively) but differ in the 'noisiness' of the LA-ICP-MS downhole profiles. In both cases, a proportion (<10%) of the analyzed material is from gangue minerals, but the 'rusty' hematite clearly shows a smooth signal for individual elements and a highly reproducible chondrite-normalized REY fractionation trend. In the second case, spot analyses from the grain-boundaries and finer-grained hematite in the matrix are broadly comparable with those displayed by the rusty hematite trends but show much higher variability in terms of ΣREY, concordant with the observation of discrete REY-bearing minerals.

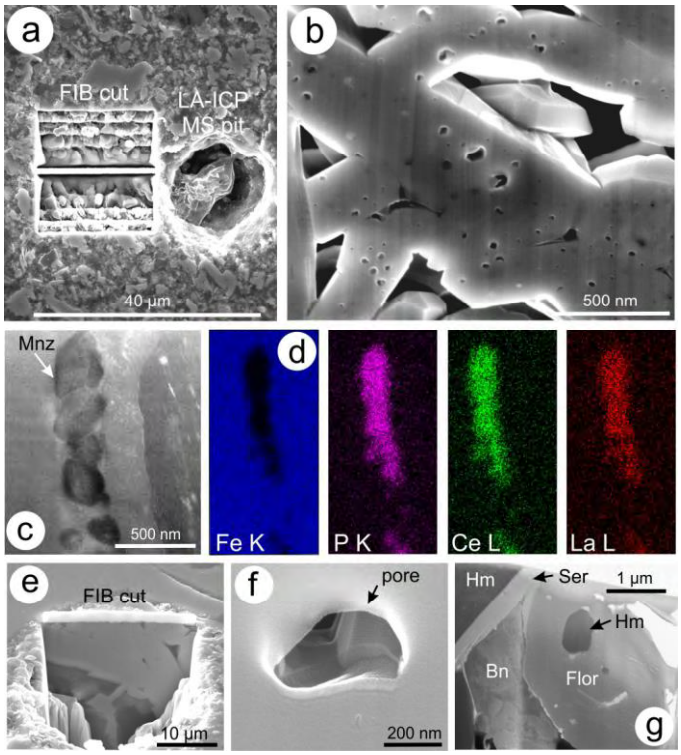

Figure 3. Mineral inclusions and porosity present in hematite from samples shown in Figure 2a,b SE images showing location of FIB-cut next to LA-ICP-MS spot in rusty hematite (**a**); and the presence of pores and inclusions within the sub-µm size lamellae (**b**); (**c**) FIB-Scanning Transmission Electron Image in Bright Field mode showing trails of sub-µm inclusions of monazite (Mnz) close to the grain boundary; (**d**) FIB-EDS maps of monazite grains in (c); (**e**,**f**) SE images showing distribution of pores and their morphology in hematite from (c) obtained after FIB-cross sectioning through the polished block; (**g**) Sub-µm-sized inclusion of hematite (Hm) in florencite (Flor) from a high-grade bornite (Bn)-bearing sample at OD. Ser—sericite.

FIB-SEM study of both types of hematite (Figure 3) feature pores and nanoscale inclusions. The latter differ in size in the rusty and coarser hematite, typically a few, or several hundred nm, respectively (Figure 3a–f). Some of these inclusions can be identified as discrete REE-minerals, notably the trail of monazite inclusions observed in the coarser hematite (Figure 3c,d). Note that the monazite grains are close to the margin of one of the lamellae, which is sputtered with nanoparticle-size

inclusions and nanopores. We also draw attention to the fact that the margins of hematite lamellae in the rusty type do not contain abundant nanoscale REE-minerals attached to them but are instead rather 'clean' and the specimen is very vuggy (Figure 2b). This implies that the bulk of the measured REY content is hosted within the hematite itself. Lattice-bound elements can be released upon supersaturation and/or interaction with fluids, and can form discrete REE-bearing minerals within crystal lattice defects. Conversely, hematite can also occur as nanoscale inclusions (several hundred nm) within REE-minerals (Figure 3g), re-emphasizing the strong genetic link between hematite and REY in iron oxide-copper-gold (IOCG) systems.

Based on this evidence, we conclude that trace element signatures in minerals (TESIM) can display consistency, and thus be used as meaningful geochemical tracers. This is true not only when the elements are lattice-bound but also when nanoscale inclusions are present, as long as the speciation of those inclusions does not vary widely.

2.5. Mineral Textures

No less important than an adequate knowledge of what has been analyzed, is an appreciation of the prevailing mineral textures, and how to compile compositional data for a given mineral into statistically meaningful groupings. Prior investigation of as large a volume of representative samples as possible by optical and scanning electron microscopy is strongly recommended prior to LA-ICP-MS microanalysis, to facilitate an adequate appreciation of multiple generations and overprinting (if present), features that might indicate compositional zoning, or evidence for mineral-mineral or mineral-fluid reactions. Single mineral grains may preserve compositionally or texturally-distinct domains that can be interpreted as multiple generations; examples include growth-zoned pyrite from metamorphosed ores that preserve pre-metamorphic grain cores (e.g., [52]), or skarn garnet recoding prograde and superposed retrograde growth cycles [53].

2.6. Spots, Rasters and Element Maps

The recent literature documents a number of different analytical approaches, notably the use of 'spots' (i.e., relatively deep craters) and 'trenches' (rasters; shallower ablation along a trajectory across a larger area). Each approach has its advantages and disadvantages and may be selected based on the target mineral and the inherent patterns to be analyzed. Spots and rasters may often be used in combination, each mode contributing information. Downhole fractionation is greater in 'spot' mode, and may affect the final results if not properly corrected for. Using raster analysis will decrease the spatial resolution of laser ablation in that the total surface area is generally larger. Spot analyses are commonly preferred when the minerals in question are small and/or compositionally zoned at the micron-size, and should be used (to keep the area analyzed as small as possible) if two or more distinct generations are present within that zoning pattern (e.g., an early core and later overgrowth). Raster analyses are certainly useful for showing variation across a single grain or assemblage, but there is always significant risk of mineral inclusions or other features that may influence the data. Raster analysis also has the advantage of allowing longer acquisition on grains that are sufficiently large and inclusion-free and can also contribute representative, average compositions for zoned minerals.

Trace element mapping by LA-ICP-MS has proven an extremely valuable technique to provide a visualization of trace element distributions within individual minerals or assemblages [54–58]. Element maps show concentration patterns with single zoned grains (Figure 1) and also facilitate a rapid visualization of the relative trace element concentrations and interpret partitioning trends among coexisting minerals (e.g., [59]).

Imaging is conducted by ablating sets of parallel lines in a grid across a sample surface. The laser spot size should match the distance between adjacent lines, and should be chosen based on the desired sensitivity of the elements of interest, as well as the desired spatial resolution. The authors typically use the open source software package 'iolite' [2] to compile and process trace element maps obtained by LA-ICP-MS data. Iolite is an add-in for the data analysis program Igor developed by WaveMetrics.

Maps can be generated to provide either qualitative or quantitative information. Qualitative trace element maps are based only on measured counts per second (cps) for each element, and variation across a mapped area is displayed only in cps. As the ablation rate for different minerals can vary over orders of magnitude, the counts for elements within different minerals also vary greatly. Thus qualitative maps are able to disclose relative concentration variations across a mineral or assemblage (e.g., compositional zoning) but actual concentration values cannot be determined, and concentration intensity cannot be compared across different phases. Quantitative trace element maps determine actual trace element concentrations and these are often displayed on a parts per million (ppm) scale bar. Quantitative maps are able to reveal both trace element variation and actual trace element concentrations in a single mineral.

Difficulties arise, however, when attempting to quantify an entire assemblage comprising multiple distinct phases. Quantifying a map with iolite requires the selection and input of an internal standard. This tells the program the concentration of one element in the mapped area, allowing calculation of all other unknown element concentrations. If, however, the mapped area contains distinct phases of vastly different composition, a single internal standard often cannot be adequately selected.

Exceptions arise when mapping assemblages comprising distinct phases with comparable concentrations of a particular element. For example, when mapping base metal sulphide assemblages comprising sphalerite, galena and chalcopyrite, an average sulfur concentration value may be used as an approximate internal standard. Figure 4 shows three quantitative LA-ICP-MS maps of an assemblage comprising co-crystallized sphalerite, galena and chalcopyrite. The LA-ICP-MS maps were quantified by using 25 wt % S as the internal standard, a value representing an approximate average sulfur concentration for the assemblage. LA-ICP-MS spot analysis was also conducted around the margins of the mapped area for comparison. As can be seen, the LA-ICP-MS spot analyses closely match the concentrations displayed by the map. Some slight discrepancies are noted, although these are typically less than 10% of the spot values and are usually less than the uncertainty of ascribing a particular concentration value to a particular color on the map.

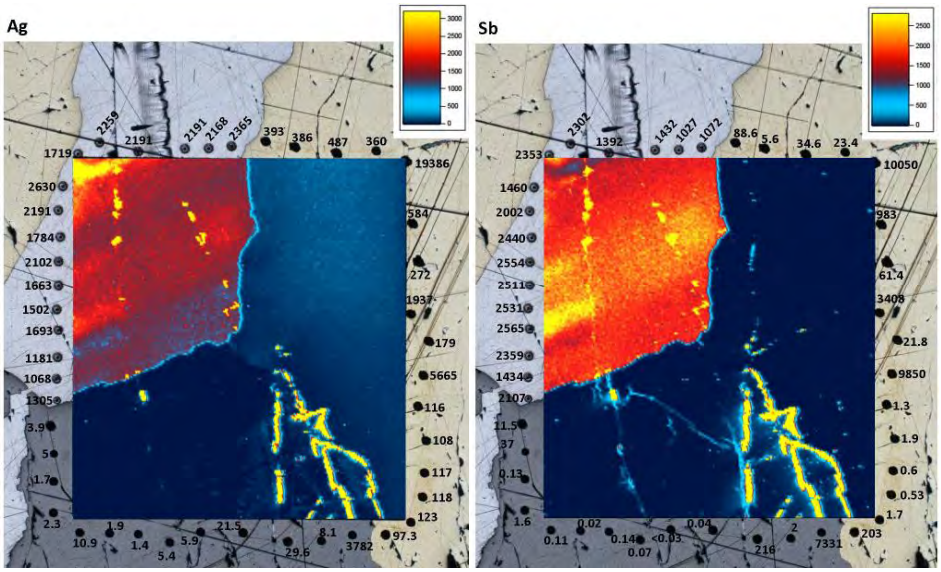

Figure 4. *Cont.*

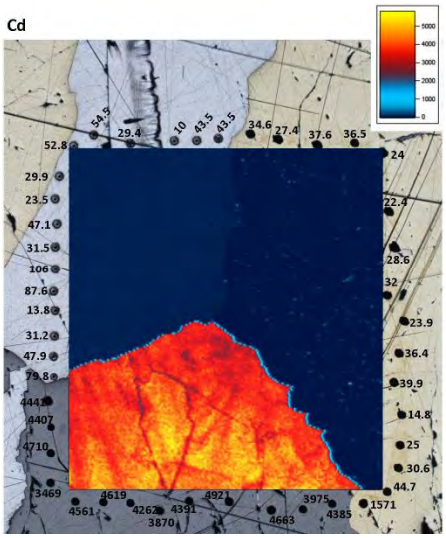

Figure 4. Comparison between quantitative LA-ICP-MS trace element maps (Ag, Sb and Cd, ppm scales) of a galena (light grey)–sphalerite (dark grey)–chalcopyrite (yellow) assemblage with spot analyses (in ppm) immediately adjacent to the mapped area. An average value for sulfur was used as the internal standard to accommodate the three distinct minerals.

LA-ICP-MS maps generated via an average internal standard value are powerful in that they display approximately real concentration values that are comparable across different minerals in an assemblage. This is ideal for determining and comparing the distribution of trace elements in a multi-mineral assemblage. Care should, however, be taken in interpreting concentrations too rigidly. If trace element concentrations look similar in different phases, other methods should be employed to determine the preferred primary host of a particular trace element with confidence. If precise concentration values are required, LA-ICP-MS spot analysis should always accompany quantitative LA-ICP-MS mapping.

Two additional points are worth making. Firstly, if the scale of zonation within a given mineral is sufficiently fine (i.e., below the resolution of the element map), electron microprobe or SEM-EDS mapping might be a more suitable option. If the zoning is on a subscale below that of the microprobe beam, synchrotron-based methods (such as μ-X-ray fluorescence spectrometry [60]) may be more appropriate. Secondly, map quality may be influenced by the orientation of the sample surface relative to zoning. Depth penetration during rastering will cause a blurring of the zoning pattern if that zoning is sharply inclined relative to the sample surface, with best results obtained if the zoning is perpendicular to the map.

3. Trace Element Distributions in Common Minerals

The range of mineral matrices in which trace element concentrations have been successfully measured by LA-ICP-MS has widened considerably in the past decade. These data, complemented by studies that have compared the trace element signatures of a particular mineral from different geological settings, provide a reasonably good understanding of which trace elements can enter specific mineral structures, and at approximately what range of concentrations. Currently available data is highly heterogeneous, keeping in mind that some minerals or mineral groups are far more thoroughly studied than others.

Table 2 provides an overview of selected studies that have contributed, through LA-ICP-MS analysis, to current understanding of the trace element geochemistry of the common sulphides, iron-oxides, rock-forming silicates and a number of accessory minerals. As more data become available, a predictive understanding of the fundamental crystal-structural controls on element partitioning into specific minerals (e.g., critical metals in sphalerite [61], controls on trace element substitution in magnetite [62]), or among co-existing minerals formed at equilibrium (e.g., coexisting sphalerite-galena-chalcopyrite assemblages [59]) can be developed. Such constraints have been complemented by empirical studies showing how lattice-scale controls aid incorporation of a broader range of trace elements, including those overlooked in broader approaches. Examples include the observation of superstructuring in hematite allowing incorporation of (U + Pb + W + Mo) [7], the incorporation of Au into bismuth chalcogenides [63], and inter-lamellar enrichment of chalcophile elements in molybdenite [64].

Table 2. Selected studies that have used LA-ICP-MS to address the trace element geochemistry of common sulphides, iron-oxides, rock-forming silicates and accessory minerals.

Minerals	Reference(s)
Sphalerite	Cook et al. (2009) [61], Ye et al. (2011) [65], Cook et al. (2012) [66], Murakami and Ishihara (2013) [67], Lockington et al. (2014) [68], Belissont et al. (2014) [69], Cook et al. (2015) [70]
Chalcopyrite	Butler and Nesbitt (1999) [71], Wohlgemuth-Ueberwasser et al. (2015) [72], George et al. (in review) [73]
Bornite, chalcocite-group	Cook et al. (2011) [74]
Galena	George et al. (2015) [75]
Pyrite	Large et al. (2007) [76], Cook et al. (2009) [47], Large et al. (2009) [77], Winderbaum et al. (2012) [78], Ingham et al. (2014) [79], Large et al. (2014) [80]
Arsenopyrite	Morey et al. (2008) [81], Sung et al. (2008) [46], Cook et al. (2013) [48], Lawley et al. (2015) [82]
Enargite	Deyell and Hedenquist (2011) [83]
Molybdenite	Ciobanu et al. (2013) [64]
Pyrrhotite–pentlandite– (pyrite, Ni-arsenides) in magmatic ores, including PGE deposits	Barnes et al. (2008) [84]; see also Table 3
Bismuth chalcogenides and sulphosalts	Ciobanu et al. (2009) [63]
Hematite	Ciobanu et al. (2013) [7]
Magnetite	Nadoll et al. (2014) [62], Dare et al. (2014) [85]
Chromite	Pagé and Barnes (2009) [86]
Gahnite	O'Brien et al. (2015) [87]
Scheelite, wolframite, ferberite	Goldmann et al. (2013) [88], Song et al. (2014) [89], Hazarika et al. (2016) [90], Raju et al. (2016) [91]
Xenotime, florencite	Cook et al. (2013) [92]
(Calcic, skarn) garnet and other skarn calc-silicates (pyroxenes, clinozoisite, etc.)	Smith et al. (2004) [93], Gaspar et al. (2008) [94], Ismail et al. (2014) [53], Xu et al. (2016) [95]
Feldspars	Kontonikas-Charos et al. (2014) [96]
Rutile and titanite	Smith et al. (2009) [97], Ismail et al. (2014) [53], Fu et al. (2016) [98]
Apatite	Ismail et al. (2014) [53], He et al. (2016) [99], She et al. (2016) [100]
Fluorite	Gagnon et al. (2003) [101]

Empirical studies aimed at understanding the fundamental ability of minerals to incorporate measurable concentrations of trace elements, the controls on trace element distributions, and partitioning behavior in multi-mineral assemblages underpin the three main applications of LA-ICP-MS trace element analysis. These are: (1) Trace element distributions in common, widely distributed phases such as pyrite, or extended mineral families, such as spinels or garnets, where variation in absolute trace

element concentrations, or their relative distributions can be valuable for understanding the nature and sequence of ore-forming processes; (2) trace element distributions in minerals that display spatial relationships at the regional or deposit scales and which can be used in a vector approach in mineral exploration; and (3) microanalysis of minerals that can potentially host elements of economic interest, or elements which are deleterious to various metallurgical processes, and where an understanding of the distribution of a particular element or group of elements is of interest in element deportment and geometallurgical studies. Each of these will be highlighted in the following sections.

4. LA-ICP-MS Analysis in Ore Petrogenesis

Trace element data for minerals is increasingly used to support models for ore genesis. Recognition of distinct trace element signatures can assist with tracking sequences of crystallization and stages of mineralization, sources of metals, evolution of ore-forming fluids over time, and overprinting during superimposed geological events. Using examples from the recent literature, we focus here on four groups of deposits for which trace element studies are advancing the understanding of ore-forming processes.

4.1. Orthomagmatic Ore Deposits

A substantial volume of literature exists on the distribution and partitioning behaviors of trace elements among sulphides and co-existing oxides and silicates in orthomagmatic ore systems. In many ways, such systems are far better understood than their hydrothermal counterparts, assisted to some degree by temperature constraints from melt compositions and predictable, relatively closed-system behavior of mineral assemblages in magmatic environments. This work has been driven by the desire to understand controls on the partitioning behavior of the platinum-group elements (PGE) and shows a surprising range of behaviors from system to system. Trace element distribution patterns have, in turn, delivered valuable evidence in support of genetic models, and the sequence of crystallization. Representative advances in the field are summarized in Table 3.

Table 3. Selected examples of LA-ICP-MS studies of trace element distribution in minerals from orthomagmatic ore systems.

Reference	Mineral(s) Analyzed	Deposit(s) Studied	Significant Findings
Barnes et al. (2008) [84]	Pentlandite, chalcopyrite, cubanite, pyrrhotite	Compilation of data from various Pt-rich ore deposits (Noril'sk, Great Dyke, Bushveld and others	Siderophile and chalcophile element distributions in pentlandite, chalcopyrite and pyrrhotite from platinum-rich ore deposits are compared. Re, Os, Ir, Ru and Rh are concentrated in both pentlandite and pyrrhotite. Pentlandite also concentrates Ni, Co and Pd. Cu, Zn, Cd and Ag are concentrated in chalcopyrite or cubanite. Au and Pt do not preferentially concentrate in any particular BMS, with very little of these elements located in BMS. Significant differences in trace element distribution between ore systems can be related to temperature evolution, abundance of sulphides and availability of other minor elements (As, Te, Bi, etc.).
Dare et al. (2010) [102]	BMS (pyrrhotite, pentlandite, chalcopyrite, pyrite)	Creighton Ni–Cu–PGE sulphide deposit, Sudbury, Canada	BMS host all Co and Se, a significant proportion (40%–90%) of Os, Pd, Ru, Cd, Sn, and Zn, but very little (<35%) of the Ag, Au, Bi, Ir, Mo, Pb, Pt, Rh, Re, Sb and Te. Os and Ru are concentrated in equal proportions in pyrrhotite, pentlandite, and pyrite. Cobalt and Pd (~1 ppm) are concentrated in pentlandite. Ag, Cd, Sn, Zn, and in rare cases Au and Te, are concentrated in chalcopyrite. Se is present in equal proportions in all three BMS. Ir Rh, and Pt are present in euhedrally zoned PGE sulph-arsenides. Enrichment of Os, Ru, Ni, and Co in pyrrhotite, pentlandite, and pyrite and Ag, Au, Cd, Sn, Te and Zn in chalcopyrite explained by fractional crystallization of MSS from sulphide liquid followed by sulphide exsolution. The bulk of Pd in pentlandite cannot be explained by sulphide fractionation alone because Pd should have partitioned into residual Cu-rich liquid and be in chalcopyrite or in PGM around chalco-pyrite. The variation of Pd among different pentlandite textures provides evidence that Pd diffuses into pentlandite during exsolution from MSS.

Table 3. *Cont.*

Reference	Mineral(s) Analyzed	Deposit(s) Studied	Significant Findings
Dare et al. (2011) [103]	Pyrrhotite, pentlandite, chalcopyrite, pyrite	McCreedy East, Sudbury, Canada	Os, Ir, Ru, Rh (IPGE), and Re concentrated in pyrrhotite, pentlandite, and pyrite. Pd present in pentlandite. Some Pt noted in oscillatory-zoned pyrite.
Dare et al. (2012) [104]	Magnetite	Sudbury, Canada	Fe-oxide geochemistry a sensitive petrogenetic indicator for the degree of fractionation of the sulphide liquid. In sulphide-bearing liquids, lithophile elements are compatible into Fe-oxide. The concentrations of these elements are highest in the early-forming titanomagnetite, which crystallized with Fe-rich MSS. Late-forming magnetite, which crystallized from residual Cu-rich liquid, is depleted in these elements. Behavior of chalcophile elements in magnetite largely controlled by the crystallization of sulphides. Local trace element redistribution occurs at subsolidus temperatures (ilmenite ex-solution from titanomagnetite, Al-spinel exsolution from magnetite).
Dare et al. (2014a) [85]	Magnetite	Compilation of data from magmatic and hydrothermal environments	Discussion of trace element partitioning behaviour between magnetite, melt/fluid, and co-crystallizing phases. Trace elements aid discrimination of magnetite formed in different environments, with applications in petrogenetic and provenance studies.
Dare et al. (2014b) [105]	BMS, also sphalerite and galena	McCreedy East, Sudbury, ON, Canada	Distribution of PGE and trace elements in different sulphides reported and comprehensive genetic model presented.
Duran et al. (2015) [106]	Pyrite	Lac des Iles Pd deposits, ON, Canada	Atypical deposits in which pyrite contains Os, Ir, Ru and Rh (also present in pyrrhotite and pentlandite), possibly redistributed during cooling. Pyrite is zoned: IPGE–Rh and As towards pyrite cores, Co and Se towards the rims. Pb, Bi and Ag present in thin overgrowths on pyrite margins (also some Pt, Te and Sn).
Godel et al. (2007) [107]	BMS (pyrrhotite, pentlandite, chalcopyrite)	Merensky Reef, Bushveld Complex	~65% up to ~85% of PGE hosted by PGM. Lesser amounts of PGE in solid solution within BMS. Pentlandite is the principal BMS host of all PGE, except Pt (preferentially enriched in Pd, Rh and Co). Pyrrhotite contains, Rh, Os, Ir and Ru, but excludes both Pt and Pd. Chalcopyrite contains very little PGE. The PGE content in the BMS varies only slightly as a function of the stratigraphy (twice as much PGE in BMS from chromitites compared to silicate rocks).
Godel and Barnes (2008) [108]	BMS (pyrrhotite, pentlandite, chalcopyrite)	J-M Reef, Stillwater Complex	Pentlandite main host for Pd. Pt occurs almost exclusively found as PGM and do not partition into BMS. Other PGE present in BMS. Highest PGE noted in samples containing secondary magnetite. Pd precipitated as an alloy, later diffusing into pentlandite.
Holwell et al. (2015) [109]	sulphide microdroplets	Platinova Reef, Skaergaard E Greenland	Extreme trace element enrichment in sulphide droplets in closed-system layered intrusions, forming unusual low-sulphide deposits.
Piña et al. (2013) [110]	Maucherite, pyrrhotite, pentlandite, chalcopyrite	Beni Bousera, Morocco	Partition coefficients for PGE, Au, Re, Ag, Se, Bi, Te, and Sb, between arsenide and sulphide phases estimated. Maucherite strongly enriched in all chalcophile elements, except Se, relative to sulphide minerals. Results highlight the strong affinity of PGE for arsenide phases and the importance of these phases as potential carriers of PGE.
Piña et al. (2015) [111]	Ni-arsenides (nickeline, maucherite, löllingite)	Serranía de Ronda, Málaga, Spain	PGE, Au, Ag, Se, Sb, Bi and Te contents of arsenide and sulphide assemblages determined. Arsenides enriched in all PGE, but especially in Ir, Rh and Pt. Se and Ag partition preferentially into the sulphide assemblage.
Piña et al. (2016) [112]	Pyrite	Main Sulphide Zone, Great Dyke, Zimbabwe	PGE and other trace element contents in pyrite reported from several mines. Two types of pyrite differentiated. Py1 is PGE rich (higher Os, Ir, Ru, Rh, and Pt contents than the associated pyrrhotite, pentlandite, and chalcopyrite); Py2 has low PGE contents. Py1 inferred to have formed by late, low temperature (<300 °C) decomposition of residual Ni-rich mss; Py2 suggested to have formed by replacement of pyrrhotite and pentlandite caused by late magmatic/hydrothermal fluids.

Table 3. *Cont.*

Reference	Mineral(s) Analyzed	Deposit(s) Studied	Significant Findings
Duran et al. (2016) [113]	Sulphides, Fe-Ti-oxides	Lac des Iles Pd deposits, ON, Canada	Trace element concentration data for pyrrhotite, pentlandite and chalcopyrite and co-existing Fe-Ti oxides (magnetite and ilmenite). The study shows how the trace element composition of sulphides can vary as a function of the degree of fractionation of the parental silicate magma. Findings carry strong implications for the petrogenesis of orthomagmatic deposits.

Abbreviations: BMS—base metal sulphides; PGE—platinum group elements; IPGE—intermediate platinum group elements (Os + Ir + Ru); PGM—platinum group minerals; MSS—monosulphide solid solution.

4.2. Skarn Formation

Calcic skarns comprise a number of gangue minerals (garnet from andradite-grossular series, pyroxene from the diopside-hedenbergite-johanssonite series, clinozoizite from the epidote supergroup and abundant accessories), which are widely distributed across skarn deposits. These minerals are known to feature significant concentrations of substituting trace elements, notably REY, opening new avenues to explore skarn evolution in space and time. Despite this, there have been relatively few published studies that specifically target trace element incorporation and partitioning in skarn minerals by LA-ICP-MS. Smith et al. (2004) [93] described garnets from the Beinn and Dubhaich contact aureoles, Scotland, which were enriched in HREE or LREE depending upon their grossular- or andradite-rich composition. High U contents (up to several hundred ppm) were also measured in such garnets. The measured REY-fractionated trends across crystal zoning in garnet were numerically modeled with respect to changes in salinity [93]. Evolving REE fractionation trends could be used as a tool to understand the evolution of metasomatic fluids. Gaspar et al. (2008) [94] studied factors that control REE incorporation into garnets and showed that evolving REE fractionation trends could be used as a tool to understand the temporal evolution of metasomatic fluids during skarn formation.

A holistic approach was taken to address the genesis of the Hillside Cu skarn-IOCG prospect, South Australia [53]. Trace element datasets covered calcic garnet, diopside, clinozoisite and accessory minerals as well as magmatic and early-hydrothermal feldspars. It was shown that prograde and retrograde assemblages can be differentiated by distinct chondrite-normalised REY fractionation trends, paralleled by changes from proximal to distal position within the deposit. Moreover, application of Zr-in-titanite geothermometry revealed the thermal evolution of the skarn from the magmatic-hydrothermal transition (~700 °C) through the main (prograde) stage of skarn formation associated with mineralization down to late, retrograde fluids (~300 °C).

In a second prospect from the same terrane (the Groundhog copper prospect, Punt Hill district), Nikolakopoulos (2013) [114] documented garnet compositional data in strongly retrogressive calcic skarn assemblages, demonstrating that a number of mineralogical and geochemical features are common to IOCG systems within the Olympic Cu-Au Province. As at Hillside, distinct textural categories of garnet, each reflecting stages in the evolution of the skarn system, are recognized. Fe-rich prograde andradite is oscillatory-zoned, with high W and As, relatively low ΣREY, and low HREE/LREE. Later, retrograde garnets, assigned to the waning stages of the hydrothermal system, are Al-rich, have ΣREY concentrations an order of magnitude higher, high HREE/LREE, and high concentrations of incompatible and high field strength elements. Marked enrichment in Cr defines the garnet rim.

In a study on the Zhibula Cu skarn deposit, Tibet, Xu et al. (in press) [95] have shown that garnet colors are largely defined by trace element concentrations. Chondrite-normalized REY fractionation trends in garnet can be correlated with the evolving salinity of ore-forming fluids. Garnets from this deposit are enriched in an extraordinary range of trace elements less commonly reported for garnet, including W, Sn, and As, but also Mo (as high as 730 ppm). Garnet compositions support a genetic connection between the Zhibula skarn and the Qulong porphyry deposit located 2 km to the

north. Trace element signatures in Zhibula garnets demonstrate the usefulness of this type of approach (see also [108]) to establish genetic links between skarn and porphyry systems.

An important point here is that although garnet, pyroxene and other minerals in calcic skarns, are characterized by trace element signatures that can be used to constrain skarn zonation and evolution in space and time, neither patterns nor trace element substitution mechanisms in garnet are necessarily identical from case to case. This has precluded development of generalized trace element models for skarn systems. These studies have also highlighted that the skarn minerals, rather than sulphides, can be significant sinks for minor metals of potential economic interest. Examples include the extraordinary enrichment of Ga in clinozosite [53], and of Mo, W and Sn is some skarn garnets [95,115], or magnetite [116].

4.3. Iron-Oxide-Apatite (IOA) and Iron-Oxide Copper Gold (IOCG) Deposits

IOA and IOCG deposit types belong to a broad spectrum of hydrothermal ore deposits with distinct characteristics underpinned by a range of common features [117]. Among these are the presence of abundant Fe-oxides (hematite and magnetite), the common phosphate, apatite, other accessory minerals such as rutile and titanite, and not least feldspar of either magmatic or hydrothermal origin. Such minerals are distributed, in varying proportions, within IOA and IOCG systems, and in each, these trace minerals have great potential for fingerprinting the magmatic to hydrothermal transition and the different origins of the protoliths to the host rocks. In IOCG systems, trace element analysis of Fe-oxides, apatite and other accessories allows recognition of distinct mineral generations formed throughout the hydrothermal lifespan of the system. Here we present existing data related to IOCG systems, including some enigmatic deposits whose affiliation to this clan is debated (e.g., Bayan Obo, El Laco, see below). What follows is a selection of examples from the recent literature intended to highlight various perspectives and the interpretation of LA-ICP-MS datasets obtained on different minerals, and in different deposits or provinces.

In a pioneering study, Smith et al. (2009) [97] used the REE trends in apatite and rutile/titanite from the Kiruna Fe-deposit, Sweden, to model deposit evolution. A number of recent publications have addressed the genesis of iron-oxide-apatite (IOA) deposits based on the trace element geochemistry of Fe-oxides and/or apatite.

Huang et al. (2015) [118] investigated magnetite and hematite compositions from banded, disseminated and massive Fe ores in the Bayan Obo Fe-REE-Nb deposit, Northern China, in an effort to understand the genesis of this world-class REE deposit. Magnetite and hematite show similar REE patterns and trace element signatures, indicating a common origin. Two stages of REE mineralization and multiple sources of Fe and REE are indicated. The authors propose a model involving sedimentary carbonates and subsequent metasomatism by REE-rich hydrothermal fluids. Magnetite chemistry has proven critical for understanding the transition from magmatic to hydrothermal conditions in Kiruna-type iron oxide-apatite (IOA) deposits [119].

LA-ICP-MS analysis of trace elements in apatite have also been used to understand the genesis of nelsonites and other apatite-oxide-rich rocks in magmatic environments [99,100]. Based on a study of rocks from the Sept-Îles Intrusive Suite, Canada, Tollari et al. (2008) [120] were able to substantiate a crystal accumulation model in which the nelsonites could have formed as dyke-like bodies.

Chen et al. (2015) [121] investigated magnetite in the Khetri copper belt in Rajasthan Province, NW India, revealing that ore-forming conditions were controlled mainly by fluid compositions and/or fO_2. Factors such as temperature, fluid–rock interaction and co-precipitating minerals were found to play negligible roles in controlling composition.

Oscillatory and sectorial zoning patterns were mapped in both hematite and magnetite from the Olympic Dam IOCG deposit, South Australia [7,122]. Such patterns involve variation in U, Pb, W, Sn, Mo and REY, elements that we group broadly as 'granitophile'. Moreover, grain-scale variation in As and Sb concentrations within hematite have also been shown [122]. The same study showed significant differences in hematite composition between the deepest and shallower parts of the Olympic Dam

deposit in terms of trace element signatures and REY content. Such trends have the potential to underpin space-time evolution models, if understood in the context of the host rocks and regional- and mine-scale alteration patterns at Olympic Dam, a deposit well-known for mineralogically- and geochemically-defined zonation patterns [123].

There is, however, one important problem when making easy generalization of LA-ICP-MS datasets for Fe-oxides in IOCG deposits—the fact that they are probably the only minerals that are continuously generated and reworked through cycles of brecciation. Such cycles will induce trace element heterogeneity associated with dissolution, recrystallization, pseudomorphic replacement and release of trace elements that will overprint pre-existing grains at the scale of the polished block. We demonstrate this variation by two contrasting examples of hematite from high-grade bornite ore at Olympic Dam, which have been dated by hematite Pb–Pb geochronology [7]. The examples differ from one another in terms of morphology, internal textures and trace element distributions (Figures 5 and 6). They do, however, represent the main categories of hematite within such ores.

The type of hematite containing high concentrations of granitophile elements occurs as acicular grains and radial aggregates that display zoning of individual lamella on the BSE images (Figure 5a,b). The same lamellae also show areas of abundant porosity and mineral inclusions (Figure 5c). The LA-ICP-MS map (Figure 5d) shows that the bright areas on BSE images correlates with high-U, Pb, Mo and W, whereas the same areas show depletion in HFSE (Nb, V, Ti), and mild increase of these elements in the porous domains. The core of the aggregates shows also an increase in LREE (Ce as a proxy).

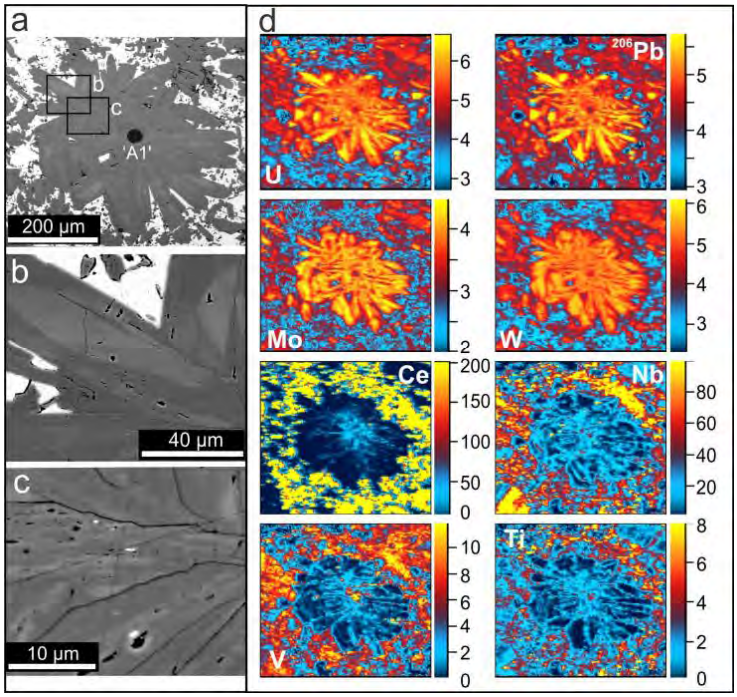

Figure 5. BSE images (**a**)–(**c**) showing textural details of a radial aggregate of hematite hosted in bornite (white in (a,b)) from Olympic Dam. Note the zoning and porosity within individual lamellae depicted on the BSE images in (b) and (c), respectively. (**d**) LA-ICP-MS element maps of the hematite aggregate shown in (a); note good correspondence between textures on BSE images and specific groups of elements, i.e., zoning with respect of U, Pb, Mo and W (middle parts of lamellae), and enrichment in HFSE in the porous, marginal parts of the same lamellae. Scales in counts-per-second ($\times 10^3$ except for Ce and Nb). Measured isotopes: ^{238}U, ^{206}Pb, ^{95}Mo, ^{182}W, ^{140}Ce, ^{93}Nb, ^{51}V, ^{47}Ti.

The second type (Figure 6) is illustrative of the abundant, coarser hematite grains that have been pseudomorphosed by fine-aggregates of hematite preserving the crystal shape, albeit with some grain rounding (Figure 6a). In detail, such hematite shows coarser, sub-micron inclusions of REE-minerals within areas of high porosity (Figure 6b,c). At the micron-scale, such porous areas show a 'channel'-like texture, which can be correlated with the element maps (Figure 6e). The maps show a correlation between the inclusions and the elements U, Y and Er (typical of coffinite-xenotime minerals), as well as an enrichment in Al, and depletion in W and V within the channel areas shown in Figure 6d.

Although Fe-oxides in certain deposit types display characteristic geochemical signatures that underpin effective discrimination schemes and can be correlated with ore-forming processes [124], there is likely to be wide variability in any particular hydrothermal deposit, or among deposits of a specific type. This is particularly true for IOCG systems where there remains an inadequate understanding of how fluid/water chemistry and specific formation conditions impact on Fe-oxide compositions.

Controls on the diversity of trace element signatures derive from different fluid sources, participation of multiple host lithologies (granites, BIF, mafic rocks), and competition for trace elements with other minerals, including accessories and REE-minerals (and also skarn minerals if the protoliths are limestone).

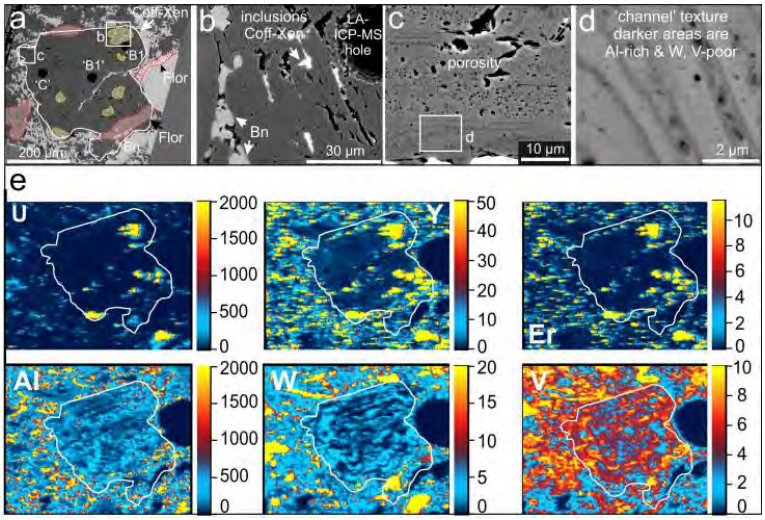

Figure 6. BSE images (**a–d**) showing the textures of coarser, sub-rounded grain of hematite from the same sample as in Figure 5 (aggregate of acicular lamellae). Note the presence of µm to sub-µm size REE-mineral inclusions (**a**,**b**), as well as the abundance of pores throughout most of the grain (**c**); (**d**) channel-like sub-texture shows a correlation between high concentrations of Al with low concentrations of W and V; (**e**) LA-ICP-MS element maps of reworked, hematite resulting in a depletion of granitophile and HFSE trace elements. Note the correlation between the maps for U, Y and Er, showing the presence of REE inclusions in (**a**,**b**), as well as the channel-like patterns on the Al, W, V maps correlating with the texture in (**d**) containing micron-scale inclusions of U- and REE-minerals, extensive porosity and chemically-defined channel textures. Concentration scales in counts-per-second ($\times 10^3$). Measured isotopes: ^{238}U, ^{89}Y, ^{166}Er, ^{27}Al, ^{182}W, ^{51}V.

Although excellent hosts for Ba, Sr, Rb, Cs, and others, plagioclase and potassium feldspars are not traditionally considered good sinks for transition metals and lanthanides. Despite relatively low absolute concentrations, the abundance of feldspars can, however, mean that they are the dominant carriers of petrogenetically valuable trace elements. Kontonikas-Charos et al. (2014) [96] have documented concentrations of as much as 200 ppm ∑(REE + Y) in feldspars from an albite-biotite schist from the Moonta-Wallaroo region, Yorke Peninsula, South Australia, associated with IOCG mineralization. Such concentrations can account for nearly all (REE + Y) in whole-rock. Chondrite-normalized REY

fractionation patterns for feldspars support the applicability of REE-fractionation trends in feldspars as geochemical tracers of regional-scale hydrothermal alteration haloes.

Apatite is a common magmatic accessory in the same intrusive rocks hosting the world-class Olympic Dam deposit and hydrothermal apatite is a locally abundant mineral throughout the altered and mineralized rocks. Krneta et al. (2016) [125] have evaluated whether changes in the morphology and chemistry (particularly REE and Y content) of apatite can be used to constrain the evolution of giant IOCG systems. At Olympic Dam, magmatic apatite commonly contains inclusion-rich cores and REY-enriched rims. The cores show a LREE-enriched chondrite-normalized fractionation trend with a strong negative Eu-anomaly. Apatite intimately associated with advanced hematite-sericite alteration and mineralization display convex, MREE-enriched patterns with a weak negative Eu-anomaly. This change in REY-partitioning behavior could be due to changes in the physiochemical character of the mineralizing fluid, or alternatively, may indicate crystallization of MREE-enriched apatite in the presence of LREE- and HREE-consuming minerals such as monazite, florencite and xenotime. These dynamics are important evidence for a change from early primitive low-grade pyrite-chalcopyrite mineralization to high-grade bornite mineralization reflected in apatite chemistry by a switch from LREE- to MREE-enriched REY-trends.

Trace element concentrations in magnetite have also been used to decipher the genesis of the enigmatic El Laco deposit, Chile [126]. El Laco magnetite was shown to have a trace element signature comparable with high-temperature hydrothermal magnetites like those in IOCG or porphyry-Cu systems, supporting a model of metasomatic replacement of andesitic lava flows, and not a magmatic origin from an effusive Fe oxide liquid.

4.4. Trace Elements in Pyrite in Hydrothermal Ore Deposits

Pyrite is the most common sulphide in a wide variety of hydrothermal ore deposits. As a refractory mineral that is stable up to relatively high temperatures, and which readily preserves trace element signatures, pyrite trace element geochemistry has proven useful for understanding the genesis of volcanogenic massive sulphides, black shale hosted deposits and others [76,77,80,127,128].

Applying LA-ICP-MS trace element mapping of pyrite within the Carbon Leader Reef, Witwatersrand Basin, South Africa, Large et al. (2013) [129] showed that "a significant proportion" of pyrite and gold in the reef was derived, via large-scale flow of basinal fluids, from sedimentary rocks stratigraphically below the reef. This is valuable evidence in support of a hybrid hydrothermal-palaeoplacer genetic model for the world's largest gold resource.

Gregory et al. (2015) [130] conducted LA-ICP-MS trace element analysis of >1400 diagenetic and syngenetic pyrites from 45 carbonaceous shale and unconsolidated sulfidic sediment samples. Despite extensive and often inconsistent variation in trace element signatures, three main groups of trace elements identified from factor analysis revealed element groupings that carry genetic implications, including recognisable signatures indicative of input from fluids associated with mafic rocks.

Steadman et al. (2015) [131] examined pyrites from black shale units in the Kalgoorlie goldfield, Western Australia, and observed complex, though generally systematic patterns of compositional zonation. These data support a genetic model for this world-class metallogenic terrane involving inter-volcanic (syn)diagenetic pre-concentration of Au-Ag-Te-Hg-As in fine-grained, sulphidic, moderate- to deep-water sediments before formation of gold-(telluride) lodes.

Trace element characterization of pyrite has been used to reconstruct the hydrothermal evolution of Archean VMS in the Abitibi Belt, Canada [132]. Five pyrite types were identified, each of which could be correlated with a distinct stage in the evolution of the mineralizing system. Recrystallization causes some early signatures to be partially obliterated, with migration of some minor elements out of pyrite. A near-mine vectoring approach to exploration is proposed based on discriminant diagrams. In a further application of pyrite trace element geochemistry, Mills et al. (2016) [133] compared compositions of pyrite from three belts within the Jiaodong gold district, Eastern China. Significant differences in pyrite geochemistry were related to style of gold mineralization, allowing a model for the timing of gold introduction, geodynamic setting, and for remobilization of gold.

5. Trace Element Vector Approaches in Mineral Exploration

Interest in using the trace element concentration in a specific mineral in a vectoring approach to mineral exploration stems from the fact that mineral compositions are more sensitive to changes associated with ore-forming processes than whole rock is. This is because the geochemical signatures of each mineral are governed by crystal structures and often-constrainable physical-chemical parameters. They are thus much less prone to averaging-out effects than is the case for whole-rock data. Successful application does depend, however, on the mineral concerned being abundant in a range of lithologies across a deposit and within the alteration envelope enclosing the deposit. A second consideration is that the variance (or 'noise') in the geochemical signal within a specific sample needs to be sufficiently low to be able to recognize trends which correlate with distance from mineralization. Several dozen recent studies have used LA-ICP-MS analysis of minerals (sulphides, oxides and in some cases, also silicates) to support a vectoring or indicator mineral approach. A selection of these is given in Table 4. Testing will be required to determine whether each can be duplicated in analogous terranes elsewhere.

In the Punt Hill district of South Australia, it was suggested [114] that trace element distributions in texturally-distinct categories of garnet can be used as vectors to mineralization within defined structural corridors. Vectors are defined by ΣREY- and W-concentrations in prograde and retrograde garnets. Understanding structures that define the direction of fluid flow is critical for application of such vectors, as is an adequate interpretation of trace element data in the contexts of textural and prograde-to-retrograde evolution of the system.

An important potential application of the approaches listed in Table 4 is that if these minerals are recovered from glacial deposits of unknown or uncertain setting, mineral compositions may indicate the presence of potential mineralization upstream, directly impacting on exploration strategies depending on the mineralization type identified.

Table 4. Selected examples of LA-ICP-MS studies of minerals as indicators of proximal and distal position, or supporting a vector approach in mineral exploration.

Vector Mineral	Reference	Geochemical Signature and Comment(s)
Magnetite	Boutroy et al. (2014) [134]	Compilation of trace element compositions in magnetite from 13 major Ni–Cu–PGE deposits. Controls on magnetite composition discussed. Discrimination diagrams introduced to distinguish primary from secondary magnetite. Magnetite considered a useful indicator mineral in exploration, particularly if used to detect eroded Ni–Cu–PGE deposits in surficial sediments.
Ni-arsenides (gersdorffite, nickeline)	Le Vaillant et al. (2015) [135]	Case study: Miitel komatiite-hosted nickel sulphide deposit, Western Australia Elevated Pd and Pt associated with Ni and As enrichment. Pd- and Pt-enriched trace arsenides in country rocks considered a proximity indicator for Ni-sulphides in hydrothermally altered terranes.
Magnetite	Acosta-Góngora et al. (2015) [136]	Major differences in the V, Ni, Cr, and Co concentrations within magnetite are reported from the Paleoproterozoic Great Bear magmatic zone. Cr/Co and V/Ni ratios are useful to distinguish barren alteration from mineralization. The results highlight potential use of magnetite as an indicator mineral in exploration for IOCG deposits.
Pyrite	Belousov et al. (2016) [137]	Pyrite compositions from VHMS and orogenic Au deposits in the Yilgarn Craton, Australia are distinct. The data are useful for distinguishing signatures at the exploration stage and have valuable implications for the deportment of precious metals in these ores.
Magnetite	Canil et al. (2016) [138]	Trace element compositions are reported from hydrothermal magnetite in 5 porphyry Cu–Mo–Au deposits and two skarns from B.C., Canada. Compositions are found to vary with temperature, redox potential, and the acidity of the ore-forming fluids. Concentrations of Mn, Sn and Mo in hydrothermal magnetite are shown to vary with fluid acidity. Variations in Ti, Al and V are inferred to depend on temperature and fO_2.

Table 4. *Cont.*

Vector Mineral	Reference	Geochemical Signature and Comment(s)
Gahnite	O'Brien et al. (2015) [87]	Major and trace element data for gahnite in the Broken Hill domain, N.S.W., Australia is reported. Gahnite chemistry may be used to distinguish prospective exploration targets from non-prospective occurrences. Principal component analysis and variation of Zn/Fe vs. Ni + Cr + V distinguishes gahnite in the Broken Hill deposit from that associated with sulphide-poor mineralization and barren rocks. Gahnite is proposed as an exploration guide to high-grade ore in analogous metamorphosed terranes.
Magnetite	Nadoll et al. (2012) [139]	Magnetite compositions from different geological settings in western Montana and northern Idaho are compared. Subtle differences are correlated with formation temperatures. Factor analysis is used to discriminate genetic types of magnetite. Magnetite is thus proposed as a useful discriminator and pathfinder for hydrothermal deposits.
Amphibole	Hanley and Bray (2009) [140]	Elevated Ni, Cu and Sn in amphiboles are noted within 10 to 20 m from sulphide veins at Sudbury, ON, Canada. The mineral is suggested to be a valuable proximity indicator for hidden footwall-style sulphide deposits.
Biotite	Warren et al. (2015) [141]	The Ni, Cr, and Cu contents of biotite vary as a function of proximity to mineralization at Sudbury, ON, Canada.
Chlorite	Wilkinson et al. (2015) [142]	Chlorite compositions reflect proximity to ore in the propylitic environment of porphyry deposits, potentially over as much as 2.5 km. The elements K, Li, Mg, Ca, Sr, Ba, Ti, V, Mn, Co, Ni, Zn and Pb, were shown to be likely incorporated in the lattice and display spatial variation. Chlorite is proposed as a precise vectoring tool in porphyry domains where few other vector tools are available.
Apatite	Mao et al. (2016) [143]	A compilation of apatite compositions shows that trace-element compositions from various magmatic-hydrothermal deposits are distinct from those in carbonatites and un-mineralized rocks. Apatite composition shows potential for identifying specific types of buried deposits.
Magnetite	Makvandi et al. (2016a, b) [144,145]	The authors compare compositional data for magnetite from VMS-type mineralization, associated bedrocks, and surrounding till samples, showing the value of preserved magnetite for prospecting in glaciated terranes.
Pyrite	Duran et al. (2015, 2016) [106,113]	The two papers show that pyrite from magmatic Ni–Cu–PGE and hydrothermal deposits, and pentlandite from Ni–Cu sulphide and PGE-dominated deposits, have distinct compositions, and can be good indicators of mineralization type.

6. Element Deportment, Geometallurgy and Forensic Applications

Exploited mineral deposits ubiquitously contain elements other than those that are the major target of a mining operation. Some of these elements are advantageous, and if present in sufficient abundance, they can be recovered economically as by-products, either directly at the processing site, or as credits in concentrates and mattes sold on to the refiner. These include the so-called 'strategic' or 'critical' metals, such as Ga, Ge, Co, In, Sn, REE, Nb, Sc, and many others. Other elements may diminish the value of the ore and represent penalty elements. High contents of As, Sb, Bi and Hg, for example, can make a copper ore difficult to process economically, or diminish the value or saleability of the concentrate [146]. LA-ICP-MS is an effective method to constrain which mineral or minerals contain the elements of interest (whether prospective by-product or penalty elements) in a specific deposit or ore province (e.g., indium in vein mineralization in SW England [147]), and the range and variation in absolute concentrations. Similarly, careful LA-ICP-MS analysis of individual minerals within mill feed or across the deposit can provide valuable information that feeds into a quantitative deportment model for penalty elements. Such approaches may require analysis of different minerals in a large number of samples, and/or examination of materials from different stages of the processing cycle. Together with microanalytical data acquired using other techniques, notably EPMA or SIMS,

and automated QEMSCAN or MLA analysis on a large number of samples, the level of understanding of key mineralogical hosts for trace elements of interest or concern has advanced significantly in the past few years. This trend is likely to continue.

Such studies need to be designed to be as holistic as possible, and consider all minerals in a given assemblage as potential hosts to the penalty or by-product elements. The distribution of certain potentially valuable trace elements (for example, In, Ga, Ge, or Sn) may be complex with the elements of interest occurring, at various concentrations, in sulphides, oxides, rock-forming silicates, and even accessory phases (e.g., [148] in the case of indium). LA-ICP-MS data can make a significant contribution to calculation of a quantitative mineralogical balance following extensive mineralogical work to understand prevailing assemblages, and ideally the sequence of ore-forming processes. Although there currently exists a sound understanding of the preferred partitioning of key trace elements in base metal sulphide ores, allowing important hosts to be predicted (e.g., [59]), substantial knowledge gaps remain, particularly with respect to trace element partitioning in complex multi-phase assemblages [149].

LA-ICP-MS analysis can provide reliable information on mineral(s) hosting contaminant elements in mine tailings and in other solid media. This knowledge can be critical, e.g., for evaluating the behavior of those waste materials under exposure to groundwater.

A growing area of interest is to use the trace element signature specific to minerals formed in a given geological environment as a fingerprint to trace the origin of a sample. Published applications include successful attempts to fingerprint so-called 'conflict diamonds' [150,151], columbite-tantalite and other sought-after ores (e.g., [152,153]). Potential can also be recognised in areas such as uranium concentrates. Related fields of application include trace element microanalysis by LA-ICP-MS to determine the likely derivation of cultural heritage objects [154].

7. Discussion

7.1. How Many Analyses?—And Which Elements?

The authors are often asked how many data points are sufficient to characterize the trace element signature of a given mineral or phase. This will vary with the complexity of ore textures, and in particular, any intra-grain compositional zoning or the presence of multiple generations of the same mineral in a given sample or suite of samples. We cannot stress enough the importance of detailed petrological characterization, by optical and scanning electron microscopy, prior to any microanalytical work. This may entail the designation of textural sub-types and should assess any major compositional zoning in the material to be analyzed (i.e., visible optically or in back-scatter electron images). Such variation is likely to be mimicked by other elements present at lower concentrations.

Routine spot analysis by EPMA or LA-ICP-MS at the centers of 'clean-looking' grain is likely to introduce a systematic bias into the dataset, with elements that concentrate towards the rim or in specific domains within individual grains being potentially over- or under-estimated. Variation can be expected between samples from different parts of a given ore, and not uncommonly within a single polished section. Meaningful, quantitative evaluation of the distribution of, e.g., Au in pyrite, may therefore only be attained by determining abundances in a large number of representative samples. Other elements and other minerals, however, often show a more limited inter- and/or intra-sample variation and an accurate appraisal may be possible with a smaller dataset. Examples include the concentration of Cd, Mn and Hg in sphalerite from metamorphosed ores, which often appear quite uniform on the deposit scale, at least in cases when only a single textural type (or generation) of sphalerite is recognized.

A further issue is the choice of isotopes to be measured. Reasonably rapid spot analysis requires sufficient dwell times for each element analyzed. The choice will be influenced by the type of mass spectrometer the number of isotopes measured; a quadrupole, for example, allows for analysis of more isotopes than a sector field instrument that may have longer magnet settling times. The maximum number of elements that can be analyzed at acceptable levels of precision using a quadrupole mass

spectrometer is, in our experience, around 25–30, exceptionally as many as 35. This may cause the user to have to choose from a larger number of elements, which might potentially be present. For common sulphides, a predictive understanding is beginning to emerge, whereby we can say with some reasonable certainty that sphalerite, for example, can contain Mn, Cd, Hg etc., even if we are unsure at what concentration levels, and that galena is likely to contain some Ag, Bi, Sb, Tl [49]. For other minerals, the choice may be more difficult—we have encountered Fe-oxides that contain more than 45 elements at measurable concentrations (authors unpublished data).

Similarly, LA-ICP-MS element maps of skarn garnet [53,95], for example, reveal recognizable patterns and measurable concentrations of more than half the periodic table (Figure 7), including several elements that were unexpected (Sb, In, etc.). The choice of elements to be analyzed can be narrowed down somewhat by considering whether the elements are present in the standard(s) to be employed, and excluding those which are not, or by considering the likelihood that concentrations are, in any case below detection limit. Nevertheless, as pointed out by Zhu et al. [13], element maps expressed in counts-per-second values can provide valuable qualitative information on the relative distributions of elements not present in a given standard.

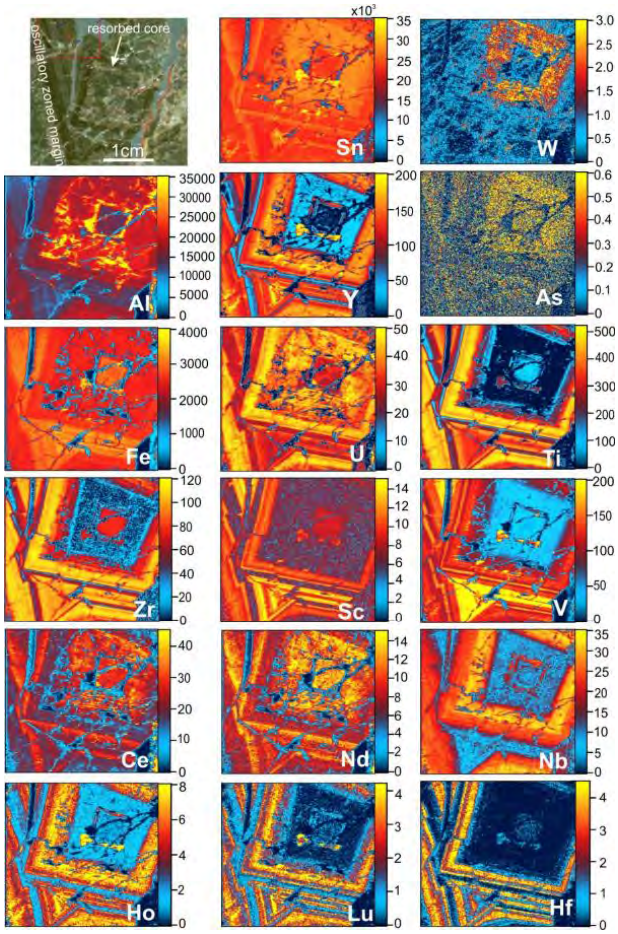

Figure 7. LA-ICP-MS element maps of zoned skarn garnet illustrating the abundance and diversity of trace elements present within the garnet structure. Scales in counts per second ($\times 10^3$). Measured isotopes: ^{118}Sn, ^{182}W, ^{27}Al, ^{89}Y, ^{75}As, ^{56}Fe, ^{238}U, ^{47}Ti, ^{90}Zr, ^{45}Sc, ^{51}V, ^{140}Ce, ^{146}Nd, ^{93}Nb, ^{165}Ho, ^{175}Lu, ^{178}Hf.

7.2. Statistical Treatment of LA-ICP-MS Data

The relative ease and speed of data collection using automated LA-ICP-MS instrumentation facilitates the generation of large data volumes. This presents its own potential pitfalls, in that innovation in data processing has not kept pace with technical development. Interpretation of multi-element datasets is reliant on the choice of statistical methods used. These have been discussed by, among others, Winderbaum et al. (2012) [78], Marques de Sá (2014) [155], Frenzel et al. (2016) [156] and Makvandi et al. (2016a, b) [144,145]. The choice of methodologies used depends on the nature of the dataset, the degree of variance at the sample or sub-population scale, and the objectives of the study. The latter may include the efficient discrimination of groupings that are rooted in temporally (genetically) distinct formation conditions, or spatial patterns that reflect systematic variation at the regional to mine scale.

For example, Winderbaum et al. (2012) [78] applied multivariate analysis to test the validity of pyrite grain classification methods based on morphological and textural factors. Parallel coordinate plots and correlation cluster analysis using Spearman's coefficients were found useful to identify unexpected elemental relationships, while principal component analysis and factor analysis demonstrate the presence of sub-classes of pyrite. Corroborated with geological data, statistical analysis provided evidence for successive generations of hydrothermal fluids, each introducing specific metals, and for partial or complete replacement of different minerals. Such weighted geochemical vectors are important for defining the evolution of geochemical signatures over time. By plotting specific components of such vectors (using, for example, Leapfrog 3D modeling software) spatial distribution can be assessed in terms of proximal to distal relative to a certain structure of interest or fluid source.

Statistical models do, however, need to account for the inherent variability and underlying relationships within such a dataset, necessitating mathematically-based, versatile, modulated approaches which could be more powerful and accurate than current approaches provided by off-the-shelf software. Such models need to acknowledge variables that do not show multivariate normal distributions and where there may be issues of scaling and tail dependency. The latter (the tendency for extreme outlying values to occur together) are crucial in the context of trace element signatures. The trace element signatures of individual minerals are governed by crystal structures and often-constrainable physical-chemical parameters making them far more sensitive to changes, and much less prone to averaging-out effects than is the case for whole-rock data. For example, if the relative concentrations and/or variation in element ratios can be correlated with the position of a mineral assemblage within a given ore system, exploration vectors can be developed for application in near-mine exploration, particularly for discrimination of proximal and distal positions relative to a hydrothermal fluid source.

7.3. Current Trends and Future Opportunities

The currently available data for many common ore and gangue minerals can assist with prediction of trace elements in the phases, and at what concentrations. As discussed above, minerals that are abundant in nature and widely distributed, and which display extensive trace element substitution, such as Fe-oxides or apatite, have particular appeal in that subtle variations in chemistry can be interpreted to reflect conditions of ore formation and represent a guide to ore in a variety of settings. Despite the considerable progress outlined above, more empirical data on a greater range of natural hydrothermal ore occurrences would be invaluable in understanding the fundamental controls on trace element distribution. This needs to be expanded to address the preferred partitioning behavior of elements valuable for petrogenetic interpretation (e.g., REE) or of potential economic value (e.g., certain 'critical' metals such as Sc, Ga or Ge).

Several recent publications have explored minerals for which little or no LA-ICP-MS trace element data have been available until now: carbonates [157,158], titanite [98,159], calcite and tourmaline [90], Ti-spinels and perovskite [160], or native gold [161]. Despite these efforts, the distribution of trace elements in certain matrices remains relatively poorly understudied. Data are particularly limited for

common gangue carbonates (e.g., calcite and siderite), sulphates (e.g., anhydrite and barite), accessory minerals (e.g., titanite) and common products of hydrothermal alteration (e.g., chlorite, epidote, sericite, amphiboles and tourmaline). Considerable opportunity therefore exists for LA-ICP-MS studies addressing the partitioning behavior of potential by-product metals, such as Ga or Sn, in multi-phase sulphide-oxide-silicate assemblages. Even for relatively well-studied minerals, more trace element data, especially for rare elements, is welcome (e.g., in sphalerite [162]). Such additional data will assist in building holistic element distribution models, and will undoubtedly highlight the importance of minor and trace minerals as hosts for specific elements. The role played by minor minerals may be disproportionately large compared to their modal abundance. Care should, however, be taken to avoid interpretation of apparent hosts for trace elements caused by isotope interference. A related future objective would be the development of trace element geothermobarometers suitable for sulphide assemblages, based on more detailed understanding of element partitioning under equilibrium conditions.

Future technical developments are likely to lead to smaller spot sizes and better spatial resolutions, in turn facilitating insights into finely-zoned or intergrown minerals that cannot, at present, be unequivocally investigated by LA-ICP-MS. It can also be reasonably expected that future work will help ease persisting uncertainties about fractionation at the site of ablation or during transport to the mass spectrometer.

Although LA-ICP-MS is a destructive technique, complementary in situ trace element microanalysis by other techniques can be used to obtain for other information. We have demonstrated how small volumes can be extracted from the surface of a sample adjacent to laser ablation craters by focused ion beam—SEM methods, thinned and investigated by TEM, resulting in the identification of nanoparticles [50]. We have also performed synchrotron-based μ-XANES investigations on sphalerite, shown by LA-ICP-MS spot analysis to contain hundreds of ppm Ge [70]. A further example is utilization of FIB-SEM-prepared foils from a sample of Bi-sulphosalts on which LA-ICP-MS spot analyses were conducted. These have been studied at the nanoscale to understand controls on trace and minor element incorporation [163].

A further topic worthy of research is the optimization of spot analysis and element mapping taking into consideration the orientation of mapped grains, given the possibility that trace elements may be preferentially incorporated along specific orientations, as has been demonstrated in fluorite [164]. This may be investigated by integrated use of LA-ICP-MS and EBSD studies. Although not using LA-ICP-MS, the multi-technique study of trace-element zoning in fluorapatite using BSE and CL imaging, and EPMA and μPIXE/μPIGE mapping [165] is exemplary of the kind of approach destined to become more common in the future.

Despite the publication of large volumes of LA-ICP-MS trace element data in recent years, and expansion of the method to new matrices and applications, there have been remarkably few studies, which have evaluated the performance of reference materials in different laboratories, or comparative studies on different mineral matrices. More standard development needs to be carried out in order to improve laboratory LA-ICP-MS practice, offer innovative strategies for preparation of reference materials [166,167], and so contribute to better LA-ICP-MS analyses. This is particularly true for standards needed to analyze the range of sulphides, oxides, phosphates and other common minerals in hydrothermal ore deposits. Ways in which this might be done include better matrix matching, homogeneity, reproducibility, and not least, accessibility to optimal reference materials. Several recent developments in standard development [168,169] show how solutions are being sought to overcome some of the limitations highlighted in this contribution.

8. Conclusions

LA-ICP-MS is a rapid, relatively inexpensive method to obtain large volumes of useful trace element data without undue time-consuming sample preparation. Comprehensive optical and SEM characterization of ore textures is, however, essential prior to analysis. Care should also be taken to

select analytical spots and to consider that if the distribution of trace elements is heterogeneous at the grain scale. Data processing and interpretation also needs to follow protocols that acknowledge the presence of outliers related to mineral inclusions. Results can underpin models of ore genesis, be applied in mineral exploration, and, indirectly, guide optimal exploitation of existing ore deposits. Rapidly expanding datasets for a variety of mineral matrices provide the foundation necessary to evaluate variations in samples from different geological settings and the issue of 'noise' within individual samples that can hamper interpretation.

Acknowledgments: We thank our colleagues and Ph.D. students for helpful discussion during preparation of this paper. Figures 1 and 7 derive from original data presented in unpublished Bachelor's and Ph.D. theses, by Matthew Fargher and Roniza Ismail, respectively. Ideas in this contribution were first raised in an invited plenary presentation at the 14th Quadrennial IAGOD meeting (Kunming, 2014). The conference organizers are thanked for their support. Nigel Cook acknowledge support from the Australian Research Council Hub for Australian Copper Uranium (project number: IH130200033), BHP Billiton Olympic Dam, OZ Minerals, and the South Australian Department of State Development (DSD). Nigel Cook acknowledges support from the 'FOX' project (Trace elements in iron oxides: deportment, distribution and application in ore genesis, geochronology, exploration and mineral processing), supported by BHP Billiton Olympic Dam and the Government of South Australia Mining and Petroleum Services Centre of Excellence. Last but not least, we gratefully acknowledge comments from three journal reviewers, which much assisted with revision of this review.

Author Contributions: Nigel Cook conceived this contribution; Cristiana L. Ciobanu contributed previously unpublished data from internal reports. Nigel Cook and Cristiana L. Ciobanu wrote the paper with contributions from Luke George, Benjamin Wade, Zhi-Yong Zhu and Kathy Ehrig.

Conflicts of Interest: The authors declare no conflict of interest.

References

1. Sylvester, P. *Laser Ablation ICP-MS in the Earth Sciences: Current Practices and Outstanding Issues*; Mineralogical Association of Canada: Québec, QC, Canada, 2008; Volume 40.
2. Paton, C.; Hellstrom, J.; Paul, B.; Woodhead, J.; Hergt, J. Iolite: Freeware for the visualisation and processing of mass spectrometric data. *J. Anal. Atom. Spectrom.* **2011**, *26*, 2508–2518. [CrossRef]
3. Gilbert, S.E.; Danyushevsky, L.V.; Rodemann, T.; Shimizu, N.; Gurenko, A.; Meffre, S.; Thomas, H.; Large, R.R.; Death, D. Optimisation of laser parameters for the analysis of sulphur isotopes in sulphide minerals by laser ablation ICP-MS. *J. Anal. Atom. Spectrom.* **2014**, *29*, 1042–1051. [CrossRef]
4. Woodhead, J.; Hergt, J.; Meffre, S.; Large, R.R.; Danyushevsky, L.; Gilbert, S. In situ Pb-isotope analysis of pyrite by laser ablation (multi-collector and quadrupole) ICPMS. *Chem. Geol.* **2009**, *262*, 344–354. [CrossRef]
5. Darling, J.R.; Storey, C.D.; Hawkesworth, C.J.; Lightfoot, P.C. In-situ Pb isotope analysis of Fe–Ni–Cu sulphides by laser ablation multi-collector ICPMS: New insights into ore formation in the Sudbury impact melt sheet. *Geochim. Cosmochim. Acta* **2012**, *99*, 1–17. [CrossRef]
6. McFarlane, C.R.M.; Luo, Y. U–Pb Geochronology using 193 nm excimer LA-ICP-MS optimized for in situ accessory mineral dating in thin sections. *Geosci. Can.* **2012**, *39*, 158–172.
7. Ciobanu, C.L.; Wade, B.; Cook, N.J.; Schmidt Mumm, A.; Giles, D. Uranium-bearing hematite from the Olympic Dam Cu–U–Au deposit, South Australia: A geochemical tracer and reconnaissance Pb–Pb geochronometer. *Precambr. Res.* **2013**, *238*, 129–147. [CrossRef]
8. Courtney-Davies, L.; Zhu, Z.Y.; Ciobanu, C.L.; Wade, B.S.; Cook, N.J.; Ehrig, K.; Cabral, A.R.; Kennedy, A. Matrix-matched iron-oxide laser ablation ICP-MS U–Pb geochronology using mixed solution standards. *Minerals* **2016**, *6*, 85. [CrossRef]
9. Thompson, J.; Meffre, S.; Maas, R.; Kamenetsky, V.; Kamenetsky, M.; Goemann, K.; Ehrig, K.; Danyushevsky, L. Matrix effects in Pb/U measurements during LA-ICP-MS analysis of the mineral apatite. *J. Anal. Atom. Spectrom.* **2016**, *31*, 1206–1215. [CrossRef]
10. Li, C.Y.; Zhang, R.Q.; Ding, X.; Ling, M.X.; Fan, W.M.; Sun, W.D. Dating cassiterite using laser ablation ICP-MS. *Ore Geol. Rev.* **2016**, *72*, 313–322. [CrossRef]
11. McFarlane, C.R.M. Allanite U–Pb geochronology by 193 nm LA ICP-MS using NIST610 glass for external calibration. *Chem. Geol.* **2016**, *438*, 91–102. [CrossRef]
12. McFarlane, C.; Lentz, D.; Dehnavi, A.S. Pb-isotopic study of galena by LA-Q-ICP-MS: Testing a new methodology with applications to base-metal sulphide deposits. *Minerals* **2016**, *6*, 96. [CrossRef]

13. Zhu, Z.Y.; Yang, T.; Ciobanu, C.L.; Cook, N.J.; Zhao, K.D.; Jiang, S.Y. Mapping of S isotopes and trace elements in sulfides by LA-(MC)-ICP-MS: Potential problems and implications. *Minerals* **2016**, *6*, 110.
14. Heinrich, C.A.; Pettke, T.; Halter, W.E.; Aigner-Torres, M.; Audétat, A.; Günther, D.; Hattendorf, B.; Bleiner, D.; Guillong, M.; Horn, I. Quantitative multi-element analysis of minerals, fluid and melt inclusions by laser-ablation inductively-coupled-plasma mass-spectrometry. *Geochim. Cosmochim. Acta* **2003**, *67*, 3473–3497. [CrossRef]
15. Zajacz, Z.; Halter, W. LA-ICPMS analyses of silicate melt inclusions in co-precipitated minerals: Quantification, data analysis and mineral/melt partitioning. *Geochim. Cosmochim. Acta* **2007**, *71*, 1021–1040. [CrossRef]
16. Watson, E.B.; Harrison, T.M. Zircon thermometer reveals minimum melting conditions on earliest Earth. *Science* **2005**, *308*, 841–844. [CrossRef] [PubMed]
17. Hayden, L.A.; Watson, E.B.; Wark, D.A. A thermobarometer for sphene (titanite). *Contrib. Mineral. Petrol.* **2008**, *155*, 529–540. [CrossRef]
18. Russo, R.E.; Mao, X.L.; Gonzalez, J.J.; Mao, S.S. Femtosecond laser ablation ICP-MS. *J. Anal. Atom. Spectrom.* **2002**, *17*, 1072–1075. [CrossRef]
19. Koch, J.; Günther, D. Femtosecond laser ablation inductively coupled plasma mass spectrometry: Achievements and remaining problems. *Anal. Bioanal. Chem.* **2007**, *387*, 149–153. [CrossRef] [PubMed]
20. Garcia, C.C.; Lindner, H.; von Bohlen, A.; Vadla, C.; Niemax, K. Elemental fractionation and stoichiometric sampling in femtosecond laser ablation. *J. Anal. Atom. Spectrom.* **2008**, *23*, 470–478. [CrossRef]
21. Ohata, M.; Tabersky, D.; Glaus, R.; Koch, J.; Hattendorf, B.; Günther, D.J. Comparison of 795 nm and 265 nm femtosecond and 193 nm nanosecond laser ablation inductively coupled plasma mass spectrometry for the quantitative multi-element analysis of glass materials. *J. Anal. Atom. Spectrom.* **2014**, *29*, 1345–1353. [CrossRef]
22. Wohlgemuth-Ueberwasser, C.C.; Jochum, K.P. Capability of fs-LA-ICP-MS for sulfide analysis in comparison to ns-LA-ICP-MS: Reduction of laser induced matrix effects? *J. Anal. Atom. Spectrom.* **2015**, *30*, 2469–2480. [CrossRef]
23. Zhu, Z.Y.; Jiang, S.Y.; Yang, T.; Ciobanu, C.L.; Cook, N.J. Sulfur isotope fractionation in pyrite during laser ablation: Implications for laser ablation multiple collector inductively coupled plasma mass spectrometry mapping. *Chem. Geol.* **2016**, in press.
24. Gilbert, S.E.; Danyushevsky, L.V.; Goemann, K.; Death, D. Fractionation of sulphur relative to iron during laser ablation-ICP-MS analyses of sulphide minerals: Implications for quantification. *J. Anal. Atom. Spectrom.* **2014**, *29*, 1024–1033. [CrossRef]
25. Günther, D.; von Quadt, A.; Wirz, A.; Cousin, H.; Dietrich, V.J. Elemental analyses using laser ablation-inductively coupled plasma-mass spectrometry (LA-ICP-MS) of geological samples fused with $Li_2B_4O_7$ and calibrated without matrix-matched standards. *Mikrochim. Acta* **2001**, *136*, 101–107. [CrossRef]
26. Jackson, S.E.; Günther, D. The nature and sources of laser induced isotopic fractionation in laser ablation-multicollector-inductively coupled plasma-mass spectrometry. *J. Anal. Atom. Spectrom.* **2003**, *18*, 205–212. [CrossRef]
27. Günther, D.; Koch, J. Formation of aerosols generated by laser ablation and their impact on elemental fractionation in LA-ICP-MS. In *Laser Ablation ICP-MS in the Earth Sciences: Current Practices and Outstanding Issues*; Sylvester, P., Ed.; Mineralogical Association of Canada: Québec, QC, Canada, 2008; Volume 40, pp. 19–34.
28. Sylvester, P.J. Matrix effects in laser ablation ICP-MS. In *Laser Ablation ICP-MS in the Earth Sciences: Current Practices and Outstanding Issues*; Mineralogical Association of Canada: Québec, QC, Canada, 2008; Volume 40, pp. 67–78.
29. Norman, M.D.; Pearson, N.J.; Sharma, A.; Griffin, W.L. Quantitative analysis of trace elements in geological materials by laser ablation ICPMS: Instrumental operating conditions and calibration values of NIST glasses. *Geostand. Newslett.* **1996**, *20*, 247–261. [CrossRef]
30. Norman, M.; Robinson, P.; Clark, D. Major- and trace-element analysis of sulfide ores by laser-ablation ICP-MS, solution ICP-MS, and XRF: New data on international reference materials. *Can. Mine.* **2003**, *41*, 293–305. [CrossRef]

31. Wohlgemuth-Ueberwasser, C.C.; Ballhaus, C.; Berndt, J.; Stotter, V.; Meisel, T. Synthesis of PGE sulphide standards for laser ablation inductively coupled plasma mass spectrometry (LA-ICP-MS). *Contrib. Mineral. Petrol.* **2007**, *154*, 607–617. [CrossRef]
32. Danyushevsky, L.; Robinson, P.; Gilbert, S.; Norman, M.; Large, R.; McGoldrick, P.; Shelley, M. Routine quantitative multi-element analysis of sulphide minerals by laser ablation ICP-MS: Standard development and consideration of matrix effects. *Geochem. Explor. Environ. Anal.* **2011**, *11*, 51–60. [CrossRef]
33. Lin, J.; Liu, Y.S.; Yang, Y.H.; Hu, Z.C. Calibration and correction of LA-ICP-MS and LA-MC-ICP-MS analyses for element contents and isotopic ratios. *Solid Earth Sci.* **2016**, *1*, 5–27. [CrossRef]
34. Gilbert, S.; Danyushevsky, L.; Robinson, P.; Wohlgemuth-Ueberwasser, C.; Pearson, N.; Savard, D.; Norman, M.; Hanley, J. A comparative study of five reference materials and the Lombard meteorite for the determination of the platinum-group elements and gold by LA-ICP-MS. *Geostand. Geoanal. Res.* **2013**, *37*, 51–64. [CrossRef]
35. Savard, D.; Barnes, S.J.; Sunder Raju, P.V. Accurate LA-ICP-MS calibration for magnetite analysis using multiple reference materials. *Geochim. Cosmochim. Acta* **2010**, *74*, A914.
36. Tabersky, D.; Luechinger, N.A.; Rossier, M.; Reusser, E.; Hametner, K.; Aeschlimann, B.; Frick, D.A.; Halim, S.C.; Thompson, J.; Danyushevsky, L.; Günther, D. Development and characterization of custom-engineered and compacted nanoparticles as calibration materials for quantification using LA-ICP-MS. *J. Anal. Atom. Spectrom.* **2014**, *29*, 955–962. [CrossRef]
37. Jochum, K.P.; Weis, U.; Stoll, B.; Kuzmin, D.; Yang, Q.; Raczek, I.; Jacob, D.E.; Stracke, A.; Birbaum, K.; Frick, D.A. Determination of reference values for NIST SRM 610–617 glasses following ISO guidelines. *Geostand. Geoanal. Res.* **2011**, *35*, 397–429. [CrossRef]
38. Nadoll, P.; Koenig, A.E. LA-ICP-MS of magnetite: Methods and reference materials. *J. Anal. Atom. Spectrom.* **2011**, *26*, 1872–1877. [CrossRef]
39. Wilson, S.A. *The Collection, Preparation, and Testing of USGS Reference Material BCR-2, Columbia River, Basalt*; Open-File Report; U.S. Geological Survey: Reston, VA, USA, 1997.
40. Jochum, H.P.; Willbold, M.; Raczek, I.; Stoll, B.; Herwig, K. Chemical characterisation of the USGS Reference Glasses GSA-1G, GSC-1G, GSD-1G, GSE-1G, BCR-2G, BHVO-2G and BIR-1G using EPMA, ID-TIMS, ID-ICP-MS and LA-ICP-MS. *Geostand. Geoanal. Res.* **2005**, *29*, 285–302. [CrossRef]
41. Flanagan, F.J. *Descriptions and Analysis of Eight New USGS Rock Standards*; U.S. Geological Survey Professional Paper; U.S. Government Printing Office: Washington, DC, USA, 1976; Volume 840.
42. Wilson, S.A.; Ridley, W.I.; Koenig, A.E. Development of sulphide calibration standards for the laser ablation inductively-coupled plasma mass spectrometry technique. *J. Anal. Atom. Spectrom.* **2002**, *17*, 406–409. [CrossRef]
43. Yuan, J.H.; Zhan, X.C.; Fan, C.Z.; Zhao, L.H.; Sun, D.Y.; Jia, Z.R.; Hu, M.Y.; Kuai, L.J. Quantitative analysis of sulfide minerals by laser ablation-inductively coupled plasma-mass spectrometry using glass reference materials with matrix normalization plus sulfur internal standardization calibration. *Chin. J. Anal. Chem.* **2012**, *40*, 201–207. [CrossRef]
44. Ding, L.; Yang, G.; Xia, F.; Lenehan, C.E.; Qian, G.; McFadden, A.; Brugger, J.; Zhang, X.; Chen, G.; Pring, A. A LA-ICP-MS sulphide calibration standard based on a chalcogenide glass. *Mineral. Mag.* **2011**, *75*, 279–287. [CrossRef]
45. Jackson, S.E.; Fryer, B.J.; Gosse, W.; Healey, D.C.; Longerich, H.P.; Strong, D.F. Determination of the precious metals in geological materials by ICP-MS with nickel sulfide fire assay collection and tellurium coprecipitation. *Chem. Geol.* **1990**, *83*, 119–132. [CrossRef]
46. Sung, Y.H.; Brugger, J.; Ciobanu, C.L.; Pring, A.; Skinner, W.; Nugus, M. Invisible gold in arsenian pyrite and arsenopyrite from a multistage Archaean gold deposit: Sunrise Dam, Eastern Goldfields Province, Western Australia. *Mineral. Depos.* **2009**, *44*, 765–791. [CrossRef]
47. Cook, N.J.; Ciobanu, C.L.; Mao, J.W. Textural control on gold distribution in As-free pyrite from the Dongping, Huangtuliang and Hougou gold deposits, North China Craton, (Hebei Province, China). *Chem. Geol.* **2009**, *264*, 101–121. [CrossRef]
48. Cook, N.J.; Ciobanu, C.L.; Meria, D.; Silcock, D.; Wade, B. Arsenopyrite-pyrite association in an orogenic gold ore: Tracing mineralization history from textures and trace elements. *Econ. Geol.* **2013**, *108*, 1273–1283. [CrossRef]

49. Ciobanu, C.L.; Cook, N.J.; Utsunomiya, S.; Pring, A.; Green, L. Focussed ion beam–transmission electron microscopy applications in ore mineralogy: Bridging micron- and nanoscale observations. *Ore Geol. Rev.* **2011**, *42*, 6–31. [CrossRef]
50. Ciobanu, C.L.; Cook, N.J.; Utsunomiya, S.; Kogagwa, M.; Green, L.; Gilbert, S.; Wade, B. Gold-telluride nanoparticles revealed in arsenic-free pyrite. *Am. Mineral.* **2012**, *97*, 1515–1518. [CrossRef]
51. Junge, M.; Wirth, R.; Oberthür, T.; Melcher, F. Mineralogical siting of platinum-group elements in pentlandite from the Bushveld Complex, South Africa. *Mineral. Depos.* **2015**, *50*, 41–54. [CrossRef]
52. Zhang, J.; Deng, J.; Chen, H.Y.; Yang, L.Q.; Cooke, D.; Danyushevsky, L.; Gong, Q.J. LA-ICP-MS trace element analysis of pyrite from the Chang'an gold deposit, Sanjiang region, China: Implication for ore-forming process. *Gondwana Res.* **2014**, *26*, 557–575. [CrossRef]
53. Ismail, R.; Ciobanu, C.L.; Cook, N.J.; Teale, G.S.; Giles, D.; Schmidt Mumm, A.; Wade, B. Rare earths and other trace elements in minerals from skarn assemblages, Hillside iron oxide-copper-gold deposit, Yorke Peninsula, South Australia. *Lithos* **2014**, *184–187*, 456–477. [CrossRef]
54. Ubide, T.; McKenna, C.A.; Chew, D.M.; Kamber, B.S. High-resolution LA-ICP-MS trace element mapping of igneous minerals: In search of magma histories. *Chem. Geol.* **2015**, *409*, 157–168. [CrossRef]
55. Ulrich, T.; Kamber, B.S.; Jugo, P.J.; Tinkham, D.K. Imaging element-distribution patterns in minerals by laser ablation—Inductively coupled plasma—Mass spectrometry (LA-ICP-MS). *Can. Mineral.* **2009**, *47*, 1001–1012. [CrossRef]
56. Agangi, A.; Hofmann, A.; Wohlgemuth-Ueberwasser, C.C. Pyrite zoning as a record of mineralization in the Ventersdorp contact Reef, Witwatersrand Basin, South Africa. *Econ. Geol.* **2013**, *108*, 1243–1272. [CrossRef]
57. Gagnevin, D.; Menuge, J.F.; Kronz, A.; Barrie, C.; Boyce, A.J. Minor Elements in Layered Sphalerite as a Record of Fluid Origin, Mixing, and Crystallization in the Navan Zn–Pb Ore Deposit, Ireland. *Econ. Geol.* **2014**, *109*, 1513–1528. [CrossRef]
58. Maslennikov, V.V.; Maslennikova, S.P.; Large, R.R.; Danyushevsky, L.V. Study of trace element zonation in vent chimneys from the Silurian Yaman-Kasy volcanic-hosted massive sulfide deposit (Southern Urals, Russia) using laser ablation-inductively coupled plasma mass spectrometry (LA-ICPMS). *Econ. Geol.* **2009**, *104*, 1111–1141. [CrossRef]
59. George, L.L.; Cook, N.J.; Ciobanu, C.L. Partitioning of trace elements in co-crystallized sphalerite–galena–chalcopyrite hydrothermal ores. *Ore Geol. Rev.* **2016**, *77*, 97–116. [CrossRef]
60. Li, K.; Etschmann, B.; Rae, N.; Reith, F.; Ryan, C.G.; Kirkham, R.; Howard, D.; Rosa, D.R.N.; Zammit, C.; Pring, A.; et al. Ore petrography using megapixel X-ray imaging: Rapid insights into element distribution and mobilization in complex Pt and U–Ge–Cu Ores. *Econ. Geol.* **2016**, *111*, 487–502. [CrossRef]
61. Cook, N.J.; Ciobanu, C.L.; Pring, A.; Skinner, W.; Danyushevsky, L.; Shimizu, M.; Saini-Eidukat, B.; Melcher, F. Trace and minor elements in sphalerite: A LA-ICP-MS study. *Geochim. Cosmochim. Acta* **2009**, *73*, 4761–4791. [CrossRef]
62. Nadoll, P.; Angerer, T.; Mauk, J.L.; French, D.; Walshe, J. The chemistry of hydrothermal magnetite: A review. *Ore Geol. Rev.* **2014**, *61*, 1–32. [CrossRef]
63. Ciobanu, C.L.; Cook, N.J.; Pring, A.; Brugger, J.; Danushevsky, L.; Shimizu, M. 'Invisible gold' in bismuth chalcogenides. *Geochim. Cosmochim. Acta* **2009**, *73*, 1970–1999. [CrossRef]
64. Ciobanu, C.L.; Cook, N.J.; Kelson, C.R.; Guerin, R.; Kalleske, N.; Danyushevsky, L. Trace element heterogeneity in molybdenite fingerprints stages of mineralization. *Chem. Geol.* **2013**, *347*, 175–189. [CrossRef]
65. Ye, L.; Cook, N.J.; Ciobanu, C.L.; Liu, Y.P.; Zhang, Q.; Gao, W.; Yang, Y.L.; Danyushevsky, L.V. Trace and minor elements in sphalerite from base metal deposits in South China: A LA-ICPMS study. *Ore Geol. Rev.* **2011**, *39*, 188–217. [CrossRef]
66. Cook, N.J.; Ciobanu, C.L.; Brugger, J.; Etschmann, B.; Howard, D.J.; de Jonge, M.; Ryan, C.G.; Paterson, D. Determination of the oxidation state of Cu in substituted Cu-In-Fe-bearing sphalerite via μ-XANES spectroscopy. *Am. Mineral.* **2012**, *97*, 476–479. [CrossRef]
67. Murakami, H.; Ishihara, S. Trace elements of indium-bearing sphalerite from tin-polymetallic deposits in Bolivia, China and Japan: A femto-second LA-ICPMS study. *Ore Geol. Rev.* **2013**, *53*, 223–243. [CrossRef]
68. Lockington, J.; Cook, N.J.; Ciobanu, C.L. Trace and minor elements in sphalerite from metamorphosed sulphide deposits. *Mineral. Petrol.* **2014**, *108*, 873–890. [CrossRef]

69. Belissont, R.; Boiron, M.-C.; Luais, B.; Cathelineau, M. LA-ICP-MS analyses of minor and trace elements and bulk Ge isotopes in zoned Ge-rich sphalerites from the Noailhac—Saint-Salvy deposit (France): Insights into incorporation mechanisms and ore deposition processes. *Geochim. Cosmochim. Acta* **2014**, *126*, 518–540. [CrossRef]
70. Cook, N.J.; Etschmann, B.; Ciobanu, C.L.; Geraki, K.; Howard, D.L.; Williams, T.; Rae, N.; Pring, A.; Chen, G.; Johannessen, B.; et al. Distribution and substitution mechanism of Ge in a Ge-(Fe)-bearing sphalerite. *Minerals* **2015**, *5*, 117–132. [CrossRef]
71. Butler, I.B.; Nesbitt, R.W. Trace element distributions in the chalcopyrite wall of a black smoker chimney: Insights from laser ablation inductively coupled plasma mass spectrometry (LA–ICP–MS). *Earth Plan. Sci. Lett.* **1999**, *167*, 335–345. [CrossRef]
72. Wohlgemuth-Ueberwasser, C.C.; Viljoen, F.; Petersen, S.; Vorster, C. Distribution and solubility limits of trace elements in hydrothermal black smoker sulfides: An in-situ LA-ICP-MS study. *Geochim. Cosmochim. Acta* **2015**, *159*, 16–41. [CrossRef]
73. George, L.L.; Cook, N.J.; Ciobanu, C.L. Trace Elements in Chalcopyrite. *Mineral. Mag.* In press.
74. Cook, N.J.; Ciobanu, C.L.; Danyushevsky, L.V.; Gilbert, S. Minor elements in bornite and associated Cu-(Fe)-sulfides: A LA-ICPMS study. *Geochim. Cosmochim. Acta* **2011**, *73*, 4761–4791. [CrossRef]
75. George, L.; Cook, N.J.; Ciobanu, C.L.; Wade, B. Trace and minor elements in galena: A reconnaissance LA-ICP-MS study. *Am. Mineral.* **2015**, *100*, 548–569. [CrossRef]
76. Large, R.R.; Maslenikov, V.V.; Robert, F.; Danyushevsky, L.V.; Chang, Z. Multistage sedimentary and metamorphic origin of pyrite and gold in the giant Sukhoi log deposit, Lena Gold Province, Russia. *Econ. Geol.* **2007**, *102*, 1233–1267. [CrossRef]
77. Large, R.R.; Danyushevsky, L.; Hollit, C.; Maslennikov, V.; Meffre, S.; Gilbert, S.; Bull, S.; Scott, R.; Emsbo, P.; Thomas, H.; et al. Gold and trace element zonation in pyrite using a laser imaging technique: Implications for the timing of gold in orogenic and Carlin-style sediment-hosted deposits. *Econ. Geol.* **2009**, *104*, 635–668. [CrossRef]
78. Winderbaum, L.; Ciobanu, C.L.; Cook, N.J.; Paul, M.; Metcalfe, A.; Gilbert, S. Multivariate analysis of an LA-ICP-MS trace element dataset for pyrite. *Mathematical Geosci.* **2012**, *44*, 823–842. [CrossRef]
79. Ingham, E.S.; Cook, N.J.; Cliff, J.; Ciobanu, C.L.; Huddleston, A. A combined chemical, isotopic and microstructural study of pyrite from roll-front uranium deposits, Lake Eyre Basin, South Australia. *Geochim. Cosmochim. Acta* **2014**, *125*, 440–465. [CrossRef]
80. Large, R.R.; Halpin, J.A.; Danyushevsky, L.V.; Maslennikov, V.V.; Bull, S.W.; Long, J.A.; Gregory, D.D.; Lounejeva, E.; Lyons, T.W.; Sack, P.J.; et al. Trace element content of sedimentary pyrite as a new proxy for deep-time ocean-atmosphere evolution. *Earth Plan. Sci. Lett.* **2014**, *389*, 209–220. [CrossRef]
81. Morey, A.A.; Tomkins, A.G.; Bierlein, F.P.; Weinberg, R.F.; Davidson, G.J. Bimodal distribution of gold in pyrite and Arsenopyrite: Examples from the Archean Boorara and Bardoc Shear Systems, Yilgarn Craton, Western Australia. *Econ. Geol.* **2008**, *103*, 599–614. [CrossRef]
82. Lawley, C.J.M.; Creaser, R.A.; Jackson, S.E.; Yang, Z.P.; Davis, B.J.; Pehrsson, S.J.; Dubé, B.; Mercier-Langevin, P.; Vaillancourt, D. Unraveling the western Churchill province Paleoproterozoic Gold Metallotect: Constraints from Re–Os Arsenopyrite and U-Pb Xenotime geochronology and LA-ICP-MS Arsenopyrite trace element chemistry at the BIF-Hosted meliadine gold district, Nunavut, Canada. *Econ. Geol.* **2015**, *110*, 1425–1454. [CrossRef]
83. Deyell, C.L.; Hedenquist, J.W. Trace element geochemistry of enargite in the Mankayan District, Philippines. *Econ. Geol.* **2011**, *106*, 1465–1478. [CrossRef]
84. Barnes, S.J.; Prichard, H.M.; Cox, R.A.; Fisher, P.C.; Godel, B. The location of the chalcophile and siderophile elements in platinum-group element ore deposits (a textural, microbeam and whole rock geochemical study): Implications for the formation of the deposits. *Chem. Geol.* **2008**, *248*, 295–317. [CrossRef]
85. Dare, S.A.S.; Barnes, S.J.; Beaudoin, G.; Méric, J.; Boutroy, E.; Potvin-Doucet, C. Trace elements in magnetite as petrogenetic indicators. *Mineral. Depos.* **2014**, *49*, 785–796. [CrossRef]
86. Pagé, P.; Barnes, S.J. Using trace elements in chromites to constrain the origin of podiform chromitites in the Thetford Mines Ophiolite, Quebec, Canada. *Econ. Geol.* **2009**, *104*, 997–1018. [CrossRef]
87. O'Brien, J.J.; Spry, P.G.; Teale, G.S.; Jackson, S.E.; Rogers, D. Major and trace element chemistry of gahnite as an exploration guide to Broken Hill-Type Pb-Zn-Ag Mineralization in the Broken Hill Domain, New South Wales, Australia. *Econ. Geol.* **2015**, *110*, 1027–1057. [CrossRef]

88. Goldmann, S.; Melcher, F.; Gäbler, H.-E.; Dewaele, S.; De Clerq, F.; Muchez, P. Mineralogy and trace element chemistry of ferberite/reinite from Tungsten Deposits in Central Rwanda. *Minerals* **2013**, *3*, 121–144. [CrossRef]
89. Song, G.X.; Qin, K.Z.; Li, G.M.; Evans, N.J.; Chen, L. Scheelite elemental and isotopic signatures: Implications for the genesis of skarn-type W–Mo deposits in the Chizhou Area, Anhui Province, Eastern China. *Am. Mineral.* **2014**, *99*, 303–317. [CrossRef]
90. Hazarika, P.; Mishra, B.; Pruseth, K.L. Scheelite, apatite, calcite and tourmaline compositions from the late Archean Hutti orogenic gold deposit: Implications for analogous two stage ore fluids. *Ore Geol. Rev.* **2016**, *72*, 989–1003. [CrossRef]
91. Raju, P.V.S.; Hart, C.J.R.; Sangurmath, P. Scheelite geochemical signatures by LA-ICP-MS and potential for rare earth elements from Hutti Gold Mines and fingerprinting ore deposits. *J. Afr. Earth Sci.* **2016**, *114*, 220–227. [CrossRef]
92. Cook, N.J.; Ciobanu, C.L.; O'Rielly, D.; Wilson, K.; Das, K.; Wade, B. Mineral chemistry and element partitioning in hydrothermal Rare Earth Element (REE) mineralization, Browns Ranges, Western Australia. *Lithos* **2013**, *172–173*, 192–213. [CrossRef]
93. Smith, M.P.; Henderson, P.; Jeffries, T.E.R.; Long, J.; Williams, C.T. The rare earth elements and uranium in garnets from the Beinn an Dubhaich Aureole, Skye, Scotland, UK: Constraints on processes in a dynamic hydrothermal system. *J. Petrol.* **2004**, *45*, 457–484. [CrossRef]
94. Gaspar, M.; Knaack, C.; Meinert, L.D.; Moretti, R. REE in skarn systems: A LA-ICP-MS study of garnets from the Crown Jewel gold deposit. *Geochim. Cosmochim. Acta* **2008**, *72*, 185–205. [CrossRef]
95. Xu, J.; Ciobanu, C.L.; Cook, N.J.; Zheng, Y.; Sun, X.; Wade, B.P. Skarn formation and trace elements in garnet and associated minerals from Zhibula copper deposit, Gangdese Belt, southern Tibet. *Lithos* **2016**, *262*, 213–231. [CrossRef]
96. Kontonikas-Charos, A.; Ciobanu, C.L.; Cook, N.J. Albitization and redistribution of REE and Y in IOCG systems: Insights from Moonta-Wallaroo, Yorke Peninsula, South Australia. *Lithos* **2014**, *208–209*, 178–201. [CrossRef]
97. Smith, M.P.; Storey, C.D.; Jeffries, T.E.; Ryan, C. In situ U–Pb and trace element analysis of accessory minerals in the Kiruna District, Norrbotten, Sweden: New constraints on the timing and origin of mineralization. *J. Petrol.* **2009**, *50*, 2063–2094. [CrossRef]
98. Fu, Y.; Sun, X.M.; Zhou, H.Y.; Lin, H.; Yang, T.J. In-situ LA-ICP-MS U–Pb geochronology and trace elements analysis of polygenetic titanite from the giant Beiya gold–polymetallic deposit in Yunnan Province, Southwest China. *Ore Geol. Rev.* **2016**, *77*, 43–56. [CrossRef]
99. He, H.L.; Yu, S.Y.; Song, X.Y.; Du, Z.S.; Dai, Z.H.; Zhou, T.; Xie, W. Origin of nelsonite and Fe-Ti oxides ore of the Damiao anorthosite complex, NE China: Evidence from trace element geochemistry of apatite, plagioclase, magnetite and ilmenite. *Ore Geol. Rev.* **2016**, *79*, 367–381. [CrossRef]
100. She, Y.W.; Song, X.Y.; Yu, S.Y.; Chen, L.M.; Zheng, W.Q. Apatite geochemistry of the Taihe layered intrusion, SW China: Implications for the magmatic differentiation and the origin of apatite-rich Fe-Ti oxide ores. *Ore Geol. Rev.* **2016**, *78*, 151–165. [CrossRef]
101. Gagnon, J.E.; Samson, I.M.; Fryer, B.J.; Williams-Jones, A.E. Compositional heterogeneity in fluorite and the genesis of fluorite deposits: Insights from LA-ICP-MS analysis. *Can. Mineral.* **2003**, *41*, 365–382. [CrossRef]
102. Dare, S.A.S.; Barnes, S.J.; Prichard, H.M. The distribution of platinum group elements (PGE) and other chalcophile elements among sulfides from the Creighton Ni–Cu–PGE sulfide deposit, Sudbury, Canada, and the origin of palladium in pentlandite. *Mineral. Depos.* **2010**, *45*, 765–793. [CrossRef]
103. Dare, S.A.S.; Barnes, S.J.; Prichard, H.M.; Fisher, P.C. Chalcophile and platinum-group element (PGE) concentrations in the sulfide minerals from the McCreedy East deposit, Sudbury, Canada, and the origin of PGE in pyrite. *Mineral. Depos.* **2011**, *46*, 381–407. [CrossRef]
104. Dare, S.A.S.; Barnes, S.J.; Beaudoin, G. Variation in trace element content of magnetite crystallized from fractionating sulfide liquid, Sudbury, Canada: Implications for provenance discrimination. *Geochim. Cosmochim. Acta* **2012**, *88*, 27–50. [CrossRef]
105. Dare, S.A.S.; Barnes, S.J.; Prichard, H.M.; Fisher, P.C. Mineralogy and geochemistry of Cu-rich ores from the McCreedy East Ni–Cu–PGE deposit (Sudbury, Canada): Implications for the behavior of platinum group and chalcophile elements at the end of crystallization of a sulfide liquid. *Econ. Geol.* **2014**, *109*, 343–366. [CrossRef]

106. Duran, C.J.; Barnes, S.J.; Corkery, J.T. Chalcophile and platinum-group element distribution in pyrites from the sulfide-rich pods of the Lac des Iles Pd deposits, Western Ontario, Canada: Implications for post-cumulus re-equilibration of the ore and the use of pyrite compositions in exploration. *J. Geochem. Explor.* **2015**, *158*, 223–242. [CrossRef]
107. Godel, B.; Barnes, S.J. Platinum-group elements in sulfide minerals and the whole rock of the J–M Reef (Stillwater complex): Implication for the formation of the reef. *Chem. Geol.* **2008**, *24*, 272–294. [CrossRef]
108. Godel, B.; Barnes, S.J.; Maier, W.D. Platinum-group elements in sulphide minerals, platinum-group minerals, and whole-rocks of the Merensky Reef (Bushveld Complex, South Africa): Implications for the formation of the reef. *J. Petrol.* **2007**, *48*, 1569–1604. [CrossRef]
109. Holwell, D.A.; Keays, R.R.; McDonald, I.; Williams, M.R. Extreme enrichment of Se, Te, PGE and Au in Cu sulfide microdroplets: Evidence from LA-ICP-MS analysis of sulfides in the Skaergaard Intrusion, east Greenland. *Contrib. Mineral. Petrol.* **2015**, *170*, 1–26. [CrossRef]
110. Piña, R.; Gervilla, F.; Barnes, S.J.; Ortega, L.; Lunar, R. Partition coefficients of platinum group and chalcophile elements between arsenide and sulfide phases as determined in the Beni Bousera Cr–Ni mineralization (North Morocco). *Econ. Geol.* **2013**, *108*, 935–951. [CrossRef]
111. Piña, R.; Gervilla, F.; Barnes, S.J.; Ortega, L.; Lunar, R. Liquid immiscibility between arsenide and sulfide melts: Evidence from a LA-ICP-MS study in magmatic deposits at Serranía de Ronda (Spain). *Mineral. Depos.* **2015**, *50*, 265–279. [CrossRef]
112. Piña, R.; Gervilla, F.; Barnes, S.J.; Oberthür, T.; Lunar, R. Platinum-group element concentrations in pyrite from the Main Sulfide Zone of the Great Dyke of Zimbabwe. *Mineral. Depos.* **2016**, in press.
113. Duran, C.J.; Barnes, S.-J.; Corkery, J.T. Trace element distribution in primary sulfides and Fe–Ti oxides from the sulfide-rich pods of the Lac des Iles Pd deposits, Western Ontario, Canada: Constraints on processes controlling the composition of the ore and the use of pentlandite compositions in exploration. *J. Geochem. Explor.* **2016**, *166*, 45–63.
114. Nikolakopoulos, D. Ore vectoring in IOCG Systems: Trace Elements in Garnets from the Groundhog Skarn, Punt Hill, South Australia. Unpublished Bachelor's Thesis, The University of Adelaide, Adelaide, Australia, 2013.
115. Peng, H.J.; Zhang, C.Q.; Mao, J.W.; Santosh, M.; Zhou, Y.M. Garnets in porphyry-skarn systems: A LA-ICP-MS, fluid inclusion, and stable isotope study of garnets from the Hongniu–Hongshan copper deposit, Zhongdian area, NW Yunnan Province, China. *J. Asian Earth Sci.* **2015**, *103*, 229–251. [CrossRef]
116. Zhao, W.W.; Zhou, M.F. In-situ LA-ICP-MS trace elemental analyses of magnetite: The Mesozoic Tengtie skarn Fe deposit in the Nanling Range, South China. *Ore Geol. Rev.* **2015**, *65*, 872–883. [CrossRef]
117. Groves, D.I.; Bierlein, F.P.; Meinert, L.D.; Hitzman, M.W. Iron oxide copper-gold (IOCG) deposits through earth history: Implications for origin, lithospheric setting, and distinction from other epigenetic iron oxide deposits. *Econ. Geol.* **2010**, *105*, 641–654. [CrossRef]
118. Huang, X.W.; Zhou, M.F.; Qiu, Y.Z.; Qi, L. In-situ LA-ICP-MS trace elemental analyses of magnetite: The Bayan Obo Fe-REE-Nb deposit, North China. *Ore Geol. Rev.* **2015**, *65*, 884–899. [CrossRef]
119. Knipping, J.L.; Bilenker, L.D.; Simon, A.C.; Reich, M.; Barra, F.; Deditius, A.P.; Heinrich, C.A.; Holtz, F.; Munizaga, R. Trace elements in magnetite from massive iron oxide apatite deposits indicate a combined formation by igneous and magmatic hydrothermal processes. *Geochim. Cosmochim. Acta* **2015**, *171*, 15–38. [CrossRef]
120. Tollari, N.; Barnes, S.-J.; Cox, R.A.; Nabil, H. Trace element concentrations in apatites from the Sept-Îles Intrusive Suite, Canada—Implications for the genesis of nelsonites. *Chem. Geol.* **2008**, *252*, 180–190. [CrossRef]
121. Chen, W.T.; Zhou, M.F.; Li, X.C.; Gao, J.F.; Hou, K.J. In-situ LA-ICP-MS trace elemental analyses of magnetite: Cu-(Au, Fe) deposits in the Khetri copper belt in Rajasthan Province, NW India. *Ore Geol. Rev.* **2015**, *65*, 929–939. [CrossRef]
122. Ciobanu, C.L.; Cook, N.J.; Ehrig, K.; Wade, B.P.; Kamenetsky, V.S. Trace element signatures in iron oxides from the Olympic Dam IOCG deposit, South Australia. In Proceedings of the 13th Biennial SGA Meeting, Mineral Resources in a Sustainable World, Nancy, France, 24–27 August 2015; Volume 3, pp. 1071–1074.

123. Ehrig, K.; McPhie, J.; Kamenetsky, V. Geology and mineralogical zonation of the Olympic Dam Iron Oxide Cu-U-Au-Ag deposit, South Australia. In *Geology and Genesis of Major Copper Deposits and Districts of the World: A Tribute to Richard H. Sillitoe*; Hedenquist, J.W., Harris, M., Camus, F., Eds.; Society of Economic Geologists Special Publication: Littleton, CO, USA, 2012; pp. 237–267.
124. Dupuis, C.; Beaudoin, G. Discrimination diagrams for iron oxide trace element fingerprinting of mineral deposit types. *Mineral. Depos.* **2011**, *46*, 319–335. [CrossRef]
125. Krneta, S.; Ciobanu, C.L.; Cook, N.J.; Ehrig, K.; Kamenetsky, V.S. *REY-Signatures in Apatite Monitor Evolution of IOCG Systems: Examples from Olympic Dam and Acropolis, South Australia*; Abstract; Australian Earth Science Convention: Adelaide, Australia, 2016.
126. Dare, S.A.S.; Barnes, S.J.; Beaudoin, G. Did the massive magnetite "lava flows" of El Laco (Chile) form by magmatic or hydrothermal processes? New constraints from magnetite composition by LA-ICP-MS. *Mineral. Depos.* **2015**, *50*, 607–617. [CrossRef]
127. Thomas, H.V.; Large, R.R.; Bull, S.W.; Maslennikov, V.; Berry, R.F.; Fraser, R.; Froud, S.; Moye, R. Pyrite and pyrrhotite textures and composition in sediments, laminated quartz veins, and reefs at Bendigo Gold Mine, Australia: Insights for ore genesis. *Econ. Geol.* **2011**, *106*, 1–31. [CrossRef]
128. Deol, S.; Deb, M.; Large, R.R.; Gilbert, S. LA-ICPMS and EPMA studies of pyrite, arsenopyrite and loellingite from the Bhukia-Jagpura gold prospect, southern Rajasthan, India: Implications for ore genesis and gold remobilization. *Chem. Geol.* **2012**, *326–327*, 72–87. [CrossRef]
129. Large, R.R.; Meffre, S.; Burnett, R.; Guy, B.; Bull, S.; Gilbert, S.; Goemann, K.; Danyushevsky, L. Evidence for an intrabasinal source and multiple concentration processes in the formation of the Carbon Leader Reef, Witwatersrand Supergroup, South Africa. *Econ. Geol.* **2013**, *108*, 1215–1241. [CrossRef]
130. Gregory, D.D.; Large, R.R.; Halpin, J.A.; Lounejeva Baturina, E.; Lyons, T.W.; Wu, S.; Danyushevsky, L.; Sack, P.J.; Chappaz, A.; Maslennikov, V.V.; et al. Trace element content of sedimentary pyrite in black shales. *Econ. Geol.* **2015**, *110*, 1389–1410. [CrossRef]
131. Steadman, J.A.; Large, R.R.; Meffre, S.; Olin, P.H.; Danyushevsky, L.V.; Gregory, D.D.; Belousov, I.; Lounejeva, E.; Ireland, T.R.; Holden, P. Synsedimentary to early diagenetic gold in black shale-hosted pyrite nodules at the golden mile deposit, Kalgoorlie, Western Australia. *Econ. Geol.* **2015**, *110*, 1157–1191. [CrossRef]
132. Genna, D.; Gaboury, D. Deciphering the hydrothermal evolution of a VMS system by LA-ICP-MS using trace elements in pyrite: An example from the Bracemac-Mcleod deposits, Abitibi, Canada, and Implications for Exploration. *Econ. Geol.* **2015**, *110*, 2087–2108. [CrossRef]
133. Mills, S.E.; Tomkins, A.G.; Weinberg, R.F.; Fan, H.R. Implications of pyrite geochemistry for gold mineralisation and remobilisation in the Jiaodong gold district, northeast China. *Ore Geol. Rev.* **2015**, *71*, 150–168. [CrossRef]
134. Boutroy, E.; Dare, S.A.S.; Beaudoin, G.; Barnes, S.J.; Lightfoot, P.C. Magnetite composition in Ni–Cu–PGE deposits worldwide: Application to mineral exploration. *J. Geochem. Explor.* **2014**, *145*, 64–81. [CrossRef]
135. Le Vaillant, M.; Barnes, S.J.; Fiorentini, M.L.; Miller, J.; McCuaig, T.C.; Muccilli, P. A hydrothermal Ni–As–PGE geochemical halo around the miitel komatiite-hosted nickel sulfide deposit, Yilgarn Craton, Western Australia. *Econ. Geol.* **2015**, *110*, 505–530. [CrossRef]
136. Acosta-Góngora, P.; Gleeson, S.A.; Samson, I.M.; Ootes, L.; Corriveau, L. Trace Element geochemistry of magnetite and its relationship to Cu–Bi–Co–Au–Ag–U–W mineralization in the great bear magmatic zone, NWT, Canada. *Econ. Geol.* **2015**, *109*, 1901–1928. [CrossRef]
137. Belousov, I.; Large, R.R.; Meffre, S.; Danyushevsky, L.V.; Steadman, J.; Beardsmore, T. Pyrite compositions from VHMS and orogenic Au deposits in the Yilgarn Craton, Western Australia: Implications for gold and copper exploration. *Ore Geol. Rev.* **2016**, *79*, 474–499. [CrossRef]
138. Canil, D.; Grondahl, C.; Lacourse, T.; Pisiak, L.K. Trace elements in magnetite from porphyry Cu–Mo–Au deposits in British Columbia, Canada. *Ore Geol. Rev.* **2016**, *72*, 1116–1128. [CrossRef]
139. Nadoll, P.; Mauk, J.L.; Hayes, T.S.; Koenig, A.E.; Box, S.E. Geochemistry of magnetite from hydrothermal ore deposits and host rocks of the mesoproterozoic belt supergroup, United States. *Econ. Geol.* **2012**, *107*, 1275–1292. [CrossRef]
140. Hanley, J.J.; Bray, C.J. The trace metal content of amphibole as a proximity indicator for Cu–Ni–PGE mineralization in the footwall of the Sudbury Igneous Complex, Ontario, Canada. *Econ. Geol.* **2009**, *104*, 113–125. [CrossRef]

141. Warren, M.R.; Hanley, J.J.; Ames, D.E.; Jackson, S.E. The Ni–Cr–Cu content of biotite as pathfinder elements for magmatic sulfide exploration associated with mafic units of the Sudbury Igneous Complex, Ontario, Canada. *J. Geochem. Explor.* **2015**, *153*, 11–29. [CrossRef]
142. Wilkinson, J.J.; Chang, Z.; Cooke, D.R.; Baker, M.J.; Wilkinson, C.C.; Inglis, S.; Chen, H.; Gemmell, J.B. The chlorite proximitor: A new tool for detecting porphyry ore deposits. *J. Geochem. Explor.* **2015**, *152*, 10–26. [CrossRef]
143. Mao, M.; Rukhlov, A.S.; Rowins, S.M.; Spence, J.; Coogan, L.A. Apatite trace element compositions: A robust new tool for mineral exploration. *Econ. Geol.* **2016**, *111*, 1043–1072. [CrossRef]
144. Makvandi, S.; Ghasemzadeh-Barvarz, M.; Beaudoin, G.; Grunsky, E.C.; McClenaghan, M.B.; Duchesne, C. Principal component analysis of magnetite composition from volcanogenic massive sulfide deposits: Case studies from the Izok Lake (Nunavut, Canada) and Halfmile Lake (New Brunswick, Canada) deposits. *Ore Geol. Rev.* **2016**, *72*, 60–85. [CrossRef]
145. Makvandi, S.; Ghasemzadeh-Barvarz, M.; Beaudoin, G.; Grunsky, E.C.; McClenaghan, M.B.; Duchesne, C.; Boutroy, E. Partial least squares-discriminant analysis of trace element compositions of magnetite from various VMS deposit subtypes: Application to mineral exploration. *Ore Geol. Rev.* **2016**, *78*, 388–408. [CrossRef]
146. Lane, D.J.; Cook, N.J.; Grano, S.R.; Ehrig, K. Selective leaching of penalty elements from copper concentrates: A review. *Miner. Eng.* **2016**, *98*, 110–121. [CrossRef]
147. Andersen, J.C.Ø.; Stickland, R.J.; Rollinson, G.K.; Shail, R.K. Indium mineralisation in SW England: Host parageneses and mineralogical relations. *Ore Geol. Rev.* **2016**, *78*, 213–238. [CrossRef]
148. Pavlova, G.G.; Palessky, S.V.; Borisenko, A.S.; Vladimirov, A.G.; Seifert, T.; Phan, L.A. Indium in cassiterite and ores of tin deposits. *Ore Geol. Rev.* **2015**, *66*, 99–113. [CrossRef]
149. Cook, N.J.; Ciobanu, C.L. Mineral hosts for critical metals in hydrothermal ores. In *Mineral Resources in a Sustainable World*, Proceedings of the 13th Biennial SGA Conference, Nancy, France, 24–27 August 2015; Volume 5, pp. 707–710.
150. Dalpé, C.; Hudon, P.; Ballantyne, D.J.; Williams, D.; Marcotte, D. Trace element analysis of rough diamond by LA-ICP-MS: A case of source discrimination? *J. Forensic Sci.* **2010**, *55*, 1443–1456.
151. Coney, L.; Moila, A.V.; Quadling, A.G. Gem-quality diamonds: Source discrimination. *S. Afr. J. Geol.* **2012**, *115*, 33–46. [CrossRef]
152. Melcher, F.; Graupner, T.; Henjes-Kunst, F.; Oberthür, T.; Sitnikova, M.; Gäbler, H.E. Analytical fingerprint of columbite-tantalite (coltan) mineralization in pegmatites: Focus on Africa. In Proceedings of the 9th International Congress for Applied Mineralogy, Australasian Institute of Mining and Metallurgy, Melbourne, Australia, 8–10 September 2008; pp. 615–624.
153. Gäbler, H.E.; Rehder, S.; Bahr, A.; Melcher, F.; Goldmann, S. Cassiterite fingerprinting by LA-ICP-MS. *J. Anal. Atom. Spectrom.* **2013**, *28*, 1247–1255. [CrossRef]
154. Giussani, B.; Monticelli, D.; Rampazzi, L. Role of laser ablation-inductively coupled plasma-mass spectrometry in cultural heritage research: A review. *Anal. Chim. Acta* **2009**, *635*, 6–21. [CrossRef] [PubMed]
155. De Marques Sá, C.; Noronha, F.; Ferreira da Silva, E. Factor analysis characterization of minor element contents in sulfides from Pb–Zn–Cu–Ag hydrothermal vein deposits in Portugal. *Ore Geol. Rev.* **2014**, *62*, 54–71. [CrossRef]
156. Frenzel, M.; Hirsch, T.; Gutzmer, J. Gallium, germanium, indium, and other trace and minor elements in sphalerite as a function of deposit type—A meta-analysis. *Ore Geol. Rev.* **2016**, *76*, 52–78. [CrossRef]
157. Debruyne, D.; Hulsbosch, N.; Muchez, P. Unraveling rare earth element signatures in hydrothermal carbonate minerals using a source—Sink system. *Ore Geol. Rev.* **2016**, *72*, 232–252. [CrossRef]
158. Li, X.F.; Cheng, H.; Wang, C.Z.; Wang, L. Genesis of the Huangshaping W–Mo–Cu–Pb–Zn polymetallic deposit in Southeastern Hunan Province, China: Constraints from fluid inclusions, trace elements, and isotopes. *Ore Geol. Rev.* **2016**, *79*, 1–25.
159. Xu, L.; Bi, X.; Hu, R.; Tang, Y.; Wang, X.; Xu, Y. LA-ICP-MS mineral chemistry of titanite and the geological implications for exploration of porphyry Cu deposits in the Jinshajiang–Red River alkaline igneous belt, SW China. *Mineral. Petrol.* **2015**, *109*, 181–200. [CrossRef]
160. Jaques, A.L. Major and trace element variations in oxide and titanate minerals in the West Kimberley lamproites, Western Australia. *Mineral. Petrol.* **2016**, *110*, 159–197. [CrossRef]

161. Velasquez, A. Trace Element Analysis of Native Gold by Laser Ablation ICP-MS: A Case Study in Greenstone-Hosted Quartz-Carbonate Vein Ore Deposits, Timmins, Ontario. Ph.D. Thesis, University of British Columbia, Kelowna, BC, Canada, 2014.
162. Kołodziejczyk, J.; Pršek, J.; Voudouris, P.; Melfos, V.; Asllani, B. Sn-bearing minerals and associated sphalerite from lead-zinc deposits, Kosovo: An electron microprobe and LA-ICP-MS study. *Minerals* **2016**, *6*, 42. [CrossRef]
163. Ciobanu, C.L.; Cook, N.J.; Maunders, C.; Wade, B.P.; Ehrig, K. Focused ion beam and advanced electron microscopy for minerals: Insights and outlook from bismuth sulphosalts. *Minerals* **2016**, *6*, 112.
164. Baele, J.-M.; Monin, L.; Navez, J.; André, L. Systematic REE Partitioning in Cubo-Dodecahedral Fluorite from Belgium Revealed by Cathodoluminescence Spectral Imaging and Laser Ablation-ICP-MS. In Proceedings of the 10th International Congress for Applied Mineralogy (ICAM), Trondheim, Norway, 1–5 August 2011; Springer: Berlin, Germany, 2012.
165. Gros, K.; Słaby, E.; Förster, H.-J.; Michelak, P.P.; Munnik, F.; Gδtze, J.; Rhede, D. Visualization of trace-element zoning in fluorapatite using BSE and CL imaging, and EPMA and μPIXE/μPIGE mapping. *Mineral. Petrol.* **2016**. [CrossRef]
166. Garbe-Schönberg, D.; Müller, S. Nano-particulate pressed powder tablets for LA-ICP-MS. *J. Anal. Atom. Spectrom.* **2014**, *29*, 990–1000. [CrossRef]
167. Garbe-Schönberg, D.; Müller, S.; Nordstad, S.; Schönberg, L. Particle size matters: A new strategy for manufacturing microanalytical reference standards from nano-particulate powder pellets. In Proceedings of the 9th International Conference on the Analysis of Geological and Environmental Materials, Leoben, Austria, 8–14 August 2015; Abstract OP-25, p. 64.
168. Onuk, P.; Melcher, F.; Walkner, C. Development of the matrix-matched sphalerite (ZnS) standards MUL-ZnS-1 and MUL-ZnS-2 for in-situ analysis of trace elements by laser ablation inductively coupled plasma-mass spectroscopy (LA-ICP-MS). In Proceedings of the 9th International Conference on the Analysis of Geological and Environmental Materials, Leoben, Austria, 8–14 August 2015; Abstract OP-26, p. 65.
169. Savard, D.; Raymond, V.; Barnes, S.J. LA-ICP-MS analysis of massive sulphides: Progress towards a new calibration material. In Proceedings of the 9th International Conference on the Analysis of Geological and Environmental Materials, Leoben, Austria, 8–14 August 2015; Abstract P-39, p. 116.

ADDITIONAL MATERIAL E

CONFERENCE ABSTRACT:

TRACE ELEMENT PARTITIONING BETWEEN SPHALERITE, GALENA AND CHALCOPYRITE

Luke L. George[1], Nigel J. Cook[2], Cristiana L. Ciobanu[2]

[1]*School of Physical Sciences, The University of Adelaide, Adelaide, S.A., 5005, Australia*

[2]*School of Chemical Engineering, The University of Adelaide, Adelaide, S.A., 5005, Australia*

Abstract Prepared for the 35th International Geological Congress, Cape Town, South Africa, August 27th – 4th September, 2016.

Trace element partitioning between sphalerite, galena and chalcopyrite

George, L.L.[1], Cook, N.J.[2] and Ciobanu, C.L.[2]

[1]School of Physical Sciences, University of Adelaide, Adelaide SA 5005, Australia; luke.george@adelaide.edu.au
[2]School of Chemical Engineering, University of Adelaide, Adelaide SA 5005, Australia

---

Despite the abundance of published trace element data for sphalerite, galena and chalcopyrite in natural systems (e.g. [1]; [2]; [3]), the partitioning behaviour of trace elements between these co-crystallizing sulphides remains poorly constrained. Laser-ablation inductively-coupled plasma mass spectrometry (LA-ICP-MS) analysis was conducted on seventeen different multicomponent base metal sulphide (BMS) assemblages from nine skarn, epithermal and sedimentary exhalative deposits. The trace elements consistently measured can be categorized into three groups based on their partitioning behaviours between co-crystallizing sphalerite, galena and chalcopyrite (See Table 1).

Table 1. *BMS hosts of various trace elements as determined from LA-ICP-MS analysis.*

Trace Element	**Mn**	**Fe**	**Co**	**Cu**	**Zn**	**Ga**	**As**	**Se**
Primary BMS Host	Sp[1]	Sp>Gn[1]	Sp>Cp[3]	Sp>Gn[3]	Cp[1]	Sp[2]	Gn>Sp[1]	Gn[1]

Trace Element	**Ag**	**Cd**	**In**	**Sn**	**Sb**	**Te**	**Hg**	**Tl**	**Bi**
Primary BMS Host	Gn[1]	Sp>Gn[1]	Sp>Cp[2]	?*	Gn>Cp[1]	Gn[1]	Sp>Cp[3]	Gn[1]	Gn[1]

Abbreviations: Sp = sphalerite, Gn = galena, Cp = chalcopyrite.
[1]Group 1 elements. Trend observed in all examined samples. [2]Group 2 elements. Recrystallization increases element concentration in Cp and may make Cp the primary host. [3]Group 3 elements. Trend generally, yet not always, true.
**Recrystallization increases Sn concentration in Cp such that Cp is usually primary host in recrystallized samples. Below recrystallization conditions, no trend is observed.*

Group 1 elements are Mn, Fe, Zn, As, Se, Ag, Cd, Sb, Te, Tl and Bi. These elements have the same primary preferred BMS host in all examined assemblages, and sometimes also an obvious secondary host as well. **Group 2** elements are Ga and In. They are primarily hosted in sphalerite in those assemblages that have not been recrystallized, whereas a relatively high concentration of these elements can be expected in chalcopyrite in recrystallized assemblages. Thus in recrystallized deposits, chalcopyrite is typically the primary host of Ga, and occasionally of In. **Group 3** elements are Co, Cu and Hg. These elements are usually preferentially hosted within sphalerite, however this trend is not observed in all assemblages. Tin exhibits partitioning behaviour similar to Group 2 elements as the concentration of Sn in chalcopyrite is higher in recrystallized assemblages. This typically makes chalcopyrite the primary host of Sn in recrystallized assemblages. However, in assemblages that have not recrystallized, Sn may be primarily hosted in sphalerite, galena or chalcopyrite, and thus does not fit neatly into any of the three groups above.

Temperature, pressure and redox conditions prevalent at the time of BMS crystallization do not appear to alter the preferred BMS host of Group 1 and 3 elements. Only high temperatures and pressures associated with upper amphibolite to granulite facies metamorphism alter the partitioning behaviour of Group 2 elements and Sn. Trace element oxidation state, ionic radius, availability and budget that a given BMS mineral can accommodate are the principal factors governing the partitioning behaviour of Group 1 elements. Ongoing research continues to investigate how the observed trends differ when other co-crystallizing sulphides, e.g. tetrahedrite-tennantite or bornite, are present.

References:

[1] Moggi-Cecchi V et al. (2002) Period Mineral 71:101-109
[2] Cook N et al. (2009) Geochim Cosmochim Acta 73:4761-4791
[3] George L et al. (2015) Am Mineral 100:548-569

ADDITIONAL MATERIAL F

CONFERENCE POSTER:

CONTROLS ON TRACE ELEMENT PARTITIONING BETWEEN SPHALERITE AND GALENA

Luke L. George[1], Nigel J. Cook[2], Cristiana L. Ciobanu[2]

[1]*School of Physical Sciences, The University of Adelaide, Adelaide, S.A., 5005, Australia*

[2]*School of Chemical Engineering, The University of Adelaide, Adelaide, S.A., 5005, Australia*

Abstract and Poster, Society of Economic Geologists Conference 2015, 'World-Class Ore Deposits: Discovery to Recovery', Hobart, TAS, Australia, September 27th – 30th.

Controls on Trace Element Partitioning between Sphalerite and Galena

Luke George[1], Nigel Cook[2] and Cristiana Ciobanu[2]

[1]School of Physical Sciences, University of Adelaide, S.A. 5005, Australia
[2]School of Chemical Engineering, University of Adelaide, S.A. 5005, Australia

Abstract

Using LA-ICP-MS trace element mapping of assemblages from a wide range of ore deposits, this study investigates the partitioning behavior of trace elements between co-crystallized sphalerite and galena. Almost all elements display a predictable, systematic partitioning between sphalerite and galena which is independent of ore type, geological environment or physiochemical conditions. Only the geochemical behavior of Sn, with respect to preferred host sulfid, remains undetermined in lower temperature ores.

Introduction

Despite an abundance of published trace element data for both sphalerite and galena in natural systems (e.g., Cook et al., 2009; George et al., 2015), the systematic partitioning behavior of trace elements between these minerals remains poorly constrained. Gaining such an understanding potentially contributes to a number of broad applications in the minerals industry: ore genesis, minerals exploration, ore processing and environmental management.

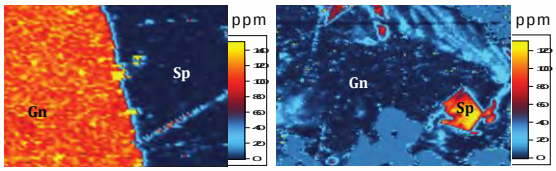

Fig. 3. *Representative LA-ICP-MS maps showing the distribution of Sn in different assemblages. Sp = sphalerite, Gn - galena.*

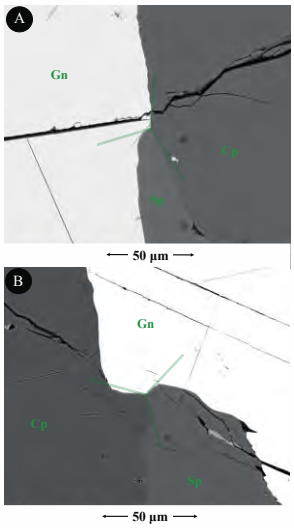

Fig. 1. *Back-scattered electron images of ~120° triple junction grain boundaries between sphalerite (Sp), galena (Gn) and chalcopyrite (Cp) at Herja (A) and Bleikvassli (B) illustrating textural evidence for co-crystallization. Note the grain boundaries curving towards the triple junction in order to approximate 120°.*

Results

LA-ICP-MS trace element maps were generated on assemblages containing co-crystallized sphalerite and galena (Fig. 1) from deposits that are representative of a range of different ore types, geologic environments and physiochemical conditions of ore formation. The LA-ICP-MS maps confirm predictable partitioning patterns that are independent of ore type, geological environment, physiochemical conditions etc. Most trace elements display predictable behavior, preferring either sphalerite or galena. Silver, for example, always prefers galena over sphalerite. Figure 2 shows the distribution of Ag in four representative multicomponent assemblages. The LA-ICPMS maps also highlight the more complicated partitioning behavior of Sn, being primarily concentrated in both sphalerite and galena in different assemblages (Fig. 3).

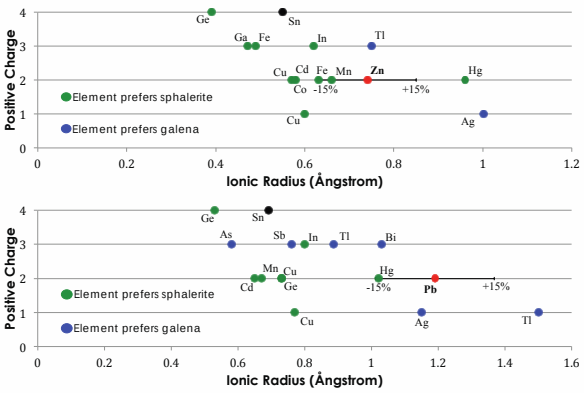

Fig. 4. *Plots showing the ionic radius of various trace element ions, both in tetrahedral coordination (as in sphalerite) compared to Zn^{2+} and octahedral coordination (as in galena) compared to Pb^{2+}. Data from Shannon 1976.*

Discussion

Sphalerite and galena both have ionic structures, in which the incorporation of trace elements is governed principally by Goldschmidt's first rule of substitution (Goldschmidt, 1954). This rule asserts that the ability of a given trace element to partition into an ionic lattice depends on the similarity of its ionic radius to that of the element it replaces. Thus most of the LA-ICP-MS mapping data can be explained by simply taking into account the ionic radius of the substituting trace element ion relative to the replaced Zn or Pb (Fig. 4). As such, the preferred host of most trace elements is largely independent of external factors. Manganese, Fe, Co, Cu, Ga, Ge, Cd, In and Hg all prefer sphalerite as host, while As, Se, Ag, Sb, Te, Tl and Bi prefer galena.

The authors are unaware of ionic radius data for either Sn^{2+} or Sn^{3+} in tetrahedral or octahedral coordination, precluding prediction of the behaviour of these ions from Goldschmidt's first rule. However, it does seem from the results here that galena becomes the preferred Sn host during syn-metamorphic recrystallization, supporting conclusions reached by George et al. (2015).

When chalcopyrite is also present, Sn, as well as Ga, move to chalcopyrite during recrystallization. Nevertheless, in lower temperature, non-recrystallized ores, the partitioning behaviour of Sn appears to vary as a function of as-yet unknown parameters.

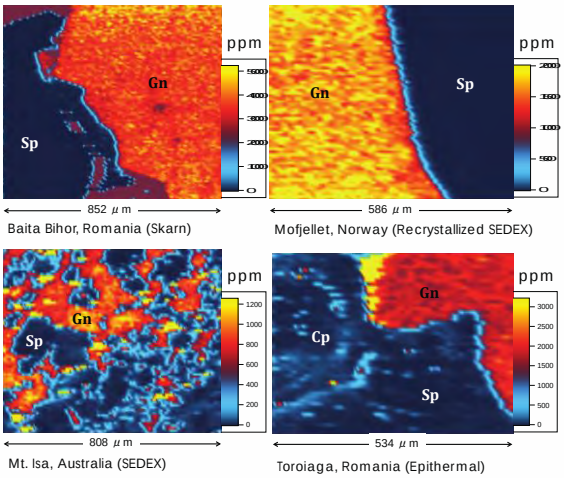

Fig. 2. *Representative LA-ICP-MS maps showing the distribution of Ag in different assemblages. Sp = sphalerite, Gn - galena, Cp = chalcopyrite.*

Discussion cont.

One question remains: why is Hg largely absent from galena, while sometimes present at relatively high concentrations in sphalerite, when the Hg^{2+} ion falls within 15% of the Pb^{2+} ionic radius in octahedral coordination, while well outside 15% of the Zn^{2+} ionic radius in tetrahedral coordination (Fig. 4). Hg^{2+} substitution into sphalerite may be aided through direct solid solution with the discrete isostructural Hg-bearing minerals metacinnabar, tiemannite and coloradoite.

In one sample from the Broken Hill deposit, Australia, which underwent syn-metamorphic recrystallization, compositional zoning was observed in both sphalerite and galena. Silver and Sb in galena, and Co in sphalerite, are depleted around grain rims and directly adjacent to fractures (Fig. 5). Growth-zoned sphalerite or galena is normally exceptionally rare in recrystallized deposits due to high temperatures and ample time for grainscale re-equilibration of trace elements. The zoning here is thus considered the result of secondary leaching following fluid-rock interaction.

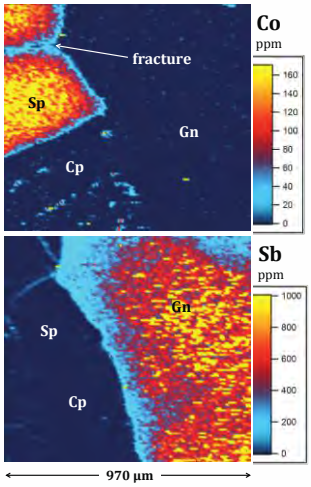

Fig. 5. *LA-ICP-MS maps showing the distribution of Co and Sb from Broken Hill, Australia (Recrystallized SEDEX). Sp = sphalerite, Gn = galena, Cp = chalcopyrite. Note the depletion of these elements around grain rims and adjacent to the fracture in sphalerite.*

References

Cook NJ, Ciobanu CL, Pring A, Skinner W, Shimizu M, Danyushevsky L, Saini-Eidukat B, Melcher F (2009) Trace and minor elements in sphalerite: A LA-ICPMS study. Geochim Cosmochim Acta 73:4761-4791

George L, Cook NJ, Ciobanu CL, Wade B (2015) Trace and minor elements in galena: A reconnaissance LA-ICP-MS study. Am Mineral 100:548:569

Goldschmidt VM (1954) Geochemistry. Soil Sci 78:156

Shannon R (1976) Revised effective ionic radii and systematic studies of interatomic distances in halides and chalcogenides. Acta Cryst A 32:751-767

Acknowledgements

Adelaide Microscopy are thanked for support with analysis. The authors express their gratitude to the numerous individuals, without whom access to many of the samples analyzed here would not have been possible.

ADDITIONAL MATERIAL G

CONFERENCE ABSTRACT:

TRACE ELEMENT PARTITIONING BETWEEN CO-EXISTING SPHALERITE, GALENA AND CHALCOPYRITE

Luke L. George[1], Nigel J. Cook[2], Cristiana L. Ciobanu[2]

[1]*School of Physical Sciences, The University of Adelaide, Adelaide, S.A., 5005, Australia*

[2]*School of Chemical Engineering, The University of Adelaide, Adelaide, S.A., 5005, Australia*

Mineral Resources in a Sustainable World. Proceedings of the 13th SGA Biennial Meeting, Nancy, France, 2015. ISBN: 978-2-85555-065-7, 24-27.

George, L., Cook, N. J., & Ciobanu, C. L. (2015). Trace element partitioning between co-existing sphalerite, galena and chalcopyrite (Extended abstract). In: André-Meyer, A.-S., et al., (Eds.), *Mineral Resources in a Sustainable World. Proceedings of the 13th SGA Biennial Meeting* (pp. 24-27), Nancy, France.

ADDITIONAL MATERIAL H

TRACE ELEMENT DISTRIBUTIONS IN SULPHIDES: PROGRESS, PROBLEMS AND PERSPECTIVES

Nigel J. Cook[2], Cristiana L. Ciobanu[2], **Luke L. George**[1], Bryony Crowe[1], Benjamin P. Wade[3]

[1]*School of Chemical Engineering, The University of Adelaide, Adelaide, S.A., 5005, Australia*

[2]*School of Physical Sciences, The University of Adelaide, Adelaide, S.A., 5005, Australia*

[3]*Adelaide Microscopy, The University of Adelaide, Adelaide, S.A., 5005, Australia*

Extended Abstract Published in Acta Geologica Sinica (English Edition), 88, 1444-1446.

Cook, N. J., Ciobanu, C. L., George, L. L., Crowe, B. & Wade, B. P., (2014). Trace Element Distributions in Sulphides: Progress, Problems and Perspectives (Extended abstract), *14th Quadrennial Symposium of the International Association on the Genesis of Ore Deposits, 'Mineral Resources: Discovery and Utilization, "Let's brainstorm"'*, Kunming, China.
Acta Geologica Sinica (English Edition), 88(s2), 1444-1446.

CHAPTER 9

REFERENCES

Acosta-Góngora, P., Gleeson, S. A., Samson, I. M., Ootes, L., Corriveau, L., 2015. Trace Element Geochemistry of Magnetite and Its Relationship to Cu-Bi-Co-Au-Ag-U-W Mineralization in the Great Bear Magmatic Zone, NWT, Canada. Econ. Geol. 109, 1901-1928.

Agangi, A., Hofmann, A., Wohlgemuth-Ueberwasser, C. C., 2013. Pyrite zoning as a record of mineralization in the Ventersdorp contact Reef, Witwatersrand Basin, South Africa. Econ. Geol. 108, 1243-1272.

Amcoff, O., 1976. The solubility of silver and antimony in galena. Neues Jahrb. Mineral. Monatsh. 6, 247-261.

Andersen, J. C. Ø., Stickland, R. J., Rollinson, G. K., Shail, R. K., 2016. Indium mineralisation in SW England: Host parageneses and mineralogical relations. Ore Geol. Rev. 78, 213-238.

Angelkov, K., Parvanov, B., 1980. The Assarel porphyry copper deposit, Bulgaria. In: Janković, S., Sillitoe, R. H., Eds., European Copper Deposits. SGA Special Publication 1, 59-62.

Apopei, A. I., Damian, G., Buzgar, N., Buzatu, A., 2016. Mineralogy and geochemistry of Pb-Sb/As-sulfosalts from Coranda-Hondol ore deposit (Romania)—Conditions of telluride deposition. Ore Geol. Rev. 72, 857-873.

Arehart, G. B., Chryssoulis, S. L., Kesler, S. E., 1993. Gold and arsenic in iron sulfides from sediment-hosted disseminated gold deposits; implications for depositional processes. Econ. Geol. 88, 171-185.

Axelsson, M. D., Rodushkin, I., 2001. Determination of major and trace elements in sphalerite using laser ablation double focusing sector field ICP-MS. J. Geochem. Explor. 72, 81-89.

Ayers, J. C., Watson, E. B., 1991. Solubility of apatite, monazite, zircon, and rutile in supercritical aqueous fluids with implications for subduction zone geochemistry. Phil. Trans. Roy. Soc. A: Math. Phys. Eng. Sci. 335, 365-375.

Ayres, R. U., Ayres, L. W., Råde, I., 2013. The life cycle of copper; Its co-products and byproducts. In: Tukker, A., Ed., Eco-Efficiency in Industry and Science, volume 13. Kluwer Academic Publishers, Dordrecht, 199 pp.

Baele, J. -M., Monin, L., Navez, J., André, L., 2011. Systematic REE Partitioning in Cubo-Dodecahedral Fluorite from Belgium Revealed by Cathodoluminescence Spectral Imaging and Laser Ablation-ICP-MS. In: Proceedings of the 10th International Congress for Applied Mineralogy (ICAM), Trondheim, Norway, 1–5 August 2011; Springer: Berlin, Germany.

Bajwah Z., Seccombe P., Offler R., 1987. Trace element distribution, Co:Ni ratios and genesis of the Big Cadia iron-copper deposit, New South Wales, Australia. Mineral. Deposita 22, 292-300.

Balić-Zunić, T., Bente, K., 1995. The two polymorphs of $TlPbSbS_3$ and the structural relations of phases in the system $TlSbS_2$-PbS. Mineral. Petrol. 53, 265-276.

Barnes, S. J., Naldrett, A. J., 1985. Geochemistry of the J-M (Howland) Reef of the Stillwater Complex, Minneapolis adit area. 1. Sulfide chemistry and sulfide-olivine equilibrium. Econ. Geol. 80, 627-645.

Barnes, S. J., Picard, C. P., 1993. The behaviour of platinum-group elements during partial melting, crystal fractionation, and sulphide segregation: an example from the Cape Smith Fold Belt, northern Quebec. Geochim. Cosmochim. Acta 57, 79-87.

Barnes, S. J., Ripley, E. M., 2016. Highly Siderophile and Strongly Chalcophile Elements in Magmatic Ore Deposits. Rev. Mineral. Geochem. 81, 725-774.

Barnes, S. J., Makovicky, E., Makovicky, M., Rose-Hansen, J., Karup-Moller, S., 1997. Partition coefficients for Ni, Cu, Pd, Pt, Rh, and Ir between monosulfide solid solution and sulfide liquid and the formation of compositionally zoned Ni–Cu sulfide bodies by fractional crystallization of sulfide liquid. Can. J. Earth Sci. 34, 366-374.

Barnes, S. J., Cox, R. A., Zientek, M. L., 2006. Platinum-group element, Gold, Silver and Base Metal distribution in compositionally zoned sulfide droplets from the Medvezky Creek Mine, Noril'sk, Russia. Contrib. Mineral. Petrol. 152, 187-200.

Barnes, S. J., Prichard, H. M., Cox, R. A., Fisher, P. C., Godel, B., 2008. The location of the chalcophile and siderophile elements in platinum-group element ore deposits (a textural, microbeam and whole rock geochemical study): Implications for the formation of the deposits. Chem. Geol. 248, 295-317.

Barrie, C. D., Boyle, A. P., Cook, N. J., Prior, D. J., 2010. Pyrite deformation textures in the massive sulfide ore deposits of the Norwegian Caledonides. Tectonophysics 483, 269-286.

Barton, P. B., 1970. Sulfide petrology. Mineral. Soc. Amer. Spec. Paper 3, 187-198.

Barton, P. B., Skinner, B. J., 1967. Sulfide mineral stabilities. In: Barnes, H. L., Ed., Geochemistry of Hydrothermal Ore Deposits, 1st edition, 236-333.

Barton, P. B., Skinner, B. J., 1979. Sulfide mineral stabilities. In: Barnes, H. L., Ed., Geochemistry of Hydrothermal Ore Deposits, 2nd edition, 278-403.

Baruah, M. K., Kotoky, P., Borah, G. C., 2014. Geochemical Association of Ni2+, Zn2+, Pb2+, Ag^{+}, Cu^{2+}, and Co^{2+} Ions in Natural Pyrite. J. Geochem. 2014. doi: 10.1155/2014/161850.

Basu, K., Bortnykov, N., Mookherjee, A., Mozgova, N., Tsepin, A. I., 1981. Rare minerals from Rajpura-Dariba, Rajasthan, India III: Plumbian tetrahedrite. Neues Jahrb. Mineral. Abh. 141, 280-289.

Basu, K., Bortnykov, N., Mookherjee, A., Mozgova, N., Sivtsov, A. V., Tsepin, A. I., Vrublevskaja, Z. V., 1984. Rare minerals from Rajpura-Dariba, Rajasthan, India V: The first recorded occurrence of a manganoan fahlore. Neues Jahrb. Mineral. Abh. 149, 105-112.

Becker, W., Lutz, H., 1978. Phase studies in the systems CoS–MnS, CoS–ZnS, and CoS–CdS. Mater. Res. Bull. 13, 907-911.

Belissont, R., Boiron, M. C., Luais, B., Cathelineau, M., 2014. LA-ICP-MS analyses of minor and trace elements and bulk Ge isotopes in zoned Ge-rich sphalerites from the Noailhac - Saint-Salvy deposit (France): Insights into incorporation mechanisms and ore deposition processes. Geochim. Cosmochim. Acta 126, 518-540.

Belousov, I., Large, R. R., Meffre, S., Danyushevsky, L. V., Steadman, J., Beardsmore, T., 2016. Pyrite compositions from VHMS and orogenic Au deposits in the Yilgarn Craton, Western Australia: Implications for gold and copper exploration. Ore Geol. Rev. 79, 474-499.

Bente, K., Doering, T., 1995. Experimental studies on the solid state diffusion of Cu+ In in ZnS and on "Disease", DIS (Diffusion Induced Segregations), in sphalerite and their geological applications. Mineral. Petrol. 53, 285-305.

Bethke, P. M., Barton, P. B., 1971. Distribution of some minor elements between coexisting sulfide minerals. Econ. Geol. 66, 140-163.

Billay, A. Y., Kisters, A. F. M., Meyer, F. M., Schneider, J., 1997. The geology of the Lega Dembi gold deposit, southern Ethiopia: Implications for Pan-African gold exploration. Mineral. Deposita 32, 491-504.

Binns, R., 1964. Zones of progressive regional metamorphism in the Willyama complex, Broken Hill district, New South Wales. J. Geol. Soc. Austral. 11, 283-330.

Bishop, A. C., Criddle, A. J., Clark, A. M., 1977. Plumbian tennantite from Sark, Channel Islands. Mineral. Mag. 41, 59-63.

Bjerkgård, T., Larsen, R. B., Marker, M., 1995. Regional geology of the Okstindene area, the Rodingsfjall Nappe Complex, Nordland, Norway. Open Rep, Nor. Geol. Unders. 95, 87.

Bjerkgård, T., Larsen, R. B., Marker, M., 1997. Regional setting of the Bleikvassli Zn-Pb deposit in Nordland, Norway. Norg. Geol. Unders. 433, 34-35.

Bjerkgård, T., Marker, M., Sandstad, J., Cook, N. J., Sørdahl, T., 2001. Ore potential with emphasis on gold in the Mofjellet Deposit, Rana, Nordland, Norway. Norges geologiske undersøkelse Report 2001.050.

Blackburn, W. H., Schwendeman, J. F., 1977. Trace element substitution in galena. Can. Mineral. 15, 365-377.

Blichert-Toft, J., Albarede, F., 1997. The Lu–Hf geochemistry of chondrites and the evolution of the mantle–crust system. Earth Plan. Sci. Lett. 148, 243–258.

Blundy, J. D., Wood, B. J., 1991. Crystal-chemical controls on the partitioning of Sr and Ba between plagioclase feldspar, silicate melts, and hydrothermal solutions. Geochim. Cosmochim. Acta 55, 193-209.

Bogdanov, B., 1987. Copper deposits in Bulgaria (in Bulgarian). Technica, Sofia, 388 pp.

Borcoş, M., 1967. Studiul geotermometric Al Mineralizatiei Din Masivul subvulcanic Neogen Toroiaga Tiganul (Maramures). Dari de Seama ale Sedintelor 53, 219-240.

Borcoş, M., Lang, B., Bostinescu, S., Gheorghita, I., 1975. Neogene hydrothermal ore deposits in the volcanic Gutai Mountains, part III. Rev. Roum. Géol. Géophys. Géogr. Ser. Géol. 19, 21-35.

Borcoş, M., Andar, P., Andar, A., Berza, T., 1982. Geochimia mineralizatiilor polimetalice din cimpul minier Toroiaga (Baia Borsa, Muntii Maramuresului). Dari de Seama ale Sedintelor 67, 55-82.

Bortnikov, N., Dobrovol'skaya, M., Genkin, A., Naumov, V., Shapenko, V., 1995. Sphalerite–galena geothermometers; distribution of cadmium, manganese, and the fractionation of sulfur isotopes. Econ. Geol. 90, 155–180.

Bortnikov, N. S., Kudryavtsev, A. S., Troneva, N. V., 1979. Bi-rich tetrahedrite from the Tary-Ekan deposit (East Karamazar, central Asia). Mineral. Zhurnal 198, 61-64. (In Russian)

Bortnikov, N. S., Cabri, L. J., Vikent'ev, I. V., McMahon, G., Bogdanov, Y. A., 2000. Invisible gold in sulfides from recent submarine hydrothermal vents. Dokl. Earth Sci. 373, 863-866.

Bos, A., 1990. Hydrothermal element distributions at high temperatures: an experimental study on the partitioning of major and trace elements between phlogopite, haplogranitic melt and vapour. Ph.D. thesis, University of Utrecht.

Both, R., Rutland, R., 1976. The problem of identifying and interpreting stratiform ore bodies in highly metamorphosed terrains: the Broken Hill example. Handbook of Stratabound and Stratiform Ore Deposits 4, 261-325.

Both, R. A., McElhinney, R., Toteff, S., 1995. The Angas Zn-Pb-Ag deposit in the Kanmantoo Group, South Australia: synsedimentary or metamorphic? In: Pasava, J., Kríbek, B., Zák, K., Eds., Mineral Deposits: From their Origin to their Environmental Impacts. A. A. Balkema, Rotterdam, 847-850.

Boudreau, A. E., Mathez, E. A., McCallum, I. S., 1986. Halogen geochemistry of the Stillwater and Bushveld Complexes: Evidence for transport of the platinum-group elements by Cl-rich fluids. J. Petrol. 27, 967-986.

Boulter, C. A., Fotios, M. G., Phillips, G. N., 1987. The Golden Mile, Kalgoorlie; a giant gold deposit localized in ductile shear zones by structurally induced infiltration of an auriferous metamorphic fluid. Econ. Geol. 82, 1661-1678.

Boutroy, E., Dare, S. A. S., Beaudoin, G., Barnes, S. J., Lightfoot, P. C., 2014. Magnetite composition in Ni-Cu-PGE deposits worldwide: application to mineral exploration. J. Geochem. Explor. 145, 64-81.

Bowles, J. F. W., Howie, R. A., Vaughan, D. J., Zussman, J., 2011. Rock-forming Minerals: nonsilicates: oxides, hydroxides and sulphides. Geol. Soc. London

Boyle, A. P., Westhead, R. K., 1992. Metamorphic peak geothermobarometry in the Furulund Group, Sulitjelma, Scandinavian Caledonides - Implications for uplift. J. Metam. Geol. 10, 615-626.

Boyle, A. P., Mason, R., Hansen, T. S., 1985. A new tectonic perspective of the Sulitjelma region. In: Gee, D. G., Sturt, B. A., Eds., The Caledonide Orogen. Scandinavia and Related Areas. Wiley, London, 529-542.

Breskovska, V. V., Tarkian, M., 1994. Compositional variation in Bi-bearing fahlores. Neues Jahrb. Mineral. Monatsh. 5, 230-240.

Brill B., 1989. Trace-element contents and partitioning of elements in ore minerals from the CSA Cu–Pb–Zn deposit, Australia. Can. Mineral. 27, 263-274.

Brookins, D. G., 1988. Eh-pH diagrams for geochemistry. Springer-Verlag Berlin Heidelberg.

Bryndzia, L. T., Scott, S. D., Spry, P. G., 1990. Sphalerite and hexagonal pyrrhotite geobarometer; correction in calibration and application. Econ. Geol. 85, 408-411.

Bürg, G., 1935. Natur des in den Pyriten nichtsichtbar enthaltenen Goldes. Zeits. prakt. Geol. 43, 17-32.

Burton, K. W., Boyle, A. P., Kirk, W. L., Mason, R., 1989. Pressure, temperature and structural evolution of the Sulitjelma Fold Nappe, Central Scandinavian Caledonides. In: Daly, J. S., Cliff, R. A., Yardley, B. W. D., Eds., Evolution of Metamorphic Belts. Geol. Soc. London Spec. Publ. 43, 391-411.

Butler, I. B., Nesbitt, R. W., 1999. Trace element distributions in the chalcopyrite wall of a black smoker chimney: insights from laser ablation inductively coupled plasma mass spectrometry (LA–ICP–MS). Earth Plan. Sci. Lett. 167, 335-345.

Buzatu, A., Damian, G., Dill, H. G., Buzgar, N., Apopei, A. I., 2015. Mineralogy and geochemistry of sulfosalts from Baia Sprie ore deposit (Romania)—New bismuth minerals occurrence. Ore Geol. Rev. 65, 132-147.

Cabri, L. J., 1987. The mineralogy of precious metals: new developments and metallurgical implications. Can. Mineral. 25, 1-7.

Cabri, L. J., 1988. The role of mineralogy in gold metallurgy. Proceedings of Symposium on Heap Leaching of Gold in a Canadian Environment Timmins, Ontario, Canada. Can. Mineral Processors, CIM, Paper No. 2, 11.

Cabri, L. J., 1992. The distribution of trace precious metals in minerals and mineral products. Mineral. Mag. 56, 289-308.

Cabri, L. J., Blank, H., El Goresy, A., Laflamme, J. G., Nobiling, R., Sizgoric, M. B., Traxel, K., 1984. Quantitative trace-element analyses of sulfides from Sudbury and Stillwater by proton microprobe. Can. Mineral. 22, 521-542.

Cabri L. J., Campbell J. L., Laflamme J. H. G., Leigh R. G., Maxwell J. A., Scott J. D., 1985. Proton-microprobe analysis of trace elements in sulfides from some massive-sulfide deposits. Can. Mineral. 23, 133-148.

Cabri, L. J., Chryssoulis, S. L., de Villiers, J. P. R., Laflamme, J. H. G., Buseck, P. R., 1989. The nature of "invisible" gold in arsenopyrite. Can. Mineral. 27, 353-362.

Cabri, L. J., McMahon, G., Bortnikov, N. S., Vikentiev, I. V., Bogdanov, Y. A., 2000. SIMS gold analyses of sea floor sulfide minerals. In: Benninghoven, A., Bertrand, P., Migeon, H. -N., Werner, H. W., Eds., SIMS XII, Proc. 12th Internat. Conf. on Secondary Ion Mass Spectrometry, Brussels, Belgium. Elsevier, 1019-1022.

Campbell, I. H., Barnes, S. J., 1984. A model for the geochemistry of the platinum-group elements in magmatic sulfide deposits. Can. Mineral. 22, 151-160.

Canil, D., Grondahl, C., Lacourse, T., Pisiak, L. K., 2016. Trace elements in magnetite from porphyry Cu–Mo–Au deposits in British Columbia, Canada. Ore Geol. Rev. 72, 1116-1128.

Cathelineau, M., Boiron, M. C., Holliger, P., Marion, P., 1988. Gold-rich arsenopyrites: crystal chemistry, gold location and state, physical and chemical conditions of crystallization. In: Proc. Gold '88 (Melbourne), 235-244.

Charnock, J. M., Garner, C. D., Pattrick, R. A. D., Vaughan, D. J., 1989. Co-ordination sites of metals in tetrahedrite minerals determined by EXAFS. J. Solid State Chem. 82, 279-289.

Charnock, J. M., Garner, C. D., Pattrick, R. A. D., Vaughan, D. J., 1989. EXAFS and Mössbauer spectroscopic study of Fe-bearing tetrahedrites. Mineral. Mag. 53, 193-199.

Chen, W. W., Zhang, J. M., Ardell, A. J., Dunn, B., 1988. Solid-state phase equilibria in the ZnS–CdS system. Mater. Res. Bull. 23, 1667-1673.

Chen, L. M., Song, X. Y., Danyushevsky, L. V., Wang, Y. S., Tian, Y. L., Xiao, J. F., 2014. A laser ablation ICP-MS study of platinum-group and chalcophile elements in base metal sulfide minerals of the Jinchuan Ni-Cu sulfide deposit, NW China. Ore Geol. Rev. 65, 955-967.

Chen, W. T., Zhou, M. F., Li, X. C., Gao, J. F., Hou, K. J., 2015. In-situ LA-ICP-MS trace element alanalyses of magnetite: Cu-(Au, Fe) deposits in the Khetri copper belt in Rajasthan Province, NW India. Ore Geol. Rev. 65, 929-939.

Chew, D. M., Sylvester, P. J., Tubrett, M. N., 2011. U-Pb and Th-Pb dating of apatite by LA-ICPMS. Chem. Geol. 280, 200-216.

Chioreanu, I., Fabricanti, M., Giurgiu, C., Groza, D., Radu, M., Råslescu, D., Surducan, A., 1993. Lithogeochemical study of primary haloes related to some mineralisations in Toroioaga Massif. Third Geological Symposium, Baia Mare, Abstracts Volume, 8-9.

Chouinard, A., Paquette, J., Williams-Jones, A. E., 2005. Crystallographic controls on trace-element incorporation in auriferous pyrite from the Pascua epithermal high-sulfidation deposit, Chile-Argentina. Can. Mineral. 43, 951-963.

Chutas, N. I., Kress, V. C., Ghiorso, M. S., Sack, R. O., 2008. A solution model for high-temperature PbS–$AgSbS_2$–$AgBiS_2$ galena. Amer. Mineral. 93, 1630–1640.

Chryssoulis, S. L., 1989. Ion probe microanalysis of gold in common sulphide minerals and implications for enhanced recovery from refractory gold ores. CANMET Contract Report # 79037-01-55.

Chryssoulis, S. L., Chauvin, W. J., Surges, L. J., 1986. Trace element analysis by secondary ion mass spectrometry with particular reference to silver in the Brunswick sphalerite. Canadian Metallurgical Quarterly 25, 233-239.

Chryssoulis, S. L., Cabri, L. J., Salter, R. S., 1987. Direct determination of invisible gold in refractory sulphide ores. In: Salter, R. S., Wyslouzil, D. M., McDonald, G. W., Eds., Gold Metallurgy--Proceedings of the International Symposium, Winnipeg, Canada, August 23-26, 1987, Pergamon Press, 235-244.

Chryssoulis, S. L., Cabri, L. J., Lennard, W., 1989. Calibration of the ion microprobe for quantitative trace precious metal analysis of ore minerals. Econ. Geol. 84, 1684-1689.

Cioacă M. E., Munteanu M., Qi L., Costin G., 2014. Trace element concentrations in porphyry copper deposits from Metaliferi Mountains, Romania: A reconnaissance study. Ore Geol. Rev. 63, 22-39.

Ciobanu, C. L., Cook, N. J., Ivascanu, P., 2001. Ore deposits of the Vorţa-Dealul Mare area, South Apuseni Mts., Romania: Textures and a revised genetic model. ABCD-Geode 2001. Rom. J. Mineral Deposits 79, 46-47.

Ciobanu, C. L., Cook, N. J., Stein, H., 2002. Regional setting and geochronology of the Late Cretaceous Banatitic Magmatic and Metallogenic Belt. Mineral. Deposita 37, 541-567.

Ciobanu, C. L., Gabudeanu, B., Cook, N. J., 2004. Neogene ore deposits and metallogeny of the Golden Quadrilateral, South Apuseni Mountains, Romania. In: Ciobanu, C. L., Cook, N. J., Eds., Gold-Silver-Telluride Deposits of the Golden Quadrilateral, South Apuseni Mts.,

Romania. Guidebook, International Field Workshop of IGCP-486, Alba Iulia, Romania, 31st August–7th September 2004. IAGOD Guidebook Series 12, 221-225.

Ciobanu, C. L., Cook, N. J., Pring, A., Brugger, J., Danushevsky, L., Shimizu, M., 2009. 'Invisible gold' in bismuth chalcogenides. Geochim. Cosmochim. Acta 73, 1970-1999.

Ciobanu, C. L., Cook, N. J., Utsunomiya, S., Pring, A., Green, L., 2011. Focussed ion beam - transmission electron microscopy applications in ore mineralogy: bridging micron- and nanoscale observations. Ore Geol. Rev. 42, 6-31.

Ciobanu, C. L., Cook, N. J., Utsunomiya, S., Kogagwa, M., Green, L., Gilbert, S., Wade, B., 2012. Gold-telluride nanoparticles revealed in arsenic-free pyrite. Amer. Mineral. 97, 1515-1518.

Ciobanu, C. L., Cook, N. J., Kelson, C. R., Guerin, R., Kalleske, N., Danyushevsky, L., 2013. Trace element heterogeneity in molybdenite fingerprints stages of mineralization. Chem. Geol. 347, 175-189.

Ciobanu, C. L., Wade, B., Cook, N. J., Schmidt Mumm, A., Giles, D., 2013. Uranium-bearing hematite from the Olympic Dam Cu-U-Au deposit, South Australia; a geochemical tracer and reconnaissance Pb-Pb geochronometer. Precambr. Res. 238, 129-147.

Ciobanu, C. L., Brugger, J., Cook, N. J., Mills, S., Elliot, P., Damian, G., Damian, F., 2014. Graţianite, $MnBi_2S_4$, a new mineral from the Băiţa Bihor skarn, Romania. Amer. Mineral. 99, 1163-1170.

Ciobanu, C. L., Cook, N. J., Ehrig, K., Wade, B. P., Kamenetsky, V. S., 2015. Trace element signatures in iron oxides from the Olympic Dam IOCG deposit, South Australia. In: Proc. 13th Biennial SGA Meeting, Mineral Resources in a Sustainable World, Nancy, France, 24–27 August 2015; Volume 3, 1071-1074.

Ciobanu, C. L., Cook, N. J., Maunders, C., Wade, B. P., Ehrig, K., 2016. Focused ion beam and advanced electron microscopy for minerals: Insights and outlook from bismuth sulphosalts. Minerals 6(4), 112; doi:10.3390/min6040112.

Cioflica, G., Lupulescu, M., 1997. Once again on the Joseite-A from the skarn deposits from Baita Bihor mine (Apuseni Mountains, Romania). Rom. J. Mineral Deposits 78, 113-116.

Cioflica, G., Vlad, S., 1981. Cupriferous mineralization at Ciclova. An Univ. Bucuresti Ser. Geol. 30, 1-17.

Cioflica, G., Vlad, S., Stoici, S., 1971. Repartition de la mineralisation dans les skarns de Baita Bihorului. Revue Roumaine de Geologie, Geophysique et Geographie, Serie de Geologie 15, 43-58.

Cioflica, G., Vlad, S., Volanschi, E., Stoici, S., 1977. Magnesian skarns and associated mineralization at Băiţa Bihor. Studii şi Cercetare Géologie Géofizică şi Géographie, Serie Géologie 22, 39-57.

Cioflica, G., Jude, R., Lupulescu, M., Simon, G., Damian, G., 1995. New data on the Bi-minerals from the mineralizations related to Palaeocene magmatites in Romania. Rom. J. Mineral. Deposita 76, 9-23.

Cioflica, G., Lupulescu, M., Shimizu, M., 1997. Bismuth minerals from the Băiţa Bihor and Valisor-Tincova Mines: New compositional data. Rom. J. Mineral Deposits 78, 13-14.

Cioflica, G., Jude, R., Berbeleac, I., Lupulescu, M., Costea, D., Costea, A., 1999. Epithermal gold mineralizations of low-sulfidation type from Baia de Aries Mine, Southern Apuseni Mountains, Romania. Rev. Roum. Géol. 43, 3-18.

Clarke, G., Burg, J., Wilson, C., 1986. Stratigraphic and structural constraints on the Proterozoic tectonic history of the Olary Block, South Australia. Precambr. Res. 34, 107-137.

Cocherie, A., Robert, M., 2008. Laser ablation coupled with ICP-MS applied to U–Pb zircon geochronology: a review of recent advances. Gondwana Res. 14, 597-608.

Coleman, R., 1959. New occurrences of ferroselite ($FeSe_2$). Geochim. Cosmochim. Acta 16, 296-301.

Coney, L., Moila, A. V., Quadling, A. G., 2012. Gem-quality diamonds: Source discrimination. S. Afr. J. Geol. 115, 33-46.

Constantinescu, E., Ilinca, G., Ilinca, A., 1988. Laramian hydrothermal alteration and ore deposition in the Oravita-Ciclova area. Southwestern Banat. DS Inst. Geol. Geofiz. 72-73, 13-26.

Cook, N. J., 1992. Antimony-rich mineral parageneses and their association with Au minerals within massive sulphide deposits at Sulitjelma, Norway. Neues Jahrb. Mineral. Montash. 3, 97-106.

Cook, N. J., 1993. Conditions of metamorphism estimated from alteration lithologies and ore at the Bleikvassli Zn-Pb-(Cu) deposit, Nordland, Norway. Norsk Geol. Tidsskr. 73, 226-233.

Cook, N. J., 1994. Post-recrystallisation phenomena in metamorphosed stratabound sulphide ores: a comment. Mineral. Mag. 58, 480-484.

Cook, N. J., 1996. Mineralogy of the sulphide deposits at Sulitjelma, northern Norway. Ore Geol. Rev. 11, 303-338.

Cook, N. J., 1997. Bismuth and bismuth-antimony sulphosalts from Neogene vein mineralisation, Baia Borsa area, Maramures, Romania. Mineral. Mag. 61, 387-409.

Cook, N. J., 2001. Ore mineralogical investigation of the Mofjell deposit (Mo i Rana, Nordland, Norway) with emphasis on gold and silver distribution. Norg. Geol. Unders. Report 2001.051, 31.

Cook, N. J., Chryssoulis, S. L., 1990. Concentrations of invisible gold in the common sulfides. Can. Mineral. 28, 1-16.

Cook, N. J., Ciobanu, C., 2001. Gold sulphosalt and telluride mineralogy of the Lega Dembi shear zone hosted gold deposit, Ethiopia. In: Piestrzynski, A., et al., Eds., Mineral deposits at the beginning of the 21st Century. Swets and Zeitlinger Publishers, Lisse, 719-722.

Cook, N. J., Ciobanu, C., 2003. Cervelleite, Ag_4TeS, from three localities in Romania, substitution of Cu, and the occurrence of the associated phase, Ag_2Cu_2TeS. Neues Jahrb. Mineral. Montatsh. 321-336.

Cook, N. J., Damian, G. S., 1997. New data on "plumosite" and other sulphosalt minerals from the Herja hydrothermal vein deposit, Baia Mare district, Rumania. Geol. Carpath. 48, 387-399.

Cook, N. J., Halls, C., Kaspersen, P. O., 1990. The geology of the Sulitjelma ore field, Northern Norway – some new interpretations. Econ. Geol. 85, 1720-1737.

Cook, N. J., Halls, C., Boyle, A. P., 1993. Deformation and metamorphism of massive sulphides at Sulitjelma, Norway. Mineral. Mag. 57, 67-81.

Cook, N. J., Spry, P. G., Vokes, F. M., 1998. Mineralogy and textural relationships among sulphosalts and related minerals in the Bleikvassli Zn-Pb-(Cu) deposit, Nordland, Norway. Mineral. Deposita 34, 35-56.

Cook, N. J., Ciobanu, C. L., Wagner, T., Stanley, C. J., 2007. Minerals of the system Bi-Te-Se-S related to the tetradymite archetype: Review of classification and compositional variation. Can. Mineral. 45, 665-708.

Cook, N. J., Ciobanu, C. L., Mao, J. W., 2009. Textural control on gold distribution in As-free pyrite from the Dongping, Huangtuliang and Hougou gold deposits, North China Craton, (Hebei Province, China). Chem. Geol. 264, 101-121.

Cook, N. J., Ciobanu, C. L., Pring, A., Skinner, W., Shimizu, M., Danyushevsky, L., Saini-Eidukat, B., Melcher, F., 2009. Trace and minor elements in sphalerite: A LA-ICPMS study. Geochim. Cosmochim. Acta 73, 4761–4791.

Cook, N. J., Ciobanu, C. L., Spry, P. G., Voudouris, P., and the participants of IGCP-486, 2009. Understanding gold-(silver)-telluride-(selenide) deposits. Episodes 32, 249-263.

Cook, N. J., Ciobanu, C. L., Danyushevsky, L. V., Gilbert, S., 2011. Minor elements in bornite and associated Cu-(Fe)-sulfides: a LA-ICPMS study. Geochim. Cosmochim. Acta 73, 4761-4791.

Cook, N. J., Sundblad, K., Valkama, M., Nygård, R., Ciobanu, C. L., Danyushevsky, L., 2011. Indium mineralisation in A-type granites in southeastern Finland: insights into mineralogy and partitioning between coexisting minerals. Chem. Geol. 284, 62-73.

Cook, N. J., Ciobanu, C. L., Brugger, J., Etschmann, B., Howard, D. J., de Jonge, M., Ryan, C. G., Paterson, D., 2012. Determination of the oxidation state of Cu in substituted Cu-In-Fe-bearing sphalerite via μ-XANES spectroscopy. Amer. Mineral. 97, 476–479.

Cook, N. J., Ciobanu, C. L., Meria, D., Silcock, D., Wade, B., 2013. Arsenopyrite-pyrite association in an orogenic gold ore: tracing mineralization history from textures and trace elements. Econ. Geol. 108, 1273–1283.

Cook, N. J., Ciobanu, C. L., O'Rielly, D., Wilson, K., Das, K., Wade, B., 2013. Mineral chemistry and element partitioning in hydrothermal Rare Earth Element (REE) mineralization, Browns Ranges, Western Australia. Lithos 172–173, 192–213.

Cook, N. J., Ciobanu, C. L., Giles, D., Wade B., 2013. Correlating textures and trace elements in ore minerals. Mineral deposit research for a high-tech world. Proceedings, 12th Biennial SGA Meeting, 12–15 August 2013, Uppsala, Sweden, 288-291.

Cook, N. J., Ciobanu, C. L., Ehrig, K., 2015. Insights into Zonation Within the Olympic Dam Cu-U-Au-Ag Deposit from Trace Element Signatures of Sulfide Minerals. Abstract, SEG 2016 Conference, Hobart, Tasmania.

Cook, N. J., Etschmann, B., Ciobanu, C. L., Geraki, K., Howard, D. L., Williams, T., Rae, N., Pring, A., Chen, G., Johannessen, B., Brugger, J., 2015. Distribution and substitution mechanism of Ge in a Ge-(Fe)-bearing sphalerite. Minerals 5, 117-132.

Cook, N. J., Ciobanu, C. L., 2015. Mineral hosts for critical metals in hydrothermal ores. In: Mineral Resources in a Sustainable World, Proceedings of the 13th Biennial SGA Conference, Nancy, France, 24–27 August 2015; Volume 5, 707-710.

Cook, N. J., Ciobanu, C. L., George, L., Zhu, Z., Wade, B., Ehrig, K., 2016. Trace element analysis of minerals in magmatic-hydrothermal ores by laser ablation inductively-coupled plasma mass spectrometry: approaches and opportunities. Minerals 6, 111.

Costagliola, P., Di Benedetto, F., Benvenuti, M., Bernardini, G. P., Cipriani, C., Lattanzi, P. F., Romanelli, M., 2003. Chemical speciation of Ag in galena by EPR spectroscopy. Amer. Mineral. 88, 1345–1350.

Courtney-Davies, L., Zhu, Z. Y., Ciobanu, C. L., Wade, B. S., Cook, N. J., Ehrig, K., Cabral, A. R., Kennedy, A., 2016. Matrix-matched iron-oxide laser ablation ICP-MS U-Pb geochronology using mixed solution standards. Minerals 6, 85. DOI: 10.3390/min6030085.

Craig, J. R., Kullerud, G., 1968. Phase relations and mineral assemblages in the copper lead sulfur system. Amer. Mineral. 53, 145-161.

Craig, J. R., Scott, S. D., 1976. Sulfide phase equilibria. In: Ribbe, P. H., Ed., Sulfide mineralogy. Reviews in Mineralogy vol. 1.

Dalpé, C., Hudon, P., Ballantyne, D. J., Williams, D., Marcotte, D., 2010. Trace element analysis of rough diamond by LA-ICP-MS: A case of source discrimination? J. Forensic Sci. 55, 1443-1456.

Danyushevsky, L., Robinson, P., Gilbert, S., Norman, M., Large, R., McGoldrick, P., Shelley, M., 2011. Routine quantitative multi-element analysis of sulphide minerals by laser ablation ICP-MS: Standard development and consideration of matrix effects. Geochem. Explor. Env. Anal. 11, 51-60.

Dare, S. A., Barnes, S. J., Prichard, H. M., Fisher, P. C., 2010. The timing and formation of platinum-group minerals from the Creighton Ni-Cuplatinum-group Element sulfide deposit, Sudbury, Canada: Early crystallization of PGE-rich sulfarsenides. Econ. Geol. 105, 1071-1096.

Dare, S. A. S., Barnes, S. J., Prichard, H. M., 2010. The distribution of platinum group elements (PGE) and other chalcophile elements among sulfides from the Creighton Ni–Cu–PGE sulfide deposit, Sudbury, Canada, and the origin of palladium in pentlandite. Mineral. Deposita 45, 765-793.

Dare, S. A., Barnes, S. J., Prichard, H. M., Fisher, P. C., 2011. Chalcophile and platinum-group element (PGE) concentrations in the sulfide minerals from the McCreedy East deposit, Sudbury, Canada, and the origin of PGE in pyrite. Mineral. Deposita 46, 381–407.

Dare, S. A. S., Barnes, S. J., Beaudoin, G., 2012. Variation in trace element content of magnetite crystallized from fractionating sulfide liquid, Sudbury, Canada: Implications for provenance discrimination. Geochim. Cosmochim. Acta 88, 27-50.

Dare, S. A. S., Barnes, S. J., Beaudoin, G., Méric, J., Boutroy, E., Potvin-Doucet, C., 2014. Trace elements in magnetite as petrogenetic indicators. Mineral. Deposita 49, 785-796.

Dare, S. A. S., Barnes, S. J., Prichard, H. M., Fisher, P. C., 2014. Mineralogy and geochemistry of Cu-rich ores from the McCreedy East Ni–Cu–PGE deposit (Sudbury, Canada): Implications for the behavior of platinum group and chalcophile elements at the end of crystallization of a sulfide liquid. Econ. Geol. 109, 343-366.

Dare, S. A. S., Barnes, S. J., Beaudoin, G., 2015. Did the massive magnetite “lava flows” of El

Laco (Chile) form by magmatic or hydrothermal processes? New constraints from magnetite composition by LA-ICP-MS. Mineral. Deposita 50, 607-617.

Darling, J. R., Storey, C. D., Engi, M., 2012. Allanite U-Th-Pb geochronology by laser ablation ICPMS. Chem. Geol. 292-293, 103-115.

Darling, J. R., Storey, C. D., Hawkesworth, C. J., Lightfoot, P. C., 2012. In-situ Pb isotope analysis of Fe–Ni–Cu sulphides by laser ablation multi-collector ICPMS: New insights into ore formation in the Sudbury impact melt sheet. Geochim. Cosmochim. Acta 99, 1-17.

Darrow, M. S., White, W. B., Roy, R., 1966. Phase relations in the system PbS-PbTe. Trans. Metall. Soc. AIME 236, 654-658.

De Marques Sá, C., Noronha, F., Ferreira da Silva, E., 2014. Factor analysis characterization of minor element contents in sulfides from Pb–Zn–Cu–Ag hydrothermal vein deposits in Portugal. Ore Geol. Rev. 62, 54-71.

De Paoli, G. R., Pattison, D. R. M., 2000. Thermobarometric calculation of peak metamorphic conditions of the Sullivan deposit. In: Lydon, J. W., Hoy, T., Slack, J. F., Knapp, M. E., Eds., The Geological Environment of the Sullivan Deposit, British Columbia. Geological Association of Canada, Mineral Deposits Division, Spec. Publ. 1, 272-280.

Debruyne, D., Hulsbosch, N., Muchez, P., 2016. Unraveling rare earth element signatures in hydrothermal carbonate minerals using a source—Sink system. Ore Geol. Rev. 72, 232-252.

Deditius, A. P., Reich, M., Kesler, S. E., Utsunomiya, S., Chryssoulis, S. L., Walshe, J., Ewing, R. C., 2014. The coupled geochemistry of Au and As in pyrite from hydrothermal ore deposits. Geochim. Cosmochim. Acta 140, 644-670.

Demir Y., Uysal I., Burhan Sadiklar M., Sipahi F., 2008. Mineralogy, mineral chemistry, and fluid inclusion investigation of Köstere hydrothermal vein-type deposit (Gümüşhane, NE Turkey). Neues Jahrb. Mineral. Abh. 185, 215-232.

Demir Y., Uysal İ., Sadıklar M. B., 2013. Mineral chemical investigation on sulphide mineralization of the Istala deposit, Gümüşhane, NE-Turkey. Ore Geol. Rev. 53, 306-317.

Deol, S., Deb, M., Large, R. R., Gilbert, S., 2012. LA-ICPMS and EPMA studies of pyrite, arsenopyrite and loellingite from the Bhukia-Jagpura gold prospect, southern Rajasthan, India: Implications for ore genesis and gold remobilization. Chem. Geol. 326-327, 72-87.

Deyell, C. L., Hedenquist, J. W., 2011. Trace element geochemistry of enargite in the Mankayan District, Philippines. Econ. Geol. 106, 1465-1478.

Di Benedetto, F., Bernardini, G. P., Costagliola, P., Plant, D., Vaughan, D. J., 2005. Compositional zoning in sphalerite crystals. Amer. Mineral. 90, 1384-1392.

Ding, L., Yang, G., Xia, F., Lenehan, C. E., Qian, G., McFadden, A., Brugger, J., Zhang, X., Chen, G., Pring, A., 2011. A LA-ICP-MS sulphide calibration standard based on a chalcogenide glass. Mineral. Mag. 75, 279-287.

Djon, M. L. N., Barnes, S. J., 2012. Changes in sulfides and platinum group minerals with the degree of alteration in the Roby, Twilight, and High Grade Zones of the Lac des Iles Complex, Ontario, Canada. Mineral. Deposita 47, 875-896.

Dmitrieva, M. T., Bojik, G. B., 1988. The crystallochemical mechanism of formation of vacancies in goldfieldite structure. Zeitschrift Krist. 185, 601.

Dobbe, R. T., 1992. Manganoan-cadmian tetrahedrite from the Tunaberg Cu-Co deposit, Bergslagen, central Sweden. Mineral. Mag. 56, 113-115.

Donnay, G., Corliss, L. M., Donnay, J. D. H., Elliott, N., Hastings, J. M., 1958. Symmetry of Magnetic Structures: Magnetic Structure of Chalcopyrite. Phys. Rev. 112, 1917-1923.

Donovan, J. J., 2014. Probe for EPMA: Acquistion, automation and analysis. Ver. 10.3.5 Xtreme Edition, Probe Software, Inc., Oregon, United States of America.

Downs, A. J., 1993. Chemistry of Aluminium, Gallium, Indium, and Thallium. Springer, Berlin, 526 pp.

Dragov, P., Petrunov, R., 1996. Elazite porphyry copper-precious metals (Au and PGE) deposit. Proceedings, Annual Meeting of IGCP Project 356, Sofia, Bulgaria, 171-175.

Duchesne, J. C., Rouhart, A., Schoumacher, C., Dillen, H., 1983. Thallium, nickel, cobalt and other trace elements in iron sulfides from Belgian lead-zinc vein deposits. Mineral. Deposita 18, 303-313.

Dupuis, C., Beaudoin, G., 2011. Discrimination diagrams for iron oxide trace element fingerprinting of mineral deposit types. Mineral. Deposita 46, 319-335.

Duran, C. J., Barnes, S. J., Corkery, J. T., 2015. Chalcophile and platinum-group element distribution in pyrites from the sulfide-rich pods of the Lac des Iles Pd deposits, Western Ontario, Canada: Implications for post-cumulus re-equilibration of the ore and the use of pyrite compositions in exploration. J. Geochem. Explor. 158, 223-242.

Duran, C. J., Barnes, S. -J., Corkery, J. T., 2016. Trace element distribution in primary sulfides and Fe–Ti oxides from the sulfide-rich pods of the Lac des Iles Pd deposits, Western Ontario, Canada: Constraints on processes controlling the composition of the ore and the use of pentlandite compositions in exploration. J. Geochem. Explor. 166, 45-63.

Edelstein, O., Bernad, A., Kovacs, M., Crihan, M., Pécskay, Z., 1992. Preliminary data regarding the K-Ar ages of some eruptive rocks from Baia Mare Neogene volcanic zone. Rev. Roum. Geol. 36, 45-60.

Ehrig, K., McPhie, J., Kamenetsky, V., 2012. Geology and mineralogical zonation of the Olympic Dam Iron Oxide Cu-U-Au-Ag deposit, South Australia. In: Geology and Genesis of Major Copper Deposits and Districts of the World: A Tribute to Richard H. Sillitoe; Hedenquist, J. W., Harris, M., Camus, F., Eds., Society of Economic Geologists Special Publication vol. 12: Littleton, CO, USA, 237-267.

Emslie, D., Beukes, G., 1981. Minor-and trace-element distribution in sphalerite and galena from the Otavi Mountainland, South West Africa. Ann. Geol. Surv. Republic of South Africa 15, 11-28.

Eugster, H. P., 1986. Minerals in hot water. Amer. Mineral. 71, 655-673.

Feng, R., Machado, N., Ludden, J., 1993. Lead geochronology of zircon by laserprobe-inductively coupled plasma-mass spectrometry (LP-ICP-MS). Geochim. Cosmochim. Acta 57, 3479–3486.

Ferry, J., Watson, E., 2007. New thermodynamic models and revised calibrations for the Ti-in-zircon and Zr-in-rutile thermometers. Contrib. Mineral. Petrol. 154, 429–437.

Fialin, M., Rémy, H., Richard, C., Wagner, C., 1999. Trace element analysis with the electron microprobe: new data and perspectives. Amer. Mineral. 84, 70-77.

Figueiredo, M. O., Silva, T. P., de Oliveira, D. P. S., Rosa, D. R. N., 2007. Searching for In-carrier minerals in polymetallic sulphide deposits: Digging deeper into the crystal chemistry of indium chalcogenides. In: Digging Deeper, Proceedings of the 9th Biennial SGA Meeting, Ferrara, Italy, 29–31 August 2007; Andrew, C. J., Ed., Irish Association Economic Geologists: Dublin, Ireland, 1355-1358.

Fiori, M., Garbarino, C., Grillo, S., Solomon, T., Valera, R., 1988. Mineral paragenesis in the Au-Ag-Cu-Zn-Pb-Te deposit of Lega Dembi (Ethiopia). Proceedings, Bicentennial Gold, Melbourne, Australia, 184-186.

Flanagan, F. J., 1976. Descriptions and Analysis of Eight New USGS Rock Standards; U.S. Geological Survey Professional Paper; U.S. Government Printing Office: Washington, DC, USA, Volume 840.

Fleet, M. E., 2006. Phase equilibria at high temperatures. Rev. Mineral. Geochem. 61, 365-419.

Fleet M. E., Mumin A. H., 1997. Gold-bearing arsenian pyrite and marcasite and arsenopyrite from Carlin Trend gold deposits and laboratory synthesis. Amer. Mineral. 82, 182–193.

Fleet, M. E., Chryssoulis, S. L., Stone, W. E., Weisener, C. G., 1993. Partitioning of platinum-group elements and Au in the Fe− Ni− Cu− S system: experiments on the fractional crystallization of sulfide melt. Contrib. Mineral. Petrol. 115, 36-44.

Fleet, M. E., Crocket, J. H., Liu, M., Stone, W. E., 1999. Laboratory partitioning of platinum-group elements (PGE) and gold with application to magmatic sulfide–PGE deposits. Lithos 47, 127-142.

Fleischer, M., 1955. Minor elements in some sulphide minerals. Econ. Geol. Fiftieth Anniversary Volume: 1905-1955. 970-1024.

Flood, B., 1967. Sulphide mineralizations within the Hecla Hoek complex in Vestspitsbergen and Bjørnøya. Norsk Polarinst. Årbok 1967, 109-127.

Foit, F. F. Jr., Hughes, M. J., 2004. Structural variations in mercurian tetrahedrite. Amer. Mineral. 89, 159-163.

Foord, E. E., Shawe, D. R., 1989. The Pb-Bi-Ag-Cu-(Hg) chemistry of galena and some associated sulfosalts; a review and some new data from Colorado, California and Pennsylvania. Can. Mineral. 27, 363–382.

Foord, E. E., Shawe, D. R., Conklin, N. M., 1988. Coexisting galena, PbSss and sulfosalts: evidence for multiple episodes of mineralization in the Round Mountain and Manhattan gold districts, Nevada. Can. Mineral. 26, 355–376.

Förster, H. J., Rhede, D., Tischendorf, G., 2002. Continuous solid-solution between mercurian giraudite and hakite. Can. Mineral. 40, 1161-1170.

Fountain, C., 2013. The whys and wherefores of penalty elements in copper concentrates. In: MetPlant 2013: Metallurgical Plant Design and Operating Strategies, Volume 5. Australasian Institute of Mining and Metallurgy, Melbourne, 502-518.

Frenzel, M., Hirsch, T., Gutzmer, J., 2016. Gallium, germanium, indium, and other trace and minor elements in sphalerite as a function of deposit type — A meta-analysis. Ore Geol. Rev. 76, 52-78.

Friedl J., Wagner F. E., Wang N., 1995. On the chemical state of combined gold in sulfidic ores: Conclusions from Mössbauer source experiments. Neues Jahrb. Mineral. Abh. 169, 279–290.

Frost, B. R., Mavrogenes, J. A., Tomkins, A. G., 2002. Partial melting of sulphide ore deposits during medium-and high-grade metamorphism. Can. Mineral. 40, 1-18.

Frost, B. R., Swapp, S. M., Gregory, R. W., 2005. Prolonged existence of sulphide melt in the Broken Hill orebody, New South Wales, Australia. Can. Mineral. 43, 479-493.

Fryer, B. J., Jackson, S., Longerich, H., 1993. The application of laser ablation microprobe-inductively coupled plasma-mass spectrometry (LAM-ICP-MS) to in situ (U)–Pb geochronology. Chem. Geol. 109, 1–8.

Fryer, B. J., Jackson, S. E., Longerich, H. P., 1995. Design, operation and role of the Laser-Ablation Microprobe coupled with an Inductively-Coupled Plasma - Mass-Spectrometer (LAM-ICP-MS) in the earth-sciences. Can. Mineral. 33, 303-312.

Fu, Y., Sun, X. M., Zhou, H. Y., Lin, H., Yang, T. J., 2016. In-situ LA–ICP–MS U–Pb geochronology and trace elements analysis of polygenetic titanite from the giant Beiya gold–polymetallic deposit in Yunnan Province, Southwest China. Ore Geol. Rev. 77, 43-56.

Fujiki, Y., 1963. Study on the Nickel-and Cobalt-bearing Sulphide Minerals from the Komori Mine by Means of Electron Probe Microanalyzer. Mining Geol. 13, 333-338.

Gäbler, H. E., Rehder, S., Bahr, A., Melcher, F., Goldmann, S., 2013. Cassiterite fingerprinting by LA-ICP-MS. J. Anal. Atom. Spectrom. 28, 1247-1255.

Gagnevin, D., Menuge, J. F., Kronz, A., Barrie, C., Boyce, A. J., 2014. Minor Elements in Layered Sphalerite as a Record of Fluid Origin, Mixing, and Crystallization in the Navan Zn–Pb Ore Deposit, Ireland. Econ. Geol. 109, 1513-1528.

Gagnon, J. E., Samson, I. M., Fryer, B. J., Williams-Jones, A. E., 2003. Compositional heterogeneity in fluorite and the genesis of fluorite deposits: Insights from LA-ICP-MS analysis. Can. Mineral. 41, 365-382.

Gallego Hernández, A. N., Akasaka, M., 2010. Ag-rich Tetrahedrite in the El Zancudo Deposit, Colombia: Occurrence, Chemical Compositions and Genetic Temperatures. Resource Geol. 60, 218–233.

Garbe-Schönberg, D., Müller, S., 2014. Nano-particulate pressed powder tablets for LA-ICP-MS. J. Anal. Atom. Spectrom. 29, 990-1000.

Garbe-Schönberg, D., Müller, S., Nordstad, S., Schönberg, L., 2015. Particle size matters: A new strategy for manufacturing microanalytical reference standards from nano-particulate powder pellets. In: Proceedings of the 9th International Conference on the Analysis of Geological and Environmental Materials, Leoben, Austria, 8–14 August 2015; Abstract OP-25, 64.

Garcia, C. C., Lindner, H., von Bohlen, A., Vadla, C., Niemax, K., 2008. Elemental fractionation and stoichiometric sampling in femtosecond laser ablation. J. Anal. Atom. Spectrom. 23, 470-478.

Gaspar, O. C., 2002. Mineralogy and sulfide mineral chemistry of the Neves-Corvo ores, Portugal: Insight into their genesis. Can. Mineral. 40, 611-636.

Gaspar, M., Knaack, C., Meinert, L. D., Moretti, R., 2008. REE in skarn systems: a LA-ICP-MS study of garnets from the Crown Jewel gold deposit. Geochim. Cosmochim. Acta 72, 185–205.

Gasparrini, C., 1983. The mineralogy of gold and its significance in metal extraction. Canad. Inst. Mining Metall. 76, 144-153.

Gena K., Chiba H., Kase K., Nakashima K., Ishiyama D., 2013. The Tiger Sulfide Chimney, Yonaguni Knoll IV Hydrothermal Field, Southern Okinawa Trough, Japan: The first reported occurrence of Pt–Cu–Fe-bearing bismuthinite and Sn-bearing chalcopyrite in an active seafloor hydrothermal system. Resour. Geol. 63, 360-370.

Genna, D., Gaboury, D., 2015. Deciphering the hydrothermal evolution of a VMS system by LA-ICP-MS using trace elements in pyrite: An example from the Bracemac-Mcleod deposits, Abitibi, Canada, and Implications for Exploration. Econ. Geol. 110, 2087-2108.

George, L., Cook, N. J., Ciobanu, C. L., Wade, B., 2015. Trace and minor elements in galena: A reconnaissance LA-ICP-MS study. Amer. Mineral. 100, 548-569.

George, L. L., Cook, N. J., Ciobanu, C. L., 2016. Partitioning of trace elements in co-crystallized sphalerite–galena–chalcopyrite hydrothermal ores. Ore Geol. Rev. 77, 97-116.

George, L. L., Cook, N. J., Crowe, B. B. P., Ciobanu, C. L., in press. Trace elements in hydrothermal chalcopyrite. Mineral. Mag.

Georgiev, G., 2008. A genetic model of the Elatsite porphyry copper deposit, Bulgaria. Geochem. Mineral. Petrol. 46, 143-160.

Geoscience Australia, 2015. Copper Fact Sheet. Australian atlas of minerals resources, mines and processing centres, Geoscience Australia, Commonwealth of Australia. Viewed 8 September 2016, <http://www.australianminesatlas.gov.au/education/fact_sheets/copper.html>

Gerth, J., 1990. Unit-cell dimensions of pure and trace metal-associated goethites. Geochim. Cosmochim. Acta 54, 363-371.

Gheorghitescu, D., 1975. Mineralogical and geochemical study of formations in the thermal, metasomatic contact at Oravita (Cosovita). DS Inst. Geol. Geofiz. 61, 59-103.

Ghiţulescu, T. P., Socolescu, M., 1941. Étude géologique et miniére des Monts Metalliféres (Quadrilatère aurifère et régions environnantes). An. Inst. Geol. 21, 181-464.

Ghosal, S., Sack, R. O., 1999. Bi-Sb energetics in sulfosalts and sulfides. Mineral. Mag. 63, 723-733.

Giaccherini, A., Montegrossi, G., Di Benedetto, F., 2016. Stability of Naturally Relevant Ternary Phases in the Cu–Sn–S System in Contact with an Aqueous Solution. Minerals 6, 79.

Gibson, G. M., Nutman, A. P., 2004. Detachment faulting and bimodal magmatism in the Palaeoproterozoic Willyama Supergroup, south–central Australia: keys to recognition of a multiply deformed Precambrian metamorphic core complex. J. Geol. Soc. 161, 55-66.

Gilbert, S., Danyushevsky, L., Robinson, P., Wohlgemuth-Ueberwasser, C., Pearson, N., Savard, D., Norman, M., Hanley, J., 2013. A comparative study of five reference materials and the Lombard meteorite for the determination of the platinum-group elements and gold by LA-ICP-MS. Geostand. Geoanal. Res. 37, 51-64.

Gilbert, S. E., Danyushevsky, L. V., Goemann, K., Death, D., 2014. Fractionation of sulphur relative to iron during laser ablation-ICP-MS analyses of sulphide minerals: implications for quantification. J. Anal. Atom. Spectrom. 29, 1024-1033.

Gilbert, S. E., Danyushevsky, L. V., Rodemann, T., Shimizu, N., Gurenko, A., Meffre, S., Thomas, H., Large, R. R., Death, D., 2014. Optimisation of laser parameters for the analysis of sulphur isotopes in sulphide minerals by laser ablation ICP-MS. J. Anal. Atom. Spectrom. 29, 1042-1051.

Giuli, G., Paris, E., Wu, Z., De Panfilis, S., Pratesi, G., Cipriani, C., 2005. The structural role of Ag in galena (PbS). A XANES study. Phys. Scripta T115, 387–389.

Giussani, B., Monticelli, D., Rampazzi, L., 2009. Role of laser ablation-inductively coupled plasma-mass spectrometry in cultural heritage research: A review. Anal. Chim. Acta 635, 6-21.

Godel, B., Barnes, S. J., 2008. Platinum-group elements in sulphide minerals and the whole rocks of the J-M Reef (Stillwater Complex): Implication for the formation of the reef. Chem. Geol. 248, 272-294.

Godel, B., Barnes, S. J., Maier, W. D., 2007. Platinum-group elements in sulphide minerals, platinum-group minerals, and whole-rocks of the Merensky Reef (Bushveld Complex, South Africa): Implications for the formation of the reef. J. Petrol. 48, 1569-1604.

Goh, S. W., Buckley, A. N., Lamb, R. N., Rosenberg, R. A., Moran, D., 2006. The oxidation states of copper and iron in mineral sulfides, and the oxides formed on initial exposure of chalcopyrite and bornite to air. Geochim. Cosmochim. Acta 70, 2210-2228.

Goldmann, S., Melcher, F., Gäbler, H. E., Dewaele, S., De Clerq, F., Muchez, P., 2013. Mineralogy and Trace Element Chemistry of Ferberite/Reinite from Tungsten Deposits in Central Rwanda. Minerals 3, 121-144.

Goldschmidt, V. M., 1954. Geochemistry. Soil Sci. 78, 156.

Gołębiowska, B., Pieczka, A., Parafiniuk, J., 2012. Substitution of Bi for Sb and As in minerals of the tetrahedrite series from Rędziny, Lower Silesia, southwestern Poland. Can. Mineral. 50, 267-279.

Gottesmann, W., Kampe, A., 2007. Zn/Cd ratios in calcsilicate-hosted sphalerite ores at Tumurtijn-ovoo, Mongolia. Chem. Erde-Geochem. 67, 323-328.

Gotz, A., Damian, G., Farbas, N., 1990. Contributii la mineralogia bournonitul associat mineralizatiilor din masivul Toroiaga-Baia Borsa. Rev. Mineral. 41, 467-471.

Graham, G. E., Kelley, K. D., Slack, J. F., Koenig, A. E., 2009. Trace elements in Zn-Pb-Ag deposits and related stream sediments, Brooks Range Alaska, with implications for Tl as a pathfinder element. Geochem. Explor. Env. A. 9, 19-37.

Greenfield, J. E., Lees, T. C., Parr, J. M., McConachy, T. F., 2003. A review of Broken Hill ore system models. Geoscience Australia Record 2003/13, 57-60.

Gregory, C. J., Rubatto, D., Hermann, J., Berger, A., Engi, M., 2012. Allanite behaviour during incipient melting in the southern Central Alps. Geochim. Cosmochim. Acta 84, 433-458.

Gregory, D. D., Large, R. R., Halpin, J. A., Lounejeva Baturina, E., Lyons, T. W., Wu, S., Danyushevsky, L., Sack, P. J., Chappaz, A., Maslennikov, V. V., Bull, S. W., 2015. Trace element content of sedimentary pyrite in black shales. Econ. Geol. 110, 1389-1410.

Gros, K., Słaby, E., Förster, H. -J., Michelak, P. P., Munnik, F., Gδtze, J., Rhede, D., 2016. Visualization of trace-element zoning in fluorapatite using BSE and CL imaging, and EPMA and μPIXE/μPIGE mapping. Mineral. Petrol. 110, 809-821.

Groves, D. I., Bierlein, F. P., Meinert, L. D., Hitzman, M. W., Iron oxide copper-gold (IOCG) deposits through earth history: Implications for origin, lithospheric setting, and distinction from other epigenetic iron oxide deposits. Econ. Geol. 2010, 105, 641–654.

Günther, D., Koch, J., 2008. Formation of aerosols generated by laser ablation and their impact on elemental fractionation in LA–ICP–MS. In: Sylvester, P., Ed., Laser Ablation ICP-MS in the Earth Sciences: Current Practices and Outstanding Issues. Mineralogical Association of Canada Short Course Volume 40, 19-34.

Günther, D., von Quadt, A., Wirz, A., Cousin, H., Dietrich, V. J., 2001. Elemental analyses using laser ablation-inductively coupled plasma-mass spectrometry (LA-ICP-MS) of geological samples fused with $Li_2B_4O_7$ and calibrated without matrix-matched standards. Mikrochim. Acta 136, 101–107.

Hackbarth, C. J., Petersen, U., 1984. A fractional crystallization model for the deposition of

argentian tetrahedrite. Econ. Geol. 79, 448-460.

Hall, S. R., Stewart, J. M., 1973. The crystal structure refinement of chalcopyrite, $CuFeS_2$. Acta Crystallogr. 29, 579-585.

Hamilton, J., Bishop, D., Morris, H., Owens, O., 1982. Geology of the Sullivan orebody, Kimberley, BC, Canada. In: Hutchinson, R. W., Spence, C. D., Franklin, J. M., Eds., Precambrian Sulphide Deposits. Geol. Assoc. Canada, Spec. Paper 25, 597-665.

Hanley, J. J., Bray, C. J., 2009. The trace metal content of amphibole as a proximity indicator for Cu–Ni–PGE mineralization in the footwall of the Sudbury Igneous Complex, Ontario, Canada. Econ. Geol. 104, 113-125.

Hannan, K. W., Golding, S. D., Herbert, H. K., Krouse, H. R., 1993. Contrasting alteration assemblages in metabasites from Mount Isa, Queensland; implications for copper ore genesis. Econ. Geol. 88, 1135-1175.

Hansen, M. K., Makovicky, E., Karup-Møller, S., 2003. Exploratory studies on substitutions in tennantite-tetrahedrite solid solution. Part IV. Substitution of germanium and tin. Neues Jahrb. Mineral. Abh. J. Mineral. Geochem. 179, 43-71.

Harris, D. C., 1990. The mineralogy of gold and its relevance to gold recoveries. Mineral. Deposita 25, S3-S7.

Harris D. C., Cabri L. J., Nobiling R., 1984. Silver bearing chalcopyrite, a principal source of silver in the Izok lake massive-sulfide deposit: confirmation by electron and proton-microprobe analyses. Can. Mineral. 22, 493-498.

Harrison, P. G., 1989. Chemistry of Tin. Blackie & Son Limited.

Hayden, L. A., Watson, E. B., Wark, D. A., 2008. A thermobarometer for sphene (titanite). Contrib. Mineral Petrol. 155, 529–540.

Haydon, R. C., McConachy, G. W., 1987. The stratigraphic setting of Pb-Zn-Ag mineralization at Broken Hill. Econ. Geol. 82, 826-856.

Hazarika, P., Mishra, B., Pruseth, K. L., 2016. Scheelite, apatite, calcite and tourmaline compositions from the late Archean Hutti orogenic gold deposit: Implications for analogous two stage ore fluids. Ore Geol. Rev. 72, 989-1003.

He, H. L., Yu, S. Y., Song, X. Y., Du, Z. S., Dai, Z. H., Zhou, T., Xie, W., 2016. Origin of nelsonite and Fe–Ti oxides ore of the Damiao anorthosite complex, NE China: Evidence from trace element geochemistry of apatite, plagioclase, magnetite and ilmenite. Ore Geol. Rev. 79, 367-381.

Hedström, P., Simeonov, A., Malmstrom, L., 1989. The Zinkgruvan ore deposit, south-central Sweden; a Proterozoic, proximal Zn-Pb-Ag deposit in distal volcanic facies. Econ. Geol. 84, 1235-1261.

Heidarian, H., Lentz, D., Alirezaei, S., Peighambari, S., Hall, D., 2016. Using the chemical analysis of magnetite to constrain various stages in the formation and genesis of the Kiruna-type chadormalu magnetite-apatite deposit, Bafq district, Central Iran. Mineral. Petrol. 110, 927-942.

Heinrich, C. A., Pettke, T., Halter, W. E., Aigner-Torres, M., Audétat, A., Günther, D., Hattendorf, B., Bleiner, D., Guillong, M., Horn, I., 2003. Quantitative multi-element analysis of minerals, fluid and melt inclusions by laser-ablation inductively-coupled-plasma mass-spectrometry. Geochim. Cosmochim. Acta 67, 3473-3497.

Helmy, H. M., Ballhaus, C., Wohlgemuth-Ueberwasser, C., Fonseca, R. O., Laurenz, V., 2010. Partitioning of Se, As, Sb, Te and Bi between monosulfide solid solution and sulfide melt–application to magmatic sulfide deposits. Geochim. Cosmochim. Acta 74, 6174-6179.

Helmy H. M., Shalaby I. M., Rahman H. A., 2014. Large-scale metal zoning in a late-Precambrian skarn-type mineralization, Wadi Kid, SE Sinai, Egypt. J. Afr. Earth Sci. 90, 77-86.

Henley, K. J., 1975. Gold-ore mineralogy and its relation to metallurgical treatment. Minerals Sci. Eng. 7, 289-312.

Hinchey, J. G., Wilton, D. H. C., Tubrett, M. N., 2003. A LAM-ICP-MS Study of the Distribution of Gold in arsenopyrite from the Lodestar Prospect, Newfoundland, Canada. Can. Mineral. 41, 353-364.

Hoda, S. N., Chang, L. L. Y., 1975. Phase relations in the systems PbS-Ag_2S-Sb_2S_3 and PbS-Ag_2S-Bi_2S_3. Amer. Mineral. 60, 621-633.

Hoffman, J. I., 1934. Preparation of pure gallium. Bur. Stand. J. Res. 13, 665.

Holwell, D. A., McDonald, I., 2007. Distribution of platinum-group elements in the Platreef at Overysel, northern Bushveld Complex: A combined PGM and LA-ICP-MS study. Contrib. Mineral. Petrol. 154, 171-190.

Holwell, D., McDonald, I., 2010. A review of the behaviour of platinum group elements within natural magmatic sulphide ore systems. Platin. Met. Rev. 54, 26–36.

Holwell, D. A., Keays, R. R., McDonald, I., Williams, M. R., 2015. Extreme enrichment of Se, Te, PGE and Au in Cu sulfide microdroplets: Evidence from LA-ICP-MS analysis of sulfides in the Skaergaard Intrusion, east Greenland. Contrib. Mineral. Petrol. 170, 1-26.

Huang, X. W., Zhou, M. F., Qiu, Y. Z., Qi, L., 2015. In-situ LA-ICP-MS trace elemental analyses of magnetite: The Bayan Obo Fe-REE-Nb deposit, North China. Ore Geol. Rev. 65, 884-899.

Huiwen, J. D. F. Z. Z., Chunpei, Z., 1988. The first Discovery of Cd-Freibergite in China. Acta Mineral. Sin. 2, 005.

Huston, D. L., Sie, S. H., Suter, G. F., Cooke, D. R., Both, R. A., 1995. Trace elements in sulphide minerals from eastern Australian volcanic-hosted massive sulphide deposits; Part I, Proton microprobe analyses of pyrite, chalcopyrite, and sphalerite, and Part II, Seleni- um levels in pyrite; comparison with delta 34 S values and implications for the source of sulfur

in volcanogenic hydrothermal systems. Econ. Geol. 90, 1167–1196.

Huston D. L., Jablonski W., Sie S. H., 1996. The distribution and mineral hosts of silver in eastern Australian volcanogenic massive sulfide deposits. Can. Mineral. 34, 529-546.

Ilinca, G., Makovicky, E., 1999. Bismuth sulphotellurides in the Banatitic Province, Romania. Mineralogy in the System of Earth Sciences, Abstract volume, University of Bucharest, 40-41.

Ilinca, G., Makovicky, E., Topa, D., Zagler, G., 2012. Cuproneyite, Cu_7Pb_{27} $Bi_{25}S_{68}$, a new mineral species from Băiţa Bihor, Romania. Can. Mineral. 50, 353-370.

Ingham, E. S., Cook, N. J., Cliff, J., Ciobanu, C. L., Huddleston, A., 2014. A combined chemical, isotopic and microstructural study of pyrite from roll-front uranium deposits, Lake Eyre Basin, South Australia. Geochim. Cosmochim. Acta 125, 440-465.

Islamov, F., Kremenetsky, E., Minzer, E., Koneev, R., 1999. The Kochbulak- Kairagach ore field. In: Shayakubov, T., Islamov, F., Kremenetshy, A., Seltmann, R., Eds., Au, Ag, and Cu deposits of Uzbekistan; Excursion Guidebook. International Field Conference of IGCP-373, Joint SGA-IAGOD symposium, Excursion B6, IGCP-SGA-IAGOD.

Ismail, R., Ciobanu, C. L., Cook, N. J., Schmidt Mumm, A., Wade, B., Giles, D., Teale, G. S., 2014. Rare Earths and other trace elements in minerals from skarn assemblages, Hillside iron oxide-copper-gold deposit, Yorke Peninsula, South Australia. Lithos 184-187, 456-477.

Ixer, R. A., Stanley, C. J., 1983. Silver mineralization at Sark's Hope mine, Sark, Channel Islands. Mineral. Mag. 47, 539-545.

Jackson, S. E., Fryer, B. J., Gosse, W., Healey, D. C., Longerich, H. P., Strong, D. F., 1990. Determination of the precious metals in geological materials by ICP-MS with nickel sulfide fire assay collection and tellurium coprecipitation. Chem. Geol. 83, 119-132.

Jackson, S. E., Günther, D., 2003. The nature and sources of laser induced isotopic fractionation in laser ablation-multicollector-inductively coupled plasma-mass spectrometry. J. Anal. Atom. Spectrom. 18, 205-212.

Janković, S., 1990. Types of copper deposits related to volcanic environment in the Bor district, Yugoslavia. Geol. Rundsch. 79, 467-478.

Janković, S., Herrington, R. J., Kozelj, D., 1998. The Bor and Majdanpek copper–gold deposits in the context of the Bor metallogenic zone (Serbia, Yugoslavia). In: Porter, T. M., Ed., Porphyry and hydrothermal copper and gold deposits; a global perspective; conference proceedings. Australian Mineral Foundation, Glenside, South Australia, 169-178.

Jaques, A. L., 2016. Major and trace element variations in oxide and titanate minerals in the West Kimberley lamproites, Western Australia. Mineral. Petrol. 110, 159-197.

Jenner, F. E., Arevalo, R. D., 2016. Major and Trace Element Analysis of Natural and Experimental Igneous Systems using LA–ICP–MS. Elements 12, 311-316.

Jenner, F. E., O'Neill, H. S. C., 2012. Major and trace analysis of basaltic glasses by laser-ablation ICP-MS. Geochem. Geophys. 13, DOI: 10.1029/2011GC003890.

Jensen, M. L., Whittle, A. W. G., 1969. Sulfur isotopes of the Nairne pyrite deposit, South Australia. Mineral. Deposita 4, 241-247.

Jeppsson, M. L., 1989. Mineral chemistry of silver in antimony and bismuth rich sulphide ore in Bergslagen, central Sweden. Neues Jahrb. Mineral. Monatsh. 5, 205–216.

Jiang, T., Ozin, G. A., 1998. New directions in tin sulfide materials chemistry. J. Mater. Chem. 8, 1099-1108.

Jochum, H. P., Willbold, M., Raczek, I., Stoll, B., Herwig, K., 2005. Chemical characterisation of the USGS Reference Glasses GSA-1G, GSC-1G, GSD-1G, GSE-1G, BCR-2G, BHVO-2G and BIR-1G using EPMA, ID-TIMS, ID-ICP-MS and LA-ICP-MS. Geostand. Geoanal. Res. 29, 285-302.

Jochum, K. P., Weis, U., Stoll, B., Kuzmin, D., Yang, Q., Raczek, I., Jacob, D. E., Stracke, A., Birbaum, K., Frick, D. A., 2011. Determination of reference values for NIST SRM 610–617 glasses following ISO guidelines. Geostand. Geoanal. Res. 35, 397-429.

Johan, Z., 1988. Indium and germanium in the structure of sphalerite: an example of coupled substitution with copper. Mineral. Petrol. 39, 211–229.

Johan, Z., Kvaček, M., 1971. La hakite, un nouveau minéral du groupe de la tétraédrite. Bull. Soc. Fr. Minéral. 94, 45-48. (In French)

Johan, Z., Picot, P., Ruhlmann, F., 1982. Evolution paragénétique de la minéralisation uranifère de Chaméane (Puy-de-Dôme) France: Chaméanite, geffroyite et giraudite, trois séléniures nouveaux de Cu, Fe, Ag, and As. Tscher. Mineral. Petrogr. Mitt. 29, 151-167. (In French)

Johnson, M. L., Burnham, C. W., 1985. Crystal structure refinement of an arsenic-bearing argentian tetrahedrite. Amer. Mineral. 70, 165-170.

Johnson, N. E., Craig, J. R., Rimstidt, J. D., 1986. Compositional trends in tetrahedrite. Can. Mineral. 24, 385-397.

Johnson, N. E., Craig, J. R., Rimstidt, J. D., 1988. Crystal chemistry of tetrahedrite. Amer. Mineral. 73, 389-397.

Jugo, P. J., Candela, P. A., Piccoli, P. M., 1999. Magmatic sulfides and Au: Cu ratios in porphyry deposits: an experimental study of copper and gold partitioning at 850 C, 100 MPa in a haplogranitic melt–pyrrhotite–intermediate solid solution–gold metal assemblage, at gas saturation. Lithos 46, 573-589.

Junge, M., Wirth, R., Oberthür, T., Melcher, F., 2015. Mineralogical siting of platinum-group elements in pentlandite from the Bushveld Complex, South Africa. Mineral. Deposita 50, 41-54.

Jurković, I. B., Garašić, V., Jurković, I. M., 2011. Geochemical characteristics of mercurian tetrahedrite, barite and fluorite from the Duboki Vagan, Glumac and Dubrave-Dugi Dol barite deposits, south of Kreševo, Mid-Bosnian Schist Mts. Geol. Croat. 64, 49-59.

Jurković, I. B., Garašić, V., Jurković, I. M., 2011. Cobalt, nickel, wolfram, cadmium, selenium, silver and gold-bearing mercurian tetrahedrite from the Saski Rad barite-siderite deposit in the Mid-Bosnian Schist Mts. Geol. Croat. 64, 223-237.

Kalbskopf, R., 1974. Synthese und Kristallstruktur von $Cu_{12-x}Te_4S_{13}$, dem Tellur-Endglied der Fahlerze. Tscher. Mineral. Petrogr. Mitt. 21, 1-10. (In German)

Kano, S., Nambu, M., 1967. The study of the equilibrium in the system FeS-S_2 (I) Dissociation equilibrium of pyrite at the low temperature. J. Jap. Assoc. Mineral. Petrol. Econ. Geol. 57, 81-97.

Karup-Møller, S., 2003. Exploratory studies on element substitutions in synthetic tetrahedrite. Part V. Mercurian tetrahedrite. Neues Jahrb. Mineral. Abh. 179, 73-83.

Karup-Møller, S., Makovicky, E., 1999. Exploratory studies of element substitutions in synthetic tetrahedrite. Part II. Selenium and tellurium as anions in Zn-Fe tetrahedrites. Neues Jahrb. Mineral. Abh. 9, 385-399.

Karup-Møller, S., Makovicky, E., 2004. Exploratory studies of the solubility of minor elements in tetrahedrite: VI. Zinc and the combined zinc-mercury and iron-mercury substitutions. Neues Jahrb. Mineral. Monatsh. 11, 508-524.

Kase, K., 1986. Tellurian tennantite from the Besshitype deposits in the Sambagawa metamorphic belt, Japan. Can. Mineral. 24, 399-404.

Kase K., 1987. Tin-bearing chalcopyrite from the Izumo vein, Toyoha Mine, Hokkaido, Japan. Can. Mineral. 25, 9-13.

Katona, I., Pascal, M. -L., Fonteilles, M., Verkaeren, J., 2003. The melilite (Gh_{50}) skarns of Oraviţa, Banat, Romania: transition to gehlenite (Gh_{85}) and to vesuvianite. Can. Mineral. 41, 1255-1270.

Keays, R. R., Campbell, I. H., 1981. Precious metals in the Jimberlana Intrusion, Western Australia: Implications for the genesis of platiniferous ores in layered intrusions. Econ. Geol. 76, 1118-1141.

Kieft, K., Damman, A. H., 1990. Indium-bearing chalcopyrite and sphalerite from the Gåsborn area, West Bergslagen, central Sweden. Mineral. Mag. 54, 109-112.

Kieft, K., Eriksson, G., 1984. Regional zoning and metamorphic evolution of the Vindfall Pb-Zn ore, east central Sweden. GFF 106, 305-317.

Klock, W., Palme, H., 1988. Partitioning of siderophile and chalcophile elements between sulfide, olivine, and glass in a naturally reduced basalt from Disko Island, Greenland. Proc. Lunar Planet. Sci. Conf. 18th, 471-483.

Klünder, M. H., Karup-Møller, S., Makovicky, E., 2003. Exploratory studies on substitutions in the tetrahedrite-tennantite solid solution series Part III. The solubility of bismuth in tetrahedrite-tennantite containing iron and zinc. Neues Jahrb. Mineral. Monatsh. 2003, 153-175.

Knipe, S. W., Foster, R. P., Stanley, C. J., 1992. Role of sulphide surfaces in sorption of precious metals from hydrothermal fluids. Trans. Inst. Min. Metall. (Sect. B) 101, 83-88.

Knipping, J. L., Bilenker, L. D., Simon, A. C., Reich, M., Barra, F., Deditius, A. P., Heinrich, C. A., Holtz, F., Munizaga, R., 2015. Trace elements in magnetite from massive iron oxide apatite deposits indicate a combined formation by igneous and magmatic hydrothermal processes. Geochim. Cosmochim. Acta 171, 15-38.

Knittel, U., 1989. Composition and association of arsenian goldfieldite from the Marian gold deposit, northern Luzon, Philippines. Mineral. Petrol. 40, 145-154.

Koch, J., Günther, D., 2007. Femtosecond laser ablation inductively coupled plasma mass spectrometry: achievements and remaining problems. Anal. Bioanal. Chem. 387, 149-153.

Kojima, S., Sugaki, A., 1984. Phase relations in the central portion of the Cu–Fe–Zn–S system between 800° and 500 °C. Mineral. J. 12, 15-28.

Kojima, S., Sugaki, A., 1985. Phase relations in the Cu–Fe–Zn–S system between 500 degrees and 300 degrees C under hydrothermal conditions. Econ. Geol. 80, 158–171.

Kołodziejczyk, J., Prsek, J., Asllani, B., Maliqi, F., 2016. The paragenesis of silver minerals in the Pb-Zn Stan Terg deposit, Kosovo: an example of precious metal epithermal mineralization. Geol. Geophys. Env. 42, 19-29.

Kołodziejczyk, J., Pršek, J., Voudouris, P., Melfos, V., Asllani, B., 2016. Sn-bearing minerals and associated sphalerite from lead-zinc deposits, Kosovo: An electron microprobe and LA-ICP-MS study. Minerals 6, 42.

Kontonikas-Charos, A., Ciobanu, C. L., Cook, N. J., 2014. Albitization and redistribution of REE and Y in IOCG systems: Insights from Moonta-Wallaroo, Yorke Peninsula, South Australia. Lithos 208-209, 178-201.

Kornicker, W. A., Morse, J. W., 1991. Interactions of divalent cations with the surface of pyrite. Geochim. Cosmochim. Acta 55, 2159-2171.

Kouzmanov, K., Bogdanov, K., Ramboz, C., 2000. Cu–Bi–Pb–Te mineral assemblage in the Elshitsa and Radka deposits, Sredna Gora zone, Bulgaria. Geodynamics and ore deposits evolution of the Alpine–Balkan–Carpathian–Dinaride Province. ABCD-GEODE Workshop, Borovets, Bulgaria, Abstracts.

Kouzmanov, K., Bailly, L., Ramboz, C., Rouer, O., Bény, J. M., 2002. Morphology, origin and infrared microthermometry of fluid inclusions in pyrite from the Radka epithermal copper deposit, Srednogorie zone, Bulgaria. Mineral. Deposita 37, 599-613.

Kovalenker, V. A., Bortnikov, N. S., 1985. Chemical composition and mineral associations of

sulphosalts in the precious metal deposits from different geological environment. Geol. Carpathica 36, 283-291.

Kovalenker, V. A., Rusinov, V. L., 1986. Goldfieldite: Chemical composition, parageneses and conditions of formation. Mineral. Zhurnal 8, 57-70. (In Russian)

Kovalenker, V., Safonov, Y., Naumov, V., Rusinov, V., 1997. The epithermal gold-telluride Kochbulak deposit (Uzbekistan). Geol. Ore Deposits 39, 107-128.

Krämer, V., Hirth, H., Hofherr, M., Trah, H. -P., 1987. Phase studies in the systems Ag_2Te–Ga_2Te_3, ZnSe–In_2Se_3 and ZnS–Ga_2S_3. Thermochim. Acta 112, 88-94.

Kremheller, A., Levine, A. K., Gashurov, G., 1960. Hydrothermal preparation of two component solid solutions from II–VI compounds. J. Electrochem. Soc. 107, 12-15.

Krismer, M., Vavtar, F., Tropper, P., Sartory, B., Kaindl, R., 2011. Mineralogy, mineral chemistry and petrology of the Ag-bearing Cu-Fe-Pb-Zn sulfide mineralizations of the Pfunderer Berg (South Tyrol, Italy). Austrian J. Earth Sci. 104, 36-48.

Krneta, S., Ciobanu, C. L., Cook, N. J., Ehrig, K., Kamenetsky, V. S., 2016. REY-Signatures in Apatite Monitor Evolution of IOCG Systems: Examples from Olympic Dam and Acropolis, South Australia; Abstract; Australian Earth Science Convention: Adelaide, Australia, 2016.

L'Heureux, I., 2013. Self-organized rhythmic patterns in geochemical systems. Phil. Trans. R. Soc. A371, http://dx.doi.org/10.1098/ rsta.2012.0356.

Laing, W., Marjoribanks, R., Rutland, R., 1978. Structure of the Broken Hill mine area and its significance for the genesis of the orebodies. Econ. Geol. 73, 1112-1136.

Lane, D. J., Cook, N. J., Grano, S. R., Ehrig, K., 2016. Selective leaching of penalty elements from copper concentrates: a review. Minerals Eng. 98, 110-121.

Lang, B., 1979. The base metals-gold hydrothermal ore deposits of Baia Mare, Romania. Econ. Geol. 74, 1336-1351.

Lang, B., Edelstein, O., Steinitz, G., Kovacs, M., Halga, S., 1994. Ar-Ar dating of adularia; a tool in understanding genetic relations between volcanism and mineralization; Baia Mare area (Gutii Mountains), northwestern Romania. Econ. Geol. 89, 174-180.

Large, R. R., Bull, S. W., McGoldrick, P. J., Derrick, G., Carr, G., Walters, S., 2005. Stratiform and strata-bound Zn–Pb–Ag + Cu deposits of the Proterozoic sedimentary basins of northern Australia. Economic Geology 100th Anniversary Volume, 931-963.

Large, R. R., Maslenikov, V. V., Robert, F., Danyushevsky, L. V., Chang, Z., 2007. Multistage Sedimentary and Metamorphic Origin of Pyrite and Gold in the Giant Sukhoi Log Deposit, Lena Gold Province, Russia. Econ. Geol. 102, 1233-1267.

Large, R. R., Danyushevsky, L., Hollit, C., Maslennikov, V., Meffre, S., Gilbert, S., Bull, S., Scott, R., Emsbo, P., Thomas, H., Singh, B., 2009. Gold and trace element zonation in pyrite using a laser imaging technique: implications for the timing of gold in orogenic and Carlin-style sediment-hosted deposits. Econ. Geol. 104, 635-668.

Large, R. R., Meffre, S., Burnett, R., Guy, B., Bull, S., Gilbert, S., Goemann, K., Danyushevsky, L., 2013. Evidence for an intrabasinal source and multiple concentration processes in the formation of the Carbon Leader Reef, Witwatersrand Supergroup, South Africa. Econ. Geol. 108, 1215-1241.

Large, R. R., Halpin, J. A., Danyushevsky, L. V., Maslennikov, V. V., Bull, S. W., Long, J. A., Gregory, D. D., Lounejeva, E., Lyons, T. W., Sack, P. J., McGoldrick, P. J., Calver, C. R., 2014. Trace element content of sedimentary pyrite as a new proxy for deep-time ocean-atmosphere evolution. Earth Plan. Sci. Lett. 389, 209-220.

Larocque, A. C. L., Jackman, J. A., Cabri, L. J., Hodgson, C. J., 1995. Calibration of the ion microprobe for the determination of silver in pyrite and chalcopyrite from the Mobrun VMS deposit, Rouyn-Noranda, Quebec. Can. Mineral. 33, 361-372.

Lawley, C. J. M., Creaser, R. A., Jackson, S. E., Yang, Z. P., Davis, B. J., Pehrsson, S. J., Dubé, B., Mercier-Langevin, P., Vaillancourt, D., 2015. Unraveling the Western Churchill Province Paleoproterozoic Gold Metallotect: Constraints from Re-Os Arsenopyrite and U-Pb Xenotime Geochronology and LA-ICP-MS Arsenopyrite Trace Element Chemistry at the BIF-Hosted Meliadine Gold District, Nunavut, Canada. Econ. Geol. 110, 1425-1454.

Lawrence, L., 1967. Sulphide neomagmas and highly metamorphosed sulphide deposits. Mineral. Deposita 2, 5-10.

Layton-Matthews D., Peter J. M., Scott S. D., Leybourne M. I., 2008. Distribution, mineralogy, and geochemistry of selenium in felsic volcanic-hosted massive sulfide deposits of the Finlayson Lake district, Yukon Territory, Canada. Econ. Geol. 103, 61-88.

Le Vaillant, M., Barnes, S. J., Fiorentini, M. L., Miller, J., McCuaig, T. C., Muccilli, P., 2015. A hydrothermal Ni–As–PGE geochemical halo around the miitel komatiite-hosted nickel sulfide deposit, Yilgarn Craton, Western Australia. Econ. Geol. 110, 505-530.

Lee, D. C., Halliday, A. N., 1995. Hafnium–tungsten chronometry and the timing of terrestrial core formation. Nature 378, 771–774.

Lefebvre, I., Lannoo, M., Olivier-Fourcade, J., Jumas, J. C., 1991. Tin oxidation number and the electronic structure of SnS-In_2S_3-SnS_2 systems. Phys. Rev. B 44, 1004.

Lepetit, P., Bente, K., Doering, T., Luckhaus, S., 2003. Crystal chemistry of Fe-containing sphalerites. Phys. Chem. Mineral. 30, 185–191.

Lewis, B., Forward, P., Roberts, J., 1965. Geology of the Broken Hill lode, reinterpreted. In: McAndrew, J., Ed., Geology of Australian Ore Deposits. 8th Comm. Min. Metall. Congr., vol. 1, 319 pp.

Leyh, W. R., Conor, C. H., 2000. Stratigraphically controlled metallogenic zonation associated with the regional redox boundary of the Willyama Supergroup—economic implications for the southern Curnamona Province. Mesa J. 16, 39–47.

Li, C., Barnes, S. J., Makovicky, E., Rose-Hansen, J., Makovicky, M., 1996. Partitioning of nickel, copper, iridium, rhenium, platinum, and palladium between monosulfide solid solution and sulfide liquid: effects of composition and temperature. Geochim. Cosmochim. Acta 60, 1231-1238.

Li, Y., Kawashima, N., Li, J., Chandra, A. P., Gerson, A. R., 2013. A review of the structure, and fundamental mechanisms and kinetics of the leaching of chalcopyrite. Adv. Colloid Interface Sci. 197, 1-32.

Li, C. Y., Zhang, R. Q., Ding, X., Ling, M. X., Fan, W. M., Sun, W. D., 2016. Dating cassiterite using laser ablation ICP-MS. Ore Geol. Rev. 72, 313–322.

Li, K., Etschmann, B., Rae, N., Reith, F., Ryan, C. G., Kirkham, R., Howard, D., Rosa, D. R. N., Zammit, C., Pring, A., Ngothai, Y., 2016. Ore petrography using megapixel X-ray imaging: Rapid insights into element distribution and mobilization in complex Pt and U–Ge–Cu Ores. Econ. Geol. 111, 487-502.

Li, X. F., Cheng, H., Wang, C. Z., Wang, L., 2016. Genesis of the Huangshaping W–Mo–Cu–Pb–Zn polymetallic deposit in Southeastern Hunan Province, China: Constraints from fluid inclusions, trace elements, and isotopes. Ore Geol. Rev. 79, 1-25.

Lin, J., Liu, Y. S., Yang, Y. H., Hu, Z. C., 2016. Calibration and correction of LA-ICP-MS and LA-MC-ICP-MS analyses for element contents and isotopic ratios. Solid Earth Sci. 1, 5-27.

Liu, H., Chang, L. L. Y., 1994. Phase relations in the system PbS–PbSe–PbTe. Mineral. Mag. 58, 567–578.

Liu, Z., Wu, F., Guo, C., Zhao, Z., Yang, J., Sun, J., 2011. In situ U-Pb dating of xenotime by laser ablation (LA)-ICP-MS. Chin. Sci. Bull. 56, 2948-2956.

Lockington, J., Cook, N. J., Ciobanu, C. L., Trace and minor elements in sphalerite from metamorphosed sulphide deposits. Mineral. Petrol. 108, 873-890.

London, D., 2011. Experimental synthesis and stability of tourmaline: a historical overview. Can. Mineral. 49, 117-136.

Lord, C. S., 1933. A study of tetrahedrite in some British Columbia ores. Doctoral dissertation, University of British Columbia.

Lottermoser, B., 1989. Rare earth element study of exhalites within the Willyama Supergroup, Broken Hill Block, Australia. Mineral. Deposita 24, 92–99.

Lueth, V. W., Megaw, P. K. M., Pingitore, N. E., Goodell, P. C., 2000. Systematic Variation in Galena Solid-Solution Compositions at Santa Eulalia, Chihuahua, Mexico. Econ. Geol. 95, 1673–1687.

Lydon, J. W., 2000. A synopsis of the current understanding of the geological environment of the Sullivan deposit. In: Lydon, J. W., Höy, T., Slack, J. F., Knapp, M. E., Eds., The Geological Environment of the Sullivan Deposit, British Columbia. Geological Association of Canada, Mineral Deposits Division, Spec. Publ. 1, 12-31.

Makovicky, E., Karup-Möller, S., 1994. Exploratory studies on substitution of minor elements in synthetic tetrahedrite. Part I. Substitution by Fe, Zn, Co, Ni, Mn, Cr, V and Pb. Unit-cell parameter changes on substitution and the structural role of "Cu^{2+}". Neues Jahrb. Mineral. Abh. 167, 89-123.

Makovicky, E., Skinner, B., 1979. Studies of the sulfosalts of copper. VII. Crystal structures of the exsolution products $Cu_{12.3}Sb_4S_{13}$ and $Cu_{13.8}Sb_4S_{13}$ of unsubstituted synthetic tetrahedrite. Can. Mineral. 17, 619-634.

Makovicky, E., Karanović, L., Poleti, D., Balić-Žunić, T., Paar, W. H., 2005. Crystal structure of copper-rich unsubstituted tennantite, $Cu_{12.5}As_4S_{13}$. Can. Mineral. 43, 679-688.

Makvandi, S., Ghasemzadeh-Barvarz, M., Beaudoin, G., Grunsky, E. C., McClenaghan, M. B., Duchesne, C., 2016. Principal component analysis of magnetite composition from

volcanogenic massive sulfide deposits: Case studies from the Izok Lake (Nunavut, Canada) and Halfmile Lake (New Brunswick, Canada) deposits. Ore Geol. Rev. 72, 60-85.

Makvandi, S., Ghasemzadeh-Barvarz, M., Beaudoin, G., Grunsky, E. C., McClenaghan, M. B., Duchesne, C., Boutroy, E., 2016. Partial least squares-discriminant analysis of trace element compositions of magnetite from various VMS deposit subtypes: Application to mineral exploration. Ore Geol. Rev. 78, 388-408.

Mao, M., Rukhlov, A. S., Rowins, S. M., Spence, J., Coogan, L. A., 2016. Apatite trace element compositions: A robust new tool for mineral exploration. Econ. Geol. 111, 1043-1072.

Marechal, C., Telouk, P., Albarede, F., 1999. Precise analysis of Cu and Zn isotopic compositions by plasma-source mass spectrometry. Chem. Geol. 156, 251–273.

Marincea, Ş., Dumitraş, D. -G., Ghineţ, C., Fransolet, A. -M., Hatert, F., Rondeaux, M., 2011. Gehlenite from three occurrences of high-temperature skarns, Romania: new mineralogical data. Can. Mineral. 49, 1001-1014.

Marques de Sá, C., Noronha, F., Ferreira da Silva, E., 2014. Factor analysis characterization of minor element contents in sulfides from Pb–Zn–Cu–Ag hydrothermal vein deposits in Portugal. Ore Geol. Rev. 62, 54-71.

Marshall, B., Spry, P. G., 2000. Discriminating between regional metamorphic remobilization and syntectonic emplacement in the genesis of massive sulfide ores. Rev. Econ. Geol. 11, 39-80.

Maslennikov, V. V., Maslennikova, S. P., Large, R. R., Danyushevsky, L. V., 2009. Study of trace element zonation in vent chimneys from the Silurian Yaman-Kasy volcanic-hosted massive sulfide deposit (Southern Urals, Russia) using laser ablation-inductively coupled plasma mass spectrometry (LA-ICPMS). Econ. Geol. 104, 1111-1141.

Mathias, B., Clark, G., 1975. Mount Isa copper and silver-lead-zinc orebodies —Isa and Hilton mines. In: Knight, C. L., Ed., Economic geology of Australia and Papua New Guinea vol. 1. AusIMM, 351-372.

Matsuhisa, Y., Goldsmith, J. R., Clayton, R. N., 1978. Mechanisms of hydrothermal crystallization of quartz at 250 C and 15 kbar. Geochim. Cosmochim. Acta 42, 173-182.

Mavrogenes, J., MacIntosh, I., Ellis, D., 2001. Partial melting of the Broken Hill galena–sphalerite ore: experimental studies in the system PbS–FeS–ZnS–(Ag_2S). Econ. Geol. 96, 205-210.

Maydagán, L., Franchini, M., Lentz, D., Pons, J., McFarlane, C., 2013. Sulfide composition and isotopic signature of the Altar Cu-Au deposit, Argentina: Constraints on the evolution of the porphyry-epithermal system. Can. Mineral. 51, 813-840.

McClenaghan, S. H., Lentz, D. R., Martin, J., Diegor, W. G., 2009. Gold in the Brunswick No. 12 volcanogenic massive sulfide deposit, Bathurst Mining Camp, Canada: Evidence from bulk ore analysis and laser ablation ICP-MS data on sulfide phases. Mineral. Deposita 44, 523-557.

McDonough, W. F., Sun, S. S., 1995. The composition of the Earth. Chem. Geol. 120, 223-253.

McFarlane, C. R. M., 2016. Allanite U-Pb geochronology by 193 nm LA ICP-MS using NIST610 glass for external calibration. Chem. Geol. 438, 91-102.

McFarlane, C. R. M., Luo, Y., 2012. U–Pb Geochronology using 193 nm excimer LA-ICP-MS optimized for in situ accessory mineral dating in thin sections. Geosci. Can. 39, 158-172.

McFarlane, C., Lentz, D., Dehnavi, A. S., 2016. Pb-isotopic study of galena by LA-Q-ICP-MS: Testing a new methodology with applications to base-metal sulphide deposits. Minerals 6, 96.

McIntyre, N. S., Cabri, L. J., Chauvin, W. J., Laflamme, J. H. G., 1984. Secondary ion mass spectrometric study of dissolved silver and indium in sulfide minerals. Scanning Electron Microsc. 3, 1139-1146.

Meinert, L. D., Dipple, G. M., Nicolescu, S., 2005. World skarn deposits. Econ. Geol. 100th Anniversary Volume, 299-336.

Melcher, F., Graupner, T., Henjes-Kunst, F., Oberthür, T., Sitnikova, M., Gäbler, H. E., 2008. Analytical fingerprint of columbite-tantalite (coltan) mineralization in pegmatites: Focus on Africa. In: Proceedings of the 9th International Congress for Applied Mineralogy, Australasian Institute of Mining and Metallurgy, Melbourne, Australia, 8–10 September 2008, 615–624.

Mikhlin, Y., Tomashevich, Y., Tauson, V., Vyalikh, D., Molodtsov, S., Szargan, R., 2005. A comparative X-ray absorption near-edge structure study of bornite, Cu_5FeS_4, and chalcopyrite, $CuFeS_2$. J. Electron Spectrosc. Relat. Phenom. 142, 83-88.

Mills, S. E., Tomkins, A. G., Weinberg, R. F., Fan, H. R., 2015. Implications of pyrite geochemistry for gold mineralisation and remobilisation in the Jiaodong gold district, northeast China. Ore Geol. Rev. 71, 150-168.

Mishin, Y., Mehl, M., Papaconstantopoulos, D., Voter, A., Kress, J., 2001. Structural stability and lattice defects in copper: ab initio, tight-binding, and embedded-atom calculations. Phys. Rev. B 63, 224106.

Moëlo, Y., Makovicky, E., Mozgova, N. N., Jambor, J. L., Cook, N., Pring, A., Paar, W., Nickel, E. H., Graeser, S., Karup-Møller, S., Balic-Žunic, T., 2008. Sulfosalt systematics: A review. Report of the Sulfosalt Sub-committee of the IMA Commission on Ore Mineralogy. Eur. J. Mineral. 20, 7-46.

Moggi-Cecchi V., Cipriani C., Rossi P., Ceccato D., Rudello V., Somacal H., 2002. Trace element contents and distribution maps of chalcopyrite: a micro-PIXE study. Period. Mineral. 71, 101-109.

Moh, G. H., 1984. Sulfosalts: Observations and mineral descriptions, experiments and applications. Neues Jahrb. Mineral. Abh. 150, 25-64.

Monteiro L. V. S., Xavier R. P., Hitzman M. W., Juliani C., de Souza Filho C. R., Carvalho E. D. R., 2008. Mineral chemistry of ore and hydrothermal alteration at the Sossego iron oxide–copper–gold deposit, Carajás Mineral Province, Brazil. Ore Geol. Rev. 34, 317-336.

Moralev, G. V., Larsen, R. B., Bjerkgård, T., 1995. Distribution of precious metals in the Bleikvassli Zn-Pb SEDEX type deposit, Nordland, Norway. Norg. Geologiske Unders. Report 95, 120.

Morey, A. A., Tomkins, A. G., Bierlein, F. P., Weinberg, R. F., Davidson, G. J., 2008. Bimodal Distribution of Gold in Pyrite and Arsenopyrite: Examples from the Archean Boorara and Bardoc Shear Systems, Yilgarn Craton, Western Australia. Econ. Geol. 103, 599-614.

Morgan, J. W., Wandless, G. A., 1980. Rare earth element distribution in some hydrothermal minerals: evidence for crystallographic control. Geochim. Cosmochim. Acta 44, 973-980.

Mozgova, N. N., Tsepin, A. I., 1983. Fahlore (Features of Chemical Composition and Properties); Nauka: Moscow, Russia, 279. (In Russian)

Mular, A. L., Halbe, D. N., Barratt, D. J., Eds., 2002. Mineral processing plant design, practice, and control. SME, 2422 pp.

Müller, W., Shelley, M., Miller, P., Broude, S., 2009. Initial performance metrics of a new custom-designed ArF excimer LA-ICPMS system coupled to a two-volume laser-ablation cell. J. Anal. Atom. Spectrom. 24, 209–214.

Mungall, J. E., Andrews, D. R., Cabri, L. J., Sylvester, P. J., Tubrett, M., 2005. Partitioning of Cu, Ni, Au, and platinum-group elements between monosulfide solid solution and sulfide

melt under controlled oxygen and sulfur fugacities. Geochim. Cosmochim. Acta 69, 4349-4360.

Murakami, H., Ishihara, S., 2013. Trace elements of indium-bearing sphalerite from tin-polymetallic deposits in Bolivia, China and Japan: A femto-second LA-ICPMS study. Ore Geol. Rev. 53, 223-243.

Nadoll, P., Koenig, A. E., 2011. LA-ICP-MS of magnetite: Methods and reference materials. J. Anal. Atom. Spectrom. 26, 1872-1877.

Nadoll, P., Mauk, J. L., Hayes, T. S., Koenig, A. E., Box, S. E., 2012. Geochemistry of Magnetite from Hydrothermal Ore Deposits and Host Rocks of the Mesoproterozoic Belt Supergroup, United States. Econ. Geol. 107, 1275-1292.

Nadoll, P., Angerer, T., Mauk, J. L., French, D., Walshe, J., 2014. The chemistry of hydrothermal magnetite: A review. Ore Geol. Rev. 61, 1-32.

Nakamoto, A., Urasima, Y., Sugiura, S., Nakano, H., Yachi, T., Tadokoro, K., 1969. Pyromorphite-mimetite minerals from the Otaru-Matsukura barite mine in Hokkaido, Japan. Mineral. J. 6, 85-101.

Naldrett, A. J., Lehmann, J., 1988. Spinel non-stoichiometry as the explanation for Ni-, Cu- and PGE-enriched sulphides in chromitites. In: Geo-platinum 87, 93-109. Springer, Netherlands.

Nash, J. T., 1975. Geochemical studies in the Park City District; II, Sulfide mineralogy and minor-element chemistry, Mayflower Mine. Econ. Geol. 70, 1038-1049.

Neubauer, N., Lips, A., Kouzmanov, K., Lexa, J., Ivaşcanu, P., 2005. Subduction, slab detachment and mineralization: The Neogene in the Apusenu Mountains and Carpathians. Ore Geol. Rev. 27, 13-44.

Nikolakopoulos, D., 2013. Ore vectoring in IOCG Systems: Trace Elements in Garnets from the Groundhog Skarn, Punt Hill, South Australia. Unpublished Bachelor's Thesis, The University of Adelaide, Adelaide, Australia.

Noddack, I., Noddack, W., 1931. Die geochemie des rheniums. Z. Phys. Chem. A 154, 207-244.

Norman, M. D., Pearson, N. J., Sharma, A., Griffin, W. L., 1996. Quantitative analysis of trace elements in geological materials by laser ablation ICPMS: Instrumental operating conditions and calibration values of NIST glasses. Geostandard. Newslett. 20, 247–261.

Norman, M., Robinson, P., Clark, D., 2003. Major- and trace-element analysis of sulfide ores by laser-ablation ICP-MS, solution ICP-MS, and XRF: New data on international reference materials. Can. Mineral. 41, 293–305.

Nriagu, J. O., 1998. Thallium in the environment. Advances in Environmental Science and Technology 29, 284 pp. Wiley, New York.

Nutman, A. P., Ehlers, K., 1998. Evidence for multiple Palaeoproterozoic thermal events and magmatism adjacent to the Broken Hill Pb-Zn-Ag orebody, Australia. Precambr. Res. 90, 203-238.

O'Brien, J. J., Spry, P. G., Teale, G. S., Jackson, S.,E., Rogers, D., 2015. Major and Trace Element Chemistry of Gahnite as an Exploration Guide to Broken Hill-Type Pb-Zn-Ag Mineralization in the Broken Hill Domain, New South Wales, Australia. Econ. Geol. 110, 1027-1057.

Oen, I. S., Kieft, C., 1976. Bismuth-rich tennantite and tetrahedrite in the Mangualde pegmatite, Viseu district, Portugal. Neues Jahrb. Mineral. Monatsh. 2, 94-96.

Offler, R., Fleming, P. D., 1968. A synthesis of folding and metamorphism in the Mount Lofty ranges, South Australia. J. Geol. Soc. Austral. 15, 245-265.

Oftedahl, I., 1940. Untersuchungen u¨ber die Nebenbestandteile von Erzmineralien norwegischer zinkblendfu¨hrender Vorkommen. Skrift. Norsk Vidensk. Akad. Oslo, Math. Naturv. Kl. 8, 1-103.

Ohata, M., Tabersky, D., Glaus, R., Koch, J., Hattendorf, B., Günther, D. J., 2014. Comparison of 795 nm and 265 nm femtosecond and 193 nm nanosecond laser ablation inductively coupled plasma mass spectrometry for the quantitative multi-element analysis of glass materials. J. Anal. Atom. Spectrom. 29, 1345-1353.

Oliver, N. H., Dipple, G. M., Cartwright, I., Schiller, J., 1998. Fluid flow and metasomatism in the genesis of the amphibolites-facies, pelite-hosted Kanmantoo copper deposit, South Australia. Amer. J. Sci. 298, 181-218.

Onuk, P., Melcher, F., Walkner, C., 2015 Development of the matrix-matched sphalerite (ZnS) standards MUL-ZnS-1 and MUL-ZnS-2 for in-situ analysis of trace elements by laser ablation inductively coupled plasma-mass spectroscopy (LA-ICP-MS). In: Proceedings of the 9th International Conference on the Analysis of Geological and Environmental Materials, Leoben, Austria, 8–14 August 2015; Abstract OP-26, 65.

Orberger, B., Pasava, J., Gallien, J. P., Daudin, L., Trocellier, P., 2003. Se, As, Mo, Ag, Cd, In, Sb, Pt, Au, Tl, Re traces in biogenic and abiogenic sulfides from Black Shales (Selwyn Basin, Yukon territories, Canada): a nuclear microprobe study. Nucl. Instr. Meth. Phys. Res. B210, 441–448.

Ortoleva, P. J., Merino, E., Moore, C., Chadam, J., 1987. Geochemical self-organization: I. Reaction-transport feedbacks and modeling approach. Amer. J. Sci. 287, 979-1007.

Painter, M. G. M., Golding, S. D., Hannan, K. W., Neudert, M. K., 1999. Sedimentologic, petrographic, and sulfur isotope constraints on fine-grained pyrite formation at Mount Isa Mine and environs, Northwest Queensland, Australia. Econ. Geol. 94, 883-912.

Pagé, P., Barnes, S. J., 2009. Using trace elements in chromites to constrain the origin of podiform chromitites in the Thetford Mines Ophiolite, Quebec, Canada. Econ. Geol. 104, 997-1018.

Pal, D. C., Chaudhuri, T., McFarlane, C., Mukherjee, A., Sarangi, A. K., 2011. Mineral Chemistry and In Situ Dating of Allanite, and Geochemistry of its Host Rocks in the Bagjata Uranium Mine, Singhbhum Shear Zone, India - Implications for the Chemical Evolution of REE Mineralization and Mobilization. Econ. Geol. 106, 1155-1171.

Park, B., 1934. Estimation of Small Amounts of Bismuth, Antimony, Tin, and Molybdenum in Copper. Industrial & Engineering Chemistry Analytical Edition 6, 189-190.

Parr, J., Plimer, I., 1993. Models for Broken Hill-type lead-zinc-silver deposits. Mineral deposits modeling. Geol. Assoc. Canada Spec. Paper 40, 245-288.

Passchier, C. W., Trouw, R. A. J., 2005. Microtectonics. 2nd edition. Springer-Verlag Berlin Heidelberg.

Paton, C., Hellstrom, J., Paul, B., Woodhead, J., Hergt, J., 2011. Iolite: Freeware for the visualisation and processing of mass spectrometric data. J. Anal. Atom. Spectrom. 26, 2508–2518.

Patten, C., Barnes, S. J., Mathez, E. A., Jenner, F. E., 2013. Partition coefficients of chalcophile elements between sulfide and silicate melts and the early crystallization history of sulfide liquid: LA-ICP-MS analysis of MORB sulfide droplets. Chem. Geol. 358, 170-188.

Pattrick, R. A., 1978. Microprobe analyses of cadmium-rich tetrahedrites from Tyndrum, Perthshire, Scotland. Mineral. Mag. 42, 286-288.

Pattrick, R. A., 1985. Pb-Zn and minor U mineralization at Tyndrum, Scotland. Mineral. Mag. 49, 671-681.

Pattrick, R. A. D., Hall, A. J., 1983. Silver substitution into synthetic zinc, cadmium and iron tetrahedrites. Mineral Mag. 47, 441-451.

Pattrick, R. A. D., van der Lann, G., Vaughan, D. J., Henderson, C. M. B., 1993. Oxidation state and electronic configuration determination of copper in tetrahedrite group minerals by L-edge X-ray absorption spectroscopy. Phys. Chem. Mineral. 20, 395-401.

Pauling, L., Brockway, L. O., 1932. The crystal structure of chalcopyrite $CuFeS_2$. Z. Kristallog.-Cryst Mater. 82, 188-194.

Pavlova, G. G., Palessky, S. V., Borisenko, A. S., Vladimirov, A. G., Seifert, T., Phan, L. A., 2015. Indium in cassiterite and ores of tin deposits. Ore Geol. Rev. 66, 99-113.

Peach, C. L., Mathez, E. A., Keays, R. R., 1990. Sulfide melt-silicate melt distribution coefficients for noble metals and other chalcophile elements as deduced from MORB: Implications for partial melting. Geochim. Cosmochim. Acta 54, 3379-3389.

Peach, C. L., Mathez, E. A., Keays, R. R., Reeves, S. J., 1994. Experimentally determined sulfide melt-silicate melt partition coefficients for iridium and palladium. Chem. Geol. 117, 361-377.

Pearce, C. I., Pattrick, R. A. D., Vaughan, D. J., Henderson, C. M. B., Van der Laan, G., 2006. Copper oxidation state in chalcopyrite: Mixed Cu d^9 d^{10} characteristics. Geochim. Cosmochim. Acta 70, 4635-4642.

Peng, H. J., Zhang, C. Q., Mao, J. W., Santosh, M., Zhou, Y. M., 2015. Garnets in porphyry-skarn systems: A LA-ICP-MS, fluid inclusion, and stable isotope study of garnets from the Hongniu–Hongshan copper deposit, Zhongdian area, NW Yunnan Province, China. J. Asian Earth Sci. 103, 229-251.

Perkins, W., 1997. Mount Isa lead-zinc orebodies: Replacement lodes in a zoned syndeformational copper-lead-zinc system? Ore Geol. Rev. 12, 61-110.

Peterson, R. C., Miller, I., 1986. Crystal structure and cation distribution in freibergite and tetrahedrite. Mineral. Mag. 50, 717-721.

Petrunov, R., Dragov, P., Neykov, H., 1991. Polyelemental (with As, Sn, V, Bi, Ag, Te, Ge, Se etc.) mineralisation in Assarel porphyry-copper deposit (in Bulgarian). Rev. Bulg. Geol. Soc. 52, 1-7.

Pfitzner, A., Evain, M., Petricek, V., 1997. $Cu_{12}Sb_4S_{13}$: A temperature-dependent structure investigation. Acta Cryst. B53, 337-345.

Phillips, G. N., 1981. Water activity changes across an amphibolite-granulite facies transition, Broken Hill, Australia. Contrib. Mineral. Petrol. 75, 377-386.

Phillips, G., Archibald, N., Wall, V., 1985. Metamorphosed high-Fe tholeiites; their alteration and relationship to sulphide mineralization, Broken Hill, Australia. S. Afr. J. Geol. 88, 49-59.

Philpotts, J. A., 1978. The law of constant rejection. Geochim. Cosmochim. Acta 42, 909-920.

Pidgeon, R., 1967. A Rubidium—Strontium Geochronological Study of the Willyama Complex, Broken Hill, Australia. J. Petrol. 8, 283-324.

Piña, R., Gervilla, F., Barnes, S. J., Ortega, L., Lunar, R., 2012. Distribution of platinum-group and chalcophile elements in the Aguablanca Ni-Cu sulfide deposit (SW Spain): Evidence from a LA-ICP-MS study. Chem. Geol. 302, 61-75.

Piña, R., Gervilla, F., Barnes, S. J., Ortega, L., Lunar, R., 2013. Partition coefficients of platinum group and chalcophile elements between arsenide and sulfide phases as determined in the Beni Bousera Cr–Ni mineralization (North Morocco). Econ. Geol. 108, 935-951.

Piña, R., Gervilla, F., Barnes, S. J., Ortega, L., Lunar, R., 2015. Liquid immiscibility between arsenide and sulfide melts: Evidence from a LA-ICP-MS study in magmatic deposits at Serranía de Ronda (Spain). Mineral. Deposita 50, 265-279.

Piña, R., Gervilla, F., Barnes, S. J., Oberthür, T., Lunar, R., 2016. Platinum-group element concentrations in pyrite from the Main Sulfide Zone of the Great Dyke of Zimbabwe. Mineral. Deposita 51, 853-872.

Pinto, A., Ferreira, A., Bowles, J. F. W., Gaspar, O. C., 1997. Mineralogical and textural characterization of the Neves-Corvo ores. Metallogenetic implications. In: Geology and VMS Deposits of the Iberian Pyrite Belt; Ser. 27; Baniga, F. J. A. S., Carvalho, D., Eds., SEG Neves Corvo Field Conference: Lisbon, Portugal, 90 pp.

Plimer, T. R., 1979. Sulphide rock zonation and hydrothermal alteration at Broken Hill, Australia. Trans. Inst. Min. Metall. (Sect. B) 88, 161-176.

Plimer, I. R., 1984. The mineralogical history of the Broken Hill Lode, NSW. Austral. J. Earth Sci. 31, 379-402.

Plimer, I. R., 1986. Sediment-hosted exhalative Pb-Zn deposits; products of contrasting ansialic rifting. S. Afr. J. Geol. 89, 57-73.

Plimer, I. R., 2007. The world's largest Zn-Pb-Ag deposit: a re-evaluation of Broken Hill (Australia). In: Andrew, C. J., Ed., Mineral deposits: Digging deeper. Irish Association for Economic Geology, Dublin, 1239-1242.

Plotinskaya, O. Y., Kovalenker, V., Seltmann, R., Stanley, C., 2006. Te and Se mineralogy of the high-sulfidation Kochbulak and Kairagach epithermal gold telluride deposits (Kurama Ridge, Middle Tien Shan, Uzbekistan). Mineral. Petrol. 87, 187-207.

Plotinskaya, O. Y., Grabezhev, A. I., Seltmann, R., 2015. Fahlores compositional zoning in a porphyry-epithermal system: Biksizak occurrence, South Urals, Russia as an example. Geol. Ore Deposits 57, 42-63.

Pohl, D., Liessmann, W., Okrugin, V. M., 1996. Rietveld analysis of selenium-bearing goldfieldites. Neues Jahrb. Mineral. Monatsh. 1996, 1-8.

Popov, P., Strashimirov, S., Kanazirski, M., 2000. Assarel-Medet ore field. In: Strashmirov, S., Popov, P., Eds., Geology and metallogeny of the Panagyurishte ore region. Guide to excursion A and C. ABCD–Geode 2000 Workshop, Borovets, May 2000, 19-25.

Prendergast, M. D., Keays, R. R., 1989. Controls of platinum group element mineralization and the origin of the PGE-rich Main Sulphide Zone in the Wedza Subchamber of the Great Dike, Zimbabwe: implications for the genesis of, and exploration for, stratiform PGE mineralization in layered intrusions. In: Prendergast, M. D., Jones, M. J., Eds., Magmatic Sulphides-the Zimbabwe Volume 43-69. Inst. M. M., London.

Prichard, H. M., Knight, R. D., Fisher, P. C., McDonald, I., Zhou, M. F., Wang, C. Y., 2013. Distribution of platinum-group elements in magmatic and altered ores in the Jinchuan intrusion, China: An example of selenium remobilization by postmagmatic fluids. Mineral. Deposita 48, 767-786.

Pring, A., Williams, T. B., 1994. A HRTEM study of defects in silver-doped galena. Mineral. Mag. 58, 455-459.

Putnis, A., Fernandez-Diaz, L., Prieto, M., 1992. Experimentally produced oscillatory zoning in the $(Ba,Sr)SO_4$ solid solution. Nature 358, 743-745.

Qian, Z., 1987. Trace elements in galena and sphalerite and their geochemical significance in distinguishing the genetic types of Pb–Zn ore deposits. Chin. J. Geochem. 6, 177-190.

Raju, P. V. S., Hart, C. J. R., Sangurmath, P., 2016. Scheelite geochemical signatures by LA-ICP-MS and potential for rare earth elements from Hutti Gold Mines and fingerprinting ore deposits. J. Afr. Earth Sci. 114, 220–227.

Ramberg, I. B., 1967. Kongsfjell-områdets geologi, en petrografisk og strukturell undersøkelse i Helgeland, Nord-Norge. Norg. Geol Unders Bulletin 240, 1-152.

Ramdohr, P., 1980. The Ore Minerals and their Intergrowths, 2nd ed. Pergamon Press, New York, 1207 pp.

Reeder, R. J., Grams, J. C., 1987. Sector zoning in calcite cement crystals: Implications for trace element distributions in carbonates. Geochim. Cosmochim. Acta 51, 187-194.

Reeder, R. J., Fagioli, R. O., Meyers, W. J., 1990. Oscillatory zoning of Mn in solution-grown calcite crystals. Earth-Sci. Rev. 29, 39-46.

Reich, M., Kesler, S. E., Utsunomiya, S., Palenik, C. S., Chryssoulis, S. L., Ewing, R.C., 2005. Solubility of gold in arsenian pyrite. Geochim. Cosmochim. Acta 69, 2781-2796.

Reich, M., Utsunomiya, S., Kesler, S.E., Wang, L., Ewing, R.C., Becker, U., 2006. Thermal behavior of metal nanoparticles in geologic materials. Geology 34, 1033-1036.

Reich M., Palacios C., Barra F., Chryssoulis S., 2013. "Invisible" silver in chalcopyrite and bornite from the Mantos Blancos Cu deposit, northern Chile. Eur. J. Mineral. 25, 453-460.

Reich, M., Deditius, A., Chryssoulis, S., Li, J. W., Ma, C. Q., Parada, M. A., Barra, F., Mittermayr, F., 2013. Pyrite as a record of hydrothermal fluid evolution in a porphyry copper system: A SIMS/EMPA trace element study. Geochim. Cosmochim. Acta 104, 42-62.

Reich, M., Simon, A. C., Deditius, A., Barra, F., Chryssoulis, S., Lagas, G., Tardani, D., Knipping, J., Bilenker, L., Sánchez-Alfaro, P., Roberts, M. P., 2016. Trace element signature of pyrite from the Los Colorados iron oxide-apatite (IOA) deposit, Chile: A missing link between Andean IOA and iron oxide copper-gold systems? Econ. Geol. 111, 743-761.

Remond, G., Cesborn, E., Traxel, K., Campbell, J. L., Cabri, L. J., 1987. Electron microprobe analysis and proton induced X-ray spectrometry applied to trace element analysis in sulfides. Problems and prospects. Scanning Microsc. 1, 1017-1037.

Renock, D., Becker, U., 2011. A first principles study of coupled substitution in galena. Ore Geol. Rev. 42, 71–83.

Repstock, A., Voudouris, P., Kolitsch, U., 2015. New occurrences of watanabeite, colusite, "arsenosulvanite" and "Cu-excess" tetrahedrite-tennantite at the Pefka high-sulfidation epithermal deposit, northeastern Greece. Neues Jahrb. Mineral. Abh. J. Mineral. Geochem.

192, 135-149.

Repstock, A., Voudouris, P., Zeug, M., Melfos, V., Zhai, M., Li, H., Kartal, T., Matuszczak, J., 2016. Chemical composition and varieties of fahlore-group minerals from Oligocene mineralization in the Rhodope area, Southern Bulgaria and Northern Greece. Mineral. Petrol. 110, 103-123.

Revan, M. K., Genç, Y., Maslennikov, V. V., Maslennikova, S. P., Large, R. R., Danyushevsky, L. V., 2014. Mineralogy and trace-element geochemistry of sulfide minerals in hydrothermal chimneys from the Upper-Cretaceous VMS deposits of the eastern Pontide orogenic belt (NE Turkey). Ore Geol. Rev. 63, 129-149.

Ringwood, A., 1955. The principles governing trace element distribution during magmatic crystallization Part I: the influence of electronegativity. Geochim. Cosmochim. Acta 7, 189-202.

Ripley, E. M., Brophy, J. G., Li, C., 2002. Copper solubility in a basaltic melt and sulfide liquid/silicate melt partition coefficients of Cu and Fe. Geochim. Cosmochim. Acta 66, 2791-2800.

Rosenberg, J. L., Spry, P. G., Jacobson, C. E., Cook, N. J., Vokes, F. M., 1998. Thermo-barometry of the Bleikvassli Zn-Pb-(Cu) deposit, Nordland, Norway. Mineral. Deposita 34, 19-34.

Rosenberg, J., Spry, P., Jacobson, C., Vokes, F., 2000. The effects of sulfidation and oxidation during metamorphism on compositionally varied rocks adjacent to the Bleikvassli Zn–Pb–(Cu) deposit, Nordland, Norway. Mineral. Deposita 35, 714–726.

Rothery, E., 2001. Tectonic origin of the shape of the Broken Hill lodes supported by their structural setting in a high-grade shear zone. Austral. J. Earth Sci. 48, 201-220.

Rozhdestvenskaya, I. V., Zayakina, N. V., Samusikov, V. P., 1993. Crystal structure features of minerals from the tetrahedrite-freibergite series. Mineral. Zhurnal 15, 9-17. (In Russian)

Rubenach, M. J., 1992. Proterozoic low-pressure/high-temperature metamorphism and an anticlockwise P–T–t path for the Hazeldene area, Mount Isa Inlier, Queensland, Australia. J. Metam. Geol. 10, 333-346.

Rubin, J. N., Kyle, J. R., 1997. Precious metal mineralogy in porphyry-, skarn-, and replacement-type ore deposits of the Ertsberg (Gunung Bijih) District, Irian Jaya, Indonesia. Econ. Geol. 92, 535-550.

Russo, R. E., Mao, X. L., Gonzalez, J. J., Mao, S. S., 2002. Femtosecond laser ablation ICP-MS. J. Anal. Atom. Spectrom. 17, 1072–1075.

Saager, R., 1967. Drei Typen von Kieslagerstätten im Mofjell-Gebiet, Nordland, und ein neuer Vorschlag zur Gliederung der Kaledonischen Kieslager Norwegens. Norsk Geol. Tidsskr. 47, 333-358.

Sack, R. O., 2000. Internally consistent database for sulphides and sulfosalts in the system Ag_2S–Cu_2S–ZnS–Sb_2S_3–As_2S_3. Geochim. Cosmochim. Acta 64, 3803–3812.

Sack, R. O., 2005. Internally consistent database for sulphides and sulfosalts in the system Ag_2S-Cu_2S-ZnS-FeS-Sb_2S_3-As_2S_3: update. Geochim. Cosmochim. Acta 69, 1157–1164.

Sack, R. O., Ebel, D. S., 2006. Thermochemistry of sulfide mineral solutions. Rev. Mineral. Geochem. 61, 265-364.

Sack, R. O., Loucks, R. R., 1985. Thermodynamic properties of tetrahedrite-tennantites: Constraints on the interdependence of the Ag ↔ Cu, Fe ↔ Zn, Cu ↔ Fe, and As ↔ Sb exchange reactions. Amer. Mineral. 70, 1270-1289.

Sadati, S. N., Yazdi, M., Mao, J., Behzadi, M., Adabi, M. H., Lingang, X., Zhenyu, C., Mokhtari, M. A. A., 2016. Sulfide mineral chemistry investigation of sediment-hosted stratiform copper deposits, Nahand-Ivand area, NW Iran. Ore Geol. Rev. 72, 760-776.

Sandiford, M., Foden, J., Zhou, S., Turner, S., 1992. Granite genesis and the mechanics of convergent orogenic belts with application to the southern Adelaide Fold Belt. Geol. Soc. Amer. Spec. Paper 272, 83-94.

Sandiford, M. I., Eraser, G., Arnold, J., Foden, J. O., Farrow, T. R., 1995. Some causes and consequences of high-temperature, low-pressure metamorphism in the eastern Mt Lofty Ranges, South Australia. Austral. J. Earth Sci. 42, 233-240.

Scaini, M. J., Bancroft, G. M., Knipe, S. W., 1997. An XPS, AES, and SEM study of the interactions of gold and silver chloride species with PbS and FeS_2: Comparison to natural samples. Geochim. Cosmochim. Acta 61, 1223-1231.

Sadati S. N., Yazdi M., Mao J., Behzadi M., Adabi M. H., Lingang X., Zhenyu C., Mokhtari M. A. A., 2016. Sulfide mineral chemistry investigation of sediment-hosted stratiform copper deposits, Nahand-Ivand area, NW Iran. Ore Geol. Rev. 72, 760-776.

Sato, M., 1992. Persistency-field Eh-pH diagrams for sulfides and their application to supergene oxidation and enrichment of sulfide ore bodies. Geochim. Cosmochim. Acta 56, 3133-3156.

Savage K. S., Tingle T. N., O'Day P. A., Waychunas G. A., Bird D. K., 2000. Arsenic speciation in pyrite and secondary weathering phases, Mother Lode gold district, Tuolumne County, California. Appl. Geochem. 15, 1219–1244.

Savard, D., Barnes, S. J., Sunder Raju, P. V., 2010. Accurate LA-ICP-MS calibration for magnetite analysis using multiple reference materials. Geochim. Cosmochim. Acta 74, A914.

Savard, D., Raymond, V., Barnes, S. J., 2015. LA-ICP-MS analysis of massive sulphides: Progress towards a new calibration material. In: Proceedings of the 9th International Conference on the Analysis of Geological and Environmental Materials, Leoben, Austria, 8–14 August 2015; Abstract P-39, 116.

Schwartz, M. O., 2000. Cadmium in Zinc Deposits: Economic Geology of a Polluting Element. Intern. Geol. Rev. 42, 445-469.

Scott K. M., Ashley P. M., Lawie D. C., 2001. The geochemistry, mineralogy and maturity of gossans derived from volcanogenic Zn–Pb–Cu deposits of the eastern Lachlan Fold Belt, NSW, Australia. J. Geochem. Explor. 72, 169-191.

Sebba, F., Pugh, W., 1937. 281. Gallium. Part II. The extraction of gallium and germanium from germanite. Journal of the Chemical Society (Resumed), 1371-1373.

Seccombe, P. K., Spry, P. G., Both, R. A., Jones, M. T., Schiller, J. C., 1985. Base Metal Mineralization in the Kanmantoo Group, South Australia: A Regional Sulfur Isotope Study. Econ. Geol. 80, 1824-1841.

Serranti S., Ferrini V., Masi U., Nicoletti M., Conde L. N., 2002. Geochemical features of the massive sulfide (Cu) metamorphosed deposit of Arinteiro (Galicia, Spain) and genetic implications. Period. Mineral. 71, 27-48.

Serranti, S., Ferrini, V., Masi, U., Cabri, L. J., 2002. Trace-element distribution in cassiterite and sulfides from rubané and massive ores of the Corvo deposit, Portugal. Can. Mineral. 40, 815-835.

Shalaby I. M., Stumpfl E., Helmy H. M., El Mahallawi M. M., Kamel O. A., 2004. Silver and silver-bearing minerals at the Um Samiuki volcanogenic massive sulphide deposit, Eastern Desert, Egypt. Mineral. Deposita 39, 608-621.

Shannon, R., 1976. Revised effective ionic radii and systematic studies of interatomic distances in halides and chalcogenides. Acta Crystallogr. Sect. A: Cryst. Phys., Diffr., Theor. Gen. Crystallogr. 32, 751–767.

Sharp, T. G., Buseck, P. R., 1993. The distribution of Ag and Sb in galena; inclusions versus solid solution. Amer. Mineral. 78, 85-95.

Sharp, T. G., Zheng, N. J., Tsong, I. S., Buseck, P. R., 1990. Scanning tunneling microscopy of defects in Ag-and Sb-bearing galena. Amer. Mineral. 75, 1438–1442.

Sharpe, M. R., 1982. Noble metals in the marginal rocks of the Bushveld Complex. Econ. Geol. 77, 1286-1295.

Sharrad, K. A., McKinnon-Matthews, J., Cook, N. J., Ciobanu, C. L., Hand, M., 2014. The Basil Cu–Co deposit, Eastern Arunta Region, Northern Territory, Australia: A metamorphosed volcanic-hosted massive sulphide deposit. Ore Geol. Rev. 56, 141-158.

She, Y. W., Song, X. Y., Yu, S. Y., Chen, L. M., Zheng, W. Q., 2016. Apatite geochemistry of the Taihe layered intrusion, SW China: Implications for the magmatic differentiation and the origin of apatite-rich Fe-Ti oxide ores. Ore Geol. Rev. 78, 151-165.

Shimizu, M., Stanley, C. J., 1991. Coupled Substitutions in Goldfieldite-Tetrahedrite Minerals from the Iriki Mine, Japan. Mineral. Mag. 55, 515-551.

Shimizu, M., Cioflica, G., Lupulescu, M., 1995. Ore mineralogy of Romanian deposits. Part I. Stanija and Baita Bihor, Apuseni Mountains and Tincova-Valisor, Banat (SW Carpathians), Romania. Japanese Mag. Mineral. Petrol. Sci. 45, 280-281.

Shore, M., Fowler, A. D., 1996. Oscillatory zoning in minerals; a common phenomenon. Can. Mineral. 34, 1111-1126.

Silinsh, E. A., 1980. Role of Structural Defects in the Formation of Local Electronic States in Molecular Crystals. In: Organic Molecular Crystals, Springer Series in Solid-State Sciences, vol. 16, 139-222.

Simon G., Huang H., Penner-Hahn J. E., Kesler S. E., Kao L. S., 1999. Oxidation state of gold and arsenic in gold-bearing arsenian pyrite. Amer. Mineral. 84, 1071–1079.

Simon, G., Kesler, S. E., Essene, E. J., Chryssoulis, S. L., 2000. Gold in porphyry copper deposits: experimental determination of the distribution of gold in the Cu-Fe-S-Au system at 400 to 700 C. Econ. Geol. 94, 259-270.

Skauli, H., 1990. The Bleikvassli zinc-lead deposit, Nordland, North Norway; petrography, geochemistry and depositional environment. Intern Skriftserie 55.

Skauli, H., 1992. On the formation of Zn-Pb deposits: a case study of the Bleikvassli deposit, northern Norway. University of Oslo (unpubl.).

Skauli, H., 1993. A metamorphosed, potassic alteration zone associated with the Bleikvassli Zn-Pb-Cu orebody, Northern Norway. Lithos 31, 1-15.

Skauli, H., Bjørlykke, A., Thorpe, R., 1992. Lead-isotope study of the sulphide ore and alteration zone, Bleikvassli zinc-lead deposit, northern Norway. Mineral. Deposita 27, 276-283.

Skauli, H., Boyce, A., Fallick, A., 1992. A sulphur isotopic study of the Bleikvassli Zn-Pb-Cu deposit, Nordland, northern Norway. Mineral. Deposita 27, 284-292.

Smith, M. P., Henderson, P., Jeffries, T. E. R., Long, J., Williams, C. T., 2004. The rare earth elements and uranium in garnets from the Beinn an Dubhaich Aureole, Skye, Scotland, UK: constraints on processes in a dynamic hydrothermal system. J. Petrol. 45, 457-484.

Smith, M. P., Storey, C. D., Jeffries, T. E., Ryan, C., 2009. In Situ U-Pb and trace element analysis of accessory minerals in the Kiruna District, Norrbotten, Sweden: New constraints on the timing and origin of mineralization. J. Petrol. 50, 2063-2094.

Smith, J. W., Holwell, D. A., McDonald, I., Boyce, A. J., 2016. The application of S isotopes and S/Se ratios in determining ore-forming processes of magmatic Ni-Cu-PGE sulfide deposits: A cautionary case study from the northern Bushveld Complex. Ore Geol. Rev. 73, 148-174.

Socolescu, M., 1952. Asupra geologiei regiunii Baia Borşa. DS Com. Geol 36, 178-186.

Sombuthawee, C., Bonsall, S., Hummel, F., 1978. Phase equilibria in the systems ZnS–MnS, ZnS–$CuInS_2$, and MnS–$CuInS_2$. J. Solid State Chem. 25, 391-399.

Song, G. X., Qin, K. Z., Li, G. M., Evans, N. J., Chen, L., 2014. Scheelite elemental and isotopic signatures: Implications for the genesis of skarn-type W-Mo deposits in the Chizhou Area, Anhui Province, Eastern China. Amer. Mineral. 99, 303–317.

Spiridonov, E. M., Sokolova, N. F., Gapeyev, A. K., Dashevskaya, D. M., Yevstigneyeva, T. L., Chvileva, T. N., Demidov, V. G., Balashov, Y. P., Shul'ga, V. I., 1986. The new mineral argentotennantite. Dokl. Akad. Nauk SSSR 290, 206-210. (In Russian)

Spiridonov, E. M., Chvileva, T. N., Borodaev, Y. S., Vinogradova, R. A., Kononov, O. V., 1986. The influence of bismuth on optical properties of gray copper. Dokl. Akad. Nauk SSSR 290, 1475-1478. (In Russian)

Spry, P. G., Rosenberg, J. L., Jacobson, C. E., Vokes, F. M., 1995. A metamorphic sulfidation-oxidation halo associated with the Bleikvassli Zn-Pb-(Cu) deposit, Nordland, Norway. In: Pasava, J., Kribek, B., Zak, K., Eds., Mineral Deposits: from their origin to their environmental impacts, 909-912, Rotterdam.

Spry, P. G., Heimann, A., Messerly, J. D., Houk, R., 2007. Discrimination of metamorphic and metasomatic processes at the Broken Hill Pb-Zn-Ag deposit, Australia: Rare earth element signatures of garnet-rich rocks. Econ. Geol. 102, 471-494.

Spry, P. G., Plimer, I. R., Teale, G. S., 2008. Did the giant Broken Hill (Australia) Zn-Pb-Ag deposit melt? Ore Geol. Rev. 34, 223-241.

Spry, P. G., Both, R. A., Ogierman, J., McElhinney, R., Heimann, A., 2010. Origin of the Angas Pb-Zn-Ag deposit, Strathalbyn, South Australia. Society of Economic Geologists SEG 2010 Conference, Keystone, Colorado, Extended Abstract.

Stanton, R., Russell, R. D., 1959. Anomalous leads and the emplacement of lead sulfide ores. Econ. Geol. 54, 588-607.

Staude, S., Mordhorst, T., Neumann, R., Prebeck, W., Markl, G., 2010. Compositional variation of the tennantite-tetrahedrite solid-solution series in the Schwarzwald ore district

(SW Germany): The role of mineralization processes and fluid source. Mineral. Mag. 74, 309-339.

Steadman, J. A., Large, R. R., Meffre, S., Olin, P. H., Danyushevsky, L. V., Gregory, D. D., Belousov, I., Lounejeva, E., Ireland, T. R., Holden, P., 2015. Synsedimentary to early diagenetic gold in black shale-hosted pyrite nodules at the golden mile deposit, Kalgoorlie, Western Australia. Econ. Geol. 110, 1157-1191.

Stephens, M. B., Gustavson, M., Ramberg, I. B., Zachrisson, E., 1985. The Caledonides of north-central Scandinavia ± a tectono-stratigraphic overview. In: Gee, D. G., Sturt, B. A., Eds., The Caledonide orogen - Scandinavia and related areas, 135-162, John Wiley & Sons.

Stevens, B., 1986. Post-depositional history of the Willyama Supergroup in the Broken Hill Block, NSW. Austral. J. Earth Sci. 33, 73-98.

Stevens, B., Barnes, R., Brown, R., Stroud, W., Willis, T., 1988. The Willyama Supergroup in the Broken Hill and Euriowie Blocks, New South Wales. Precambr. Res. 40, 297-327.

Stillwell, F., 1959. Petrology of the Broken Hill lode and its bearing on ore genesis. The Australasian Institute of Mining and Metallurgy, Proceedings 190, 1-84.

Stillwell, F. L., Edwards, A. B., 1956. Uralite dolerite dykes in relation to the Broken Hill lode. The Australasian Institute of Mining and Metallurgy, Proceedings 178, 213-228.

Stoiber, R. E., 1940. Minor elements in sphalerite. Econ. Geol. 35, 501-519.

Strashimirov, S., 1993. Features in distribution of the ore minerals in the western periphery of the porphyry-copper deposit Assarel (in Bulgarian). Ann HIMG 39, 79-93.

Strashimirov, S., Popov, P., 2000. Geology and metallogeny of the Panagyurishte Ore region (Srednogorie Zone, Bulgaria). Geodynamics and ore deposits evolution of the Alpine-Balkan-Carpathian-Dinaride Province. (ABCD-GEODE Workshop, Brovets, Bulgaria, Guide to excursions A and C). Publishing House St Ivan Rilski, Sofia.

Strashimirov, S., Petrunov, R., Kanazirski, M., 2002. Porphyry-copper mineralisation in the central Srednogorie zone, Bulgaria. Mineral. Deposita 37, 587-598.

Stüwe, K., Ehlers, K., 1997. Multiple metamorphic events at Broken Hill, Australia. Evidence from chloritoid-bearing parageneses in the Nine-Mile Mine region. J. Petrol. 38, 1167-1186.

Stwertka, A., 1998. "Tin". Guide to the Elements, revised edition. Oxford University Press, U.K.

Subba Rao, D. V., Naqvi, S. M., 1997. Geological setting, mineralogy, geochemistry and genesis of the Middle Archaean Kalyadi copper deposit, western Dharwar craton, southern India. Mineral. Deposita 32, 230-242.

Sugaki, A., Shima, H., Kitakaze, A., 1970. Fundamental study on the quantitative analysis of sulphide minerals by electron probe microanalyser (I). Research report, faculty of engineering, Yamaguchi University 21, 87-209.

Sung, Y. H., Brugger, J., Ciobanu, C. L., Pring, A., Skinner, W., Nugus, M., 2009. Invisible gold in arsenian pyrite and arsenopyrite from a multistage Archaean gold deposit: Sunrise Dam, Eastern Goldfields Province, Western Australia. Mineral. Deposita 44, 765-791.

Sylvester, P., Ed., 2001. Laser Ablation ICP-MS in the Earth Sciences: Principles and Applications. Mineralogical Association Canada Short Course Volume 29, 243 pp.

Sylvester, P., Ed., 2008. Laser Ablation ICP-MS in the Earth Sciences: Current Practices and Outstanding Issues. Mineralogical Association of Canada Short Course Volume 40, 364 pp.

Sylvester, P. J., 2008. Matrix effects in laser ablation ICP-MS. In: Sylvester, P., Ed., Laser Ablation ICP-MS in the Earth Sciences: Current Practices and Outstanding Issues. Mineralogical Association of Canada Short Course Volume 40, 67-78.

Sylvester, P. J., Jackson, S. E., 2016. A brief history of Laser Ablation Inductively Coupled Plasma Mass Spectrometry (LA-ICP-MS). Elements 12, 307-310.

Szoke, A., Steclaci, L., 1962. Regiunea Toroiaga-Baia-Borsa. Studiu Geologic, Petrografic, Mineralogic si Geochimic. Editura Academiei Republicii Populare Romine, Bucharest, 240 pp.

Tabersky, D., Luechinger, N. A., Rossier, M., Reusser, E., Hametner, K., Aeschlimann, B., Frick, D. A., Halim, S. C., Thompson, J., Danyushevsky, L., Günther, D., 2014. Development and characterization of custom-engineered and compacted nanoparticles as calibration materials for quantification using LA-ICP-MS. J. Anal. Atom. Spectrom. 29, 955-962.

Takenouchi, S., Fujiki, Y., 1968. Experimental study on Cu-Fe-S minerals (1st report) – Application of EPMA to synthetic products. Mineral. J. (Japan) 84, 1-6.

Tauson, V. L., Paradina, L. F., Andrulaitis, L. D., 1986. The entry of mercury into galena and the new galena-sphalerite geothermometer. Geochem. Internat. 23, 55-61.

Tauson, V. L., Parkhomenko, I. Y., Babkin, D. N., Men'shikov, V. I., Lustenberg, E. E., 2005. Cadmium and mercury uptake by galena crystals under hydrothermal growth: A spectroscopic and element thermo-release atomic absorption study. Eur. J. Mineral. 17, 599-610.

Thole, R. H., 1976. The geology of the Shamrocke mine, Rhodesia - a stratiform copper deposit. Econ. Geol. 71, 202-228.

Thomas, R., 2013. Practical Guide to ICP-MS: A Tutorial for Beginners. CRC Press, Boca Raton, 446 pp.

Thomas, H. V., Large, R. R., Bull, S. W., Maslennikov, V., Berry, R. F., Fraser, R., Froud, S., Moye, R., 2011. Pyriteand pyrrhotite textures and composition in sediments, laminated quartz veins, and reefs at Bendigo Gold Mine, Australia: Insights for ore genesis. Econ. Geol. 106, 1-31.

Thompson, J., Meffre, S., Maas, R., Kamenetsky, V., Kamenetsky, M., Goemann, K., Ehrig, K., Danyushevsky, L., 2016. Matrix effects in Pb/U measurements during LA-ICP-MS analysis of the mineral apatite, J. Anal. Atom. Spectrom. 31, 1206-1215.

Thomson, B. P., 1975. Kanmantoo trough-regional geology and comments on mineralization. In: Knight, C. L., Ed., Economic Geology of Australia and Papua New Guinea – I Metals. Australasian Institute of Mining and Metallurgy Monograph 5, 555-560.

Todd, E. C., Sherman, D. M., 2003. Surface oxidation of chalcocite (Cu_2S) under aqueous (pH = 2–11) and ambient atmospheric conditions: mineralogy from Cu L-and O Kedge X-ray absorption spectroscopy. Amer. Mineral. 88, 1652-1656.

Todd, E., Sherman, D., Purton, J., 2003. Surface oxidation of chalcopyrite ($CuFeS_2$) under ambient atmospheric and aqueous (pH 2–10) conditions: Cu, Fe L-and O K-edge X-ray spectroscopy. Geochim. Cosmochim. Acta 67, 2137-2146.

Tollari, N., Barnes, S. -J., Cox, R. A., Nabil, H., 2008. Trace element concentrations in apatites from the Sept-Îles Intrusive Suite, Canada—Implications for the genesis of nelsonites. Chem. Geol. 252, 180-190.

Toteff, S., 1999. Cambrian sediment-hosted exhalative base metal mineralization, Kanmantoo Trough, South Australia. Geological Survey of South Australia, Report of Investigations 57, 41.

Trudu, A. G., Knittel, U., 1998. Crystallography, mineral chemistry and chemical nomenclature of goldfeldite, the tellurian member of the tetrahedrite solid-solution series. Can. Mineral. 36, 1115-1137.

Ubide, T., McKenna, C. A., Chew, D. M., Kamber, B. S., 2015. High-resolution LA-ICP-MS trace element mapping of igneous minerals: In search of magma histories. Chem. Geol. 409, 157-168.

Ulrich, T., Golding, S. D., Kamber, B. S., Zaw, K., Taube, A., 2002. Different mineralization styles in a volcanic-hosted ore deposit: the fluid and isotopic signatures of the Mt Morgan Au–Cu deposit, Australia. Ore Geol. Rev. 22, 61-90.

Ulrich, T., Kamber, B. S., Jugo, P. J., Tinkham, D. K., 2009. Imaging element-distribution patterns in minerals by laser ablation—Inductively coupled plasma—Mass spectrometry (LA-ICP-MS). Can. Mineral. 47, 1001-1012.

United States Geological Survey, 2016. Microanalytical Reference Materials and Accessories. Available online: <http://crustal.usgs.gov/geochemical_reference_standards/microanalytical_RM.html> (accessed on 6 October 2016).

Urasima, Y., 1968. Gold-bearing ores of the Oe ore deposits in Hokkaido. Mining Geol. 17, 328-339.

Van Achterberg, E., Ryan, C. G., Jackson, S. E., Griffin, W. L., 2001. Data reduction software for LAICP-MS. In: Sylvester, J. P., Ed., Laser-ablation-ICPMS in the Earth Sciences; Principles and applications. Mineralogical Association of Canada, Short Course Series 29, 239-243.

Van Hook, H. J., 1960. The ternary system Ag_2S-Bi_2S_3-PbS. Econ. Geol. 55, 759–788.

Vanhaecke, F., Degryse, P., Eds., 2012. Isotopic Analysis: Fundamentals and Applications using ICP-MS. Wiley-VCH Verlag GmbH & Co, Weinheim, 550 pp.

Vaughan, D. J., Craig, J. R., 1997. Sulfide ore mineral stabilities, morphologies, and intergrowth textures. In: Barnes, H. L., Ed., Geochemistry of Hydrothermal Ore Deposits 3rd edition, 367-434.

Vavelidis, M., Melfos, V., 1997. Two plumbian tetrahedrite-tennantite occurrences from Maronia area (Thrace) and Milos island (Aegean sea), Greece. Eur. J. Mineral. 9, 653-658.

Velasquez, A., 2014. Trace Element Analysis of Native Gold by Laser Ablation ICP-MS: A

Case Study in Greenstone-Hosted Quartz-Carbonate Vein Ore Deposits, Timmins, Ontario. Ph.D. Thesis, University of British Columbia, Kelowna, BC, Canada.

Verwoerd, P. J., Cleghorn, J. H., 1975. Kanmantoo copper orebody. In: Knight, C. L., Ed., Economic Geology of Australia and Papua New Guinea – I Metals. Australasian Institute of Mining and Metallurgy Monograph 5, 560-565.

Vlad, Ş., Borcoş, M., 1997. Alpine metallogenesis of the Romanian Carpathians. Rom. J. Mineral Deposits 78, 5-20.

Vokes, F. M., 1963. Geological studies on the Caledonian pyritic zinc-lead orebody at Bleikvassli, Norland, Norway. Norg. Geol. Unders. 222, 1-126.

Vokes, F. M., 1966. On the possible modes of origin of the Caledonian sulfide ore deposit at Bleikvassli, Nordland, Norway. Econ. Geol. 61, 1130-1139.

von Cotta, B., 1864. Erzlagerstätten im Banat und in Serbien. Braumüller.

Von Quadt, A., Moritz, R., Peytcheva, I., Heinrich, C. A., 2005. 3: Geochronology and geodynamics of Late Cretaceous magmatism and Cu–Au mineralization in the Panagyurishte region of the Apuseni–Banat–Timok–Srednogorie belt, Bulgaria. Ore Geol. Rev. 27, 95-126.

Voropayev, A. V., Spiridonov, E. M., Shchibrik, V. I., 1988. Cd-Tetrahedrite, first find in the USSR. Dokl. Acad. Sci. USSR. 300, 1446-1468.

Voudouris, P. C., Spry, P. G., Sakellaris, G. A., Mavrogonatos, C., 2011. A cervelleite-like mineral and other Ag-Cu-Te-S minerals [Ag_2CuTeS and $(Ag, Cu)_2TeS$] in gold-bearing veins in metamorphic rocks of the Cycladic Blueschist Unit, Kallianou, Evia Island, Greece. Mineral. Petrol. 101, 169-183.

Wang, Y., Merino, E., 1992. Dynamic model of oscillatory zoning of trace elements in calcite: double layer, inhibition, and self-organization. Geochim. Cosmochim. Acta 56, 587-596.

Wang G., Wang Z. Q., Shi R., Zhang Y. L., Wang K. M., 2015. Mineralogy and isotope geochemical characteristics for Xiaozhen copper deposit, Langao County, Shaanxi Province and their constraint on genesis of the deposit. Geosci. J. 19, 281-294.

Wang, Z., Xu, D., Zhang, Z., Zou, F., Wang, L., Yu, L., Hu, M., 2015. Mineralogy and trace element geochemistry of the Co-and Cu-bearing sulfides from the Shilu Fe–Co–Cu ore district in Hainan Province of South China. J. Asian Earth Sci. 113, 980-997.

Warren, H. V., 1932. Relation between silver content and tetrahedrite in the ores of the North Cananea Mining Co., Cananea, Sonora, Mexico. Econ. Geol. 27, 737-743.

Warren, H. V., Loofbourow, R. W., 1932. The occurrence and distribution of silver in the silver king coalition mines, Park City, Utah. Econ. Geol. 27, 644-650.

Warren, M. R., Hanley, J. J., Ames, D. E., Jackson, S. E., 2015 The Ni–Cr–Cu content of biotite as pathfinder elements for magmatic sulfide exploration associated with mafic units of the Sudbury Igneous Complex, Ontario, Canada. J. Geochem. Explor. 153, 11-29.

Watson, E. B., 1991. Diffusion in fluid-bearing and slightly-melted rocks: experimental and numerical approaches illustrated by iron transport in dunite. Contrib. Mineral. Petrol. 107, 417-434.

Watson, E. B., Harrison, T. M., 2005. Zircon thermometer reveals minimum melting conditions on earliest Earth. Science 308, 841–844.

Watson, E. B., Lupulescu, A., 1993. Aqueous fluid connectivity and chemical transport in clinopyroxene-rich rocks. Earth Planet. Sci. Lett. 117, 279-294.

Watson, E. B., Chemiak, D. J., Hanchar, J. M., Harrison, T. M., Wark, D. A., 1997. The incorporation of Pb into zircon. Chem. Geol. 141, 19-31.

Watson, E., Wark, D., Thomas, J., 2006. Crystallization thermometers for zircon and rutile. Contrib. Mineral. Petrol. 151, 413–433.

Webster, A. E., 2006. The geology of the Broken Hill lead-zinc-silver deposit, New South Wales, Australia. ARC Centre of Excellence in Ore Deposits (CODES), CODES Monograph 1, 278.

Wernick, J. H., 1960. Constitution of the $AgSbS_2$-PbS, $AgBiS_2$-PbS, and $AgBiS_2$-$AgBiSe_2$ systems. Amer. Mineral. 45, 591-598.

White, W. M., Albarède, F., Télouk, P., 2000. High-precision analysis of Pb isotope ratios by multi-collector ICP-MS. Chem. Geol. 167, 257-270.

Wilkinson, J. J., Chang, Z., Cooke, D. R., Baker, M. J., Wilkinson, C. C., Inglis, S., Chen, H., Gemmell, J. B., 2015. The chlorite proximitor: A new tool for detecting porphyry ore deposits. J. Geochem. Explor. 152, 10-26.

Wilson, S. A., 1997. The collection, preparation, and testing of USGS reference material BCR-2, Columbia River, Basalt. U.S.G.S. Open File Report, 98-00x.

Wilson, S. A., Ridley, W. I., Koenig, A. E., 2002. Development of sulfide calibration standards for the laser ablation inductively-coupled plasma mass spectrometry technique. J. Anal. Atom. Spectrom. 17, 406–409.

Winderbaum, L., Ciobanu, C. L., Cook, N. J., Paul, M., Metcalfe, A., Gilbert, S., 2012. Multivariate Analysis of an LA-ICP-MS Trace Element Dataset for Pyrite. Math. Geosci. 44, 823-842.

Wittmann, A., 1974. Indium. 49-A Crystal Chemistry. In: Wedepohl, K. H., Ed

., Handbook of geochemistry: Berlin, Springer-Verlag, v. II/4, 49-A-1-49-A-8.

Wohlgemuth-Ueberwasser, C. C., Jochum, K. P., 2015. Capability of fs-LA-ICP-MS for sulfide analysis in comparison to ns-LA-ICP-MS: reduction of laser induced matrix effects? J. Anal. Atom. Spectrom. 30, 2469-2480.

Wohlgemuth-Ueberwasser, C. C., Ballhaus, C., Berndt, J., Stotter, V., Meisel, T., 2007. Synthesis of PGE sulphide standards for laser ablation inductively coupled plasma mass spectrometry (LA-ICP-MS). Contrib. Mineral. Petrol. 154, 607-617.

Wohlgemuth-Ueberwasser, C. C., Viljoen, F., Petersen, S., Vorster, C., 2015. Distribution and solubility limits of trace elements in hydrothermal black smoker sulfides: An in-situ LA-ICP-MS study. Geochim. Cosmochim. Acta 159, 16-41.

Woodhead, J., Hergt, J., Meffre, S., Large, R. R., Danyushevsky, L., Gilbert, S., 2009. In situ Pb-isotope analysis of pyrite by laser ablation (multi-collector and quadrupole) ICPMS. Chem. Geol. 262, 344-354.

Woodhead, J. D., Horstwood, M. S. A., Cottle, J. M., 2016. Advances in isotope ratio determination by LA-ICP-MS. Elements 12, 317-322.

Wuensch, B. J., 1964. The crystal structure of tetrahedrite, $Cu_{12}Sb_4S_{13}$. Zeitschrift Krist. Cryst. Mater. 119, 437-453.

Wuensch, B. J., Tackeuchi, Y., Nowacki, W., 1966. Refinement of the crystal structure of binnite, $Cu_{12}As_4S_{13}$. Zeitschrift Krist. Cryst. Mater. 123, 1-20.

Xu, L., Bi, X., Hu, R., Tang, Y., Wang, X., Xu, Y., 2015. LA-ICP-MS mineral chemistry of titanite and the geological implications for exploration of porphyry Cu deposits in the Jinshajiang–Red River alkaline igneous belt, SW China. Mineral. Petrol. 109, 181-200.

Xu, J., Ciobanu, C. L., Cook, N. J., Zheng, Y., Sun, X., Wade, B. P., 2016. Skarn formation and trace elements in garnet and associated minerals from Zhibula copper deposit, Gangdese Belt, southern Tibet. Lithos 262, 213-231.

Ye, L., Cook, N. J., Ciobanu, C. L., Liu, Y. P., Zhang, Q., Gao, W., Yang, Y. L., Danyushevsky, L. V., 2011. Trace and minor elements in sphalerite from base metal deposits in South China: a LA-ICPMS study. Ore Geol. Rev. 39, 188–217.

Yuan, J. H., Zhan, X. C., Fan, C. Z., Zhao, L. H., Sun, D. Y., Jia, Z. R., Hu, M. Y., Kuai, L. J., 2012. Quantitative analysis of sulfide minerals by laser ablation-inductively coupled plasma-mass spectrometry using glass reference materials with matrix normalization plus sulfur internal standardization calibration. Chin. J. Anal. Chem. 40, 201-207.

Zack, T., Stockli, D. F., Luvizotto, G. L., Barth, M. G., Belousova, E., Wolfe, M. R., Hinton, R.W., 2011. In situ U-Pb rutile dating by LA-ICP-MS ^{208} Pb correct ion and prospects for geological applications: Contrib. Mineral. Petrol. 162, 515-530.

Zajacz, Z., Halter, W., 2007. LA-ICPMS analyses of silicate melt inclusions in co-precipitated minerals: Quantification, data analysis and mineral/melt partitioning. Geochim. Cosmochim. Acta 71, 1021-1040.

Zanetell, Z. A., 2007. Penalty element separation from copper concentrates utilizing froth flotation. Masters thesis, Colorado School of Mines, Colorado, USA.

Zhang, J., Deng, J., Chenb, H. Y., Yang, L. Q., Cooke, D., Danyushevsky, L., Gong, Q. J., 2014. LA-ICP-MS trace element analysis of pyrite from the Chang'an gold deposit, Sanjiang region, China: Implication for ore-forming process. Gondwana Res. 26, 557-575.

Zhao, W. W., Zhou, M. F., 2015. In-situ LA-ICP-MS trace element alanalyses of magnetite: The Mesozoic Tengtie skarn Fe deposit in the Nanling Range, South China. Ore Geol. Rev. 65, 872-883.

Zhdanov, Y. Y., Amuzinskii, V. A., Andrianov, N. G., 1992. Discovery of a natural Ag-rich fahlore with the highest parameter of the unit cell. Dokl. Akad. Nauk SSSR 326, 337-340. (In Russian)

Zhu, Z. Y., Yang, T., Ciobanu, C. L., Cook, N. J., Zhao, K. D., Jiang, S. Y., 2016. Mapping of S isotopes and trace elements in sulfides by LA-(MC)-ICP-MS: Potential problems and implications. Minerals 6, 110.

Zhu, Z. Y., Jiang, S. Y., Yang, T., Ciobanu, C. L., Cook, N. J., 2017. Sulfur isotope fractionation in pyrite during laser ablation: Implications for Laser Ablation Multiple Collector Inductively Coupled Plasma Mass Spectrometry mapping. Chem. Geol. 450, 223-234.

Zielinski, R. A., Frey, F. A., 1974. An experimental study of the partitioning of a rare earth element (Gd) in the system diopside—aqueous vapour. Geochim. Cosmochim. Acta 38, 545-565.

Zimmerman, A., Stein, H. J., Hannah, J. L., Kozely, D., Bogdanov, K., Berza, T., 2008. Tectonic configuration of the Apuseni–Banat—Timok–Srednogorie belt, Balkans-South Carpathians, constrained by high precision Re–Os molybdenite ages. Mineral. Deposita 43, 1-21.